CONTENTS

Part 1

PREFACE . . . . iii 1/A6

1. INTRODUCTORY REMARKS 1 1/A12
Roger L. Winblade

SESSION 1 - TERMINAL-AREA OPERATIONS
Cochairmen: T. M. Walsh and R. L. Kurkowski

2. TEST RESULTS OF FLIGHT GUIDANCE FOR FUEL CONSERVATIVE DESCENTS IN A TIME-BASED METERED AIR TRAFFIC ENVIRONMENT 7 1/B4
Charles E. Knox and Lee H. Person, Jr.

3. A PILOT'S SUBJECTIVE ANALYSIS OF A COCKPIT DISPLAY OF TRAFFIC INFORMATION (CDTI) 29 1/C12
Gerald L. Keyser, Jr.

4. GUIDANCE AND CONTROL SYSTEM RESEARCH FOR IMPROVED TERMINAL AREA OPERATIONS 51 1/E6
R. M. Hueschen, J. F. Creedon, W. T. Bundick, and J. C. Young

5. OPERATIONAL CONSIDERATIONS IN UTILIZATION OF MICROWAVE LANDING SYSTEM APPROACH AND LANDING GUIDANCE 83 1/G10
William F. White and Leonard V. Clark

6. AUTOMATED PILOT ADVISORY SYSTEM TEST AND EVALUATION AT MANASSAS MUNICIPAL AIRPORT 113 2/B4
John L. Parks, Jr.

7. A METHOD FOR DETERMINING LANDING RUNWAY LENGTH FOR A STOL AIRCRAFT 127 2/C14
D. M. Watson, G. H. Hardy, D. F. Moran, and D. N. Warner, Jr.

8. FLIGHT TESTS OF IFR LANDING APPROACH SYSTEMS FOR HELICOPTERS 145 2/E4
J. S. Bull, D. M. Hegarty, L. L. Peach, J. D. Phillips, D. J. Anderson, D. C. Dugan, and V. L. Ross

9. A HEAD-UP DISPLAY FORMAT FOR TRANSPORT AIRCRAFT APPROACH AND LANDING 165 2/F10
Richard S. Bray and Barry C. Scott

MICROFILMED FROM BEST
AVAILABLE COPY

SESSION II - AVIONICS AND HUMAN FACTORS
Cochairmen: M. D. Montemerlo and A. B. Chambers

10. AN EVALUATION OF HEAD-UP DISPLAYS IN CIVIL TRANSPORT OPERATIONS 197 **3/B2**
John K. Lauber, Richard S. Bray, and Barry C. Scott

11. GENERAL AVIATION SINGLE PILOT IFR AUTOPILOT STUDY 201 **3/B6**
Hugh P. Bergeron

12. APPLICATION OF THE EPIDEMIOLOGICAL MODEL IN STUDYING HUMAN ERROR IN AVIATION 219 **3/C10**
Ed S. Cheaney and Charles E. Billings

13. HOW A PILOT LOOKS AT ALTITUDE 237 **3/D14**
Amos A. Spady, Jr., and Randall L. Harris, Sr.

SESSION III - ATMOSPHERIC ENVIRONMENT
Cochairmen: D. W. Camp and L. J. Ehernberger

14. SUMMARY OF FLIGHT TESTS OF AN AIRBORNE LIGHTNING LOCATOR SYSTEM AND COMPARISON WITH GROUND-BASED MEASUREMENTS OF PRECIPITATION AND TURBULENCE 251 **3/E14**
Bruce D. Fisher and Norman L. Crabill

15. WALLOPS SEVERE STORMS MEASUREMENT CAPABILITY 279 **4/A3**
Robert E. Carr and John C. Gerlach

16. THE 1979 CLEAR AIR TURBULENCE FLIGHT TEST PROGRAM 293 **4/B3**
E. A. Weaver, L. J. Ehernberger, B. L. Gary,
R. L. Kurkowski, P. M. Kuhn, and E. P. Stearns

17. PULSED DOPPLER LIDAR FOR THE DETECTION OF TURBULENCE IN CLEAR AIR 313 **4/C9**
E. A. Weaver, J. W. Bilbro, J. A. Dunkin, S. C. Johnson
W. D. Jones, C. E. Harris, and C. A. DiMarzio

18. FLIGHT TESTS OF A CLEAR-AIR TURBULENCE ALERTING SYSTEM 329 **4/D11**
Richard L. Kurkowski, Peter M. Kuhn, and Ernest P. Stearns

19. CLEAR AIR TURBULENCE STUDIES WITH MICROWAVE RADIOMETERS 351 **4/F5**
Bruce L. Gary

20. IN-FLIGHT DIRECT-STRIKE LIGHTNING RESEARCH 359 **4/F13**
Felix L. Pitts and Mitchel E. Thomas

21. MAGNITUDE AND FREQUENCY OF WIND SPEED SHEARS AND ASSOCIATED DOWNDRAFTS 373 **4/G13**
Margaret B. Alexander and C. Warren Campbell

MICROFILMED FROM BEST
AVAILABLE COPY

APR 2 1981
Item 830-H-10
NAS 1.55:2170/pt 1

NASA Conference Publication 2170
Part 1

1980 Aircraft Safety and Operating Problems

ORIGINAL

COMPLETED

Proceedings of a conference
held at NASA Langley Research Center
Hampton, Virginia
November 5-7, 1980

NASA Conference Publication 2170
Part 1

1980 Aircraft Safety and Operating Problems

Joseph W. Stickle, *Compiler*
Langley Research Center
Hampton, Virginia

Proceedings of a NASA conference
held at Langley Research Center
Hampton, Virginia
November 5-7, 1980

NASA
National Aeronautics
and Space Administration

Scientific and Technical
Information Office

1981

BLANK PAGE

BLANK PAGE

PREFACE

This Conference Publication contains the proceedings of the 1980 NASA Aircraft Safety and Operating Problems Conference held at the Langley Research Center, Hampton, VA, on November 5-7, 1980. The purpose of the conference was to report results of research activities within NASA in the field of aircraft safety and operating problems. The last conference reporting on this subject was held at Langley on October 18-20, 1976.

The 1980 conference contained sessions on: Terminal-Area Operations; Avionics and Human Factors; Atmospheric Environment; Operating Problems and Potential Solutions; Flight Experiences and Ground Operations; and Acoustics and Noise Reduction. In many instances the verbal presentations summarized the work of several researchers in a particular area. The published proceedings provided for individual reporting of the research efforts. In addition, a few research activities which were not selected for presentation due to other recent exposure have been included in order to more accurately portray the scope of the Aircraft Safety and Operating Problems Program within NASA.

The size of the compilation necessitated publication in two parts (Parts 1 and 2). A list of attendees, by organizational affiliation, is included at the back of Part 2.

Use of trade names or names of manufacturers in this report does not constitute an official endorsement of such products or manufacturers, either expressed or implied, by the National Aeronautics and Space Administration.

Joseph W. Stickle
Allen R. Tobiason
Conference Cochairmen

BLANK PAGE

BLANK PAGE

CONTENTS

Part 1

PREFACE iii

1. INTRODUCTORY REMARKS 1
Roger L. Winblade

SESSION I - TERMINAL-AREA OPERATIONS
Cochairmen: T. A. Walsh and R. L. Kurkowski

2. TEST RESULTS OF FLIGHT GUIDANCE FOR FUEL CONSERVATIVE DESCENTS IN A TIME-BASED METERED AIR TRAFFIC ENVIRONMENT 7
Charles E. Knox and Lee H. Person, Jr.

3. A PILOT'S SUBJECTIVE ANALYSIS OF A COCKPIT DISPLAY OF TRAFFIC INFORMATION (CDTI) 29
Gerald L. Keyser, Jr.

4. GUIDANCE AND CONTROL SYSTEM RESEARCH FOR IMPROVED TERMINAL AREA OPERATIONS 51
R. M. Hueschen, J. F. Creedon, W. T. Bundick, and J. C. Young

5. OPERATIONAL CONSIDERATIONS IN UTILIZATION OF MICROWAVE LANDING SYSTEM APPROACH AND LANDING GUIDANCE 83
William F. White and Leonard V. Clark

6. AUTOMATED PILOT ADVISORY SYSTEM TEST AND EVALUATION AT MANASSAS MUNICIPAL AIRPORT 113
John L. Parks, Jr.

7. A METHOD FOR DETERMINING LANDING RUNWAY LENGTH FOR A STOL AIRCRAFT 127
D. M. Watson, G. H. Hardy, J. F. Moran, and D. N. Warner, Jr.

8. FLIGHT TESTS OF IFR LANDING APPROACH SYSTEMS FOR HELICOPTERS 145
J. S. Bull, D. M. Hegarty, L. L. Peach, J. D. Phillips, D. J. Anderson, D. C. Dugan, and V. L. Ross

9. A HEAD-UP DISPLAY FORMAT FOR TRANSPORT AIRCRAFT APPROACH AND LANDING. 165
Richard S. Bray and Barry C. Scott

SESSION II - AVIONICS AND HUMAN FACTORS

Cochairmen: M. D. Montemerlo and A. B. Chambers

10. AN EVALUATION OF HEAD-UP DISPLAYS IN CIVIL TRANSPORT OPERATIONS 197
John K. Lauber, Richard S. Bray, and Barry C. Scott

11. GENERAL AVIATION SINGLE PILOT IFR AUTOPILOT STUDY 201
Hugh P. Bergeron

12. APPLICATION OF THE EPIDEMIOLOGICAL MODEL IN STUDYING HUMAN ERROR IN AVIATION 219
Ed S. Cheaney and Charles E. Billings

13. HOW A PILOT LOOKS AT ALTITUDE 237
Amos A. Spady, Jr., and Randall L. Harris, Sr.

SESSION III - ATMOSPHERIC ENVIRONMENT

Cochairmen: D. W. Camp and L. J. Eherenberger

14. SUMMARY OF FLIGHT TESTS OF AN AIRBORNE LIGHTNING LOCATOR SYSTEM AND COMPARISON WITH GROUND-BASED MEASUREMENTS OF PRECIPITATION AND TURBULENCE 251
Bruce D. Fisher and Norman L. Crabill

15. WALLOPS SEVERE STORMS MEASUREMENT CAPABILITY 279
Robert E. Carr and John C. Gerlach

16. THE 1979 CLEAR AIR TURBULENCE FLIGHT TEST PROGRAM 293
E. A. Weaver, L. J. Ehernberger, B. L. Gary,
R. L. Kurkowski, P. M. Kuhn, and L. P. Stearns

17. PULSED DOPPLER LIDAR FOR THE DETECTION OF TURBULENCE IN CLEAR AIR 313
E. A. Weaver, J. W. Bilbro, J. A. Dunkin, S. C. Johnson
W. D. Jones, C. E. Harris, and C. A. DiMarzio

18. FLIGHT TESTS OF A CLEAR-AIR TURBULENCE ALERTING SYSTEM 329
Richard L. Kurkowski, Peter M. Kuhn, and Lois P. Stearns

19. CLEAR AIR TURBULENCE STUDIES WITH MICROWAVE RADIOMETERS 351
Bruce L. Gary

20. IN-FLIGHT DIRECT-STRIKE LIGHTNING RESEARCH 359
Felix L. Pitts and Mitchel E. Thomas

21. MAGNITUDE AND FREQUENCY OF WIND SPEED SHEARS AND ASSOCIATED DOWNDRAFTS 373
Margaret B. Alexander and C. Warren Campbell

Part 2*

SESSION IV - OPERATING PROBLEMS AND POTENTIAL SOLUTIONS
Chairman: H. W. Schmidt

22. WAKE VORTEX ATTENUATION FLIGHT TESTS: A STATUS REPORT 387
Marvin R. Barber and Joseph J. Tymczyszyn

23. BASIC RESEARCH IN WAKE VORTEX ALLEVIATION USING A VARIABLE TWIST WING 409
Dana J. Morris and G. Thomas Holbrook

24. PNEUMATIC BOOT FOR HELICOPTER ROTOR DEICING 425
Bernard J. Blaha and Peggy L. Evanich

25. AIRCRAFT OPERATING EFFICIENCY ON THE NORTH ATLANTIC - A CHALLENGE FOR THE 1980'S 445
Robert Steinberg

26. FIREWORTHINESS OF TRANSPORT AIRCRAFT INTERIOR SYSTEMS 453
John A. Parker and D. A. Kourtides

27. COMBUSTION TOXICOLOGY OF EPOXY/CARBON FIBER COMPOSITES 481
D. E. Cagliostro

28. THE USE OF ANTIMISTING KEROSENE (AMK) IN TURBOJET ENGINES 499
Harold W. Schmidt

29. NASA/FAA GENERAL AVIATION CRASH DYNAMICS PROGRAM 511
Robert G. Thomson, Robert J. Hayduk, and Huey D. Carden

SESSION V - FLIGHT EXPERIENCES AND GROUND OPERATIONS
Chairman: J. L. McCarty

30. CURRENT RESEARCH IN AIRCRAFT TIRE DESIGN AND PERFORMANCE 543
John A. Tanner and John L. McCarty

31. REVIEW OF ANTISKID AND BRAKE DYNAMICS RESEARCH 555
Sandy M. Stubbs and John A. Tanner

32. STUDIES OF SOME UNCONVENTIONAL SYSTEMS FOR SOLVING VARIOUS LANDING PROBLEMS 569
T. J. W. Leland, J. R. McGehee, and R. C. Dreher

33. RECENT PROGRESS TOWARDS PREDICTING AIRCRAFT GROUND HANDLING PERFORMANCE 583
Thomas J. Yager and Ellis J. White

---

*Papers 22 to 40 are published under separate cover.

34. THE NASA DIGITAL VGH PROGRAM - EARLY RESULTS 613
Norman L. Crabill and Garland J. Morris

35. EVALUATION OF EMERGENCY-LOCATOR-TRANSMITTER PERFORMANCE IN REAL AND SIMULATED CRASH TESTS 625
Huey D. Carden

36. EXTINGUISHING IN-FLIGHT ENGINE FUEL-LEAK FIRES WITH DRY CHEMICALS 655
Robert L. Altman

SESSION VI - ACOUSTICS AND NOISE REDUCTION
Chairman: H. G. Morgan

37. RECENT DEVELOPMENTS IN AIRCRAFT ENGINE NOISE REDUCTION TECHNOLOGY 671
James R. Stone and Charles E. Feiler

38. SOURCES, CONTROL, AND EFFECTS OF NOISE FROM AIRCRAFT PROPELLERS AND ROTORS 699
John S. Mixson, George C. Greene, and Thomas K. Dempsey

39. NASA PROGRESS IN AIRCRAFT NOISE PREDICTION 721
J. P. Raney, S. L. Padula, and W. E. Zorumski

40. AIRPORT NOISE IMPACT REDUCTION THROUGH OPERATIONS 759
Richard DeLoach

ATTENDEES 779

INTRODUCTORY REMARKS

by

Roger L. Winblade
Manager, Transport Aircraft Office
Aeronautical Systems Division
NASA Headquarters
Washington, DC 20546

It is with great pleasure that I welcome you to this Conference on behalf of NASA Headquarters and the NASA Centers represented here today. The purposes of this Conference are to update the aviation community on significant NASA research accomplishments in aircraft safety, operating problems and human factors since the last Conference in 1976 and gain feedback from the aviation community.

Based on previous conferences, I believe these next few days will be both enjoyable and profitable to you, representing the aviation industry, and the NASA Centers and Headquarters. We see in this Conference a continuation of a unique and vital relationship between government, industry and the military that started here at Langley some 65 years ago. It is interesting to note a supporting conclusion reached at this summer's workshop conducted by the National Research Council's Aeronautics and Space Engineering Board, which deliberated on NASA's future role in aeronautics: A conclusion reached at the workshop was the NASA/Industry relationship is a model of a successful Government-industry partnership.

As you can see from the Conference agenda, there will be a wide range of topics discussed and the available time only allows summarizing research of wide interest. The Conference proceedings will also contain papers not presented here. Fewer presentations this year will allow more time for interaction between you and the NASA researchers. We need your feedback, both here and following this Conference, and I encourage you to establish a solid one-on-one relationship with NASA in your areas of interest so that we can maintain the most useful research program for industry, military, and government needs.

By any measure, aviation is by far the safest means of public transportation and many categories of aircraft users are continuing to improve an already enviable safety record. But aviation has its critics and we should try to learn from them that which is useful. In the last year or so, there have been three formal reports, by the Government Accounting Office, National Academy of Sciences and the SAFER Committee, which have made recommendations on improving aviation safety. These studies concentrated on specific issues such as safety management, human factors, airworthiness and fireworthiness. In some cases, these reports have noted the high level of aviation safety and also recognize safety improvements will be incremental.

We learn a lot from formal studies such as these about safety problems and issues as well as our own perceptions. Some of you may be aware that NASA, on a selective basis, participates in on-scene accident investigations because of a particular unique NASA capability or facility. An example of this means of real world experience is Langley's research on aircraft ground handling problems.

Even though the safety record is excellent, we must collectively pursue research that will help make the record even better. NASA views the entire aviation community as its reason for being and wishes to be responsive to its needs. However, in some cases, we must exercise our own judgment, for we recognize that the perceived needs of the aviation community can be driven by near-term problems and events.

It is difficult to clearly categorize aircraft operating problems, human factors and safety. Much of NASA's research involves all three categories, and the first paper, "Test Results of Flight Guidance for Fuel Conservative Descents in a Time-Based Metered Air Traffic Environment," is an example showing the important inter-relationships between man, the machine and the environment, whether the environment be man-made or natural. The first session, "Terminal-Area Operations," also demonstrates the cooperative interactions between NASA and the FAA in developing new technology concepts for future aircraft systems in future ATC environments.

A number of new research programs have been initiated since the last Conference in 1976, while others have been developed into a more mature and productive research. An example of maturing research is the concept of improving safety by increased situation awareness by flight crews using new technology displays for flight guidance and conflicting traffic evolving from the early MLS demonstrations by the Langley B-737 Terminal Configured Vehicle (TCV). The entire air transport industry, in particular, will benefit from TCV research that has established the credibility of advanced avionics and display concepts for the third generation fuel-efficient transport now under development. Other examples of maturing research include the Aviation Safety Report System (ASRS) and Fireworthiness and Head-up Display research at Ames; Anti-Misting Kerosene and Icing research at Lewis; and Severe Storms and Aircraft Noise and Aircraft Ground Handling research at Langley.

A significant opportunity now exists to exploit NASA research in operating problems and safety in advanced flight training simulators now required by the FAA. NASA research on aircraft performance on abnormal runway surfaces, in wind shear and icing conditions, and profile descents and aircraft operations in the terminal environment should be useful in advanced simulators.

In closing, I think you will find that significant and useful progress has been achieved in aircraft safety, operating problems and human factors research since our last Conference, and that you will gain some insight into future research that will involve many industry and Government organizations represented here this week. We welcome comments you may have on how the Conference met your expectations and needs. On behalf of the Conference organizing committee, NASA Headquarters, and the NASA researchers, I thank you for taking time from your busy schedules to attend this Conference.

BLANK PAGE

BLANK PAGE

SESSION I - TERMINAL-AREA OPERATIONS

BLANK PAGE

BLANK PAGE

TEST RESULTS OF FLIGHT GUIDANCE FOR FUEL CONSERVATIVE DESCENTS IN A TIME-BASED METERED AIR TRAFFIC ENVIRONMENT

Charles E. Knox and Lee H. Person, Jr.
Langley Research Center

ABSTRACT

The NASA has developed, implemented, and flight tested a flight management algorithm designed to improve the accuracy of delivering an airplane in a fuel-conservative manner to a metering fix at a time designated by air traffic control. This algorithm provides a 3-D path with time control (4-D) for the TCV B-737 airplane to make an idle-thrust, clean configured (landing gear up, flaps zero, and speed brakes retracted) descent to arrive at the metering fix at a predetermined time, altitude, and airspeed. The descent path is calculated for a constant Mach/airspeed schedule from linear approximations of airplane performance with considerations given for gross weight, wind, and nonstandard pressure and temperature effects. This report describes the flight management descent algorithms and presents the results of the flight tests.

SUMMARY

The Federal Aviation Administration has developed an automated time-based metering form of air traffic control for arrivals into the terminal area called local flow management/profile descent (LFM/PD). The LFM/PD concept provides fuel savings by matching the airplane arrival flow to the airport acceptance rate through time control computations and by allowing the pilot to descend at his discretion from cruise altitude to the metering fix. Substantial fuel savings have resulted from LFM/PD but air traffic control workload is high since the radar controller maintains time management for each airplane through either speed control or path stretching with radar vectors. Pilot workload is also high since the pilot must plan the descent to the metering fix using various rules-of-thumb.

The NASA has implemented and flight tested a flight management descent algorithm designed to improve the accuracy of delivering the airplane to a metering fix at a time designated by air traffic control in its Terminal Configured Vehicle (TCV) Boeing 737 airplane. This algorithm provides a 3-D path with time control (4-D) for the TCV Boeing 737 airplane to make an idle-thrust, clean-configured descent to arrive at the metering fix at a predetermined time, altitude, and airspeed. The descent path is calculated for a constant Mach/airspeed schedule using linear approximations of airplane performance accounting for gross weight, wind, and nonstandard pressure and temperature effects.

Flight test data were obtained on 19 flight test runs to the metering fix. The standard deviation of metering fix arrival time error was 12 sec with no arrival time error greater than 29 sec. Comparable statistics for time error accumulated between the top of descent and the metering fix (approximately 40 n.mi.) are a 6.9-sec standard deviation with no error greater than 15 sec. The airspeed and altitude error at the metering fix have standard deviations of 6.5 KCAS and 23.7 m (77.8 ft), respectively, and the maximum errors were less than 12.9 KCAS and 51.51 m (169 ft).

INTRODUCTION

Rising fuel costs combined with other economic pressures have resulted in industry requirements for more efficient air traffic control and aircraft operations. The Federal Aviation Administration (FAA) has developed an automated form of time-based metering air traffic control (ATC) for arrivals into airport terminals called local flow management/profile descent (LFM/PD). This concept provides for increased airport capacity and fuel savings by combining time-based metering with profile descent procedures. Time-based metering procedures provide for sequencing airport arrivals through time control of airplanes at metering fixes located 30 to 40 n.mi. from the airport. Time metering airplanes at these fixes reduce the low altitude vectoring (and subsequent fuel burned) required to position the airplanes into a final queue for landing. In addition, delays due to terminal area sequencing may be absorbed at higher altitudes further minimizing fuel usage (refs. 1 and 2).

Profile descent procedures allow the pilot to descend at his discretion so that he passes the metering fix at a specified altitude and airspeed. This procedure allows the pilot to plan his descent in a fuel-conservative manner accounting for the performance characteristics of his particular airplane.

In the original operational concept of the time based metering LFM/PD program, the flight crew was responsible for both the descent and time navigation to the metering fix. However, the pilots had little, or no, electronically computed guidance to aid them with this highly constrained (fuel efficient descent with a fixed time objective), 4-D navigation problem. Flight crews were forced to rely on past experience and various rules-of-thumb to plan descents. This resulted in unacceptably high cockpit workloads and the full potential of fuel savings from a planned descent not being obtained (ref. 3).

In an effort to reduce the cockpit workload, the responsibility of delivering the airplane to the metering fix at an assigned time was transferred to the ATC controller. The ATC controller directs each airplane to arrive at the metering fix at the assigned time through path stretching radar vectors and/or speed control commands to the pilot. These operations have resulted in airplane arrival time accuracy at the metering fix of approximately ±2 min (ref. 4). This arrival time accuracy may be improved with a significant increase in workload for the ATC controller, but an even further reduction of the time dispersions at the metering fix can produce further fuel savings.

Splitting the navigation responsibilities between the flight crew and ATC controller reduced the pilot's workload. However, when the ATC controller must apply path stretching or speed control for time management purposes, the pilot is forced to deviate from his planned descent profile; thus, more than the minimum fuel required is used.

The NASA has flight tested in its Terminal Configured Vehicle (TCV) Boeing 737 research airplane a flight management descent algorithm designed to increase fuel savings by improving the accuracy of delivering the airplane to the metering fix at an ATC designated time and by transferring the responsibility of time navigation from the radar controller to the flight crew. The algorithm computes a profile descent to the metering fix based on airplane performance at idle-thrust and in a clean configuration (landing gear up, flaps zero, and speed brakes retracted). Time and path guidance is provided to the pilot for a constant Mach, constant airspeed descent to arrive at the metering fix at a predetermined (ATC specified) time, altitude, and airspeed.

Flight tests using the flight management descent algorithm were conducted in the Denver, Colorado, LFM/PD ATC environment. The purpose of these flight tests was to quantify the accuracy of the airplane's descent algorithm and to investigate the compatibility and pilot acceptability of an airplane equipped with a 4-D navigation system in an actual ATC environment. This report will present the results of these tests.

SYMBOLOGY

ACLT	actual computed landing time
ARTCC	air route traffic control center
ATC	air traffic control
CLR	clearance
CRT	cathode ray tube
EADI	electronic attitude director indicator
EHSI	electronic horizontal situation indicator
ETA	estimated time of arrival
GW	gross weight
h_{AP}	altitude at the aim point
h_C	altitude at cruise
h_{MF}	altitude at the metering fix

h_{XO}	altitude to transition from a constant Mach to a constant airspeed descent
KCAS	calibrated airspeed, knots
LFM/PD	local flow management/profile descent
MF	metering fix
M_C	Mach number at cruise
M_d	Mach number in descent
NCDU	navigation control and display unit
NCU	navigation computer unit
RNAV	area navigation
TAT	total air temperature
TCV	terminal configured vehicle
VORTAC	very high frequency omnidirectional range and distance measuring equipment facility

ARTCC AUTOMATED LOCAL FLOW MANAGEMENT/PROFILE DESCENT DESCRIPTION

The ATC concept of automated local flow management/profile descents utilizing time-based metering is designed to permit operators of high performance turbine-powered aircraft to descend in a clean configuration at idle thrust to a point within the airport terminal area. Significant fuel savings are accomplished on a fleet-wide (all users) basis by matching the airplane arrival rate into the terminal area to the airport's arrival acceptance rate which reduces the need for holding and low altitude vectoring for sequencing. Fuel savings are also achieved on an individual airplane basis by permitting the pilot to descend in a fuel efficient manner at his discretion. In addition to arrival fuel savings, safety, noise abatement, and standardization of arrival procedures are all enhanced (ref. 5).

The Denver Air Route Traffic Control Center's (ARTCC) automated version of LFM/PD employs four metering fixes located around the Stapleton International Airport. All arriving high performance aircraft are time-based metered to one of these four metering fixes. Metering is accomplished with the ARTCC computer with consideration given to the following parameters:

1. Airport acceptance rate specified by the Stapleton International Airport tower (number of arrivals per unit time).

2. Nominal paths and airspeed profiles associated with each of the four metering fixes to the runways.

3. True airspeed filed on the airplane's flight plan.

4. Airplane position detected by ATC radar.

5. Forecast winds-aloft data from several stations in the Denver ARTCC area and/or measured winds from pilot reports.

These parameters are processed by the ARTCC computer to determine an estimated time of arrival (ETA) that each metered airplane would land on the runway assuming no conflicts. The ETA's for all metered airplanes are chronologically ordered and compared to determine if any of the airplanes are in conflict. Landing times are reassigned by the computer to resolve any time conflicts. The adjusted landing time is referred to as the actual computed landing time (ACLT). If the ACLT and the ETA are different, the difference indicates the delay that an airplane must accommodate prior to the metering fix through holding, speed control or path stretching. The metering fix arrival time (MFT) assigned to each airplane is found by subtracting a nominal transition time from the metering fix to the runway from the ACLT.

FLIGHT MANAGEMENT DESCENT ALGORITHM DESCRIPTION

The flight management descent algorithm computes a five segment descent profile (fig. 1) between an arbitrarily located entry fix to an ATC defined metering fix. A sixth segment from the metering fix to the next fix (specified by ATC and called the aim point) is also generated. Time and path guidance descent information based on these six segments is provided to the pilot.

The first segment after the entry fix is a level flight and constant Mach segment. The remaining level flight segments in the profile are for speed changes. The descent is divided into two segments, the first being an upper altitude constant Mach segment followed by a transition to the second which is a constant calibrated airspeed segment. The constant Mach/airspeed descent and the level flight airspeed change segments were used to be consistent with standard airline operating practices. The descent profile calculations are based on linear approximations of airplane performance for an idle-thrust, clean configuration. Airplane gross weight, maximum and minimum operational speed limits, wind, and nonstandard temperature and pressure effects are also considered in the calculations. A complete discussion of the equations and their development may be found in reference 6.

The flight management descent algorithm may be used in either of two modes. In the first mode, the pilot may input the Mach/airspeed descent schedule to be flown. This mode does not require a metering fix time assigned for the descent profile to be calculated. Once the profile is generated, a metering fix time may be assigned for time guidance. However, some time error, which must be nulled by the pilot, may result since an arbitrary specification of the descent speed schedule will not satisfy the time boundary conditions.

In the second mode, the entry fix and the metering fix times are pilot inputs which are time constraints that the algorithm must satisfy through an iterative process to determine an appropriate Mach/airspeed schedule. The initial Mach/airspeed schedule is proportional to the difference in times specified for the entry fix and the metering fix and the times required to fly between these fixes at the lower and the upper Mach/airspeed operational limits (0.62/250 KCAS and 0.78/340 KCAS, respectively). Subsequent iterations produce the descent Mach/airspeed profile that lies within the specified operational speed limits. The convergence criterion is that the computed metering fix arrival time error be less than 5 sec. This convergence criterion was normally satisfied in less than five iterations.

The algorithm checks to ensure that the final Mach/airspeed schedule selected is within the operational speed limit range. If a selected metering fix time requires a speed which violates one of these speed limits, the descent parameters are computed using the exceeded speed limit and the resultant difference in desired time and programmed time of arrival at the metering fix is displayed to the pilot.

DESCENT ALGORITHM INPUT/OUTPUT REQUIREMENTS

Data required for profile descent calculations are obtained from the NCU navigation data base, from pilot inputs through the NCDU, and from real-time sensor inputs through a data bus to the NCU.

Parameters contained in the NCU navigation data base include

(1) Aim point: location (latitude and longitude), programmed altitude, and programmed airspeed

(2) Metering fix: location (latitude and longitude), maximum and minimum programmed altitudes, and programmed airspeed

(3) Maximum and minimum airplane operational descent Mach number and airspeed

(4) Wind speed and direction gradients

Inputs required for the profile descent calculations inserted through the NCDU by the pilot include

(1) Entry fix description: location, programmed altitude, programmed ground speed, and programmed crossing time; the entry fix is the last waypoint the pilot has defined on his path before using the LFM/PD algorithm

The remaining pilot inputs through the NCDU are made on the profile descent display format shown in figure 2. Data entry is accomplished by pushing the appropriate numeric key corresponding to the data labels on the display followed by the actual data entry. The data may be entered in any order, or changed at any time, prior to the profile descent algorithm calculations.

(2) Descent Mach/CAS schedule (not allowed if both the metering fix and entry fix times are specified)

(3) Metering fix time (not allowed if the pilot selects the descent Mach/CAS schedule)

(4) Surface winds (zero is not data entered)

(5) Airport altimeter setting (29.92 if no data entered)

(6) Airplane gross weight (limited to not less than 333 600 N (75 000 lb) and not greater than 444 800 (100 000 lb))

(7) Total air temperature

Information required for the profile descent calculations input to the navigation computer automatically through a data bus include (magnitudes at time of profile descent calculation)

(1) Winds-aloft speed and direction

(2) Cruise Mach number

(3) Cruise altitude

The flight management descent algorithm calculates and outputs the following parameters to be used by the guidance and display system:

(1) All descent way-point distances relative to the metering fix, programmed altitudes, and programmed ground speeds

(2) The magnetic direction of the entry fix relative to the metering fix (all waypoints used to describe the descent profile lie in the vertical plane defined between the metering fix and entry fix)

(3) Mach/CAS descent schedule

FLIGHT TEST OBJECTIVES

The objectives of the flight tests were to (1) document the descent path parameters determined by the descent flight management algorithms including wind modeling effects, (2) establish the compatibility of the airborne flight management descent concept with time control in the cockpit while operating in the time-based metered LFM/PD air traffic control environment, (3) determine pilot acceptance of the cockpit procedures to program and fly a fuel efficient, time controlled descent, and (4) obtain data for estimates of fuel usage. These objectives were achieved using qualitative data in the form of pilot and ARTCC radar controller comments, audio recordings of controller, cockpit, and air-to-ground conversations, and video recordings from the ARTCC radar scope and with quantitative data in the form of speed, altitude, and time error recorded onboard the airplane.

DESCRIPTION OF AIRPLANE AND EXPERIMENTAL SYSTEMS

The test airplane is the TCV Boeing 737 research airplane (a twin-jet commercial transport). The experimental systems consist of a digital flight control system, a digital navigation and guidance system, and an electronic CRT display system integrated into a separate research flight deck. The research flight deck, shown in figure 3, is full-scale and located in the airplane cabin just forward of the wing (ref. 7).

The triply redundant digital flight control system provides both automatic and fly-by-wire control wheel steering options. The velocity vector control wheel steering mode (ref. 7) was utilized during these flight tests.

The navigation computer is a general purpose digital computer designed for airborne computations and data processing tasks. It utilizes a 24-bit word length and has a 32K word directly addressable core memory.

Major software routines (refs. 8 and 9) in the navigation computer include the (1) navigation position estimate, (2) flight route definition, (3) guidance commands to the flight control computer system, (4) piloting display system computations, and (5) flight data storage for navigation purposes. The flight management descent algorithm software was also included in the navigation computer.

The captain and the first officer each have three CRT displays and conventional airspeed and altimeter instrumentation for guidance. The three CRT displays include the EADI, the EHSI, and a digital display of various navigation information in the NCDU.

The EADI display is formatted much like a conventional attitude indicator but has numerous additional symbology to help the pilot navigate and control the airplane. A detailed explanation of the EADI display may be found in reference 8. Two options of the EADI display used for lateral and vertical path navigation on these flight tests are the vertical and lateral course deviation indicators and the "star and flight path angle wedges."

The vertical and lateral course deviation indicators are presented in a conventional needle and tape format shown in figure 4. The vertical tape on the right hand side of the EADI shows the vertical path error. A standard "fly to" deviation convention is employed where the needle represents the desired path and the center of the tape represents the airplane (i.e., if the airplane is below the desired path the needle will be displaced above the center of the tape). The indicated range of the tape scale is 152.4 m (500 ft.)

The lateral course deviation indicator is displayed on the bottom of the EADI. The "fly to" deviation convention is utilized and the indicated range of the horizontal tape is ±1829 m (6000 ft.)

The second EADI navigation option used during this test was the "star and flight path angle wedges" shown in figure 4. The star represents the next waypoint on the programmed route. The star's vertical displacement on the EADI pitch grid represents the flight path angle at which the airplane must be flown to arrive at the programmed altitude at the next waypoint. The star is also displaced laterally in the same manner to provide lateral path tracking guidance.

The flight path angle wedges used with the star display represent the inertially referenced flight path of the airplane. If the airplane flight path angle and track angle are adjusted so that the flight path angle wedges center directly on the star, the airplane will be flying directly to the waypoint.

Figure 5 shows a drawing of the CRT EHSI display operated in a track-up mode. This display is a plan view of the desired route and optionally displayed features such as radio fixes, navigation aids, airports, and terrain drawn relative to a triangular airplane symbol. A trend vector has been drawn in front of the airplane symbol to aid the pilot with route capture and tracking and with time guidance utilization. The trend vector is composed of three consecutive 30-sec lines which predict where the airplane will be in the next 30, 60 and 90 sec based on the airplane's current ground speed and bank angle. The EHSI display also provides the pilot with time guidance and an altitude predictive arc to aid the pilot during altitude changes.

Time guidance is provided on the EHSI by a box that moves along the programmed path. The time box represents the position along the route where the airplane should be based on the programmed ground speeds and the time profile. The pilot nulls the time error by maneuvering the airplane so that the airplane symbol is inside the time box.

During climbs and descents, the pilot may select the range/altitude arc option to be drawn on the CRT EHSI. This option generated an arc on the EHSI, as shown in figure 5, that depicts the range in front of the airplane where a pilot selected reference altitude will be achieved. This symbol is drawn based on the airplane's current altitude and flight path angle and the desired reference altitude.

The range/altitude arc was used on the descent profile during these tests by setting the magnitude of the reference altitude to the programmed altitude of the next waypoint. Then the pilot would adjust the flight path angle of the airplane so that the arc would lie on top of the next waypoint displayed on the EHSI. This would result in the airplane crossing the next waypoint at the programmed altitude.

The NCDU display contains numerous navigational data for the pilot to select including programmed route information, tracking and navigational error information, and systems status checks. This information is presented in digital form. A complete description of the NCDU and its operations may be found in reference 8.

DATA ACQUISITION

Data were recorded onboard the airplane by a wide-band magnetic tape recorder at 40 samples/sec. These data include 93 parameters describing the airplane configuration, attitude, control surface activity, and 32 selectable parameters from the navigation computer. Airborne video recordings of the EADI and the EHSI displays were made throughout the flight. In addition, audio records of test crew conversations and air/ground communications were recorded.

On the ground, the radar controller's scope presentation and the ARTCC computer generated time-based metering update list were video recorded.

FLIGHT TEST CREW

The flight test crew consisted of a captain and first officer. The captain was responsible for flying the airplane in the velocity vector control wheel steering mode and for operation of the thrust levers. The first officer was responsible for program inputs to the navigation computer, selecting appropriate display guidance, and assisting the captain as requested. In addition, the first officer recorded flight notes of various parameters describing the profile descent for post-flight analysis.

Two NASA test pilots and four management/line airline pilots served as captain during the flight tests. Both NASA pilots had extensive previous flight and simulation experience with the TCV airplane and its experimental flight control and display systems. The four airline pilots each had approximately 6 hours of simulator training prior to the flight tests. One of the airline pilots had 4 hours of flight time in the TCV airplane on unrelated flight tests 9 months earlier.

A NASA engineer served as first officer on all flights. He had previous flight crew experience in simulation and flight with the TCV airplane and its experimental systems.

TASK

Other than requiring the time navigation responsibility to be in the cockpit, the experiment task required the flight crew to operate the airplane as a normal arrival flight to the Denver airport participating in the time-based metered LFM/PD air traffic control system. Each test run was started with the airplane at cruise altitude and speed on a 4-D programmed path to an entry fixed 100 n.mi. from Denver. Prior to passing the entry fix, the flight crew received a profile descent clearance and an assigned metering fix time from the Denver ARTCC. The flight crew then keyed the appropriate parameters into the NCDU so that an idle thrust descent path to the metering fix would be generated. Then the crew flew to the metering fix using 4-D path guidance presented on the EADI and EHSI displays. Each test run was terminated at the metering fix and the airplane was repositioned for another test run (or flown back to the airport).

The flight crew was expected to null lateral and vertical path errors throughout the test and null the time error prior to the top of descent waypoint. During the descent to the metering fix, thrust was at flight idle and speed brakes were not used regardless of any time error so that the effects of wind modeling on the predicted descent path could be observed. Path deviations for air traffic control purposes or for weather were accepted and accommodated during the test runs.

The flight test path, including the profile descent segments, flown for each run is shown in figure 6. This test path was 420 n.mi. long and took approximately 1 hour to fly. The first officer would program path guidance to the entry fix prior to arriving at the Gill VORTAC. After the final metering fix arrival time was computed by the Denver ARTCC and radioed to the airplane, guidance for the profile descent between the entry fix and the aim point was computed with the navigation computer using the flight management descent algorithm.

The pilot was instructed to null small time errors (less than 20 sec) through speed control and larger time errors through path stretching (with ATC concurrence) maneuvers. However, the pilot was to have attained the programmed ground speed and altitude at the top-of-descent waypoint regardless of the time error.

Between the top-of-descent and the metering fix waypoints, the airplane was flown at idle thrust and the use of speed brakes was not permitted. The captain used path guidance on the EHSI display and the lateral path deviation indicator on the EADI for lateral path guidance. For vertical guidance, he used the star and flight path angle wedges on the EADI and the range altitude arc on the EHSI display. It was the responsibility of the first officer to select the desired altitude for the range/altitude arc option so that the captain could devote his full attention to flying the airplane.

The captain would anticipate leveling the airplane for the programmed altitude at the bottom-of-descent waypoint with reference to a conventional barometric altitude and then would proceed to the meeting fix. After passing the metering fix, the test run was complete and the captain would turn the airplane to reposition for another test run (or continue to the airport for landing).

RESULTS AND DISCUSSION

Airborne Algorithm Flight Performance

The prime indicator of performance of the flight management descent algorithm and concept of time control in the cockpit was the accuracy in terms of time, airspeed, and altitude with which the airplane passed the metering fix. This accuracy was quantified through the calculation of the mean and standard deviation of the altitude error, airspeed error, and time error for 19 test runs.

The mean, standard deviation, and maximum value for the altitude, airspeed, and time errors are summarized in the following table:

	Altitude error, m (ft)	Airspeed error, KCAS	Absolute time error, sec
Mean	10.2(33.6) high	0.3 slow	6.6 late
Std Dev	23.7(77.8)	6.5	12.0
Maximum Error	51.5(169) high	12.9 fast	29.0 late

The values of these errors were judged by the pilots to be very good for this flight environment. These data demonstrated that highly accurate fuel efficient descent profiles that satisfy terminal time boundary constraints can be generated and flown using a relatively simple and straightforward empirical model for the aerodynamic and performance characteristics of the airplane. Because of the simplicity of modeling these characteristics, this algorithm could be applied to various flight management/planning systems that are much less sophisticated than the NASA TCV Boeing 737 experimental system.

The standard deviation and the maximum value of the altitude error were slightly higher than expected. This was attributed to the fact that the pilots had been instructed not to make minor altitude corrections after the initial level-off at the bottom of descent waypoint so that the difference between the actual and predicted airspeed change between the bottom of descent and metering fix waypoints could be accurately assessed.

The absolute time error of the airplane crossing the metering fix resulted in a significant error reduction with time control in the cockpit (6.6 sec compared to approximately ±2 min). The pilots felt that they could have reduced the time error even further had they been allowed to modulate thrust and/or speed brakes during the descent. Since the thrust was at flight idle and the speed brakes not employed during the descent, the absolute time error was a function of the initial time error at the top of descent as well as a function of the flight management descent algorithms (which included wind modeling).

The time error accumulated between the top of descent and the metering fix waypoints more appropriately reflects the accuracy with which the performance of the airplane and the winds had been modeled in the flight management descent algorithm. The mean and standard deviation of the accumulated time error for the 19 test runs were 2.5 sec and 6.9 sec, respectively. The maximum accumulated time error was 15 sec, but typically less than 9 sec.

The mean and standard deviation of the time errors associated with crossing the metering fix may have been influenced by the time error in the Mach/airspeed descent speed schedule convergence test. During these flights, the descent speed schedule was computed based upon a 5-sec time error convergence criterion. Five sec was chosen because the descent speed schedule could be computed in less than six iterations and would result in a reasonable bound upon the time error with the resulting descent speed schedule. However, if more computational iterations to compute the descent speed schedule are permissible, then the convergence criterion could be reduced and a corresponding reduction of the time error crossing the metering fix expected.

Wind Modeling

The direction and speed gradients of a two-segment linear wind model were entered into the descent flight management software each day prior to flight. The gradients for the wind model were based on the winds aloft forecast for the Denver area for the time period of the test flights. Since the winds aloft forecast was made 6 to 8 hours before the flight tests, the actual winds aloft measured onboard were recorded during the climb to cruise altitude on the first test run of the day. This wind information was plotted and compared to the forecast to determine if the wind model gradients should be modified. The gradients could be changed in flight for succeeding test runs, if required. The wind speed gradient was changed on only two of the test runs - one of these changes is shown on figure 7.

Figure 7 shows the original and modified wind models used and the winds measured for two consecutive test runs. The first test run used a model based on the winds aloft forecast obtained before the flight. The second run used a wind model based on the winds measured during the first test run. The wind speed gradient on the first model was not steep enough and resulted in wind speeds modeled faster than encountered during the run. The accumulated time error resulting on this run was 15 sec.

The gradient of the wind speed model was steepened for the second test run. The direction gradient was unchanged. The resulting accumulated time error was reduced to 2 sec.

While the wind model had predetermined speed and direction line gradients, the position of these lines was defined by the magnitudes of the inertially measured wind speed and direction when the profile descent was calculated by the flight management descent algorithm. These measured initial conditions are shown in figure 7 with a circle around the data point. During these test flights this point of calculation was typically 100 n.mi. before the top of descent waypoint. This resulted in the possibility of a bias error in the modeled wind speed and/or direction due to a wind shift between the point where the descent calculation was executed and the top of descent. This phenomena occurred in the direction gradient of the second run as shown in figure 7. The measured wind direction at the point of descent calculation (115 n.mi. from the top of descent) was 304° and at the top of descent the measured wind direction was 291°. Hence, a 13° bias error in direction resulted. The resulting accumulated time error during descent due to a wind direction error is dependent upon the magnitude of the wind, the wind's direction relative to the airplane's path (headwind component error), and the total time required for descent.

Airborne and Ground System Compatibility

The profile descent calculated by the flight management descent algorithm, pilot's guidance, and cockpit procedures was designed to be compatible with current time-based metering LFM/PD ATC procedures and with other traffic participating in the ATC system. The test airplane was treated by the automated time-based metering LFM/PD computer program in the same manner as other airplanes inbound to the Denver airport. The only ATC procedural difference during the flight tests was that the test airplane pilots were responsible for time management, which resulted in no path stretching radar vectors or speed control commands required for sequencing purposes. Controller comments indicated that this difference allowed a reduction in their workload due to less required ground-to-air radio transmissions.

Pilot comments indicated the task of flying profile descents with time control using the electronic displays was very easily accomplished. The descent algorithm and the path guidance substantially reduced the pilot's workload, no cockpit calculations were required to determine the top of descent point, and guidance presented to the pilot made it easy to maintain good time control. Computer inputs prior to descent were direct and simple.

Video tape recordings of the ATC controller's radar scope have shown that the test airplane operated compatibly with other traffic. The TCV airplane merged with, and remained in, a queue of other airplanes bound for the metering fix. This compatibility resulted due to the Mach/airspeed descent schedule and resulting time profile calculated with the descent management algorithm based on the assigned metering fix time. This assigned metering fix time was based upon the position and metering fix time assigned to the airplanes landing prior to the TCV airplane. Proper spacing between these airplanes and the test airplane would result if the time profile was followed.

Fuel Savings

Total fuel savings are accomplished on both a fleet-wide basis and an individual airplane basis. Time-based metering procedures produce fleet-wide fuel savings by reducing extra vectoring and holding of aircraft at low altitude for sequencing into an approach queue. Profile descent procedures produce individual airplane fuel savings by allowing the pilot to plan for a fuel efficient descent to the metering fix.

No attempt was made to quantify the increased fleet-wide fuel savings due to the reduction of time dispersion crossing the metering fix since the TCV vehicle was the only airplane that utilized onboard generated 4-D guidance during these tests. It is apparent, however, that a reduction in time dispersion between airplanes merged into an approach queue can produce an increase in fuel savings by a reduction of the extra maneuvering for longitudinal spacing and can produce an increase in runway utilization by narrowing larger than required time gaps between airplanes.

Fuel savings at the Denver airport as a result of profile descent operations have been estimated to be as high as three and a quarter million dollars per year (ref. 5). Additional fuel savings as a result of the airborne algorithms were quantified through an analytical comparison of a descent calculated by the flight management descent algorithm and a conventional descent typical of those airplanes observed on the ARTCC radar display. Fuel usage for each descent was based on fuel flow for a Boeing 737 airplane.

Figure 8 shows the vertical profile of both the calculated and conventional descents. Identical initial and final boundary conditions (location, altitude, speeds, and time) were used for both descents so that a valid comparison of fuel usage could be made. Both descents begin at the entry fix, 76 n.mi. from the metering fix, at an altitude of 10668 m (35000 ft), and at a cruise Mach of 0.78. The descents end at the metering fix at an altitude of 5944 m (19500 ft) and at a calibrated airspeed of 250 knots. Flying time for both descents is 11.7 min.

The conventional descent is based on idle thrust at a Mach of 0.78 with a transition to 340 knots airspeed. The descent from cruise altitude is started at a point 60 n.mi. from the metering fix which is consistent with various pilot rules-of-thumb for descent planning. At the bottom of descent, the airplane is slowed until reaching an airspeed of 250 knots. Thrust is then added as required to maintain the 250 knots airspeed.

The descent calculated by the flight management descent algorithm is based upon an 11.7 min time constraint. The calculated Mach/airspeed descent schedule for this profile is 0.62/250 knots. Thrust is set to flight idle approximately 7 n.mi. prior to the descent so that the airplane may slow from the cruise to the descent Mach. A constant 0.62 Mach descent segment is started 40.6 n.mi. from the metering fix with a transition to a constant 250 KCAS airspeed descent segment to the metering fix.

Both descents, by definition of the comparison, require the same length of time to fly between the entry fix and the metering fix. This time objective is achieved with similar ground speeds on both descents. Even though the calculated descent is flown at a slower indicated Mach/airspeed descent schedule, similar ground speeds result since the airplane stays at altitudes higher than on the conventional descent.

Fuel usage on these two descents is substantially different, however. The descent calculated by the flight management descent algorithm required approximately 28 percent less fuel to fly between the entry fix and the metering fix (2989 N (672 lb) on the conventional descent and 2148 N (483 lb) on the calculated descent). Approximately two-thirds of this fuel savings was attributed to the lower indicated airspeeds and one-third to flight at higher altitudes.

CONCLUSIONS

An airborne flight management descent algorithm designed to define a flight profile subject to the constraints of using idle-thrust, a clean airplane configuration (landing gear up, flaps zero, and speed brakes retracted), and fixed time end conditions was developed and flight tested in the NASA TCV Boeing 737 research airplane. The research test flights, conducted in the Denver ARTCC automated time-based metering LFM/PD ATC environment, demonstrated that time guidance and control in the cockpit was acceptable to the pilots and ATC controllers and resulted in delivery of the airplane over the metering fix with standard deviations of 6.5 knots of airspeed error, 23.7 m (77.8 ft) of altitude error, and 12 sec of arrival time accuracy. Fuel savings may be obtained on a fleet-wide basis through a reduction of the time error dispersions at the metering fix and on a single airplane basis by presenting the pilot guidance for a fuel efficient descent. Pilot workload was reduced by automating those processes that required use of rule-of-thumb and/or extensive experience to achieve a solution to a complex 4-D navigation problem and through steering guidance for 4-D path following. ATC controller workload was reduced through a reduction of required ground-to-air communications and through the transfer of time navigation responsibilities to the cockpit.

REFERENCES

1. Stein, Kenneth J.: New Procedures Key to Fuel Savings. Aviat. Week & Space Technol., vol. 111, no. 9, Aug. 27, 1979, pp. 105-111.

2. Stein, Kenneth J.: Advanced Systems Aid Profile Descents. Aviat. Week & Space Technol., vol. 111, no. 8, Aug. 20, 1979, pp. 57-62.

3. Ames Research Center and Aviation Safety Reporting System Office: NASA Aviation Safety Reporting System: Fifth Quarterly Report April 1 - June 30, 1977. NASA TM-78476, 1978.

4. Heimbold, R. L.; Lee, H. P.; and Leffler, M. F.: Development of Advanced Avionics Systems Applicable to Terminal-Configured Vehicles. NASA CR-3280, 1980.

5. Cunningham, F. L.: The Profile Descent. AIAA Paper 77-1251, Aug. 1977.

6. Knox, Charles E.; and Cannon, Dennis G.: Development and Test Results of a Flight Management Algorithm for Fuel-Conservative Descents in a Time-Based Metered Traffic Environment. NASA TP 1717, October 1980.

7. Staff of NASA Langley Research Center and Boeing Commercial Airplane Company: Terminal Configured Vehicle Program - Test Facilities Guide. NASA SP-435, 1980.

8. Cosley, D.; and Martin, A. J.: ADEDS Functional/Software Requirements. SST Technology Follow-On Program - Phase II. Rep. No. FAA-SS-73-19, Dec. 1973. (Available from DTIC as AD B000 287.)

9. McKinstry, R. Gill: Guidance Algorithms and Non-Critical Control Laws for ADEDS and the AGCS. Doc. D6-41565, Boeing Co., 1974.

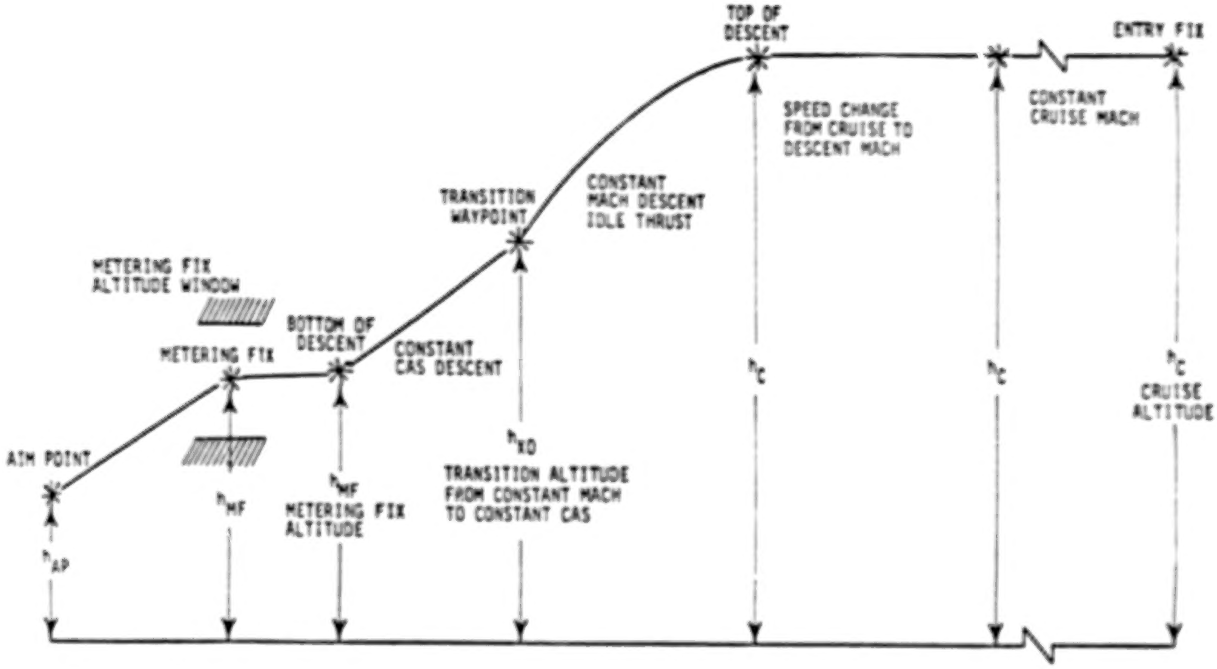
TOP OF DESCENT
ENTRY FIX
CONSTANT CRUISE MACH
SPEED CHANGE FROM CRUISE TO DESCENT MACH
TRANSITION WAYPOINT
CONSTANT MACH DESCENT IDLE THRUST
METERING FIX ALTITUDE WINDOW
BOTTOM OF DESCENT
METERING FIX
CONSTANT CAS DESCENT
h_C
h_C
h_C
CRUISE ALTITUDE
AIM POINT
h_{XD}
TRANSITION ALTITUDE FROM CONSTANT MACH TO CONSTANT CAS
h_{MF}
METERING FIX ALTITUDE
h_{MF}
h_{AP}

Figure 1.- Vertical plane geometry associated with LFM/PD algorithms.

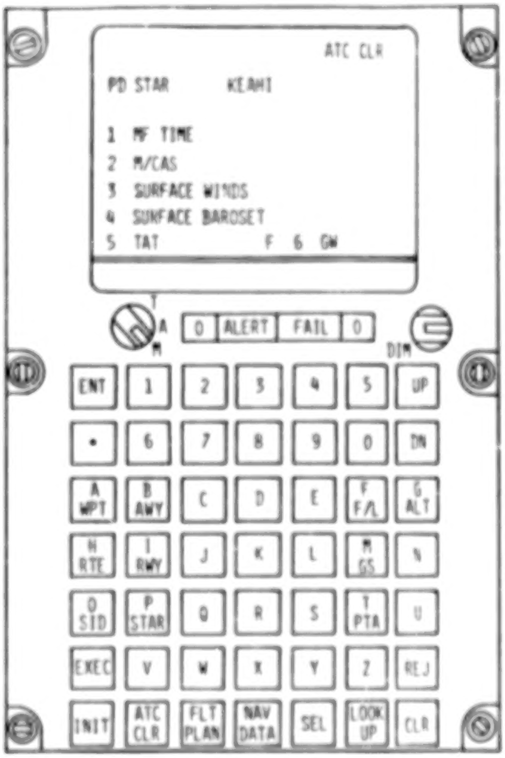
ATC CLR
PD STAR KEAHI
1 MF TIME
2 M/CAS
3 SURFACE WINDS
4 SURFACE BAROSET
5 TAT F 6 GW
T A M
0 ALERT FAIL 0
DIM
ENT 1 2 3 4 5 UP
• 6 7 8 9 0 DN
A WPT B AWY C D E F F/L G ALT
H RTE I RWY J K L M GS N
O SID P STAR Q R S T PTA U
EXEC V W X Y Z REJ
INIT ATC CLR FLT PLAN NAV DATA SEL LOOK UP CLR

Figure 2.- Profile descent display format on the NCDU.

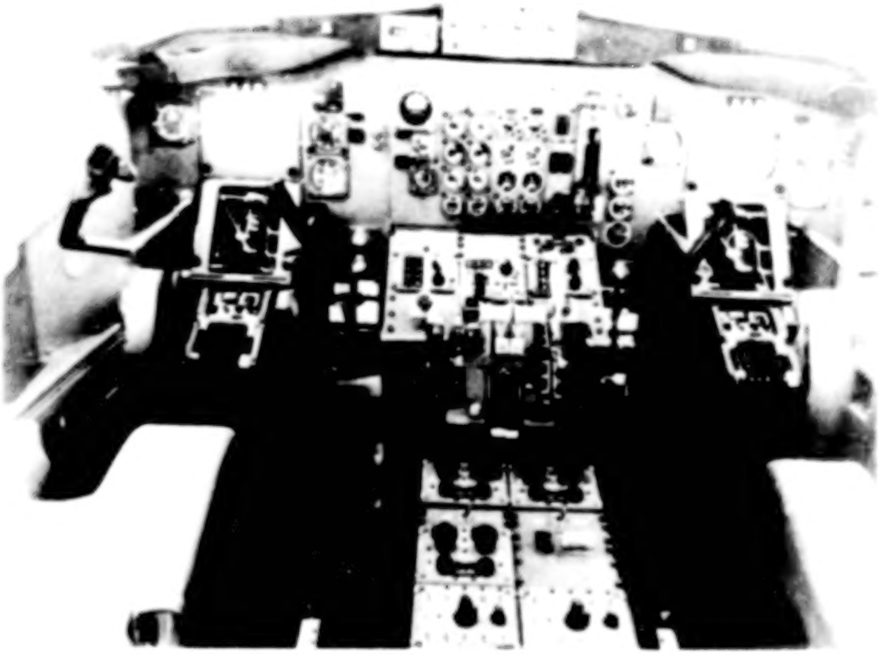

Figure 3.- Research flight deck instrument panel.

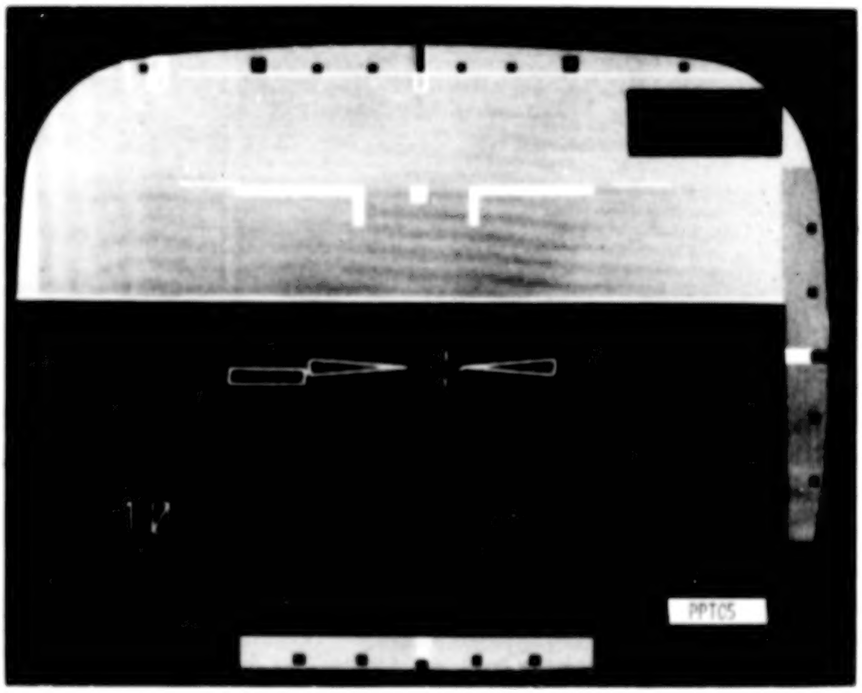

Figure 4.- EADI display with the course deviation indicators and the star and wedges guidance symbology.

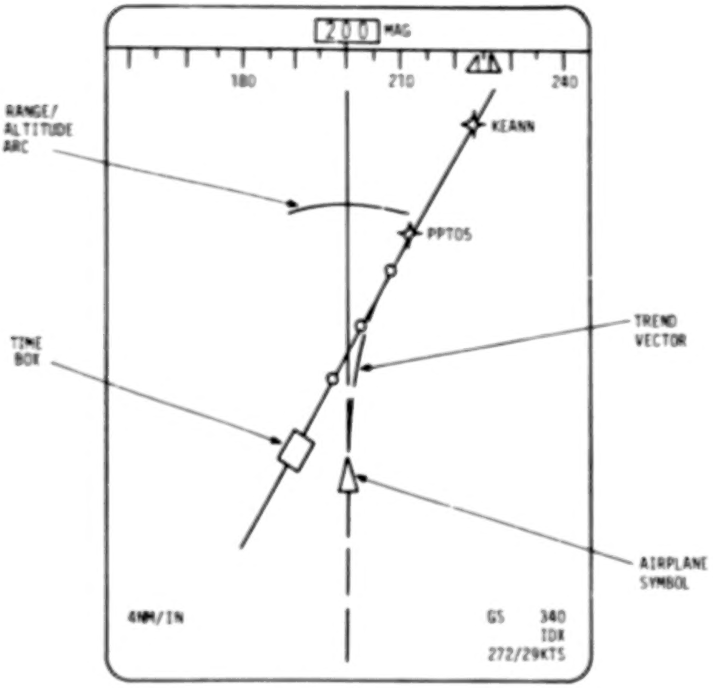
200
MAG
180
210
240
RANGE/ ALTITUDE ARC
KEANN
PPTO5
TREND VECTOR
TIME BOX
AIRPLANE SYMBOL
4NM/IN
GS 340
IDX
272/29KTS

Figure 5.- EHSI display with the trend vector, range/altitude arc, and time guidance symbology. (Note: 1 in. = 2.54 cm.)

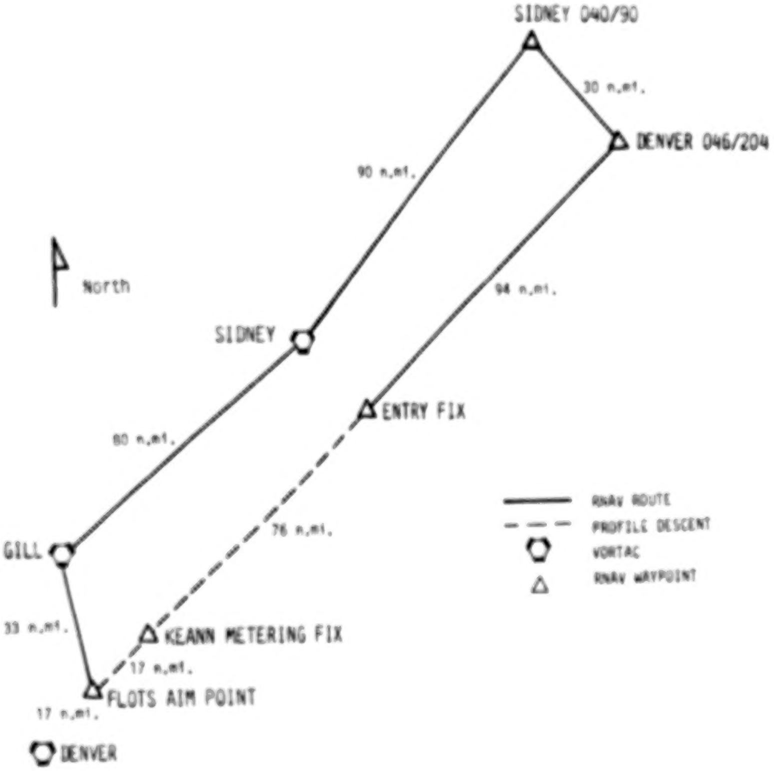
SIDNEY 040/90
30 n.mi.
DENVER 046/204
90 n.mi.
North
94 n.mi.
SIDNEY
ENTRY FIX
80 n.mi.
RNAV ROUTE
PROFILE DESCENT
VORTAC
RNAV WAYPOINT
76 n.mi.
GILL
33 n.mi.
KEANN METERING FIX
17 n.mi.
FLOTS AIM POINT
17 n.mi.
DENVER

Figure 6.- LFM/PD flight test path.

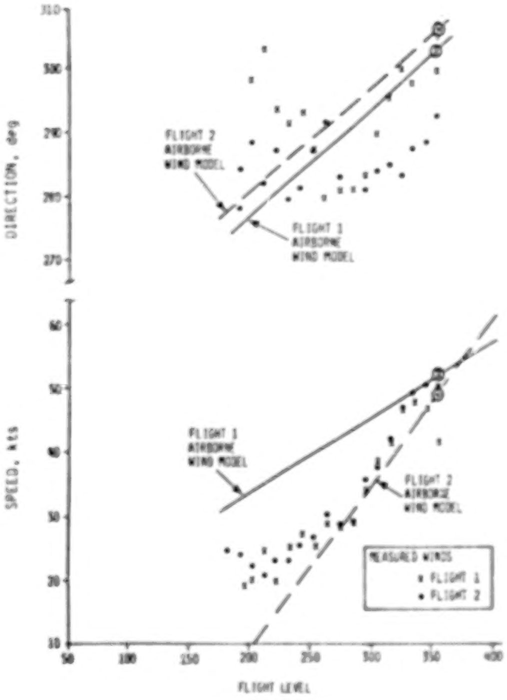

Figure 7.- Modelled and measured wind speed and direction (relative to magnetic north) for two flights.

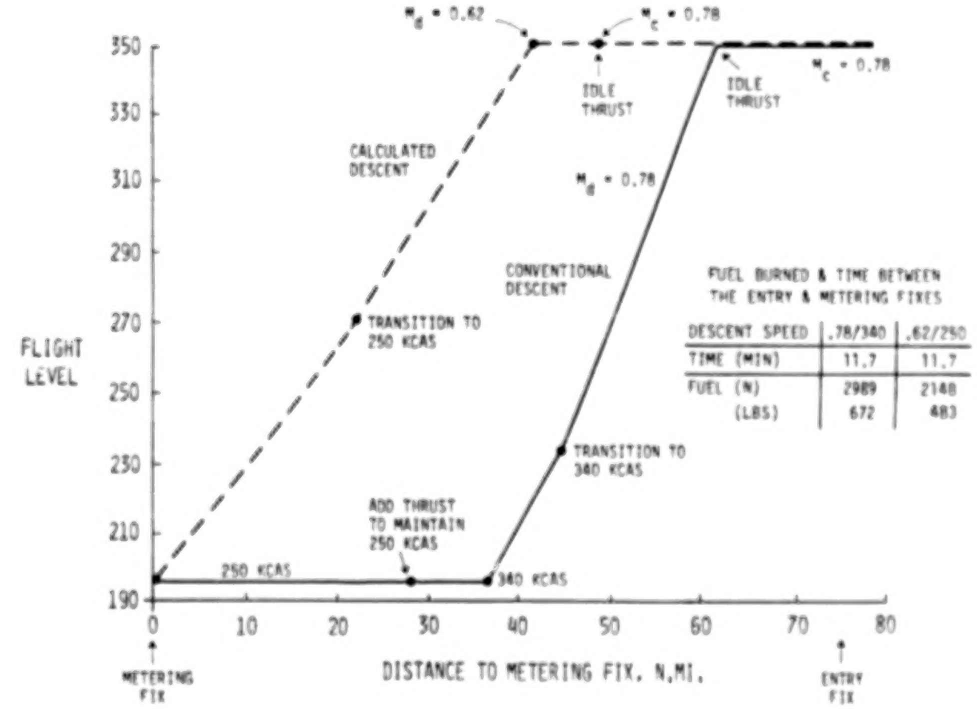

FUEL BURNED & TIME BETWEEN THE ENTRY & METERING FIXES

DESCENT SPEED	.78/340	.62/250
TIME (MIN)	11.7	11.7
FUEL (N)	2989	2148
(LBS)	672	483

Figure 8.- A comparison of a conventional descent profile typically flown and a descent profile calculated by the flight management descent algorithm.

BLANK PAGE

BLANK PAGE

A PILOT'S SUBJECTIVE ANALYSIS OF A COCKPIT DISPLAY OF TRAFFIC INFORMATION (CDTI)

Gerald L. Keyser, Jr.
Major, United States Air Force
Langley Research Center

SUMMARY

During recent years, aviation growth rates have been outstripping the ability of the air traffic control (ATC) system to effectively accommodate the ever-increasing demand. Human error has been found to be a casual or contributing factor in a large percentage of aviation accidents--both air carrier and general aviation. Recent accidents and incidents indicate the interface between the cockpit and the air traffic control system is a major problem area contributing to human error problems for both pilots and controllers.

Reduction in human errors may be achievable through better integration of the pilot into the information loop by the exploitation of recent technological advances. Both the advent of electronic displays for cockpit applications and the availability of high-capacity data transmission systems, linking aircraft with ATC ground computers, offer the opportunity of expanding the pilots' role in the distributive management process. A critical element in the distributive management process is believed by many to be the presentation to the pilot of his traffic situation, i.e., CDTI.

Although the CDTI concept has obvious potential benefits, it must be examined in an operational environment to assess the conditions under which the crew can effectively utilize it, the effect on controller procedures and efficiency, and the overall impact on system safety, efficiency, and capacity. As part of a joint NASA/FAA effort, CDTI flight tests were recently conducted with a research aircraft equipped with advanced cockpit displays.

This paper briefly presents the results of these flight tests and summarizes one of the test subject's subjective analysis of the CDTI concept.

INTRODUCTION

During recent years, aviation growth rates have been outstripping the ability of the air traffic control (ATC) system to efficiently accommodate the ever-increasing demand for capacity. One method that has been proposed to alleviate this problem is to provide traffic information in the cockpit to allow the pilot to interact more directly in the ATC process and thereby permit the use of more efficient procedures. This concept was first proposed during the 1940's (ref. 1). Early tests of this concept, however, involving TV broadcast of the controllers' radar scope, resulted in numerous deficiencies related to the mechanization scheme employed. Recent technological advances, including the Discrete Address Beacon System (DABS), Beacon Collision Avoidance System (BCAS), and electronic display systems, have resulted in a resurgence of interest in exploring potential benefits to safety, efficiency, and capacity offered by such a concept.

Studies initiated during the early 1970's by the Massachusetts Institute of Technology, under Federal Aviation Administration sponsorship, provided initial exploration of traffic-situation display concepts in a simulation environment and demonstrated pilot acceptance of traffic information (ref. 2). More recently, a joint FAA/NASA program has been undertaken to explore potential cockpit display of traffic information (CDTI) applications through the use of full-system studies (i.e., the real-world environment would be closely approximated). A first step under the joint program was a study (ref.3) to obtain a set of guidelines for display content, symbology, and format that would be used for subsequent research, the general intent being to provide a basis for standardizing a display for use in follow-on CDTI experiments. That study, involving commercial airline pilots in group sessions during which static displays were viewed on a projection screen and rated, resulted in the definition of a preferred encoding scheme for depicting altitude and other information as part of the basic traffic symbol.

The primary objective of the present study was to assess the benefit of coded traffic symbology and to obtain an initial assessment of the impact of workload on pilot ability to monitor the traffic display, using simulated traffic in a flight environment. The coded symbology, based on the results of reference 3, was displayed on the pilot's electronic horizontal situation indicator (EHSI) and flight tested in the Terminal Configured Vehicle (TCV) research airplane. Workload variations were accomplished by use of two levels of airplane control automation. The tests consisted of 29 curved, decelerating approaches flown by research pilot flightcrews. The traffic scenarios involved both conflict and conflict-free situations. Subjective pilot commentary was obtained through the use of a questionnaire and extensive debriefing sessions.

THE CDTI CONCEPT

CDTI offers a possible means for providing the needed assurance for the pilot, as well as a possible means for providing a major breakthrough for improved operating efficiency through increased pilot participation in the distributive management of the ATC system. The CDTI concept is illustrated in figure 1, wherein a real-world situation is depicted, and a conceptual sketch of the CDTI is shown for the corresponding situation. As indicated by the sketch, CDTI is generally conceived to include not only traffic information, but also weather, terrain, and other map information required for navigation. Many believe it may ultimately provide the pilot with a capability equaling, or even exceeding, visual flight capability during instrument meterological conditions, in short, electronic VFR. On the other hand, there are some who believe it could lead to chaos, a sort of do-it-yourself ATC system.

RESEARCH SYSTEM

Research Airplane

These experiments were conducted in the NASA TCV airplane, a Boeing 737 jet transport modified for advanced control and display research. This research airplane is shown in figure 2 and described in reference 4. Principal features of the airplane, pertinent to this study, included the advanced cockpit environment provided by the aft flight deck (AFD) (fig. 3), from which a two-man crew could operate the airplane under instrument like conditions using electronic displays and a fly-by-wire control system.

Displays.- The primary flight displays for the AFD were monochromatic cathode-ray tubes (CRT), driven by the navigation/guidance and electronic display computers. Two CRT's functioned as electronic attitude director indicators (EADI); the two other CRT's functioned as electronic horizontal situation indicators (EHSI). They were located on the cockpit panel in the same general area as their mechanical counterparts (fig. 3). A description of the EADI is presented in reference 4. The EHSI, which measured 12.7 by 17.8 cm (5 by 7 in.), was basically a moving map display on which traffic information was superimposed to provide the CDTI for this study.

Control modes.- Two levels of pilot workload were achieved through the use of two flight control modes that were available in the TCV airplane. The higher level of workload corresponded to the use of the attitude control mode (ACM), which was essentially a rate command/attitude hold system. Specifically, the ACM provided a rate response proportional to control deflection whenever the control was positioned outside an electrical deadband, the center of which was defined by a mechanical detent. Within the deadband, the ACM maintained the commanded angle. The lower level of workload corresponded to the velocity vector control mode (VVCM), which was essentially a rate command/flightpath hold system. Like the ACM, the VVCM provided a rate response whenever the control was positioned outside the dead band. Within the deadband, however, the VVCM maintained both the vertical-flightpath and ground-track angles. Throughout the tests, speed was controlled using an autothrottle system wherein the crew manually selected the desired speed by use of a control panel.

Traffic Generation

The displayed traffic was generated from an onboard data tape which had been previously recorded using the Langley Real-Time Simulation System. Specifically, the traffic tape was created by using a piloted simulation capability, wherein approaches were made along each of the routes that corresponded to the airway structure prescribed by the test scenarios. These individual approaches were recorded and were then merged into a set of data that was both position and time correlated. Finally, the resulting data were geographically correlated and adjusted to match the runway and terrain configuration of the area of Wallops Flight Center where the flight tests were conducted. The output of these merged data was the representation of numerous airplanes following several flightpaths and landing with a nominal separation of 2 1/2 n. mi. at the runway threshold. This traffic-generation technique was developed for use in the study described in reference 5.

CDTI DISPLAY FORMAT

General Format

The general format for the EHSI was a "track-up" display with a fixed own-ship symbol that was centered laterally on the display and was positioned longitudinally such that two-thirds of the viewing area was ahead of own-ship. A magnetic-course indication was presented along the upper portion of the display, and various digital information was shown in the lower corners (fig. 4).

A sufficiently high update rate was used so that motion of the EHSI map appeared to be continuous with respect to own-ship. Geographical-position updating of the traffic, on the other hand, was done at 4 second intervals in order to simulate the current terminal-area radar sweep rate.

The test subjects had direct control over several aspects of the CDTI. Of primary importance were the capability for selecting traffic data blocks and map-scale factors. The six map scales, ranging from 0.4 to 12.6 n. mi./cm (1 to 32 n. mi./in.), could be selected by using a rotary knob. (Because of limited computer capacity, independent selection of map scale for the captain's and first officer's CDTI displays was not possible.) The traffic-data-block option, which provided airplane identification, altitude, and ground-speed information, was selected by using a push button. Selection of this option caused the data blocks for all displayed traffic to appear simultaneously. The capability to select individual data blocks for specific traffic, as suggested in reference 3, was not available.

Traffic Symbology

In addition to tests with the coded traffic symbology, uncoded traffic symbols were used during tests to obtain a comparative evaluation. Both the coded and uncoded traffic symbology are presented in figure 5. The basic characteristic of the uncoded traffic symbol, based upon a previous (unpublished) TCV program investigation, is that ground-track angle is explicitly shown. The coded symbology explicitly identified altitude relative to own-ship, indicated whether the traffic was under ATC control, and indicated whether it was CDTI equipped. With regard to altitude encoding, an altitude band of ±150 m (±500 ft.) was used to define "at" own-ship altitude.

Additionally, as shown in figure 6, the traffic symbology included a position predictor, position history, and an airplane data block. In all cases, the position history depicted airplane position for the three previous updates. The position predictor, for the coded-symbology case, was simply a velocity vector, scaled to represent either a 30- or 90- sec prediction, the longer prediction being used in conjunction with the 0.8 n. mi./cm (2 n. mi./in.) and larger scale factors. For the uncoded-symboloby case, and for own-ship in all cases, the prediction vectors included roll-angle information.

Terminal-Area Route Structure

The overall route structure is shown in figure 7. The three routes indicated by the dashed lines were alternate arrival paths and were provided to represent a typical terminal area. The route indicated by the solid line was used by own-ship; it was based on an experimental Standard Terminal Arrival Route (STAR) developed for the TCV program. This route was designed to exploit the expanded coverage provided by advanced landing aids such as the microwave landing system (MLS). In addition to specifying the route, the STAR contained waypoints for which nominal altitudes and speeds were prescribed as shown in figure 8.

Traffic Scenario

Four traffic scenarios used in this study are shown in figures 9 to 12. In all the scenarios, which involved seven landing airplanes, own-ship was positioned to be fifth in the landing sequence. An eighth airplane was programmed to overfly the terminal area at a high altitude. The altitude and speed profiles were the same for all landing airplanes; they were specified as a function of ground-track distance from the runway threshold as specified in figure 8.

Figure 10 illustrates the general traffic arrangement, where the numerals designate the landing sequence for airplanes 1 to 7; airplane 8 is a constant velocity, constant altitude overflight of the simulated terminal area. The intended flightpath of airplane 8, unlike the STAR and the alternate routes, was not displayed. In an effort to provide additional realism, airplane 4 did not follow the proposed path exactly, but delayed its first turn, and then paralleled the desired path until it intercepted the straight-in portion.

Conflict-Free Scenarios

Two conflict-free scenarios were generated for this study, their differences being the initial position and flightpath of airplane 6. For scenario A, airplane 6 was positioned on one of the alternate routes (fig. 9) and was programmed to merge 2 1/2 n. mi. beyond own-ship in the landing sequence. For scenario B, airplane 6 was positioned on another of the alternate paths behind airplane 4 (fig. 10) and was programmed to follow the same flightpath as airplane 4, again merging 2 1/2 n. mi. beyond own-ship.

Conflict Scenarios

A conflict scenario was generated from each of the two conflict-free scenarios so that airplane 6 would violate own-ship's airspace. Scenario C, the conflict situation derived from scenario A, was produced by adjusting the initial position of airplane 6 along its route, and then changing its flightpath to delete the last turn. This path and the point of conflict are shown in figure 11. The other conflict situation, scenario D, was created by adjusting the initial conditions of airplane 6 in scenario B and modifying its flightpath to a straight line (fig. 12.) In both conflict scenarios, the vertical path of the conflicting airplane was adjusted to coincide with the altitude profile of own-ship at the point of conflict.

RESULTS AND DISCUSSION

The results of this test can best be shown by putting the reader in the pilot's seat and systematically running through a typical curved approach to landing. The approach selected was previously described as scenerio C, which had a conflict situation materialize on base leg just prior to the turn to final.

The approach is started as shown in figure 13 with own-ship on downwind leg in straight and level flight at approximately 1524 m (5000 ft) with a ground speed of 209 knots and an airspeed of approximately 179 KIAS. Figure 13 shows own-ship to be 13 seconds from Waypoint MERCI which is the start of descent point. The wind at altitude is shown to be from 252° at 26 knots. The map scale is shown as 1.6 n. mi./cm (4 n. mi./in.) and the aircraft is coupled in 4D for guidance. Four other aircraft can be seen, two below own-ship's altitude and one above. The fourth aircraft is landing on the runway. No conflicts are apparent at this time.

Figure 14 shows own-ship now under MLS coverage in a descending left turn on track both vertically and horizontally. Once under MLS coverage, the vertical and horizontal deviation tapes automatically appear. The horizontal situation is displayed in a track-up mode and as can be seen own-ship has made an approximate 90° left turn. The current altitude is just over 823 m (2700 ft), the ground speed is 159 knots and the airspeed is approximately 171 KIAS. The scale factor has been changed to 0.8 n. mi./cm (2 n. mi./in.) and the guidance is still 4D. Three aircraft are shown on the display, only two of which have tracks which will intersect that of own-ship. The coded symbol of the aircraft closest to own-ship indicates that he is 152 m (500 ft) or more above own-ship's altitude. Without the airplane data block selected, nothing else is known about his vertical position. The coded symbol does indicate that he is not under ATC control and not equipped with CDTI. The other airplane with an intersecting path is within 152 m (500 ft) of own-ship's altitude, is under ATC control, but is not equipped with CDTI. The pilot's attention is naturally drawn to this airplane in the upper right hand corner because it can be seen that, even if he follows his intended flightpath, the spacing at the runway threshold is probably going to be close.

Figure 15 depicts the approach scenario approximately 50 seconds later. The pilot has called up the airplane data tags and immediately sees that the airplane closest to own-ship (DA 495) is indeed no factor because he is overflying the scenario at 2438 m (8000 ft). The real potential conflict is Trans World 80 (TW 080) because he has been descending at approximately the same rate and his altitude has been approximately the same as own-ship. If he follows his projected path the longitudinal separation will not be adequate when both airplanes arrive on the final approach segment. Own-ship's pilot has switched to 2 D guidance (horizontal only), has essentially stopped his descent and is commencing an early slowdown to final approach speed in order to increase both the horizontal and vertical separation between own-ship and Trans World 80. This is the logical thing to do because Trans World 80 is slightly ahead of own-ship and own-ship has no traffic immediately behind him.

Figure 16 depicts the scenario approximately 40 seconds later. The vertical separation between own-ship and Trans World 80 is now approximately 152 m (500 ft) with own-ship currently crossing his projected flightpath. It should be noted that the actual position of own-ship is the apex of the triangle. Trans World 80 has missed the turn to final and is currently tracking straight ahead through the scene at 488 m (1600 ft). On his present course he will pass behind and approximately 152 m (500 ft) below own-ship. The potential conflict has successfully been avoided. The pilot of own-ship has resumed his descent in order to recapture his vertical path. The EADI shows his gamma wedges below the -3.0° reference line and the NAV Data page shows that he has a 2.1° intercept angle established in order to recapture his vertical profile. The EHSI indicates in the lower left hand corner that he is still coupled in 2 D and is manually controlling the selection of Flightpath Angle (gamma) and Indicated Airspeed (IAS).

Figure 17 depicts the scenario approximately 50 seconds later. The pilot of own-ship has switched the EHSI to the 0.4 n. mi./cm (1 n. mi./in.) scale. All of the other aircraft have flown out of the area of coverage except for the airplane just short of the threshold of runway 22. The pilot of own-ship can now devote all of his attention to the task of recapturing his vertical profile, making his turn to final and assuring that his airplane is properly configured for landing. It can also be seen that when the 0.4 n. mi./cm (1 n. mi./in.) scale factor is selected only 30 seconds worth of trend vector extends from the nose of the own-ship symbol.

The NAV Data page shows the own-ship altitude at 379 m (1244 ft) with the altitude error decreased from 157 m (516 ft) in figure 16 down to 51 m (166 ft) in figure 17. The pilot of own-ship is still maintaining a flightpath angle error (FPAE) or vertical path intercept angle of just over 2°.

Figure 18 depicts own-ship in a left 8° bank turn to the final straight in segment of the approach. The EADI shows the aircraft at a radar altitude of 180 m (590 ft) and back on the path both horizontally and vertically. The flightpath angle is approximately 3° below the horizon and the acceleration cue indicates a slight deceleration along this flightpath. The pilot has selected the speed error option and set the desired approach speed as a target. The dark bar seen on the left wing of the airplane symbol indicates that the current airspeed is slightly faster than the set approach speed. As the airplane slows the bar will decrease in height and disappear when on speed. If the airspeed decreases below the set approach speed the bar will appear below the left wing of the aircraft symbol and function in the same manner. The perspective runway and extended center lines can also be seen moving into the picture as the aircraft progresses around the final turn. The perspective runway, with correct and accurate microwave or navigation signals, will exactly overlay the actual runway.

The EHSI also depicts Runway 22 in a planform view. The airplane at the far end of the runway is the airplane that own-ship has been following on the approach. It is not obvious from this photo but the autoland system has been armed, the glideslope has been captured and the localizer signal should capture as the airplane completes the final turn.

Figure 19 depicts own-ship at a radar altitude of 28 m (92 ft). The box around the airplane symbol in the EADI indicates that the autoland control laws have been implemented and the airplane is within Category II landing criteria at 30 m (100 ft).

Figure 20 shows the view out the front cockpit windshield with the airplane at approximately the same position on final approach.

Figure 21 depicts the airplane at 8 feet radar altitude. Both the pilot when flying manually, and the airplane automatics when flying a coupled approach commence the flare at approximately 15 m (50 ft) above the runway. In figure 21, it may be possible to see that the low light level TV has been switched on. The horizon line can be seen to exactly describe the real world horizon and the perspective runway can be seen to overlay just slightly right of the actual runway. The flare task is accomplished manually by simply bringing the flightpath angle wedges up to a point just slightly below the horizon line. The aircraft automatics perform the task basically the same way. A manual over rotation and resulting aircraft "float" in ground effect will be immediately evident because the flightpath angle wedges will raise to a point slightly above the horizon line.

The perspective runway and tracking guidance remain available to the pilot during runway rollout.

CONCLUDING REMARKS

A representative Cockpit Display of Traffic Information (CDTI) system has been presented as viewed from the pilot in the cockpit, and the research results from these flight tests have been presented in reference 6. The use of advanced controls and displays allows for presentation to the pilot, large quantities of information that he has not had before. It can be easily seen that with this large quantity of data available a fine line exists between the display of valid, necessary information and clutter.

Figure 22 presents three needs that the pilot in the cockpit must have in order for a CDTI system to work effectively, efficiently and safely. These are the need to maximize the lead time for detection, the need to quantify the vertical situation, and most importantly the need for total situational awareness. The real challenge in the design of an operational CDTI system will be the satisfaction of these needs and the presentation to the pilot of all the necessary information, but only the necessary information, in a useable format in order to avoid clutter. Even though a reasonably large display was utilized in these tests, display clutter was the primary problem from the standpoint of information assimilation.

Some of the other specific conclusions drawn by the pilots particpating in the flight test are:

1. For both the coded- and uncoded-symbology cases, ample leadtime for detecting and resolving conflicts was provided by the traffic display.

2. Although it was generally felt that encoding the symbology improved the overall traffic information presented, some of the encoded information, specifically, CDTI equipage and ATC control encoding, was of little interest from a pilot's viewpoint.

3. The most beneficial element in the encoded symbology was altitude; it provided a convenient means for the pilot to formulate a three-dimensional assessment of the situation without continuously displaying airplane data blocks.

4. The additional task of monitoring traffic did not adversely affect the traditional pilot task, with traffic observation falling naturally into the pilot's normal scan pattern.

5. The 2 1/2 n. mi. nominal traffic separation, used during this flight test, does not appear to be the lower limit if something could be done to eliminate the wake vortex problem.

REFERENCES

1. Ewing, D. H.; and Smith, R. W. K.: Teleran-Air Navigation and Traffic Control by Means of Television and Radar. RCA Rev., Vol. VII, no. 4, Dec. 1945, pp. 601-621.

2. Connelly, Mark E.: Simulation Studies of Airborne Traffic Situation Display Applications - Final Report. Rep. ESL-R-751 (Contract FA71-WAI-242 (Task F)), Massachusetts Inst. Technol., May 1977.

3. Hart, Sandra G.; and Wempe, Thomas E.: Cockpit Display of Traffic Information: Airline Pilots' Opinions About Content, Symbology, and Format. NASA TM-78601, 1979.

4. Staff of NASA Langley Research Center and Boeing Commercial Airplane Company: Terminal Configured Vehicle Program - Test Facilities Guide. NASA SP-435, 1980.

5. Steinmetz, George G.: A Simulation Investigation of Cockpit Display of Aircraft Traffic During Curved, Descending, Decelerating Approaches. NASA TM-80098, 1979.

6. Abbott, Terence S.; Moen, Gene C.; Person, Lee H., Jr.; Keyser, Gerald L., Jr.; Yenni, Kenneth R.; and Garren, John F., Jr.: Flight Investigation of Cockpit-Displayed Traffic Information Utilizing Coded Symbology in an Advanced Operational Environment. NASA Technical Paper 1684, July 1980.

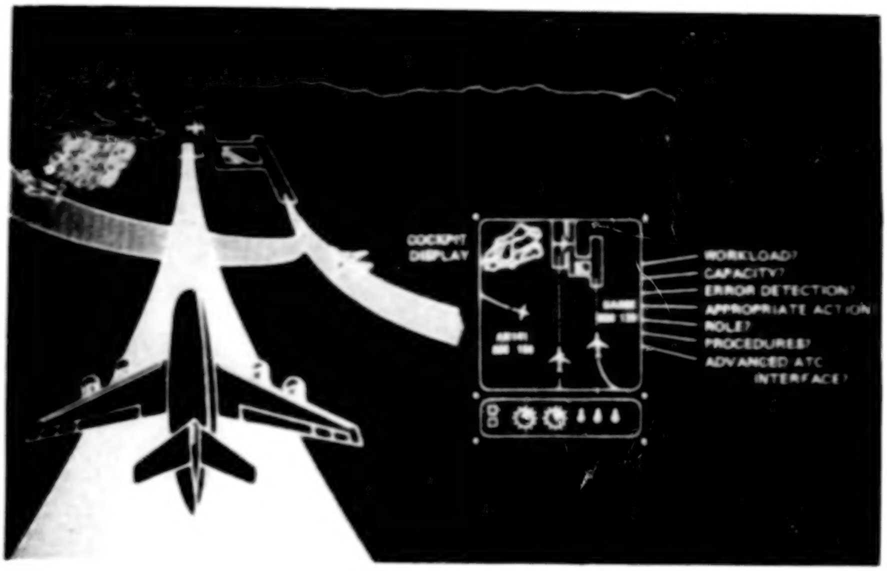
COCKPIT
DISPLAY
WORKLOAD?
CAPACITY?
ERROR DETECTION?
APPROPRIATE ACTION?
ROLE?
PROCEDURES?
ADVANCED ATC
INTERFACE?

Figure 1.- CDTI concept.

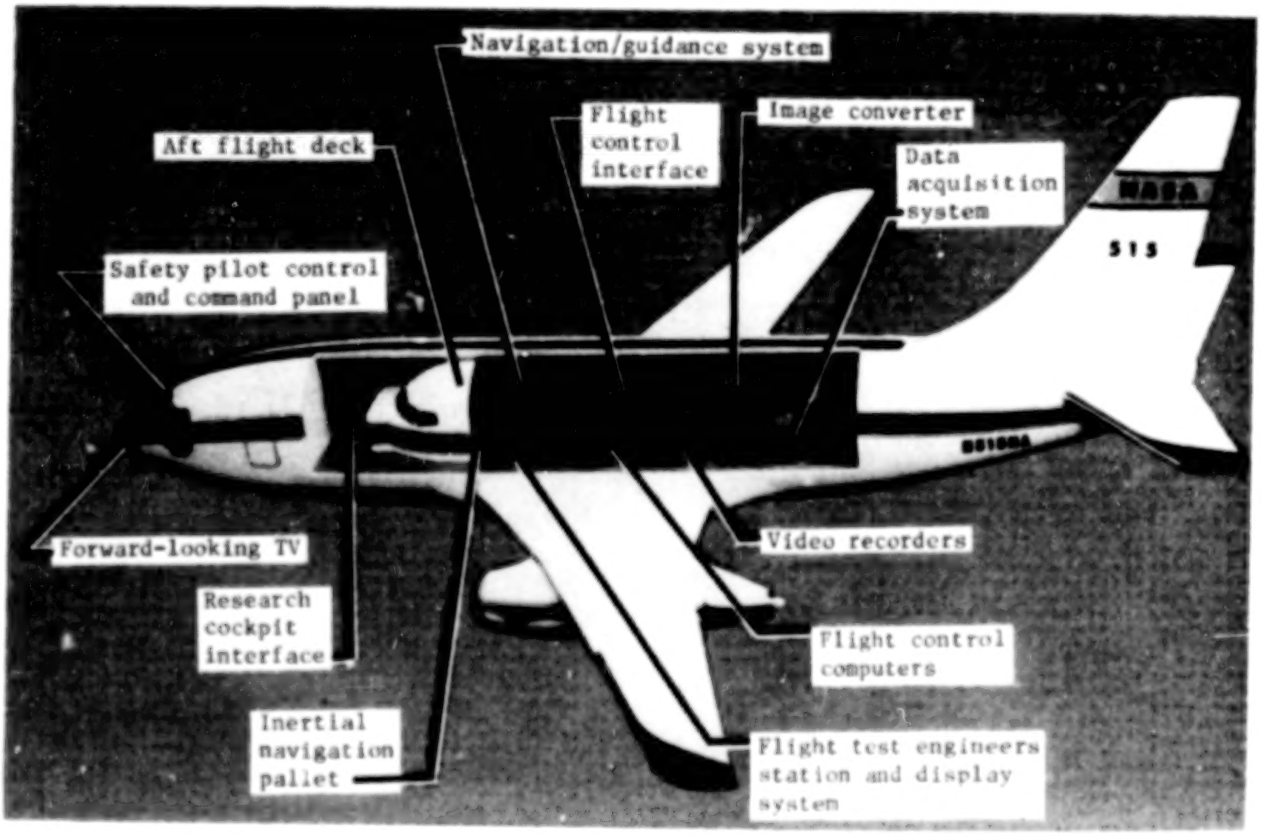
Navigation/guidance system
Aft flight deck
Flight control interface
Image converter
Data acquisition system
Safety pilot control and command panel
NASA
515
Forward-looking TV
Video recorders
Research cockpit interface
Flight control computers
Inertial navigation pallet
Flight test engineers station and display system

Figure 2.- Research airplane.

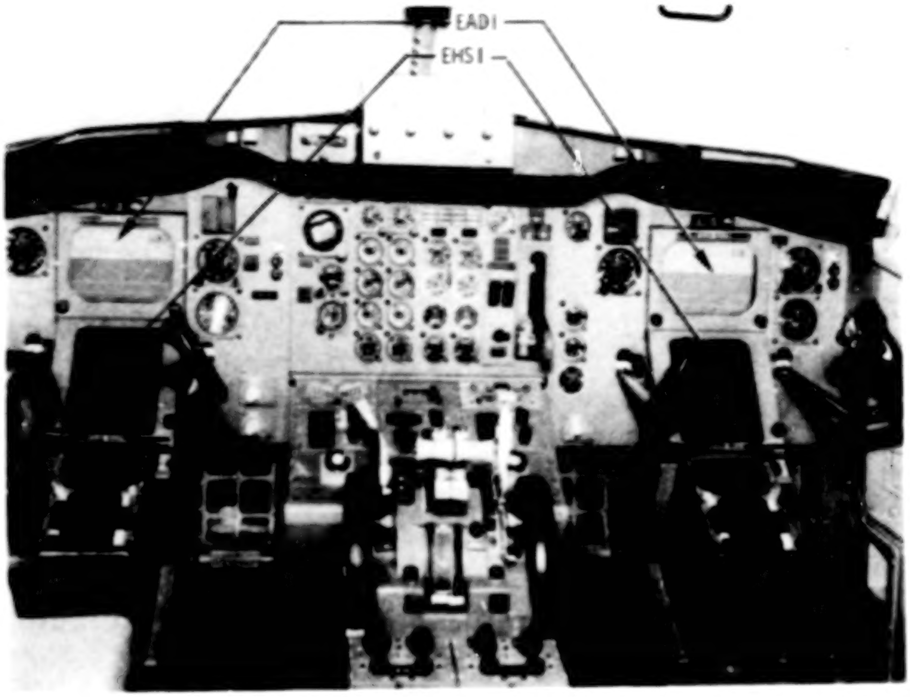

Figure 3.- Aft-flight-deck instrument panel.

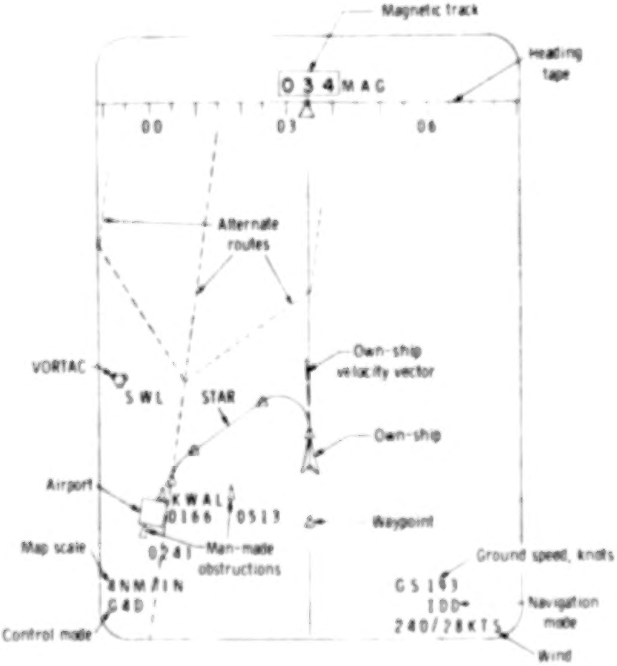
Magnetic track
Heading tape
034 MAG
00
03
06
Alternate routes
VORTAC
SWL
STAR
Own-ship velocity vector
Own-ship
Airport
KWAL
0166
0513
Waypoint
Map scale
0241
Man-made obstructions
Ground speed, knots
8NM/IN
C4D
Control mode
GS 143
IDD
240/28KTS
Navigation mode
Wind

Figure 4.- Electronic situation indicator format. (1 inch = 2.54 cm.)

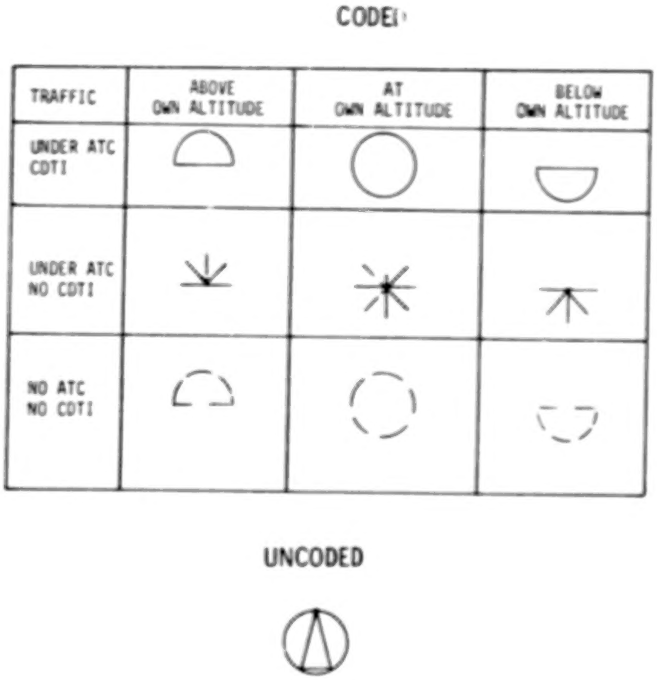
CODED
TRAFFIC
ABOVE OWN ALTITUDE
AT OWN ALTITUDE
BELOW OWN ALTITUDE
UNDER ATC CDTI
UNDER ATC NO CDTI
NO ATC NO CDTI
UNCODED

Figure 5.- Traffic symbology.

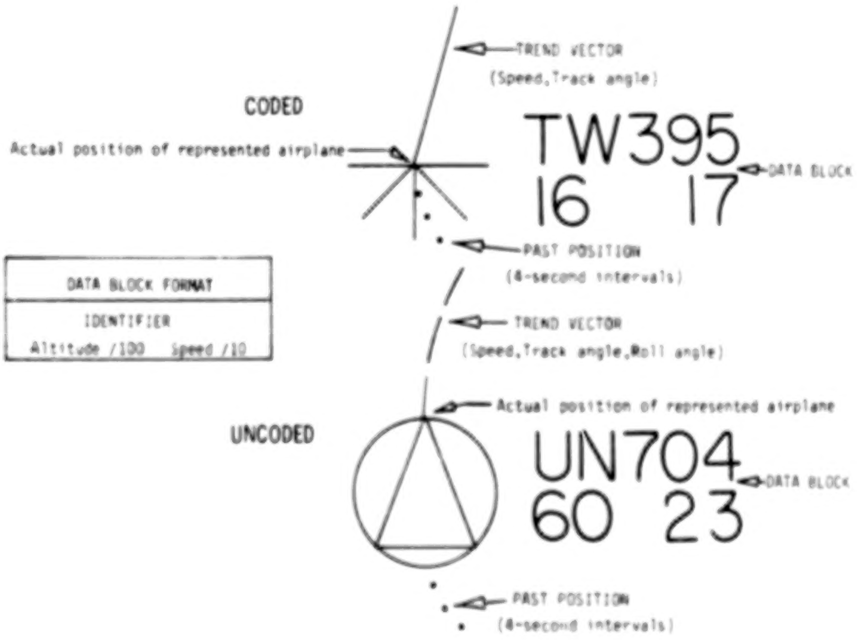
TREND VECTOR
(Speed,Track angle)
CODED
Actual position of represented airplane
TW395
16 17
DATA BLOCK
PAST POSITION
(4-second intervals)
DATA BLOCK FORMAT
IDENTIFIER
Altitude /100 Speed /10
TREND VECTOR
(Speed,Track angle,Roll angle)
Actual position of represented airplane
UNCODED
UN704
60 23
DATA BLOCK
PAST POSITION
(4-second intervals)

Figure 6.- Traffic symbology with situational information.

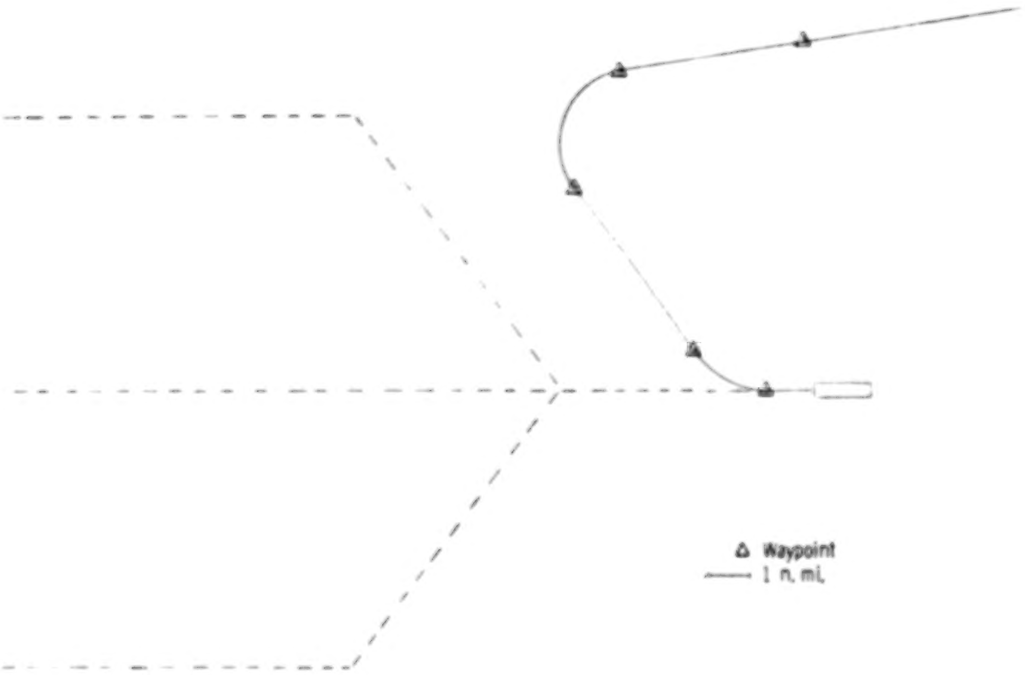
△ Waypoint
1 n. mi.

Figure 7.- Route structure.

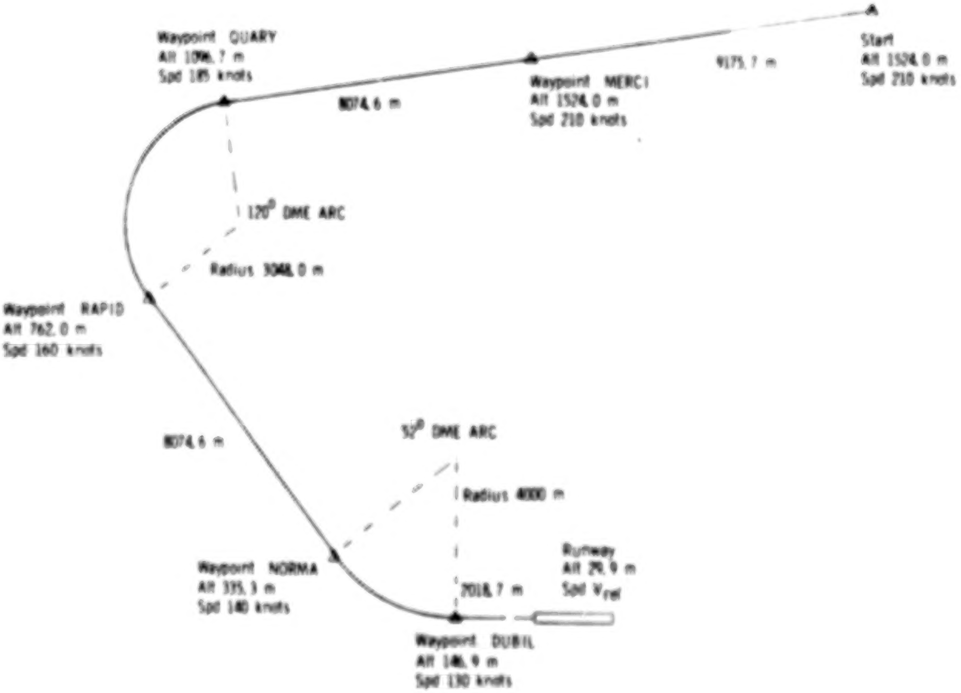
Waypoint QUARY
Alt 1096.7 m
Spd 185 knots
8074.6 m
Waypoint MERCI
Alt 1524.0 m
Spd 210 knots
9175.7 m
Start
Alt 1524.0 m
Spd 210 knots
120° DME ARC
Radius 3048.0 m
Waypoint RAPID
Alt 762.0 m
Spd 160 knots
8074.6 m
52° DME ARC
Radius 4000 m
Waypoint NORMA
Alt 335.3 m
Spd 140 knots
2018.7 m
Runway
Alt 29.9 m
Spd V_{ref}
Waypoint DUBIL
Alt 146.9 m
Spd 130 knots

Figure 8.- Experimental standard terminal arrival route (STAR). (V_{ref} is reference velocity.)

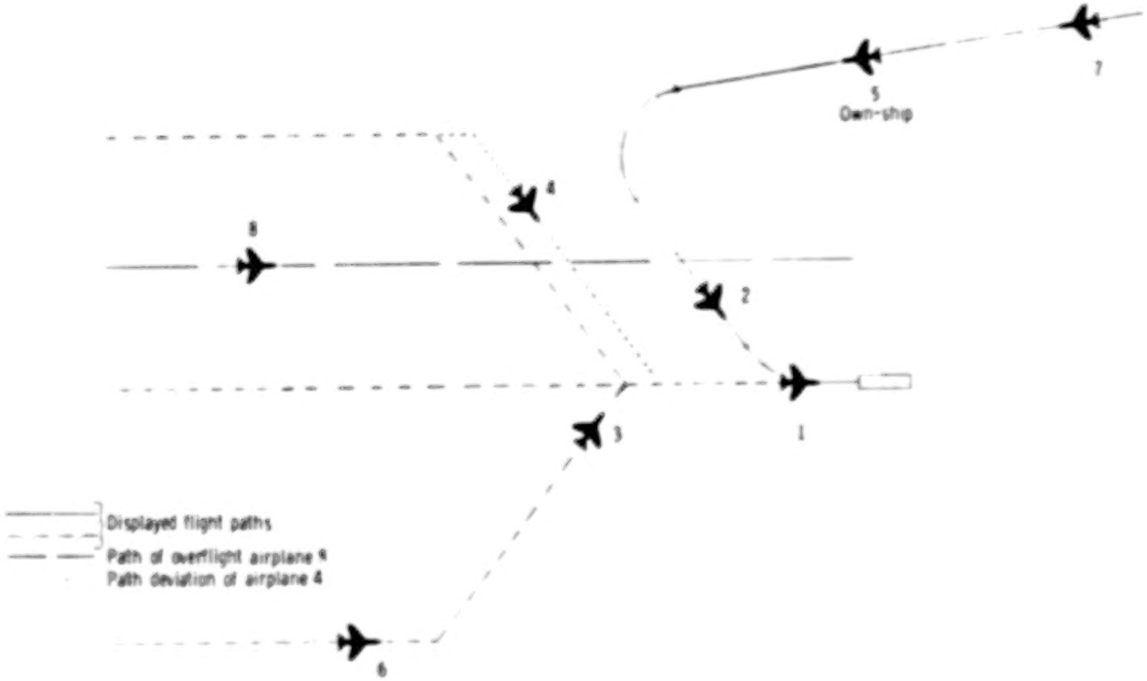
7
5
Own-ship
4
8
2
1
3
6
Displayed flight paths
Path of overflight airplane 8
Path deviation of airplane 4

Figure 9.- Traffic scenario A.

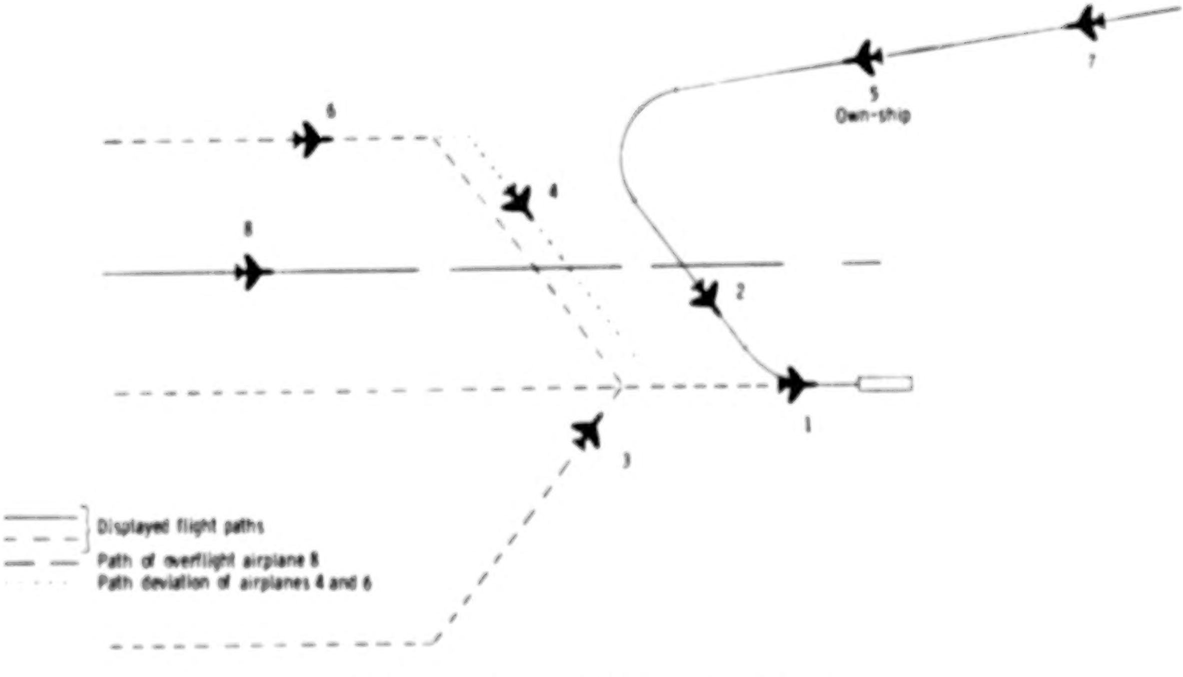
7
5
Own-ship
6
4
8
2
1
3
Displayed flight paths
Path of overflight airplane 8
Path deviation of airplanes 4 and 6

Figure 10.- Traffic scenario B.

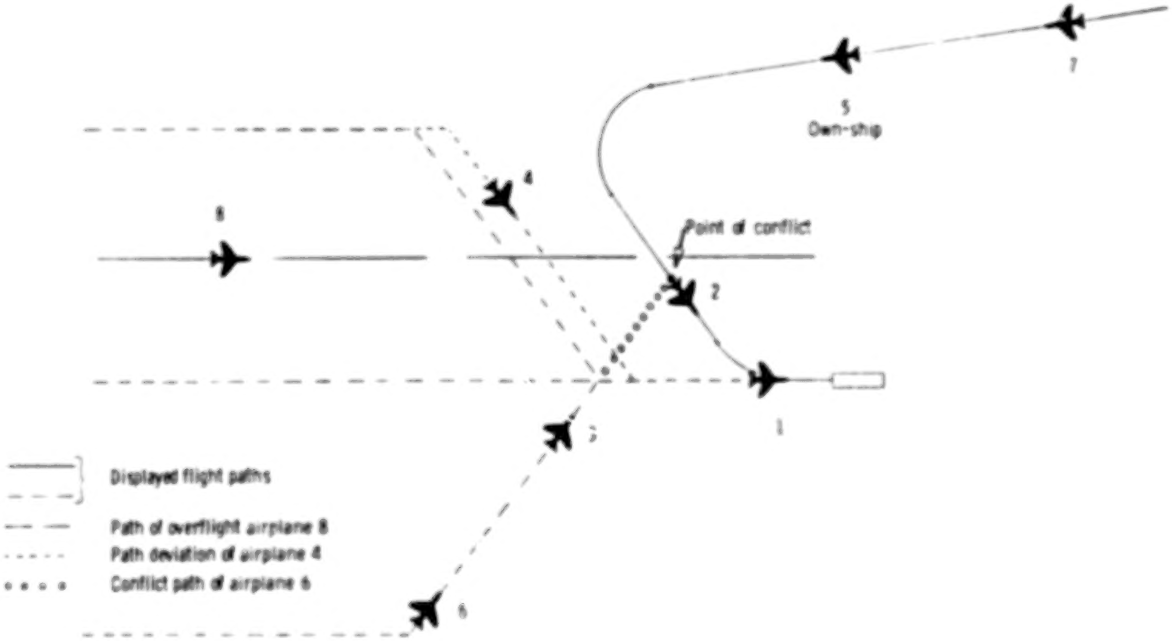
7
5
Own-ship
4
8
Point of conflict
2
1
3
6
Displayed flight paths
Path of overflight airplane 8
Path deviation of airplane 4
Conflict path of airplane 6

Figure 11.- Traffic scenario C.

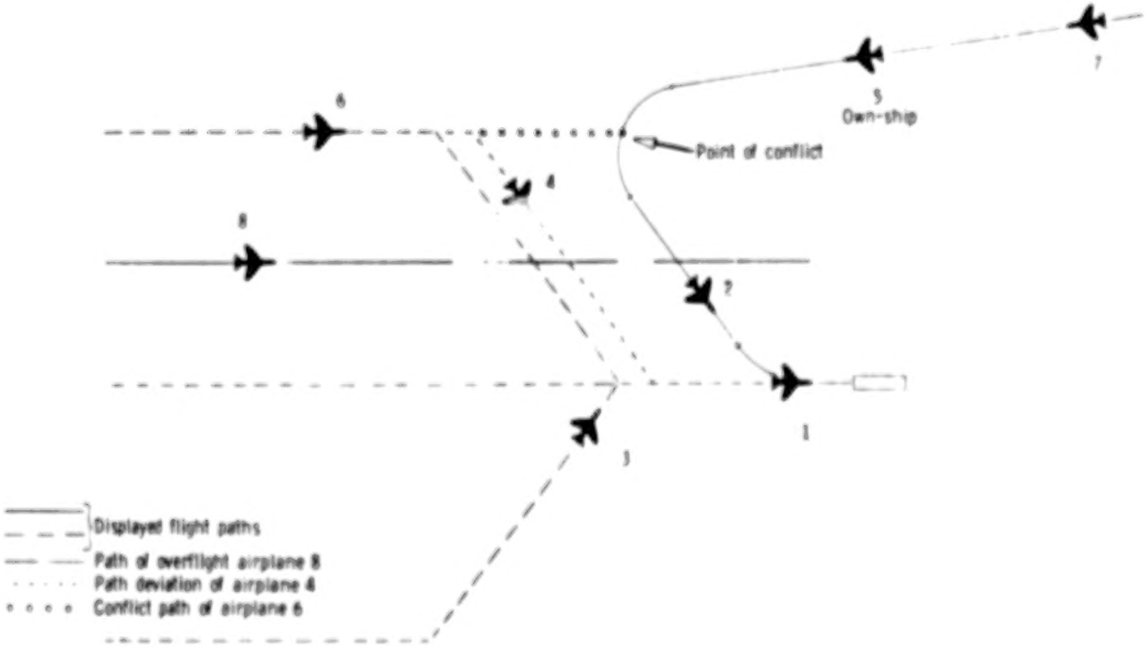
7
5
Own-ship
6
Point of conflict
4
8
2
1
3
Displayed flight paths
Path of overflight airplane 8
Path deviation of airplane 4
Conflict path of airplane 6

Figure 12.- Traffic scenario D.

Figure 13.- Starting approach on downwind leg.

Figure 14.- Descending left turn to base leg. Potential conflict starts to become apparent.

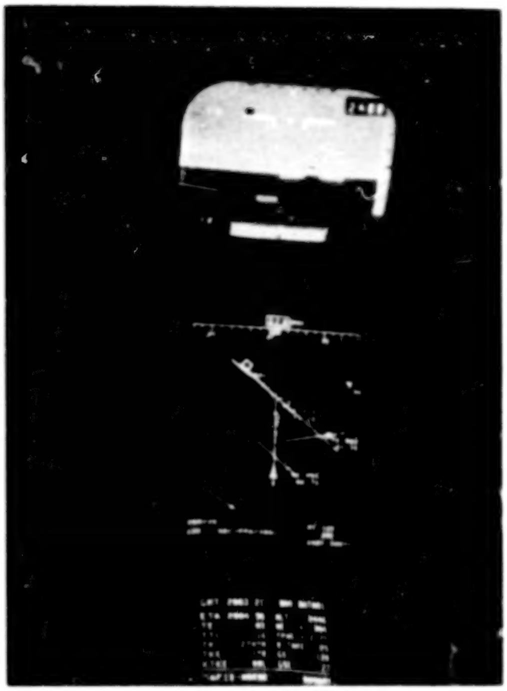

Figure 15.- Conflict imminent. Own-ship pilot levels and starts early slowdown.

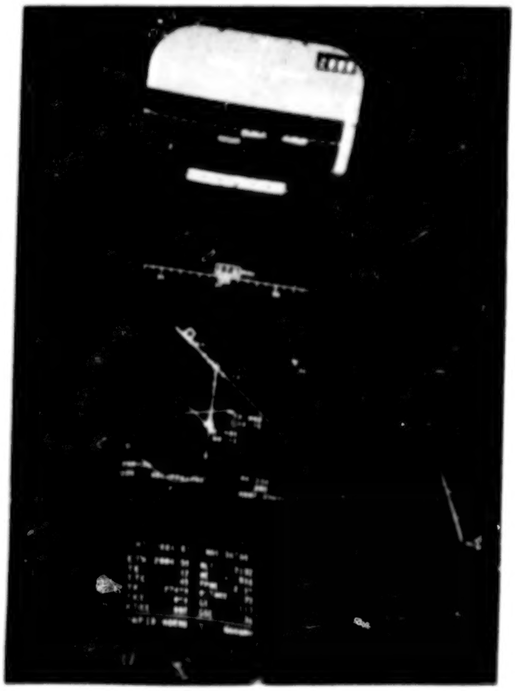

Figure 16.- Conflict avoided. Pilot resumes descent to recapture vertical path.

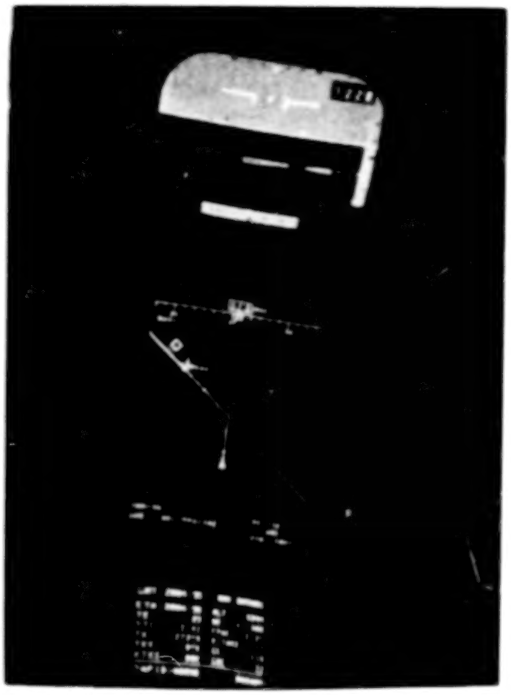

Figure 17.- Own-ship just prior to final turn. Vertical path capture imminent.

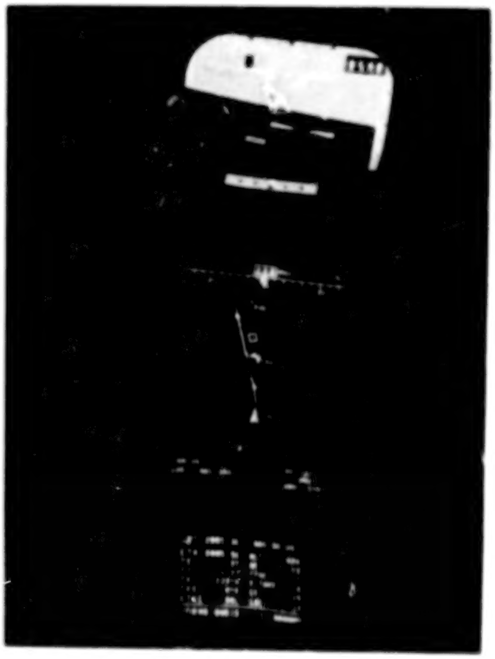

Figure 18.- Own-ship in left turn to final. Vertical path recaptured.

Figure 19.- Own-ship on short final. Autoland control laws implemented.

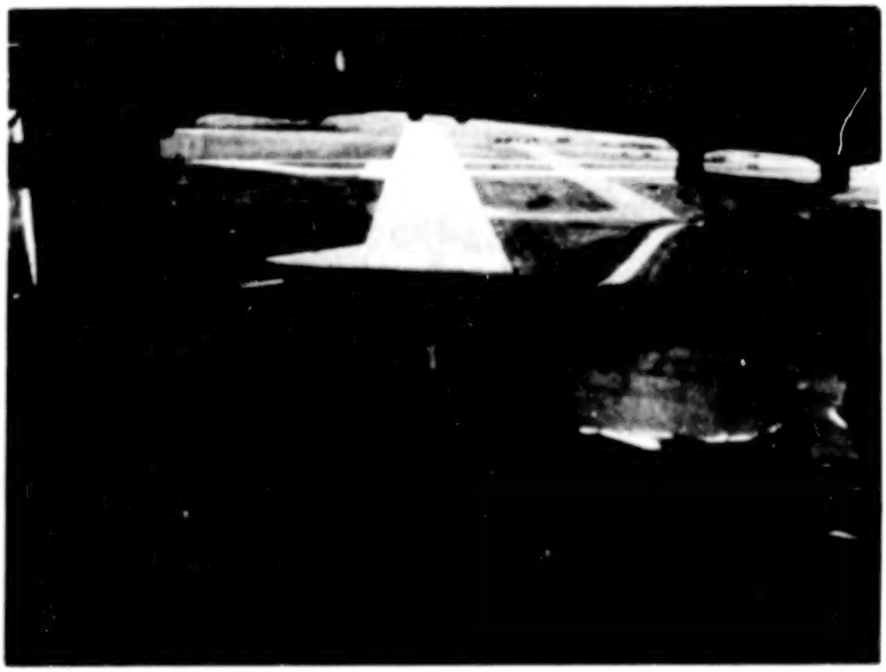

Figure 20.- View from front cockpit on short final.

Figure 21.- Own-ship in the flare for landing.

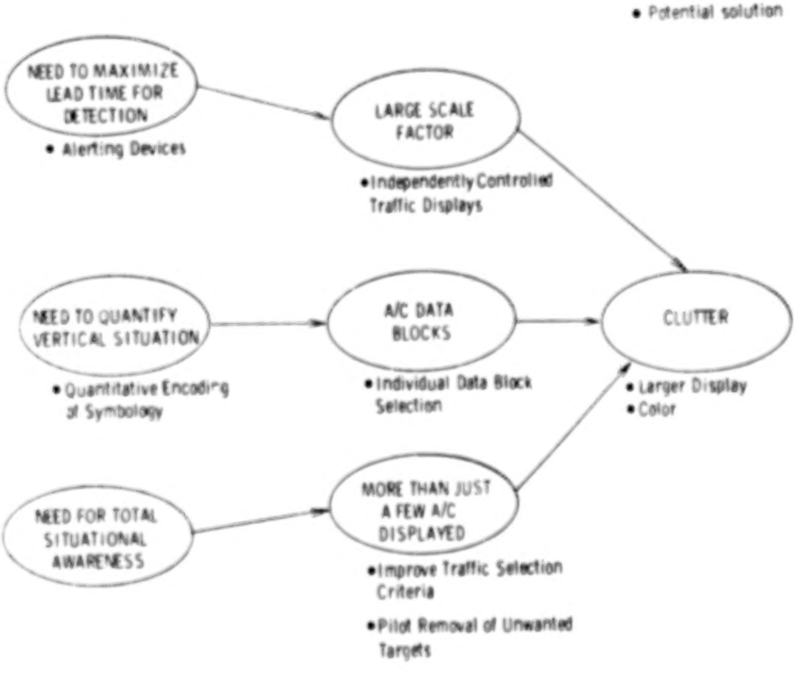
• Potential solution
NEED TO MAXIMIZE LEAD TIME FOR DETECTION
• Alerting Devices
LARGE SCALE FACTOR
• Independently Controlled Traffic Displays
NEED TO QUANTIFY VERTICAL SITUATION
• Quantitative Encoding of Symbology
A/C DATA BLOCKS
• Individual Data Block Selection
CLUTTER
• Larger Display
• Color
NEED FOR TOTAL SITUATIONAL AWARENESS
MORE THAN JUST A FEW A/C DISPLAYED
• Improve Traffic Selection Criteria
• Pilot Removal of Unwanted Targets

Figure 22.- Summary of display clutter factors.

BLANK PAGE

BLANK PAGE

GUIDANCE AND CONTROL SYSTEM RESEARCH FOR IMPROVED TERMINAL AREA OPERATIONS*

R. M. Hueschen, J. F. Creedon, W. T. Bundick, and J. C. Young

NASA Langley Research Center

ABSTRACT

Several guidance and control system research and development activities aimed at improving the operational capabilities of commercial aircraft in the terminal area are described. The guidance and control systems have been designed to improve the capacity and efficiency of terminal area operations, enhance the approach and landing capability of aircraft in adverse weather conditions, and reduce the impact of aircraft noise perceived on the ground. Specific performance features include the ability to capture and track steep glideslopes, use short final approaches, perform flares with reduced longitudinal touchdown dispersion and execute high speed runway rollout and turnoff. Results obtained from simulation studies or flight tests are shown for each of the algorithms.

INTRODUCTION

Significant improvements in the terminal area operational capability of commercial aircraft are being sought to alleviate crowded conditions at major airports and to enhance safety and schedule reliability. The Terminal Configured Vehicle (TCV) program being pursued at Langley Research Center has the goal of providing flight management and CTOL aircraft technology to increase terminal area capacity and efficiency, to improve the approach and landing capability of aircraft operating in adverse weather conditions, and to reduce the aircraft-generated noise perceived on the ground. This paper presents some results obtained from a coordinated guidance and control system development effort directed to support the TCV program.

---

* The work presented comprises the results of both in-house and contractual research efforts. In particular, the DIALS design effort was performed by Dr. N. Halyo currently of the Information and Control Systems, Inc.; two flare law algorithms were developed by A. A. Lambregts of the Boeing Co.; and the initial rollout and turnoff guidance and control law was developed by S. Pines of the Analytical Mechanics Associates, Inc.

Automatic guidance and control systems are presented for glideslope and localizer capture and track, flare and landing, rollout, and runway exit. For all flight phases considered, the aircraft sensors providing acceleration, attitude, altitude, and body rate data are augmented by information derived from the Time Referenced Scanning Beam Microwave Landing System (MLS) under development by the FAA. The MLS consists of a precision DME providing range information and discrete azimuth and elevation signals available within the specified volumetric coverage. In cooperative efforts between NASA and the FAA, many automatic approaches and landings have been performed by the TCV B-737 aircraft to demonstrate the utility of this information in flying curved approaches to relatively short finals (refs. 1, 2, 3, 4, and 5). To enhance and extend the autoland capability and performance levels previously demonstrated, a digital, integrated automatic landing system (DIALS) has been developed using a modern control theoretic approach. The DIALS algorithm provides rapid capture and precise tracking of glideslope and localizer--including the capability of simultaneously performing both capture maneuvers. This feature enhances the efficient use of terminal area airspace by permitting aircraft to be flown along separate curved approach paths and merged only for short final approaches. The control law also permits tracking of pilot selectable steep glideslopes. The lower thrust levels required for steep glideslopes reduce the noise emanating from the aircraft and the greater attenuation afforded by the increased altitudes further reduces the noise levels perceived on the ground. To improve passenger comfort and control performance in adverse weather conditions, the DIALS algorithm generates estimates of wind velocities and uses these estimates in the control loop.

Several research efforts were pursued to increase runway landing capacity by reducing the time each aircraft occupies the runway. To limit the occupancy time, each inbound aircraft would flare to a landing at a prescribed distance from the desired exit. The aircraft would then be automatically controlled to follow a closed-loop deceleration program during rollout and perform a high speed turnoff. Reduction of the longitudinal touchdown footprint is essential since short landings requiring large occupancy times or long landings resulting in missed turnoffs would disrupt the flow of traffic and decrease the landing rate achieved. To obtain improved flare performance, two algorithms were developed and flight tested. The first flare law commands altitude as a function of sink rate to achieve an exponential path. The time constant is varied as a function of ground speed to ameliorate the effect of variations in ground speed on touchdown location. The second flare algorithm commands the aircraft to follow an explicitly defined path-in-space. This approach has the potential to further reduce touchdown dispersions by also minimizing the effects of glideslope tracking errors on touchdown location.

To extend automatic operations through rollout and turnoff, the aircraft is commanded to follow a prescribed path. The path is defined by a magnetic leader cable imbedded in the runway and turnoff. Signals obtained from a three coil magnetic sensor mounted on the aircraft are processed to yield measurements of the aircraft's heading and lateral deviation from the desired path. These measurements are used in a rollout and turnoff guidance and control law which provides deceleration and steering commands for both wet and dry runway conditions.

In the subsequent sections, descriptions are given of each of the control algorithms and results are given for simulation, prototype evaluation or flight testing. The DIALS design philosophy and performance advantages are discussed. Results of detailed simulation studies are given to demonstrate significantly improved performance relative to existing autoland system designs. The flare algorithms are described and the effect of the design concepts on touchdown dispersion is illustrated. Results of extensive flight tests of the flare laws are reviewed. Both theoretical and field test results for the magnetic leader cable and the associated sensor are presented. The deceleration program is given along with rollout and turnoff guidance and control performance results obtained from a simulation study using a detailed model of the sensor derived from the field tests.

DIALS

Current operational autoland systems perform well the task they were designed to accomplish. However, increased capabilities are being demanded for autoland systems to solve some of the problems of the increasingly crowded terminal area airspace. These demands include improved performance in adverse weather conditions, tracking of steep and selectable glideslopes for noise reduction, avoidance of wake vortices, and reduced fuel consumption. The current systems have limitations which make it impossible for them to meet the demands for increased capabilities. The DIALS design was undertaken to provide a system with expanded capabilities free of the current limitations. The DIALS is a complete software algorithm designed and developed for the automatic landing of a commercial type aircraft. The tasks performed by the DIALS (see figure 1) are: (1) close-in simultaneous capture of the localizer and glideslope including steep glideslopes up to 6 degrees, (2) tracking of the localizer and glideslope, (3) a sideslip decrab maneuver (the same type decrab maneuver performed manually by pilots), (4) the flare maneuver from the various selected glideslopes, (5) precision touchdown, (6) calibrated airspeed (CAS) hold, (7) stabilizer trim, and (8) inner loop damping including the yaw rate damper function. First, some of the limitations of the current systems will be given and then the approach and methods used in the design of the DIALS will be presented.

The current autoland systems use the Instrument Landing System (ILS) for guidance along the localizer and glideslope paths. The ILS restricts guidance to one fixed glideslope and also often has characteristic beam bends on the localizer signal. In addition, these systems use the classical approach to control system design in which the gains are determined through root locus techniques and specified gain and phase margin criteria. These techniques can be applied only to single-input single-output portions of the system--a limitation of the classical approach. Thus after the initial determination the gains must be adjusted by trial and error procedures to account for the interaction between the multiple inputs and outputs of the system. One final point to be made concerning the present systems is that the systems are analog. Special programming efforts and analyses are generally required to implement an analog system on a digital computer.

The DIALS differs from systems currently being flown in several ways. First, it was designed to use the MLS rather than the ILS. The MLS provides the information necessary to fly different glideslopes as well as providing signals relatively free of beam bends (multipath effects). Second, the system was designed using modern digital control theory techniques and methods as opposed to the classical approach. The modern control theory approach provides a means for defining the total system and control requirements within a unified set of equations. Then from the total set of equations all the system feedback gains are mathematically determined simultaneously. The simultaneous solution of the gains is referred to as an integrated design--the second character of the DIALS acronym. For DIALS this method was applied once to a unified set of lateral system equations and then to a set of longitudinal equations (refs. 6, 7, and 8). The integrated design results in commands coordinated among the longitudinal controls as well as commands coordinated between the lateral controls. For instance, if a reduction in airspeed is desired while maintaining glideslope track, DIALS will produce coordinated throttle and elevator commands. The throttle reduction will be accompanied by an elevator command calling for a pitch up to maintain the glideslope track (reduced airspeed results in reduced lift and subsequent movement below the glideslope).

Another feature of the DIALS is that it is a digital or discrete design--the first character of the acronym. This means that the differential equations describing the system were discretized into a system of difference equations. The difference equations were then used in the modern control theory approach to determine the system control gains and the filter gains for estimating the state variables of the system from one sampling instant to the next. The digital design results in a set of difference equations for updating the guidance and control commands and a set for updating the filter equations.

There were several reasons for choosing a digital design. First, aircraft avionics technology is moving toward the use of digital flight control computers and the control laws would ultimately be discretized anyway for implementation on the flight computer. Second, the MLS system used by DIALS provides the aircraft's position at discrete intervals of time rather than continuously. Also, the aircraft sensor measurements will only be available at discrete sampling instants on a digital computer. For these reasons, a digital design was chosen for the DIALS.

A feature of the digital design is that the update interval or rate of the flight control computer is specified in the formulation of the set of system difference equations. This results then in a set of control system gains which take into account the update rate of the computer. Another important feature of the DIALS design is that the continuous cost function (the means of weighing the control law performance in the modern control theory design) was discretized in a manner such that the system dynamics between sampling instants is included in the discrete cost function (ref. 6). The inclusion of the system dynamics between sampling instants makes it possible to use larger sampling intervals than generally used. Thus the real-time computational requirements on the flight control computer are reduced. For the DIALS the update rate is 10 times per second.

The DIALS consists of three basic functions--navigation/filtering, guidance, and control about a desired path. (The relationship of these functions is illustrated in figure 2.) The navigation/filtering function estimates the aircraft position and other parameters using a steady-state Kalman filter, that is, a Kalman filter whose gains remain constant for a given approach and landing. The filter determines the aircraft position in a runway coordinate frame using aircraft sensors and measurements of azimuth, elevation, and range from the MLS. The filter also provides estimates of the aircraft attitude, velocity, accelerometer biases, barometric altitude and barometric sink rate biases, and wind velocities. The DIALS was also formulated to take into account the effects of wind disturbances on the aircraft. The wind states were weighed in the discrete cost function and thus the control commands are a function of the wind state estimates. Wind velocity estimates are provided for the steady state, gust, and shear wind components. The aircraft sensor measurements used by the filter are attitudes, attitude rates, body-referenced accelerations, barometric altitude and sink rate, radar altitude, and calibrated airspeed.

The guidance function determines the tracking errors from the desired flight path (trajectory) using the aircraft state and wind estimates. The generation of the desired flight path, which was formulated to be a function of several selectable parameters, is also part of the guidance function. Pilot selectable parameters include the desired glideslope angle and the calibrated airspeed. Other parameters which can be changed to tailor the flare trajectory are the glide path intercept point (GPIP), the touchdown point, touchdown sink rate, and the airspeed reduction during flare. The control function determines the control commands necessary (1) to null the errors or deviations from the commanded trajectory, (2) to maintain aircraft trim, and (3) to damp the inherent natural frequency modes of the aircraft (inner loop damping). The commands computed are elevator and aileron position and rudder, stabilizer, and throttle rate. The stabilizer rate commands are converted through logic equations to trim up and trim down discretes to interface with the aircraft's stabilizer trim motor.

The use of rate commands provided a means for formulating an automatic trim capability into the control law. By using rate commands no penalty is incurred on position changes, but only on excessive rates of change. Aileron and elevator position commands were used to provide quickness of response. Also, the use of position commands in the cost function prevents large standoff position commands which could result in large undesirable hinge-moments for these control surfaces.

The control commands are functions of the aircraft states, wind velocities, nominal flight path, and commanded path deviations from the nominal flight path as illustrated in figure 3. The nominal trajectory or flight path consists of the straight line localizer and glideslope path as well as the nominal aircraft state. Deviations from the nominal trajectory are commanded during the decrab and flare maneuvers.

The DIALS has been tested via a digital computer simulation which used a six degree of freedom non-linear model of the TCV B-737 aircraft. The simulation included sensor noises and biases, such as accelerometer misalignment and scaling errors, and various wind conditions--steady state, gust, and shear. The servos were modeled as first order lags.

Simulation results are shown in figures 4 and 5. Figure 4 compares the capture and track of the localizer with the current TCV B-737 localizer capture and track algorithm. It can be seen that the DIALS capture occurs within 40 seconds as opposed to the 120 seconds or so for the current algorithm. This capability to fly short final approach paths is important for efficient air traffic control operations. Also note that the overshoot performance is much lower for DIALS. This performance, which has been demonstrated for various simulated wind conditions, is important in achieving reduced runway spacing for parallel runway operations. The sideslip decrab maneuver is also illustrated in the roll and yaw plots. Figure 5 compares the capture of a six degree glideslope by DIALS with the capture of a three degree glideslope by the TCV B-737 ILS glideslope capture algorithm. Note that the capture and settling time for DIALS is 5 seconds while at least 30 seconds is required for the TCV B-737 algorithm. It is also noted that this capture occurred simultaneously with the localizer capture. Simultaneous capture is important because it contributes to reducing the length of the final approach path. However, the DIALS can perform the captures independently. The capability to fly various glideslope angles, including steep final approaches, provides the means for noise reduction along the ground track and avoidance of trailing vortices.

FLARE LAW DEVELOPMENT

Certification under FAA AC 20-57A for commercial aircraft requires automatic landing systems to meet a $\pm 2\sigma$ longitudinal touchdown dispersion of 457.2 m (1500 ft). Flare laws which provide touchdown dispersions smaller than this requirement are desirable for several reasons. The precise flare performance can be combined with a capability to perform high-speed exits and thus increase runway landing capacity by limiting runway occupancy time. In addition, reduction in touchdown dispersion is an effective means of reducing the operational field length requirement. The TCV program has established a longitudinal touchdown dispersion criterion of $1\sigma \leq 30.5$ m (100 ft) as being commensurate with their specific goals for improved terminal area performance. To attain this goal, factors contributing to touchdown dispersion have been evaluated and several flare concepts have been identified to ameliorate the effects of specific sources of dispersion.

Many flare laws in current use command sink rate as a function of altitude. Algorithms of this type, designated here as $\dot{h}$ (h) flare laws, are designed to provide an exponential flare path. To obtain transient-free initiation the flare is started at the altitude at which the commanded flare sink rate becomes equal to the measured sink rate. The TCV B-737 used a flare law of this type during autoland demonstrations performed for the ICAO all-weather operations panel at the FAA's National Aviation Facilities Experimental Center

(NAFEC) in May 1976 (refs. 1 and 2). The touchdown performance for 56 landings performed during this demonstration was:

Longitudinal dispersion (1σ) = 94.2 meters (309 ft)

Sink rate (mean/1σ) = .713/.430 m/sec (2.34 / 1.41 ft/sec)

This performance was achieved with average wind velocities of 8.23-10.29 meters/sec (16-20 knots) and relatively large gusts and tail winds (ref. 1). While the longitudinal dispersion was better than the FAA requirement, it fell short of the TCV goal. Accordingly, a detailed study, to be described in a contractor report, was performed by the Boeing Company to identify factors which contribute to touchdown dispersion. Flare law designs were then sought to reduce their effects. One such factor is that approaches in different steady wind conditions are performed at different ground speeds; consequently, the flare initiation altitude and touchdown point can vary significantly. Figure 6 shows a variation of over 152.4 meters (500 ft) in touchdown location for approaches flown at $V_{ref.}$ + 2.57 meters/sec (5 knots) in steady wind conditions ranging from a 12.86 meters/sec (25 knots) headwind to a 7.72 meters/sec (15 knot) tail wind. These results were obtained from a simulation of the TCV B-737 for an $\dot{h}$ (h) flare law of the type used during TCV autoland demonstrations. It is noted that the flare initiation altitude varies by over six meters during these conditions--a variation which increases the difficulty experienced by pilots in monitoring flare performance. Glideslope tracking errors and errors in the estimates of aircraft sink rate can also make significant contributions to touchdown dispersion. To reduce longitudinal touchdown dispersions, two flare concepts have been developed and evaluated. The concepts, called the variable time constant flare law and the fixed-path flare laws, are described in the following sections.

Variable Time Constant Flare Law

Figure 6 illustrates the effect on flare performance of variations in approach speed to accommodate steady wind conditions. To reduce the resulting dispersion, several approaches were investigated. In the selected approach, the time constant (ratio of the control gain on sink rate to the gain on altitude) is defined as

$$T = \frac{T_o \quad V_{Go}}{V_G} \qquad (1)$$

where T is the time constant, V_{Go} is the nominal approach ground speed and V_G is the actual approach ground speed. This modification provides transient free initiation at a fixed altitude--chosen as 12.8 m (42 ft) during this study. Simulation results for this algorithm are shown in figure 7 for the various head wind/tail wind conditions used in the simulation illustrated in figure 6. These results confirm the ability of this flare law, designated as the $\dot{h}$ (h, V_G) or variable time constant flare law, to eliminate the effects of steady winds on touchdown dispersion. Prior to flight evaluation, an improved inner loop was designed and the $\dot{h}$ signal was developed as the output of a first order complementary filter using vertical acceleration from the INS and altitude from the radar altimeter. Selection of 12.8 m as the flare initiation altitude, insures that the aircraft will be over the runway at most airports and the radar altimeter signal will not be affected by uneven approach terrain during the flare. In production configurations the $\dot{h}$ signal derivation would be made an implicit function of the $\ddot{h}$, $\dot{\theta}$ inner loop filter. Implicit h derivation and initialization of the filter at the time of flare avoids carrying pre-flare terrain history, stored on the complementary filter, into the flare.

Flight evaluation of the $\dot{h}$ (h, V_G) flare law was performed using the TCV B-737 aircraft and the associated experimental system (ref. 9). The flare algorithm was implemented in the triple channel fail-operational flight control computers which computed flare commands at 20 iterations/second and performance data was obtained during automatic landing demonstrations performed at Dorval Airport in Montreal, Canada during 1978. During the demonstrations, flare data was obtained for 58 landings on 10 days while carrying passengers connected with an ICAO All-Weather Operations Division meeting. Several equipment configurations were used; however, over the last 40 runs both the equipment and system configuration were unchanged. A summary of the flare law performance at touchdown for these runs is:

Longitudinal dispersion (1σ) = 41.8m (137 ft)

Sink rate (mean/1σ) = .87/.19 m/sec (2.84 / .62 ft/sec)

All touchdowns were located in a 196 m (641 ft) range. This compares very favorably with 1500 ft (457.2 m) FAA $\pm$ 2σ footprint requirement and indicates that the flare law did not experience any extremely short or long landings. A more detailed discussion of both the flare design concept and flight test performance is contained in reference 10.

Fixed-Path Flare Law

A second approach to reducing touchdown dispersion involves commanding the aircraft to fly a fixed flare trajectory that is explicitly defined as a function of runway distance. Flares of this type, designated path-in-space or h(x) flare laws, have several advantages. The path is unchanged for variations in approach speed. The explicitly defined path may be altered independently of the gains used to achieve damping and turbulence response. Conversely the effects of feedback gains can be studied without changing the flare path. When an estimate of aircraft position is available such as can be provided by MLS, the flare is initiated at a preselected value of x and the path may be made a continuous extension of the glide path. This approach would enable the flare law to reduce the effect of glideslope tracking errors at flare initiation on touchdown location. Finally, commands for h (x), $\dot{h}$ (x), and $\ddot{h}$(x) can be developed to provide close tracking of the desired trajectory.

Two path-in-space trajectories have been studied. The first, designed for use with a nominal 3° glideslope, specifies the first path as:

$$h_c(x) = \frac{K_1}{K_2^2} e^{-K_2 x} - \frac{K_1}{4K_2^2} e^{-2K_2 x} + K_3 x + K_4 \qquad (2)$$

The four constants K_1 through K_4 were chosen to satisfy the boundary conditions

$$\dot{h}_1 = \dot{h}_{\text{GLIDE PATH}} \qquad \text{at flare initiation} \qquad (3)$$

$$h_1 = 12.8 \text{ m } (42 \text{ ft}) \qquad (4)$$

$$\dot{h} = \dot{h}_{\text{DESIGN VALUE}} \qquad \text{at touchdown} \qquad (5)$$

$$x = x_{\text{DESIGN}} \qquad (6)$$

The corresponding $\dot{h}_1$ and $\ddot{h}_1$ commands are developed by differentiating the $h_1(x)$ command and dropping terms involving $\ddot{x}$. This formulation provides transient free flare initiation at fixed altitude for fixed glideslope approaches as well as specifying a gradual increase of $\ddot{h}_1$ to a maximum followed by a smooth reduction. Figure 8 shows the $h_1(x)$ trajectory for the aircraft dynamics and wind conditions used in generating figures 6 and 7.

The $h_1(x)$ flare law was evaluated during 1978 at NAFEC. For these tests the value of x was obtained from MLS measurements as described in reference 2. MLS configurations both with and without the flare elevation antenna were used. Performance was better with the flare elevation antenna--primarily as a result of onboard processing resolution. With the flare elevation antenna, 32 runs were made with touchdown performance of

Longitudinal dispersion (1σ) = 28.0 meters (92 ft)

Sink rate (mean/1σ) = .78 / .16 m/sec (2.56 / .51 ft/sec)

All flares which can be logically grouped together are summarized even though during the first part of the h(x) test program, several minor configuration changes were made. The performance during the latter portion of the testing, in which the configuration was held constant, indicates that the system was improved by these changes. For example, the last 18 landings using guidance derived from the flare elevation antenna were performed with a constant configuration. For these landings, a longitudinal dispersion of 48.3 ft was obtained with no degradation in the mean and standard deviation of touchdown sink rate.

This fixed-path flare concept was also evaluated in an ILS mode. When using the ILS the aircraft's position is not known; consequently, the flare was initiated at a radar altimeter reading of 12.8 m. The value of x required to generate $h_1(x)$, $\dot{h}_1(x)$ and $\ddot{h}_1(x)$ was obtained by integrating ground speed from the INS. For this configuration 23 runs were made resulting in

Flare distance (1σ) = 28.7 m (94 ft)

Sink rate (mean/1σ) = .71/.15 m/sec (2.33 / .50 ft/sec)

The variation in flare distance does not represent the total variation in touchdown position since errors in glideslope tracking at flare affect only the latter. Other flight tests with this aircraft indicated that the 1σ longitudinal dispersion attributable to glideslope tracking errors is 14.9 m (49 ft). This value was combined in an RSS manner with the 1σ value for flare distance to obtain an estimate of 32.3 m (106 ft) (1σ) in touchdown position.

An alternative h(x) formulation has been developed to accommodate the DIALS approaches which have selectable, steep-glideslope capability. In this approach $\ddot{h}_2(x)$ was specified as a 1-Cosine function. The $\dot{h}_2(x)$ and $h_2(x)$ commands were obtained though expressions formulated from off line integration of the $\ddot{h}_2(x)$ function. Constants are selected to provide transient free initiation for the glideslope being flown and to achieve the specified touchdown point and flight path angle. The flare initiation altitude is determined on line as a function of the selected glide path and specified touchdown parameters.

Simulation studies have been performed to evaluate the performance of this flare law. The studies used a nonlinear aircraft model and included sensor noise and atmospheric disturbances. The touchdown performance obtained for twenty flares from a 6° glideslope was

Longitudinal dispersion (1σ) = 34.4 m (113 ft)

Sink Rate (mean/1σ) = .66/.26 m/sec (2.18 / .85 ft/sec)

A graphical presentation of the performance results for the $h_1(x)$ fixed path and $\dot{h}(h, V_G)$ flare law is shown in figure 9. This figure also contains the performance of the baseline $\dot{h}(h)$ flare law.

In summary, both the variable time constant and specified trajectory laws can achieve significant reductions in longitudinal touchdown dispersion with reasonable values for the mean and standard deviation of touchdown sink rate. The flare laws performed well using currently available guidance sources and sensors as well as with the MLS guidance system. The results are thus applicable to both current and future commercial aircraft operations.

MAGNETIC LEADER CABLE

To extend the automatic operations described in the preceding sections through rollout and turnoff, a guidance signal for following a prescribed ground path is required. One potential source of the required guidance information during rollout, turnoff, and taxi is the Magnetic Leader Cable. The cable, or wire, would be in the runway, turnoff, and taxiway along the path which the aircraft is to follow, as in figure 10. An audio frequency current in the cable sets up a magnetic field, which is detected in magnitude and direction by a set of three orthogonal coils mounted in the aircraft. The voltage outputs of the three coils are then amplified, filtered, and detected to produce three varying d.c. voltages V_x, V_y, and V_z which are proportional to the x-, y-, and z- components of the magnetic field. It can be shown theoretically that, assuming the leader cable is an infinitely long straight wire, the ratio of the voltages V_z/V_y is a measure of the lateral displacement y of the coils (and aircraft) from the cable as in figure 11, that is

$$\hat{y}_1 = k_y \, V_z/V_y \tag{7}$$

Similarly, it can be shown that within a small angle approximation the ratio of voltages V_x/V_y is a measure of the aircraft heading ψ relative to the cable, that is,

$$\hat{\psi} = k_\psi \, V_x/V_y \tag{8}$$

A sensor of this type has been investigated analytically and experimentally.

Analytical Studies

Since the current in the cable must have a return path, a practical cable installation would be neither infinite nor straight, but must be some form of closed loop, such as a rectangle. The analytical investigation has emphasized an examination of the effects of a rectangular loop configuration on the sensor performance.

The components of the magnetic field were computed theoretically for various sizes of the loop and for various displacements and headings of an aircraft relative to the cable. The ratios of the components were computed according to equations (7) and (8), and the following results were obtained. The voltage ratio V_z/V_y is no longer a linear function of displacement y as in equation (7). Thus, an exact measure of y would require that the sensor utilize a non-linear calibration curve. Furthermore, the measurement $\hat{\psi}$ is only exact at a point midway between the ends of the loop. However, it may be possible to reduce these effects sufficiently to allow use of the linear relationships by making the rectangular loop large enough such that the return wire is at least 200 meters from the centerline and the ends of the rectangle are at least 200 meters beyond the ends of the runway. Furthermore, errors produced by using a linear calibration become very small near the cable.

Experimental Studies

Tests were conducted using an experimental sensor based on a design by Ohio State University. The processor was designed and fabricated using analog circuits, and the coils were wound on a four-inch wooden cube. For ease and economy of testing, the sensor and support instrumentation were installed in a passenger van modified for this use. An aluminum structure, shown in figure 12, was attached to the rear of the van to support the coils and preamplifier. The processor output signals together with the output of a time code generator were recorded on magnetic tape for post-test data analysis. Tests with the van were conducted at Wallops Flight Center. Leader cables in the form of rectangular loops 305 meters (1,000 ft) long were temporarily installed on various taxiways and runways at Wallops to examine the effects of different runway construction materials on the processor signals.

In general, two types of tests were conducted: static during which the van was stopped at a specified point, and dynamic during which the van was driven along a desired path. For both types, cable current frequencies of 150 Hz, 165 Hz, and 990 Hz were employed, and currents from 0.25 Amperes to 2.0 Amperes were used. Coil heights varied from 1.2 meters (4 ft) to 3.7 meters (12 ft) with most data taken at 2.41 meters (8 feet).

For the dynamic tests the van was driven along the desired path at speeds of approximately 3.6, 8.9, and 22.4 m/sec (8, 20, and 50 mph) with most of the runs being made at 8.9 m/sec. While 8.9 m/sec was somewhat arbitrary, it did afford a compromise among realistic aircraft speed, ability to accurately drive the path, and a desirable data record length in terms of time. Most of the paths were parallel to the cable at displacements from the cable of as much as 21.3 m (70 ft).

The test procedure for each parallel run normally consisted first of recording static data and setting the gains for the paper chart and magnetic tape recorders with the vehicle aligned with the proper parallel mark and at the center of the test area. Then dynamic data was recorded while the van was driven along the selected parallel marker at a constant speed.

Test Results

Plotted in figure 13 is an example of static data taken at Wallops with a cable current of 0.25 A at 990 Hz. The signal V_y and V_z are the d. c. voltages in the y- and z- channels, respectively, after detection. Also shown are the theoretical values computed as part of the analytical studies. As can be seen, the experimental and theoretical data agree quite well. In figure 14 is plotted the corresponding experimental data for the processor $\hat{y}_1$ output, that is, the output obtained by taking the ratio V_z/V_y, as in equation (7). As predicted by the analytical studies of a rectangular loop, the output is a slightly non-linear function of the displacement y. To obtain an accurate measure of displacement, the sensor (or the guidance and control computer) would store and utilize this calibration curve.

In figure 15 is shown a time history plot of dynamic data recorded with the loop installed on the southwest end of taxiway 04/22, part of which is constructed of concrete and part of asphalt. The van was driven at 8.9 m/sec along a path 7.62 m (25 ft) from the cable. The current frequency was again 990 Hz. Using calibration curves, such as the one in figure 14 for $\hat{y}_1$, the data has been converted to engineering units.

Several characteristics of this data are worth noting. First, the $\hat{y}_1$-output is a promising measurement of the displacement y, but the $\hat{\psi}$-output does not accurately measure the heading ψ, which was close to zero for this run. The bias in the heading measurement was judged to be caused, at least in part, by distortion of the magnetic field by the van. In the $\hat{\psi}$ - output there is an obvious ripple which has the same spatial frequency as the sections of concrete and which is apparently caused by the metal reinforcement in the concrete. In both outputs there is a transient near the concrete/asphalt junction, and there is a bias shift of three to four feet in the $\hat{y}_1$-output between the two sections.

Aircraft Tests

To obtain some preliminary data on the effect of the metal aircraft structure and of aircraft electrical systems on sensor performance, limited static tests were conducted using the TCV B-737 aircraft. A magnetic leader cable loop was set up on a taxiway in front of the NASA hangar at LaRC. Static data was taken just as in the van tests with the following exceptions: The coils and pre-amplifier were removed from the van support structure and temporarily installed in one of two locations in the B-737. One of the coil locations was inside the nosecone at a height of about 2.4 m (8 ft), and the other location was below the nosewheel well at a height of .91 m (3 ft). The pre-amplifier was connected via extended cables to the processor and instrumentation in the van. The overall installation can be seen in the photograph in figure 16, and the nosecone installation is shown in figure 17. The aircraft was positioned at the test point using a tug and power to the aircraft electrical systems was supplied by the aircraft APU.

In figure 18 are plotted static $\hat{\psi}$ - output voltage as a function of displacement y for the aircraft oriented at 0° heading and at 5° heading relative to the cable. Due to distortion of the field by the aircraft, the $\hat{\psi}$ - output is a stronger function of y than of ψ at both 150 Hz and 990 Hz. These results were obtained with the coils in the nosecone location. With the coils located below the nosewheel well, the y- dependence is even more dramatic.

The preceding data was taken with no aircraft electrical system operating. Additional static data was taken and the processor outputs were recorded on magnetic tape as various aircraft electrical and avionics systems were turned "on." Analysis of this data indicates that considerable filtering may be required to reduce the interference produced by other avionics, particularly when operating at 990 Hz. Additional tests are required to determine if this filtering is effective.

In summary, the analysis and test results to date indicate that because of the effects of the metal aircraft, an accurate measure of heading probably cannot be obtained with the Magnetic Leader Cable system. However, measurement of lateral displacement from the desired path looks promising. A new experimental sensor suitable for flight test on the B-737 is being designed and fabricated using a combination of analog and digital circuits for increased processing flexibility. Additional tests with the van and then with the aircraft will be conducted to further assess performance and to select such parameter values as the cable frequency and bandpass filter bandwidth.

AUTOMATIC ROLLOUT AND TURNOFF

The automatic rollout and turnoff guidance and control system performs the following tasks: It controls the aircraft from touchdown along the runway centerline and desired high speed turnoff exit, and it decelerates the aircraft to the desired turnoff speed. The basic elements of the system are shown in figure 19 and consist of (1) the filter, (2) the magnetic leader cable processor, and (3) the guidance and control law.

The filter provides estimates of the aircraft position and velocity components in the runway coordinate frame. The inputs to the filter are the MLS measurements of azimuth and range, lateral and longitudinal acceleration, aircraft attitude, and body rates. In simulation studies both a time-varying Kalman filter and a third order complementary filter were used. The Kalman filter and complementary filter were previously designed for use in the automatic approach and landing phases of flight.

The magnetic leader cable processor provides outputs of lateral displacement and relative heading from the cable. These outputs can be provided through either a hardware or software processor given the coil output voltages as inputs.

The guidance and control law is a modified design of the TCV B-737 rollout law which uses the ILS localizer signal for runway centerline location. The modified law consists of two parts--the path tracking law, similar to the localizer law, and a new part, the braking law. Like the localizer law, the modified law commands the rudder and nose wheel positions. In addition, the modified law commands the desired deceleration for input to the autobrake system and the desired nominal reverse thrust.

The inputs to the path tracking law are the position and velocity estimates from the filter, the magnetic leader cable processor outputs, the aircraft heading, and the specified path information (magnetic leader cable location). The law uses these inputs to compute estimates of cross-track error (lateral displacement from the cable), cross-track rate, and heading error. The estimated cross-track error is determined by computing a linear combination of the cross-track error from the filter and the magnetic leader cable processor output. The estimated heading error is a linear combination of relative track angle determined by the filter outputs and heading error from the magnetic leader cable. Using the guidance signals of cross-track error, cross-track rate, and yaw error, the path tracking law determines the commanded rudder and nose wheel positions.

The guidance law also contains a logic section. At touchdown, a determination is made as to whether or not the aircraft can decelerate safely to the desired exit speed using the estimated distance to go, ground speed, and aircraft weight. If the aircraft is unable to decelerate safely, an alternate turnoff exit further down the runway is used in calculating the deceleration profile. When the logic determines that the exit speed is safely achievable, the guidance calculates the total deceleration force necessary to achieve the desired exit speed. If the force is greater than the maximum specified reverse thrust, it sets the commanded reverse thrust to the specified maximum and computes the nominal braking required. If the total force is less than the specified maximum thrust, the reverse thrust is set to slightly less than the total force required and the required nominal braking is computed as previously described. In either case, the reverse thrust command remains constant while the deceleration command to the autobrake system maintains the closed loop control about the desired deceleration. The logic and calculations also take into account wet and dry runway conditions. In addition, the logic triggers computations to estimate the DME bias when crossing over a known position (calibrated position) on the runway. The discrete telling the logic that the calibrated position is being crossed over perhaps could be determined from detecting the magnetic field of a small current driven loop buried in the runway. In the development of this system, this measurement was simulated with an error of 2 to 3 meters.

The braking control law was designed to compute a brake command which would control the aircraft about a desired fixed deceleration, $\ddot{X}_D$, according to the following equation:

$$\ddot{X}_D = \frac{\dot{X}_T^2 - \dot{X}^2}{2\ (d-d_B)}$$

where $\dot{X}_T$ is the desired turnoff speed, $\dot{X}$ is the estimated speed, d is the estimated distance to go to the turnoff or exit, and d_B is the distance before the turnoff at which it is desired to reach the exit speed. This formulation results in a linear decrease in speed. The desired acceleration is then compared with the measured acceleration to determine the acceleration error.

The braking control law integrates the acceleration error and then multiplies the integrator output by a constant gain to compute the command level of braking. At initiation of braking, the auto-brake system is commanded to the nominal braking required in one second. After one second the integrator is initialized and engaged to integrate the acceleration error. The brake command is limited to a constant value for dry runways and to a variable limit for wet runways. The variable limit, which is a function of ground speed, was determined from hydroplane data.

The following summarizes the sequence of events that occur during the automatic rollout and turnoff guidance and control:

- Deploy the ground and speed brakes (spoilers) at main gear compression.
- At two seconds:
  - Compute the nominal reverse thrust and braking if not achievable, recompute the same parameters for the alternate exit.
  - Then initiate the nominal reverse thrust, steering and braking commands.
- Determine DME bias and update position estimates 396 meters (1300 ft) from turnoff
- Deactivate reverse thrust 2.6 m/sec (5 knots) above desired exit speed.
- Continue braking to desired exit speed and turnoff at runway exit.

The performance of the rollout and turnoff system was evaluated using a nonlinear aircraft simulation similar to that described earlier in the DIALS. One addition to the simulation was a model for the landing gear and tire dynamics and preliminary error models for the buried magnetic leader cable signals. The models used for the cable were obtained from the experimental test results described earlier. Figure 20 shows the time histories of four longitudinal parameters--thrust, percent of specified maximum braking, deceleration, and the ground and airspeed. The runway configuration simulated was the Wallop Flight Center (WFC) high speed exit 1158 meters (3800 ft) from threshold - 914 meters (3000 ft) radius. This case was for a dry runway, 5.1 m/sec (10 knot) headwinds and gusts. Note that the braking increases at first to compensate for the reverse thrust which is lagging the desired command. Also note that as the reverse thrust is reduced to idle, the level of braking increases to compensate. Figure 21 is a time history plot of the aircraft yaw with respect to the runway centerline, the cross-track error from the desired path, and the side acceleration of the aircraft. The cross-track error plot shows the true error, the error measured from the magnetic leader cable, and the error determined from filter estimate. For this run the control system used the cross-track error from the magnetic cable only and the heading error computed only from the filter estimates. The cross-track error plot illustrates that much better accuracy is obtained from the magnetic cable measurement than that computed from the estimates. Note that the lateral acceleration is smooth and that it's slightly greater than .1 g for this 30.9 m/sec (60 knot), 914 m (3000 ft) radius turn. It can be seen that the aircraft reaches its desired turnoff speed just before 15 seconds (see figure 20, percent braking) and begins its turn off the runway about 1 second later as indicated by the yaw plot. Figures 22 and 23 are similar time history plots for a wet runway. Note the lower level of braking as compared to the dry runway case. Also note the longer time it takes to turnoff the wet runway in going to the alternate exit -- approximately 25 seconds. It can be seen from the ground speed trace that the aircraft was decelerated smoothly to its exit speed just before it reached the turn. In both plots (wet and dry) it can be seen that the aircraft tracks the desired path very close during the straight line positions and stands off to the outside of the turns, but within three meters of the desired track.

The simulation results have shown that the automatic guidance and control system provides acceptable performance for both wet and dry runway conditions. In addition, this performance was demonstrated in the presence of aircraft sensor noises and biases, MLS noises and biases, magnetic cable errors modeled from the van tests described earlier and wind disturbances. Further simulation studies still remain to check the performance of the system using a refined landing gear model. These studies should also include tests to determine the effects on performance due to thrust imbalance in the engines.

SUMMARY

Several results have been obtained from a coordinated guidance and control system development effort. The overall objective of the effort is to contribute to the Terminal Configured Vehicle Program goal of increasing terminal area capacity and efficiency, improving approach and landing performance of aircraft in adverse weather conditions, and reducing the aircraft noise perceived on the ground. Using the Microwave Landing System, a magnetic leader cable and airborne sensors as inputs, automatic guidance and control algorithms have been developed for glideslope and localizer acquisition and tracking, flare, rollout and turnoff. In extensive simulation studies, a Digital Integrated Automatic Landing System (DIALS) has demonstrated the capability to perform rapid acquisition of the glideslope and localizer with small overshoots. The DIALS can also accurately track the localizer and preselected glideslopes. This performance and flexibility permits use of short finals and steep noise-abatement approaches. Specific design features have been incorporated to estimate winds and reduce their effect on performance, to reduce computational requirements, and to produce control maneuvers that should result in pilot acceptance of the design.

Two flare concepts have been developed and evaluated. Flight test results have demonstrated significant reductions in longitudinal touchdown dispersion with reasonable values for sink rate. The flare algorithms have been shown to perform well with either the ILS or MLS landing guidance systems. An advanced rollout and turnoff capability has been developed to complement the precision flare algorithm development in reducing runway occupancy time and thereby increasing airport capacity. A sensor, currently under development, has shown a promise, in both van and limited aircraft tests, of measuring lateral deviation from the desired ground track. A rollout guidance and control system has been developed, using the developmental sensor measurements, to provide acceptable performance for rollout and turnoff under both wet and dry runway conditions. Further simulation studies and flight tests are currently planned for each of the research topics which have been described.

REFERENCES

1. Walsh, T. M.; and Weener, E. F.: Automatic Flight Performance of a Transport Airplane on Complex Microwave Landing System Paths, Presented at the AGARD 25th GCP Symposium on Guidance and Control Design Considerations for Low Altitude and Terminal Area Flight, Dayton, Ohio, October 17-20, 1977.

2. White, W. F.; et al: Flight Demonstrations of Curved Descending Approaches and Automatic Landings, Using Time Referenced Scanning Beam Guidance, NASA TM 78745, May 1978.

3. White, W. F.; and Clark, L. V.: Flight Performance of the TCV B-737 Airplane at Kennedy Airport Using TRSB/MLS Guidance, NASA TM 80148, July 1979.

4. White, W. F.; and Clark, L. V.: Flight Performance of the TCV B-737 Airplane at Jorge Newbery Airport, Buenos Aires, Argentina, Using TRSB/MLS Guidance, NASA TM 80233, January 1980.

5. White, W. F.; and Clark, L. V.: Flight Performance of the TCV B-737 Airplane at Montreal Dorval International Airport, Montreal, Canada, Using TRSB/MLS Guidance, NASA TM 81885, September 1980.

6. Halyo, N.: Development of an Optimal Automatic Control Law and Filter Algorithm for Steep Glideslope Capture and Glideslope Tracking, NASA CR-2720, August 1976.

7. Halyo, N.: Development of a Digital Automatic Control Law for Steep Glideslope Capture and Flare, NASA CR-2834, June 1977.

8. Halyo, N.: Development of a Digital Guidance and Control Law for Steep Approach Automatic Landings Using Modern Control Techniques, NASA CR-3074, February 1979.

9. Staff of Langley Research Center and Boeing Commercial Airplane Company: Terminal Configured Vehicle Program Test Facilities Guide, NASA SP 435, 1980.

10. Lambregts, A. A.; and Creedon, J. F.: Development and Flight Evaluation of Automatic Flare Laws with Improved Touchdown Dispersion, presented at the AIAA Guidance and Control Conference, Danvers, Massachusetts, August 11-13, 1980.

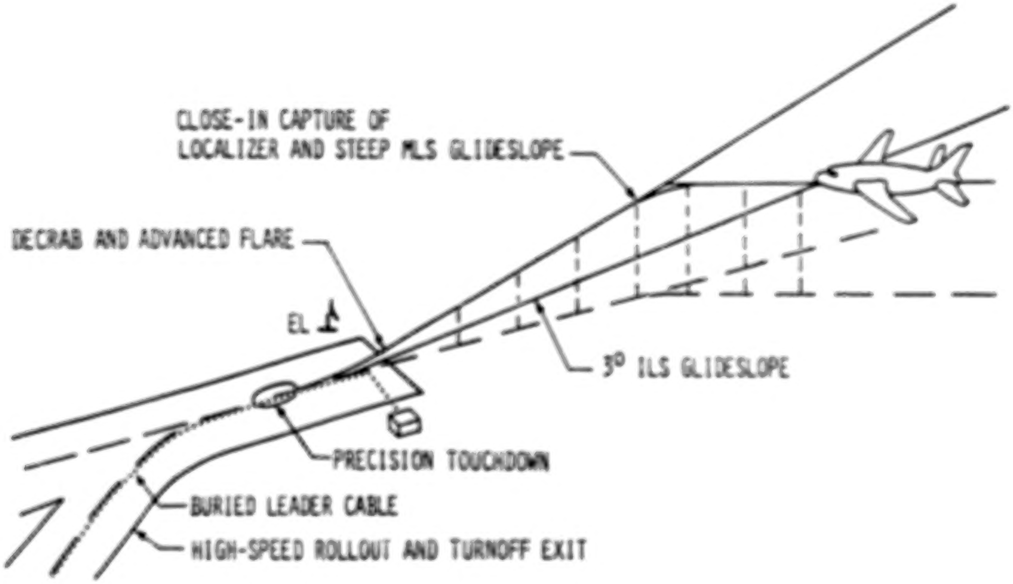
CLOSE-IN CAPTURE OF
LOCALIZER AND STEEP MLS GLIDESLOPE
DECRAB AND ADVANCED FLARE
EL
3° ILS GLIDESLOPE
PRECISION TOUCHDOWN
BURIED LEADER CABLE
HIGH-SPEED ROLLOUT AND TURNOFF EXIT

Figure 1.- Pictorial of the DIALS tasks.

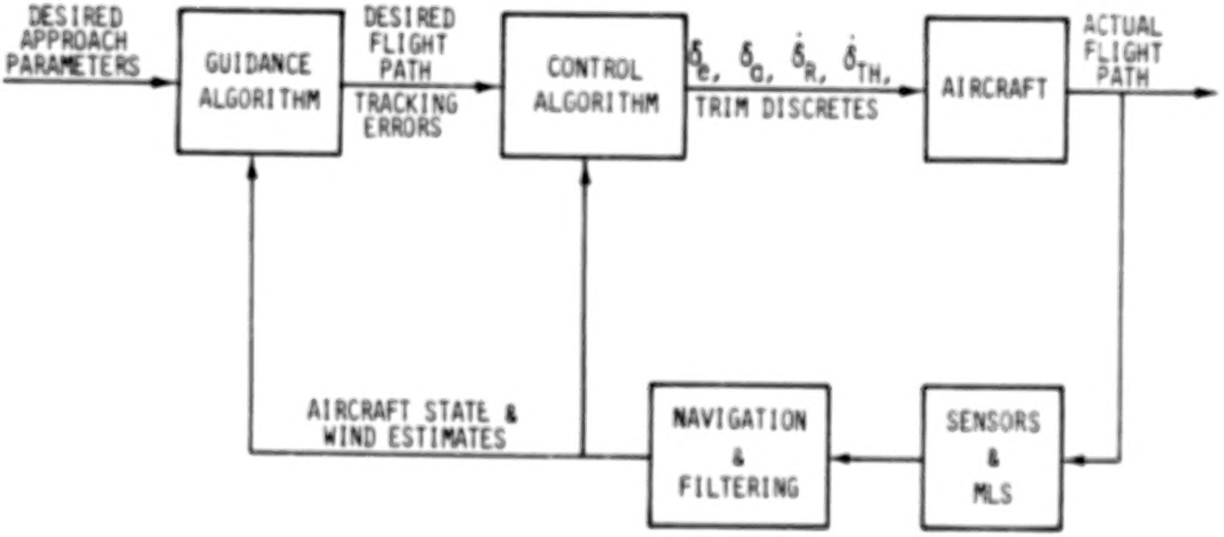
DESIRED APPROACH PARAMETERS
GUIDANCE ALGORITHM
DESIRED FLIGHT PATH
TRACKING ERRORS
CONTROL ALGORITHM
δ_e, δ_a, $\dot{\delta}_R$, $\dot{\delta}_{TH}$,
TRIM DISCRETES
AIRCRAFT
ACTUAL FLIGHT PATH
AIRCRAFT STATE & WIND ESTIMATES
NAVIGATION & FILTERING
SENSORS & MLS

Figure 2.- The DIALS block diagram.

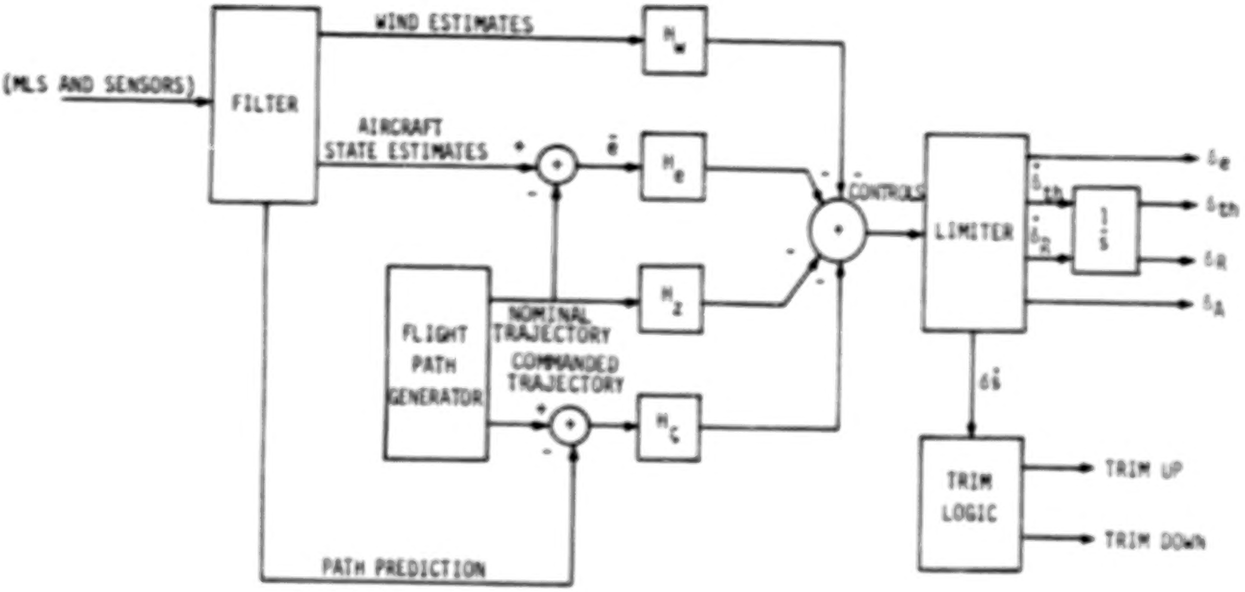
(MLS AND SENSORS)
FILTER
WIND ESTIMATES
AIRCRAFT STATE ESTIMATES
H_w
H_e
H_z
H_c
$\dot{e}$
FLIGHT PATH GENERATOR
NOMINAL TRAJECTORY
COMMANDED TRAJECTORY
CONTROLS
LIMITER
$\dot{\delta}_{th}$
$\dot{\delta}_R$
$\frac{1}{s}$
δ_e
δ_{th}
δ_R
δ_A
$d\dot{\delta}$
TRIM LOGIC
TRIM UP
TRIM DOWN
PATH PREDICTION

Figure 3.- Block diagram of feedback loop.

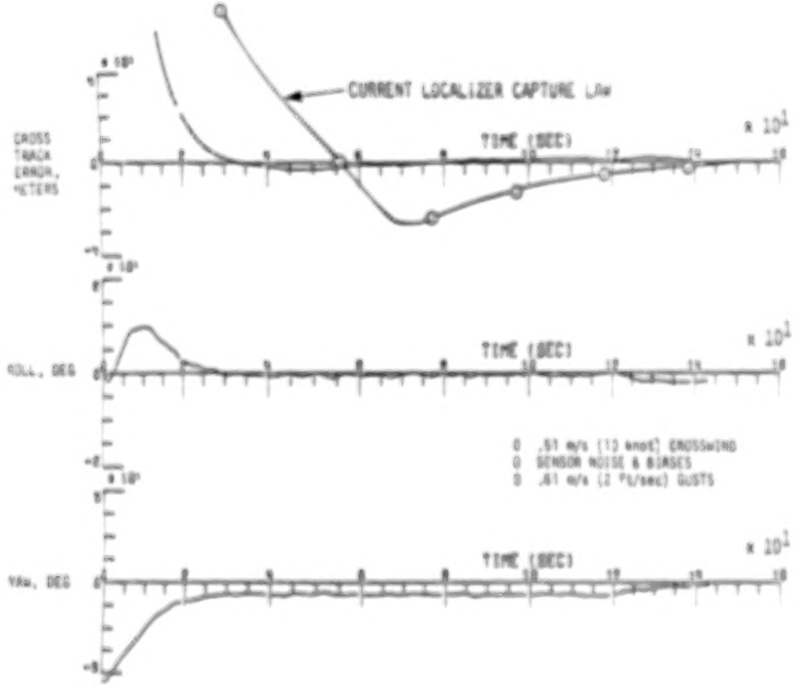

Figure 4.- Capture, track, and decrab of localizer path.

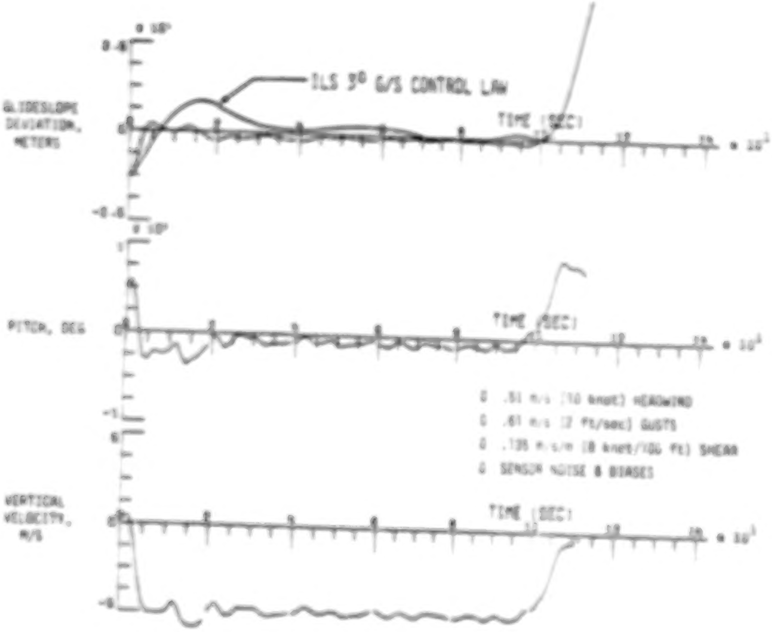

Figure 5.- Capture, track, and flare for 6° glideslope.

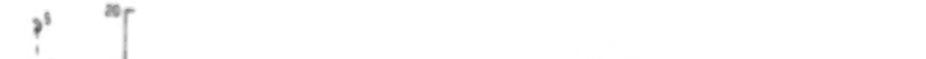

Figure 6.- Variation of $\dot{h}(h)$ flare trajectory with steady state winds.

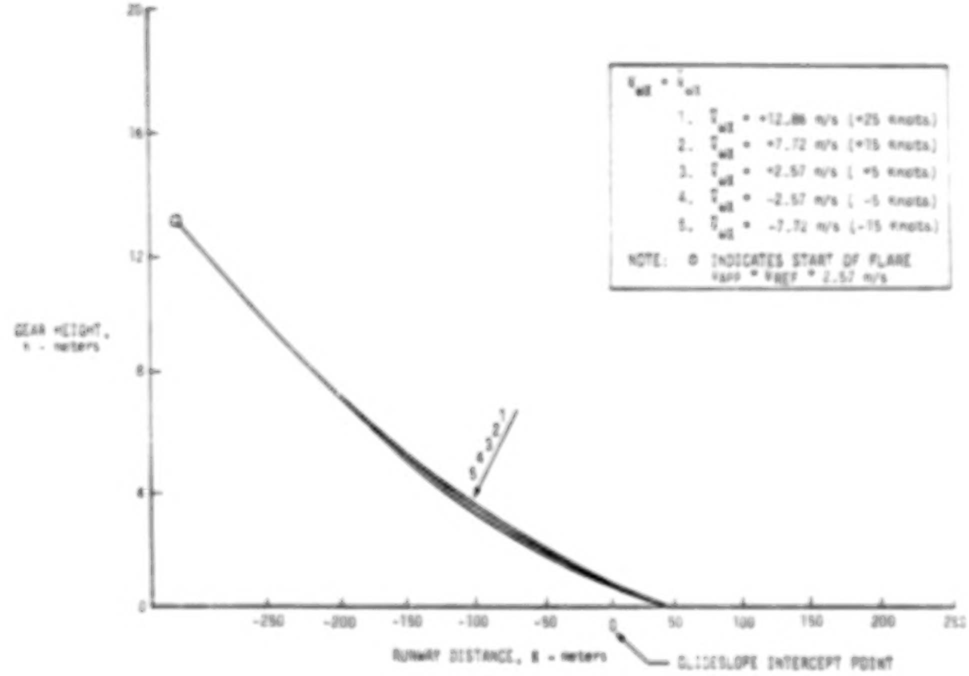

Figure 7.- Variation of $\dot{h}(h,V_G)$ flare trajectory with steady state winds.

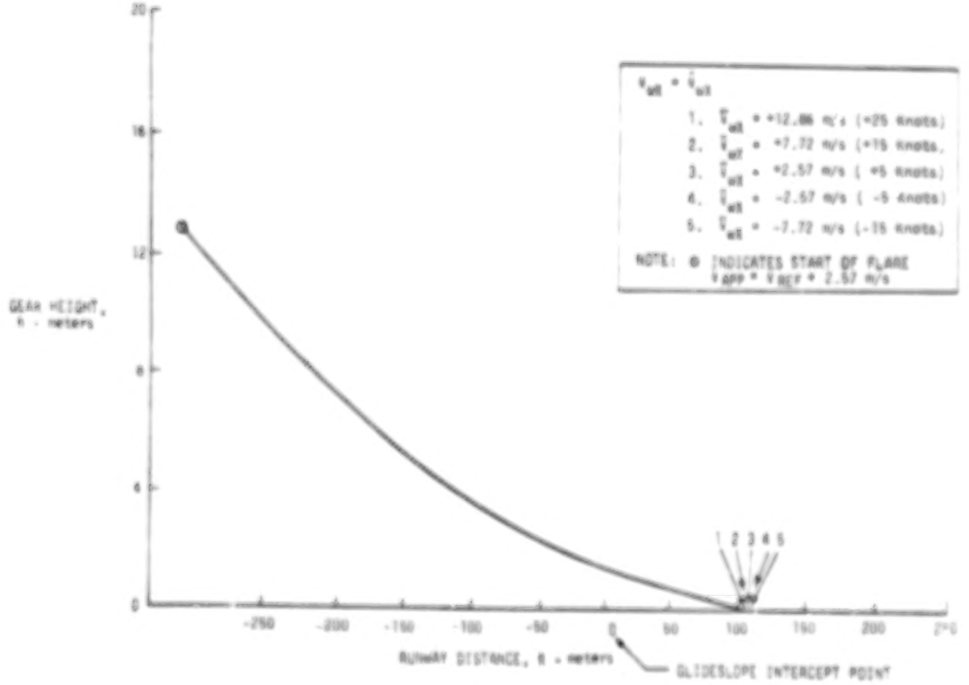

Figure 8.- Variation of $h_1(x)$ flare trajectory with steady state winds.

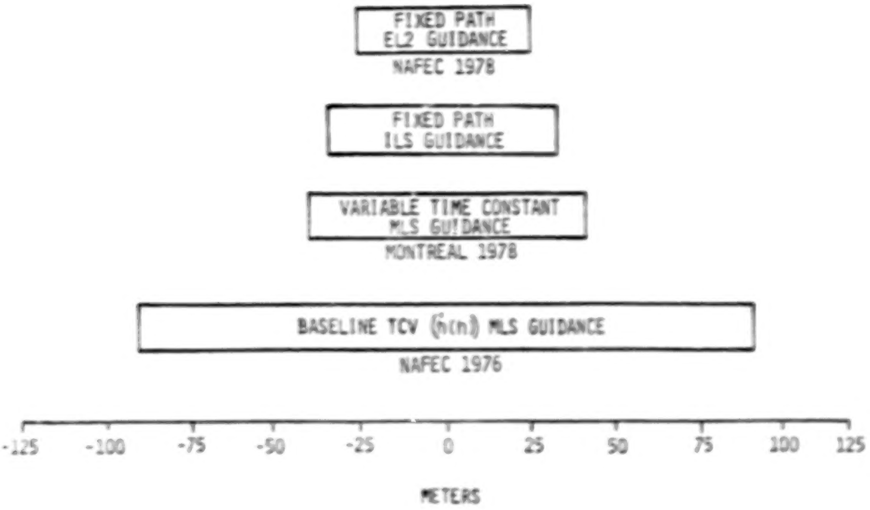

Figure 9.- Flight test $\pm 1\sigma$ longitudinal dispersions for the $\dot{h}(h)$, variable time constant, and fixed path flare laws.

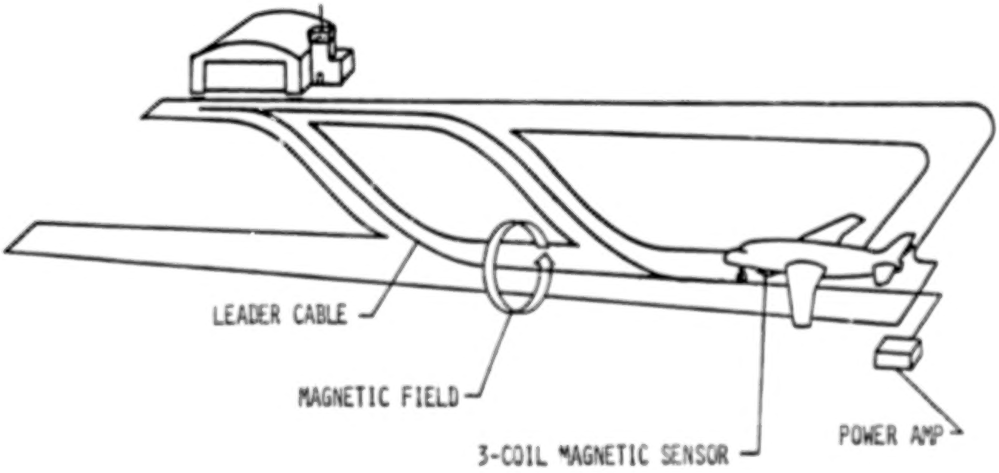
LEADER CABLE
MAGNETIC FIELD
3-COIL MAGNETIC SENSOR
POWER AMP

Figure 10.- Magnetic leader cable system.

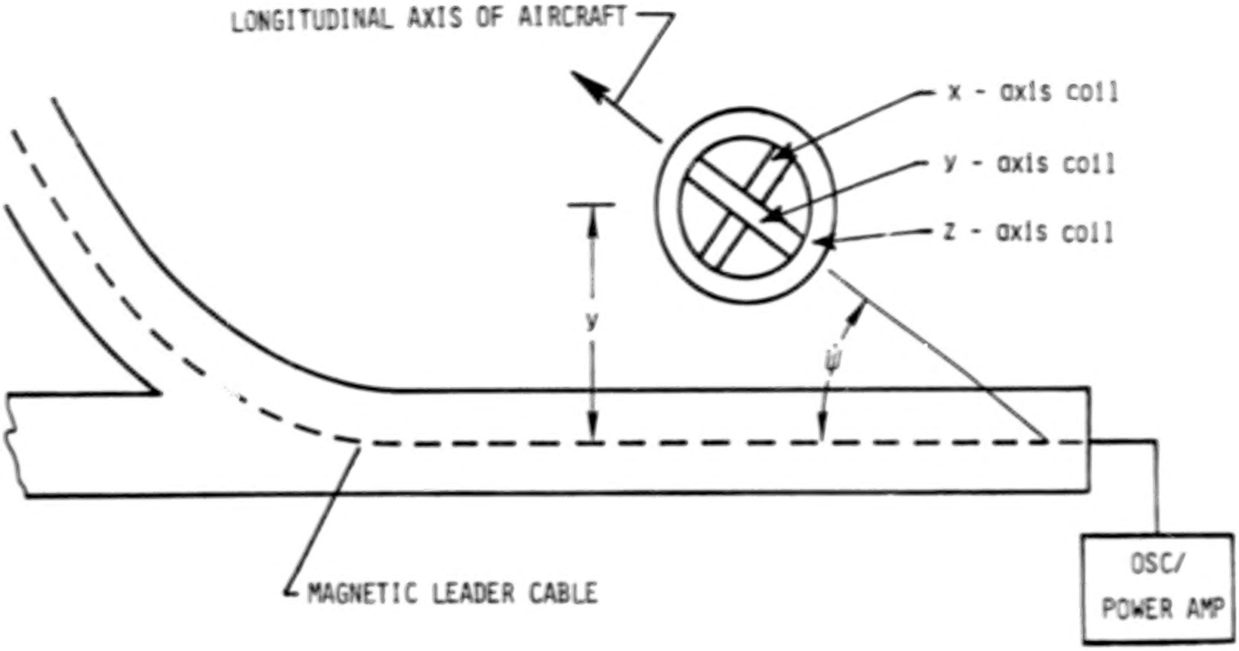
LONGITUDINAL AXIS OF AIRCRAFT
x - axis coil
y - axis coil
z - axis coil
y
ψ
MAGNETIC LEADER CABLE
OSC/
POWER AMP

Figure 11.- Displacement and heading of aircraft relative to the cable.

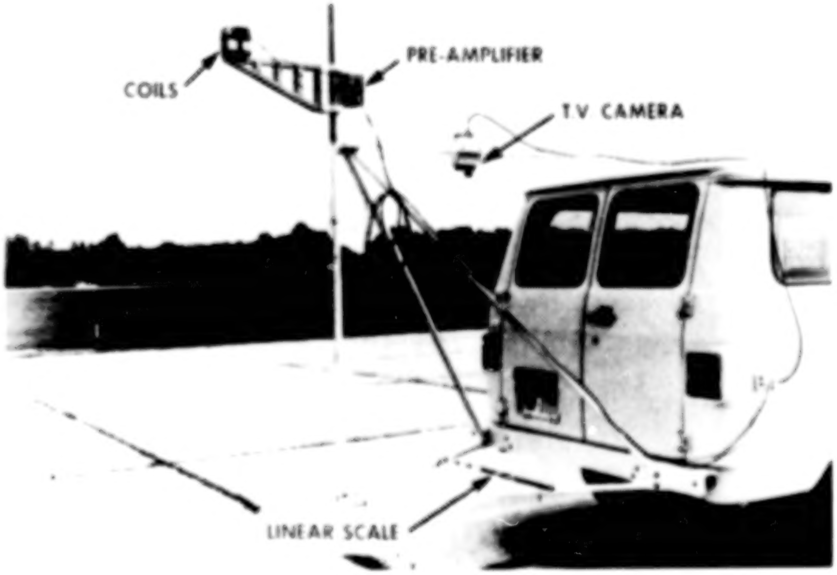
COILS
PRE-AMPLIFIER
T.V. CAMERA
LINEAR SCALE

Figure 12.- Van support structure with coils and pre-amplifier.

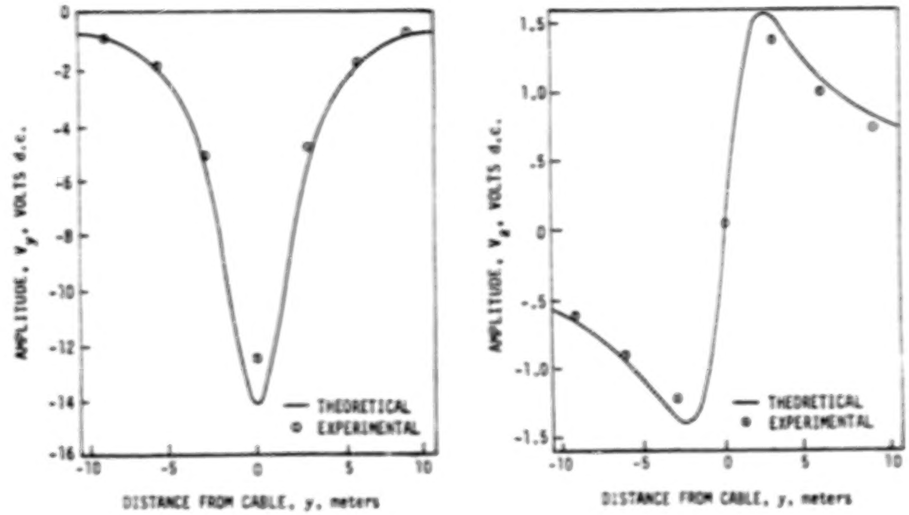

(a) y - channel. (b) z - channel.

Figure 13.- Comparison of theoretical and experimental signal amplitudes.

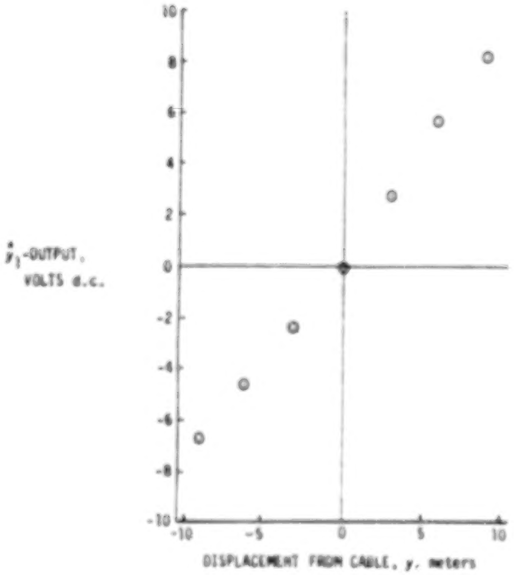

Figure 14.- A typical experimental calibration curve for y_1.

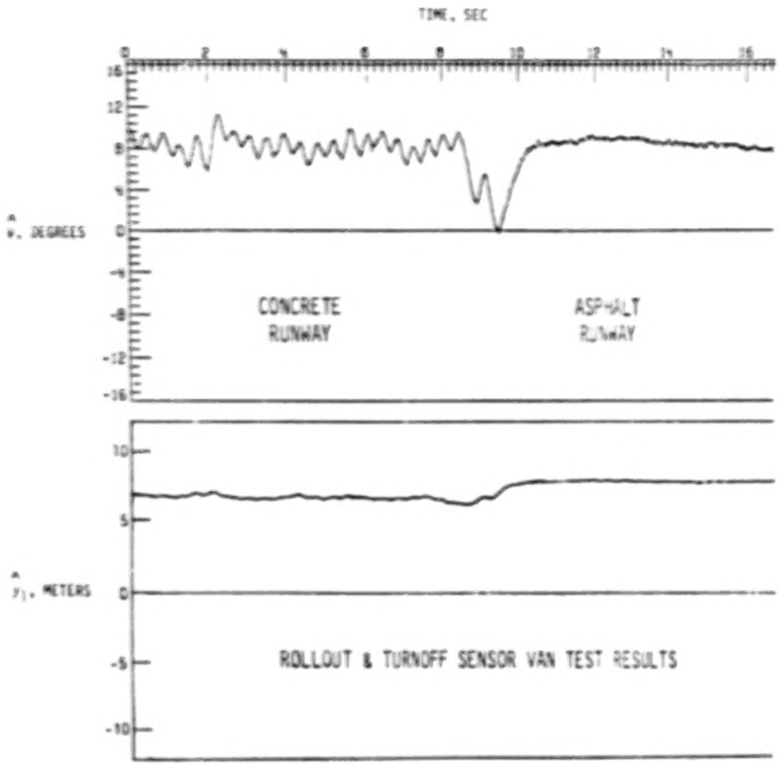

Figure 15.- Time history plot of dynamic data showing effects of taxiway construction material.

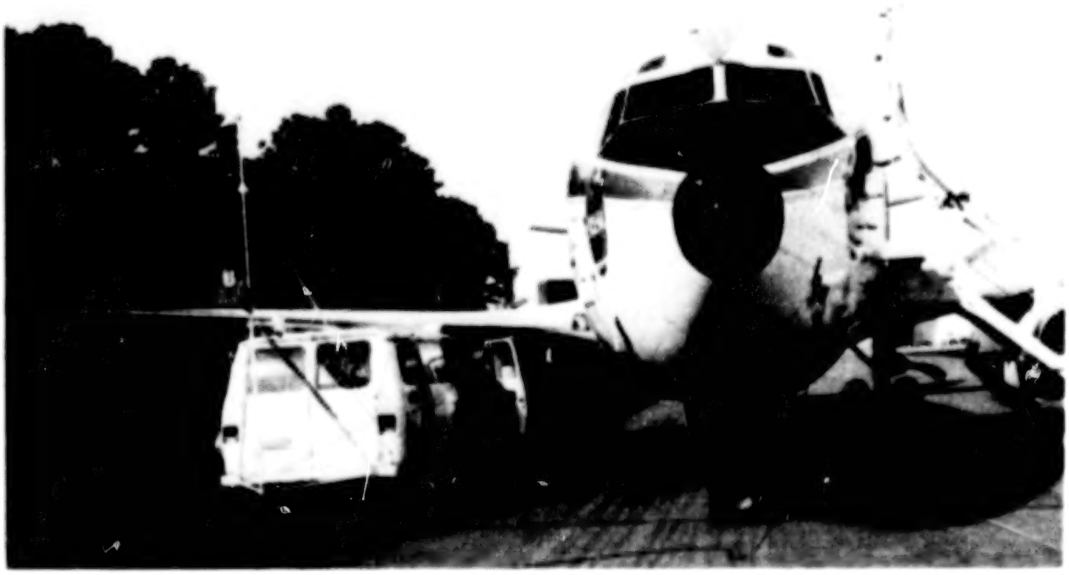

Figure 16.- Experimental set-up for aircraft tests.

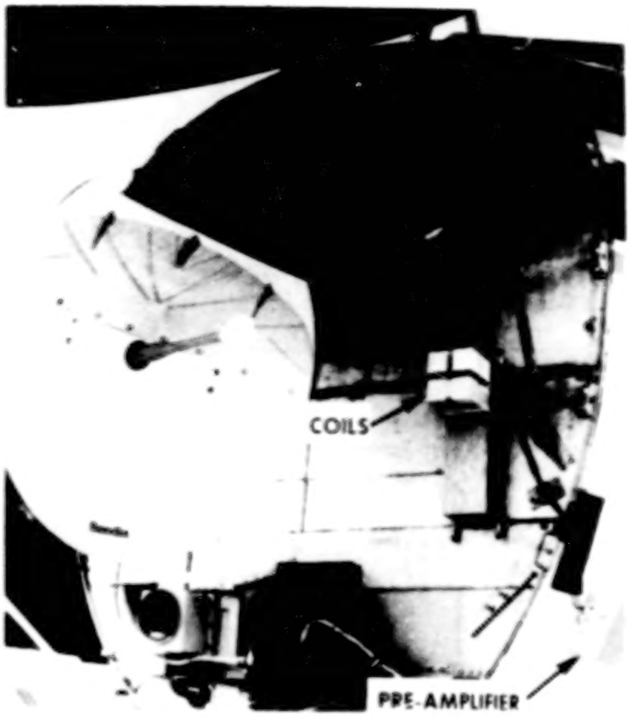
COILS
PRE-AMPLIFIER

Figure 17.- Sensor location for aircraft tests.

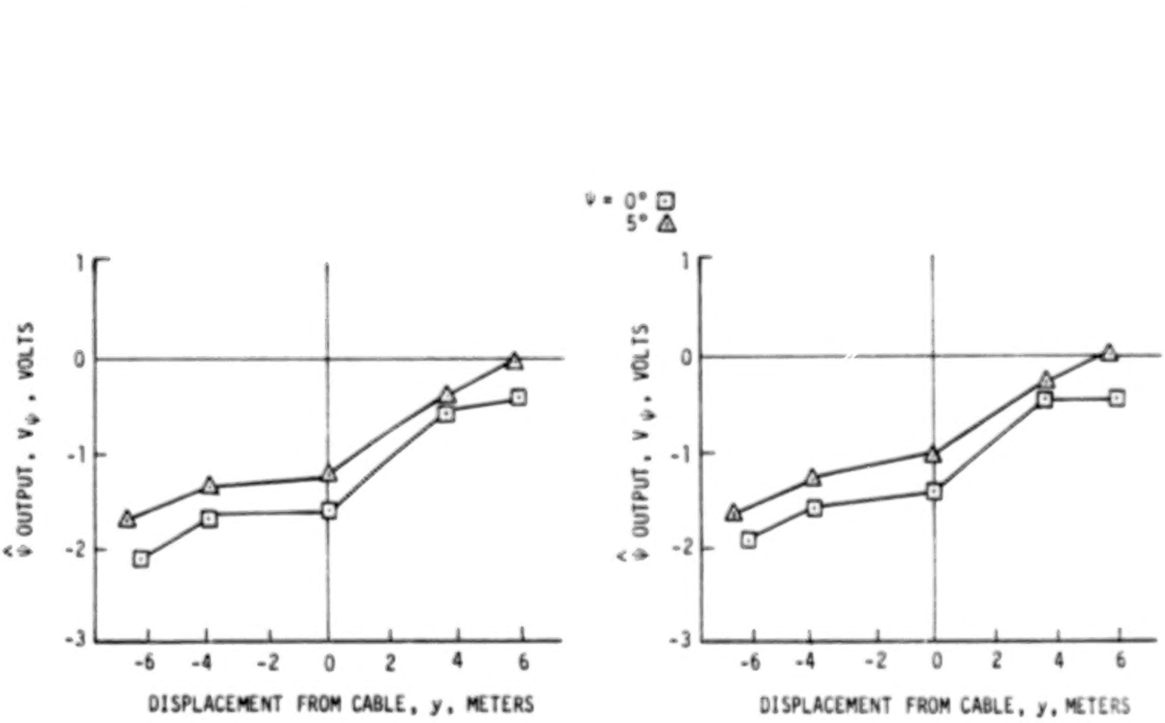

(a) 990 Hz.

(b) 150 Hz.

Figure 18.- Static heading data taken with coils in nose of B-737 aircraft.

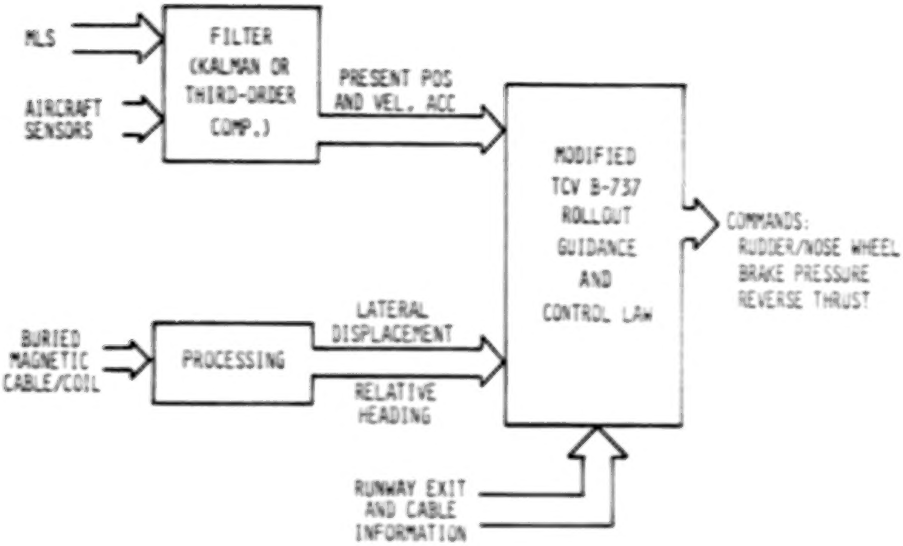
MLS
AIRCRAFT SENSORS
FILTER (KALMAN OR THIRD-ORDER COMP.)
PRESENT POS AND VEL, ACC
MODIFIED TCV B-737 ROLLOUT GUIDANCE AND CONTROL LAW
COMMANDS:
RUDDER/NOSE WHEEL
BRAKE PRESSURE
REVERSE THRUST
BURIED MAGNETIC CABLE/COIL
PROCESSING
LATERAL DISPLACEMENT
RELATIVE HEADING
RUNWAY EXIT AND CABLE INFORMATION

Figure 19.- Automatic rollout and turnoff system.

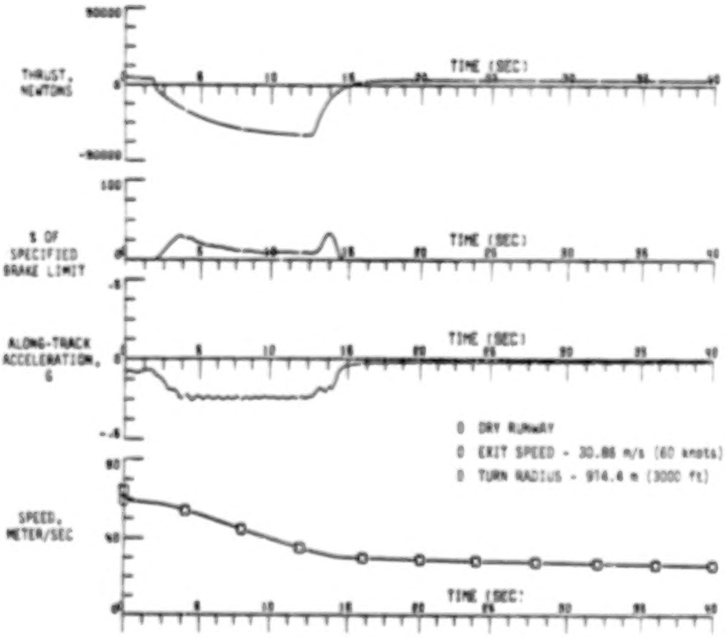

Figure 20.- Automatic rollout and turnoff - longitudinal. Dry runway.

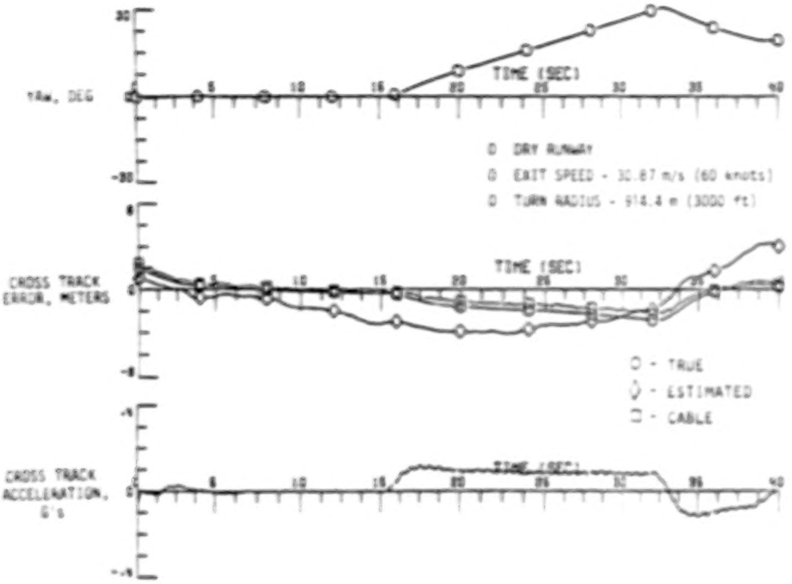

Figure 21.- Automatic rollout and turnoff - lateral. Dry runway.

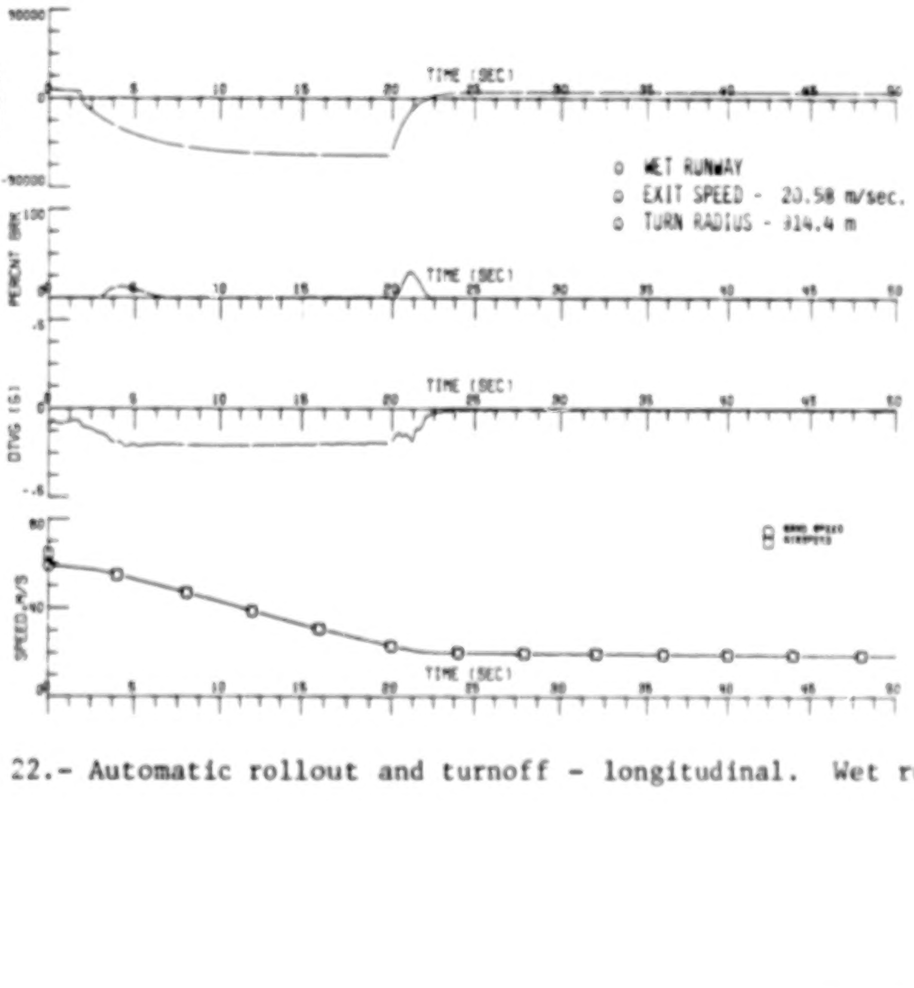

Figure 22.- Automatic rollout and turnoff - longitudinal. Wet runway.

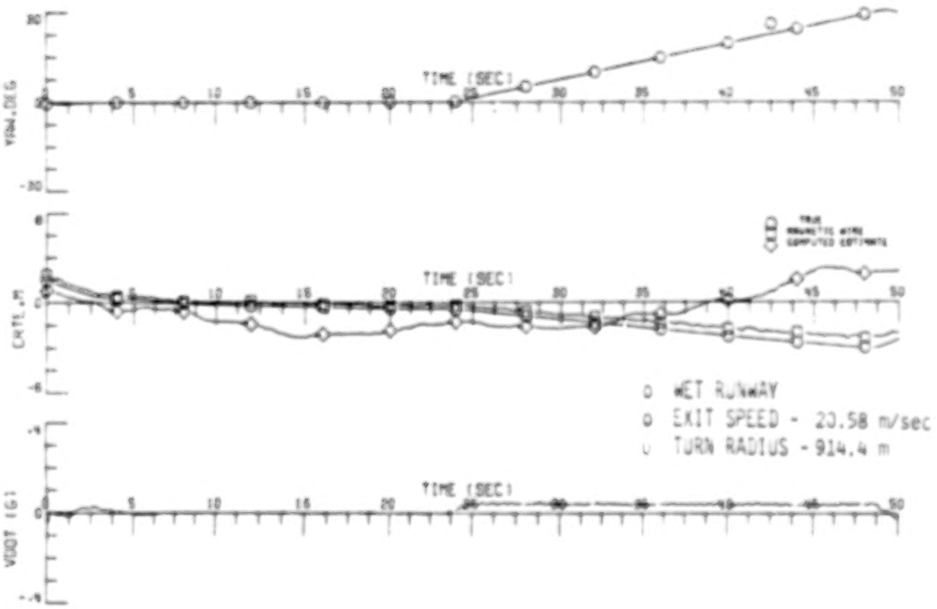

Figure 23.- Automatic rollout and turnoff - lateral. Wet runway.

BLANK PAGE

OPERATIONAL CONSIDERATIONS IN UTILIZATION OF MICROWAVE LANDING SYSTEM APPROACH AND LANDING GUIDANCE

William F. White and Leonard V. Clark
Langley Research Center

SUMMARY

Nearly five years of flight experience has been gained with the TCV B-737 using MLS guidance to fly curved, descending intercepts of final approaches as short as 0.8 km (0.44 n. miles). During that time the United States MLS has been adopted as the world standard, and development of operating performance standards and practices is under way. This paper briefly reviews the present characteristics of MLS equipment and summarizes TCV flight performance, then considers some possible uses of MLS to solve current noise abatement problems and the requirements for service area in light of TCV experience.

It is suggested that existing visual approach procedures could be improved by the use of MLS guidance, and that the experience and confidence necessary for air traffic controller and pilot acceptance of new MLS procedures could be gained in this manner. Examples are given using published approaches to San Francisco and two New York airports, as well as experimental curved approaches at Buenos Aires. For one of the approaches, a minimum coverage (±40°) system is inadequate. In another case, even the maximum coverage of ±60° is not sufficient unless the service region is skewed to provide asymmetric coverage.

MLS altitude is preferable to radio or barometric altitude at the lower levels for purposes of obstacle clearance, flying curved or segmented constant descent paths, and landing. However, the disagreement between MLS and barometric altitudes at upper levels during non-standard atmospheric conditions may create transition problems and a requirement for greater vertical separation between aircraft than is presently used.

Examples of need for a 360° azimuth function are given, but this option is still only in the conceptual stage. Some flight experience has been gained with experimental back azimuth and flare elevation systems, but there are still questions as to how both functions should be used.

Currently, most attention is directed towards the initial introduction of MLS in a manner most compatible with existing ILS practice. This is a desirable objective in order to minimize confusion during a period when MLS and ILS will be in simultaneous use. However, further effort is needed to establish practices and procedures by which the full capabilities of MLS can be utilized, and to insure that they do not conflict with conventional uses.

INTRODUCTION

In October, 1976 some operational aspects of initial experiments with the Microwave Landing System (MLS) were presented at the Aircraft Safety and Operating Problems Conference (reference 1). In the succeeding four years, considerable additional experience has been obtained with more difficult flight paths and using MLS ground equipment of varied capabilities at Buenos Aires, New York, Montreal and NAFEC (recently renamed FAATC). Also during that period the time reference scanning beam MLS has been adopted by ICAO as the new international standard landing system, and several national and international organizations are in the process of defining standards and practices for ground and airborne equipment. It therefore seems timely to review MLS characteristics in light of earlier operational requirements (e.g. reference 2), TCV flight experience, and present and expected operational procedures and problems.

This paper briefly summarizes the characteristics and performance of MLS equipment utilized by the TCV B-737. Several classes of MLS service and approach procedures are discussed in light of TCV experience. Since the early uses of MLS will involve procedures identical to ILS, most of this discussion is concerned with exploitation of MLS capabilities not possessed by ILS. Examples are given of how this could be done by using MLS to enhance the safety and utility of procedures presently in use for noise abatement. Finally, some areas which require definition of new procedures and conventions are indicated.

SYMBOLS AND ACRONYMS

AZ	Approach Azimuth
BAZ	Back Azimuth
CAT I	Category I Landing Minima {71 m (200 ft) decision height, 732 m (2400 ft) runway visual range}
CAT II	Category II Landing Minima {30.5 m (100 ft) decision height, 366 m (1200 ft) runway visual range}
CDI	Course Deviation Indicator
CMN	Control Motion Noise
CRI	Location identifier for Canarsie VORTAC
DME	Distance Measuring Equipment
DME-M	Precision Distance Measuring Equipment associated with MLS
DME-N	Standard Distance Measuring Equipment

EL	Approach Elevation
FAA	Federal Aviation Administration
FAATC	Federal Aviation Administration Technical Center
FAF	Final Approach Fix
GPIP	Glidepath Intercept Point
h	Height at which transition is made from approach elevation to flare elevation guidance
ICAO	International Civil Aviation Organization
IFR	Instrument Flight Rules
ILS	Instrument Landing System
JFK	John F. Kennedy International Airport; Location identifier for Kennedy VORTAC
LF	Low Frequency
LOM	Outer Compass Locator/Outer Marker
MLS	Microwave Landing System
MSL	Mean Sea Level
NAFEC	National Aviation Facilities Experimental Center
PDME	Precision Distance Measuring Equipment
PFE	Path Following Error
R	Radial
RNAV	Area Navigation
RWY	Runway
SFO	San Francisco International Airport; Location identifier for San Francisco VORTAC
STAR	Standard Terminal Arrival Route
T	time
TCV	Terminal Configured Vehicle

TD	Touchdown
VFR	Visual Flight Rules
VHF	Very High Frequency
VNAV	Area navigation with vertical guidance included
VOR	Very High Frequency Omnidirectional Range
VORTAC	Colocated VOR and military Tactical Air Navigation system providing both azimuth and range information
X_{TD}	Distance from runway threshold to aircraft MLS antenna at touchdown
α	Elevation angle
θ	Azimuth angle
σ	Standard deviation

MLS CHARACTERISTICS AND ACCURACY

Equipment

MLS Ground Equipment. Figure 1 shows the MLS installation colocated with ILS at Buenos Aires, Argentina, which the TCV B-737 used in the fall of 1977. The system illustrated used the Basic Narrow (aperture) equipment, with a proportional azimuth coverage of ±40°. The currently favored practice for minimizing elevation signal multipath contamination involves centerline emphasis for the elevation antenna. That is, an antenna pattern similar to the one shown at the right side of figure 2 is used to concentrate power along the runway centerline, reducing reflections from buildings or other obstacles to the sides. With such an antenna, a typical MLS installation will provide the minimum lateral coverage indicated in figure 2. The required lateral coverage area is at least ±40° (not necessarily all proportional) measured from the MLS datum point, a point on the runway adjacent to the elevation antenna. However, it is readily seen from figures 1 and 2 that the azimuth coverage angle must actually be measured with respect to the azimuth antenna, located at a typical distance of 2 to 4 km (≈1 to 2 n. miles) from the datum point. The resulting strips of coverage on either side of the specified service area are important for MLS approaches on downwind or base legs near the airport.

An operationally significant region is the volume in which azimuth and DME signals are available, but not elevation. This information can be used for accurate area navigation in combination with barometric altitude. The volume appears to be insignificant in figure 2, but may actually extend over the entire coverage area for as much as half the coverage volume, since the current proposals (reference 3) specify a minimum azimuth coverage of 15° above the horizontal, but the minimum requirement for the elevation scanning beam is only 7.5°. The subject of RNAV position updating with MLS and of MLS versus barometric altitudes will be discussed later.

One of the advantages of MLS is that the antenna patterns may be tailored to minimize radiation near the surface, thereby reducing multipath effects caused by reflections from the ground. However, this characteristic may have implications for the ability to test an MLS airborne installation on the ground prior to takeoff, since coverage is required only down to 2.4 m (8 ft) above a line of sight to the azimuth antenna. This may also be a factor to be considered in the use of MLS for guidance during landing and rollout phases, especially on humped runways.

Three range options are currently possible for MLS installations. The first would provide MLS angle guidance only and follow ILS practice by the use of marker beacons or other radio fixes to provide distance to touchdown information. The second option would provide conventional L-band DME, which has been designated DME-N. This could be substituted for marker information, as it is with ILS, and could be used with the MLS angle data to provide RNAV position data for the initial approach phase. Finally, precision range data can be provided by a modified L-band DME, designated DME-M. This information would be sufficiently accurate for use in autoland computations and in RNAV position updating where accurate flight path following might be critical.

MLS Airborne Equipment. The simplest MLS receiving equipment will probably be operationally indistinguishable from ILS. However, most receivers will at least have selectable azimuth and elevation reference angles and some sort of basic data display. The more sophisticated equipment, for use with airborne computers, will have digital angle data outputs and capability for decoding auxiliary data transmissions. A conventional DME may be used with either DME-N or DME-M ground stations but will not provide the accuracy required for flare and landing computations. A precision DME may also be used with either DME-N or DME-M ground equipment and will provide precision range data where DME-M is installed.

Airborne antennas will likely be a more critical item with MLS than with VHF systems and may restrict allowable maneuvers or procedures unless multiple antenna installations are used. Considerable analysis and experimentation has been conducted and sponsored by the Langley Research Center on antenna patterns and locations. Figure 3 shows the antenna locations which have been flight tested on the TCV B-737. Several of these have also been extensively studied analytically and by scale model measurements, and a technique has been verified for accurately predicting volumetric coverage of airborne antennas. The bottom front antenna is a location used only for experiments using the optional MLS flare subsystem at NAFEC (recently renamed FAATC), where it was desired to make measurements near the ground to test a multipath reduction processing technique for the FAA. This location is undesirable because it is more likely to provide degraded signals while operating on or near the runway, and interference from landing gear doors is experienced with omnidirectional antennas. The fin-mounted antenna provides good omnidirectional coverage but requires long cable runs and is subject to

CONTENTS

Part 1

PREFACE . . . . iii 1/A6

1. INTRODUCTORY REMARKS 1 1/A12
Roger L. Winblade

SESSION I - TERMINAL-AREA OPERATIONS
Cochairmen: T. A. Walsh and R. L. Kurkowski

2. TEST RESULTS OF FLIGHT GUIDANCE FOR FUEL CONSERVATIVE DESCENTS IN A TIME-BASED METERED AIR TRAFFIC ENVIRONMENT 7 1/B4
Charles E. Knox and Leo H. Person, Jr.

3. A PILOT'S SUBJECTIVE ANALYSIS OF A COCKPIT DISPLAY OF TRAFFIC INFORMATION (CDTI) 29 1/C12
Gerald L. Keyser, Jr.

4. GUIDANCE AND CONTROL SYSTEM RESEARCH FOR IMPROVED TERMINAL AREA OPERATIONS 51 1/E6
R. M. Hueschen, J. F. Creedon, W. T. Bundick, and J. C. Young

5. OPERATIONAL CONSIDERATIONS IN UTILIZATION OF MICROWAVE LANDING SYSTEM APPROACH AND LANDING GUIDANCE 83 1/G10
William F. White and Leonard V. Clark

6. AUTOMATED PILOT ADVISORY SYSTEM TEST AND EVALUATION AT MANASSAS MUNICIPAL AIRPORT 113 2/B4
John L. Parks, Jr.

7. A METHOD FOR DETERMINING LANDING RUNWAY LENGTH FOR A STOL AIRCRAFT 127 2/C14
D. M. Watson, G. H. Hardy, J. F. Moran, and D. N. Warner, Jr.

8. FLIGHT TESTS OF IFR LANDING APPROACH SYSTEMS FOR HELICOPTERS 145 2/E4
J. S. Bull, D. M. Hegarty, L. L. Peach, J. D. Phillips, D. J. Anderson, D. C. Dugan, and V. L. Ross

9. A HEAD-UP DISPLAY FORMAT FOR TRANSPORT AIRCRAFT APPROACH AND LANDING. 165 2/F10
Richard S. Bray and Barry C. Scott

MICROFILMED FROM BEST
AVAILABLE COPY

SESSION II - AVIONICS AND HUMAN FACTORS
Cochairmen: M. D. Montemerlo and A. B. Chambers

10. AN EVALUATION OF HEAD-UP DISPLAYS IN CIVIL TRANSPORT OPERATIONS 197 3/B2
John K. Lauber, Richard S. Bray, and Barry C. Scott

11. GENERAL AVIATION SINGLE PILOT IFR AUTOPILOT STUDY 201 3/B6
Hugh P. Bergeron

12. APPLICATION OF THE EPIDEMIOLOGICAL MODEL IN STUDYING HUMAN ERROR IN AVIATION 219 3/C10
Ed S. Cheaney and Charles E. Billings

13. HOW A PILOT LOOKS AT ALTITUDE 237 3/D14
Amos A. Spady, Jr., and Randall L. Harris, Sr.

SESSION III - ATMOSPHERIC ENVIRONMENT
Cochairmen: D. W. Camp and L. J. Ehernberger

14. SUMMARY OF FLIGHT TESTS OF AN AIRBORNE LIGHTNING LOCATOR SYSTEM AND COMPARISON WITH GROUND-BASED MEASUREMENTS OF PRECIPITATION AND TURBULENCE 251 3/E14
Bruce D. Fisher and Norman L. Crabill

15. WALLOPS SEVERE STORMS MEASUREMENT CAPABILITY 279 4/A3
Robert E. Carr and John C. Gerlach

16. THE 1979 CLEAR AIR TURBULENCE FLIGHT TEST PROGRAM 293 4/B3
E. A. Weaver, L. J. Ehernberger, B. L. Gary,
R. L. Kurkowski, P. M. Kuhn, and L. P. Stearns

17. PULSED DOPPLER LIDAR FOR THE DETECTION OF TURBULENCE IN CLEAR AIR 313 4/C9
E. A. Weaver, J. W. Bilbro, J. A. Dunkin, S. C. Johnson
W. D. Jones, C. E. Harris, and C. A. DiMarzio

18. FLIGHT TESTS OF A CLEAR-AIR TURBULENCE ALERTING SYSTEM 329 4/D11
Richard L. Kurkowski, Peter M. Kuhn, and Lois P. Stearns

19. CLEAR AIR TURBULENCE STUDIES WITH MICROWAVE RADIOMETERS 351 4/F5
Bruce L. Gary

20. IN-FLIGHT DIRECT-STRIKE LIGHTNING RESEARCH 359 4/F13
Felix L. Pitts and Mitchel E. Thomas

21. MAGNITUDE AND FREQUENCY OF WIND SPEED SHEARS AND ASSOCIATED DOWNDRAFTS 373 4/G13
Margaret B. Alexander and C. Warren Campbell

MICROFILMED FROM BEST AVAILABLE COPY

pattern lobing due to reflections from the fuselage and wings.

The two remaining antennas can provide complete coverage for most normal maneuvers, as shown by the patterns in figure 4. Both are simple ¼-wavelength stubs providing omnidirectional coverage in the plane tangent to the mounting surface. This results in the blind spots shown due to blockage by the fuselage in the principal plane. However, when the aircraft is pitched up in climb attitude either antenna provides nearly full coverage horizontally for a wide range of roll attitudes. In practice, the cabin-top antenna has been used exclusively for all flight operations except two experiments and has rarely failed to provide sufficient signal. Studies by both Langley Research Center and Boeing have indicated that the cabin-top location is preferred for most transport aircraft, with an optional bottom rear antenna for full coverage if required. It is assumed that the wheel-height-over-threshold requirement can be met by electronic biasing of the antenna position. If that is not the case, then a directional antenna on or under the nose will be required for some aircraft on final approach.

Light jets and small general aviation aircraft may often operate at small airports without radar vectoring, where procedure turns will be required. Smooth radiation patterns such as those of figure 4 are more difficult to achieve on this class of aircraft due to the sharper curvatures of surfaces and the relatively larger solid angles subtended by wings, engine nacelles, and the like. It may be desirable to investigate instrument approach procedures such that outbound maneuvering can be eliminated, rather than requiring the penalty of multiple antenna installations. This is true even of transport aircraft, where the cable runs may be quite long and require the installation of a preamplifier to obtain sufficient signal strength, in addition to causing a weight and installation cost penalty from the cable itself.

MLS Accuracy

Since MLS is an angle of measurement system, it was formerly the practice to define errors in terms of angular bias and noise. This method has been modified and errors are now specified by the method illustrated in figure 5. The MLS measurement is compared to an absolute position reference and a time history of the error is obtained which is then fed into standard filters. The path following filter is a low-pass filter with an output containing only errors with low enough frequencies to affect the aircraft's position. The path following error (PFE) consists of a mean course error (equivalent to an average bias error over the region of measurement) and path following noise. The control motion noise (CMN) filter is a high-pass filter which passes the frequencies which can cause rapid control motion but are of too short duration to result in an aircraft position displacement. In either case, a maximum error in either degrees or feet is specified, and as the sliding window is moved over the time history, this maximum error may not be exceeded more than 5% of the time. This method takes into account the fact that errors are not constant throughtout the coverage volume due to multipath or propagation effects.

An illustration of the effects of PFE and CMN is shown in figure 6. This is a portion of the data obtained during Boeing simulations in which the MLS deviation signals were directly substituted for ILS in the B-747 lateral autopilot. A direct channel propagation model produced the simulated MLS azimuth signal shown. The high frequency noise produced aileron deflections with a peak to peak amplitude af about 3° and a period somewhat larger than 1 second and rudder deflections of less than 1° with a somewhat longer period. As the bottom portion of the figure shows, the airplane displacements were of much longer period and were excited by the low frequency components of the azimuth noise. The maximum bank angle was less than 2° for this run. Preliminary results from this simulation indicate a lateral touchdown standard deviation of about 1.5 m (4.9 ft) for 10 runs.

Considerable data has been published giving error time histories and statistical error analyses of the TCV B-737 performance on various MLS paths (references 4-8). One example is given here: figure 7 summarizes the flight technical errors of the TCV B-737 autoland system at the Categories I (61 m (200 ft)) and II (30.5 m (100 ft)) decision heights, for approaches at Buenos Aires, New York, and Montreal. The performance is much better than required for FAA certification of Category II autopilots even though the final approach legs and lengths ranging from 3 km down to 0.8 km (1.6 to 0.44 n. miles). More significant is that these flight technical errors are also a good indication of absolute position errors, as discussed in references 6-8. The cross track errors were larger at the Category I decision height mainly because of the short final approach legs. In fact, for over 30 of the approaches (at JFK), the data are representative of RNAV delivery error rather than autoland tracking performance since the intercept of final approach occurred near the Category I decision height.

Errors at large distances and off centerline will probably be larger than those indicated in the preceding discussion. However, the MLS worst case accuracy should be equal to or better than the best performance which can be expected from VHF navigation and barometric altitude. Throughout most of its coverage volume the MLS will have much smaller linear errors than any other means of navigation.

CLASSES OF MLS USEAGE

Conventional ILS-type Approaches

MLS will initially be installed at many locations along with existing ILS. To prevent confusion during the early phases when both types of systems will be in use, the procedures are expected to be identical with present ILS practice. Pilots will probably notice very little difference from ILS under these conditions, other than possibly a more stable signal with fewer course bends. Depending on the airborne antenna coverage characteristics, there may be more flag activity during initial maneuvering than pilots are accustomed to with VHF or LF navaids. Signals may be lost or not acquired on outbound headings with single-antenna installations.

Cockpit instrumentation will probably be the same as that used for ILS, except that if the wider proportional coverage of MLS is to be used to assist in capture of the final approach course, provisions will be necessary for either reducing CDI sensitivity during the capture phase or for providing some auxiliary display of azimuth angle to provide lead information. The minimum, or operationally preferred, glideslope angle will be a part of basic data transmitted from the ground equipment. This information must either [illegible] used to automatically set the receiver's elevation reference angle, or m[illegible] displayed to the pilot with provisions for preventing the use of lo[illegible]s. There is still some question as to whether the MLS should always us[illegible] glideslope unless a larger angle is required for safety or if the gl[illegible] should be set to match a lower ILS glideslope in the cases where MLS is colocated with such an ILS. If the MLS glideslope does not match the ILS, may require higher weather minima since the approach lights and Visual Approach Slope Indicators are set to match the ILS angle.

Advanced Applications

Off-centerline Approaches. MLS receiving equipment with selectable azimuth and elevation reference angles will allow approaches on other than the 0° azimuth angle using conventional cockpit displays and techniques. An example of how such an approach might be used is given in figure 8, which is a published noise abatement procedure used extensively at San Francisco during the after-midnight hours. A conventional ILS approach to either runway 28L or 28R brings aircraft in over residential areas near the San Mateo bridge. The Quiet Bridge approach depicted uses VOR/DME in the early stages but is basically a visual approach requiring good weather. There is no positive vertical guidance, since the ILS glideslopes of 2.7° and 3° are both below the minimum altitude of 579.1 m (1900 ft) at the bridge.

An example of how MLS could be used for this approach is given in figure 9. The MLS is assumed to be colocated with the ILS on runway 28L. The vertical scale has been exaggerated since the angles are small. Note that an approach along the -6° azimuth radial closely adheres to the desired flight track. By selecting the 3.3° elevation reference angle, a stabilized descent with precise guidance may be started well before reaching the bridge at the specified altitude. After passing the bridge, a shallow left turn allows intercept of the final approach course 4 to 6 km (2.1 to 3.2 n. miles) from threshold, and elevation guidance is available throughout the entire procedure. Rather than intercepting the extended centerline for runway 28L, the transition may be made to the -3° azimuth angle. Accurate guidance is then furnished laterally and vertically to cross the final approach course for runway 28R approximately at the middle marker at a 3° angle. The improved guidance could enhance safety and reduce missed approaches for either runway, and as sufficient experience was gained the weather minima could be reduced.

Segmented Approaches. For aircraft with RNAV capability, MLS waypoints could be specified on the Bridge approach such that positive guidance was provided during the transition from the -6° to the -3° or 0° azimuth angles. Aircraft with more sophisticated computational capability and displays could easily make manual or automatic approaches through touchdown.

Curved Approaches. A proposed solution to the San Francisco noise problem would require approaches over the bay with a left turn of greater than 90° to final approach to runway 19. Because of Oakland traffic conflicts, this must be accomplished at or within about 11 km (6 n. miles). Existing navaids are inadequate for this task, and it was determined that the weather conditions deemed necessary to make this approach visually at night do not exist during a majority of the hours of interest. Such an approach could be easily handled with the wider proportional coverage of MLS.

An example of an over-water approach is shown in figure 10, which depicts two MLS approaches flown at Buenos Aires by the TCV B-737. These paths avoid overflying a city area with numerous high-rise apartment buildings, as the ILS approach does at altitudes as low as 305 m (1000 ft). The final approach legs here were 2 and 3 km (1.1 and 1.6 n. miles) in length. Figures 11 and 12 are photographs taken from the pilot's window on base leg and in the turn to final approach, respectively, on the path ABE05. The aircraft track is toward the right hand edge of the photo, and the runway may be seen at the left. The final approach course is intercepted over the athletic field beyond the two large buildings.

As performed by the TCV B-737, this type of approach is explicitly defined in 3 dimensions and the waypoint and altitude data are stored in the navigation computer bulk data in the form of a Standard Terminal Arrival Route (STAR). The path is easily entered into the flight plan by the pilot by merely calling for the STAR by name. This not only reduces workload by eliminating the necessity for entering each waypoint, but allows the waypoint locations to be defined more accurately than the 0.1' of latitude and longitude which is normal with present-day control and display units. This resolution does not take advantage of MLS accuracy, and is insufficient for curved, close-in intercepts of final approach.

In order to allow the definition of curved, continuously descending flight paths, the TCV MLS signal processing used a coordinate conversion from the MLS conical coordinates to a runway-based rectangular coordinate system. After filtering, the rectangular coordinate data were again transformed into Inertial Navigation System-equivalent data for input to the existing navigation computer system, and to ILS-like deviation data for the autoland system and displays. This is a rather cumbersome process, with the added disadvantage that no MLS data can be used unless all angle and range data are available. However, it does allow the definition of complex flight paths and touchdown points independent of ground station geometry so long as the path stays within coverage of all signals. In future system designs a capability to use azimuth and range information of RNAV along with barometric altitude and to intercept and track specific azimuth and elevation angles directly is desirable.

An important factor when an explicit path is to be followed is the navigation error existing at the time MLS coverage is entered and a change is made to MLS guidance. Depending on the available navaids and geometry, and the aircraft navigation capability, large discrepancies may exist between the position estimate and the actual aircraft position. Similarly, there are likely to be altitude errors due to aircraft instrumentation errors and non-standard atmospheric conditions. Flight path design must take the size of these errors and the MLS coverage characteristics into consideration so that sufficient flight time within MLS coverage is allowed for a smooth and gentle correction prior to attempting the final intercept turn, since correcting track errors in a turn is more difficult and may result in undesirable aircraft maneuvering. This is especially true if the aircraft happens to be on the outside of the turn. Figure 13 illustrates a typical situation during entry of the TCV airplane into MLS coverage and a 130° turn to a 5.6 km (3 n. miles) final approach leg. This is the same path described for other flights at NAFEC in references 4 and 5. The error data was obtained by phototheodolite tracking from the ground. At the beginning of the plot, waypoint DD135, the airplane was to begin a 3° descent. A cross track position error of about 100 m is apparent, with a standard deviation of about 75 m. A larger along-track error is implied by the rapid increase of altitude error initially, indicating that the aircraft passed the waypoint before beginning descent. At the edge of the MLS coverage region, the mean cross track error has decreased to near zero but the dispersion is unchanged. The altitude error has settled at about 30.5 m (100 ft). At this point the cross track error dispersion is seen to begin decreasing as the switch is made to MLS guidance. The mean altitude error rapidly decreases to near zero and at the same time the dispersion is reduced. Further improvement in the dispersion is seen as the final approach leg is intercepted and the autoland system takes over. During these flights no special provision was made for the transition from conventional to MLS guidance. Rather, any existing error was fed to the guidance algorithms as a step input when the MLS guidance switch was enabled. This proved acceptable for most of the flights, since navigation errors are a minimum with a dual DME updated inertial navigation system such as used on the TCV B-737. However, with the occasional larger errors experienced, maneuvers tend to become abrupt and it is desirable to provide a blanding technique for smooth transition to the MLS guidance. Such techniques are planned for flight testing on the TCV B-737.

A summary of the cross track and altitude errors experienced by the TCV airplane during flights at Buenos Aires, New York and Montreal is given in figure 14. The mean cross track error of -79 m can be expected to approach zero as data is included for additional locations and flight geometries, but the dispersion is probably representative of what can be expected using this type of inertial/DME/DME navigation. On the few occasions when VOR data has been used, errors of about 2 km have been seen. The altitude error here also shows a bias, which could be due in part to the fact that the flights at JFK and Montreal were performed in cold weather when the barometric altimeter would tend to read low. Other factors could be along track navigation errors for any approaches where MLS entry occurred during a descent, or errors in the MLS equipment or on-board processing.

Canarsie Approach to JFK. A published curved instrument approach procedure, the VOR RWY 13L/13R (Canarsie) approach to John F. Kennedy airport is shown in figure 15. Although this is an instrument approach, the curved portions must be flown by visual reference to a series of flashing lead-in lights; thus relatively high ceilings and visibilities are required. The approach to runway 13R, in particular, requires basic VFR weather conditions. The approaches are difficult to fly since the curved path must be tracked by reference to a few visual cues, which may be difficult to pick out from the city lights at night, and at the same time a descent must be made with no vertical guidance. Pilots frequently overshoot the curve and fly over the residential district, which the approach is designed to avoid.

Figure 16 shows an experimental MLS installation at JFK which was used by the TCV B-737 to demonstrate the conversion of the Canarsie approach to a precision approach to touchdown. The azimuth antenna provided ±60° coverage. Two different elevation antennas were tested at JFK by the FAA. The one in use during the TCV flights was the Basic Narrow system with centerline emphasis so that elevation coverage was not matched to the azimuth system and was marginal in the vicinity of CRI. The result was that the elevation signal was sometimes lost for brief periods early in the approach as the airplane maneuvered. The black triangles show the points at which the pilots switched to MLS guidance. This varied widely for several reasons, but a contributing factor was loss of confidence when the pilots coupled to the MLS early and then lost the elevation signal in the resulting transition maneuver. With an operational system this should not be a problem since the elevation and azimuth coverages would be matched.

If a ±40° azimuth system had been used, all transitions to MLS guidance would have been delayed until near the turn entry, often leaving insufficient time to correct the navigation errors before entering the turn. Further, if terminal procedures were to require that MLS approach procedure design could include only the ±40° sector originating at the datum point, as illustrated in figure 2, MLS could not be assumed valid prior to reaching the start of the turn, which is the missed approach point in today's procedure. Thus only a ±60° system can be used for this approach. Even as measured from the datum point, this allows adequate time to acquire the signals in the vicinity of CRI and correct any navigation and altitude errors.

The MLS on runway 13L could be used to provide VNAV approaches to both runways, allowing lower weather minima than are presently required and improving the utility and accuracy of the approaches. With TCV type signal processing, autolands would be possible on either runway using the same MLS ground station. For runway 13R the final approach course could be simply offset using the same technique which was used at Montreal, where the azimuth antenna was installed off-centerline to allow installation of the British Doppler MLS on the same runway. While the use of such methods may be questioned today, the technical feasibility was clearly demonstrated over two years ago. The use of an MLS for RNAV or VNAV approaches to more than one runway could increase the utility of these types of approaches without the added cost of complete systems on every runway. However, in the beginning, confidence can probably be best gained by using the MLS primarily to improve the accuracy and safety of the visual portions of these approaches and to reduce the weather minima later as experience shows to be appropriate.

La Guardia Expressway Approach. A final example of a current curved, descending noise abatement approach is the La Guardia Expressway Approach in figure 17. The curved portion is even less well defined than the JFK approaches just discussed, since there are no lead-in lights or other visual cues to define the curve. The pilot must locate and visually follow a particular highway system, turning over Flushing Meadow Park to intercept a very short final approach, all the while making a steeper than normal descent without guidance. The procedure calls for a ceiling of 914.4 m (3000 ft) and visibility of at least 8 km (5 mi), considerably greater than basic VFR requirements. The problem with making this an MLS approach is that even a standard $\pm 60^0$ MLS does not provide sufficient coverage due to the large turn and very short final approach leg.

There are some possible ways in which MLS could be used for the Expressway Approach. Illustrated in figure 17 is a way to do it with a single $\pm 60^0$ MLS on runway 31. The azimuth and elevation antennas are rotated by about 40^0 toward the side on which additional coverage is required. This would allow the signals to be acquired during the initial inbound leg toward the airport in plenty of time to establish accurate path tracking and a stabilized descent before reaching DIALS intersection and turning to base leg. However, any conventional users approaching along the runway centerline would be required to track the -40^0 azimuth angle rather than 0^0. It is technically a simple matter to set this reference angle into the receiver automatically using data transmitted by the ground equipment, or the pilot could be required to select the proper reference angle as part of the cockpit procedure. This technique would still allow 20^0 of proportional coverage on the north side of the runway, well in excess of the required 10^0 minimum. It would also allow VNAV approaches to runway 4 using the same installation. This technique would require that the present proposed practice be modified, since it calls for the 0^0 azimuth angle to be aligned with the runway centerline.

A second possibility would be the installation of another MLS on runway 4 in addition to the one on 31. The runway 4 system could be used during the initial part of the approach to provide accurate VNAV guidance and the runway 31 system used for final approach. The disadvantages are that twice as much ground equipment is required, and the airborne equipment would require either an additional MLS receiver dedicated to area navigation or frequency retuning at a critical point in the approach.

A final potential solution is the 360^0 azimuth option, which is considered a possible growth feature of the MLS. Assuming that the accuracy would be comparable to the approach azimuth, this would solve the lateral guidance problem. However, there would still be a problem with altitude errors. Recall from figure 14 that errors of a few hundred feet would not be uncommon. An error of this magnitude needs to be detected and corrected before reaching DIALS intersection because of the shortness of the path and the fact that the approach is already somewhat steeper than 3^0 and a fly-down error indication might result in higher than desirable descent rates. Since much of this error is caused by non-standard atmospheric conditions, the size of the transition is to some extent determined by the altitude at which it occurs. Figure 14 included data on transitions occurring from 610 to 1524 m (2000 to 5000 ft) MSL. Table I summarizes the differences between barometric, radio and MLS altitudes at several points along the final approach path at Buenos Aires. These points were all below 182.9 m (600 ft) MSL. The mean difference between barometric and MLS altitudes this near the ground is seen to be about 12.2 to 15.2 m (40 to 50 ft), with a standard deviation of 15.2 to 18.3 m (50 to 60 ft). An attempt was made to correct radio altitude for the approximate terrain elevation, and the results show good agreement with the MLS altitude. The larger dispersions of 3.7 and 4.0 m (12 and 13 ft) at two points show the terrain dependence of the radio altimeter. These were due to the effects of street traffic and trees at one point, and a double row of approach lights at the other.

The conclusion which may be drawn is that MLS altitude accuracy is comparable to that of radio altimeters, and MLS is preferable for obstacle clearance and landing guidance since it is terrain independent. However, there is a transition which may be hundreds of feet in magnitude required to change from barometric to MLS altitude. This transition problem increases with altitude, and must be considered in the design of MLS approaches.

USE OF MLS AT COVERAGE LIMITS

Lateral Coverage

All discussions to this point have been concerned with MLS near the airport traffic pattern. The minimum specified coverage extends to a range of 20 n. miles and an altitude of 6096 m (20 000 ft). During normal conditions, the signals will probably be received at much greater distances. During the first TCV B-737 tests using MLS, valid signals were received in excess of 55 km (30 n. miles). Since it has been implied that it is desirable to correct navigation errors as early as practical in an approach, let us consider the use of MLS at the coverage limits.

Figure 18 illustrates a hypothetical installation of two ±60° systems at Denver, which provide coverage for all arrival routes. The Denver terminal area is of interest because of the experiments with traffic metering and profile descents, which may result in similar traffic arrival patterns being used more widely in the future. Note that even the minimum system range of 37 km (20 n. miles) allows MLS use during the last part of the profile descent, and it is quite likely that under most conditions signals will be acquired much further out--perhaps at the metering fixes. The question, then, is what use might be made of MLS under those conditions.

It is obviously advantageous to use MLS to update the navigation position estimate as early as possible so that any necessary corrections can be made smoothly and expeditiously. The procedure depicted is the high profile descent, which would be in use for traffic being routed to a downwind leg for landing opposite the initial approach direction. With only the two systems shown, aircraft would temporarily leave MLS coverage on downwind leg. If MLS were installed on the east-west runways, a switch to that system could be made on downwind for continuous MLS guidance. In either event, another frequency change would be required for the final approach phase. If the 360° azimuth and DME option were available, the landing MLS could be tuned initially and accurate lateral guidance would be available continually with no further action.

MLS Altitude

In the case illustrated in figure 18, it would be possible to compute MLS altitude at initial entry to the MLS coverage region. However, an area navigation study done for the FAA several years ago (reference 9) showed that vertical separation would be compromised by mixing traffic using barometric altitude with traffic using MLS altitude, and it is not reasonable to expect all traffic in the terminal area to be using MLS altitude. The problem is mainly due to the large errors in barometric altitude which can occur under non-standard conditions. These errors affect all aircraft in the same vicinity by approximately the same amount, so that relative separation is not affected. Absolute errors are accounted for by the requirement for a minimum altitude of 305 m (1000 ft) above the highest obstacle within 8 km (5 mi) (610 m (2000 ft) in mountainous areas). One conclusion of that study was that with mixed barometric and MLS altitudes, a vertical separation of 2000 ft would be required. This study limited the conditions to an altitude of 3048 m (10 000 ft) and an airspeed of 250 kts. As just shown in figure 18, aircraft will be within MLS coverage at altitudes of 6096 m (20 000 ft) or more and in many cases they mat by at airspeeds greater than 250 kts. Table II shows a summary of the results from reference 9 and an extension of the analysis to include an altitude of 20 000 ft and airspeed of 350 kts. A slightly larger MLS error is also used to conform more closely to current proposals, but this is an insignificant perturbation. The column labelled "noise error" is composed primarily of the maximum random errors which can occur due to non-standard temperatures, lapse rates and horizontal pressure gradients. By the rule of thumb given in the reference, the vertical separation must be increased by about 1000 ft over that calculated for the lower altitude and airspeed. A possible need to change terminal area vertical separation from 305 to 914 m (1000 to 3000 ft) would appear to be a good argument against the early use of MLS altitude.

A second disadvantage of early use of MLS altitude would be the magnitude of the correction necessary after switching from barometric to MLS altitude. This could occur during the profile descent phase and result in either a loss of some of the fuel savings or inability to correct the error, if a fly-down error signal were received while descending at idle power. Transition methods would have to be very gradual to compensate for altitude errors of 1000 ft or more in a reasonable fashion. One simple way to achieve a gradual reduction of altitude error to a more reasonable value is to wait until reaching a lower altitude before making the switch.

To summarize, MLS altitude is essential for purposes such as curved, descending flight paths and is very desirable for obstacle clearance and guidance in the final approach phases and landing. However, its use at higher levels creates problems which do not appear to have a ready solution. Further analysis and experimentation is required to define the conditions under which MLS altitude should be used.

OPTIONAL MLS FEATURES

Little or no experience has been gained with the use of the proposed MLS growth features. Therefore, only a few general comments will be made about their possible applications or characteristics.

360° Azimuth

This paper has mentioned several potential applications for an omni-directional azimuth function, and the MLS signal format does contain growth potential to allow its implementation. At this time, however, it is strictly in the conceptual stage. In the early planning stages of MLS, a ±90° coverage was felt to be an operational requirement for a full service system (reference 1), but this was modified to ±60° because of practical considerations regarding implementation. The emphasis at present is concentrated on the lesser capability systems with proportional coverage of ±40° down to ±10° (reference 3). Every reduction from ±90° coverage increases the need for a 360° azimuth subsystem, and the requirements for accuracy become more stringent to insure that navigation problems can be corrected before reaching a critical phase in the approach. The problem of transition from barometric altitude, however, will not be solved by the implementation of this function.

Back Azimuth

Flight tests have been conducted using MLS installations which had an azimuth subsystem installed in the back amimuth location, and performance standards for this function are under development. Some questions remain as to the use of this function. Figure 19 illustrates the proposed azimuth scanning conventions. This convention will result in a change of sign of the deviation signal at a change from approach to back azimuth. This can be easily handled by having the receiver reverse output polarity for the back azimuth function, so that the CDI deflections will follow the same conventions as for ILS. However, the angular course deviations as measured by the two systems will not be of the same magnitude except midway between the antennas. A switch from approach to back azimuth will therefore usually result in a change, perhaps large, of CDI deflection; or in the case of automatic flight operations will result in a step error input to the autopilot. Figure 20 shows that during much of the time the aircraft is over the runway, there will be a choice of using either approach or back azimuth information. It must yet be established whether the switch to back azimuth is to be made automatically in the receiver or initiated by the pilot. In either case, criteria for making the switch must be defined and some transition method developed to smooth the possible jump in error magnitude.

In the TCV B-737 flight tests, the back azimuth signal was used only as a sensor input for updating the RNAV position solution after the approach azimuth signal was lost. A desirable feature of this technique is that the pilot always follows the same procedures and uses the same displays regardless of the availability of back azimuth guidance. The back azimuth here has no effect except to improve the accuracy of the RNAV position.

MLS Flare Guidance

The MLS flare elevation function has been flight tested in two versions by the TCV B-737. Performance standards for this function are presently being developed. The primary function of the flare elevation system is to provide a source of altitude data equal to or better than a radio altimeter during the flare and landing phase, when the approach DME and computational capability are also required. During most of the TCV flights, flare elevation was substituted for approach elevation whenever it became available rather than waiting until the latter was about to be lost. This eliminated any possibility of problems arising from changing altitude guidance in a critical flight phase near the ground, and performance on the glidepath was somewhat better due to the narrower beam width of the flare elevation system.

One alternate use that could be made of the flare elevation system by aircraft without precision DME or computations is the segmented glidepath approach illustrated in figure 21. In this procedure a normal glidepath would be flown on the approach elevation system, and a transition would be made to a smaller angle glidepath upon intercepting the desired angle from the flare elevation antenna. This angle would be chosen to provide the desired touchdown sink rate, thus eliminating the need for a final flare maneuver. Several examples are given for the TCV B-737, assuming an MLS antenna height of 4 m above the runway at touchdown. The transition altitudes and touchdown sink rates for the 0.6 to 0.7° glidepaths are comparable to the normal flare, except that the latter is a gradual continuous maneuver rather than a discrete transition to a flatter glidepath. This type of landing maneuver has been tested on an earlier experimental guidance system. One of the potential problems with such a procedure is that the touchdown dispersion would probably be greater than that achieved using present TCV flare control laws (reference 10). An estimate of touchdown dispersion for each glidepath is given in the figure. It was obtained by using the glidepath tracking dispersion from figure 7 and the tangent of the glidepath angle. In practice, the values might be either better or worse depending on how closely the glidepath was tracked at these shorter ranges and what the effects of transitioning to a new glidepath were. There might also be problems in providing a single ground antenna geometry suitable for a wide range of aircraft characteristics.

CONCLUDING REMARKS

Many of the uses originally envisioned for a new precision approach and landing aid, such as curved approaches for noise abatement purposes and automatic landings, have been clearly demonstrated to be technically feasible by TCV B-737 flights. With regard to the technical requirements, there is no reason why such procedures could not be put into use within a few years, since the new aircraft which are currently on production lines will have electronic displays and computational capabilities suitable for emulating or improving on the TCV experience. Reasons why these capabilities may not be exploited soon are the lack of defined procedures and conventions, opposition by pilots and air traffic controllers without training and experience in these types of operations, and possible deficiencies in ground station and/or airborne equipment capabilities.

It has been TCV program experience that during the MLS flight tests, most air traffic controllers and guest pilots developed confidence in the airplane's ability to follow complex flight paths and traffic clearances, after they were briefed on the aircraft systems and saw from actual flight operations that they worked as advertised. It is suggested in this paper that a good way to smooth the way for the use of MLS for complex noise abatement procedures is to start with existing visual approaches. This would cause a negligible perturbation to present air traffic control procedures and could reduce pilot workload (with the proper displays), increase safety and flight path accuracy, and reduce missed approach frequency. The resulting operational experience would help to provide the confidence needed for the reduction of weather minima on existing approaches and influence the design for new procedures.

The other factors which could delay or prevent the full realization of the potential of MLS are technical ones involving coverage volume and the provision for special techniques to increase coverage asymmetrically where required. While it is desirable to simplify the transition from ILS to MLS by the use of common procedures, it must be emphasized that a "minimum" performance standard is exactly that. Many proposed uses of MLS will require additional capability, and may require special techniques or data transmissions. These should be carefully considered and coordinated with the needs of early conventional users of MLS to insure that future applications are not inadvertently restricted.

REFERENCES

1. Walsh, Thomas M., Morello, Samuel A., and Reeder, John P.: Review of Operational Aspects of Initial Experiments Utilizing the U. S. MLS. NASA SP-416, 1976, pp. 3-30.

2. A New Guidance System for Approach and Landing. Radio Technical Commission for Aeronautics Document No. DO-148, December, 1970.

3. Non-Federal Navigation Facilities; Proposed Microwave Landing System Requirements. Notice of Proposed Rulemaking No. 80-15, Federal Aviation Administration, DOT. Federal Register 45, no. 175, Sept. 8, 1980.

4. The TCV B-737 Flight Performance During the Demonstration of the Time Reference Scanning Beam Microwave Landing System to the International Civil Aviation Organization All Weather Operations Panel. Boeing Commercial Airplane Company Document no. D6-44291, February, 1977.

5. White, William F., et al.: Flight Demonstrations of Curved, Descending Approaches and Automatic Landings Using Time Reference Scanning Beam Guidance. NASA TM 78745, May, 1978.

6. White, William F., and Clark, Leonard V.: Flight Performance of the TCV B-737 Airplane at Kennedy Airport Using TRSB/MLS Guidance. NASA TM 80148, July, 1979.

7. White, William F., and Clark, Leonard V.: Flight Performance of the TCV B-737 Airplane at Jorge Newbery Airport, Buenos Aires, Argentina Using TRSB/MLS Guidance. NASA TM 80223, January, 1980.

8. White, William F., and Clark, Leonard V.: Flight Performance of the TCV B-737 Airplane at Montreal/Dorval International Airport, Montreal, Canada Using TRSB/MLS Guidance. NASA TM 81885, September, 1980.

9. Hemesath, N. B., et al.: Three and Four Dimensional Area Navigation Study. Federal Aviation Administration Report RD-74-150, June, 1974.

10. Hueschen, R. M., Creedon, J. F., Bundick, W. T., and Young, J. C.: Guidance and Control System Research for Improved Terminal Area Operations. 1980 Aircraft Safety and Operating Problems, NASA CP-2170, 1981. (Paper 4 of this compilation).

TABLE I. - COMPARISON OF MLS WITH BAROMETRIC AND RADIO ALTITUDES

Location	No. of Points	Barometric minus MLS Altitude, ft	Radio minus MLS Altitude, ft
3 km Final Approach Fix	43	53.1 ± 47.5	17.1 ± 3.6
2 km Final Approach Fix	10	14.5 ± 67.3	15.5 ± 2.4
Cat I DH	53	41.8 ± 56.0	12.6 ± 3.2
Decrab Initiation	53	46.4 ± 51.9	6.9 ± 13.1
Cat II DH	52	41.0 ± 57.6	2.7 ± 12.1
Flare Initiation	52	39.2 ± 56.8	0.2 ± 2.3
Touchdown	34	27.1 ± 63.6	0.5 ± 1.8

TABLE II. - RELATIVE POSITION ERRORS FOR MLS VERSUS BAROMETRIC ALTITUDE AT A RANGE OF 20 NAUTICAL MILES

	Bias Error, ft	Noise Error, ft	Minimum Separation, ft
(1) Altitude $\leq$ 10 000 ft Airspeed $\leq$ 250 kts	330	895	1 710
(2) Altitude = 20 000 ft Airspeed = 350 kts	570	1 720	2 720

(1) Data from reference 9.
(2) Assumes maximum PFE of 300 ft, treated as bias error, and 350 ft static defect error.

(Note: 1 ft = 0.3048 m.)

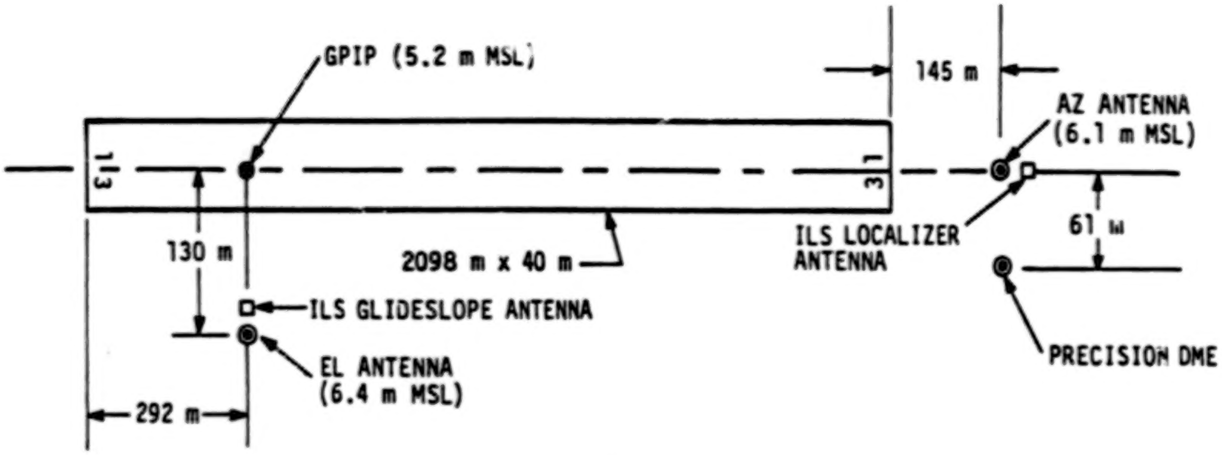
GPIP (5.2 m MSL)
145 m
AZ ANTENNA
(6.1 m MSL)
13
31
61 m
130 m
2098 m x 40 m
ILS LOCALIZER
ANTENNA
ILS GLIDESLOPE ANTENNA
EL ANTENNA
(6.4 m MSL)
PRECISION DME
292 m

Figure 1.- MLS configuration for runway 13 at Jorge Newbery Airport, Buenos Aires, Argentina.

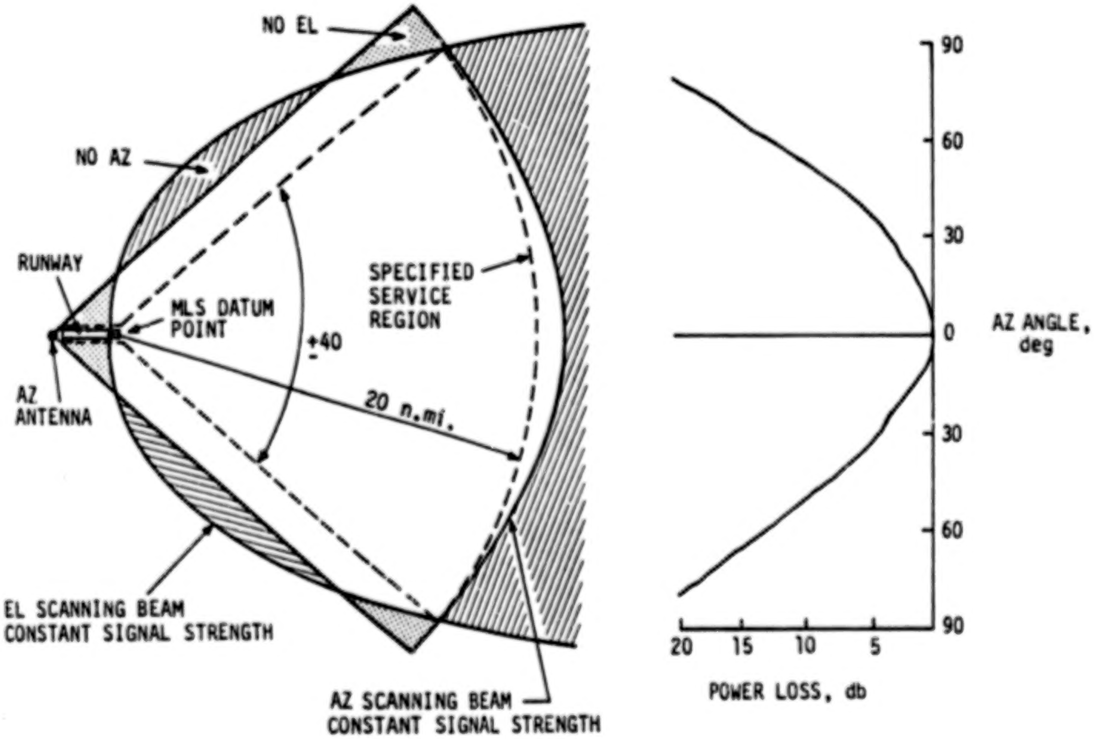
NO EL
NO AZ
RUNWAY
MLS DATUM
POINT
±40
SPECIFIED
SERVICE
REGION
20 n.mi.
AZ
ANTENNA
EL SCANNING BEAM
CONSTANT SIGNAL STRENGTH
AZ SCANNING BEAM
CONSTANT SIGNAL STRENGTH
90
60
30
0
30
60
90
AZ ANGLE,
deg
20
15
10
5
POWER LOSS, db

Figure 2.- Typical MLS centerline emphasis antenna pattern and resulting lateral coverage area.

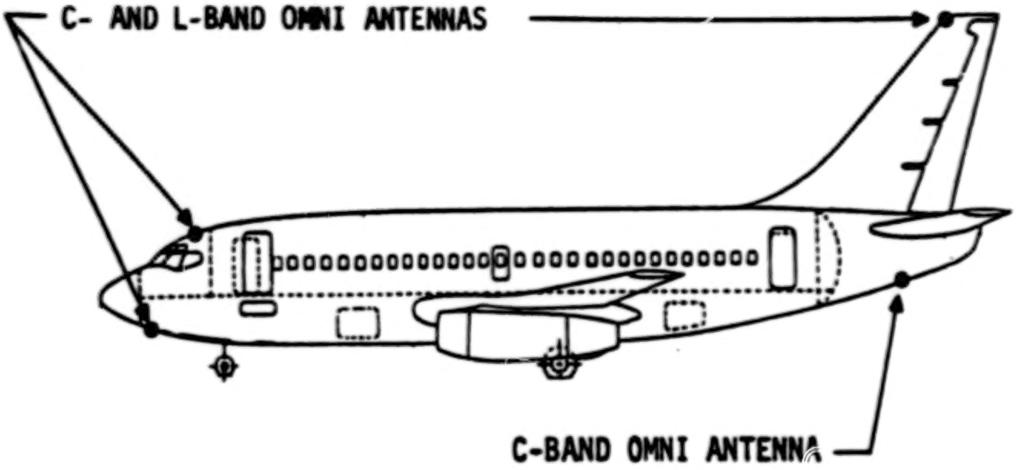
C- AND L-BAND OMNI ANTENNAS
C-BAND OMNI ANTENNA

Figure 3.- MLS antenna locations which have been flight tested on the TCV B-737.

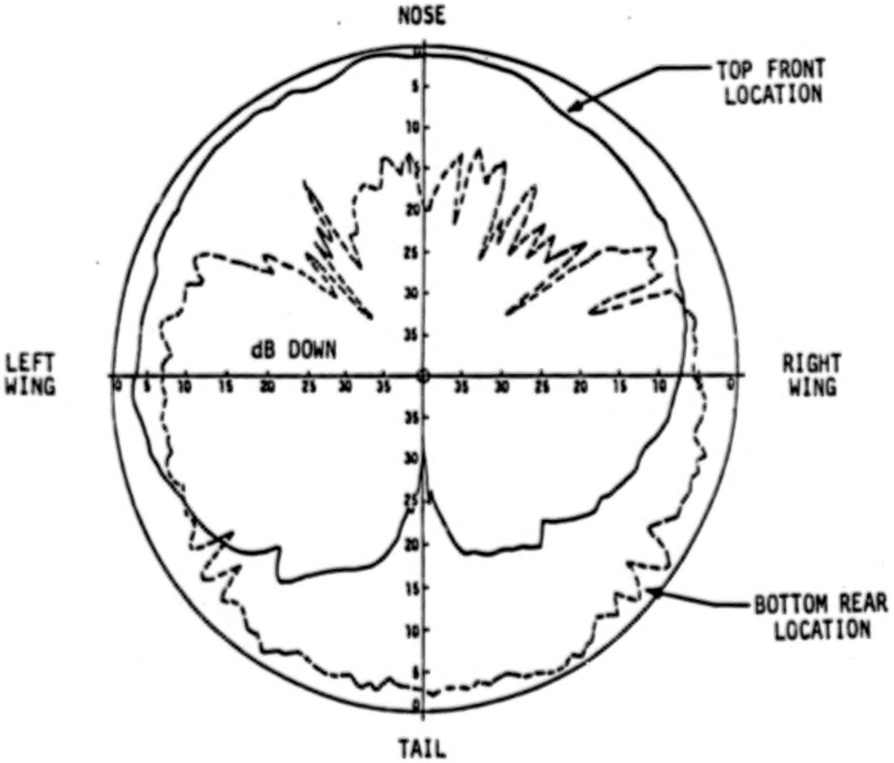

Figure 4.- Azimuthal plane radiation patterns of monopole antennas on TCV B-737.

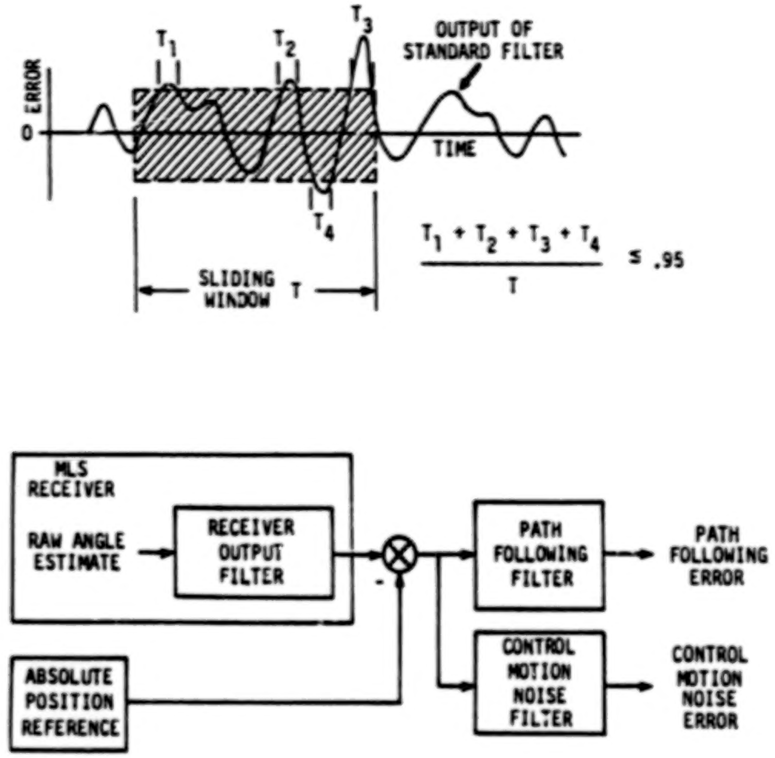
ERROR
0
T_1
T_2
T_3
T_4
OUTPUT OF STANDARD FILTER
TIME
SLIDING WINDOW T
$\frac{T_1 + T_2 + T_3 + T_4}{T} \leq .95$
MLS RECEIVER
RAW ANGLE ESTIMATE
RECEIVER OUTPUT FILTER
-
ABSOLUTE POSITION REFERENCE
PATH FOLLOWING FILTER
PATH FOLLOWING ERROR
CONTROL MOTION NOISE FILTER
CONTROL MOTION NOISE ERROR

Figure 5.- MLS error specification methodology.

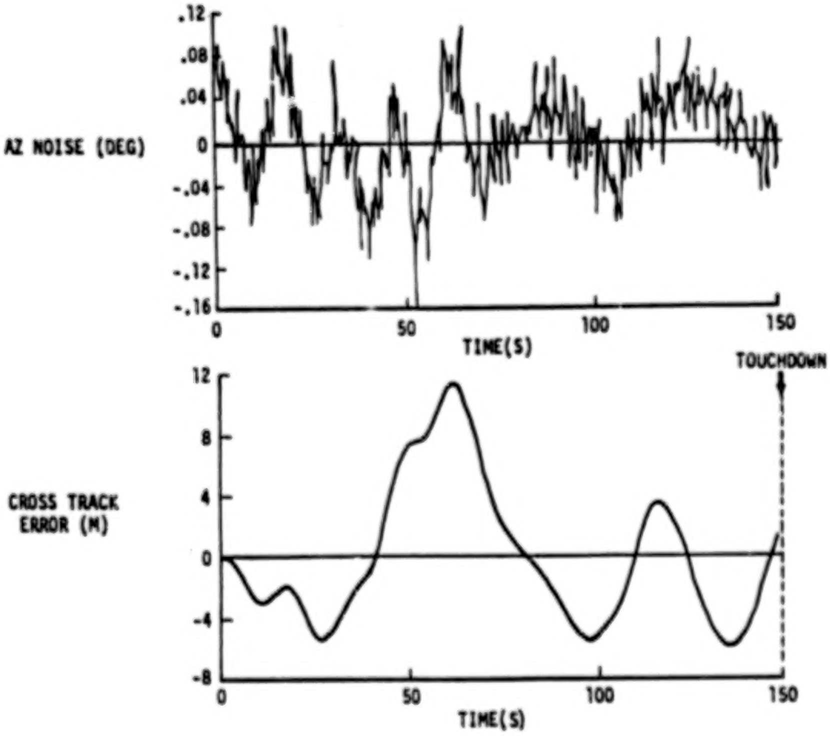

Figure 6.- Example of simulated B-747 lateral autopilot performance with MLS substituted for ILS.

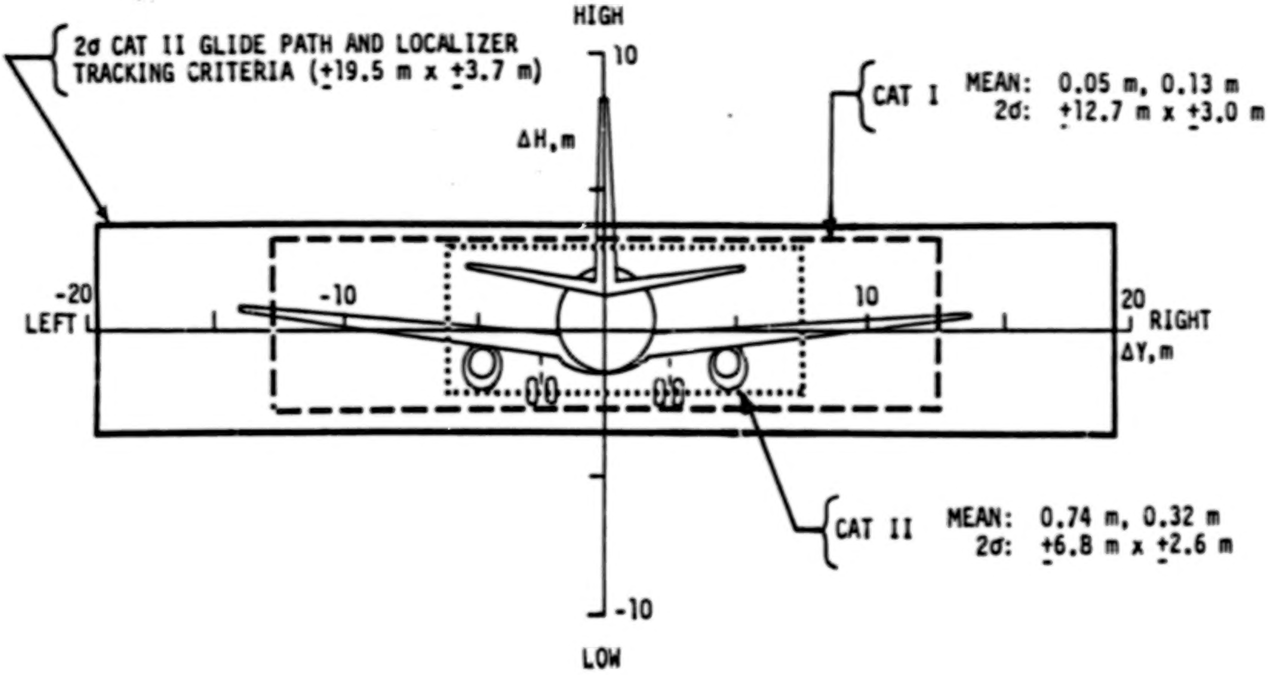

Figure 7.- Summary of TCV B-737 autopilot performance utilizing MLS guidance.

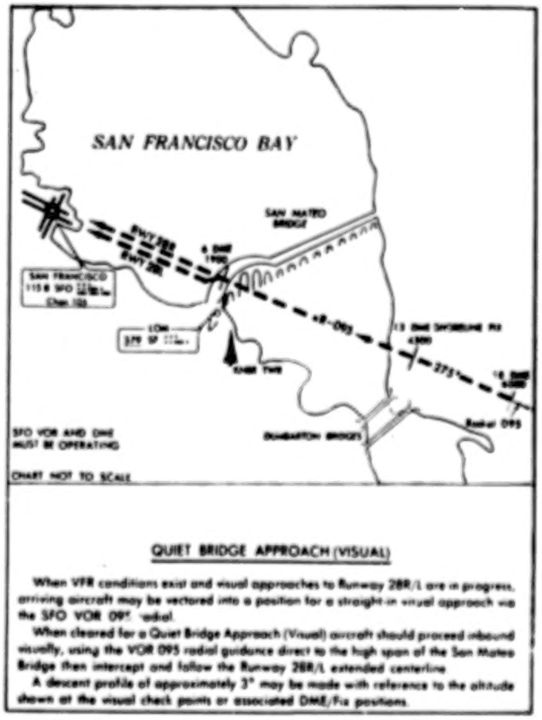
SAN FRANCISCO BAY
SAN MATEO BRIDGE
DUMBARTON BRIDGES
Radial 095
SFO VOR AND DME MUST BE OPERATING
CHART NOT TO SCALE

QUIET BRIDGE APPROACH (VISUAL)

When VFR conditions exist and visual approaches to Runway 28R/L are in progress, arriving aircraft may be vectored into a position for a straight-in visual approach via the SFO VOR 095 radial.

When cleared for a Quiet Bridge Approach (Visual) aircraft should proceed inbound visually, using the VOR 095 radial guidance direct to the high span of the San Mateo Bridge then intercept and follow the Runway 28R/L extended centerline.

A descent profile of approximately 3° may be made with reference to the altitude shown at the visual check points or associated DME/Fix positions.

Figure 8. - Example of off-centerline noise abatement approach. (Note: 1 ft = 0.3048 m.)

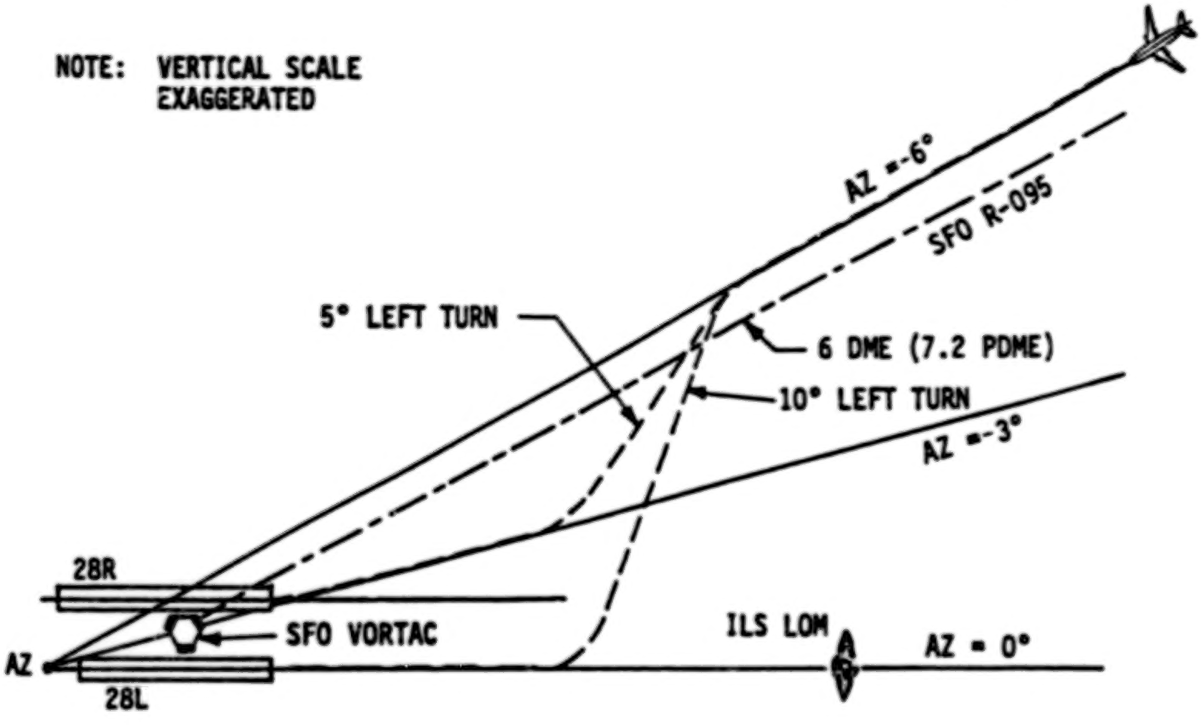
NOTE: VERTICAL SCALE EXAGGERATED
AZ =-6°
SFO R-095
5° LEFT TURN
6 DME (7.2 PDME)
10° LEFT TURN
AZ =-3°
28R
SFO VORTAC
ILS LOM
AZ = 0°
AZ
28L

Figure 9.- Possible MLS version of San Francisco Quiet Bridge Approach.

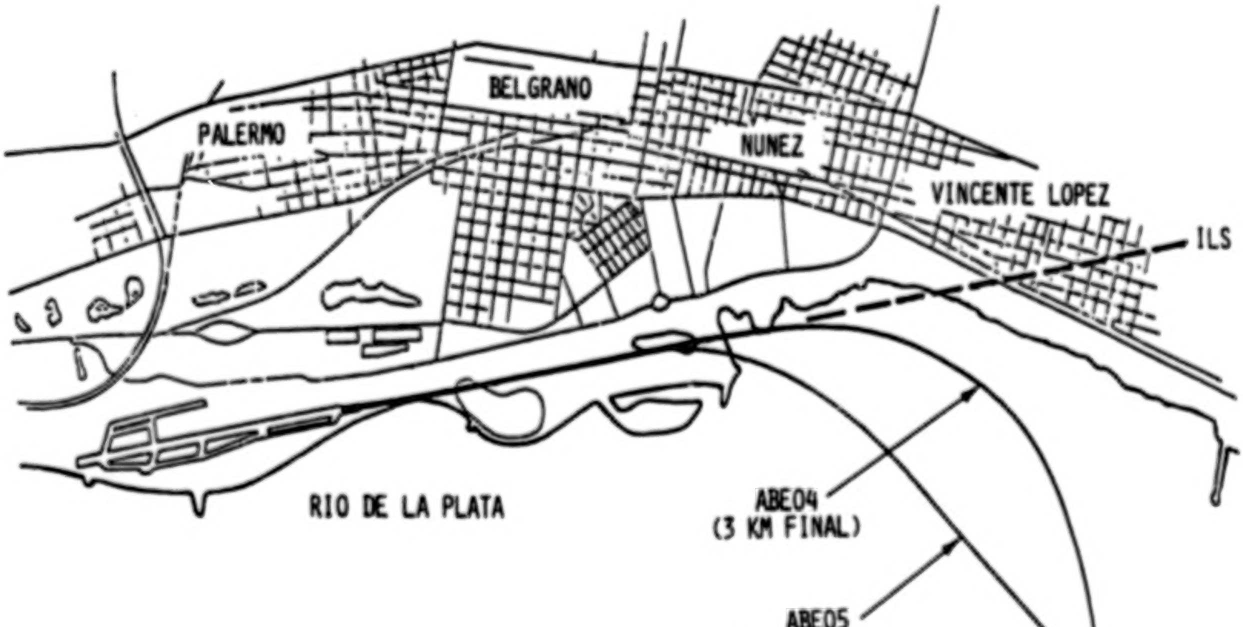
PALERMO
BELGRANO
NUNEZ
VINCENTE LOPEZ
ILS
RIO DE LA PLATA
ABE04
(3 KM FINAL)
ABE05
(2 KM FINAL)
MLS

Figure 10.- Approach paths for automatic MLS landings by TCV B-737 at Jorge Newbery Airport, Buenos Aires, Argentina.

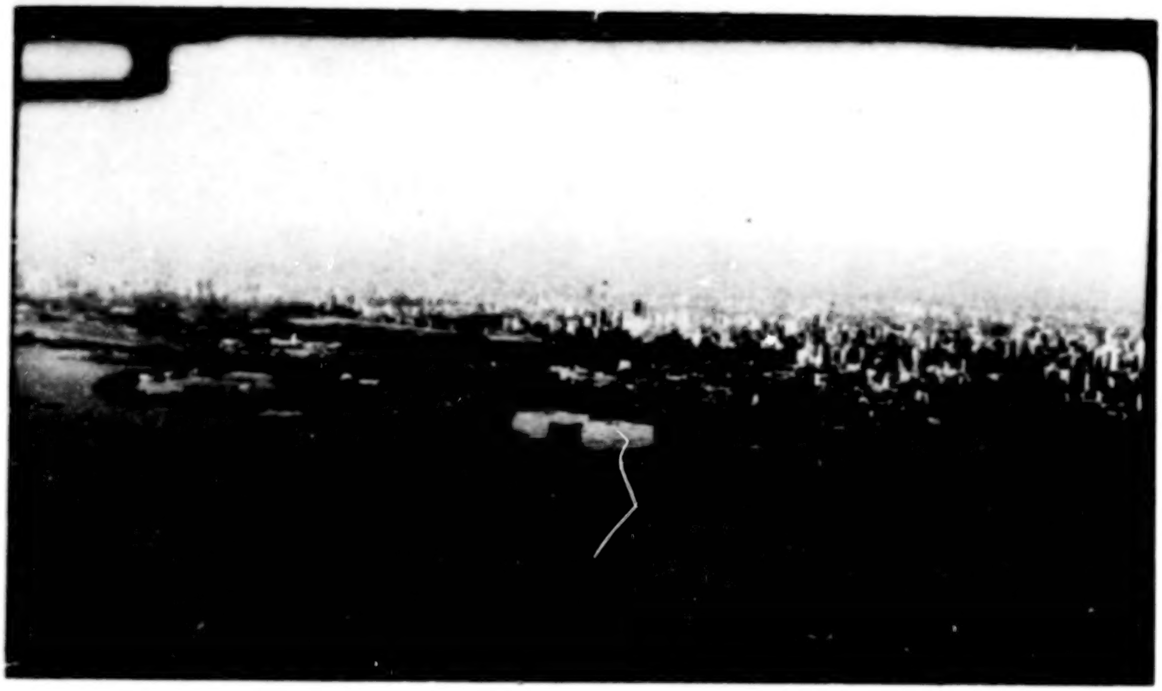

Figure 11.- View from TCV B-737 cockpit on base leg of noise abatement approach at Buenos Aires, Argentina.

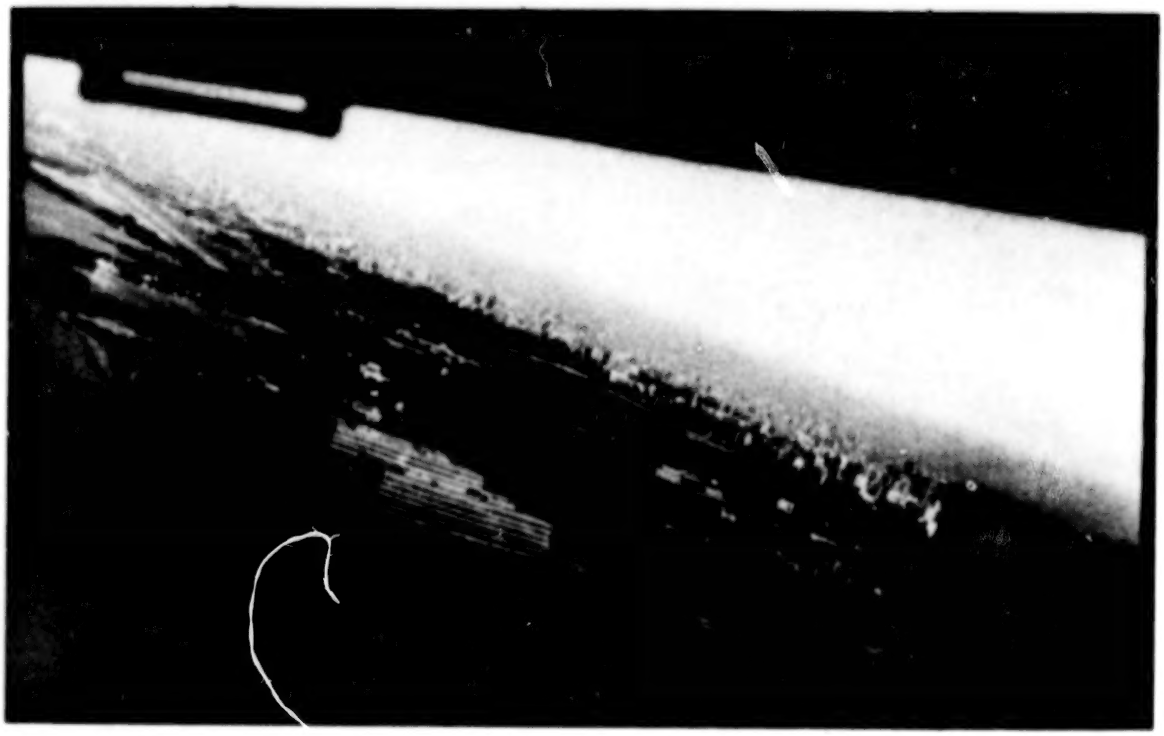

Figure 12.- View from cockpit of TCV B-737 intercepting 2 km (1.1 n. mile) final approach at Buenos Aires, Argentina.

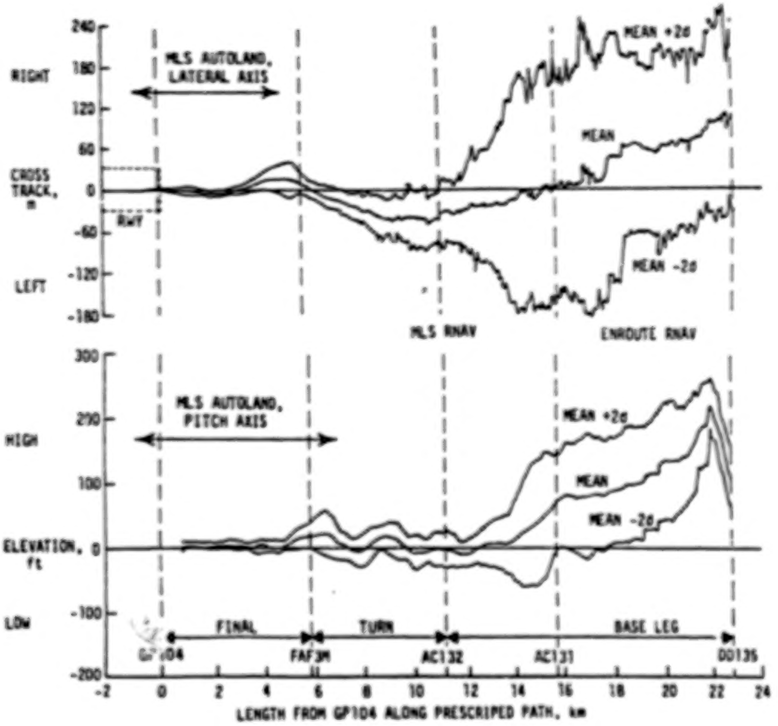

Figure 13.- TCV B-737 path deviation for 130° turn to 5.6 km (3 n. mile) final approach leg. (Note: 1 ft = 0.3048 m.)

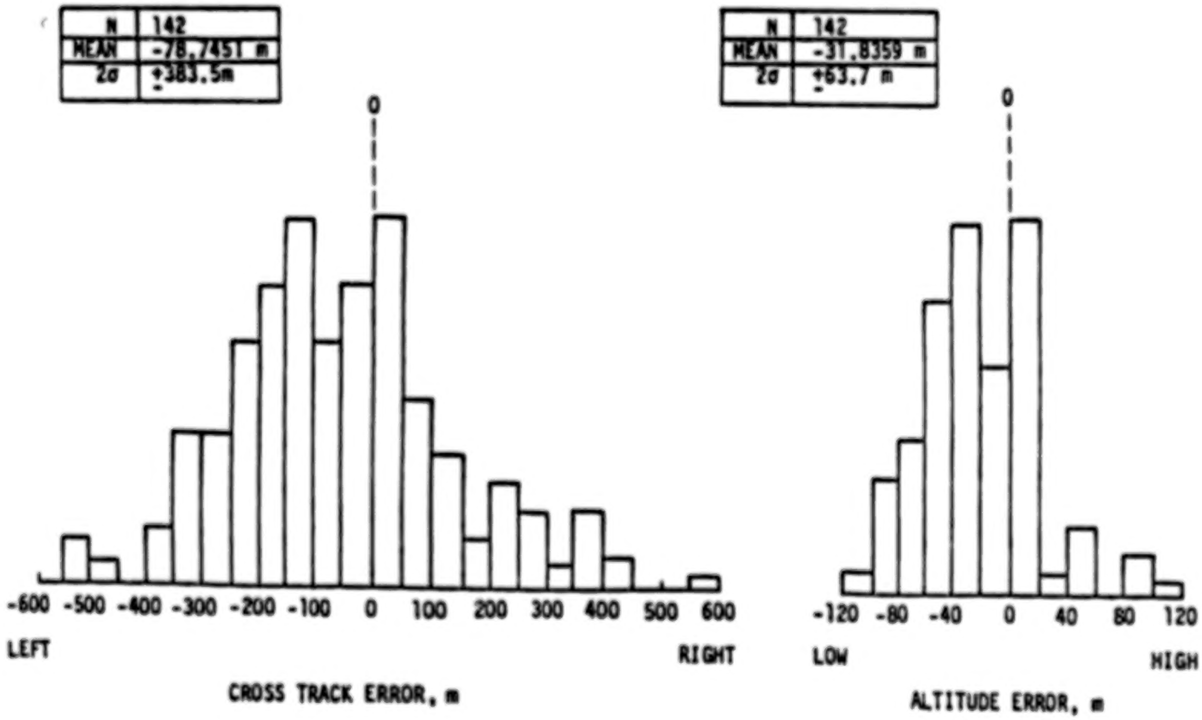

Figure 14.- Summary of conventional-to-MLS RNAV path differences for TCV B-737 approaches to JFK, Jorge Newbery, and Montreal/Dorval International Airports.

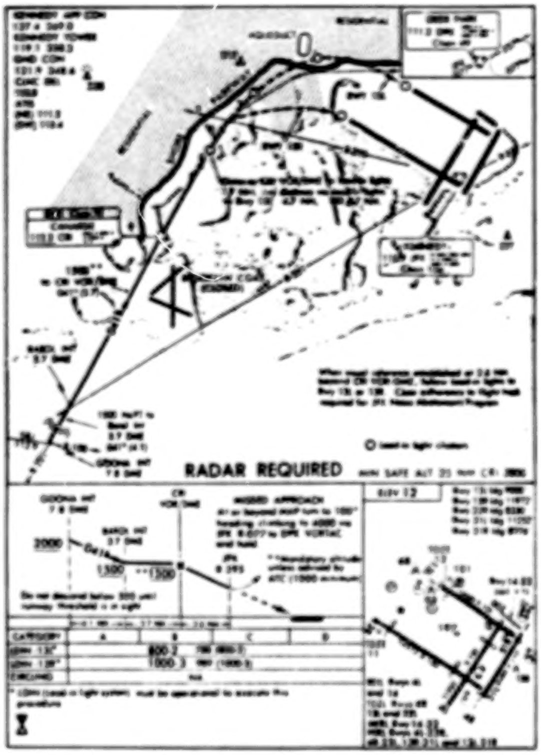
RADAR REQUIRED
2000
1500
1500

Figure 15. - Example of current curved noise abatement approach procedure. (Note: 1 ft = 0.3048 m.)

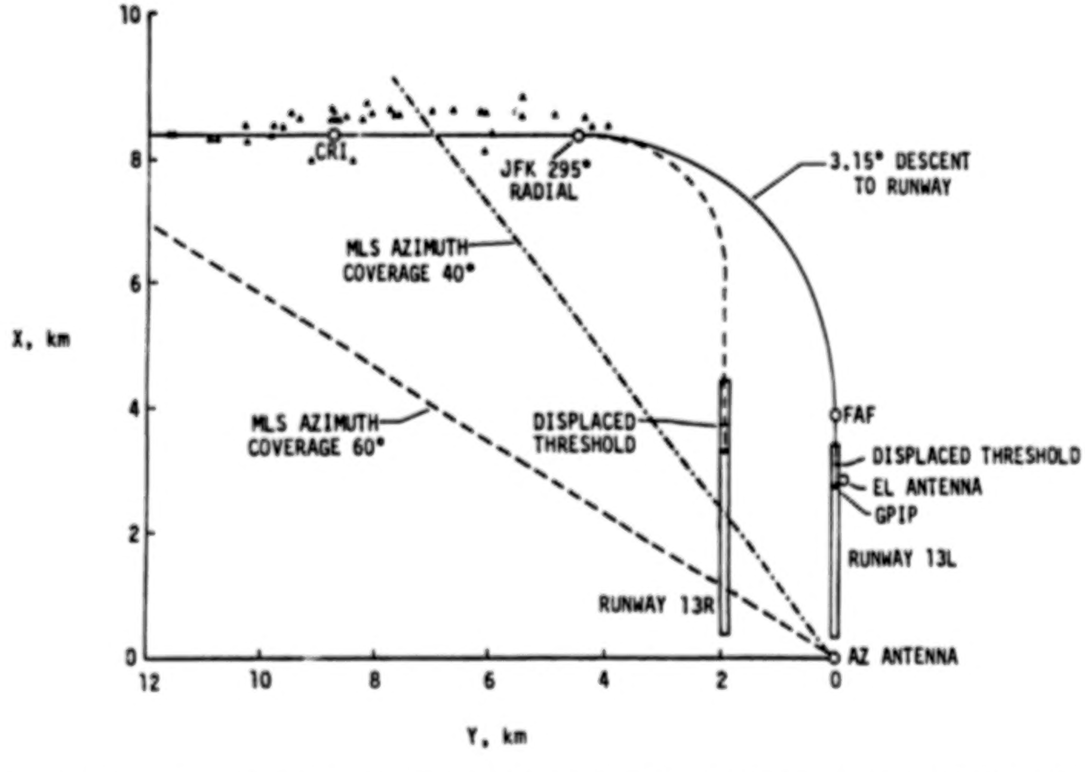

Figure 16.- Summary of conventional-to-MLS RNAV lateral transitions for TCV B-737 approaches to JFK.

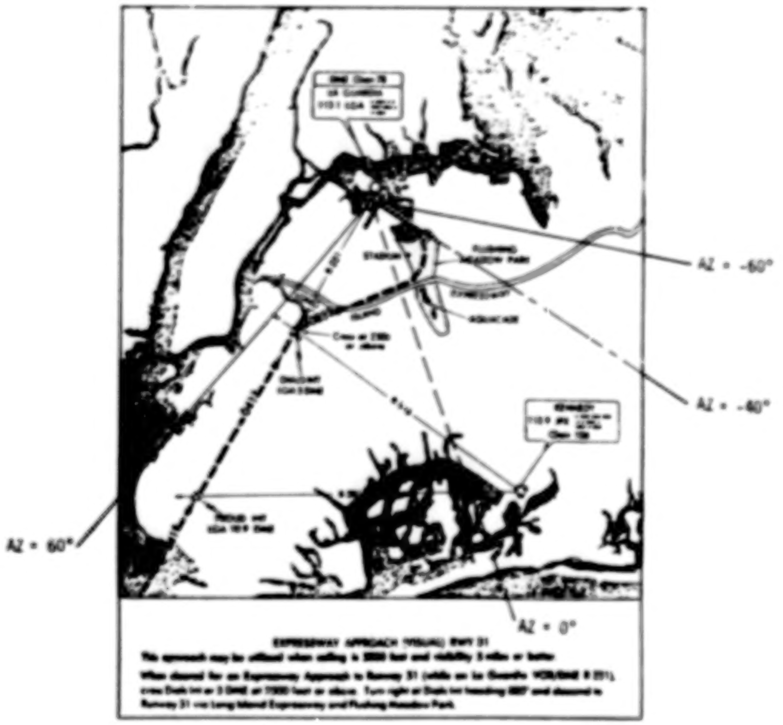
AZ = -60°
AZ = -40°
AZ = 60°
AZ = 0°
EXPRESSWAY APPROACH (VISUAL) RWY 31

Figure 17.- Possible solution to coverage volume problem for La Guardia noise abatement. (Note: 1 ft = 0.3048 m and 1 mi = 1.61 km.)

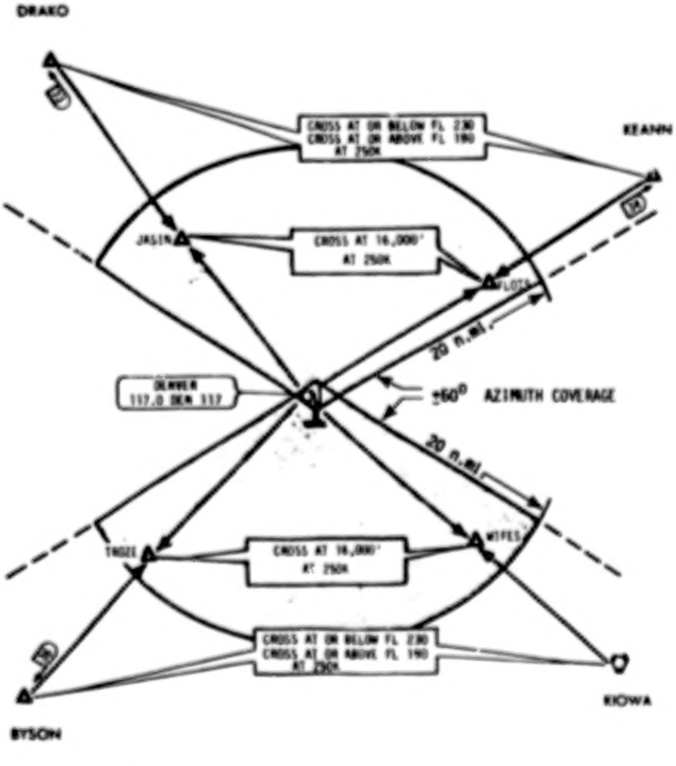
DRAKO
KEANN
CROSS AT OR BELOW FL 230
CROSS AT OR ABOVE FL 190
AT 250K
JASIN
CROSS AT 16,000'
AT 250K
FLOTS
20 n.mi
DENVER
117.0 DEN 117
±60° AZIMUTH COVERAGE
20 n.mi
TROZE
CROSS AT 16,000'
AT 250K
WIFES
CROSS AT OR BELOW FL 230
CROSS AT OR ABOVE FL 190
AT 250K
BYSON
KIOWA

Figure 18.- Possible MLS configuration for Denver terminal area. (Note: 1 ft = 0.3048 m.)

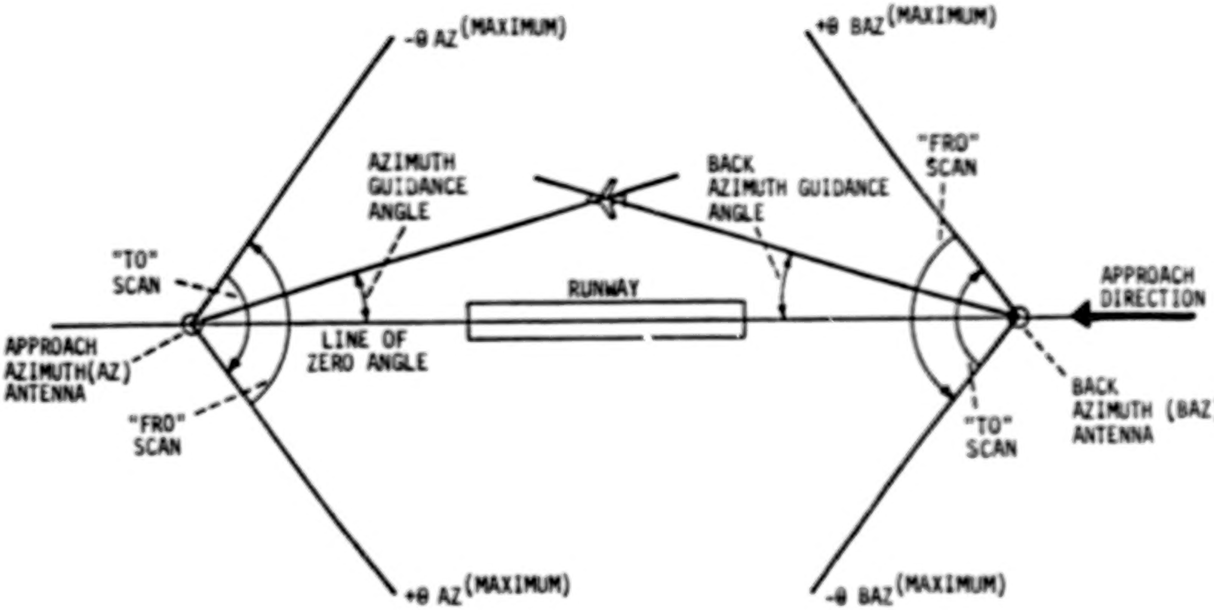
-θ AZ (MAXIMUM)
+θ BAZ (MAXIMUM)
AZIMUTH GUIDANCE ANGLE
BACK AZIMUTH GUIDANCE ANGLE
"FRO" SCAN
"TO" SCAN
RUNWAY
APPROACH DIRECTION
APPROACH AZIMUTH(AZ) ANTENNA
LINE OF ZERO ANGLE
"FRO" SCAN
"TO" SCAN
BACK AZIMUTH (BAZ) ANTENNA
+θ AZ (MAXIMUM)
-θ BAZ (MAXIMUM)

Figure 19.- Azimuth guidance functions scanning conventions.

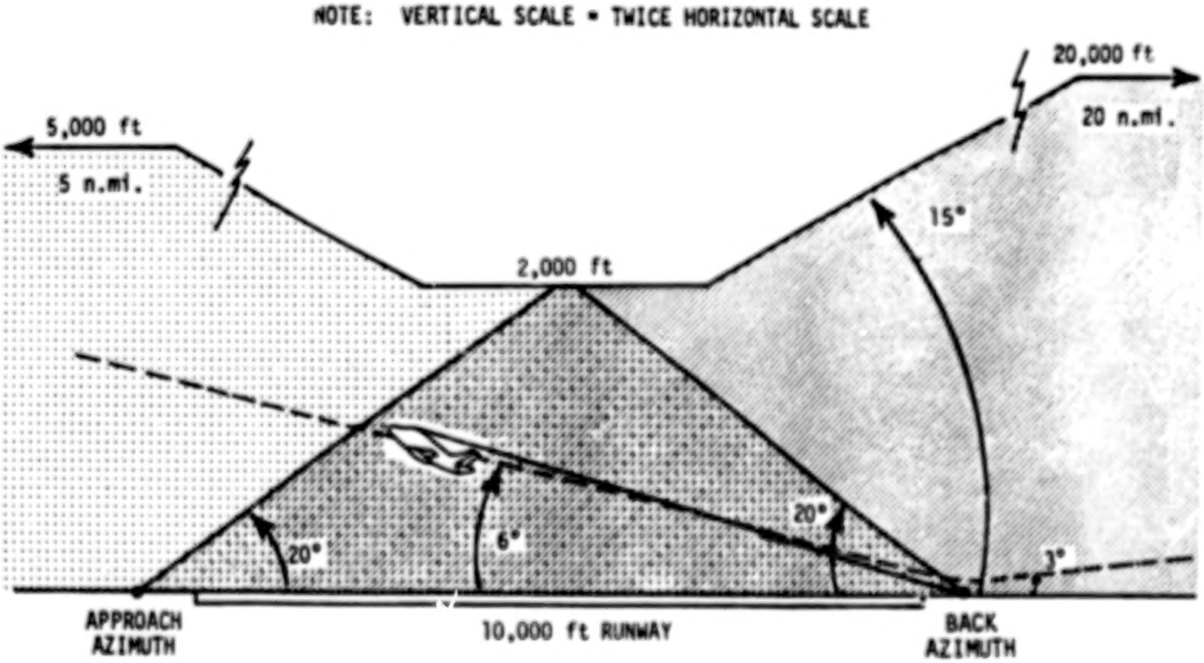
NOTE: VERTICAL SCALE = TWICE HORIZONTAL SCALE
20,000 ft
20 n.mi.
5,000 ft
5 n.mi.
15°
2,000 ft
20°
20°
6°
3°
APPROACH AZIMUTH
10,000 ft RUNWAY
BACK AZIMUTH

Figure 20.- Example of missed approach vertical MLS coverage.
(Note: 1 ft = 0.3048 m.)

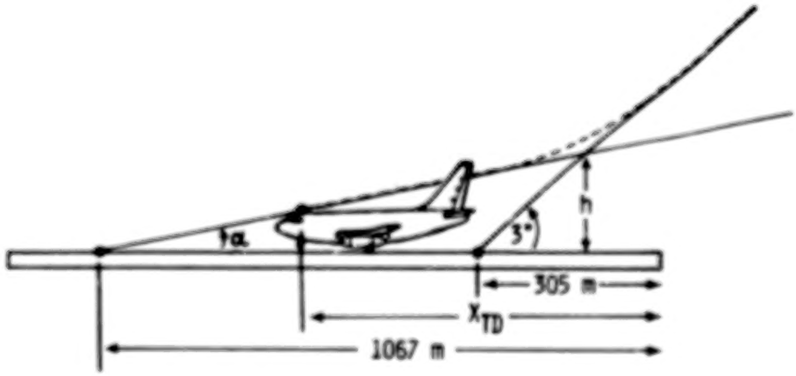

α, deg.	SINK RATE FOR 120 KTS TD, m/s (ft/s)	X_{TD}, m	σ_{TD}, m	h, ft
0.5	0.54 (1.77)	560	149	26
0.6	0.65 (2.12)	645	124	33
0.7	0.75 (2.47)	705	106	40
0.8	0.86 (2.83)	750	93	48

Figure 21.- Alternative method for use of flare guidance system. (Note: 1 ft = 0.3048 m.)

AUTOMATED PILOT ADVISORY SYSTEM TEST AND EVALUATION

AT

MANASSAS MUNICIPAL AIRPORT

John L. Parks, Jr.
Wallops Flight Center
National Aeronautics and Space Administration

INTRODUCTION

It is anticipated that the growth of aviation in the next decade will occur primarily in general aviation thereby placing greater traffic demands on the uncontrolled airport system. Since Air Traffic Control (ATC) services are not normally provided at these airports, automated systems are being evaluated as a means of ensuring safe and orderly air traffic flow at high density uncontrolled airports.

The National Aeronautics and Space Administration (NASA), in cooperation with the Federal Aviation Administration (FAA), has developed an experimental Automated Pilot Advisory System (APAS) (reference 1) to provide airport and air traffic advisories at high density uncontrolled airports. The APAS concept is to utilize low cost automated systems to provide the necessary information for pilots to more safely plan and execute approach and landing at uncontrolled high density airports. The system is designed to be a natural extension of the procedural Visual Flight Rules (VFR) system used at uncontrolled airports and, as an advisory system, will enhance the "see-and-be-seen" rule.

The current system used at uncontrolled airports is for pilots to "self-announce" (traffic advisory) over a UNICOM radio channel and request the active runway (airport advisory) from the Fixed Base Operator (FBO). The UNICOM radio channel is also used for general information and requests, and can be shared by several different airports. For example, the UNICOM at Manassas airport is shared by Manassas, Montgomery County, Warrenton, and Freeport. The problems with this type of system are (1) not all pilots self-announce; (2) the active runway information may not be available (FBO may be absent from the radio performing other jobs, etc.); (3) there may be radio interference due to multiple transmissions; and (4) self-announcement at one airport may be interpreted by pilots at another airport.

The experimental APAS was designed to be a test instrument in which its concept could be evaluated and experiments could be performed to determine the specifications for an operational system. Testing of the experimental system was initially performed at NASA's Wallops Flight Center (WFC) using NASA test pilots, but in late May 1980, the APAS was moved to Manassas Municipal Airport, Manassas, Virginia. This airport was selected because it is a high density uncontrolled airport with an estimated 200,000 operations per year. From June 23, to August 16, 1980, the experimental APAS was operated daily between 9 a.m. and 5 p.m. (9 a.m. to 10 p.m. the week of August 11), and an evaluation of the APAS concept was obtained from pilots who used the system. These evaluations and the system performance are presented.

APAS DESIGN AND CONFIGURATION

In order to implement the APAS concept, the APAS was required to have the following design features:

(1) Low Cost - The system must be affordable to most of the county, municipal, or privately-owned airports in the nation. (A cost limit of $50,000 in 1975 dollars was imposed for the APAS.)

(2) Airport Advisory System - This system should be capable of:

  (a) Issuing a report at least once every two minutes which would include an airport identifier, time of day, favored runway, wind speed, direction and gust, altimeter setting, and ambient and dew point temperatures.

  (b) Automatically selecting the runway and having self-checking features.

  (c) Manual control over runway select and sensor fault via an operator control panel.

  (d) Handling at least five additional sensors.

(3) Traffic Advisory System - This system should be capable of:

  (a) Issuing a report every 20 seconds to identify the number of aircraft on each pattern leg and the position, bearing, and heading of non-pattern aircraft.

  (b) Radar surveillance of a non-cooperative aircraft via a skin tracking radar.

  (c) Radar coverage to five nautical miles.

  (d) Height detection.

  (e) Reporting at least ten (10) aircraft and tracking at least twenty (20) aircraft.

(4) Interface - The APAS should require only a standard Very High Frequency (VHF) radio.

To meet these requirements, the experimental APAS configuration (Figure 1) used at the Manassas airport included a radar set, mini- and micro-computers, weather sensors, a VHF transmitter, and an operator control panel.

Ideally, an APAS radar system should have the following features: solid-state electronics, a Moving Target Indicator (MTI) or Doppler processor for ground clutter elimination, capable of detecting a 0.5 m^2 target at three nautical miles with a 300 meter range resolution, and costing $30,000 in production runs. Studies performed (reference 2) to select the APAS radar indicated that MTI and Doppler type radars were either cost prohibitive (>$250,000) or had insufficient range capability (<1.8 nautical miles). From these studies, it was concluded that the most suitable radar for APAS was the Marine Pathfinder surveillance radar. This non-coherent radar is solid-state, except for a magnetron and modulator switch tube, and requires targets to be detected and tracked in a ground clutter environment. To accomplish this, the APAS used clutter suppression techniques (narrow beam width antennas, Sensitivity Time Control (STC) for each antenna, and a clutter screen set to attenuate Radio Frequency (RF) signals below two degrees elevation), and software target detection algorithms (clutter mapping, thresholding, and mean level).

A single transmit and multiple receive antenna were selected for the APAS to enable the system to determine whether aircraft were at pattern altitude, above pattern altitude, or so high that they were of no interest. For the Manassas configuration, three receive antennas were used and set at 5, 10, and 20 degrees elevation with beam widths of 4, 6, and 13 degrees, respectively. One antenna was scanned 360 degrees every two seconds resulting in a six second target update rate. (Under certain conditions, the signal returned from a target was received in two of the three antennas.)

The mini- and micro-computers were used to provide target detection and tracking, pattern classification, evaluation of weather sensory data, and generation of audio voice messages for transmission to aircraft. The operator control panel provided manual control over runway selection and weather sensory status.

SYSTEM PERFORMANCE EVALUATION

An evaluation of the APAS performance in a high density uncontrolled environment was one of the primary objectives of the Manassas testing. The purpose of this evaluation was to determine the adequacy of system specifications and to ascertain whether any system degradation would occur due to high traffic density or other factors. The primary areas of concern were system cycle time, target detection, tracking, and message rates.

The methods used to evaluate APAS performance included a continual verification of advisory reports and the maintenance of a system anomalies and pertinent data log. Additionally, during two 90-minute periods each day, all traffic advisory reports were recorded and a count was obtained of those reports verified or unverified by radar or visual spotters. Throughout the six-week test period, 95 percent of the APAS reports were verified during the 90-minute counts. The breakdown on the five percent incorrect reports showed that one percent was loss of track on the final leg, one percent were late reports on departing aircraft, two percent were false tracks caused by large earth-moving equipment being used to construct a parallel runway, and one percent was for various other causes. The occurrences of the incorrect final and departure reports were enhanced by earth-moving equipment and site location problems unique to the experimental APAS. These two factors caused a higher-than-normal radar signal to be required for target detection, therefore, decreasing the probability of detection. It should be noted that the APAS software contains a computer code to eliminate problems produced by roadways, but it could not be utilized because the "roadway" for the earth-moving equipment was one-half mile wide.

During the test period, the maximum traffic density occurred on Sunday, July 13, 1980. The total track rate, operation rate, and traffic report histogram data for this day are presented in Figures 2, 3, and 4, respectively. (Total track rate is the number of APAS validated tracks per hour; the operation rate is the sum of take-offs and landings per hour; the traffic report histogram depicts the number of traffic reports containing "N" number of aircraft). This data indicates that the APAS operated for five hours at an operational rate exceeding 50 operations per hour with a peak rate of 70 operations during a one-hour period. Additionally, the system reported its design limit of 10 aircraft on several occasions. System performance measurements during this period indicated: (1) the two-second system cycle time was maintained; (2) no degradation occurred in traffic report accuracy rates (the highest accuracy rate achieved during the six-week test occurred during the five-hour high density period on July 13); and (3) the time for a traffic advisory message exceeded the 20-second period several times, but system software handled this situation by delaying the next advisory by the time overrun.

During this test period, the APAS performance in marginal VFR conditions was mixed. On two occasions, during very hazy conditions, the APAS experienced no performance degradation; on other occasions, in light to moderate rain, the traffic advisory system was turned off because of numerous false target reports. The APAS contains computer software which detects the existence of rain and attempts to maintain pattern reports while deleting traffic reports outside the pattern in the area where the rain occurs. This software was used with favorable results on several occasions during isolated thunderstorms. Although the computer software in the experimental APAS did not contain the proper messages, it appears that the rain detection software could be expanded to handle the moderate rain problems.

The experimental APAS had a seven-to-eighteen second system delay which resulted in aircraft completing a pattern leg turn being reported on the previous pattern leg. This time delay was caused by a combination of the traffic advisory reporting time, the six-second target update rate, and target coast mode following a missed detection. Initial users of APAS expressed concern about the delay, but pilots who continually used the system indicated that, if they didn't locate the traffic reported in a pattern leg, they would instinctively look for traffic on the next pattern leg and, therefore, the delay wasn't a problem.

During the APAS operational period, the Manassas UNICOM voice traffic was significantly reduced. This condition was illustrated by a comparison between the voice traffic which occurred immediately before to that which occurred during short periods in which APAS messages were terminated to store tracking data. During these periods pilots used the self-announcement system. Although measurements were not made to quantize it, the reduction was significant enough to make it obvious to those who monitored the UNICOM frequency.

The only APAS anomaly occurred in the runway selection algorithm, which caused a runway change three times over a five minute period in light and variable winds. An analysis of the problem indicated that the number of runways impacted several input numbers in unforeseen ways. An immediate fix to the problem was implemented by changing the value of an input number, but this fix would negate the universality of the algorithm. A solution to this problem has been proposed but has not been tested.

PILOT EVALUATION

The second objective of the Manassas testing was to obtain pilot evaluations of the APAS concept in the uncontrolled high density environment. To accomplish this, the experimental APAS was operated for an eight-hour period each day for six weeks. An informational package, including a questionnaire was distributed to pilots who used the system and one hundred pilots responded to the questions (Q). Their responses (R) and an authors comment (C) are presented:

Q: Date and time of experience?

R: Not applicable.

Q: Pilot Hours?

R: 50 - 5%
100 - 6%
200 - 12%
500 - 18%
1000 - 17%
>1000 - 42%

Q: a. Function?

R: Pilot - 99%
Co-Pilot - 1%

b. Rating?

Private - 7%
Commercial - 2%
Instrument - 12%
SEL - 28%
Multiple - 51%

Q: Type of aircraft?

R: SEL - 81%
MEL - 16%
Other - 3%

Q: APAS Voice Quality?

R: Unusable - 0%
Confusing - 1%
Satisfactory - 39%
Excellent - 53%
Other - 7% (4% favorable and 3% unfavorable)

Q: Was the airport advisory two minute rate satisfactory?

R: Yes - 89%
No - 11%

C: Most of the no reponses occurred on hazy days when pilots indicated they needed favored runway information more often. The two-minute rate was insufficient because pilots were released from a controlled condition to VFR and tuned to the APAS broadcast after they had the airport in sight. Invariably, some pilots had to fly around the airport for almost two minutes to learn the favored runway from the next airport advisory.

Q: Was the airport advisory message format acceptable?

R: Yes - 92%
No - 8%

Q: Any improvements in airport advisory?

R: No improvement - 38%
Repeat runway more often - 12%
Runway change confusing - 10%
Temperature and dew point information not necessary - 6%
Other - 34%

Q: a. Did you experience a change in active runway?

R: Yes - 18%
No - 82%

C: The APAS selects the favored runway by a technique which is a function of the prevailing winds. When conditions occur which produce a change in the favored runway, the APAS initiates the change by announcing it on the next airport advisory message. On each of the next six traffic advisory reports, which occur between airport advisories, the runway change is announced following the traffic report. The process is completed on the next airport advisory when the favored runway is announced to be the new one.

Q: b. If so, describe your reaction.

R: Dangerous - 22%
Confusing - 28%
Satisfactory - 28%
Orderly - 22%

C: Two occurrences contributed negative responses to this question. The first was the runway change anomoly described in the system performance evaluation where several aircraft were forced to taxi back-and-forth on the taxiway, while the APAS kept changing the favored runway. This occurrence caused several responses that the runway change method was confusing.

The second occurrence resulted from a breakdown in control over the favored runway. Since controlling the runway would be part of any APAS evaluation, an agreement was made with the Manassas airport authorities, whereby the Manassas FBO would direct anyone requesting the favored runway to obtain the information from APAS broadcast. On two occasions this procedure failed and a favored runway, different than the one selected by APAS, was announced on the UNICOM frequency. On both occasions, the result produced was two aircraft simultaneously attempting to land on opposite runways. Announcements were made to divert the aircraft, but several "dangerous" responses were received from pilots.

Q: Was the traffic advisory rate satisfactory?

R: Yes - 89%
No - 11%

C: A non-limiting method was chosen to announce traffic information for the APAS. Non-pattern reports were ordered by azimuth so that pilots could differentiate potential conflicting and non-conflicting aircraft. This method would produce numerous target reports in high traffic densities so the next several questions were designed to evaluate the method.

Q: a. Were you able to identify yourself in the traffic advisory?

R: Yes - 95%
No - 5%

b. How many other aircraft were being reported?

1 - 9%
2 - 13%
3 - 24%
4 - 19%
5 - 19%
6 - 10%
7 - 4%
8 - 1%

Q: Were you able to locate all other traffic in the advisory?

R: Yes - 46%
No - 54%

If no, were you able to locate all traffic presenting a potential conflict?

Yes - 86%
No - 14%

Q: What is your opinion of the traffic advisory?

R: Disastrous - 3%
Confusing - 8%
Satisfactory - 34%
Wonderful - 30%
Other - 25% (19% favorable and 6% unfavorable)

Q: Did you experience any false target reports?

R: Yes - 14%
No - 86%

If yes, was it a problem?

Yes - 45%
No - 55%

Q: Did you site any traffic that was not reported by the system?

R: Yes - 20%
No - 80%

Q: Was the traffic advisory information in a format that you fully understood?

R: Yes - 95%
No - 5%

Q: What is your opinion of the APAS messages vs. self-announcement?

R: Favored APAS - 87.5%
Favored self-announcement - 12.5%

Q: Comments:

R: Favorable - 86.5%
Unfavorable - 13.5%

C: The favorable comments indicated that pilots thought that APAS was a safer system than the self-announcement procedure. The unfavorable comments were in two general areas: system delay and lack of knowledge about pilot intentions.

CONCLUDING REMARKS

The testing at Manassas was the first attempt to evaluate an APAS in a high density uncontrolled environment. As a minimum, this test proved that low-cost automated systems can provide airport and air traffic advisory information at high density uncontrolled airports, and a large majority of the users preferred the APAS over a self-announcement procedure.

The operational performance of the APAS indicated that additional investigations should be conducted in the following areas:

Clutter Suppression.- - Enhancements in clutter suppression will decrease the false target report rate and could solve the final and departing aircraft reporting problem. The enhancements could be made in several ways, such as increasing the height of the antenna platform and optimizing the transmit and receive antennna elevation beam width. It is recognized that an MTI type of radar would solve the clutter problem, and this type radar may be required at some "trouble" airports, but the cost of this solution should be analyzed vs. system affordability.

System Delay.- - Decreasing the system time delay appears feasible without significantly increasing system cost by using a dual receiver radar system and concurrently processing two receive antennas. It is suggested that the lowest elevation antenna be processed every cycle and the two upper elevation antennas be alternately processed. This method should result in a three-to-seven second system delay and have additional benefits such as to increase the range of initial target reporting and decrease the false target report frequency.

Channel Assignments. - - The decrease in UNICOM voice traffic during APAS operations and the APAS requirement of only a 10- to 20-nautical mile broadcast coverage area are significant factors in accessing frequency channel assignments for an operational system. Additional channels for the APAS broadcast may be obtained by assigning more uncontrolled airports the same UNICOM frequency.

The initial objectives of the APAS program have been accomplished in that concept feasibility has been demonstrated and a system description can be defined. It is recommended that a Phase II program be initiated to incorporate the results of the Manassas testing into a follow-on system.

REFERENCES

1. Parker, L. C., et al.: "An Automated Pilot Advisory System," (A paper presented at the 1978 IEEE Region 3 Conference and Exhibit in Atlanta GA, April 10-12, 1978).

2. Haidt, J. G., et al.: "Pilot Advisory System Feasibility Definition Study," Research Triangle Institute, February 1977.

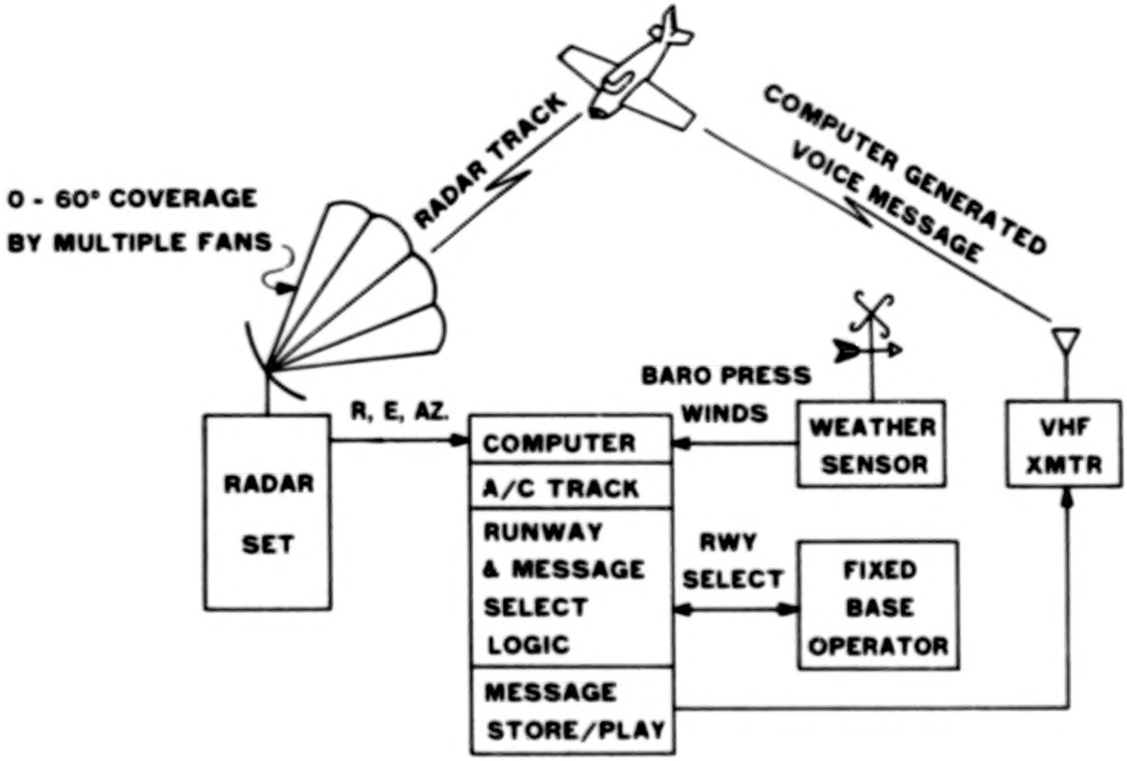
0 - 60° COVERAGE
BY MULTIPLE FANS
RADAR TRACK
COMPUTER GENERATED
VOICE MESSAGE
BARO PRESS
WINDS
R, E, AZ.
RADAR
SET
COMPUTER
A/C TRACK
RUNWAY
& MESSAGE
SELECT
LOGIC
MESSAGE
STORE/PLAY
WEATHER
SENSOR
VHF
XMTR
RWY
SELECT
FIXED
BASE
OPERATOR

Figure 1.- Automated pilot advisory system.

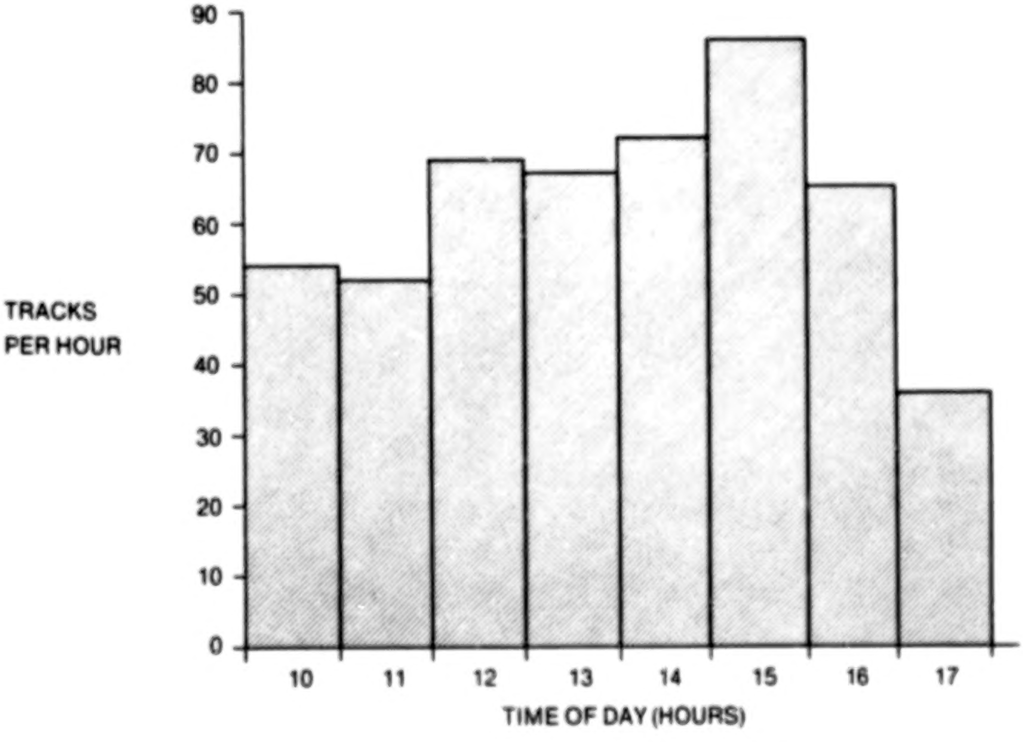

Figure 2.- Track rate - July 13, 1980.

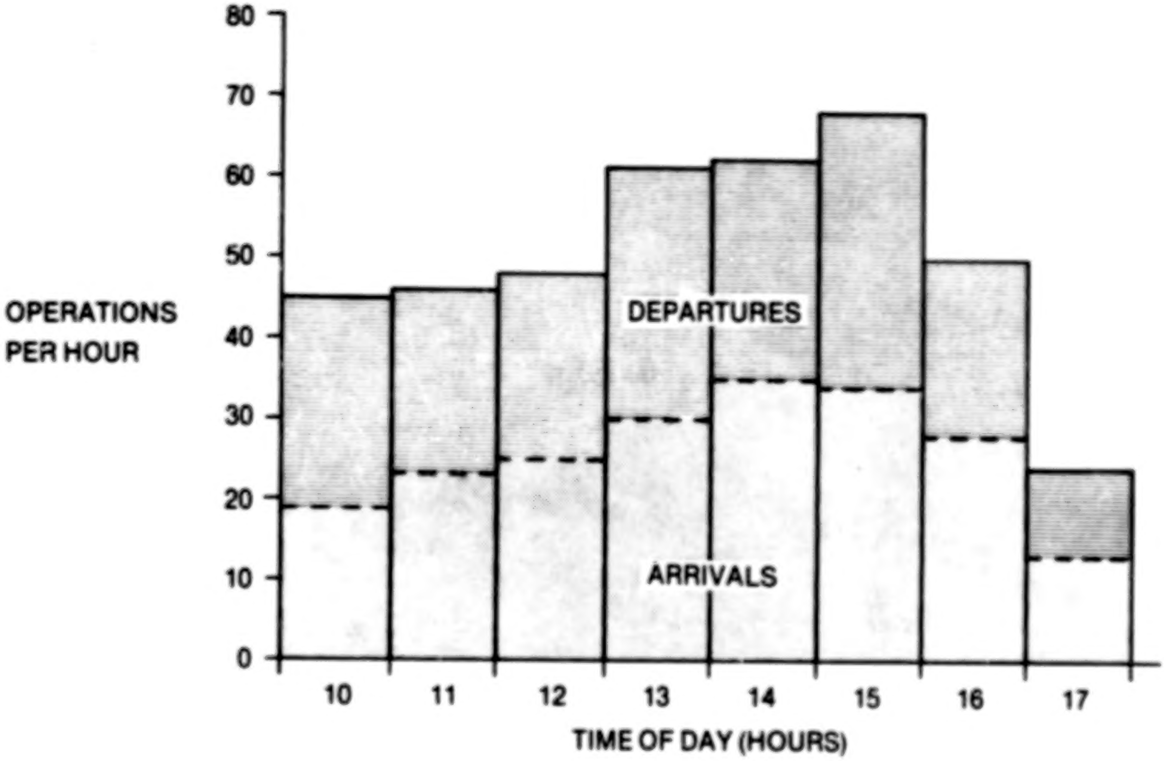

Figure 3.- Operational rate - July 13, 1980.

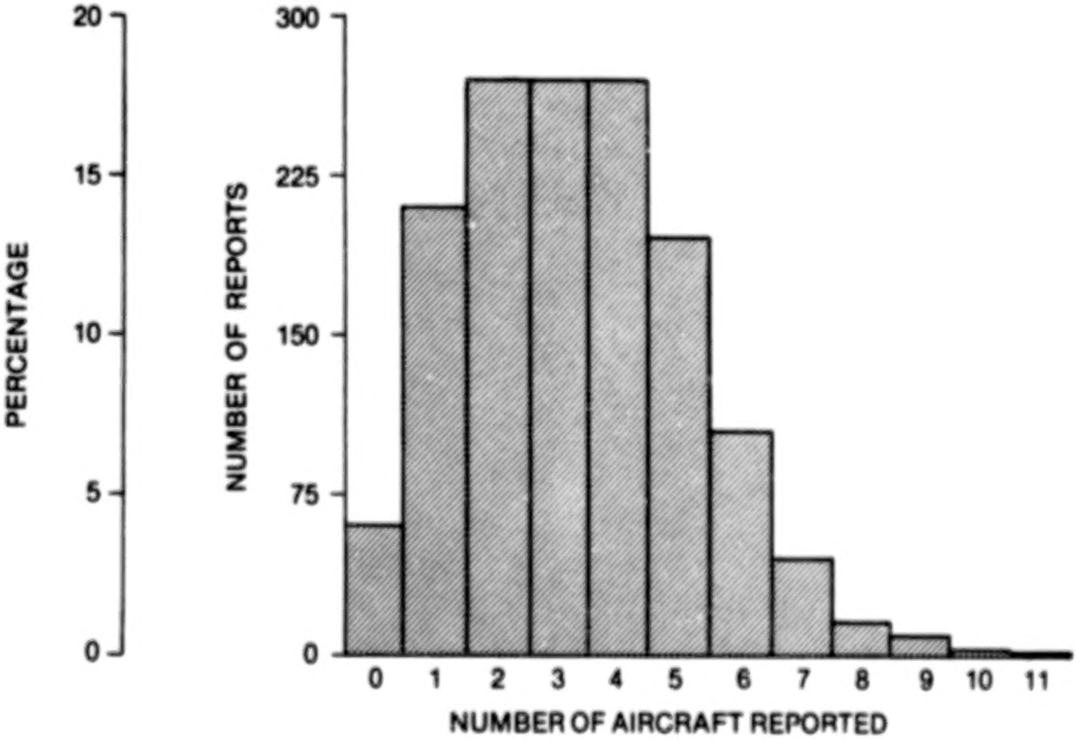

Figure 4.- Traffic report histogram - July 13, 1980.

BLANK PAGE

BLANK PAGE

A METHOD FOR DETERMINING LANDING RUNWAY LENGTH FOR A STOL AIRCRAFT

D. M. Watson, G. H. Hardy, J. F. Moran, and D. N. Warner, Jr.
Ames Research Center

SUMMARY

The certification method that is presently used by the FAA for determining runway landing lengths for conventional transports and that might be applied to STOL aircraft would require longer STOL runways than those envisioned by designers for a metropolitan STOL-port. During the development and evaluation of an automatic landing system for the Augmentor Wing Jet STOL Research Airplane (AWJSRA) this matter of runway lengths was examined. Based on data obtained from flight tests of the AWJSRA, a new method is proposed for determining the length of the landing runway for powered-lift STOL aircraft. The suggested method determines runway landing length by summing three segments: the touchdown-dispersion distance, the transition distance from touchdown to application of brakes, and the stopping distance after brakes are applied. In addition, it is shown how the landing field length can be reduced either through improved autoland system design or by providing the pilot with appropriate information to allow him to identify a "low probability" long or short landing and to execute a go-around.

INTRODUCTION

STOL aircraft have been envisioned as the main element in a high-speed transportation system connecting metropolitan centers, major hub airports, and outlying communities. Basic to such a system is the requirement for safe routine operation into STOL runways. At the present time, the general basis for determining the landing distance performance of a transport category STOL airplane is the airworthiness requirement of Federal Air Regulations (FAR) Part 25 (ref. 1). The operating rule for determining the landing runway length is contained in FAR Part 121 (ref. 2). However, there are developments that might lead to FAR revisions in this area. For example another method, which has been considered for determining an operational runway length requirement, takes into account a specific aircraft and various runway characteristics. To date this method, known as the rational method, has only been applied to the Concorde supersonic transport (ref. 3). The FAA has recognized the need for new airworthiness standards for powered lift STOL transport category aircraft. Proposed Airworthiness Standards for Powered Lift Transport Aircraft, Part XX (ref. 4) presents a method for determining the required landing runway length based on a variation of FAR Part 25 (ref. 1).

Rational method concepts for determining the landing distance are recommended in reference 5. Airport planning recommendations for metropolitan STOL-ports are presented in reference 6.

In addition to the above developments, flight experience has been accumulated for light-wing-loading as well as powered-lift STOL aircraft. For example, reference 7 presents data for a FAA Twin Otter flight-test program that uses a 549-m (1,800-ft) STOL runway with 30-m (100-ft) safety overruns. These data indicate that the Twin Otter is capable of routine operations into the type of STOL-port recommended in reference 6. Considerable data were collected on the landing performance of a specially equipped Twin Otter in the Canadian Air Transportation Administration, Ministry of Transport demonstration program (refs. 8, 9). Satisfactory operation into a 610-m (2,000-ft) STOL runway with 134-m (440-ft) safety overruns was demonstrated. Since the Canadian STOL demonstration, another light-wing-loading turboprop STOL airplane, the deHavilland DHC-7, has begun service into a high-density hub airport (ref. 10). A proposed "stub" runway concept is being evaluated in which the DHC-7 and conventional takeoff and landing (CTOL) aircraft would be allowed to fly simultaneous approaches; the CTOL airplane would land on the main runway, and the DHC-7 would land on an intersecting runway and then stop short of the main runway. Under special STOL conditions for the DHC-7 certification (ref. 11), the airplane can operate into a 594-m (1,950-ft) runway.

Experience with one powered-lift STOL airplane, the McDonnell Douglas Model 188 (Breguet B.R. 941S) has been reported in references 12 and 13. Reference 12, which describes a demonstration program conducted by American Airlines, presents general performance numbers for the airplane but makes no recommendation about the landing runway length. Reference 13 presents landing distance performance data for 60 landings; it notes the need for special factors to cover the effects of wind disturbances, runway conditions, and landing technique for each type of STOL airplane and recommends that a demonstration procedure for rationally determining landing performance replace the current procedures of FAR Parts 25 and 121.

This paper discusses the present runway length certification methods including FAR Parts 25 and 121, special conditions for the DHC-7, the rational method, and the CTOL autoland certification process. This is followed by a detailed discussion of a proposed method for establishing the runway length for STOL aircraft. The present and proposed methods are then compared, using the example of the propulsive-lift STOL aircraft. The report concludes with a discussion of techniques for reducing runway length requirements for STOL aircraft through high touchdown sink rates, or by using special pilot displays to facilitate go-arounds when the pilot sees an out-of-tolerance situation.

PRESENT RUNWAY LENGTH CERTIFICATION METHODS

The certification method used in FAR Parts 25 and 121 and in the rational method can be characterized as a deterministic method. That is, the manufacturer works with the FAA to conduct a limited number of landings and uses data from those landings to arrive at a certified landing distance. The FAA adopts another method, a statistical method, in certifying automatic landing systems, as discussed in Advisory Circular AC 20-57A (ref. 14). The specification states that no more than a certain percentage of the total number of landings shall be outside a specified touchdown region. An application of the statistical method for autoland certification is presented for the L-1011 in reference 15.

A statistical method that has been proposed for determining the landing distance for a STOL transport is discussed in references 16 and 17. Parameters important to the determination of landing distance, such as approach airspeed, touchdown distance, and stopping distance, are evaluated in terms of probabilities. Safety limits are assigned to each parameter. If the pilot determines that any critical parameter exceeds safe limits, he must either execute a go-around or prepare to engage an emergency arresting gear for stopping. The airplane manufacturer must establish through design and testing that the probability of exceeding safety limits on critical parameters is acceptable to the FAA and operators.

Several key issues emerge from a review of references 1 through 17. A conservative method of determining the landing distance performance for transport aircraft is presently used that requires relatively little flight data, is applicable to existing types of operational aircraft, and yet insures safe operations. For STOL aircraft in which heavy emphasis is on maximizing landing performance, investigators of that performance indicate a preference for the rational method but note the difficulty of evaluating the effects of a wide range of atmospheric conditions, runway conditions, and airplane characteristics. Many flight-test landings, supplemented by considerable simulation work, are needed to investigate the performance of each type of airplane. The probabilistic approach presented in references 16 and 17 provides the tool for determining the landing runway length needed for the STOL airplane.

FAR Part 25

Figure 1(a) outlines the procedure presently contained in FAR Part 25 (ref. 1) for determining the flight manual reference landing distance (RLD). The RLD is determined from maximum-effort flight-test data as the horizontal distance required to land and come to a full stop from a point 15 m (50 ft) above the landing surface. As noted earlier, this method is broadly applied to transport aircraft.

FAR Part 121

FAR Part 121 (ref. 2) provides the operating factors that determine the runway length required at the destination airport before a commercial transport can be dispatched to that destination. As shown in figure 1(a), the destination airport runway length required is RLD/0.6 for a dry runway and (RLD/0.6) × 1.15 for a wet runway.

Special Condition for DHC-7

The deHavilland DHC-7 has been certified in the United States under special conditions developed by the FAA (ref. 11). Under this special condition, the STOL landing distance for the DHC-7 is determined for a 7.5° glide slope from the lowest point of the airplane at an altitude of 11 m (35 ft) to stop. The 0.6 factor for the destination airport dry runway length of FAR Part 121 is retained for the DHC-7.

Rational Method for Concorde

The rational method (ref. 3) was developed for transport certification; however, it has been applied only to the Concorde supersonic transport. This method, outlined in figure 1(b), specifies the separate determination of an air segment, a transition segment, and a stopping segment. The air segment begins with the lowest part of the airplane at an altitude of 15 m (50 ft) on a 2.5° glidepath and ends at the point of touchdown. The transition segment begins at the point of touchdown and ends when a deceleration device is applied. The stopping segment is from the point where the braking device is applied to the point where the airplane comes to a stop. The operating portion of the rational method requires that a multiplication factor of 1.15 be applied only to the stopping segment for determining the dry runway length. A wet runway correction factor, determined for each specific runway, can range from 1 to 4. Figure 1(b) shows that the landing runway length is the sum of the air segment, the transition segment, and the factored stopping segment.

CTOL Autoland Certification Process

The autoland certification process for a CTOL jet transport (from ref. 14) is illustrated in figure 1(c). This autoland process provides the method for determining the touchdown zone requirement that is adopted as part of the proposed procedure described in the next section.

PROPOSED METHOD FOR ESTABLISHING THE RUNWAY LENGTH FOR STOL AIRCRAFT

The new method proposed here for determining the landing runway length for a STOL aircraft is a combination of the statistical method used by the FAA for autoland certification (ref. 14) and the rational method developed for the Concorde landing distance certification (ref. 3). Probabilistic data like those used for autoland certification determine the length of runway that must be reserved to accommodate touchdown dispersions. Deterministic data from the rational method determine the distance from touchdown to brake application and the distance from brake application to point of stop.

The touchdown data from the automatic landing system flight tests provide an example for the application of the proposed method. These tests were conducted by Ames Research Center using a powered-lift STOL airplane. The test airplane, which is referred to as the Augmentor Wing Jet STOL Research Airplane (AWJSRA), is shown in figure 2 and is described in reference 18. These flight tests were conducted using a microwave landing system (MLS). An automatic landing system (described in ref. 19) was utilized in the tests. An operationally oriented flight-director system for flying curved descending approaches (described in ref. 20) has also been flight-tested on the AWJSRA.

General Method

The landing runway length needed for a powered-lift STOL airplane is proposed to be determined as the sum of three segments (fig. 3): a touchdown-probability-dispersion distance, a transition-segment distance, and a factored stopping-segment distance. The touchdown-dispersion distance is determined using the method that is used for automatic landing system certification (ref. 14); it is illustrated in figure 1(c).

The rationale for the use of the transition and stopping segments in the determination of runway landing length is well established in connection with the rational method (ref. 3) and will be adapted for determining the STOL runway landing length. However, the rationale for use of touchdown-probability dispersion requires some explanation.

From the outset, in considering this problem, it appeared that a conservative approach must be used, with emphasis on taking maximum advantage of the capability of an automatic landing system to accurately control the landing touchdown point. As previously noted, it appeared that the "Automatic Landing System Criteria" of reference 14 meet the above requirements. Moreover, enough experience has been gained in the certification of autoland systems for CTOL aircraft, using the criteria of reference 14, to make this approach a credible one.

In essence, the longitudinal touchdown dispersions about a nominal point on the runway must be demonstrated in flight. Sufficient flight-test data are usually obtained to define the $2\text{-}\sigma$ probability landing dispersions. These flight-test results are then backed up by a suitable computer or simulation analysis, which extends the landing dispersion estimate to the $4\text{-}\sigma$ to $5\text{-}\sigma$ level; that is, to the determination of the improbable-event touchdown distance. This latter "dispersion" distance is the third segment, which is summed with the transition and stopping segments to define the proposed landing runway length for STOL aircraft.

The method of determining the touchdown probability distribution is well established for automatic landing systems. Unfortunately, a comparable method applicable to manual landings has not been developed. In order for this proposed method to be useful for a manually flown airplane, a suitable procedure for extrapolating manual flight-test data to account for the improbable event will be needed. Extrapolating flight data on the basis of an assumed probability distribution is the procedure employed in reference 7. Another possible procedure would require the development of a suitable pilot model for use in a high-speed simulation. Still a third possible procedure is to accumulate operating experience from a large number of landings, using instrumented airplanes.

The next four sections will describe the determination of the touchdown dispersion, the transition segment, and the stopping segment from the AWJSRA autoland flight test and simulation data.

Touchdown Dispersion

Figure 4 shows touchdown data presented in the form of a probability distribution plot. The data are plotted on paper on which a normal probability distribution appears as a straight line. These data were obtained from both flight test and high-speed computer simulation for the best performing of several autoland control laws examined (ref. 19). The circles in figure 4 represent the probability distribution data for 31 flight-test automatic landings; the solid line represents more than 10,000 samples of data obtained from high-speed computer simulation. The abscissa shows the touchdown distance measured with respect to the MLS glidepath intercept point (GPIP). The ordinate shows the probability that the touchdown distance will exceed the abscissa value. The shaded vertical band in figure 4 represents the 61-m (200-ft) STOL-port marked touchdown zone shown in figure 2. The touchdown dispersion for any probability level can be read from the simulation data in figure 4. For example, there is a 97.7% ($2\text{-}\sigma$ short landing) probability that the airplane will land longer than 34 m (110 ft) and a 2.3% ($2\text{-}\sigma$ long landing) probability that the airplane will land longer than 157 m (515 ft). The difference between the $2\text{-}\sigma$ short landing and the $2\text{-}\sigma$ long landing is the $2\text{-}\sigma$ touchdown dispersion.

The 31 flight-test landings provide (1) a good estimate of the mean value and the $1\text{-}\sigma$ performance of the autoland system, (2) a poorer estimate of the $2\text{-}\sigma$ performance, and (3) no estimate at all of the low-probability performance. The low-probability performance is estimated by first validating the simulation with flight-test data and then using the simulator to generate the low-probability performance. Figure 4 shows agreement between the flight and simulation data, provided differences in the flight and simulation wind disturbances are taken into account. The wind disturbances encountered in flight were less than the reference 14 wind model disturbances used for the simulation. The steeper slope of the flight data probability distribution curve in figure 4 is the result of lighter wind disturbances. The difference in the mean touchdown distance between flight and simulation is the result of a residual modeling discrepancy coupled with the fact that the range was not explicitly controlled in the AWJSRA autoland system. The match between the simulation and flight data is believed to be adequate to establish the validity of the simulation data.

The FAA has allowed 10^{-6} to define the improbable event for a recent autoland certification (ref. 15). Figure 4 shows that the touchdown dispersion for a 10^{-6} probability is 297 m (970 ft); this is the value that will be used later to define the STOL runway landing length. References 16 and 17 present another view on the probability level to use in determining the required runway landing length for a STOL-port. If the pilot had the means of detecting that the airplane would land outside an acceptable touchdown region, a go-around could be executed. References 16 and 17 state that from an airline point of view no more than 1×10^{-3} approaches should result in a go-around. One landing in 1,000 means that the probability of landing short is $1 - (0.5\times10^{-3})$ and the probability of landing long is 0.5×10^{-3}. Using the simulation data from figure 4, the touchdown dispersion for 1×10^{-3} landings is 203 m (665 ft).

Transition and Stopping Segments

Transition and stopping segment time histories are shown in figure 5 for three levels of braking performance: maximum, moderate, and minimum. To execute a maximum-performance stop, the pilot applied the antiskid brakes installed on the main wheels of the AWJSRA as firmly as possible until the airplane came to a stop. It should be noted that the pilots object to maximum antiskid operation because of attendant longitudinal jerk (i.e., rate of change of acceleration).

Figure 5(a) shows a typical maximum-performance time history of longitudinal acceleration and distance from touchdown to stop. A maximum-performance stop is characterized by a rapid change in deceleration from 0 to -0.4 g in 0.5 sec followed by two cycles of antiskid brake operation before a near steady state -0.42 g is achieved.

Figure 5(b) shows a moderate-performance time history. The pilot applied brakes gradually to avoid antiskid brake cycling, taking 10 sec to achieve a steady-state deceleration of -0.42 g. The difference between maximum and moderate performance appears to be the rate of onset of deceleration rather than the steady-state deceleration. A typical time for achieving the steady-state deceleration was 2.5 sec; this onset time will be used for subsequent stopping segment calculations.

Figure 5(c) shows another type of stop that can be denoted either as a minimum-performance stop or as "turn off at the next taxiway" (located beyond the end of the STOL runway markings). In this case, following an initial deceleration, the airplane was allowed to coast until near the second turnoff after the touchdown zone, at which time light braking was applied just before the turn.

Transition segment- During the transition segment, the pilot of the AWJSRA must reduce thrust, lower the nose of the airplane from the 6° pitch attitude, which was commanded by the automatic landing system, and begin applying the brakes.

Figure 6 shows transition-segment data as a function of groundspeed for minimum-performance stops and for maximum- and moderate-performance stops. The transition-segment distance varied randomly from 40 m (131 ft) to 88 m (290 ft) for the maximum- and moderate-performance stops and was beyond 91 m

(300 ft) for the minimum-performance stops. The transition-segment samples obtained during the flight tests do not show a trend with groundspeed; nevertheless, such a trend would be expected. This trend might have become evident if the pilots had been asked to minimize transition-segment distance as well as the overall touchdown-to-stop distance. In any case, the transition-segment distance for the maximum- and moderate-performance landings never exceeded 91 m (300 ft); this number will be used for subsequent determinations of required runway landing length.

Stopping segment- The distance that must be available for stopping an airplane is simply computed by integrating a longitudinal acceleration profile. Figure 7 shows the stopping distance computed for a range of wind speeds and for an assumed moderate longitudinal acceleration profile like that seen in figure 5(b). The braking commences at the end of the transition segment with a typical AWJSRA calibrated airspeed V_c of 55 knots. Accelerometer data recorded during AWJSRA performance landing stops show peak deceleration levels of -0.42 g. However, the -0.35 g deceleration profile curve matches the recorded moderate stopping distance apparently because of reduced average deceleration associated with antiskid brake cycling.

Figure 7 shows that the longest stopping distance occurs in a tailwind. The pilot will generally avoid a tailwind situation, but in rapidly changing wind conditions, a tailwind can develop during the approach. Therefore, a conservative runway landing length should be based on a 10-knot tailwind. For a 10-knot tailwind and a -0.35-g deceleration profile, the dry runway stopping distance is 204 m (670 ft).

References 21 and 22 show that very long stopping distances can occur due to hydroplaning if the runway is flooded. These references also indicate that if the runway is grooved, a flooded runway need only be 10% longer than a dry runway to insure equivalent stopping performance. References 6, 16, and 17 conclude that a grooved and heated runway will be a necessary feature of an all-weather STOL-port. In the comparison of methods of determining runway landing length that follows, a division factor of 0.9 is assumed to be adequate for determining the length of the grooved runway needed in wet conditions.

References 21 and 22 also indicate that a maximum deceleration of -0.55 g is possible if the airplane is equipped with antiskid brakes on the nosewheel as well as on the main wheels. If the AWJSRA had been equipped with antiskid brakes on all wheels, a steady-state deceleration of -0.45 g would probably have been possible. Figure 7 shows that the stopping distance in a 10-knot tailwind with a -0.45-g average deceleration is 169 m (555 ft).

COMPARISON OF METHODS

Figure 8 summarizes the runway landing lengths needed for both the FAR Parts 25 and 121 method and the proposed method. Based on a maximum-performance landing conducted with the AWJSRA, the FAR Part 25

15-m-altitude-to-stop (50-ft-altitude-to-stop) reference landing distance would be near 409 m (1,340 ft). Applying the FAR Part 121 destination-airport factor of 0.6 results in a required dry runway landing length of 680 m (2,230 ft). Applying the 1.15 factor results in a wet runway landing length of 782 m (2,570 ft). Both the dry and wet runway landing lengths exceed the recommended (ref. 6) STOL-port runway length of 457 m (1,500 ft) to 549 m (1,800 ft).

If the 11-m-to-stop (35-ft-to-stop) provision of the special STOL condition for certification of the DHC-7 is applied to the maximum-performance landing of the AWJSRA, the reference landing distance would be 366 m (1,200 ft). The destination-airport factor of 0.6 results in a required runway landing length of 610 m (2,000 ft). This distance also exceeds the runway length recommended in reference 6.

The proposed-method runway landing length is the sum of a touchdown-probability distribution determined as for autoland certification (ref. 14), a transition-segment distance, and a factored stopping-segment distance from the rational method (ref. 3). The 10^{-6} improbable-event touchdown probability distribution of 296 m (970 ft) summed with the 91 m (300 ft) transition segment distance and a factored stopping distance of 204 m (670 ft) results in a dry runway landing length of 622 m (2,040 ft), which still exceeds the recommended STOL-port length. In this case, the stopping distance is based on the main wheel and antiskid brakes installed on the AWJSRA and on the 1.15 factor applied only to the stopping distance as adopted from the rational method. The assumed additional 10% factor for a wet grooved and heated runway increases the runway landing length to 649 m (2,130 ft).

If the airline point of view from references 16 and 17 is adopted (1 out of 1,000 approaches can result in a go-around) and if the airplane is assumed to be equipped with antiskid brakes on all wheels, the runway landing length is within the STOL-port runway length recommended in reference 6. In this case, the dry runway landing length is 488 m (1,601 ft) and the grooved-and-heated wet runway length is 510 m (1,673 ft).

TECHNIQUES FOR REDUCING RUNWAY LENGTH REQUIREMENTS

The touchdown dispersion results presented in this paper were obtained with an automatic landing system that was designed to produce the low touchdown sink rates (near 1 m/sec (3 ft/sec)) found in contemporary CTOL autoland systems, but to do so for a powered-lift STOL airplane flying a 7.5°-glideslope landing approach. Improved touchdown dispersions can probably be achieved by using a range feedback term in the autoland control law and by accepting higher touchdown sink rates. However, such improvements in automatic landing system design are no aid in reducing the touchdown dispersion for manually flown approaches. There is an acute need to find a way — equally applicable to both automatic and manually flown systems — to reduce touchdown dispersion.

As noted earlier, one way to reduce the runway landing length needed for a STOL airplane is to execute go-arounds for those landing approaches that will be outside a desired touchdown region. The key element in this procedure is a display that will provide the pilot with an indication of the touchdown point.

Some form of cockpit display, perhaps integrated into a head-up display, is needed for approaches in near-zero visibility and ceiling conditions. Two such display concepts have undergone preliminary evaluations on the AWJSRA, which was equipped with an electronic attitude display indicator (EADI) as shown in figure 9 and described in reference 23. The EADI incorporated a perspective runway and a path-deviation box. The perspective runway was intended to provide the pilot with a simple picture of the runway during the approach. This display provides some measure of both range and range rate. The path-deviation box shows glide slope and localizer error on the approach down to the flare height. This sort of raw data information is presently used down to the decision height but not below. For the AWJSRA evaluation the path-deviation window was mechanized to show errors from a reference flare path throughout the flare maneuver, thereby providing the pilot with an indication of a long or short landing. A brief evaluation of this mechanization of the path-deviation window was conducted with the AWJSRA. Although the EADI displays appeared to provide the desired range-error information, the pilot was not inclined to ride through the flare with his head down. Further research in conjunction with a head-up display is needed to determine if the pilot can perceive and react to a range-error display in time to execute a satisfactory go-around maneuver.

CONCLUDING REMARKS

A systematic method for defining the runway landing length for a STOL transport has been developed. In this method the runway length is composed of the sum of three segments: the touchdown-dispersion distance, the transition-segment distance from touchdown to the application of a braking device, and the stopping-segment distance after a braking device is applied. The method combines statistical and deterministic data.

The proposed method appears to determine a safe runway landing length for the STOL application and offers the potential for reducing runway length if great emphasis is placed on a short-runway capability. FAR Parts 25 and 121 appear conservative and suitable for the situation where no great emphasis is placed on reducing the runway length requirement.

Work directed at techniques to shorten the landing runway length requirement is under way. Cockpit displays, which would permit the pilot to reject long or short landings, appear to have the greatest potential for reducing required runway landing lengths.

REFERENCES

1. Federal Air Regulations, Part 25.125.

2. Federal Air Regulations, Part 121.195.

3. Merritt, Leslie R.: Concorde Landing Requirement Evaluation Tests. Report No. FAA-FS-160-74-2, Federal Aviation Administration, Aug. 1974.

4. Tentative Airworthiness Standards for Verticraft/Powered Lift Transport Category Aircraft. Flight Standards Service, Department of Transportation, Federal Aviation Administration, Part XX, July 1968.

5. Scott, Barry C.; Hynes, Charles S.; Martin, Paul W.; and Bryder, Ralph B.: Progress Towards Development of Civil Airworthiness Criteria for Powered-Lift Aircraft. FAA-RD-76-100; also NASA TM X-73124, 1976.

6. Planning and Design Criteria for Metropolitan STOL Ports. FAA, AC 150/5300-8, Federal Aviation Administration, Nov. 1970.

7. Spangler, Roman M., Jr.: Simulated Ground-Level STOL Runway/Aircraft Evaluation. FAA-RD-73-110, Federal Aviation Administration, Sept. 1973.

8. Bentham, Richard P.: Some DHC-6 Twin Otter Approach and Landing Experience in a STOL System. AGARD-CP-160, 4 Apr. 1974, pp. 19-1 to 19-11.

9. Rosewarne, H. P.; and Spruston, D. D.: The Canadian STOL Demonstration — The Data Collection, The Findings and Their Applications. ICAS Paper 76-53, Oct. 1976.

10. Ransome Begins Dash 7 Service Today. Business Aviation, Oct. 16, 1979, p. 123.

11. Special Conditions for DeHavilland Aircraft of Canada Model DHC-7 Airplane. Special Conditions, No. 25-53-EA-10, Federal Aviation Administration.

12. Final Report - Inter-Metropolitan STOL Evaluation (Phase X). American Airlines Development Engineering Report No. 50, Jan. 1970.

13. Innis, Robert C.; Holzhauser, Curt A.; and Quigley, Hervey C.: Airworthiness Considerations for STOL Aircraft. NASA TN D-5594, 1970.

14. Automatic Landing Systems (ALS). FAA, AC 20-57A, Federal Aviation Administration, 12 Jan. 1971.

15. Shah, N. M.; Gevaert, G.; and Lykken, L. O.: The Effect of Aircraft Environment on Category III Autoland Performance and Safety. AIAA Paper 72-811, Danvers, Mass., 1972.

16. Ransone, R. K.: Proposed STOL Definition and Field Length Criteria. J. Aircraft, vol. 8, no. 12, Dec. 1971, pp. 971-976.

17. Ransone, R. K.: STOL - Creating a Good Neighbor. Astronaut. & Aeronaut., Dec. 1970, pp. 30-35.

18. Ashleman, R. H.; and Skavdahl, H.: The Development of an Augmentor Wing Jet STOL Research Airplane (Modified C-8A), vol. I - Summary. NASA CR-114503, 1972.

19. Feinreich, B.; Gevaert, G.; Hardy, G. H.; and Watson, D. M.: A Comparison of Flight and Simulation Data for Three Automatic Landing System Control Laws for the Augmentor Wing Jet STOL Research Airplane. NASA CR-152365, 1980.

20. Hindson, W. S.; Hardy, G. H.; and Innis, R. C.: Evaluation of Several STOL Control and Flight Director Concepts from Flight Tests of a Powered-Lift Aircraft Flying Steep, Curved Approaches. NASA TP-1641, 1980.

21. Drinkwater III, F. J.; Major Price, C.; Patton, J. M. Jr.: Research Pilot's Observations of Aircraft Performance on a Grooved Runway. NASA SP-5073, 1968, pp. 115-122.

22. Yager, Thomas J.: Comparative Braking Performance of Various Aircraft on Grooved and Ungrooved Pavements at the Landing Research Runway, NASA Wallops Station. NASA SP-5073, Nov. 1968, pp. 35-65.

23. Neuman, Frank; and Warner, David N., Jr.: A STOL Terminal Area Navigation System. NASA TM X-62348, 1974.

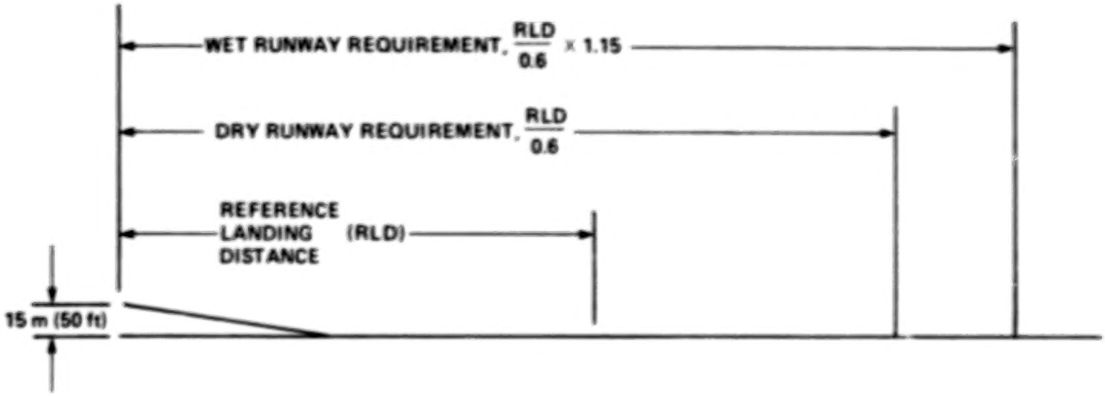
WET RUNWAY REQUIREMENT, $\frac{RLD}{0.6} \times 1.15$
DRY RUNWAY REQUIREMENT, $\frac{RLD}{0.6}$
REFERENCE LANDING DISTANCE (RLD)
15 m (50 ft)

(a) Method of FAR Parts 25 and 121.

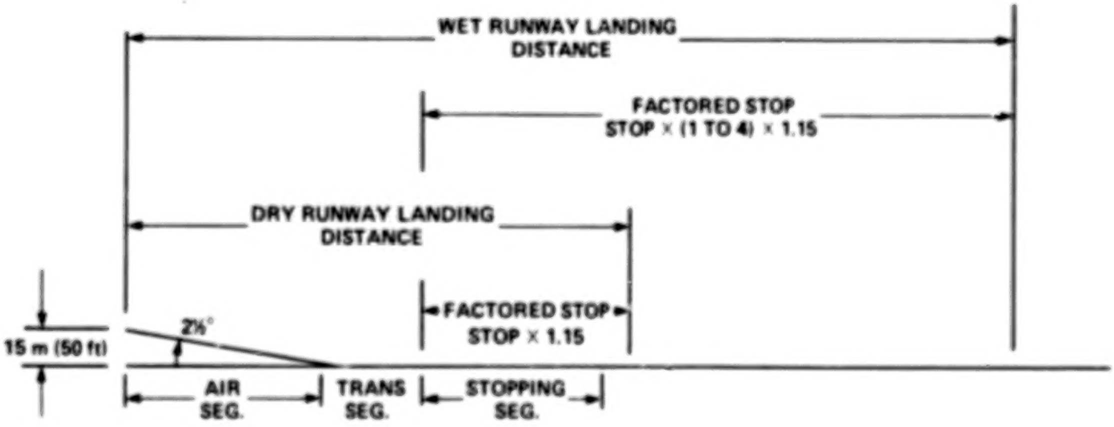
WET RUNWAY LANDING DISTANCE
FACTORED STOP
STOP × (1 TO 4) × 1.15
DRY RUNWAY LANDING DISTANCE
FACTORED STOP
STOP × 1.15
2½°
15 m (50 ft)
AIR SEG.
TRANS SEG.
STOPPING SEG.

(b) Rational method for Concorde.

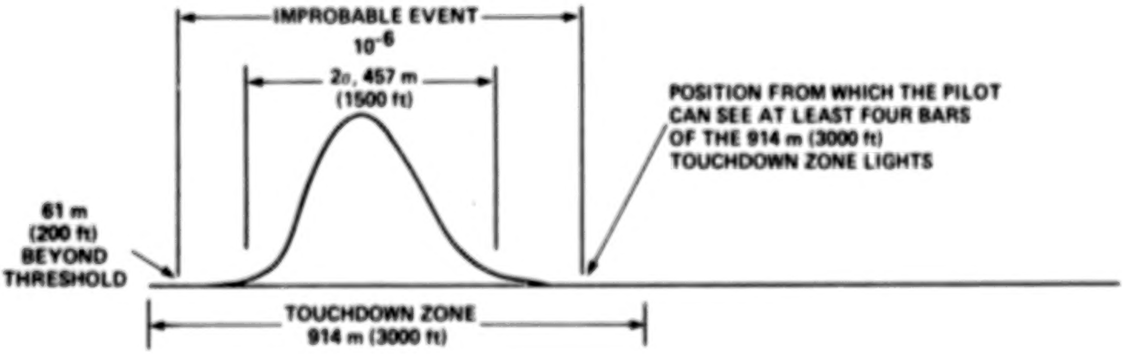
IMPROBABLE EVENT
10^{-6}
2σ, 457 m (1500 ft)
POSITION FROM WHICH THE PILOT CAN SEE AT LEAST FOUR BARS OF THE 914 m (3000 ft) TOUCHDOWN ZONE LIGHTS
61 m (200 ft) BEYOND THRESHOLD
TOUCHDOWN ZONE 914 m (3000 ft)

(c) Autoland requirement.

Figure 1.- Present certification methods.

Figure 2.- The Augmentor Wing Jet STOL Research Airplane on an automatic landing approach to a 518-m (1,700-ft) microwave-landing-system-equipped STOL-port located at the Crows Landing Navy Auxiliary Landing Field, California.

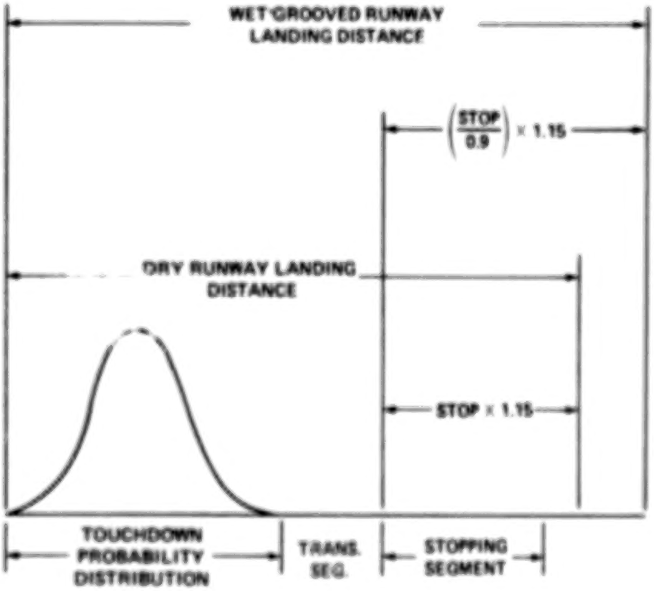
WET GROOVED RUNWAY LANDING DISTANCE
$\left(\frac{STOP}{0.9}\right) \times 1.15$
DRY RUNWAY LANDING DISTANCE
STOP × 1.15
TOUCHDOWN PROBABILITY DISTRIBUTION
TRANS. SEG.
STOPPING SEGMENT

Figure 3.- Proposed method for STOL autoland.

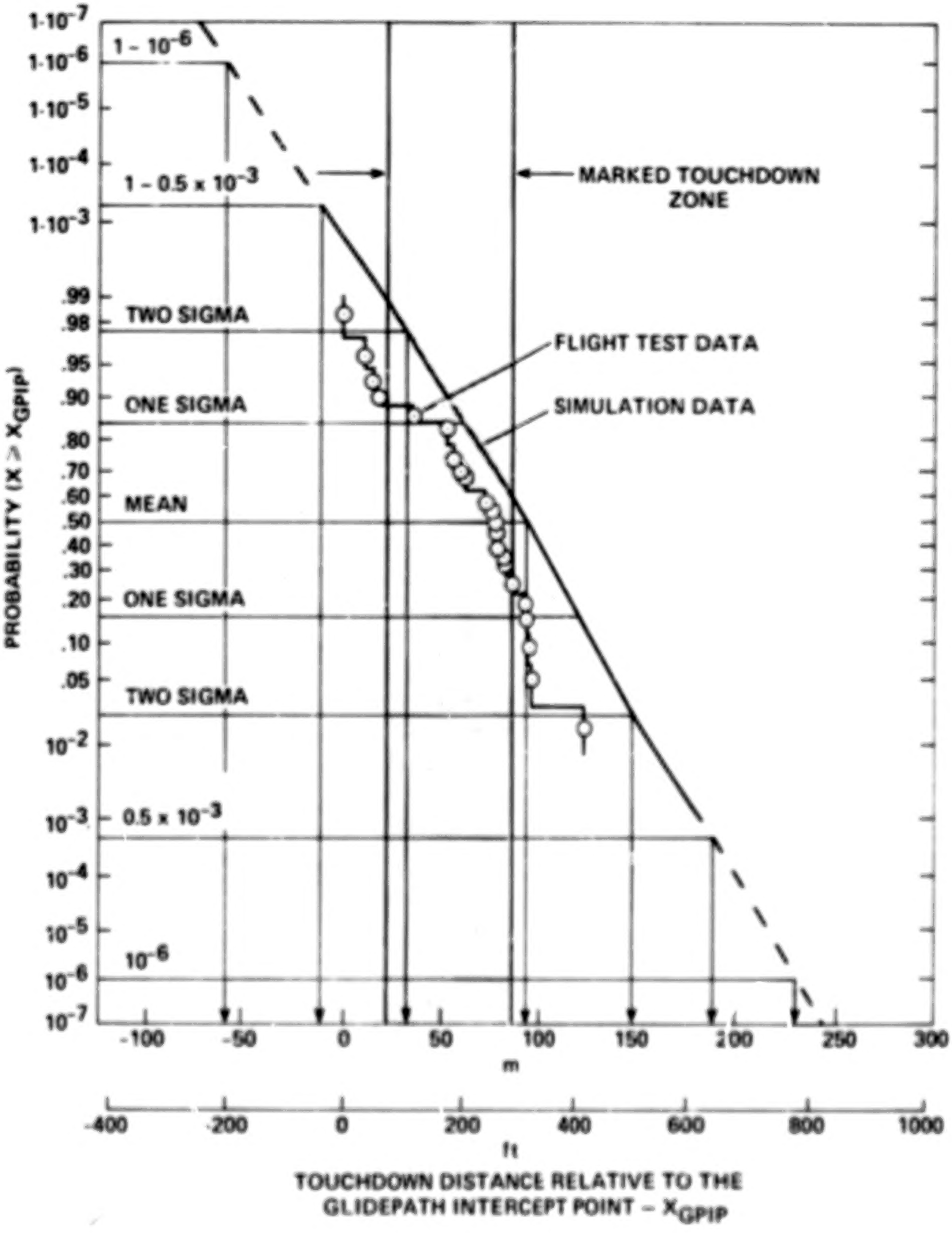

Figure 4.- Touchdown probability distribution for the AWJSRA autoland system.

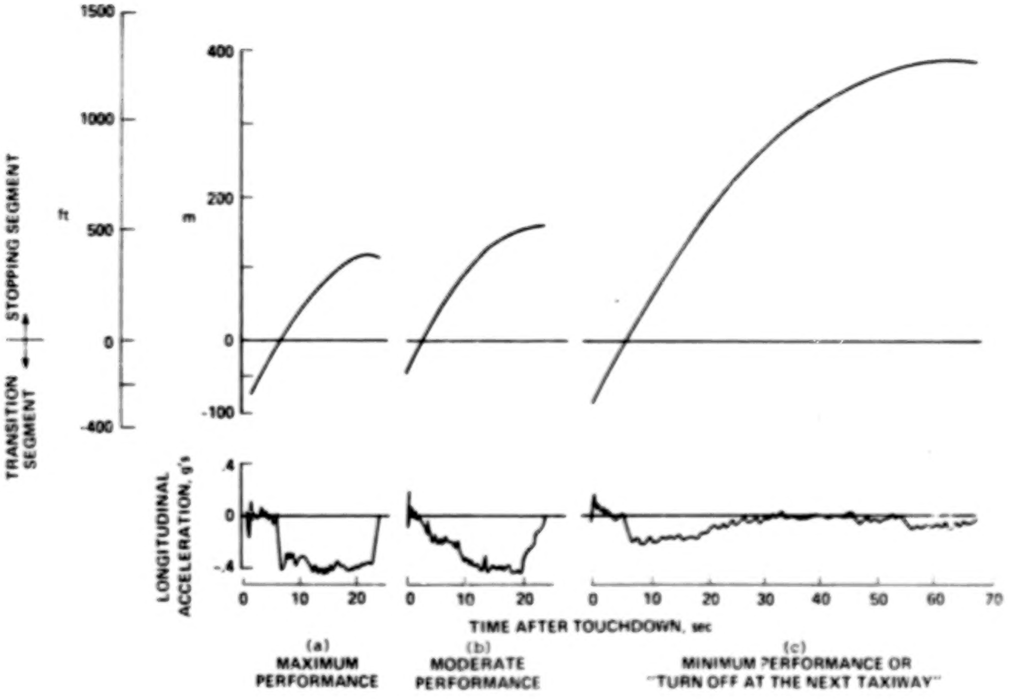

Figure 5.- Transition and stopping segment time histories.

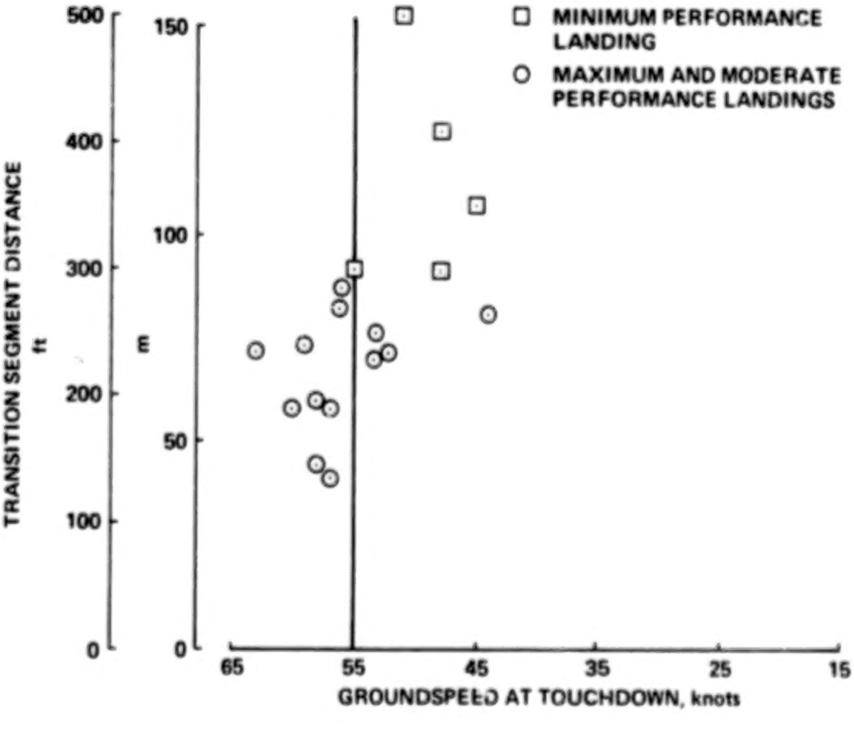

Figure 6.- Transition segment distance as a function of touchdown groundspeed.

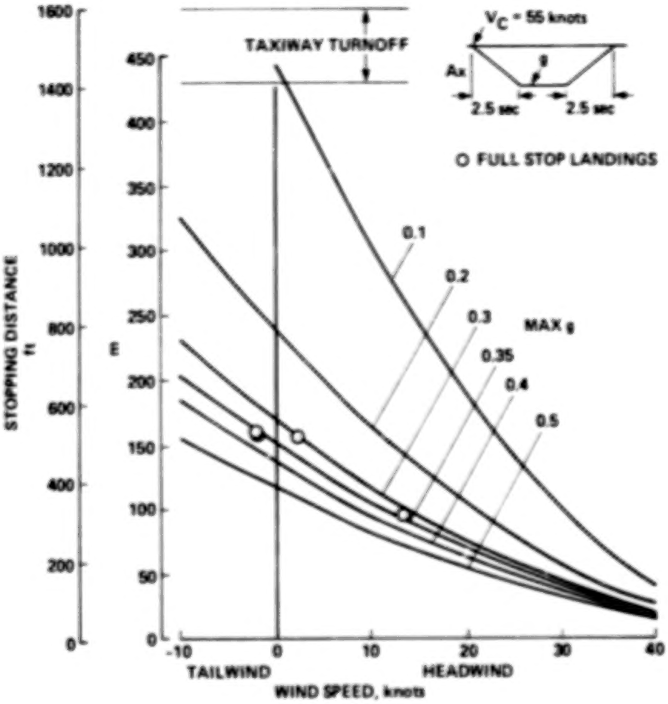

Figure 7.- Moderate-performance stopping distance as a function of windspeed.

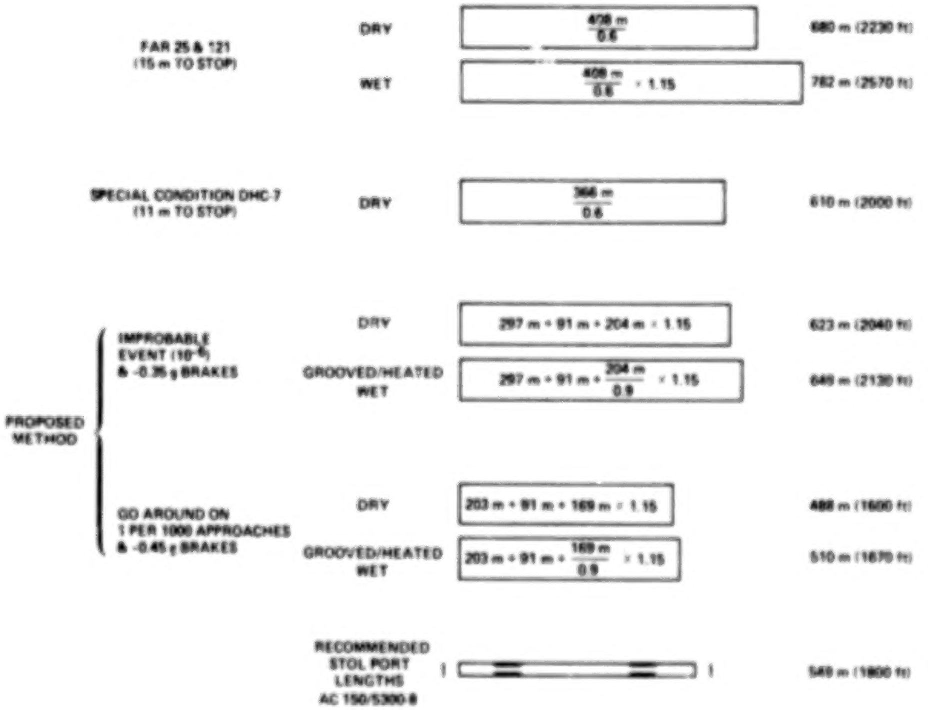
FAR 25 & 121
(15 m TO STOP)
DRY
$\frac{408\ m}{0.6}$
680 m (2230 ft)
WET
$\frac{408\ m}{0.6} \times 1.15$
782 m (2570 ft)
SPECIAL CONDITION DHC-7
(11 m TO STOP)
DRY
$\frac{366\ m}{0.6}$
610 m (2000 ft)
PROPOSED
METHOD
IMPROBABLE
EVENT (10^{-6})
& -0.35 g BRAKES
DRY
297 m + 91 m + 204 m × 1.15
623 m (2040 ft)
GROOVED/HEATED
WET
$297\ m + 91\ m + \frac{204\ m}{0.9} \times 1.15$
649 m (2130 ft)
GO AROUND ON
1 PER 1000 APPROACHES
& -0.45 g BRAKES
DRY
203 m + 91 m + 169 m × 1.15
488 m (1600 ft)
GROOVED/HEATED
WET
$203\ m + 91\ m + \frac{169\ m}{0.9} \times 1.15$
510 m (1670 ft)
RECOMMENDED
STOL PORT
LENGTHS
AC 150/5300-8
549 m (1800 ft)

Figure 8.- Comparison of methods for determining landing runway length.

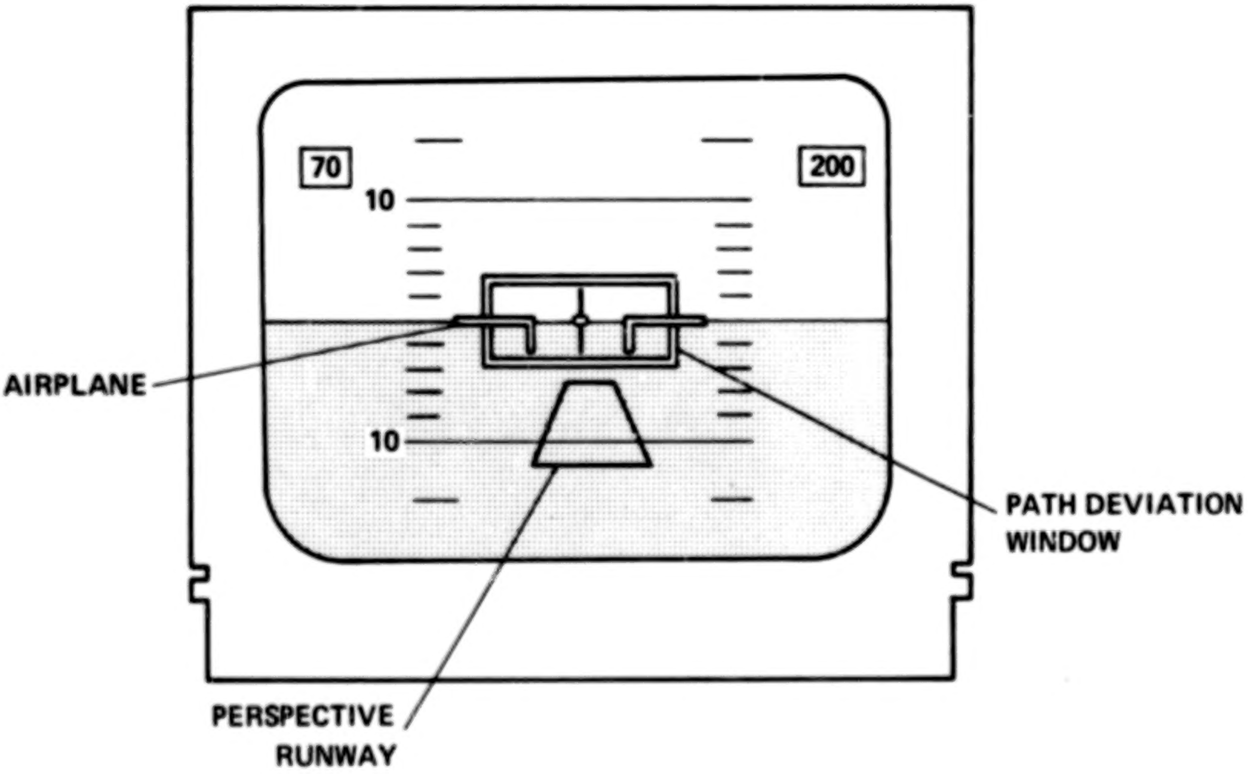
70
200
10
10
AIRPLANE
PATH DEVIATION WINDOW
PERSPECTIVE RUNWAY

Figure 9.- Electronic attitude director indicator.

FLIGHT TESTS OF IFR LANDING APPROACH SYSTEMS FOR HELICOPTERS

J. S. Bull, D. M. Hegarty, L. L. Peach, J. D. Phillips,
D. J. Anderson, D. C. Dugan, and V. L. Ross
Ames Research Center

SUMMARY

The helicopter section of the U.S. Standard for Terminal Instrument Procedures (TERPS) was first issued in 1970, when only a few civilian helicopters were IFR certified and operations under Instrument Flight Rules (IFR) were very limited. In the subsequent decade, there has been considerable technological progress in the helicopter industry, and there has been a significant increase in civilian IFR operations. Thus, there exists a need to update the existing helicopter TERPS criteria in order that civilian operators may take maximum advantage of the helicopter's unique flight capabilities.

In response to this need for the establishment of new helicopter TERPS criteria, the Ames Research Center and the FAA Flight Standards National Field Office have conducted two joint flight-test investigations: (1) airborne radar approaches (ARA) and (2) microwave landing system (MLS) approaches. The first flight-test investigation consisted of helicopter IFR approaches to offshore oil rigs in the Gulf of Mexico, using weather/mapping radar, operational pilots, and a Bell 212 helicopter. The second flight-test investigation consisted of IFR MLS approaches at Crows Landing (near Ames Research Center), with a Bell UH-1H helicopter, using NASA, FAA, and operational industry pilots. The purposes of the flight tests were to (1) provide the FAA with statistical data for establishment of TERPS criteria and (2) provide NASA with a data base to serve as a performance measure for advanced guidance and navigation concepts.

INTRODUCTION

In the past decade, there has been increased utilization of the helicopter for transportation into remote sites as well as into high-traffic-density hub airports. Concurrent with this increased transportation utilization is a significant increase in operation under instrument flight rules (IFR). For example, the growth of the helicopter offshore transportation industry has been stimulated in recent years by the accelerated development and exploration of the Nation's offshore oil resources (ref. 1). To avoid flight cancellations or delays caused by unfavorable weather conditions, airborne weather/mapping radar has been developed by the operators as a "self-contained" navigation aid for landings on sites where there are no ground-based navigation aids. Operational implementation of the new National Microwave Landing System, which is also under way (ref. 2), will provide an expanded IFR landing approach capability particularly suited to the helicopter's unique flight characteristics. The airborne selectable glide slope and offset radial features of the microwave landing system (MLS) will permit greater approach-path flexibility, which can be utilized in noise abatement, minimum airspace, and traffic separation procedures for high-density hub airport operations.

The current edition of the U.S. Standard for Terminal Instrument Procedures (TERPS) (ref. 3) contains no criteria relative to helicopter instrument approaches that utilize either airborne radar or MLS as the primary navigation source. Operators are currently using airborne radar approach (ARA) procedures that have been approved by the FAA on a regional basis; however, these procedures have not been approved as a national standard, as would be set by TERPS. In addition, since precision MLS instrument approaches will offer many advantages to helicopter operators over the conventional instrument landing system (ILS) approach, there is a need to update existing helicopter TERPS criteria in order that civilian operators may take maximum advantage of ARA and MLS instrument approach procedures.

In response to this need, Ames Research Center and the FAA Flight Standards National Field Office have conducted two joint flight-test investigations: (1) airborne radar approaches (ARA) (refs. 4, 5, 6) and (2) microwave landing system (MLS) approaches (ref. 7). The first flight-test investigation consisted of helicopter IFR approaches to offshore oil rigs in the Gulf of Mexico, using weather/mapping radar, operational pilots, and a Bell 212 helicopter. The second flight-test investigation consisted of IFR MLS approaches at Crows Landing (near Ames Research Center), with a Bell UH-1H helicopter flown by NASA, FAA, and operational industry pilots. The purposes of the flight tests were to (1) provide the FAA with statistical data for establishment of TERPS criteria and (2) provide NASA with a data base to serve as a performance measure for development of advanced guidance and navigation concepts. The specific flight test objectives were to:

1. Develop procedures
2. Measure total system errors
3. Measure navigation equipment errors
4. Measure flight technical errors
5. Determine acceptable weather minimums

This paper presents the results of these two Joint NASA/FAA helicopter flight tests.

TEST DESCRIPTION

General Test Plan

The general plan for conducting both flight tests was to (1) include operational pilots in the tests, (2) conduct approaches "under the hood" for IFR simulation, (3) conduct both landings and missed approaches, and (4) conduct a sufficient number of approaches to allow for statistical analysis of flight envelopes.

Airborne Radar Approach (ARA) Test Description

Flight tests of helicopter airborne radar approaches were conducted using a Bell 212 helicopter (fig. 1); a cluster of seven oil platforms, located about 15 miles south of Intracoastal City, Louisiana, in the Gulf of Mexico, was used as landing sites. The tests consisted of 15 flights, 15 pilots, and 120 approaches, with both pilot and copilot hooded for simulated instrument conditions. A "chase" plane insured separation from traffic in the test area. Aircraft tracking was accomplished by triangulating range data from responders located on three separate oil rigs such that the approach area was totally covered. Cameras in the helicopter were used to photograph the cockpit radar display and a radar repeater display. The test aircraft was also equipped with a palletized data acquisition system for recording basic flight data. Pilot acceptability ratings were recorded for each approach; questionnaires, filled out by the pilots after their flights, provided more detailed comments and recommendations.

Microwave Landing System Test Description

Flight tests of MLS approaches were conducted using a NASA Bell UH-1H helicopter (fig. 2) and a simulated STOLport at Crows Landing, an Ames Research Center flight-test facility. Crows Landing is equipped with a basic narrow time reference scanning beam (TRSB) MLS ground system. The approach envelope provided by the MLS system was ±40° in azimuth and 0-15° in elevation. Fourteen pilots from various elements of the helicopter community flew 140 manual-mode (without stability augmentation) simulated instrument approaches under the "hood." Various performance parameters and radar tracking data were monitored in real time, and pilot opinion ratings were recorded during the flight tests. Digital tape recordings of these and other data were provided for postflight analysis. A comprehensive pilot questionnaire was also completed by participating pilots.

TEST RESULTS: AIRBORNE RADAR APPROACH

ARA Procedures

A typical airborne radar approach flight profile is depicted in figure 3. The instrument approach is a high workload operation that requires two pilots. The copilot operates and interprets the radar display and acts as a "GCA" controller in giving the pilot heading and altitude commands. As the aircraft approaches the target oil platform, the copilot first determines the wind direction and plans the approach so that the final approach segment will be flown directly into the wind. If the destination rig is in a cluster of platforms, the approach is planned to a platform on the downwind edge of the cluster so that the final approach segment is clear of obstructions.

After "overheading" the target rig, a descending turn is made to 152 m (500 ft) and to a heading within ±10° of the reciprocal of the final approach heading. The distance flown on the outbound leg is "dead reckoned" because the target rig "blip" is lost from the radarscope after passing overhead. The outbound heading is held for 3 min and a level procedure turn is made, at an altitude of 152 m (500 ft) and an airspeed of about 90 knots, to the final approach inbound heading.

The final approach begins after the aircraft crosses the downwind final approach fix (DWFAF) located 4 n. mi. from the target rig. The aircraft is slowed to an airspeed of 60 knots, and a rate of descent is initiated that will allow the aircraft to be leveled off at a minimum-descent altitude for missed-approach altitude, at about 1-2 n. mi. from the target rig. At the missed-approach point (MAP), the copilot commands the pilot to execute a missed approach if the copilot does not have the target rig in sight. If the copilot has the target rig in sight at the missed-approach point he takes command of the aircraft and performs the landing.

Two different types of MAPs were investigated: (1) a MAP located on the straight-in final approach path, and (2) a MAP laterally offset from the straight-in final approach path. The lateral offset MAP is arrived at by making a 15° aircraft heading change at 1 n. mi. from the target platform and holding the heading until the MAP range is reached. In either case the missed-approach procedure consists of a climbing turn to clear adjacent rigs in the cluster and return to the initial approach fix.

ARA Display on Typical Approach

The weather-mapping radar used in these tests had two modes of operation: beacon and primary. In the beacon mode the radar displays only those signals that are received from radio beacon transponders. In the primary mode the radar displays all radar target returns and is commonly referred to as a "skin paint" mode. The radar display presented to the copilot as the aircraft headed south from Intracoastal City across the Gulf coastline is shown in figure 4. The radar is being operated in the primary mode ("skin paint") on the 40-n. mi.-range scale which has 10-n. mi. range-mark increments. The high density of oil platforms and clusters of oil platforms in the Gulf of Mexico, which is apparent in figure 4, presents the copilot with a difficult task in correctly identifying the destination platform. In order to satisfactorily identify the target platform, the copilot must be intimately familiar with the local area or have additional position information provided by some other available navigation aid, such as VOR/DME, Loran-C or a beacon transponder located on or near the target rig. The destination cluster of seven oil platforms used in these tests is shown on the display at a range of about 18 n. mi. from the aircraft and about 5° left of the aircraft heading.

The radar display that results as the aircraft completes the procedure turn and initiates the final approach segment is shown in figure 5. The target oil platform is shown dead ahead of the aircraft at about 4-1/4 n. mi. Radar display "blips" for three oil platforms are separated; however, display "blips" for three other platforms are still merged at about 5 n. mi. as one target due to poor resolution and excessive gain control. Also showing, on the radar display, merged as one target at about 5-1/2 n. mi., are two ships that were passing through the area.

The radar display that results after the aircraft has progressed far enough on final approach for the copilot to switch to the 5-n. mi.-range scale (1-n. mi. range-mark increments) is shown in figure 6. The target oil platform is still dead ahead at about 3-1/2 n. mi., and three platforms are still merged; however, the two ships are now displayed as separate targets.

The radar display resulting after switching to the 2.5-n. mi.-range scale (0.5-n. mi. range-mark increments) is shown in figure 7. The target platform is dead ahead at about 1-1/4 n. mi., and all platforms are now displayed as separate targets. One platform has passed off the scope down and to the left. The copilot would continue to give the pilot heading commands to bring the target platform "blip" down the center cursor of the radar display until the leading edge of the target met the 1/2-n. mi. range mark, at which point a landing or missed approach would be executed.

ARA Target Mididentification

The test crews unanimously agreed in their postflight pilot questionnaires that the most difficult task in making an airborne radar approach to a cluster of oil platforms is target identification. This conclusion is strongly supported by the test results. Of the 90 approaches conducted in primary mode to the seven-rig test cluster, 5 were made to wrong target platforms, and 5 others were made to ships in the area; that is, 11% of the primary-mode radar approaches were conducted to incorrect targets. The difficulty of target identification is illustrated in the typical display shown in figure 7. Due to the wide radar antenna beam width (8°), targets are elongated in azimuth, making pattern recognition very difficult; there is further confusion if ships are in the area. If a beacon is located in the destination oil rig cluster, use of the beacon mode can aid target identification. However, there are very few beacons at offshore oil rigs, and future installations are uncertain because of the expense and possible conflict of beacons with maritime radars.

There is usually no hazard associated with incorrect target identification, if a missed approach is not required; the pilot can simply locate himself upon arrival at the wrong platform and fly to the correct platform in the cluster. A serious problem can be created, however, in the event a missed approach is executed from the wrong target because the aircraft may not have sufficient obstruction clearance.

In contrast with an approach to an oil rig cluster, an approach to single rig does not present such a serious target-identification problem. In the case of a single-rig approach, transient shipping presents the only target identification difficulty.

ARA Final Approach Lateral Flight Envelope

The minimum descent altitude in these tests was not based on vertical obstacle clearance, as is the case in conventional instrument approaches. Rather the aircraft was flown at minimum descent altitudes on final approach that placed it below the tops of some surrounding oil rigs. This was made possible by relying on the airborne radar to provide sufficient lateral clearance from obstacles in the area and using the radar altimeter to provide necessary vertical clearance from the water surface. Thus, to help establish criteria that will provide satisfactory lateral obstacle clearance, it is important to analyze statistically the actual ground track relative to the intended ground track of the final approach (ground track that passes through the downwind final approach fix). An ensemble plot of individual final approaches is shown in figure 8. The individual final approach ground tracks indicate that the aircraft crews accepted initial cross-track deviation at the DWFAF and simply flew homing-type approaches by keeping the target platform centered on the radar display. The mean and 2-sigma cross-track deviations of final approach ground track relative to intended final approach ground track are shown in figure 9. The 2-sigma "envelope" can be closely approximated by a ±30° sector about the intended final approach track. Thus, if the final approach area is clear of known oil platforms within ±30° of the selected final approach ground track, there is a 95% probability (2-sigma) of incurring only shipping or other transient obstacles.

ARA Missed Approach Lateral Flight Envelope

The acceptability of weather minimums for instrument approaches is largely determined by resulting obstacle clearance provided in the missed-approach procedure. Lateral obstacle clearance from the target platform of missed approaches conducted in these tests, using the laterally offset MAP, is shown in figure 10. The mean missed-approach ground track had a minimum lateral clearance from the target platform of 625 m (2,050 ft) with a 2-sigma deviation of ±427 m (±1,400 ft). Based on these statistics, the probability of overflying the target platform into the cluster area is 0.2%, if the distribution is assumed to be normal.

ARA Weather Minimums

Weather minimums recommended by the subject test pilots are shown in table 1. It is significant that although 25% of the approaches were conducted to 1/4-n. mi. minimums for test purposes, none of the 15 pilots recommended that 1/4-n. mi. minimums be operationally approved for either primary- or beacon-mode approaches. Most of the pilots recommended that 61 m (200 ft), 1/2-n. mi. weather minimums be approved, but a considerable number felt that 91 m (300 ft), 1/2-n. mi. minimums would be appropriate; a few thought that the approved minimums should even be higher in both altitude and visibility.

TEST RESULTS: MICROWAVE LANDING SYSTEM

MLS Approach Procedures

In order to determine "worst case" airspace requirements, MLS approaches were flown using raw data guidance (glide slope and localizer only) without the aid of stability augmentation, flight director, or DME. The flight profiles flown by the 14 evaluation pilots included 3°, 6°, and 9° glide-slope, centerline approaches to decision heights of 15, 30, and 46 m (50, 100, and 150 ft), respectively. A 20°, lateral-offset approach was also flown on a 3° glide slope to a decision height of 61 m (200 ft).

Approach plates for each of the flight-test profiles were provided to the evaluation pilots for use during the approaches. A typical approach plate is shown in figure 11 depicting the appropriate headings, fixes, decision heights, and missed-approach procedures. The final approach was conducted at constant airspeed, and deceleration for landing was performed under visual conditions after the decision height was reached.

Decision heights for the runway centerline approaches were established to provide an approximate constant range of 305 m (1,000 ft) from the DH to glidepath intercept point (GPIP). A 15-m (50-ft) DH for 3° glide slope, 20° offset radial approach was not possible at this facility because MLS glide-slope guidance signal was lost on the 20° azimuth radial at an altitude just under 61 m (200 ft) (because of antenna coverage geometry of the "split-site" facility - azimuth antenna 1341 m (4,400 ft) past the elevation antenna). Thus, a 61-m (200-ft) DH was used for the 20° offset radial approaches.

MLS Final Approach Lateral Flight Envelope

A composite plot of the lateral tracking for 6° glide-slope approaches on runway centerline is shown in figure 12(a). The 2-sigma lateral flight envelope for the approaches in the composite plot is shown in figure 12(b). Shown on both approach plots is a plan view of the STOLport to which the approaches were conducted. The short dashes on either side extend from runway threshold to the end of the STOLport (610 m (2,000 ft)) and represent the lateral course window (±107 m (±350 ft)) at the 30 m (100-ft) decision height. The reference flightpath is depicted by the dashed line; the dotted lines indicate the full-scale limits of the course deviation indicator (CDI) instrument. Therefore, the lateral flightpath plots show graphically the relative position of the CDI needle displacement, throughout the approach, as seen by the pilot.

In figure 12(b), the mean ground track and small 2-sigma flight envelope for the approaches indicate good lateral tracking performance. The slight bias to right of centerline is probably related to the prevailing left-to-right cross winds which occurred during most of the flight tests. The 2-sigma lateral flight envelope boundary corresponds to about a 1/2 dot deflection on the pilot's CDI instrument. The lateral dispersion at the 30-m (100-ft) decision height window is shown in figure 13. Also shown in figure 13 for comparison are the "2-dot" CDI window and the conventional ILS CAT II window. The mean lateral flightpath at the 30 m (100-ft) decision height window was 5 m (17-ft) to right of centerline; the 2-sigma lateral flight envelope at the 30 m (100-ft) decision height window was ±37 m (±120 ft) about the mean. The lateral tracking performance for the 3° and 9° glide-slope approaches was essentially equivalent to that of the 6° glide-slope approaches. It should be noted that missed approaches were conducted outside the MLS coverage area under dead reckoning. Thus, the wide missed-approach path variations evident on the composite approach plot (fig. 12(a)) resulted from lack of navigation guidance during this procedure. The MLS system can provide back-azimuth guidance for missed approaches when optional equipment is provided.

MLS Final Approach Vertical Flight Envelope

A composite plot of the vertical tracking for 6° glide-slope approaches on runway centerline is shown in figure 14(a). The 2-sigma flight envelope for the approaches in the composite plot is shown in figure 14(b). The zero point roughly corresponds to the glide-path intercept point (GPIP), or the extension of the glide slope to its intersection with the runway. The reference flightpath is depicted by the dashed line, and the vertical wedge defined by the dotted lines represents the full-scale limits (±2 dots) of the pilot's vertical deviation indicator (VDI). Thus, the vertical flightpath plots provide a graphic indication of the relative position of the glide-slope indicator through the complete approach.

The mean glidepath and small 2-sigma deviations shown in figure 14(b) indicate good glide-slope tracking performance. The 2-sigma vertical flight envelope boundary corresponds to generally about 3/4 of a dot deflection on the pilot's VDI instrument. However, there was a tendency for the aircraft to arrive at the 30 m (100-ft) decision height window slightly high on glide slope, as illustrated in figure 13. The mean flightpath at the 30 m (100-ft) decision height window was 6 m (21 ft) high, corresponding to about 1-1/2 dots deflection on the pilot's VDI instrument. The 2-sigma vertical flight envelope at the 30 m (100-ft) decision height window ranged from a lower boundary of 22 m (71 ft) to an upper boundary of 53 m (173 ft). The vertical flightpath dispersions for the 3°, 6°, and 9° glide slopes were essentially equivalent, as seen on the pilot's VDI. However, full-scale VDI deflection sensitivity was varied with glide slope (full-scale deflection = GS°/3). Therefore, for equivalent VDI deflection, the actual flight envelope of the 3° glide slope was about 50% less than that of the 6° glide slope, and the 9° glide-slope vertical flight envelope was about 50% greater than that of the 6° glide slope.

MLS Minimum Missed Approach Altitude

The minimum altitude to which an aircraft descends after initiation of the missed approach is an important parameter, for it affects the establishment of an acceptable decision height for a particular flightpath geometry.

Flight-test data for the 3°, 6°, and 9° runway centerline approaches were analyzed to determine the statistical means and 2-sigma deviations of the minimum altitude to which the aircraft descended after initiation of the missed approach procedure. These data are shown in table 2.

As one would expect, the means and 2-sigma deviations of the minimum missed-approach altitude increase with increasing sink rate (steeper glide slopes). The mean minimum missed-approach altitudes were 13, 23, and 36 m (43, 77, and 118 ft) for decision heights of 15, 30, and 46 m (50, 100, and 150 ft), respectively. The 2-sigma (95% probability) missed-approach vertical envelopes for the same decision heights were bounded by minimum altitudes of 8, 18, and 27 m (26, 58, and 87 ft), respectively.

MLS Decision Height Pilot Ratings

The pilot acceptability ratings of the decision heights for the 3°, 6°, and 9° runway centerline approaches are shown in table 3. Eleven pilots rated the 15 m (50-ft) decision height for the 3° glide slope acceptable. High airspeeds, tracking errors, unacceptable obstacle clearance, wind gusts, and turbulence were stated as reasons by three pilots who felt the 15 m (50-ft) decision height was "too close to the ground for manual flight." All 14 pilots rated the 30 m (100-ft) decision height "acceptable" for the 6° glide-slope approaches. Twelve pilots considered the 46-m (150-ft) decision height acceptable for the 9° approaches, and two rated it unacceptable. Excessive sink rate and pilot workload were stated as the reasons for the unacceptable ratings.

CONCLUDING REMARKS

Joint NASA/FAA helicopter flight tests have been conducted to investigate airborne radar approaches (ARA) and microwave landing system (MLS) approaches. Flight-test results have been utilized to provide (1) NASA with a data base to be used as a performance measure for advanced guidance and navigation concepts and (2) FAA with data for establishment of TERPS criteria. NASA is using the ARA test data to develop flight director concepts which will be superimposed on the radar display for improved tracking and reduced pilot workload. The FAA has used the ARA test data to draft an Advisory Circular for use of Airborne Radar for instrument approaches to offshore oil rigs, which will serve as a forerunner to actual TERPS publication. NASA is using the MLS test data to develop advanced concepts for high-traffic density operations such as 3D/4D, helical, decelerating approaches. The FAA is using the MLS test data as a basis for suggested helicopter landing criteria in their System Test and Evaluation Program (STEP), a program designed to accomplish operational implementation of the new National Microwave Landing System.

REFERENCES

1. Parrish, Robert: The Offshore Transportation Industry. Business and Commercial Aviation, Jan. 1979.

2. National Plan for Development of the Microwave Landing System. FAA-ED-07-2A, June 1978.

3. United States Standard for Terminal Instrument Procedures. FAA Handbook 8260.3B, July 1976.

4. Bull, J. S.; Hegarty, D. M.; et al.: Flight Investigation of Helicopter IFR Approaches to Oil Rigs Using Airborne Weather and Mapping Radar. Paper 79-52, 35th Annual Forum of the American Helicopter Society, May 1979.

5. Phillips, J. D.; Bull, J. S.; Hegarty, D. M.; and Dugan, D. C.: Navigation Errors Encountered Using Weather Mapping Radar for Helicopter IFR Guidance to Oil Rigs. Paper 80-16, 36th Annual Forum of the American Helicopter Society, May 1980.

6. Pate, D. P.; and Yates, J. H.: Airborne Radar Approach FAA/NASA Gulf of Mexico Helicopter Flight Test Program. FAA Report No. AFO-507-78-2, Jan. 1980.

7. Peach, L. L.; Bull, J. S.; et al.: NASA/FAA Flight Test Investigation of Helicopter Microwave Landing System Approaches. Paper 80-55, 36th Annual Forum of the American Helicopter Society, May 1980.

TABLE 1.- ARA WEATHER MINIMUMS RECOMMENDED BY SUBJECT TEST PILOTS

Weather minimum	Recommended number of pilots	
	Primary mode	Beacon mode
200 ft, 1/4 n. mi.	0	0
200 ft, 1/2 n. mi.	7	10
300 ft, 1/2 n. mi.	4	3
Higher	4	2
Total	15	15

TABLE 2.- MLS MINIMUM MISSED-APPROACH ALTITUDE STATISTICS

	3° glide slope	6° glide slope	9° glide slope
	50-ft decision height	100-ft decision height	150-ft decision height
Mean minimum missed-approach altitude, ft AGL	43.5	57.5	118.0
2-sigma deviation, ft	17.0	20.0	31.0
2-sigma (95% probability) minimum altitude, ft AGL	26.5	57.5	87.0

TABLE 3.- MLS DECISION HEIGHT RATINGS (14 PILOTS)

Decision height, ft	Glide slope, deg	Rating, number of pilots	
		Acceptable	Unacceptable
150	9	12	2
100	6	14	0
50	3	11	3

1 FOOT = 0.3048 METERS

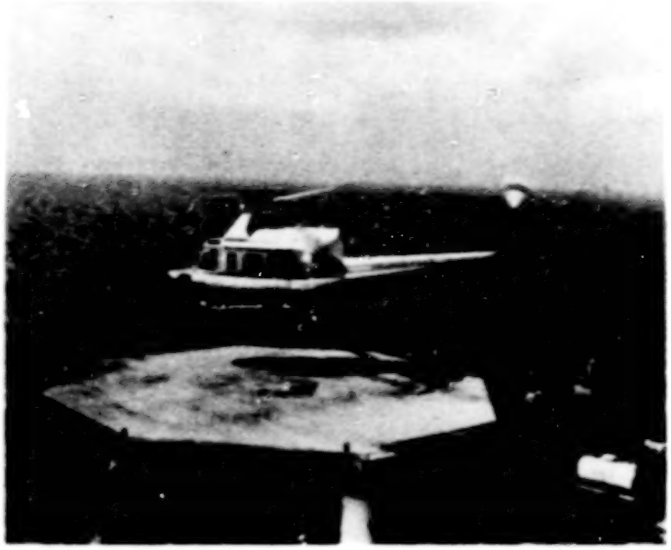

Figure 1.- Bell 212 helicopter landing on oil rig in the Gulf of Mexico.

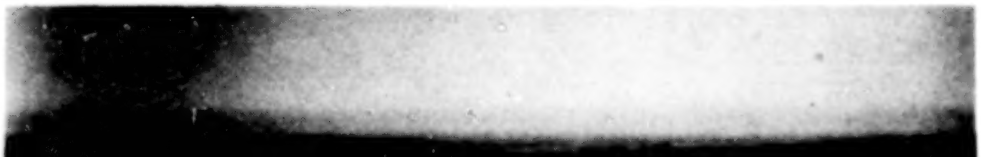

Figure 2.- NASA UH-1H helicopter on MLS approach (selected approach angle = 9°).

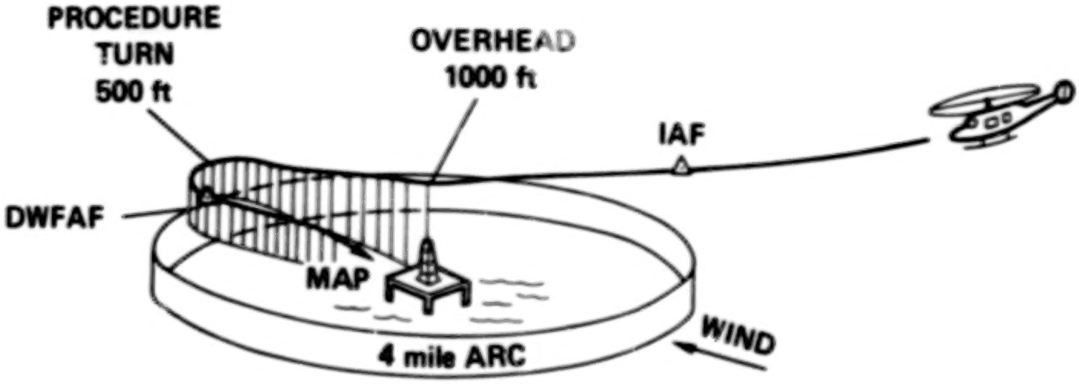
PROCEDURE TURN 500 ft
OVERHEAD 1000 ft
IAF
DWFAF
MAP
WIND
4 mile ARC

Figure 3.- Airborne radar approach to offshore oil rig. 1 ft = 0.3048 m.

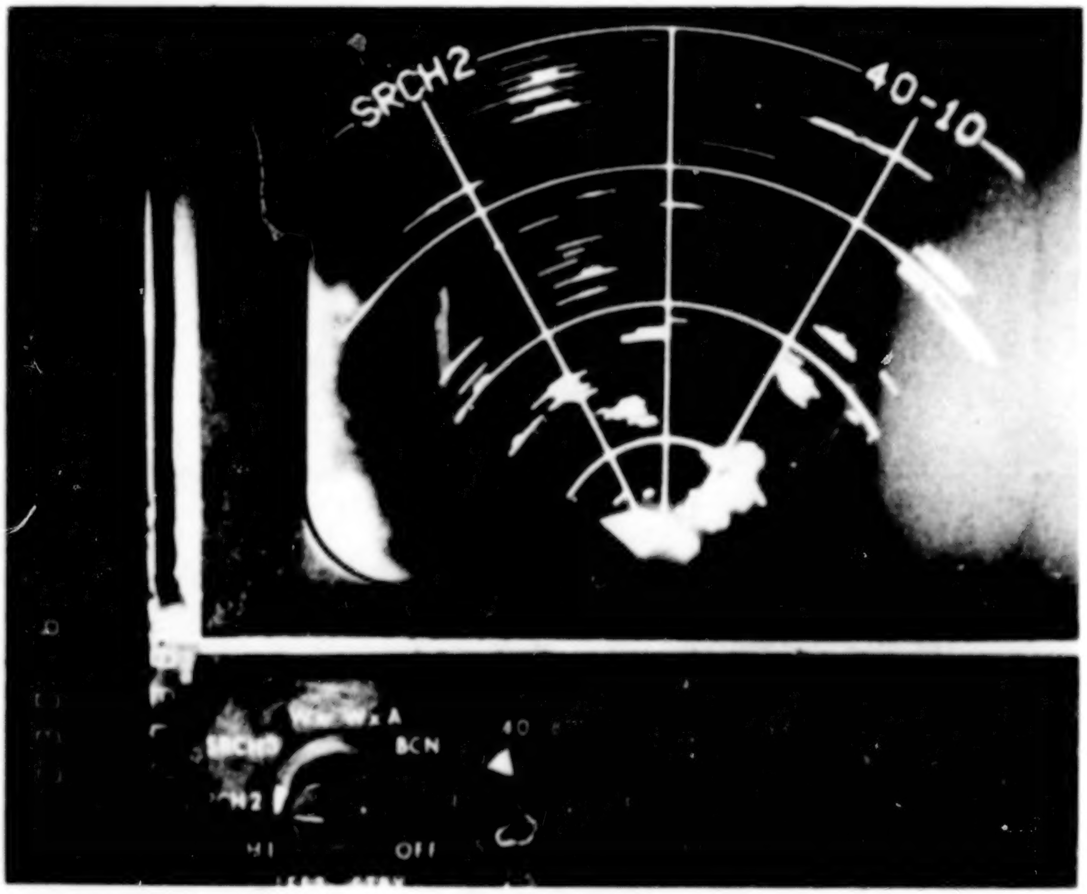
SRCH2
40-10
BCN
40
OFF

Figure 4.- Primary radar return display looking south over Gulf coastline south of Intracoastal City, Louisiana (40-n. mi.-range scale).

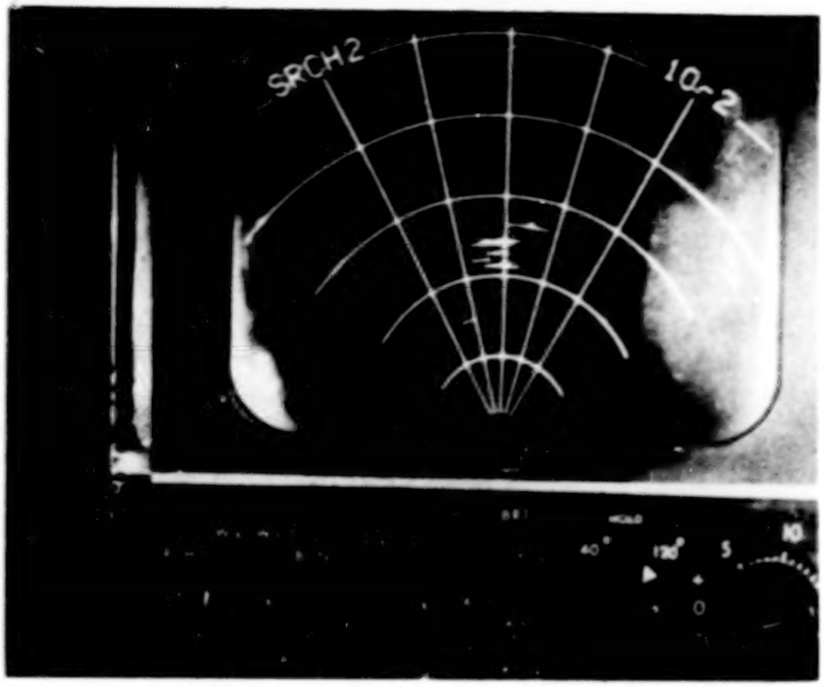
SRCH2
10-2
BRT
HOLD
40°
120°
5
10
0

Figure 5.- Primary radar return display on final approach (10-n. mi.-range scale).

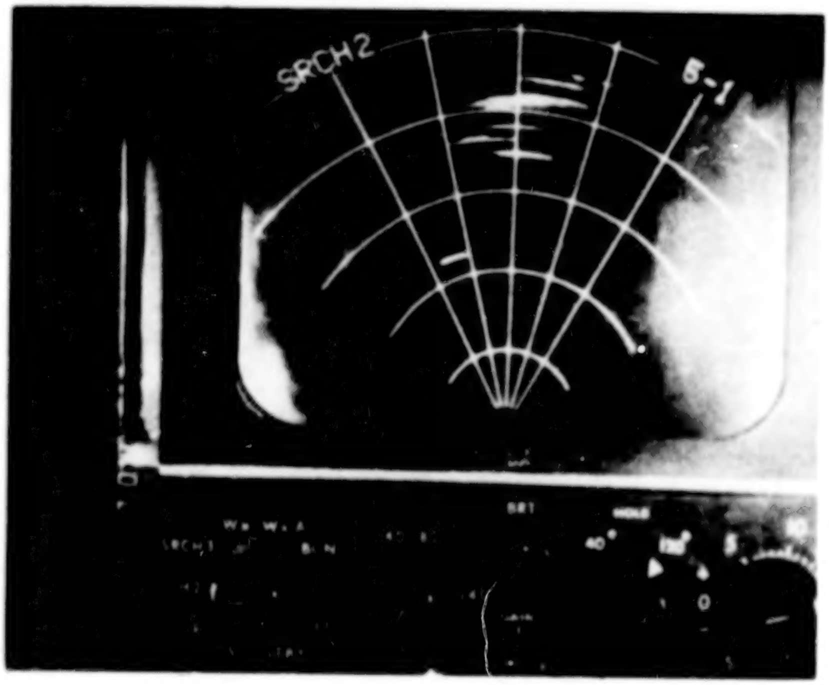
SRCH2
5-1
BRT
HOLD
40°
120°
5
10
0

Figure 6.- Primary radar return display on final approach (5-n. mi.-range scale).

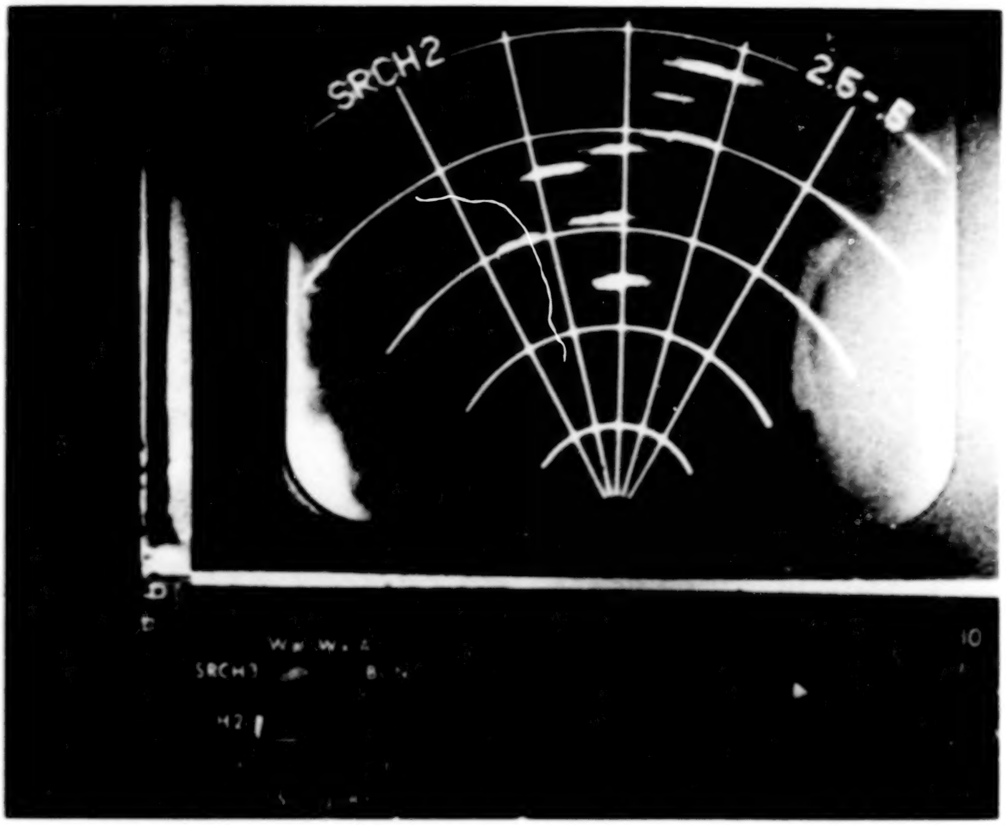

Figure 7.- Primary radar return display on final approach (2.5-n. mi.-range scale).

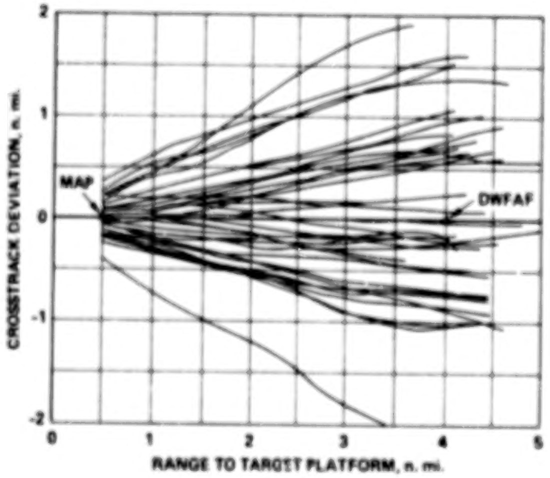

Figure 8.- ARA individual final approach ensemble plot.

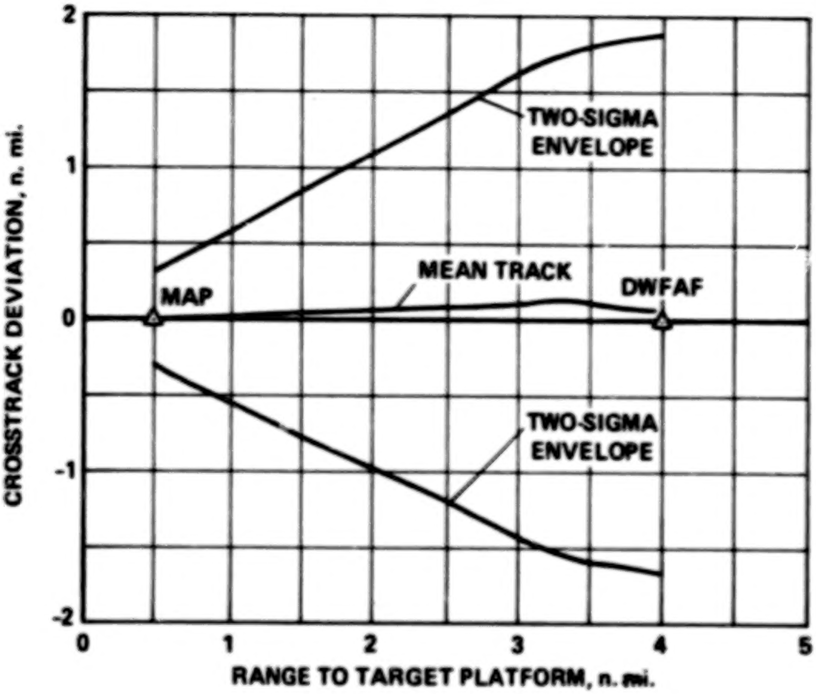

Figure 9.- ARA final approach envelope.

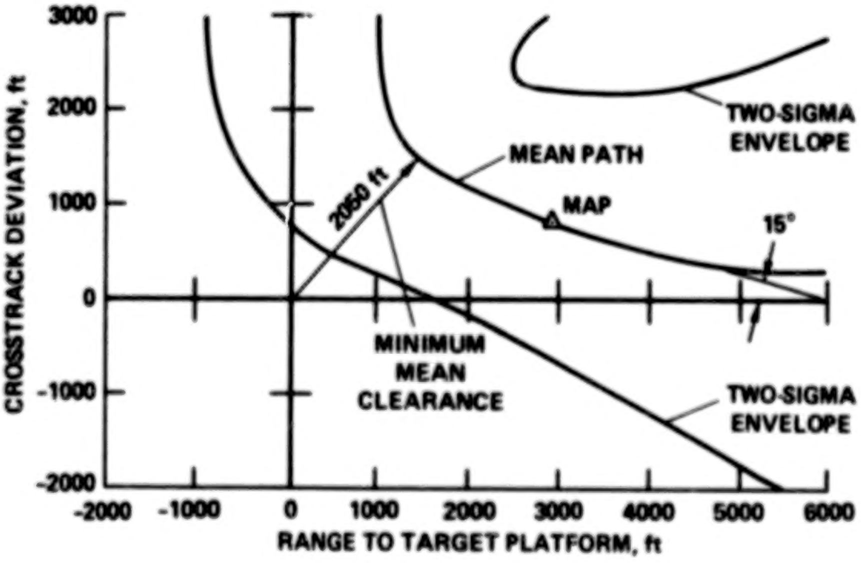

Figure 10.- ARA missed-approach envelope (laterally offset MAP).
1 ft = 0.3048 m.

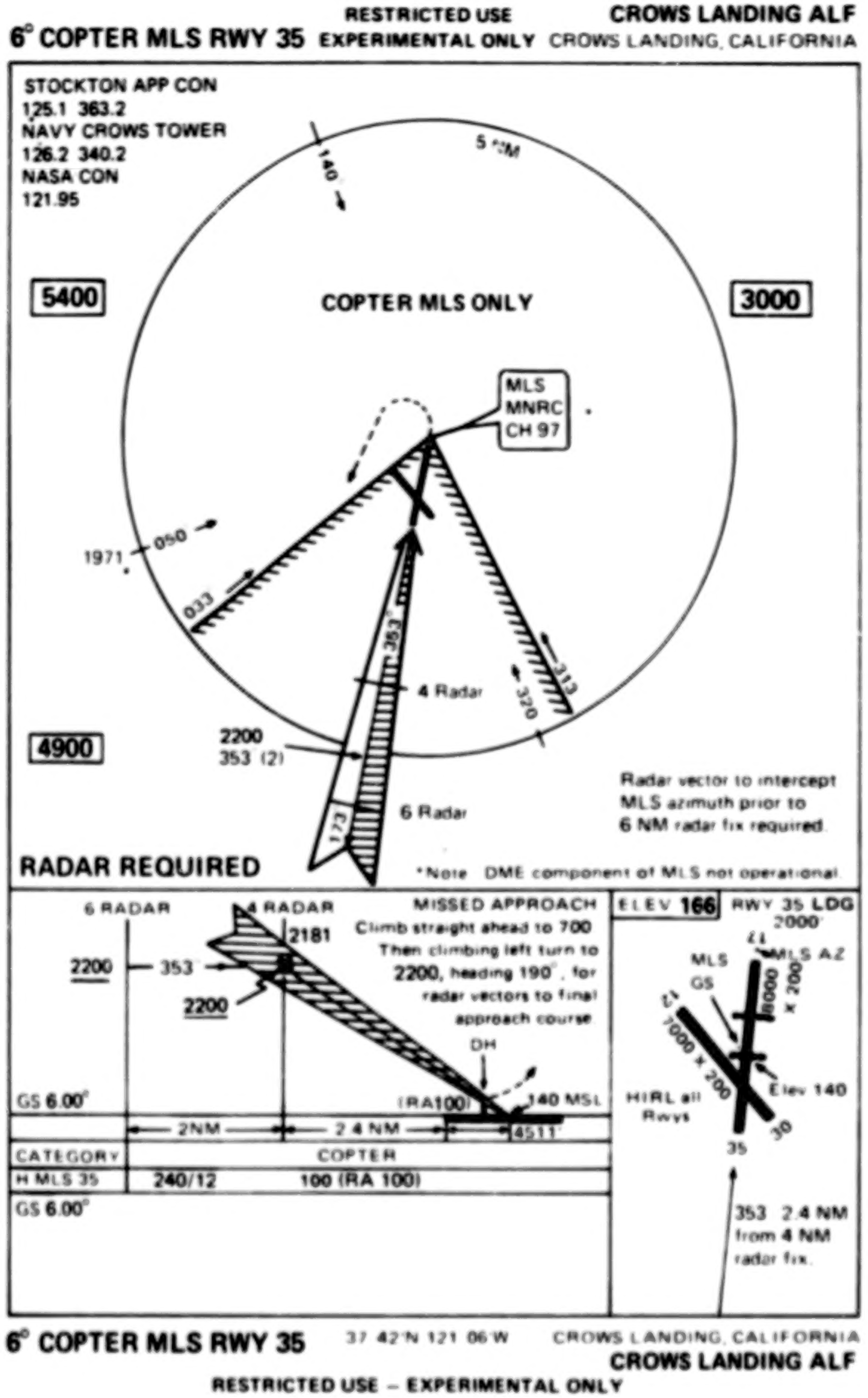
RESTRICTED USE
EXPERIMENTAL ONLY
CROWS LANDING ALF
CROWS LANDING, CALIFORNIA
6° COPTER MLS RWY 35
STOCKTON APP CON
125.1 363.2
NAVY CROWS TOWER
126.2 340.2
NASA CON
121.95
140
5 NM
5400
COPTER MLS ONLY
3000
MLS
MNRC
CH 97
1971
050
033
353
313
320
4 Radar
4900
2200
353 (2)
173
6 Radar
Radar vector to intercept MLS azimuth prior to 6 NM radar fix required.
RADAR REQUIRED
*Note DME component of MLS not operational.
6 RADAR
4 RADAR
2181
2200
353
2200
MISSED APPROACH
Climb straight ahead to 700. Then climbing left turn to 2200, heading 190°, for radar vectors to final approach course.
DH
GS 6.00°
(RA100)
140 MSL
2NM
2.4 NM
4511
CATEGORY
COPTER
H MLS 35
240/12
100 (RA 100)
GS 6.00°
ELEV 166
RWY 35 LDG 2000'
17
MLS AZ
MLS GS
8000 x 200
12
7000 x 200
Elev 140
HIRL all Rwys
30
35
353 2.4 NM from 4 NM radar fix.
6° COPTER MLS RWY 35
37 42'N 121 06'W
CROWS LANDING, CALIFORNIA
CROWS LANDING ALF
RESTRICTED USE – EXPERIMENTAL ONLY

Figure 11.- MLS 6° glide-slope approach plate. 1 ft = 0.3048 m.

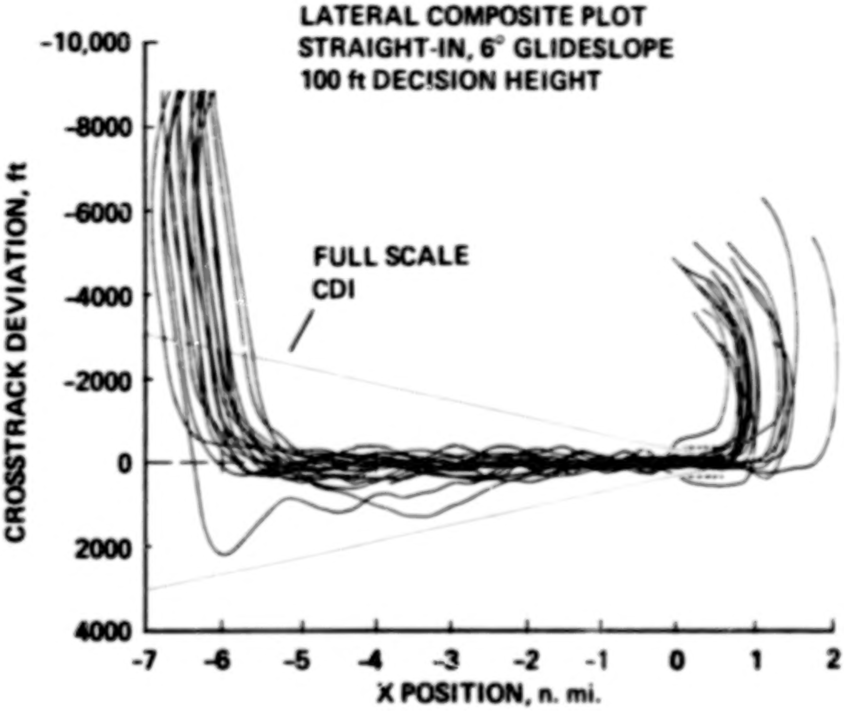

(a) Lateral composite.

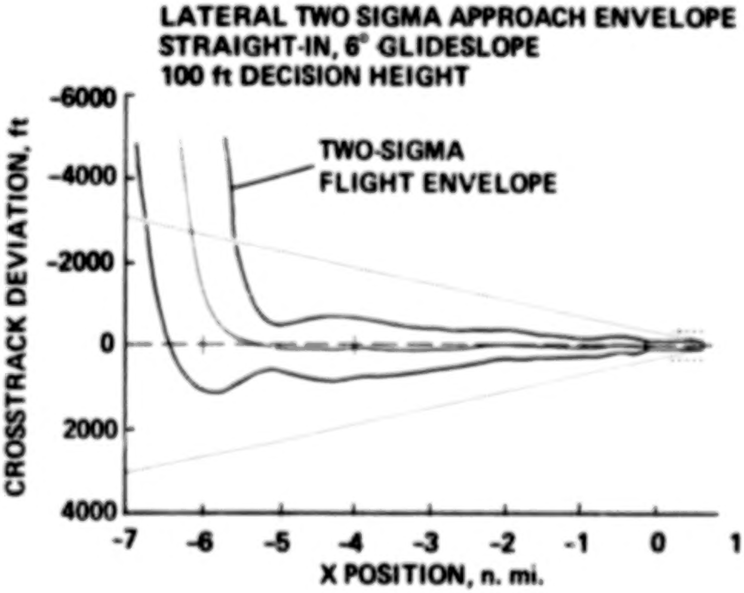

(b) Lateral 2-sigma approach envelope.

Figure 12.- MLS composite individual approach and 2-sigma envelope plots of lateral tracking: centerline, 6^o glide slope. 1 ft = 0.3048 m.

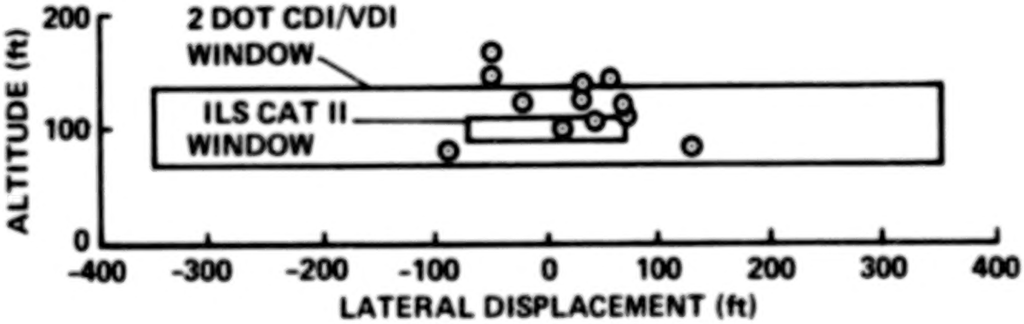

Figure 13.- MLS flightpath dispersions at 100-ft decision height window for 6° glide-slope approaches. 1 ft = 0.3048 m.

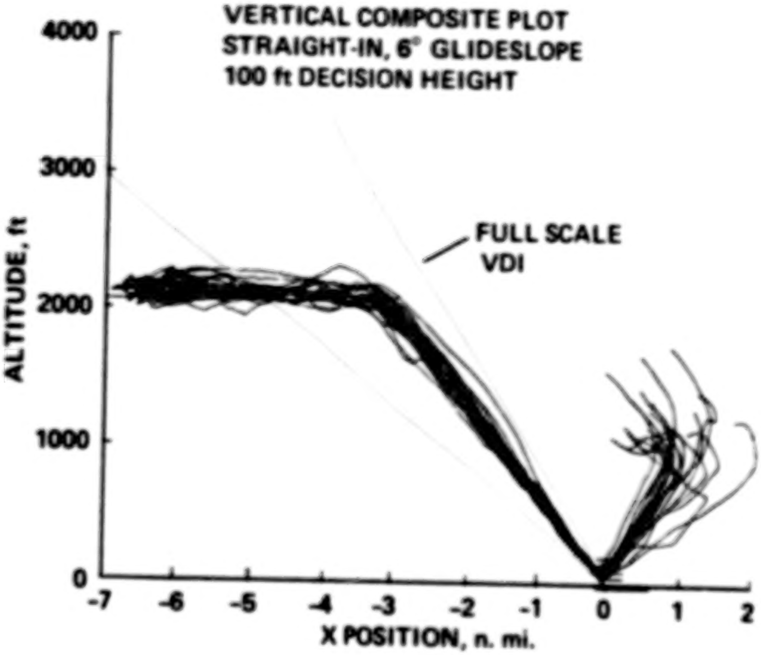

(a) Vertical composite.

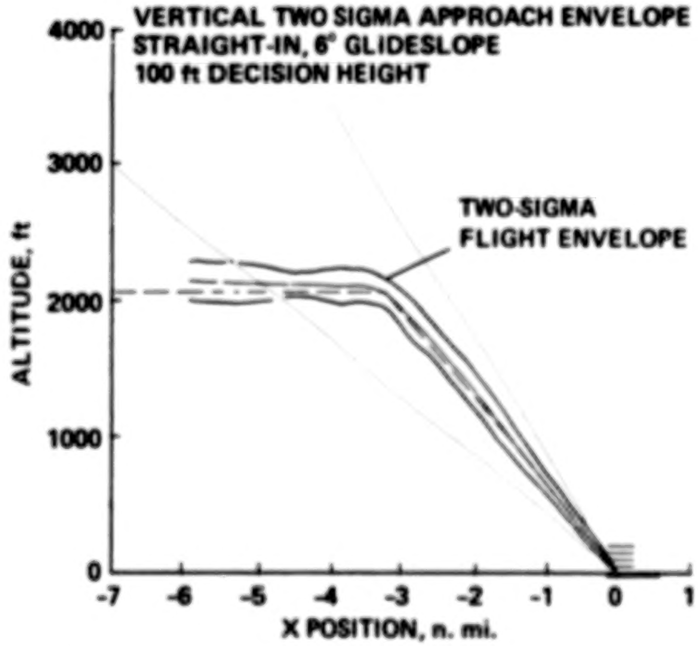

(b) Vertical 2-sigma approach envelope.

Figure 14.- MLS composite individual approach and 2-sigma envelope plots of vertical and lateral tracking: centerline, 6° glide slope. 1 ft = 0.3048 m.

A HEAD-UP DISPLAY FORMAT FOR TRANSPORT AIRCRAFT

APPROACH AND LANDING

Richard S. Bray
Ames Research Center

Barry C. Scott
Federal Aviation Administration

SUMMARY

An electronic flight-guidance display format was designed for use in evaluations of the collimated head-up display concept applied to transport aircraft landing. In the design process of iterative evaluation and modification, some general principles, or guidelines, applicable to electronic flight displays were suggested. The usefulness of an indication of instantaneous inertial flightpath was clearly demonstrated. Evaluator pilot acceptance of the unfamiliar display concepts was very positive when careful attention was given to indoctrination and training.

INTRODUCTION

The electronic flight-guidance display discussed in this paper was developed for use in a NASA/FAA program studying the potential benefits and problems associated with the application of head-up displays (HUD) to landing operations of civil-transport aircraft. Another paper in these proceedings (ref. 1) reports the reactions and performances of airline pilots using this display in flight-simulation experiments. It is the purpose of this paper to describe the display and its development and to point out the factors that influenced its design. The display format evolved over a period of several years in a process that included iterative evaluations in flight simulators. Initial formats borrowed significantly from military HUD experience and from the very limited experience with HUD in transport-category aircraft. Experience with these formats in flight simulation inspired many modifications, and in the process some basic "design principles" were suggested. The experimental displays were designed to function as the pilot's primary instrumentation in a broad range of operational situations, not just the final approach; thus, it is probable that many observations discussed are appropriate to forms of integrated electronic flight-guidance displays other than HUD.

After a brief description of the simulator facilities and procedures used in the development process, this paper addresses the HUD symbology content as influenced by the flight modes in which it is to be used. The logic employed in the dynamics of some of the display elements is described, and the pilot's use of the full display in several types of approaches is demonstrated. The design of selected display elements is discussed to substantiate suggested HUD design principles. The paper concludes with observations regarding a few unresolved questions exposed in the simulator exercises and the training requirements associated with new display concepts.

TEST FACILITIES AND PROCEDURES

Simulation

Equipment- Most of the simulator tests were conducted in the Ames Flight Simulator for Advanced Aircraft (FSAA), which incorporates a transport-type cockpit on a larger amplitude six-degree-of-freedom cockpit motion system. In this simulator, a *Redifon* TV-model board visual simulation system provides a 46° by 34° representation of the forward view of the terrain from the cockpit.

The optical collimating system of the cockpit visual simulation display was used to provide the collimated head-up instrumentation display superimposed upon the outside scene. The physical arrangement is illustrated in figure 1. In a flight installation, the display system must place the optical combiner relatively close to the pilot's eyes to present a satisfactory field of view with equipment of practical size. For some of the simulator tests, a dummy combiner having typical combiner transmissivity was mounted as shown in figure 1. With or without the dummy combiner, the binocular field of view of the HUD was 24° wide and 18° high and it was not affected by head motion. The HUD display written on the cockpit cathode ray tube (CRT) was generated by a general purpose computer-graphics system linked to the similator computer. An example of the pilot's visual scene, including the HUD, is illustrated in figure 2.

Aircraft models- The initial simulator tests utilized a dynamic model of the Boeing 737 airplane, but the more recent work was conducted with a simulation that incorporates the flight dynamics of the Boeing 727-200 airplane. The simulations were optimized for dynamic fidelity in approach and landing maneuvers. Instrument landing system (ILS) approach-coupling and autoland capability were provided with the 727 model.

Simulation of landing environments- The objectives of the display development called for efforts to simulate with some fidelity the reduced-visibility conditions accompanying low clouds and fog. Appropriate selective electronic occlusion of the simulated visual scene provided constant or varying visual conditions to as low as a 150-m (~500-ft) runway visual range (RVR). In addition to standard wind, wind-gradient, and turbulence models, a library of discrete atmospheric disturbances (shears and downdrafts) was utilized. In some instances, shear and downdraft profiles were combined with intermittent visibility conditions to simulate conditions known to be associated with specific aircraft accidents.

Evaluation Procedures

In general, the evaluation procedures during the development of display formats were considerably less formal than those of the "operational evaluation" reported in reference 1. After an experimental display format had been assembled and tested by the Ames project staff, engineering pilots from the air transport industry and the Federal Aviation Administration (FAA) were invited to participate in the simulations and offer their evaluations and suggestions for improvements. In all the evaluations, a variety of approach types and environmental situations were experienced with and without the HUD. Without the HUD, approaches were conducted with instrument panel displays including an attitude-director indicator (ADI) and a horizontal situation indicator (HSI) typical for the aircraft and operation categories. Performance of the simulated aircraft and comments of the evaluator pilot were recorded. Over the past several years, about 250 hr of piloted simulation have been devoted to development of the subject display. At least 20 industry and government-agency pilots have participated in the extended evaluation sessions, and more than twice that number have experienced less extended exposure to the HUD simulations.

HUD DESIGN CONSIDERATIONS

Introduction

Two interrelated design objectives characterize the evolution of a head-up display. The first involves the *superposition* of displayed information on the outside scene to form unique flight-guidance information in visual meteorological conditions (VMC). The allied objective is the optimal *integration* of attitude, energy, and guidance information, taking advantage of the electronic medium and modern sensors to provide the pilot with the means for improved precision of control in low-visibility approach and landing. The following discussion uses the particular details of the subject HUD to demonstrate how these objectives can be met. It should be pointed out that the individual logics and symbology details utilized in the display are not claimed to be unique to this display nor are they claimed to be uniquely effective, but simulation experience to date indicates that they do meet the design objectives. A complete technical description of the display is the subject of reference 2.

Military experience (particularly with the Viggen in Sweden), experimental work with head-up displays in transport-category aircraft in France, and experience with the panel-mounted electronic display of the Terminally Configured Vehicle (TCV) program at the Langley Research Center have demonstrated the virtues of a representation of the instantaneous direction of flight of the airplane (flightpath symbol) relative to visible earth references. To provide this "conformality," attitude information of a quality normally associated with inertial navigation systems (INS) is desired. The following discussion assumes the availability of such information, as well as inertial velocity and acceleration data sufficient to determine vertical flightpath angle and ground-track angle relative to heading. A later discussion addresses the options available when inertial velocity information is nonexistent.

Approach Guidance

VMC glidepath control- The most obvious method of providing precise VMC glidepath guidance with a conformal display of flightpath is illustrated in figure 3. A "fixed-depression" line below the horizon is utilized to determine whether the aircraft is above or below the intended glidepath. In figure 3(a) the aircraft is above the intended glidepath of -3° and is in level flight. In figure 3(b) the flightpath of the aircraft is being directed at a point short of the runway, thus descending toward the desired glidepath. As the -3° line lowers to the intended touchdown point, the flightpath symbol is raised to aim at the touchdown point (fig. 3(c)). If necessary the flightpath is adjusted further to maintain the -3° line on the touchdown point. The effectiveness of this scheme has been thoroughly demonstrated in flight by G. Klopfstein of the French Air Force (ref. 3) and more recently in the Calspan T-33 airplane associated with the Air Force/Navy Display Evaluation Flight Test (DEFT) program in this country. With the visible runway, lateral lineup is assumed to be straightforward, requiring no additional aids. However, the indication of track does offer increased precision in the lateral steering mode.

IMC guidance- As might be deduced from figure 3, instrument meteorological conditions (IMC) guidance can be provided by a symbolic representation (in true perspective and location) of the runway. Such a symbol can be constructed from the ILS glide-slope and localizer error measurements, together with range-to-runway information either measured directly or deduced from the altitude above the runway and the ILS error. In fact, Klopfstein's display functions in just this manner in the IMC mode.

With the subject display, however, it was desired to explore a more explicit form of guidance, one that did not depend on the symbolic runway remaining in the display field of view. The guidance concept chosen is illustrated in figure 4. ILS localizer error is indicated by the lateral displacement of a display element with respect to the approach course heading reference, as shown in figure 4(a). Glide-slope error is indicated by the vertical displacement of another element with respect to the horizontal elements 3° below the horizon (or the path angle of the ILS system in use). These error indications are gained so that they combine to define a point in the visual field that corresponds to a position of an object on the ILS glidepath approximately one-fifth of the distance from the aircraft to the runway. The explicit guidance principle inherent in this error-display concept is illustrated in figure 4(b). By directing the flightpath of the aircraft at the combined error indication (i.e., flying a "pursuit course" at the symbolic moving point on the approach path) a convergence to the path is effected, and the aircraft falls in trail "behind" the ILS symbology on the desired path (fig. 4(c)). The same guidance principle appears in a newer French HUD development (ref. 4). A symbolic runway is shown in these figures to assist in illustrating the guidance principle, but it is not essential to the pilot's control task. It was retained in the display for its contribution to "situation awareness."

Energy Management

To this point, the basic-approach guidance functions of the display in IMC and VMC have been defined. Displays of energy state are now required in order to provide the desired independence of instrument panel information while using the head-up display. As shown in figure 5, four separate items of information, three of which are normally found on the instrument panel, are added in association with the flightpath symbol, moving with it to form a single major element of the display. A digital readout of indicated airspeed appears to the left and below the flightpath reference. A "tape" extends vertically above or below the left "wing" of the flightpath symbol to indicate fast or slow relative to a reference speed. A small chevron-shaped symbol moving vertically with respect to the left wing indicates acceleration along the flightpath. With the appropriate scaling, the position of this symbol indicates the constant-speed flightpath for the current thrust and airplane configuration. Other mechanizations of this concept have been termed "potential flightpath." A digital display of altitude, of definition appropriate to the flight regime, is located below and to the right of the flightpath symbol. A separate vertical rate indication is deemed unnecessary since the vertical flightpath presentation provides that function.

Additional Display References

The format of figure 5, with the addition of the ILS symbology discussed earlier, contains the information desired for the final IMC approach. However, additional symbology is added (fig. 6) to accommodate the more generalized maneuvering of approach-path intercept or go-around. Additional pitch and heading references are provided, together with a fixed symbol relating the longitudinal reference of the aircraft ("boresight") to the other display elements. It can be noted that the lateral position of the flightpath symbol relative to the "aircraft" symbol defines the drift angle of the airplane, and the vertical relationship of these two symbols is an approximate indication of angle of attack. The latter relationships suggested another symbol, intended as a warning of approach to limit angle of attack. As the angle of attack is increased, as indicated by increasing deflection of the flightpath symbol downward in the display field, a flashing line is displayed at a vertical position representative of the angle of attack associated with the primary stall-warning device of the airplane. When appropriate, a distance-measuring-equipment (DME) measure and a marker-beacon annunciation appear near the aircraft reference symbol. All these features are illustrated in figure 6, which depicts the display as it might appear if the aircraft were recovering from a sudden severe wind shear at low altitude.

Two elements in the display provide altitude references. Radio altitude of the main gear above the runway is indicated by the deflection of a two-line-segment symbol below the horizon. A satisfactory landing flare is effected if this symbol is tracked with the flightpath symbol. In the absence of an ILS glide-slope signal, a similar symbol is used to provide an altitude "command" or capture function.

This display did include the means for localizer intercept in duplication of the basic function of the horizontal situation indicator (HSI) of the panel. A line symbolic of the runway centerline extended, in perspective, defines whether the aircraft is left or right of course and whether the aircraft is on a converging or diverging track relative to the approach course. An approach to course from a left-of-course position is illustrated in figure 7. When the approach course heading is outside the field of view, as in this case, the point of intersection of the symbol with the horizon is constrained to remain at the edge of the field, and the approach course heading is defined beneath the flightpath symbol. In figure 7, the localizer-error symbol and the 1° pitch marks are used to designate the desired intercept heading (135°). At "localizer capture," these symbols assume their localizer-error function, indicating a turn toward the approach course.

OPERATIONAL PROCEDURES

The operational use of the display in an ILS approach is demonstrated in figures 8(a) through 8(h), which are photographs taken during simulator tests of the display. Prior to the approach, the pilot has entered into his guidance-display computer the runway heading and altitude, ILS glide-slope descent angle, decision height, speed reference, and desired ILS course-intercept heading. In figure 8(a), the pilot is maintaining an altitude of 1500 ft by flying the flightpath symbol on the horizon. He is tracking an intercept heading of 155° toward the ILS localizer associated with a runway having a heading of 090°. The DME reading indicates that he is 15 km (9.3 mi) from station, which in this case is at the airport. Acceleration and speed-error indications show a steady speed about 10 knots above the reference. For this series of photographs, the option to use angle of attack as the speed-error reference is being exercised, and the extension of the tape represents a negative angle-of-attack increment corresponding to a 10-knot speed surplus. The glide-slope signal is being received, as indicated by the presence of the symbol near the top of the display. It should be pointed out that the runway is at sea-level elevation; thus, the barometric altitude shown corresponds to altitude above the runway.

In figure 8(b), the airplane is in a localizer-intercept turn. As the localizer error is reduced below 2.5°, the localizer symbol moves left from its preset intercept heading position. The pilot pursues the localizer symbol while maintaining his desired altitude. His acceleration symbol shows speed to be decreasing at about 0.5 knots/sec.

In figure 8(c), convergence on the localizer is nearing completion and the runway symbol is in the field of view. The glide-slope symbol is descending, indicating an imminent crossing of the glide slope.

Figure 8(d) shows the aircraft on localizer, on course, in level flight just slightly below the ILS glide slope. This is the optimum moment to initiate the pushover to the 3° descent path. The flaps have been lowered to final-approach configuration, resulting in the reduction of the target speed to that corresponding to the reference angle of attack.

Figure 8(e) is a configuration of the display representing the stabilized on-localizer, on-glide-slope situation that is sought and effected by directing the flightpath symbol to the localizer and glide-slope symbols. The aircraft is "in trail" behind the intersection circle. Note that the aircraft heading is left of the aircraft track, in this case the result of a crosswind component from the left.

In figure 8(f), the airplane has just passed the middle-marker position 900 m (0.5 mi) short of the runway threshold. The runway symbol overlays the runway, which is just becoming visible. Within a second after this situation, the runway symbol disappears, indicating descent through "decision height." For the remainder of this approach, radio altitude is indicated.

Figure 8(g) shows the airplane descending toward flare-initiation altitude and shows the ground-proximity symbol rising in the display, while in figure 8(h) the ground-proximity symbol is being tracked in the landing flare.

In figures 9(a) through 9(e), a localizer-only "nonprecision" approach (NPA) is demonstrated. From the approach fix (in this case, the outer marker beacon), a 5° descent is flown to minimum descent altitude (MDA), which in this approach was set at 135 m (440 ft). In figure 9(a), the target-altitude symbol is shown rising toward the flightpath symbol. Tracking the line pair produces the convergence on the MDA shown in figure 9(b). Level flight is continued until the intended touchdown area is nearly 3° below the display horizon, as shown in figure 9(c). A descent is initiated with the flightpath symbol aimed at the touchdown area (fig. 9(d)). Adjustments are made in the flightpath as necessary to maintain the touchdown point on the runway depressed 3° below the horizon. Again, flare altitude is being approached in figure 9(e).

The go-around maneuver requires no unique symbology or procedure relative to the approach modes of use. The flightpath is expeditiously raised to a modest positive value (2°-3°) as the thrust is increased to climb power. When the desired climb speed is attained, the flightpath is elevated to correspond to the position of the acceleration symbol, assuring a constant-speed climbout. If climb performance is threatened by engine malfunction or atmospheric disturbance, optimum action can be effected with the closely integrated displays of altitude, speed, flightpath, and acceleration. Speed decay is avoided by matching the flightpath with the acceleration indication. If terrain clearance is temporarily critical, intelligent trade-offs between speed and altitude are aided because the pilot is directly controlling an indication proportional to vertical velocity, and he has speed and acceleration indications in close visual proximity.

DISCUSSION OF DESIGN DETAILS

The previous sections of this report have described a display format developed over a period of time that reflects experience with a variety of individual display-element concepts. The following discussions of individual features are offered with the hope that they suggest design principles applicable to head-up displays and to integrated electronic displays generally.

Symbol Form

Airspeed and altitude display- The first display format evaluated in the program nearly 3 years ago is illustrated in figure 10. Its design borrowed heavily from military experience in general layout, with airspeed and altitude scales, or "thermometer readings," boldly evident. At that time, the display was designed with the assumption that ground track was not available, and lateral guidance was aided by a symbol which duplicated the function of a flight director "steering bar." The only features of this display that are retained in the final display configuration are the ILS glide-slope guidance scheme and the fast-slow tape.

The speed and altitude scales were quickly assessed as awkward and cluttered in the landing approach. In fact, they were often ignored because the fast-slow tape and an expanding runway representation at least partially met the immediate demands of the pilot. The first major revision of the display presented digital readouts of speed and altitude fixed in the lower portion of the display frame (fig. 11). These were retained through the next-to-final configuration, illustrated in figure 12. Efforts to move these indications closer to the flightpath symbol for easier scanning resulted in undesirable dynamic "conflicts" until McDonnell-Douglas Corp., in the development of their DC9 HUD, demonstrated the virtue of tying the digits directly to the flightpath symbol. On no occasion have evaluation pilots cited a desire to return to scales or electronic representations of their panel airspeed and altitude instruments. Several pilots missed a vertical rate indication until they recognized that the displayed flightpath angle provided that function.

Symbol "weight"- The state of current technology discourages the use of color to improve discrimination between symbols in head-up displays; and to minimize obscuration of the outside scene, as well as to minimize display-writing time, line or outline symbols are favored over solid opaque symbols. Simulator experience with the display of figure 11 pointed out the hazard resulting from inadequate differentiation between a controlled element (flightpath symbol) and the display element to which it is being referenced (glide-slope error line). On a number of occasions, under stressful, dynamic conditions, pilots suffered abrupt divergences of flightpath because they momentarily reversed the roles of these two symbols. With the current display format, which features a return of the flightpath circle and the attachment of the speed and altitude digits to form a relatively massive array, such occurrences have been rare. A "reversal" tendency was noted with the energy-control symbology of a foreign experimental head-up format in which the controlled and reference elements were similar in type and size.

Pitch scales- The earlier versions of the display included the traditional pitch "ladder," with references at 5° intervals, that moved in pitch and roll with respect to the aircraft reference symbol. It was found that such clutter can be satisfactorily avoided by limiting the pitch references to those required for the nominal approach tasks, except in cases of severe nosedown upset where additional references can be programed to appear. The final display format reflects this finding, and in addition gives a heading degree of freedom to the pitch references. This latter feature is visually gratifying. All major earth-oriented symbols have the full three-degrees of angular freedom, reducing the slight tendencies toward disorientation that were experienced with the earlier configurations under conditions of combined high pitch and yaw rates.

Speed control- The fast-slow tape, attached directly to the primary symbol, was derived from earlier electronic display experience and received consistently favorable reviews throughout the course of the subject development. The attachment of the symbol to its reference may be as important to its success as is its easily scanned location. Even under the most dynamic circumstances, it does not have to be sought, and its size is a direct indication of the error to be nulled. Selection of upward extension to indicate "fast" reflects the decision to remain consistent with the usual ADI fast-slow indication.

The acceleration (or "potential flightpath") symbol did not appear in the first format. Among the criticisms of that design was lack of a thrust reference. The acceleration symbol satisfied most evaluators, although some observed that an indication of overboost would be valuable. The weight of the symbol was kept low in accordance with its role as an aid or guide, not as a measure that was continuously monitored and controlled to a specific reference.

The acceleration indication was probably the single most unfamiliar feature in the display to those pilots who had not been previously exposed to electronic flight displays; however, its acceptance was unanimous, as it has been in other flightpath display mechanizations. Because of its novelty, pilots varied in their techniques and skill in using the measure, and their appreciation of its usefulness grew with their experience. No obvious, systematic misuses of the symbol were noted.

Symbol Dynamics

Flightpath- With the subject display, the pilot's primary task is direct control of the flightpath symbol to what are normally considered attitude references, or to guidance elements. The dynamic behavior of the flightpath of the center of gravity of the airplane in response to pitch-control inputs lags that of pitch attitude by more than 1.5 sec at approach speeds. Thus, without some form of compensation, precise control of an indication of the vertical flightpath of the aircraft c.g. location is quite difficult. However, if the flightpath is measured or computed to be that of the cockpit area of a large aircraft (25.9 m (85 ft) forward of the c.g. in the 727-200), the dynamics of the symbol are very good. A small amount of additional pitch-attitude "lead" can be used to optimize the response without producing any undesirable consequences. Vertical flightpath angle in the subject display is defined as

$$\tan^{-1}\left(\frac{\text{vertical velocity of cockpit}}{\text{velocity along track}}\right) + \theta\left(\frac{0.4s}{0.4s + 1}\right)$$

where θ is pitch attitude and s is Laplace operator.

In the simulation exercises, direct control of this "augmented" flightpath indication was seen to be analogous to that of pitch attitude, and it substituted completely and gracefully for that normal mode. When the significance of the flightpath indication is fully appreciated by the pilot, control of vertical flightpath in the presence of speed or configuration changes, as well as atmospheric disturbances, is instinctive and precise. A unique virtue is seen in the response of the flightpath indication to the vertical gust component of turbulence. As configured, the indication represents the flightpath of a point forward of the cockpit, in the vicinity of the center of the natural rotational response as the airplane heaves and "weathercocks" in response to vertical gusts; thus, the flightpath indication is stabilized relative to pitch attitude, and the need for higher frequency pitch-control inputs is minimized. While the indication of pitch attitude provided in the display by the aircraft reference symbol becomes of secondary importance, the relationship of this symbol to the flightpath symbol, reflecting angle of attack, strongly complements the speed indications of the display.

Acceleration along the flightpath- The definition of the acceleration indicated by the deflection of the chevron relative to the flightpath symbol reflects the objective of providing for improved energy management in severe atmospheric disturbances. To provide wind-shear sensing attributes while also assisting in routine thrust management, a combination of inertial acceleration and rate of change of indicated airspeed was derived in a complementary filter of the form

$$\text{indicated acceleration} = \left(\frac{\text{airspeed}}{\tau} + \text{inertial acceleration}\right)\left(\frac{\tau s}{\tau s + 1}\right)$$

where τ is a time constant (3 to 5 sec). This logic prevents the masking of continuing shear indications by inertial acceleration, while sufficiently filtering the noise inherent in the derivative of airspeed in turbulence.

Lateral flightpath dynamics- As indicated earlier, the final format, and the one immediately preceding it, were configured and evaluated with the assumption that INS-derived ground-track information was available. The pilot's task in the ILS approach was to direct his track (flightpath symbol) at a particular instantaneous heading reference indicated by the localizer-error symbol. Some difficulties were anticipated because of the unfamiliar response of the track indication in lateral maneuvering (it is almost decoupled from heading in short period motions) and because the "track command" relationship of the localizer-error symbol to the flightpath symbol resembles that of the roll-command vertical needle in a conventional flight director. No major difficulty was encountered, although the pilots demonstrated a need for some familiarization with the new control mode. A few of the pilots experienced undesirably persistent tendencies to oscillate slightly in roll when tracking the localizer. Some of these pilots felt that their behavior was the result of inadequate bank-angle references in the display. It is possible that these pilots possessed styles of control that did not accommodate readily to the unfamiliar tracking dynamics, or they may have carried into the task some of their flight director habits. These oscillatory tendencies diminished with increased exposure to the display.

Some of the most recent experience with the final configuration has utilized a display mode that again assumes the unavailability of INS-derived ground speed or track. In this mode, the flightpath symbol remains associated laterally with aircraft reference (indicated track the same as heading) until a valid localizer error of less than 3° is sensed. Localizer-error rate is then used, in the manner of a flight-director computer, to deduce an approximation to ground track which is used to position the flightpath symbol. This technique is effective in the simulator for localizer-guided approaches; however, a fully satisfactory mechanization of the lateral behavior of the flightpath symbol for approaches without track measures or localizer has not yet been identified.

Symbol excursion limits- If the guidance elements of the display, which are referenced to the approach course heading, were to remain strictly conformal with the outside world, they would leave the limited field of view of the display in many situations when they are most needed. The same fact is true of the flightpath symbol itself; a very strong crosswind can produce a drift (or crab) angle that will place the flightpath outside the display field. Excursions of these symbols must be limited to the display field in a manner that does not produce ambiguities or irritating dynamic behavior and does not require a significantly revised mode of operation. In the subject display, when the flightpath symbol is against a lateral excursion limit, the positioning of the guidance elements reflects that condition so as to continue the same dynamic relationships. The experience with the subject display suggests that these excursion-limiting considerations are among the most challenging in the design of a conformal head-up display.

Unresolved Issues

Localizer-intercept display- The attempt to include in the display format indications adequate for intercept of a localizer course may have been more appropriate for panel instrumentation than for a head-up display, but the opportunity to address the question of combining ADI and HSI functions in one format could not be ignored. The "runway centerline" mechanization described in figure 7 is as technically unambiguous and descriptive of the flight situation as the conventional HSI; however, it consistently inspired criticism from pilots, especially in their early experience. Resistance to acceptance of the runway-centerline perspective interpretation is probably caused by confusion with the error indication in the familiar HSI. As illustrated in figure 13, the angular relationship of the error symbol to the "frame" of the HSI is a measure of the difference between localizer course and aircraft headings, while in the HUD the angle is a measure of lateral displacement from course and is independent of aircraft heading. The disorientations experienced by the pilots with this feature of the display argue strongly for avoidance of such perceptual conflicts with conventional display logic, or at least for indoctrination and training to effect full familiarity with the new logic.

Flare guidance- The provision for continuous vertical guidance in the landing flare was included in all the formats and was effectively utilized by most of the evaluating pilots. However, it is the personal observation of the author, supported by solicited views of pilots similarly experienced with the display, that the use of the flare guidance to touchdown in manually controlled landing is accomplished at the expense of reduced perception and use of the cues normally derived from visual scanning of the runway. This is understandable if one accepts the reasonable assumption that in normal landings, without HUD, pilots fully saturate their visual perception capabilities in support of their conduct of the flare maneuver. In a pilot's early experience with the display, presentation of a second field of information inspires an either/or decision, conscious or subconscious. The development of a scan that includes both fields of information to effect optimal control of the flare seems to require much practice. The possibility is raised that the willingness to concentrate on the display in the flare is exaggerated in simulation, where outside visual cues are somewhat degraded relative to those of flight. Thus a question still remains regarding the value of a continuous flare cue in the manual landing, but very recent experiences with simulations of very-low-visibility automatic landings support its presence as a performance monitoring aid.

Provisions for display simplification- All versions of the format were accompanied by one or more submodes, suitable for the final VMC portion of the approach, that contained considerably less symbology than the all-up display. A "decluttered" version of the final display is illustrated in figure 14. These modes were acquired by depression of a sequencer button on the pilot's control wheel. When introduced to this feature, all the evaluator pilots reacted favorably; however, in the total simulator experience, only a few of the pilots actually adopted the procedure of simplifying the display late in the approach. Apparently either the full display did not constitute a significant visual burden to most pilots, or the declutter option was simply forgotten in the high work load of low final approach.

PILOT ACCEPTANCE AND LEARNING

To most of the evaluator pilots, the HUD format represented an arrangement of information radically different from any they had used in flight. The rapidity of acceptance of most of these unfamiliar forms is considered a measure of their effectiveness. The designation of the flightpath symbol as the primary controlled element of the display presented no problems to the pilots in the aircraft control modes used in this development (full manual or ILS-coupled autoland). Its use was dynamically comfortable, and sufficiently analogous to that of their conventional instruments to require a minimum of familiarization prior to the conduct of precise instrument approaches, at least in nominal conditions. The observation is offered that many pilots tended initially to demonstrate more confidence in than technical comprehension of the display, and thus were sometimes slow to appreciate and employ the full potential of the flightpath information offered them. Continued instruction and practice past the first several hours of experience proved rewarding in terms of demonstrated performance in high-workload situations posed by turbulence and shears. It should be expected that the development of scan patterns and control strategies with a completely new layout of flight information requires practice. The simulator experience associated with this display development very strongly points out the advisability of exposing pilots to thorough indoctrination, practice, and testing as part of their evaluation procedure.

CONCLUDING REMARKS

The display development program described in this paper enjoyed the periodic availability of sophisticated flight simulation in which demanding piloting tasks could be realistically represented. The experience suggests that there is no rational alternative; the evaluator must get into the control loops, with ample time to develop a performance plateau. However, the program would have benefited from the availability of a simpler simulator in which a greater variety of display concepts could have been given preliminary inspection. Such improved flexibility in the design process might protect against the natural tendency to concentrate on, and overrefine, a single concept.

The subject conformal flightpath-based head-up display format was developed and evaluated under the assumption that in the aircraft it would, under the most favorable circumstances, be supplied precise attitude, velocity, and acceleration data from modern sensors, including INS. A quite different display concept might result if assumed sensors remained limited to those found on most of our presently operating domestic-transport aircraft.

Most of the air-transport-community pilots exposed to the HUD formats demonstrated an encouraging acceptance of unfamiliar concepts when effectiveness was demonstrated in high-quality flight simulation. However, from this design and evaluation experience comes the warning that with radically new displays pilot performance can precede pilot understanding, with the result that inadequate emphasis is placed on instruction, testing, and practice.

REFERENCES

1. Lauber, John K.; Bray, Richard S.; and Scott, Barry C.: An Evaluation of Head-Up Displays in Civil Transport Operations. 1980 Aircraft Safety and Operating Problems, NASA CP-2170, 1981. (Paper 10 of this compilation.)

2. Bray, Richard S.: A Head-Up Display Format for Application to Transport Aircraft Approach and Landing. NASA TM-81199, 1980.

3. Head-Up Display Systems Evaluated. Aviation Week and Space Technology, Jan. 10, 1977, pp. 70-79.

4. Mirage 2000 Head-Up Display. Flight International, April 12, 1980, p. 1124.

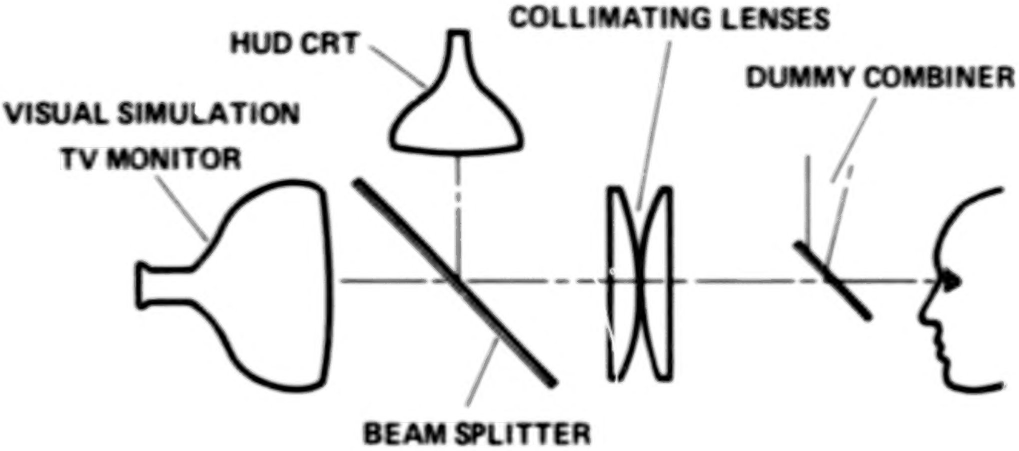
COLLIMATING LENSES
HUD CRT
DUMMY COMBINER
VISUAL SIMULATION
TV MONITOR
BEAM SPLITTER

Figure 1.- Optical combining of HUD with visual scene in simulator.

Figure 2.- Head-up display in simulated low-visibility approach.

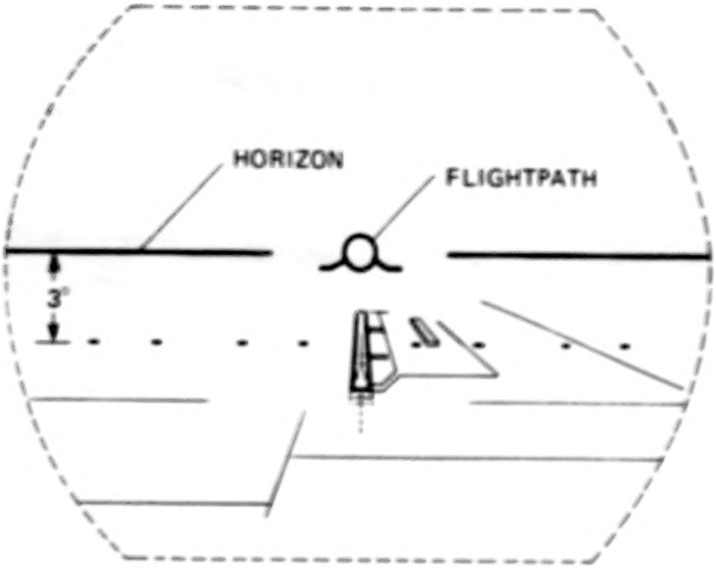
HORIZON
FLIGHTPATH
3°

(a) Level flight, above 3° path to touchdown point.

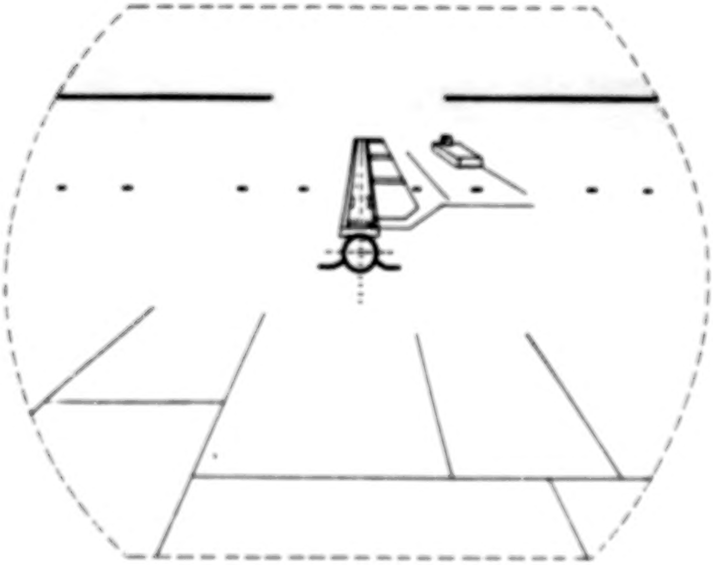

(b) Descending at 5° to establish 3° approach flightpath.

Figure 3.- Approach-path guidance provided by conformal display of flightpath vector.

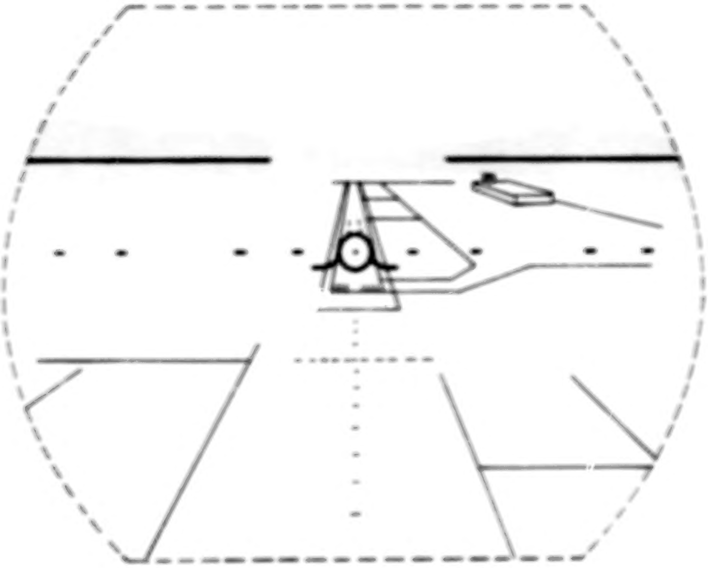

(c) On 3° approach flightpath.

Figure 3.- Concluded.

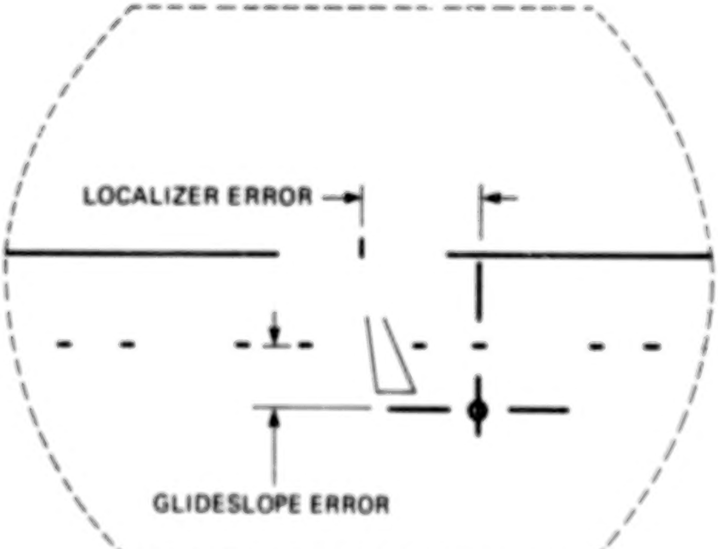
LOCALIZER ERROR
GLIDESLOPE ERROR

(a) Glide-slope and localizer-error indications.

Figure 4.- ILS guidance.

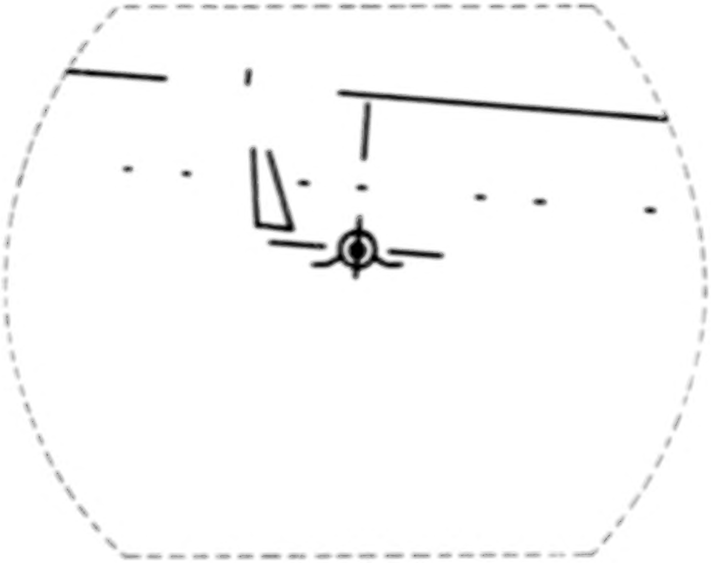

(b) Tracking combined error signals to effect convergence to ILS path.

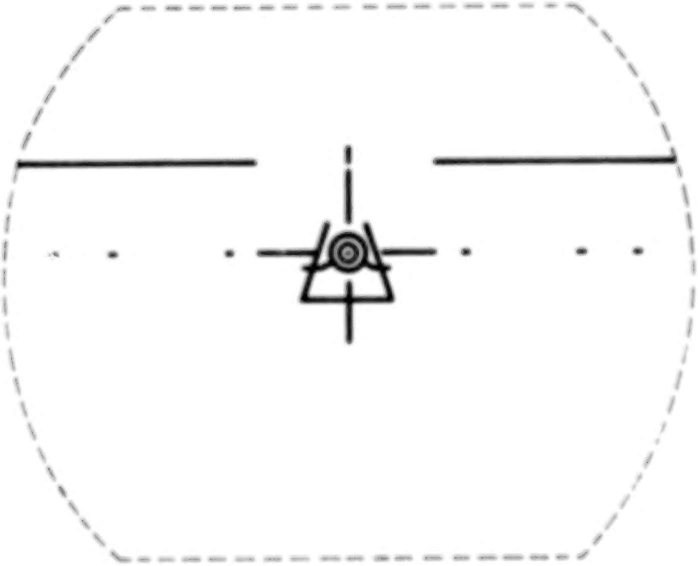

(c) On ILS approach path.

Figure 4.- Concluded.

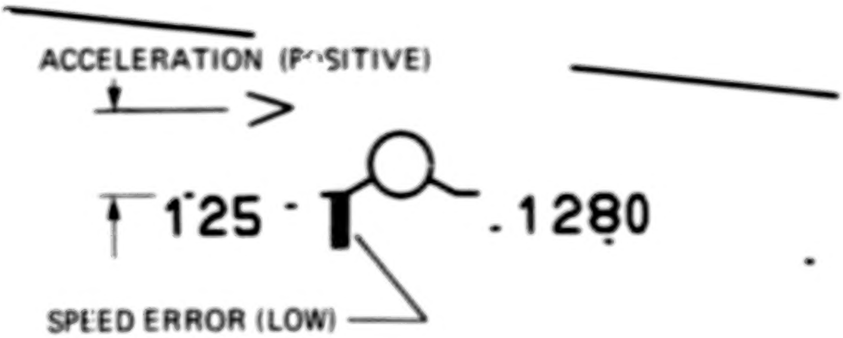
ACCELERATION (POSITIVE)
125
1280
SPEED ERROR (LOW)

Figure 5.- Fligthpath symbol and associated array of speed and altitude indications.

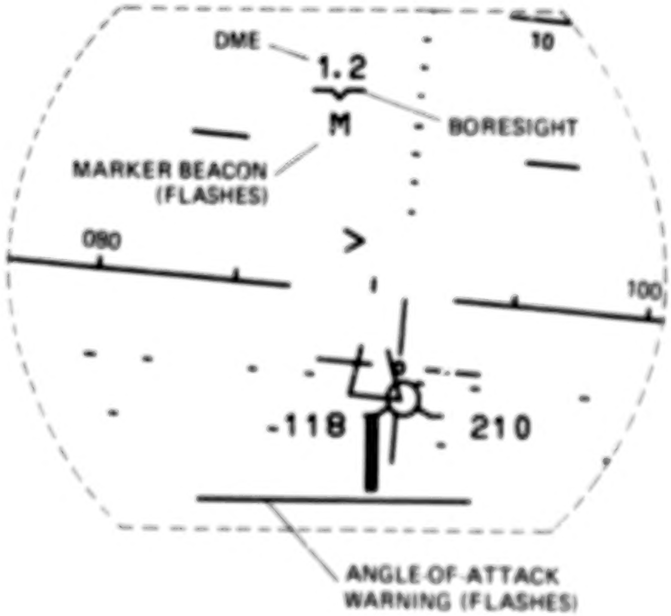
DME
1.2
10
BORESIGHT
M
MARKER BEACON (FLASHES)
090
100
-118
210
ANGLE-OF-ATTACK WARNING (FLASHES)

Figure 6.- Additional display references.

CONTENTS

Part I

PREFACE . . . . iii 1/A6

1. INTRODUCTORY REMARKS 1 1/A12
Roger L. Winblade

SESSION I - TERMINAL-AREA OPERATIONS
Cochairmen: T. A. Walsh and R. L. Kurkowski

2. TEST RESULTS OF FLIGHT GUIDANCE FOR FUEL CONSERVATIVE DESCENTS IN A TIME-BASED METERED AIR TRAFFIC ENVIRONMENT 7 1/B4
Charles E. Knox and Lee H. Person, Jr.

3. A PILOT'S SUBJECTIVE ANALYSIS OF A COCKPIT DISPLAY OF TRAFFIC INFORMATION (CDTI) 29 1/C12
Gerald L. Keyser, Jr.

4. GUIDANCE AND CONTROL SYSTEM RESEARCH FOR IMPROVED TERMINAL AREA OPERATIONS 51 1/E6
R. M. Hueschen, J. F. Creedon, W. T. Bundick, and J. C. Young

5. OPERATIONAL CONSIDERATIONS IN UTILIZATION OF MICROWAVE LANDING SYSTEM APPROACH AND LANDING GUIDANCE 83 1/G10
William F. White and Leonard V. Clark

6. AUTOMATED PILOT ADVISORY SYSTEM TEST AND EVALUATION AT MANASSAS MUNICIPAL AIRPORT 113 2/B4
John L. Parks, Jr.

7. A METHOD FOR DETERMINING LANDING RUNWAY LENGTH FOR A STOL AIRCRAFT 127 2/C14
D. M. Watson, G. H. Hardy, J. F. Moran, and D. N. Warner, Jr.

8. FLIGHT TESTS OF IFR LANDING APPROACH SYSTEMS FOR HELICOPTERS 145 2/E4
J. S. Bull, D. M. Hegarty, L. L. Peach, J. D. Phillips, D. J. Anderson, D. C. Dugan, and V. L. Ross

9. A HEAD-UP DISPLAY FORMAT FOR TRANSPORT AIRCRAFT APPROACH AND LANDING. 165 2/F10
Richard S. Bray and Barry C. Scott

MICROFILMED FROM BEST
AVAILABLE COPY

SESSION II - AVIONICS AND HUMAN FACTORS

Cochairmen: M. D. Montemerlo and A. B. Chambers

10. AN EVALUATION OF HEAD-UP DISPLAYS IN CIVIL TRANSPORT OPERATIONS 197 3/B2
John K. Lauber, Richard S. Bray, and Barry C. Scott

11. GENERAL AVIATION SINGLE PILOT IFR AUTOPILOT STUDY 201 3/B6
Hugh P. Bergeron

12. APPLICATION OF THE EPIDEMIOLOGICAL MODEL IN STUDYING HUMAN ERROR IN AVIATION 219 3/C10
Ed S. Cheaney and Charles E. Billings

13. HOW A PILOT LOOKS AT ALTITUDE 237 3/D14
Amos A. Spady, Jr., and Randall L. Harris, Sr.

SESSION III - ATMOSPHERIC ENVIRONMENT

Cochairmen: D. W. Camp and L. J. Ehernberger

14. SUMMARY OF FLIGHT TESTS OF AN AIRBORNE LIGHTNING LOCATOR SYSTEM AND COMPARISON WITH GROUND-BASED MEASUREMENTS OF PRECIPITATION AND TURBULENCE 251 3/E14
Bruce D. Fisher and Norman L. Crabill

15. WALLOPS SEVERE STORMS MEASUREMENT CAPABILITY 279 4/A3
Robert E. Carr and John C. Gerlach

16. THE 1979 CLEAR AIR TURBULENCE FLIGHT TEST PROGRAM 293 4/B3
E. A. Weaver, L. J. Ehernberger, B. L. Gary,
R. L. Kurkowski, P. M. Kuhn, and L. P. Stearns

17. PULSED DOPPLER LIDAR FOR THE DETECTION OF TURBULENCE IN CLEAR AIR 313 4/C9
E. A. Weaver, J. W. Bilbro, J. A. Dunkin, S. C. Johnson
W. D. Jones, C. E. Harris, and C. A. DiMarzio

18. FLIGHT TESTS OF A CLEAR-AIR TURBULENCE ALERTING SYSTEM 329 4/D11
Richard L. Kurkowski, Peter M. Kuhn, and Lee P. Stearns

19. CLEAR AIR TURBULENCE STUDIES WITH MICROWAVE RADIOMETERS 351 4/F5
Bruce L. Gary

20. IN-FLIGHT DIRECT-STRIKE LIGHTNING RESEARCH 359 4/F13
Felix L. Pitts and Mitchel E. Thomas

21. MAGNITUDE AND FREQUENCY OF WIND SPEED SHEARS AND ASSOCIATED DOWNDRAFTS 373 4/G13
Margaret B. Alexander and C. Warren Campbell

MICROFILMED FROM BEST AVAILABLE COPY

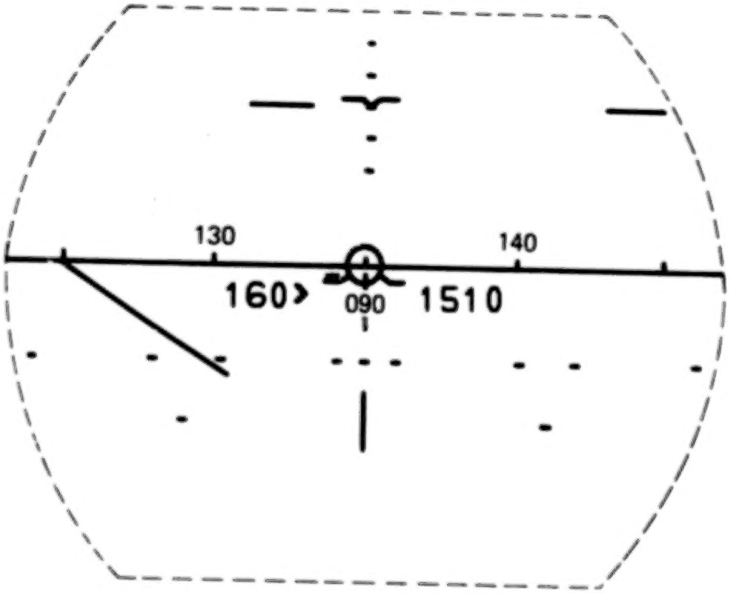
130
140
160>
090
1510

Figure 7.- Lateral guidance prior to localizer capture.

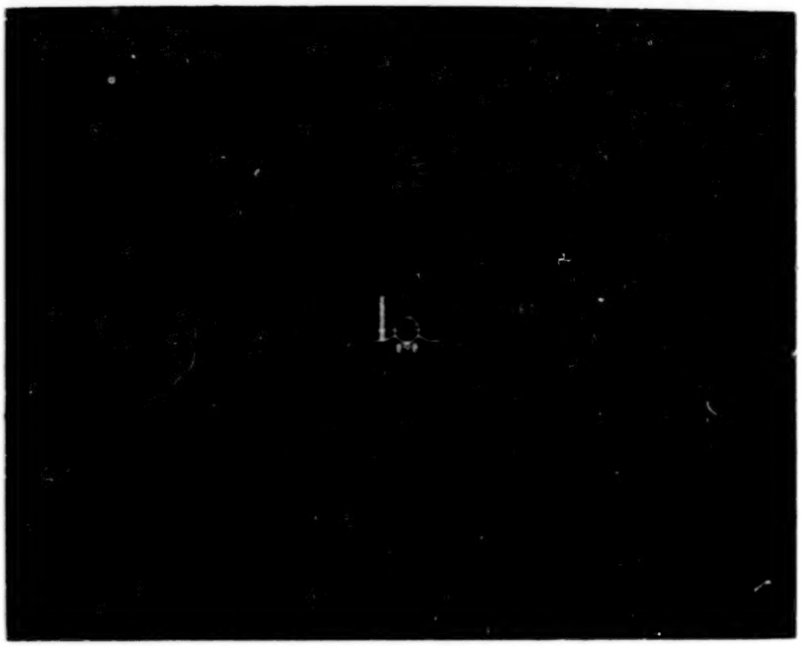

(a) Level flight on intercept heading.

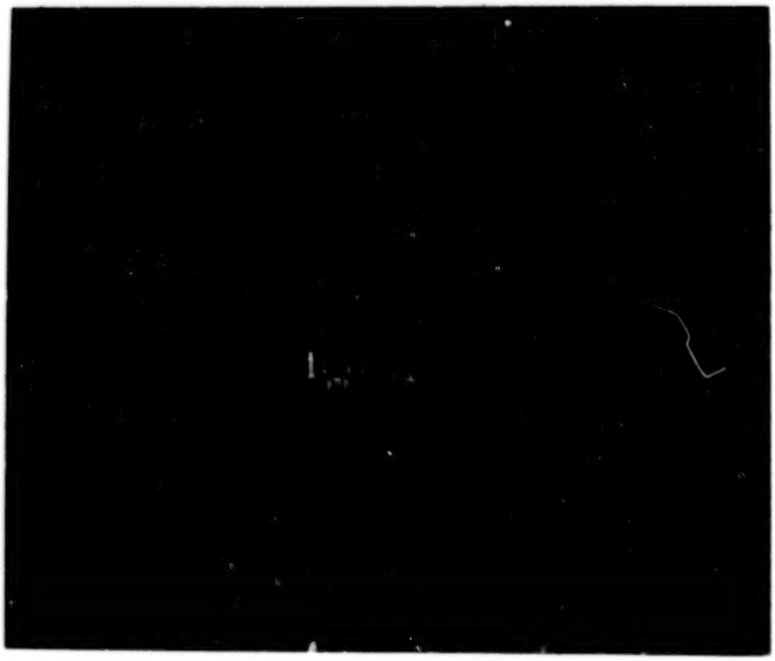

(b) Turning to localizer course.

Figure 8.- Photographs of HUD during simulated ILS approach.

(c) Near completion of localizer capture.

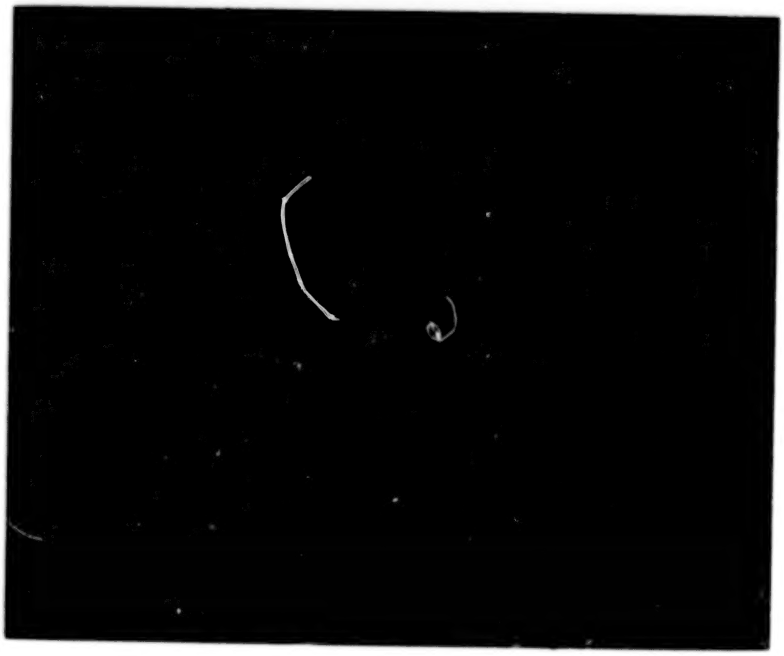

(d) Initiating pushover to ILS glidepath.

Figure 8.- Continued.

(e) On approach path.

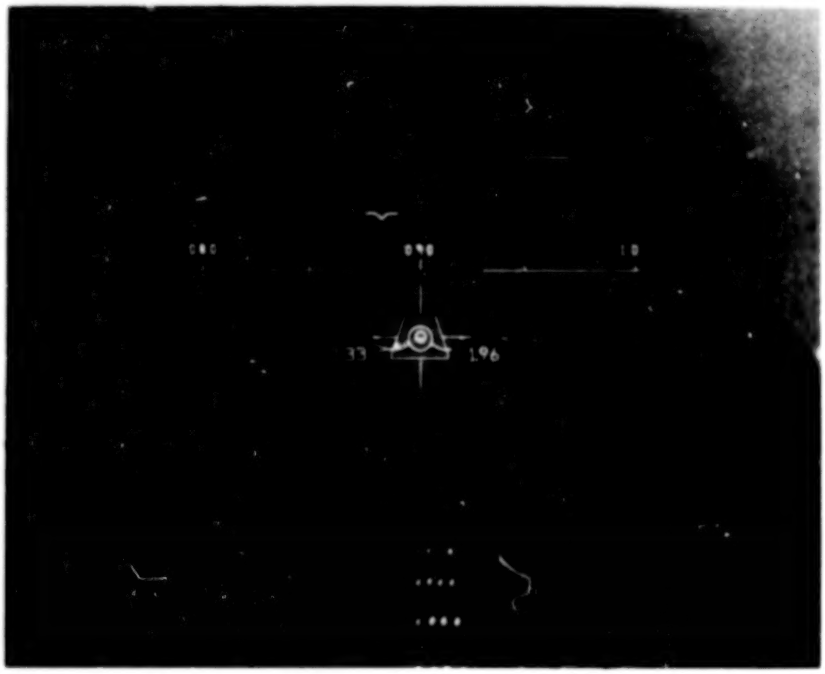

(f) Runway in sight, 900-m (0.5-mi) visibility.

Figure 8.- Continued.

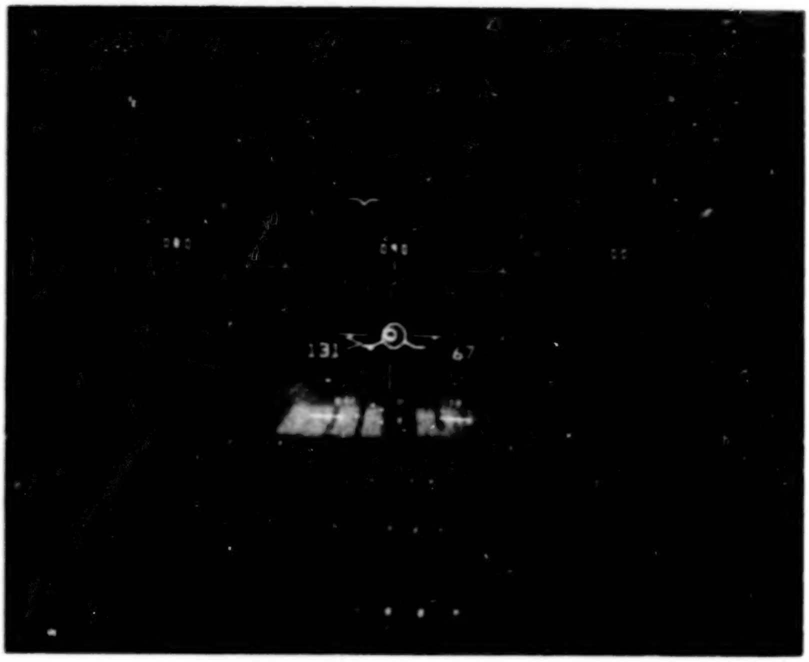

(g) Ground-proximity symbol rising.

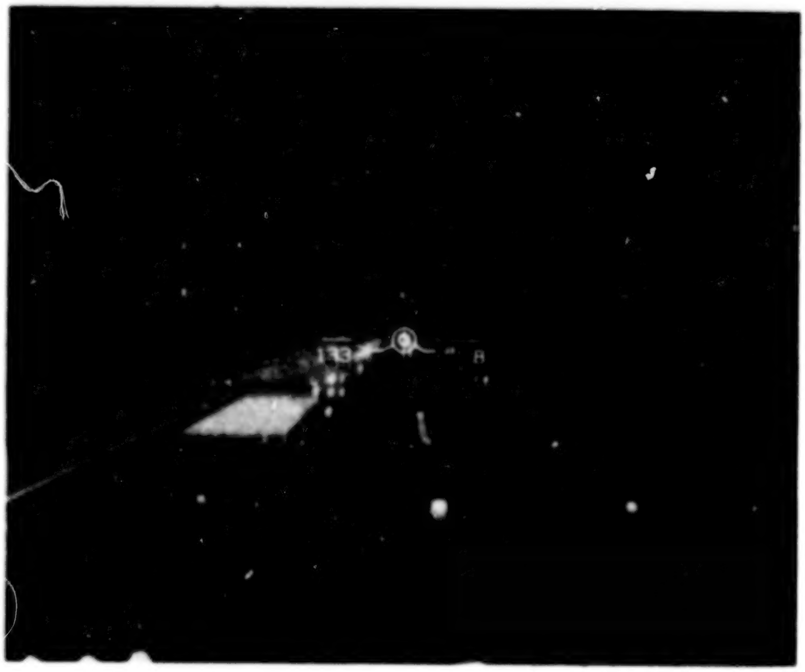

(h) Tracking ground-proximity symbol in flare.

Figure 8.- Concluded.

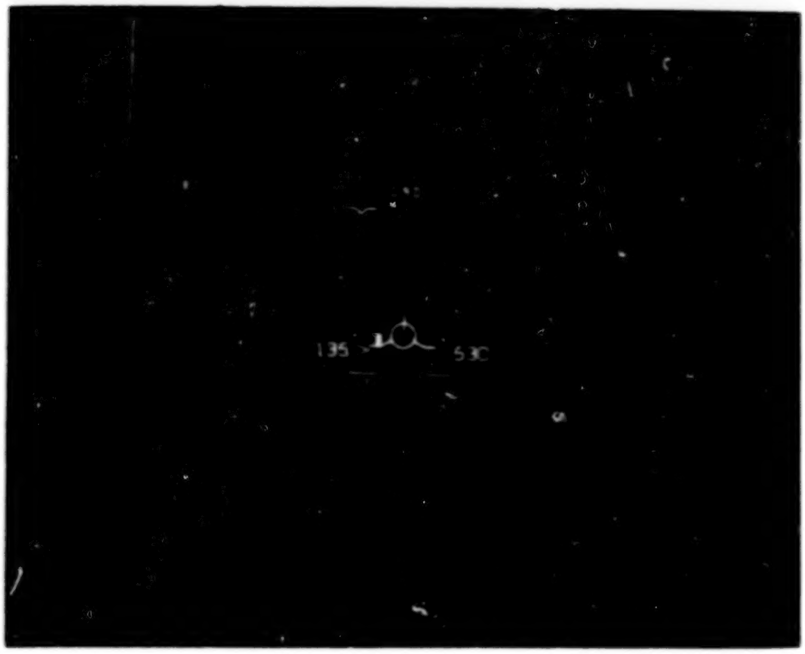

(a) Descending to MDA, target-altitude symbol rising.

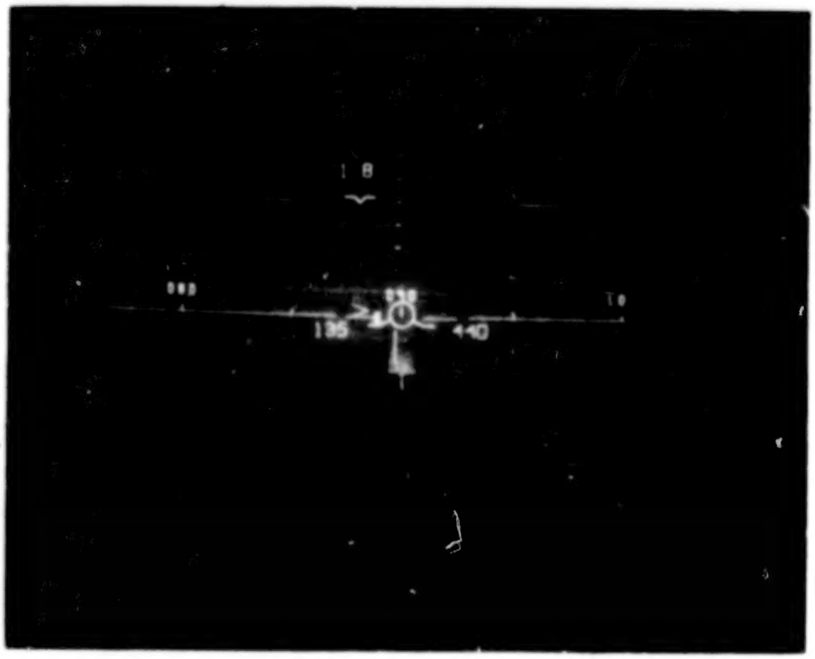

(b) Holding MDA by tracking altitude symbol.

Figure 9.- HUD in localizer-only nonprecision approach (NPA).

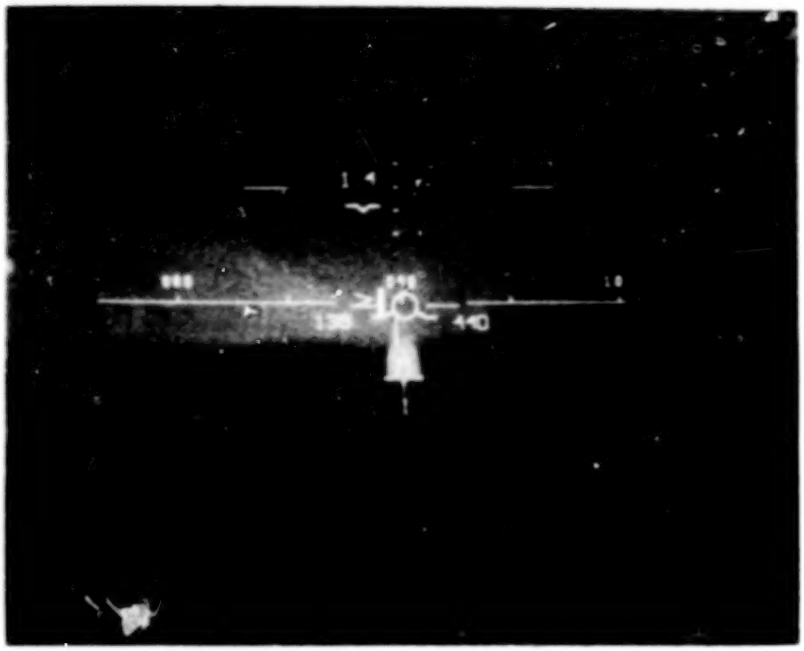

(c) Nearing 3° path to runway.

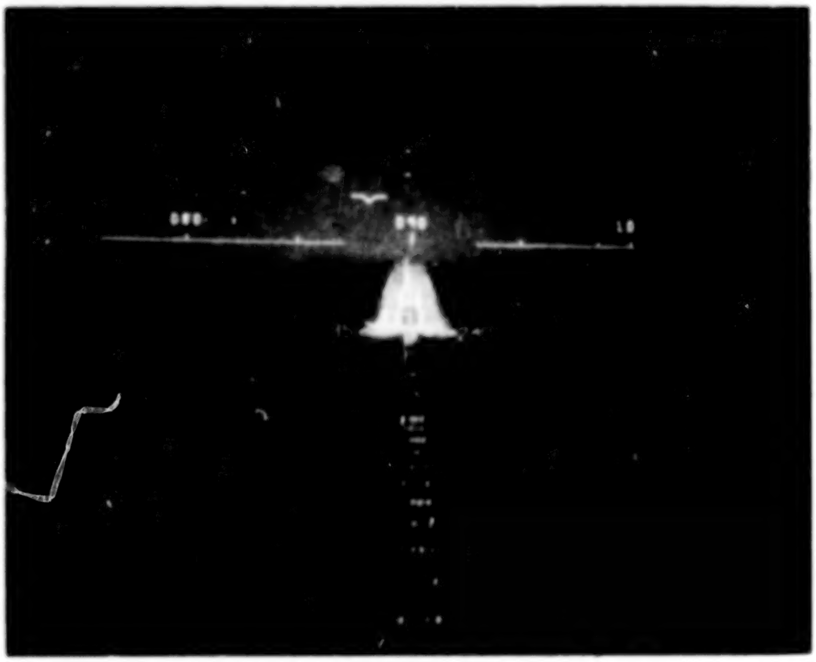

(d) Tracking intended touchdown area.

Figure 9.- Continued.

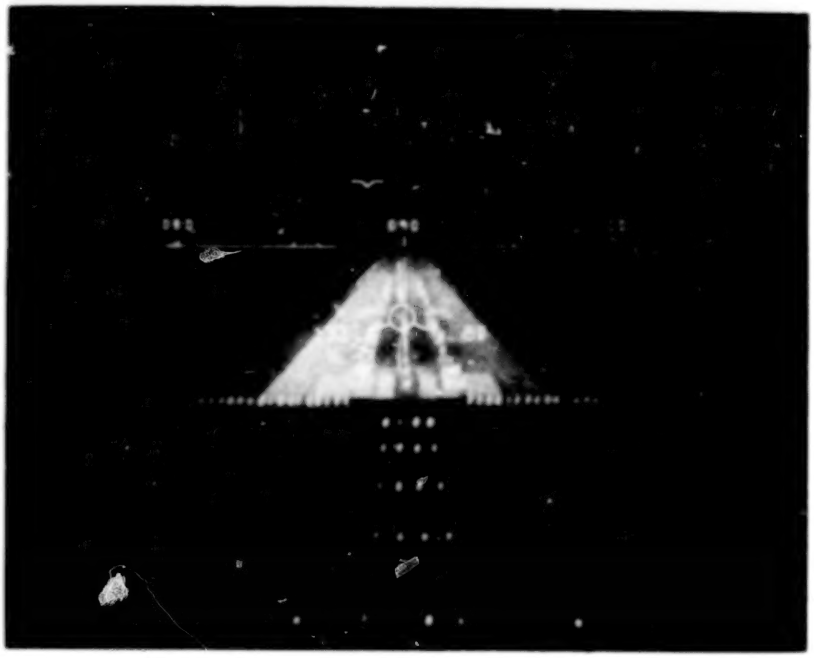

(e) Completing approach.

Figure 9.- Concluded.

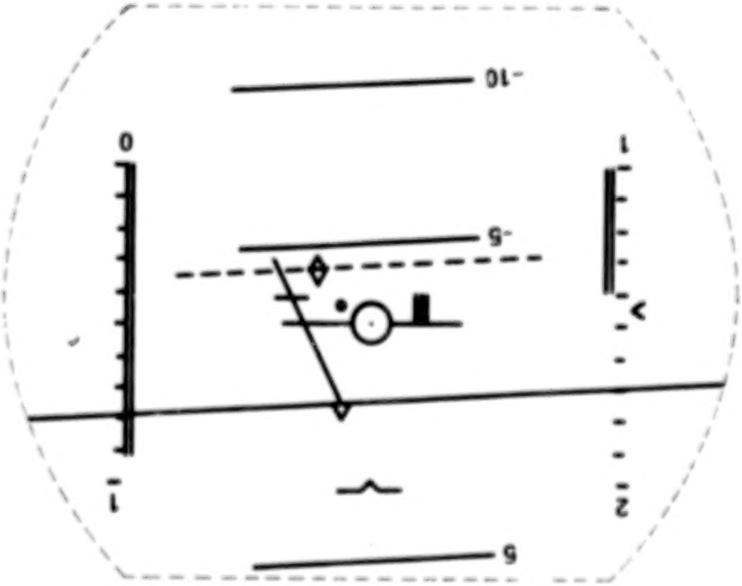

Figure 10.- Initial flightpath format of NASA-Ames HUD studies.

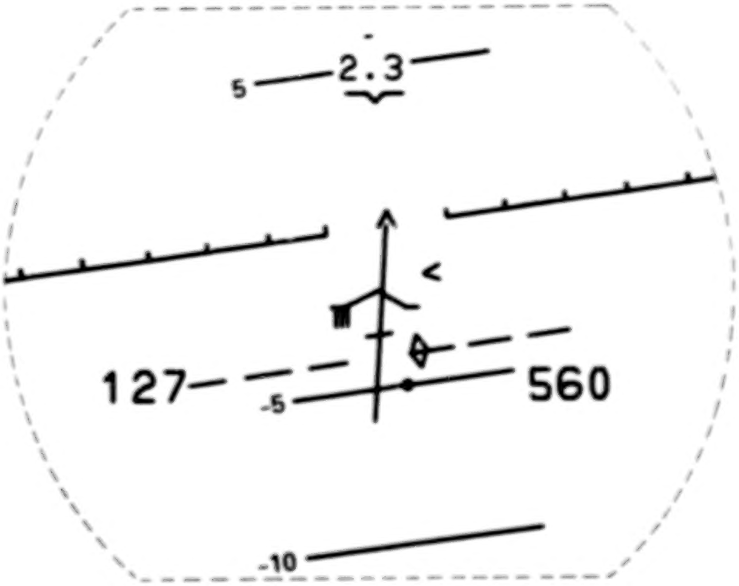
5
2.3
127
-5
560
-10

Figure 11.- First major variation of HUD format.

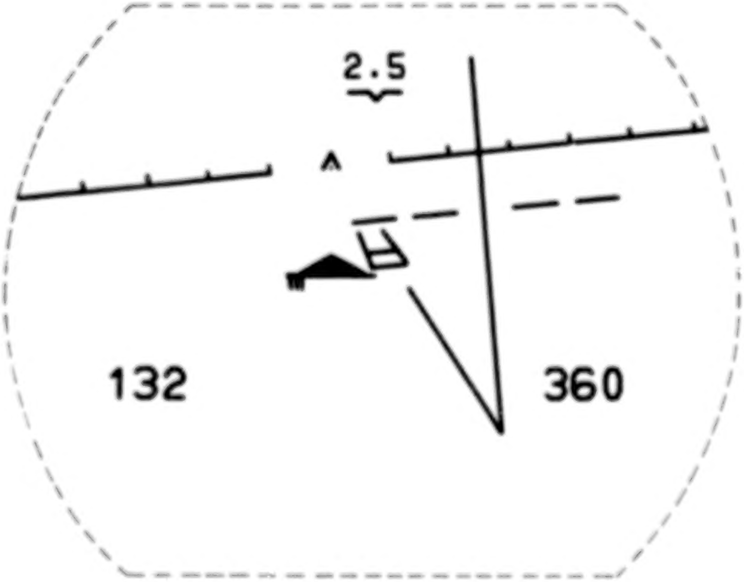

Figure 12.- Second variation of HUD format; assumes definition of ground track.

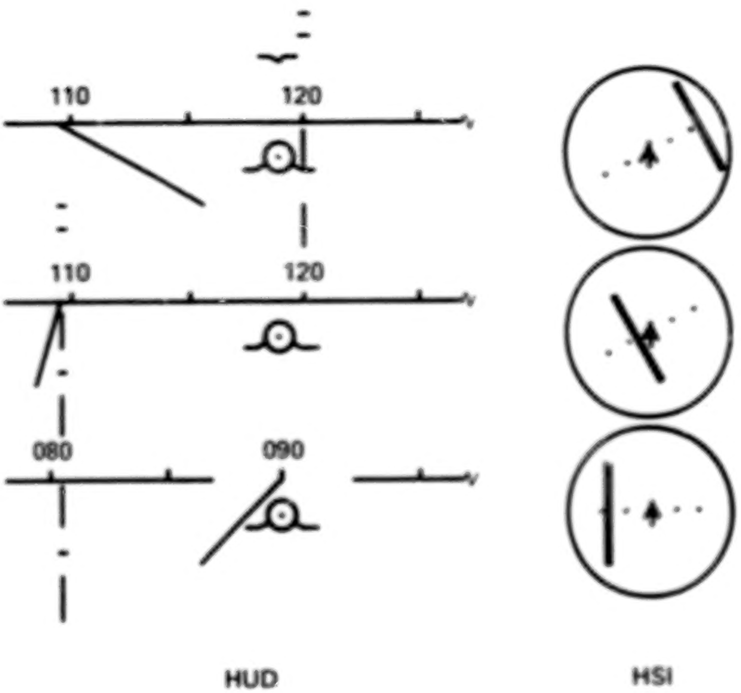
110
120
110
120
080
090
HUD
HSI

Figure 13.- Comparison of HUD and HSI indications of aircraft position and heading relative to ILS localizer course.

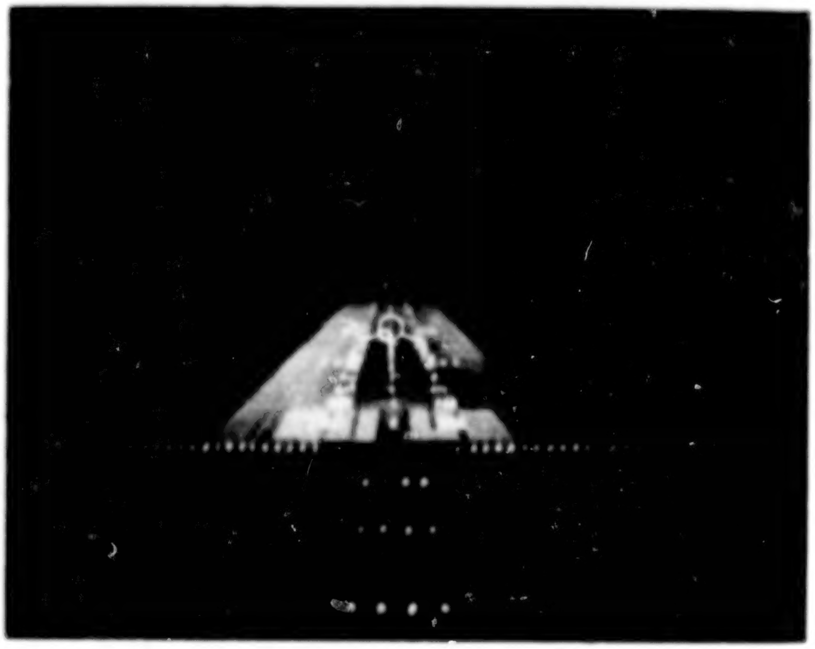

Figure 14.- "Decluttered" display.

BLANK PAGE

BLANK PAGE

SESSION II - AVIONICS AND HUMAN FACTORS

BLANK PAGE

BLANK PAGE

AN EVALUATION OF HEAD-UP DISPLAYS IN CIVIL TRANSPORT OPERATIONS

John K. Lauber, Richard S. Bray
Ames Research Center

and

Barry C. Scott
Federal Aviation Administration

SUMMARY

As part of a joint NASA/FAA program to determine the advantages and disadvantages of Head-Up Displays (HUD) in civil transport approach and landing operations, an operational evaluation was conducted on the Flight Simulator for Advanced Aircraft at Ames. Two HUD concepts were evaluated during this study: (a) a non-conformal HUD which contained raw data and Flight Director command information; and (b) a conformal, flight path HUD. Both HUD concepts were designed to permit terminal area maneuvering, intercept, final approach, flare, and landing operations. Twelve B-727 line pilots (Captains) flew a series of precision and non-precision approaches under a variety of environmental and operational conditions, including wind shear, turbulence and low ceilings and visibilities. A preliminary comparison of various system and pilot performance measures as a function of display type (Flight Director HUD, Flight Path HUD, or No HUD) has indicated improvements in precision and accuracy of aircraft flight path control when using the HUDs. The results also demonstrated some potentially unique advantages of a flight path HUD during non-precision approaches.

INTRODUCTION

The experiment reported in this paper is one of a series of studies conducted under a joint agreement between the FAA and NASA. The program was organized into four major phases: Phase I, for which the FAA had major responsibility, was a review of the relevant literature, and an analysis of the major issues surrounding HUD; Phase II, conducted at Ames Research Center, focussed upon fundamental human factors issues related to HUD and upon the development of candidate HUD concepts to be further evaluated in Phase III, which focussed upon the major operational issues associated with HUD and which is the subject of this report. Phase IV of the program consists of flight tests conducted in an FAA aircraft; this part of the program is currently underway, and will be reported in a future report. The following is an overview of the Phase III operational evaluation only. No attempt has been made here to summarize the entire Phase III study, and for complete details, the reader is referred to the final report for that project (ref. 1).

OBJECTIVES

The primary objectives of this study were to determine the benefits of HUDs during manually flown, visually referenced approaches and landings, and to determine potential problems associated with their use. Secondary objectives included a preliminary evaluation of various ancillary issues, including flight crew operating procedures and flight crew training requirements associated with the use of HUD in jet transport operations.

APPROACH

Two candidate HUDs were developed for use in the Phase III evaluation: (1) a flight path HUD, described in the paper appearing elsewhere in these proceedings by Bray and Scott (ref. 2); and (2) a flight director display, described in reference 3. Both of these HUDs were designed to be capable for use during precision and non-precision approaches. In addition, both displays were designed so that limited terminal area maneuvering and intercept of the final approach guidance could be accomplished using only information on the HUD.

Ten line qualified B-727 captains served as subject pilots for this experiment. Following completion of a comprehensive training program which consisted of handout material, lecture and 35 mm slides, video tapes and simulator training, subject pilots flew a series of precision and non-precision approaches under a variety of environmental and operational conditions, including head-, cross- and quartering tail-winds, ceilings and visibilities near the appropriate minima for the approach type, and various other conditions, including wind shear, variable visibilities and simulated runway incursions. An identical series of approaches was flown for each of the three display conditions (flight path HUD, flight director HUD, and no HUD). In addition to objective measures of aircraft flight path and airspeed control, subject pilots were asked to complete several questionnaires and rating scales during the course of the experiment.

RESULTS

Objective performance measures were analyzed by phase of approach and display type. Statistically significant differences in performance as a function of display type were observed for 23 variables at various stages of the approach and landing. All were measures of either airspeed, lateral flight path, or vertical flight path control. Generally, performance using either of the two HUDs showed improved precision and accuracy when compared to normal, no-HUD approach and landing operations. Significant improvements in vertical flight path control were particularly noticeable for non-precision approaches conducted using the flight path HUD.

Pilot opinion and rating data show strong preferences for the flight path display compared to conventional panel instruments. Opinion was divided with respect to the flight director HUD.

CONCLUSIONS

The preliminary results of the study have indicated that the use of a HUD can result in improvements in the precision and accuracy of flight path control under a variety of circumstances. These benefits were particularly noticeable for the flight path display during non-precision approaches. Other observations and conclusions were made regarding HUD design, training requirements, and operational procedures.

REFERENCES

1. Lauber, J. K.; Bray, R. S.; Harrison, R. L.; Hemingway, J. C.; and Scott, B. C.: An Operational Evaluation of Head-Up Displays For Civil Transport Operations: NASA/FAA Phase III Final Report. NASA TP-1815, 1981.

2. Bray, Richard S.; and Scott, Barry C.: A Head-Up Display Format For Transport Aircraft Approach and Landing. 1980 Aircraft Safety and Operating Problems, NASA CP-2170, 1981. (Paper 9 of this compilation.)

3. Naish, J. M.: A Review of Some Head-Up Display Formats. NASA TP-1499, 1979.

BLANK PAGE

BLANK PAGE

GENERAL AVIATION SINGLE PILOT IFR AUTOPILOT STUDY

Hugh P. Bergeron
Langley Research Center

SUMMARY

Five levels of autopilot complexity were flown in a single engine IFR simulation for several different IFR terminal operations. A comparison was made of the five levels of complexity ranging from no-autopilot to a fully coupled lateral and vertical guidance mode to determine the relative benefits vs. complexity/cost of state-of-the-art autopilot capability in the IFR terminal area. Of the five levels tested, the heading select mode made the largest relative difference in decreasing workload and simplifying the approach task. It was also found that the largest number of blunders was detected with the most highly automated mode. The data also showed that, regardless of the autopilot mode, performance during an IFR approach was highly dependent on the type of approach being flown. These results indicate that automation can be useful when making IFR approaches in a high workload environment, but also that some disturbing trends are associated with some of the higher levels of automation found in state-of-the-art autopilots.

INTRODUCTION

General aviation IFR operations have been increasing rapidly in the past few years. This increase is expected to continue and estimates are that the number of operations will double within the next 10 years. Along with this increasing IFR activity is a corresponding increase in accidents.[1]

A review of incident and accident data during IFR flights[1,2] shows several areas where incidents and/or accidents are most likely to occur. IFR flight in the terminal area, for example, during approach and landing, is usually associated with one of the highest incident and accident rates in single pilot IFR operations.[1-4] In many of these cases it appears that some level of automation might help reduce pilot workload and increase the safety of the flight. General aviation pilots, especially those flying single engine aircraft, however, have frequently resisted purchasing an autopilot for many reasons, (complexity/cost, reliability, pilot acceptance, etc). It is suggested that a simple low-cost partial capability autopilot can frequently provide sufficient benefits in an IFR environment to justify its use, whereas, a complete highly automated autopilot may be undesirable or unaffordable. This study compares relative benefits versus complexity/cost of state-of-the-art autopilot capability in the IFR terminal area.

The paper reports on research comparing various levels of autopilot complexity flown in a single engine IFR simulation for several different IFR approaches. The analysis reported in the paper represents an overview of the results. Examples are presented to illustrate some of the conclusions.

ABBREVIATIONS

ADF	automatic direction finder
BC	back course
CDI	course deviation indicator
COM	communication
DG	directional gyro
DH	decision height
GS	glideslope
HAC	heading select with lateral nav coupler and altitude hold with vertical nav coupler
HC	heading select with lateral nav coupler
HS	heading select
IFR	instrument flight rules
ILS	instrument landing system
K	kilometers
LOC	localizer
N	nautical
NA	no-autopilot
NAV	navigation
NDB	nondirectional radio beacon
OBS	omni bearing selector
PIO	pilot induced oscillation
VOR	very high frequency omni range
WL	wing leveler
WX	weather

Simulation Facility

The tests were performed on the NASA Langley general aviation simulator. The simulator, flown in the fixed-base mode, was configured and programmed as a typical high wing single engine aircraft. Figure 1 shows an outside view of the simulator. The cockpit was outfitted with typical basic aircraft instruments. In addition to these instruments, the following were also included: an ADF receiver, two NAV COM systems with corresponding CDI's, and a complex autopilot system. Figure 2 shows an inside view of the cockpit. The simulation also incorporated a video out-the-window visual presentation, a programmed navigational area encompassing the landing approaches flown, a realistic engine and airstream noise system, and a force feel wheel and column control loader.

The visual out-the-window scene was used for breakout and landing, weather permitting. The scene is a video presentation of a map model that encompassed a scaled area of approximately 4.4 km (2.4 N miles) by 13.9 km (7.5 N miles).[5] Although two airports were located in the scene, all approaches were set up for only one of the airports. However, the second airport did play an unplanned part in some of the tests. This will be discussed later. Landing and taxiing can be accomplished with this visual presentation.

The programmed navigation area on the computer encompassed the five airports used in this study. All the programmed NAV facilities duplicated the local real-world NAV environment. All radio aids, magnetic variation, etc, were included in the simulation. The simulation did not, however, include some of the anomalies associated with the specific real world NAV installation (i.e., scalloping, multiple glideslope paths, etc).

Method

Five levels of autopilot automation were tested. The five, in order of increasing levels of automation, consisted of: (1) no-autopilot (NA); the basic aircraft, (2) wing leveler (WL); the WL mode used in this study did not have a centering detent on the roll command knob, (3) heading select (HS); a course selector directional gyro was used in this mode, (4) heading select with lateral NAV coupler (HC); this mode included lateral guidance for both VOR and ILS navigation, and (5) heading select with lateral NAV coupler and altitude hold with vertical NAV coupler (HAC); in addition to the previously discussed capabilities this mode also included a choice of pitch attitude hold, altitude hold, or vertical NAV guidance (i.e., glideslope coupler).

Five airports and their associated radio NAV aids located in the general vicinity of Langley Research Center were programmed and used in this study. The types of approaches included two ILS approaches, one VOR approach, one LOC BC approach, and one NDB approach. These approaches, and other pertinent information, are given in more detail in table I.

The ceiling and visibility for each data run were randomly chosen from three conditions predefined for each of the five approaches. They were: (1) 15.2 m (50 ft) ceiling and 0.8-km (0.5-mi) minimums for the given approach, (2) published minimums for the given approach, or (3) 61 m (200 ft) above ceiling and double visibility of published minimums for the given approach. All the runs were flown in moderate turbulence (1.2 m/sec (4 ft/sec)) and 20 kt winds from a predefined direction. (See table I.)

Seven subjects were used in the tests: Two NASA test pilots and five IFR rated pilots with various levels of IFR and autopilot experience. Each subject flew a total of 27 data runs. This included the 25 different combinations of five autopilot modes and five different approaches. The extra two runs per subject were repeats for replication purposes. The order or presentation was randomly determined for each pilot. Simulation sessions were scheduled for 2-1/2 hours with a 15-minute break halfway through the session. Except for one subject, no two sessions were on the same day. Four to five sessions were usually required to complete one pilot's set of runs.

Prior to making any data runs, the subjects were scheduled for a session during which they were able to practice all autopilot modes until they were satisfied with their performance with the autopilot. The approaches used for data (table I) were not used in the practice sessions.

TABLE I.- APPROACHES

Airport	Runway	Approaches	Display	Wind
Norfolk, VA	5	ILS	CDI	091°/20 kt
Atlanta, GA	8	ILS	CDI	225°/20 kt
Newport News, VA	25	LOC/BC (Holding)	CDI	290°/20 kt
Franklin, VA	9	VOR	CDI	332°/20 kt
Wakefield, VA	20	NDB	Fixed compass card	155°/20 kt

Data Acquisition

The piloting task consisted of flying the specified approach (table I), making the required pilot reports, and performing a side task. The pilot reports were specified for the particular approach being flown. The side task was a self-pacing velocity/distance/time problem solved by using a hand held E6B type flight computer. For the side task, the subject would, upon his request, be given a problem. He would solve the problem, when time was available, and report the answer. The radio communication system in the simulator was used for this process. The subject was told to perform the side task only when it would not interfere with or change the quality of the approach being flown. The problems and answers for each run were recorded.

The pilots were given handouts which included all five approach charts, their aircraft location, the initial conditions for each approach, and the required reporting points. Table II shows typical initial conditions for one of the approaches.

TABLE II.- INITIAL CONDITIONS

Newport News LOC BC Rwy 25	
Altitude	61 m (2000 ft)
Heading	065 deg
Airspeed	100 kts
Wind velocity*	20 kts
Wind direction	290 deg

*From 305 m (1000 ft) to ground wind velocity goes from 20 kts to 10 kts.

TABLE II.- INITIAL CONDITIONS (cont'd)

Newport News LOC BC Rwy 25

Turbulence	moderate (1.2 m/sec (4 ft/sec))
WX conditions	day time/ceiling and visibility as specified
Flaps	0
NAV1	110.1 mc
OBS 1	--
NAV 2	116.9 mc
OBS 2	342 deg
ADF	375 kc

NOTE: Use tear drop entry

The initial conditions positioned the aircraft at a location where a final approach and landing clearance would typically be received for that approach.

At the beginning of each day's session, the subject was given a practice run. Also, prior to each data run, the subjects were given sufficient time to review the approach chart, conditions, and procedures. They were then given an IFR clearance and reporting points for the approach and the simulation was started. The runs were ended after landing and rollout or 10 to 20 seconds after initiation of the missed approach.

The data taken during each approach consisted of flight technical error, ground track and profile plots, pilot workload rating and comments, and side task results.

RESULTS AND DISCUSSION

A review of the data disclosed several events and trends associated with pilot performance in flying the various autopilot modes. The following analysis is based on pilot comments, pilot ratings, side task results, and ground track and profile plots. In analyzing the data, it is necessary to consider the interrelationship of several of the above data to fully understand the results. Results from a single source of data can often be misleading. For example, the side task results are dependent not only on task difficulty but also on total time required to complete the approach, whereas the time required to complete the approach is dependent on the specific approach being flown, piloting technique in flying the approach, and the difficulty of the approach. Also, the total time to fly the approach may be either longer or shorter if the pilot blunders or deviates from the normal approach path.

The following discussion includes a brief comparison of the five levels of autopilot complexity. This is followed by a discussion of the effects of the different approaches. Finally, an indepth discussion of trends, as related to the various levels of automation, is presented.

Autopilot Comparison

Side Tasks.- The side task results, figure 3, in general are representative of all the data. This figure shows the average number of problems completed per run during all the approaches for all the subjects at each level of autopilot complexity. The upper and lower limit bars represent the maximum and minimum of the averages of the individual subjects at each level of autopilot complexity. Implicit in using a secondary task is the assumption that the more difficult the task, the fewer problems completed, hence, the higher the workload associated with the primary task. As can be seen by the data, the workload tends to decrease (increased secondary task performance) as automation level is increased. Significant, however, is the leveling off of the workload for automation levels greater than the HS mode. One interpretation of this phenomenon is that beyond the HS mode the subject trades off the workload associated with flying the control task for the workload required to monitor the autopilot's control of the flight task. This results in little net difference in primary task workload beyond the HS mode.

Pilot Workload Ratings.- Figure 4 shows a similar relationship with respect to subjective pilot workload ratings. At the end of each run the subject rated the primary task on a workload scale of 1 to 7 with 1 designated as the easiest and 7 as the hardest. It should be realized that this type of rating technique typically produces a relative workload rating of difficulty rather than an absolute workload rating. The format of figure 4 is similar to that of figure 3, i.e., figure 4 shows the average workload rating per run during all the approaches for all the subjects at each level of autopilot complexity. The upper and lower limit bars represent the maximum and minimum of the averages of the individual subjects at each level of autopilot complexity. These results tend to agree with the side task results, i.e., increased automation decreases workload. There is also a slight leveling off of the workload beyond the HS mode, but it is not as dramatic as in the side task data.

Ground Track Plots.- Figures 5, 6, and 7 show typical pilot control of flight ground tracks. The three ground track plots shown are for the NA, WL, and HS autopilot modes. All are for the Atlanta ILS approach and were all flown by the same subject. An altitude profile plot is also included in figure 5. These figures illustrate the differences in the frequency characteristics. The NA mode, figure 5 for example, exhibits two frequencies; a high frequency with low damping and a low frequency. As the level of automation increases, see figures 6 and 7, the high frequency component decreases, in both amplitude and frequency. This results in an apparent smoothing of the ground track trace. This smoothing trend with automation was characteristic for all the different approaches flown in this study.

No-autopilot (NA) Mode.- In the NA mode the pilot flew the basic aircraft without assistance from any autopilot mode. The data, including pilot comments and ratings, show this mode to be the most difficult to fly. Typically, the biggest problem in flying the NA mode was high workload (as measured by the side task and pilot ratings) and less precise flying. Figure 8 shows an example of this characteristic for the Newport News LOC BC approach. The holding pattern during this run does not conform to a typical pattern. Also, the ground track of the NA mode exhibits relatively high frequency and low damping characteristics.

Wing Leveler (WL) Mode.- This mode was slightly easier than the no-autopilot mode, but some characteristics of the mode were disconcerting. Many of the subjects found the WL inputs disturbing when trying to control pitch. The control wheel moving in roll interfered with pitch inputs. Also, the particular autopilot used in this study did not incorporate a centering detent on the roll command knob. This lack of accurate centering frequently resulted in the aircraft being in a slight bank with the pilot having to continually make inputs to keep wings level. A centering detent is considered very desirable, especially when flying in turbulence. An interesting side issue is that those subjects not intimately familiar with the WL mode commented that it took considerable practice to become comfortable with this mode. Even considering all the above, however, all pilots preferred this mode to the no-autopilot mode.

Heading Select (HS) Mode.- The HS mode was considered, by the subjects, to be much easier to fly than the WL mode. Of the five levels of autopilot complexity tested, the HS mode was found to make the largest difference in decreasing workload and simplifying the approach task. It was also observed that the workload, as measured by the side task, leveled off for the HS, HC, and HAC modes (see figure 3).

Heading Select with Lateral NAV Coupling (HC) Mode.- The next level of complexity, the HC mode, was considered somewhat easier than the HS mode but not by a large margin. One interesting point, however, is that in this mode no comments were made about roll inputs interfering with the pilot's control of pitch. These comments were made in the WL and, to a lesser degree, the HS modes. These may be due to the fewer inputs required in these two latter modes.

Heading Select with Lateral NAV Coupling and Altitude Hold with Vertical NAV Coupling (HAC) Mode.- The most fully automated mode tested, HAC, as expected, was somewhat easier to fly than the HC mode, but again not by a large margin over the HC mode. In addition, several problems associated with the HAC mode, especially in a high pilot workload environment, became apparent. To a lesser degree some of these problems also existed for the HC mode. This will be discussed later.

Approaches

In addition to the varying levels of difficulty in flying the approach task due to a given level of autopilot automation, the different types of approaches were also found to be a factor in difficulty of flying the task. This was taken into consideration in analyzing and comparing the autopilot data. In general, the data show that the ILS approach (LOC and GS) was the easiest to fly. The ILS data included the runs from both the Norfolk and Atlanta approaches.

The Newport News LOC BC and Franklin VOR approaches were about the same in overall task difficulty. They were, however, more difficult than the ILS approach. Some variability did exist for the two approaches from pilot to pilot and from autopilot mode to autopilot mode. It is difficult to make a point to point direct comparison of the two approaches due to the difference in display sensitivity, the mental gymnastics of reverse sensing, and the added task of holding in the LOC BC approach.

The Wakefield NDB approach was found to be the most difficult by the majority of the subjects. This is partly due to the different display used in this approach, i.e., the typical ADF relative bearing needle on a fixed compass card. This lack of a computed, displayed error for the desired path makes the tracking task more difficult. The pilot must continually compute error information mentally, using the relative bearing and DG information. The differences in difficulty in flying the various approaches can, to a large degree, be related to differences in display format, information, and sensitivity and to procedures.

General Trends

Several disturbing trends were noted as the level of autopilot automation was increased. In general, an increased level of automation tends to take the pilot out of the aircraft control loop. He becomes a manager of the autopilot functions. The effects of this change in duty appear to be emphasized in the HAC mode. The subjects were more likely to lose track of where they were in the approach. It seemed that in monitoring the autopilot they would associate instrument readings with the autopilot functions rather than to situational awareness. Therefore, if the autopilot functions were either set incorrectly or interpreted incorrectly, the subject would frequently perform the wrong task, thinking that everything was normal. This would frequently lead to an incident or blunder. An example is shown in figure 9 (Franklin VOR approach, HAC mode). The run began with the autopilot set in the heading select mode. After crossing the VOR, a right turn to the outbound course was initiated. At this point the autopilot was switched to omni coupler to intercept and track the outbound course. However, the subject had neglected to reset the correct bearing on the CDI. Therefore, the autopilot reintercepted and tracked the original bearing of the CDI. Eventually, he realized his mistake and set the correct outbound bearing. The aircraft then took up a 45° intercept path to the new bearing. After a fair amount of time he still had not intercepted the outbound course but due to the time into the approach he decided to make a pseudo procedure turn using heading select. At this point in time he also set in the correct inbound heading on the CDI. Upon completion of the procedure turn he continued in heading select until the CDI needle came alive. He than selected omni coupler and completed the approach without further incident. It is likely this incident would not have been detected in the real world.

Another subject (figure 10, Wakefield NDB approach, HAC mode) made his final let down on an outbound heading. He leveled off and made his missed approach without ever realizing his mistake. Another interesting facet related to this run is the fact that the NDB at Wakefield is located on the airport. The missed approach should have been executed when, if in this case, the NDB was crossed. In fact several, otherwise normal, runs were also flown at Wakefield in which the missed approach was executed prior to crossing the NDB inbound. It seems that the subjects would time their outbound leg and use this time, rather than the NDB crossing, to execute their missed approach. The 45° left headwind on the inbound heading was obviously a contributing factor in these incidents. This situation implies a lack of positional awareness.

Several other comments about the HAC mode are considered relevant at this point. A couple of subjects commented that, while flying the HAC mode, they had a tendency, at times, to forget to perform the side task. Another subject felt that the altitude hold and glideslope coupler could create a safety issue. The pilot can be lulled into a false sense of security or complacency with all the automatic features. The problem appears to be almost as if the pilot thinks of the autopilot as a copilot and expects it to think for itself. He allows himself to become completely engrossed in other tasks once the autopilot is set. Hence, he is frequently late in resetting new functions or he may become confused as to exactly where he is in the approach and not reset all the necessary functions or controls. Still another subject commented that the more automated his autopilot the less he trusted it. He stated he had trained himself to expect and look for problems of an insidious nature when using complex autopilots.

The above comments agreed with the relationship of blunders versus autopilot automation. The HAC mode encompassed the largest number of detectable blunders.

Remember also that the type of approach was a factor on the prevalence of incidents or blunders, the fewest exhibited during the ILS approaches and the most during the NDB approach. One notable exception was during an Atlanta ILS approach where the subject got into a PIO at the middle marker and impacted the ground. (The PIO characteristic of ILS sensitivities associated with the middle marker has been observed in independent work at NASA LaRC.) The no-autopilot mode was being used for this run. The DH for the approach was 61 m (200 ft) above the ground. However, this was only one of two blunders for the more than 70 ILS runs flown. The second was when the subject executed a missed approach at the outer marker thinking he was at the middle marker. The altitude at the outer marker was 853.4 m (2800 ft), whereas at the middle marker it would have been 365.8 m (1200 ft). This latter run was flown with the HAC mode.

Several other incidents or blunders not related directly to the autopilot mode are worth mentioning at this point. One subject executed his missed approach early for three of the five runs he flew on the Newport News LOC BC approach. The wind for this approach was a 45° right headwind to final approach. The subject stated that he intentionally does not use reported winds in his missed approach timing. Another problem in LOC BC approach was positional disorientation due to reverse sensing on the CDI. One subject became so confused he became lost on one run and had to abort.

The Franklin VOR approach demonstrated similar problems. In several runs, for example, the subjects overshot the outbound heading on the approach course by a fairly large margin. Also, the procedure turn was, on several occasions, considerably larger and out of porportion to the desired path. The approach had a 20 knot, 45° tail wind relative to the final approach heading. This tail wind apparently also caused a larger number of missed approaches. The subjects would not compensate for the tail wind in their approach timing, would descend too slow, and breakout beyond the airport.

During the Wakefield NDB approach two subjects landed at a second airport which just happened to be part of visual model. The second airport was located approximately 4.8 km (3 mi) from the destination airport at about 0.8 km (0.5 mi) to the left side of the desired approach path. Figure 11 shows the ground track and profile plots of one of these runs. The location of a second airport in the vicinity of the destination airport was not planned as part of the experiment. Therefore, the subjects were not previously told about the location of the second airport. This incident, having occurred, however, emphasizes the problem associated with airports located in the vicinity of each other.

CONCLUDING REMARKS

A total of 189 IFR approaches were flown on the NASA Langley general aviation simulator to compare various levels of automation of autopilot systems. Seven IFR rated pilots flew five different airport/approaches with five levels of autopilot complexity.

Of the five levels of autopilot complexity tested, the subjects rated each level of added automation to be somewhat easier to fly than the previous level, except for one mode. This mode, heading select, was considered to be much easier than its next lower level of automation. Also, the data show that the heading select mode made the largest difference in decreasing workload and simplifying the approach task. The most fully automated mode, which included altitude hold and vertical nav coupling, exhibited some disturbing aspects, i.e., the largest number of blunders was detected with this mode. Also, the side task results showed no decrease in workload from its next lower level of automation.

The data show that the overall quality of performance during an approach was highly dependent on the type of approach being flown. The ILS approach, localizer, and glideslope were found to be the least difficult. The VOR and localizer back course approaches were rated about the same in difficulty, but were considered more difficult than the ILS approach. The NDB approach was considered to be the most difficult of those tested.

The results of this study indicate that automation is desirable when making IFR approaches in a high workload environment, but also that some disturbing trends are associated with the higher levels of automation as presently implemented in state-of-the-art autopilots. It is believed however, that a better man/machine interface could alleviate these problems. The data further suggest that the heading select mode may currently be the best choice for the IFR approach task when considering both benefits and costs.

REFERENCES

1. Forsyth, Donna L.; and Shaughnessy, John D.: Single Pilot IFR Operating Problems Determined from Accident Data Analysis. NASA TM-78773, September 1978.

2. Bergeron, Hugh P.: Analysis of General Aviation Single Pilot IFR Incident Data Obtained from the NASA Aviation Safety Reporting System. NASA TM-80206, October 1980.

3. Ames Research Center and ASRS Office: NASA Aviation Safety Reporting System: Second Quarterly Report. July 15 - October 14, 1976. NASA TM X-3494, December 1976.

4. Ames Research Center and ASRS Office: NASA Aviation Safety Reporting System: Third Quarterly Report. October 15, 1976 - January 14, 1977. NASA TM X-3456, May 1977.

5. Rollins, John D.: Description and Performance of the Langley Visual Landing Display System. NASA TM-78742, August 1978.

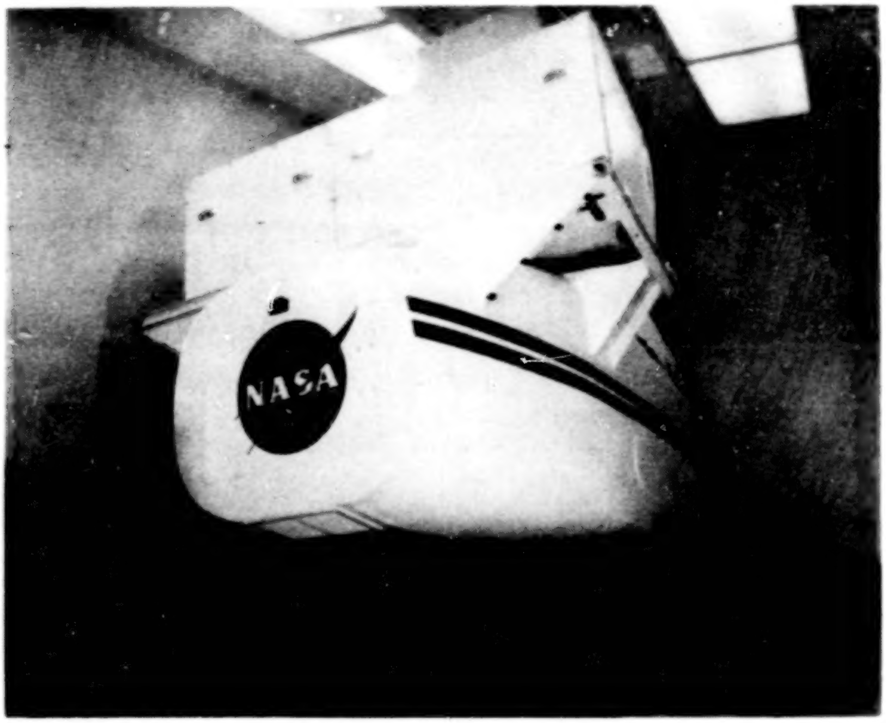

Figure 1.- Outside view of simulator.

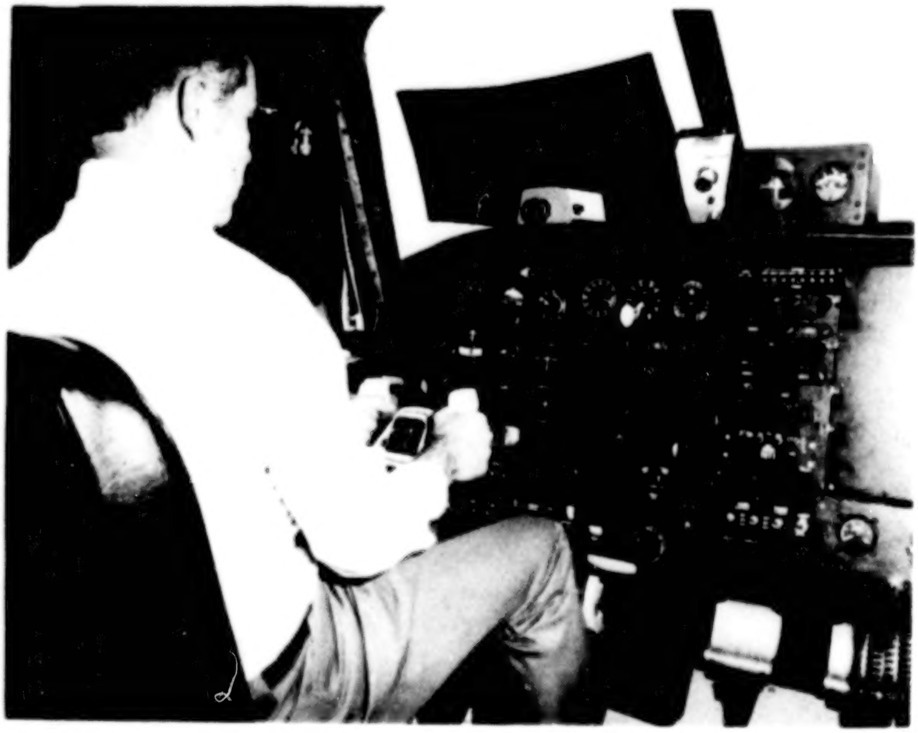

Figure 2.- Inside view of simulator.

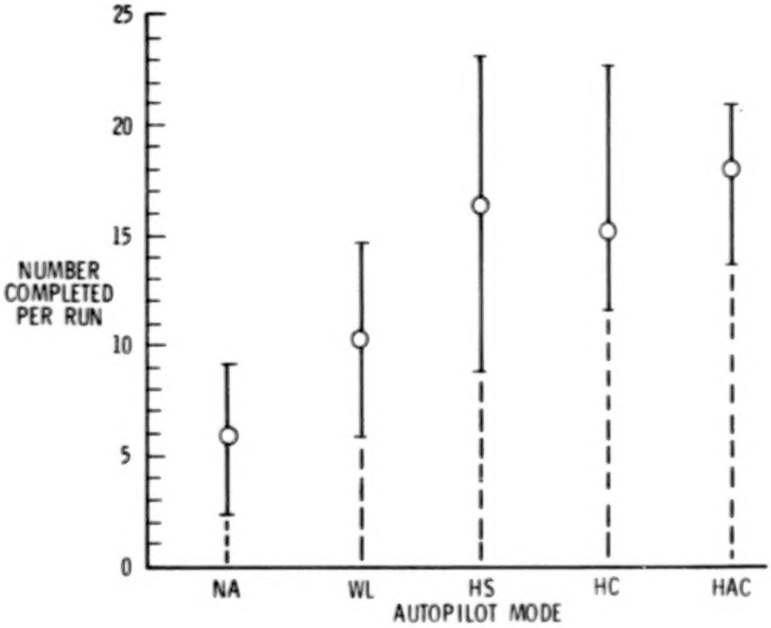

Figure 3.- Average number of side tasks.

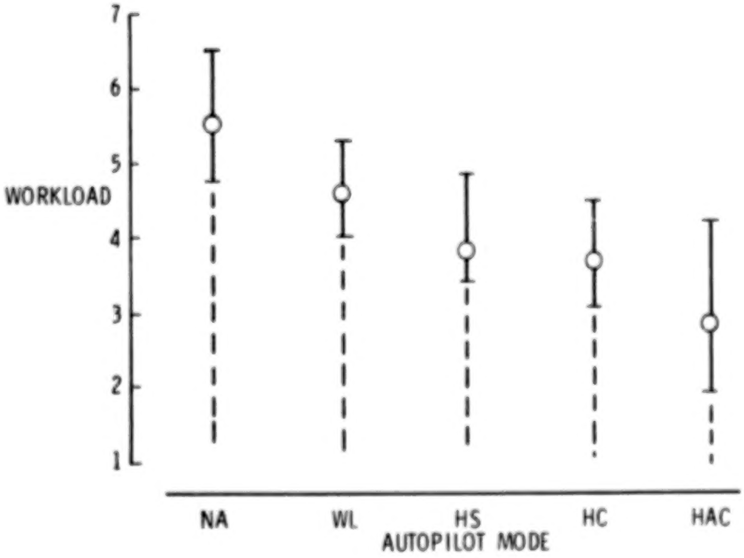

Figure 4.- Workload ratings.

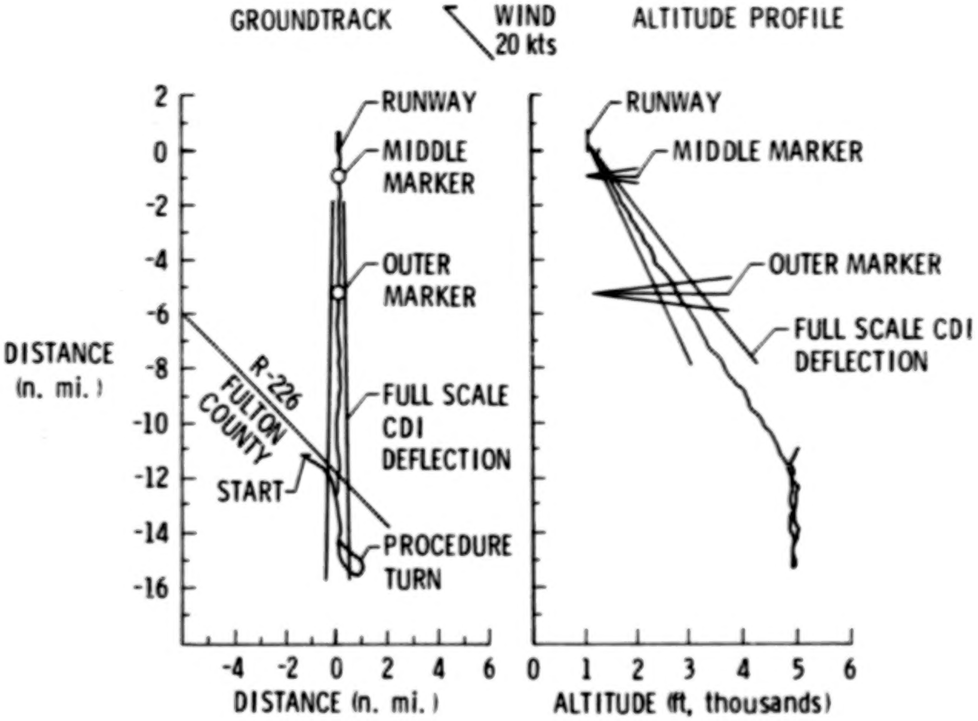

Figure 5.- Atlanta ILS appraoch. No-autopilot mode. (Note: 1 ft = 0.3048 m.)

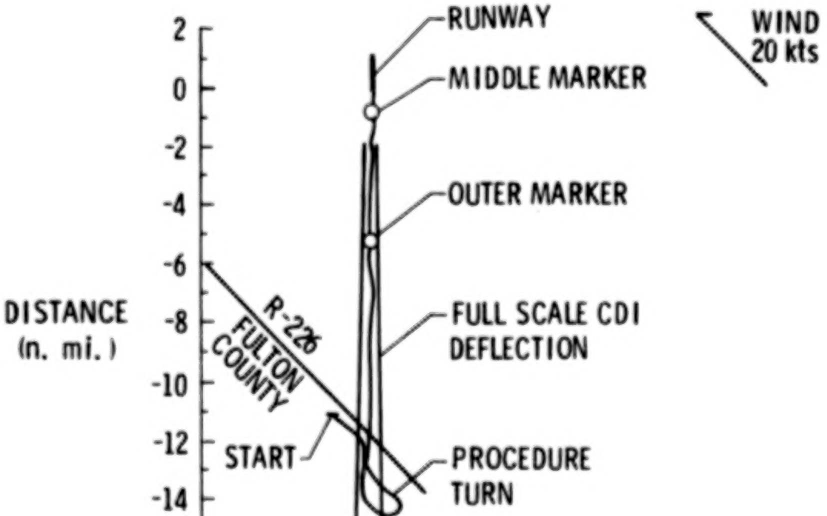

Figure 6.- Groundtrack Atlanta ILS approach. WL autopilot mode.

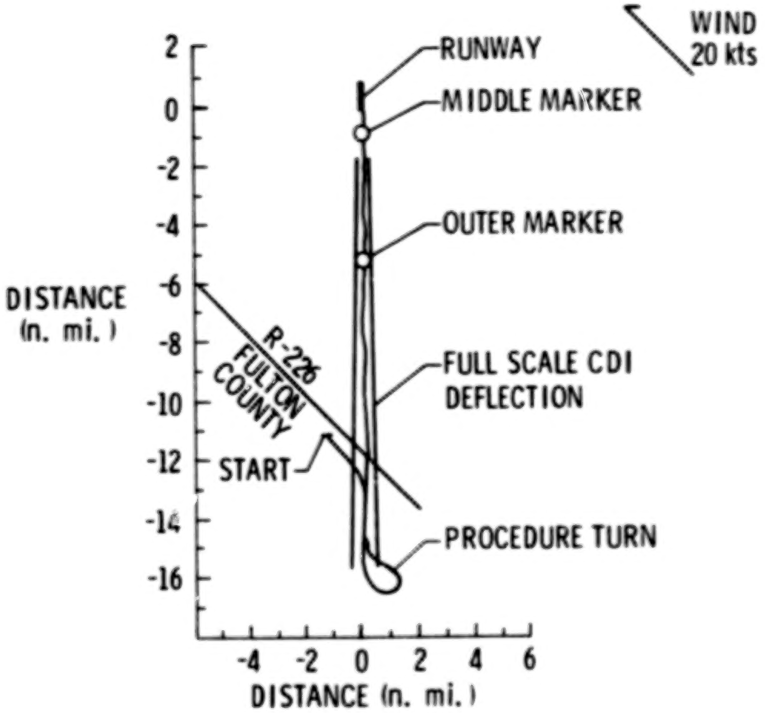

Figure 7.- Groundtrack Atlanta ILS approach. HS autopilot mode.

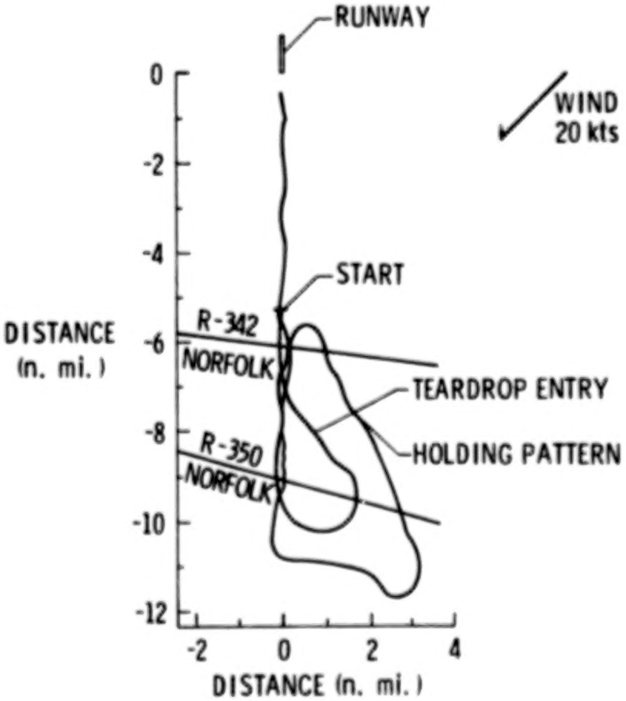

Figure 8.- Groundtrack Newport News LOC BC approach. No-autopilot mode.

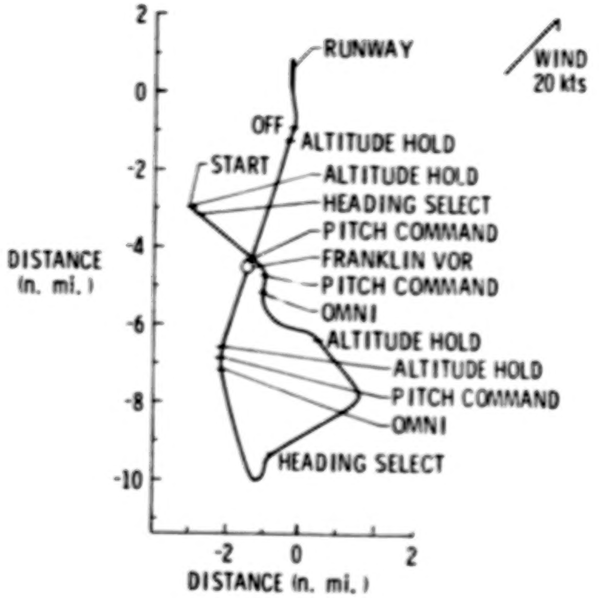

Figure 9.- Groundtrack Franklin VOR approach. HAC autopilot mode.

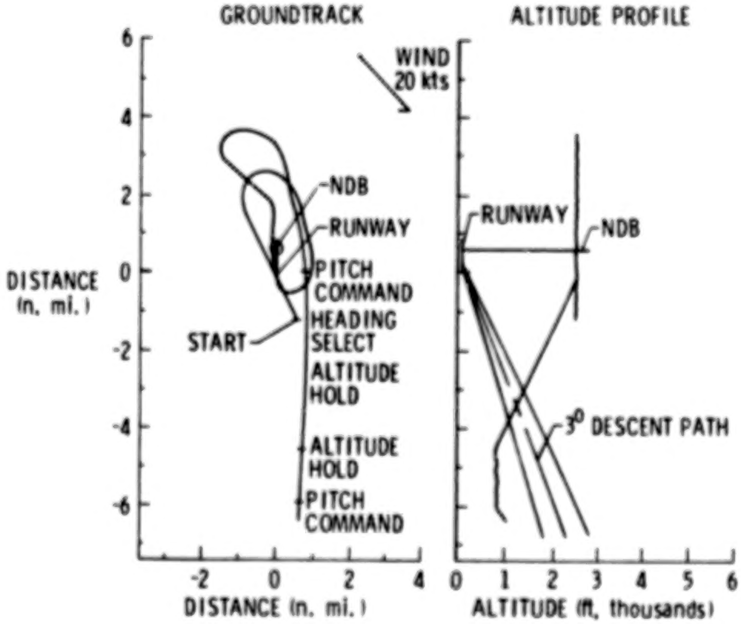

Figure 10.- Wakefield NDB approach. HAC autopilot mode.
(Note: 1 ft = 0.3048 m.)

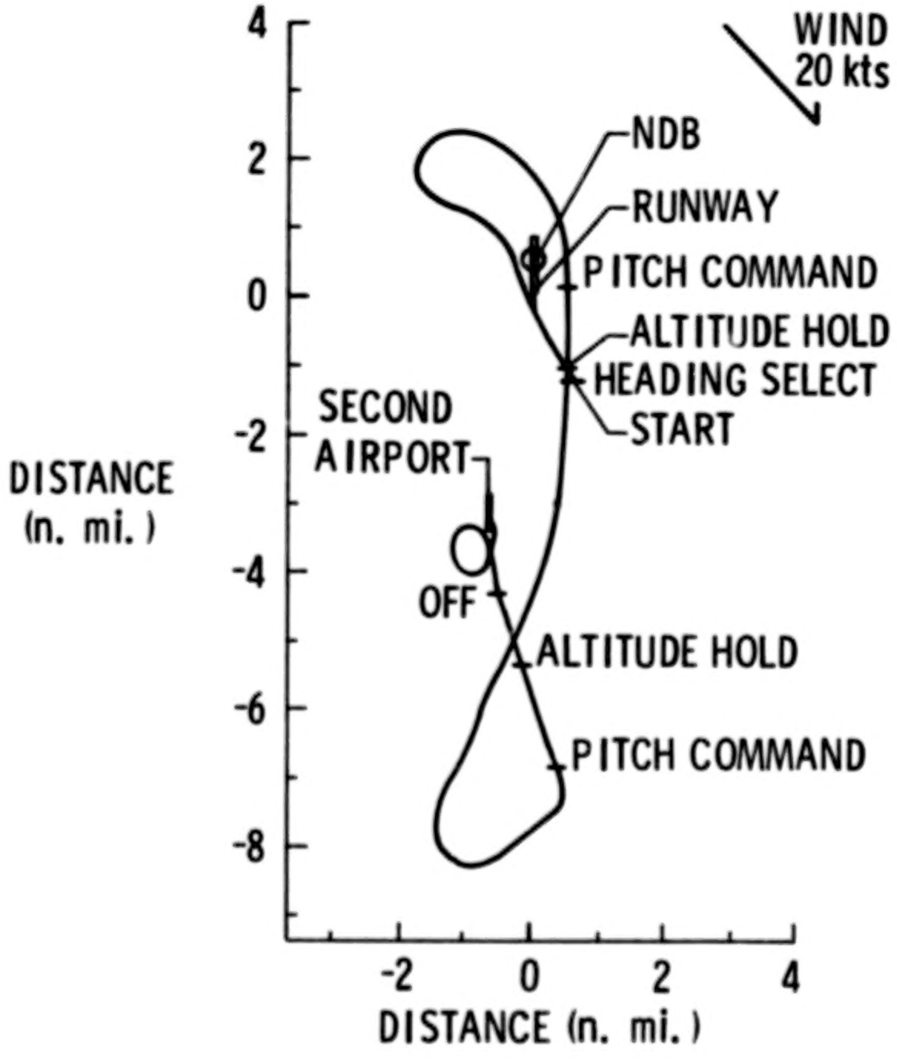

Figure 11.- Groundtrack Wakefield NDB approach. HAC autopilot mode.

BLANK PAGE

BLANK PAGE

APPLICATION OF THE EPIDEMIOLOGICAL MODEL IN STUDYING HUMAN ERROR IN AVIATION

Ed S. Cheaney* and Charles E. Billings**

SUMMARY

The classic methods of epidemiology provided one basis for the original design of NASA's Aviation Safety Reporting System (ASRS) and have figured importantly in the subsequent research investigations conducted where ASRS information was used. An epidemiological model is described in conjunction with the analytical process through which aviation occurrence reports are decomposed into the events and factors pertinent to it. Discussion of three research investigations, each of which manifests the application of the epidemiological method, exemplifies its use and effectiveness.

INTRODUCTION

Four years ago, at this conference, Dr. Billings presented a paper (ref. 1) in which he and his associates at Ames outlined an approach to the study of operational safety problems in air transportation. In that approach an epidemiological method analyzing the causes of disease propagation was to be used in conjunction with aviation occurrence reports. The reasoning set forth in that paper provided the conceptual foundation of the NASA program known as the Aviation Safety Reporting System (ASRS) which had at that time been in operation only four months. This paper is a review of the still-continuing development of the program, generally along the lines expected then, and a discussion of the current embodiment of the method in ASRS program activity.

---

*Project Manager, Battelle Columbus Laboratories' ASRS Office, Mountain View, California, 94043

**Assistant Chief for Research, Man-Vehicle Systems Research Division, Ames Research Center, NASA, Moffett Field, California 94035

EPIDEMIOLOGICAL METHOD

Figure 1 illustrates schematically the epidemiological model and its aviation system analogy. The model represents a process in which disease, emanating from environmental conditions, manifests itself in symptoms that may lead to fatal illness, recoverable illness, or no illness depending on individual circumstances of patient vulnerability, preventive actions, and intervention. In the aviation system the analogy of the disease process is the predilection for error of human participants. This arises from factors in the operating or physical environment and results in errors of commission or omission that, again depending on the individual circumstances, may lead to accidents, system perturbations, or harmless corrections.

Epidemiology was described by Waller (ref. 2) as "... the study of the distribution and determinants of disease or other pheonomena in a population". The method of study is to obtain data on real world populations (as opposed to theoretical or controlled experiment situations), detect in them non-random distributions of phenomena, and then identify the reasons for the non-random distributions. The role of the model and its aviation system analogy as depicted here is to categorize the factors whose distributions are studied by the epidemiological method. The method has been used successfully for more than a century to examine factors in the environment that contribute to a great variety of problems besetting humans and animals. Its application to the study of human error appeared conceptually feasible provided a sufficient study population could be obtained. The aviation accident database assembled from NTSB investigations, although containing many instances of human error, was not considered suitable for the purpose because of its relatively small size and the impossibility of retrospectively examining, or even determining, the causes of many of the errors. Recognition of the need for a large population of occurrences susceptible to more exhaustive study of its error content was the stimulus for institution of the ASRS program.

ASRS PROGRAM

In the four-plus years of its operational existence, the ASRS program has received more than 25,000 reports covering a large variety of safety-related occurrences and situations. Of these, more than 22,000 have been studied by aviation safety analysts and the abstracted safety related information, including the original narratives and followup data, has been stored in a computerized information system.

The reports, usually presented on standard NASA forms, have been submitted voluntarily by pilots and controllers in roughly equal numbers. The existence and purposes of the program were publicized throughout the aviation community by means of Advisory Circulars and various informal means including, recently, the publication of a monthly newsletter.

Reporters are guaranteed anonymity and, as a further incentive to report, they are accorded a limited form of immunity from penalties for FAR violations if they can show that report submission has been timely and meets certain other reasonable conditions.

These three tenets: voluntary reporting, anonymity of reporters, and limited immunity, have had a very important effect on the evolution of the ASRS program. More than 80 percent of the reports received describe human errors on the part of aircrew or controllers. The remainder deal with equipment failures or difficulties involving ground facilities, publications, and other material conditions. Even these, however, are often associated with human errors that either caused the failures or occurred in dealing with the problems resulting from them. Thus the need for an extensive population of human error occurrences has been met. The main reason for this human error focus is that many reporters appear not only willing but eager, under the anonymous, non-punitive conditions of reporting, to reveal their own errors and those of others. Because of the voluntary aspect the reports are not of uniform quality. They vary considerably in accuracy, readability, and background coverage. Some do not reveal the pre-disposing conditions or environmental factors causing the errors disclosed but many others do; these are of inestimable value in analysis using the epidemiological method.

The database is mounted on Battelle's BASIS software which provides a flexible retrieval capability in the on-line mode. Datasets consisting of specified report records pertaining to a large variety of topics can be assembled readily using search terms from the 150-plus information fields in the report record architecture.* The system is also capable of rapid sorting to expose statistical distributions. Three tabulations--cross sections of the database from various viewpoints--will give some feeling for what is there.

Table 1 shows the distribution of sources of the reports. It is noteworthy that controllers are reporting about as much as are pilots and other crew members and that together they account for over 90 percent of the reports received. The Air Force and Navy sources denote the reports received from those organizations via official channels. This distribution of sources shows that ASRS receives reports principally from the flight operations sector of the aviation system (as opposed to maintenance, equipment supply, etc.) and this is reflected in the contents of the reports, which deal almost exclusively with operational matters.

---

*The reports are coded sufficiently richly that they can be retrieved at quite detailed indentures. For example the following retrieval can be made directly without inferential searching strategy: all reports describing deviations from assigned altitude on the part of heavy air carriers in passenger service in the state of California occurring between the hours of midnight and 0600 during the Captain's leg where the deviation was caused by an error on the part of the flight crew but no conflict resulted from the deviation (one report).

Table 2 shows the distribution of the reports in the database as to the "primary problem"* with which they are concerned. Each report is given a unique classification from this group. The significance of the tabulation lies in the definition of the first two items as human error occurrences. This is the quantitative confirmation of the earlier assertion: the ASRS database is overwhelmingly concerned with human error. However, the holdings on equipment failures, navigation aid problems, etc. are not negligible and have given rise to the issuance of more than 700 Alert Bulletins advising the aviation community of reported hazards embedded in conditions or failures in these categories.

Table 3 shows the distribution of reports as to their final outcomes. The final outcome is the last link in the chain of events comprising an occurrence before recovery (chance or some kind of human intervention) takes place. Several kinds of final outcomes are tabulated. Some represent instances where the event chain has progressed to the point where all the elements of an accident are present. The "aircraft separation anomalies", "controlled flight toward terrain", and "aircraft out of control" items fall in this category. Another kind of outcome includes a variety of intermediate events: human errors, aircraft out of position, and equipment failures--cases where the event chain ended without all elements of an accident being present. Thus, the table indicates that 10.1 percent of the reports in the database describe occurrences that culminated in a controller error which was corrected before it could cause further difficulty. There are, of course, many other controller errors contained in the occurrences whose final outcomes were aircraft separation anomalies or controlled flight toward terrain. Finally, the category "situations" refers to reports that describe continuing hazards at specific locations (i.e., inadequate lighting at an airport) as opposed to the occurrence reports making up the rest of the database.

Figure 2 names and describes the generic categories of human error identified in the ASRS database. Although the consequences of human error recorded in ASRS reports vary widely, this list of categories is relatively small because effort has been devoted to isolating and defining generic categories of error at a useful level of detail. The thinking leading to this listing is based on definitions of behavioral functions in aviation from Barnhart, et al (ref. 3). These, then, are the elements considered at the human error node of the epidemiological model of the aviation system, Figure 1.

---

*The "primary problem", not to be confused with probable cause, is defined in the ASRS Operations Manual as "a judgement as to the type of problem leading to or revealed by a particular occurrence or situation."

A TAXONOMY OF AVIATION OCCURRENCES

To apply the epidemiological method in aviation safety analysis, it is necessary to order the information contained in the human error reports in categories commensurate with the elements of the model. This means that the narrated occurrences must be decomposed into outcomes, human errors, predisposing conditions, etc.

A means of doing this generally applicable to all occurrence reports was found in viewing the occurrences as chains of discrete events. A great many different kinds of events are depicted in the reports. Some are near-accidents, as when two aircraft narrowly avoid colliding, or a pilot's faulty navigation heads an aircraft toward high terrain instead of the proper approach track. Others describe potentially hazardous irregularities in the operation of the aviation system, such as deviation from an assigned altitude or course, failures in coordination between ATC facilities, failures of many kinds in air-ground communications, or events reflecting procedural or operational mistakes on the part of pilots or controllers. Finally, some reports describe hazardous conditions deeply embedded--latent--in the system such as a deficiency in a letter of agreement between two ATC facilities, poor training procedures, visually confusing lighting at an airport, or easily misread charts. Nearly all the reports describe sequences of such events and many cover the full spectrum running from the existence of a latent hazard condition through a series of irregularities to the onset of a near-accident.

Figure 3 illustrates an event sequence involving an altitude deviation that led to a conflict. The occurrence was reported to ASRS in this way:

> Captain was flying. I was copilot. He began descent far enough out to make altitude restrictions but did not keep descent rate high enough to comply with STAR (profile descent). He made several corrections and comments which led me to think he was going to make the prescribed altitude/fix but he didn't keep the corrections in long enough. I was distracted by turbulence and weather. We were several thousand feet high at the fix. Controller advised he lost separation between us and an outbound but we didn't see the other aircraft. A factor was that we had a 0500 departure which means (for me) getting up at 0230 to leave home by 0300 and I have difficulty getting enough sleep prior to that kind of schedule. Although I didn't feel sleepy during the descent and he didn't appear to be, we apparently weren't sharp as usual. Although I mentioned the crossing altitude once or twice, I should have "bugged" him more about it.

This occurrence scenario is representative of the large body of reported altitude anomalies now in the database. In this case, the deviation was caused by simultaneous performance failures of the pilot and copilot in which the pilot missed a crossing restriction while flying an approach and the copilot, momentarily relaxing from his monitoring role, failed to observe and call out the error. The altitude deviation resulted in a conflict because of the chance event that the aircraft's actual altitude was occupied by another aircraft. The crew error was attributed to fatigue.

The "occurrence" in this case was reported to ASRS as a single entity but is readily decomposed into the seven events depicted. Each event is discrete, involving an actor and a related action taking place in a finite interval of time and having a definite beginning and ending. Each event could occur in quite different sequences (i.e., with different precedent and subsequent events) and the particular sequence depicted here could have terminated at any point (i.e., a fatigued crew might not necessarily make any errors so the sequence would have stopped at the second event--and yet could have drawn an ASRS report from one of the crewmembers describing fatigue resulting from long, boring flights). An important aspect of the event chain concept is that each discrete event can be viewed as a cause of the subsequent one and an effect of the preceding one.

In the course of analyzing a large number of reported occurrences in this way, the ASRS research staff developed the event classification schema indicated in Figure 3. It is termed the "time/sequence event classification" and has been of great usefulness to the research staff in framing trend analysis studies and in other tasks where it was necessary to deal in terms of event frequencies rather than report or occurrence frequencies. Figure 4 presents the definitions for the four categories.

The significance of the time/sequence event classification, however, lies in its pertinence to the epidemiological model. This is indicated in the lower part of Figure 3 showing how the two classifications interrelate. Although the registration is not exact (the "latent hazards" group includes both the "environment" and "predisposition" components), it does reveal how well the event chain concept lends itself to decomposing the occurrences into the separate components of the model. The event chain elements in each occurrence have been identified by separate descriptors entered into the record for each report. Reports can be retrieved by searching the database with each descriptor of interest. The example report, for instance, would have the descriptors: "WORK SCHEDULING/FLIGHT CREW", "FLIGHT CREW FATIGUE", "ALTITUDE CROSSING RESTRICTION", "CLEARANCE INTERPRETATION", "COCKPIT COORDINATION/MONITORING", "ALTITUDE DEVIATION/ALTITUDE UNDERSHOT", "UNAUTHORIZED DESCENT THROUGH OCCUPIED ALTITUDE", "POTENTIAL CONFLICT". Datasets consisting of all reports coded with each of these event descriptors could readily be formed with the retrieval powers of the BASIS software. Thus, there are 5 reports in the present database in which the work scheduling descriptor appeared, 17 with flight crew fatigue, 149 crossing restrictions, etc. These are the "counts" of model components present in the database relevant to the type of occurrence depicted above.

Figure 5 shows the most prevalent events or conditions in the present ASRS database at each of the model component locations. It is significant that the most frequently reported human error is faulty operating technique in communicating; perceptual and vigilance problems are next in rank. The leading predisposing condition reported is distraction which, of course, takes many forms in the cockpit and the ATC control facility. Distraction is followed closely by excess workload and there is an obvious relationship between these two conditions. Complacency, although most difficult to define because of its subjectivity, is frequently reported or implied as is the existence of strained interpersonal relationships among the human participants. The prevalent sources cited in the operational and physical environments are self explanatory but it is noteworthy that in the context of studying human error in aviation, equipment failure is treated as an environmental factor capable of setting up a predisposing condition for errors.

At the outcomes level in the model, the only kind of near-accidents reported frequently to ASRS are aircraft separation anomalies (conflicts). This is confirmed by the data in Table 3. Many aircraft position anomalies are reported of which altitude deviations ("busts") are most prevalent. Cases where an aircraft inadvertently gets into an incorrect category of airspace, as when ATC mishandles a handoff between sectors, are frequently reported. As indicated in the upper right part of the figure, human errors are most often corrected before a system perturbation can occur by timely intervention on the part of controllers or by the quick response of flight crews.

The citations in Figure 5 show only the more prevalent events or factors at the various model component locations. There are many others reported; the database index contains thousands of terms. However, there is no explicit causal relationship among the events and factors in Figure 5--they are merely independent listings at each component. The way the model actually manifests itself in the conduct of a research investigation is best understood through examination of past studies in which epidemiological methods were employed.

EPIDEMIOLOGY IN ASRS RESEARCH

Three example ASRS studies will illustrate the use of the method. Reports on two of them appeared in NASA ASRS Quarterly Reports; the third was separately reported.

- o Human Factors Associated With Profile Descents (ref. 4)
- o Distraction--A Human Factor in Air Carrier Hazard Events (ref. 5)
- o Fatigue and Associated Performance Decrements in Air Transport Operations (ref. 6)

Epidemiology is not mentioned in any of these reports nor are the model's structure or terminology employed explicitly in the discussions of the investigative steps or conclusions. As will be shown, epidemiology was the underlying method used in obtaining the results in each case even though it was not discussed in their descriptions.

Human Factors Associated With Profile Descents

Profile descents are published terminal arrival procedures intended to save time and fuel. They provide an unrestricted descent from cruising altitude or flight level to interception of glide slope. Headings and crossing altitudes during the descent are specified. The procedures were experimentally implemented at several terminals during 1976. Shortly, a considerable number of reports arrived at ASRS indicating difficulties with the profile descents, the majority of which were altitude deviations. ASRS then performed a study with the purpose of discovering the nature and causes of the problems.

In terms of the epidemiological model, the only known factors at the outset of this study were outcomes--primarily system perturbations in the form of altitude deviations, some of which progressed to near-accidents when the deviant altitudes proved to be occupied. The study hypothesis was that the profile descent procedures were operational environment factors related to these undesirable outcomes by some chain of human error and predisposing condition. The study consisted of examining reports on the profile descent problems at two terminal areas (Denver and Atlanta) to catalogue the errors and conditions present.

The occurrence analyses resulted in identification of five "problem areas" that clearly connected the outcomes with the profile descent procedures thus establishing logically the validity of the hypothesis that the procedures and observed outcomes were causally related. The five problem areas were:

- Profile descent charts
- Profile descent clearances
- Profile descent rules and procedures
- Aircraft operations in profile descents
- Human factors in profile descents

The chart problems were crewmembers' misreading or selecting the wrong chart for the assigned descent--perceptual errors related to the poor design of the charts which made them complex and cluttered. The descent clearance problems were all flight crew errors in communications technique whereas the problems with rules and procedures pertained to flight crew misunderstanding of them due to complexity and/or ambiguity. The problems cited regarding aircraft operations reflected misjudgement errors involving descent rates. Thus, the first four of the problem areas were enumerations of the various human errors causing the observed outcomes.

The fifth problem area was mainly a recitation of the predisposing conditions causing the errors. Several were logically relatable to the profile descent procedures themselves; i.e., poor chart design giving rise to chart complexity and clutter, extra workload and distraction imposed by the nature of the procedures, and unfamiliarity with the procedures all were present and interacting factors. Superimposed on these, in several cases, were flight crew fatigue or weather factors that were not directly related to the profile descent procedures but exacerbated those adverse conditions that were.

These findings not only supported the hypothesis convincingly but identified the most serious of the factors causing the errors. This was a predisposing condition--the complex and cluttered design of the charts available to the flight crews. This condition was rectified and shortly afterwards a notable decrease in profile descent error reports at the pertinent terminals was observed at ASRS.

Distraction--A Human Factor in Air Carrier Hazard Events

An ASRS study of flight crew distraction, observed to be the most frequently cited factor in air carrier reports, began in the fall of 1978 as a part of a series of human factor investigations. The purpose of the study was to discover the kinds of distractions that affect flight crew performance, their sources, the seriousness of their effects, and to comment on possible remedies. The epidemiological method was used in the study to associate the cause and effect chain.

In terms of the model, the starting point for this study, in contrast to the one previously described, was the arbitrary identification of distraction as a predisposing condition for errors. Epidemiology was used descriptively to classify distractions by generic type and then to associate those types with the environmental factors cited as causing them and the types of errors and outcomes described as resulting from them. Statistical techniques were not employed; the ingredient used in making the classifications and confirming the cause-effect associations was the expertise of the investigator, an experienced airline pilot and safety researcher.

Analysis of the dataset of 169 reports resulted in the following classifications and associations among factors:

- Flight crew distractions fall into two generic classes: (1) Those arising from non-flight operations activities (public address announcements, on/off block messages, logbook paper-work, handling flight-service/passenger problems, and untimely cockpit conversations) and (2) those imposed by flight operations tasks internal to crew functioning and frequently cited in reports as "excessive workload" (running checklists, looking for traffic, communicating with ATC, coping with minor malfunctions, avoiding weather buildups, and monitoring radar).

- The sources of distraction as a predisposing condition were traced to operational environment factors. The two most significant were (1) company rules and procedures directed to maximizing passenger comfort and service and (2) the inherent complexity of the flight crew's job mandated by the technology of the modern jet airplane and the ATC system in which it functions.

- Two kinds of human errors arose from distractions: failures on the part of individuals to perform an essential task such as traffic watch and, even more critical, breakdowns in crew coordination or crew management. Both are failures in operating technique involving controlling, communicating and monitoring behaviors.

- Overwhelmingly, in the dataset used in this study, the outcomes of the distraction occurrences were system perturbations in the form of altitude deviations, many of which led into conflict situations. Other outcomes consisted of failures to see traffic -- also productive of conflicts -- unauthorized penetrations of airspace, landings or takeoffs without clearance, and, in a few cases, successful correction of an error.

The average quality of the reports in this dataset was excellent; many of them depicted associations among distractions, errors, and outcomes with precision and detail. The study results not only served to delineate the problems involved with distraction but suggested considerations important to remedial action. The causes of nonoperational distractions, for example, may be minimized by continued emphasis on cockpit priorities through both written procedures as in flight operations manuals, and constant command attention to optimum use of cockpit resources. Trends in cockpit design are aimed at simplification of the tasks involved and many of the reports indicate that this, if achieved, would significantly reduce the distraction burden. It is noteworthy that regulatory measures aimed at reducing non-operational activity distractions in air carrier cockpits are being actively considered (ref. 7). ASRS data indicate that there is a considerable opportunity for safety improvement in controlling distractions and they are acknowledged to have pointed the way toward achieving that control.

Fatigue and Associated Performance Decrements in Air Transport Operations

Although relatively few reports about fatigue in aviation operations have been received, public and Congressional concern prompted the conduct of an ASRS study on the topic during the summer of 1980. The purpose was to assess the effects of fatigue on air crew performance by examining the hypothesis that skill fatigue and associated performance decrements occur and are associated with some combination of such factors as sleep deficit, work schedules, circadian desynchronosis (effects of jet lag), and the like.

The reader will discern the outline of the epidemiological model in the preceding statement of purpose. Fatigue was hypothesized to be the predisposing condition arising from a variety of operational environmental factors having to do with trans-meridian flights and various scheduling issues. Further, the hypothesis assumed that fatigue was capable of producing performance decrements -- human errors -- leading to potentially hazardous outcomes.

The epidemiological method was used somewhat more rigorously in this study than in the two described previously since some statistical analysis entered the study procedure as well as descriptive analysis to establish associations. The fatigue-related dataset of 77 occurrences was compared in several respects with a similarly retrieved set of reported performance errors where fatigue was not present. These comparisons showed that the fatigue-related occurrences involved patterns of error and outcome significantly different from the non-fatigue-related ones. The descriptive analysis coupled with the statistical comparisons supported seven conclusions regarding fatigue.

- Fatigue-associated performance decrements occur;
- Fatigue-associated performance decrements can produce potentially hazardous conditions;
- Only a small fraction of performance decrements reported to ASRS are associated with fatigue by their reporters;
- The performance decrements associated with fatigue differ in frequency, but not in kind, from those occurring in its absence;
- Failures in monitoring tasks are described frequently in fatigue-associated performance decrements reports;
- Long duty periods, large numbers of flight segments, and disturbed sleep are frequently reported as the reasons for fatigue associated with performance decrements;
- The ASRS data do not permit a conclusion as to the effect of circadian desynchronosis on flying performance.

In this study, the practice of epidemiological analysis in conjunction with ASRS data may be said to have reached some degree of maturity since the classic case history comparison procedure (comparison of a population having a phenomenon with a similar one not having it) was employed for the first time. It is of course, not yet known whether ASRS data will consistently be capable of supporting analysis in this somewhat more rigorous way but it is indicative that, at the time of preparation of this paper, two other ASRS research investigations are proceeding using case history comparison procedures.

CONCLUSIONS

The ASRS program has developed successfully along the lines originally envisioned. It has secured and retained the confidence of the members of the aviation community so that submission of the voluntary reports has not only continued but has increased in volume since the beginning of the program. The average quality of the reports is high and they are primarily concerned with human error in operations. It has proved feasible to analyze the reports, to abstract pertinent information from them, and to store it in highly retrievable form in a computerized database. The design of the database has provided an effective means for arranging the data in ways that facilitate the application of the epidemiological method.

Epidemiology has been an effective tool in the conduct of research investigations using ASRS information. It has been present either implicitly or explicitly in all of the studies performed to date and has provided the principal strategic approach in many. The results obtained validate fully the design of the ASRS. Information and new knowledge about aviation safety matters gleaned from these studies are flowing to the aviation community in the form of published technical reports. Sixteen such reports have been published -- all but two in NASA Quarterlies. All have contained information useful to the operating community and in several cases, as exemplified in Reference 7, ASRS research results are being used in bringing about changes to increase aviation safety.

REFERENCES

1. Billings, C. E.; Lauber, J. K.; Cooper, G. E.; Ruffell-Smith, H. P.: "Retrospective Studies of Operating Problems in Air Transport". Paper No. 33, Proceedings of the Annual Safety and Operating Problems Conference, October, 1976, National Aeronautics and Space Administration Report No. NASA SP-416.

2. Waller, J.A.: "Epidemiological Approaches to Injury Research". Proceedings of a Workshop on Rare Event/Accident Research Methodology, pp. 29-46, NBS Special Publication 482, National Bureau of Standards, May 1976.

3. Barnhart, W.; Billings, C. E.; Cooper, G.; Gilstrap, R.; Lauber, J.; Orlady, H.; Puskas, B.; Stephans, W.: "A Method for the Study of Human Factors in Aircraft Operations". NASA Technical Memorandum No. NAS TMX 62472, NASA-Ames Research Center, September, 1975.

4. Ames Research Center, Aviation Safety Reporting System Office: "Human Factors Associated with Profile Descents". NASA Aviation Safety Reporting System: Fifth Quarterly Report, NASA Technical Memorandum 78476, NASA-Ames Research Center, April, 1978.

5. Monan, Wm. P.: "Distraction--A Human Factor in Air Carrier Hazard Events". NASA Aviation Safety Reporting System: Ninth Quarterly Report, NASA Technical Memorandum 78608, NASA-Ames Research Center, Moffett Field, CA 94035, June, 1979.

6. Lyman, E. G.; Orlady, H. W.: "Fatigue and Associated Performance Decrements in Air Transport Operations--An Aviation Safety Reporting System Study". Paper prepared for a fatigue effects workshop held at NASA-Ames in August, 1980, NASA-Ames Research Center, Moffett Field, CA 94035, September, 1980.

7. U. S. Department of Transportation, Federal Aviation Administration: "Proposed Elimination of Duties and Activities of Flight Crew Members not Required for the Safe Operation of Aircraft", Notice of Proposed Rulemaking No. 80-12, Docket No. 20659, Federal Register, Vol. 45, No. 169, August 28, 1980.

TABLE 1. - SOURCES OF REPORTS

Reporter	Percent of total reports
Controllers	48.1
Pilots	40.7
Air Force	5.0
Crew members	4.0
Navy	1.3
Observers	.7
Passengers	.2
Unknown	neg.

TABLE 2. - PRIMARY PROBLEMS

Problem description	Percent of total reports
Human error -- flight crew	45.4
Human error -- ATC	39.8
Ground navigation or communication equipment failure	4.5
Airport physical or institutional problem	3.4
Aircraft or aircraft equipment failure	3.1
Publications problems	1.6
Other (including weather related)	2.2

TABLE 3. - OCCURRENCE OUTCOMES

Outcome	Percent of total reports
Aircraft/Aircraft Separation Anomaly	51.1
Flight crew errors	14.3
Controller errors	10.1
Aircraft out of position	7.9
Situations	7.9
Ground equipment failures	3.6
Airborne equipment failures	2.4
Controlled flight toward terrain	.5
Aircraft out of control	.4
Other	1.8

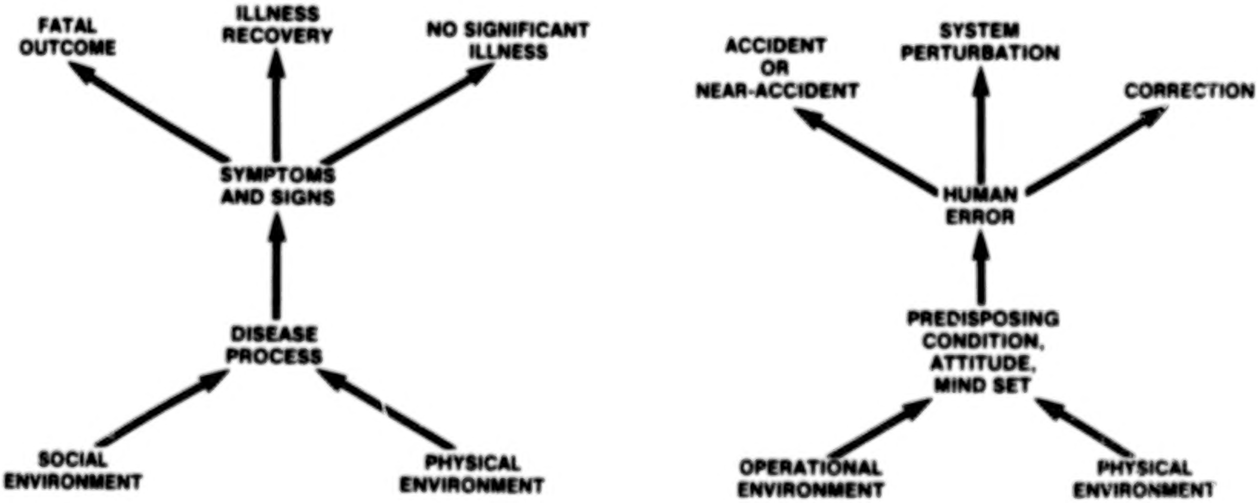
FATAL OUTCOME
ILLNESS RECOVERY
NO SIGNIFICANT ILLNESS
SYMPTOMS AND SIGNS
DISEASE PROCESS
SOCIAL ENVIRONMENT
PHYSICAL ENVIRONMENT
ACCIDENT OR NEAR-ACCIDENT
SYSTEM PERTURBATION
CORRECTION
HUMAN ERROR
PREDISPOSING CONDITION, ATTITUDE, MIND SET
OPERATIONAL ENVIRONMENT
PHYSICAL ENVIRONMENT

Figure 1.- The epidemiological model and its aviation system analogy.

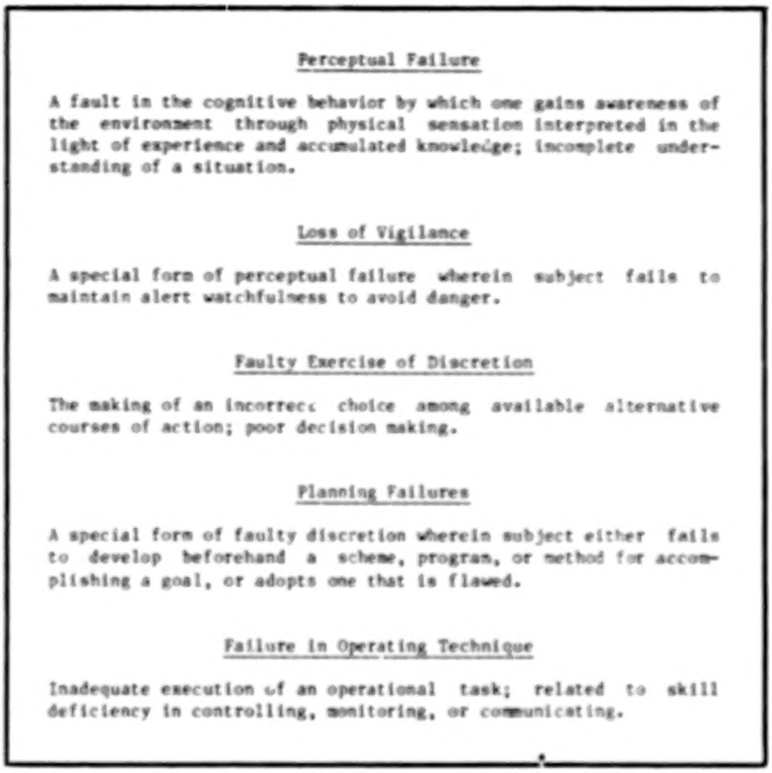

Perceptual Failure

A fault in the cognitive behavior by which one gains awareness of the environment through physical sensation interpreted in the light of experience and accumulated knowledge; incomplete understanding of a situation.

Loss of Vigilance

A special form of perceptual failure wherein subject fails to maintain alert watchfulness to avoid danger.

Faulty Exercise of Discretion

The making of an incorrect choice among available alternative courses of action; poor decision making.

Planning Failures

A special form of faulty discretion wherein subject either fails to develop beforehand a scheme, program, or method for accomplishing a goal, or adopts one that is flawed.

Failure in Operating Technique

Inadequate execution of an operational task; related to skill deficiency in controlling, monitoring, or communicating.

Figure 2.- Human error listing.

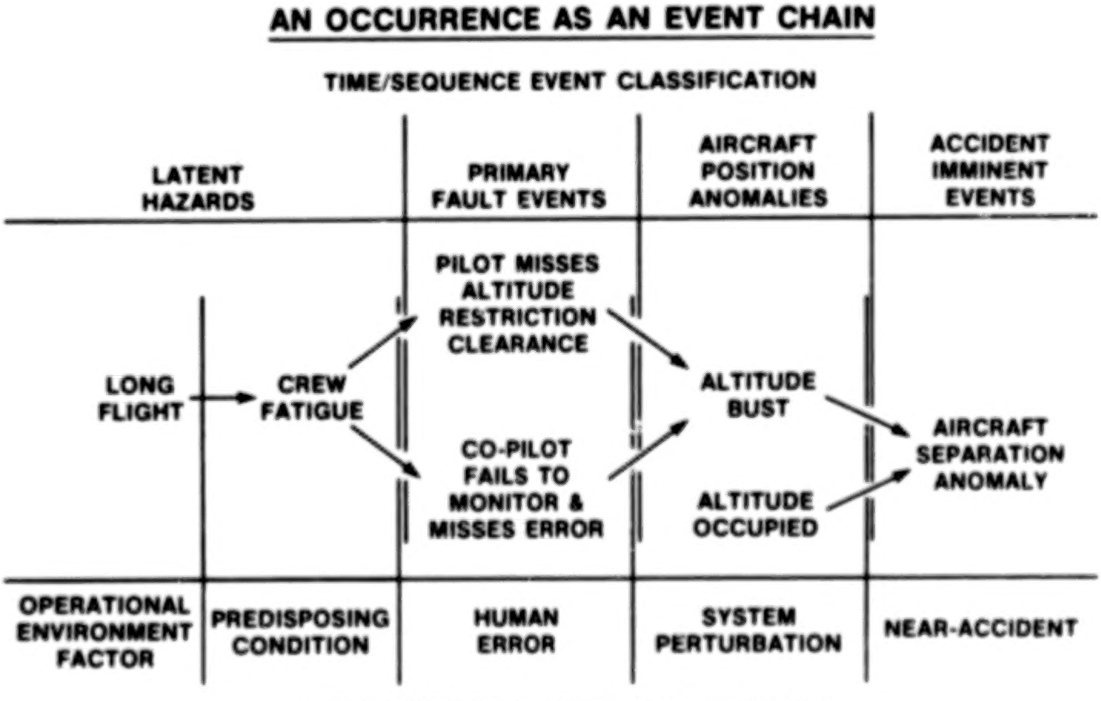
AN OCCURRENCE AS AN EVENT CHAIN
TIME/SEQUENCE EVENT CLASSIFICATION
LATENT HAZARDS
PRIMARY FAULT EVENTS
AIRCRAFT POSITION ANOMALIES
ACCIDENT IMMINENT EVENTS
LONG FLIGHT
CREW FATIGUE
PILOT MISSES ALTITUDE RESTRICTION CLEARANCE
CO-PILOT FAILS TO MONITOR & MISSES ERROR
ALTITUDE BUST
ALTITUDE OCCUPIED
AIRCRAFT SEPARATION ANOMALY
OPERATIONAL ENVIRONMENT FACTOR
PREDISPOSING CONDITION
HUMAN ERROR
SYSTEM PERTURBATION
NEAR-ACCIDENT
EPIDEMIOLOGICAL EVENT CLASSIFICATION

Figure 3.- Event classifications.

LATENT HAZARD CONDITION

A condition in the system continuing in time with the potential of triggering a hazardous chain of events but not, in itself, usually regarded as an event.
EXAMPLE: UNDETECTED CHART ERROR

SYSTEM IRREGULARITIES--PRIMARY EVENTS

Events reflecting mistakes in procedures or execution, or failures of equipment, that can lead to accident.
EXAMPLE: MISINTERPRETED CONTROL CLEARANCE

SYSTEM IRREGULARITIES--AIRCRAFT POSITION ANOMALIES

Events in which an aircraft is unsafely mispositioned, as by being flown into the wrong airspace or deviating from correct altitude, course, or speed.
EXAMPLE: ALTITUDE DEVIATION

ACCIDENT IMMINENT EVENTS

Events that are proximate to the occurrence of an actual accident; all the elements of an accident are in place so the next event in sequence would be an accident unless an intervening recovery event takes place or the accident is avoided by chance.
EXAMPLE: NEAR MIDAIR COLLISION

Figure 4.- Time/sequence event classification.

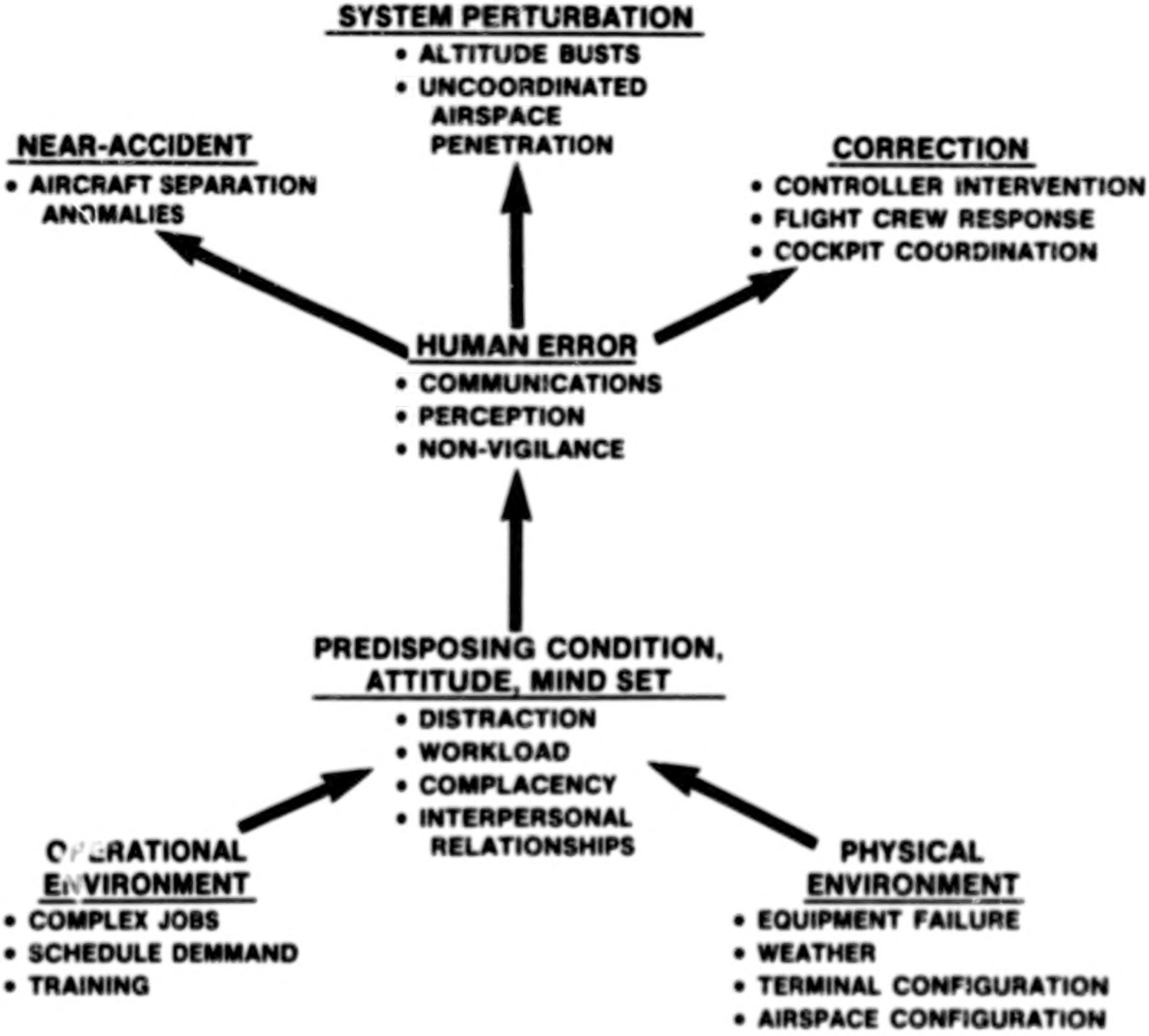
SYSTEM PERTURBATION
• ALTITUDE BUSTS
• UNCOORDINATED AIRSPACE PENETRATION
NEAR-ACCIDENT
• AIRCRAFT SEPARATION ANOMALIES
CORRECTION
• CONTROLLER INTERVENTION
• FLIGHT CREW RESPONSE
• COCKPIT COORDINATION
HUMAN ERROR
• COMMUNICATIONS
• PERCEPTION
• NON-VIGILANCE
PREDISPOSING CONDITION, ATTITUDE, MIND SET
• DISTRACTION
• WORKLOAD
• COMPLACENCY
• INTERPERSONAL RELATIONSHIPS
OPERATIONAL ENVIRONMENT
• COMPLEX JOBS
• SCHEDULE DEMMAND
• TRAINING
PHYSICAL ENVIRONMENT
• EQUIPMENT FAILURE
• WEATHER
• TERMINAL CONFIGURATION
• AIRSPACE CONFIGURATION

Figure 5.- Prevalent factors in the ASRS database.

HOW A PILOT LOOKS AT ALTITUDE

Amos A. Spady, Jr. & Randall L. Harris, Sr.
Langley Research Center

SUMMARY

Altitude information is very important to pilots. Although on the instrument landing approach, pilots only look at the altimeter 3% to 6% of the time, they obtain relative altitude information from glideslope and command bar needles. One pilot questionnaire survey has indicated that altimeters are misread by almost all pilots. Commercial pilot eye scanning data previously collected were reanalyzed to evaluate how pilots used the drum pointer altimeter. The results of these tests showed that the pilots seldom used the drum window apparently because it was difficult to read as indicated by average drum window dwell times of .6 seconds. It is suggested that pilot scanning data be collected for other types of altimeters in order to find those with good scanning characteristics.

INTRODUCTION

Altitude is one of the prime bits of information needed by a pilot during any phase of flight. Misreading of the altimeter can result in incidents and accidents. Consequently, a number of altimeter designs have been tried over the years. The tests conducted and the reports written on the subject are numerous; in fact, a number of summary reports have been written such as references 1 and 2. In 1975, A. N. Du Zeu (ref. 3) wrote that "the altimeter is one of the most important aircraft instruments and is likely to remain so for many years to come. It is pertinent, therefore, to attempt to forecast what the future holds for this instrument." In summarizing he wrote "no great change is foreseen in display presentation of altimeters, the counter pointer type will become universal except for low performance, low altitude aircraft. Solid state displays are likely to supplant mechanical displays, but still with an imitation of mechanical displays. It is possible that the advent of CRT presentation will result in presentations of optimum displays for each phase of flight, but still there is no sign of an acceptable completely new presentation on the horizon." Even though no completely new presentation is forecast, the current altimeter designs are not totally adequate as evidenced by the number of accidents, near accidents, and incidents due to pilots misreading altimeters.

This paper will discuss an analysis of pilot scanning characteristics of a drum pointer altimeter. Correlations will be made to past research on altimeters in an effort to understand how a pilot uses an altimeter. Also, suggestions to help improve the readability of the altimeters thereby reducing the number of misreads will be discussed.

EQUIPMENT AND TEST PROCEDURE

The tests were performed in a Boeing 737 simulator at Piedmont Airline's Training Facility. The simulator is FAA certified and used for initial and recurrent training. The only change in the instrument panel was the incorporation of an oculometer optical head which was mounted below the Automatic Direction Finder (ADF) behind the instrument panel. A TV camera was mounted behind the pilot to view the instrument panel and a TV monitor was located behind the pilot's seat to allow the test conductor to observe the pilot lookpoints superimposed in the instrument panel scene.

The oculometer has two primary subsystems: the electro-optical system and the signal processing unit. The electro-optical system mounted in the instrument panel generates a beam of infrared light which is directed through a beam splitting mirror toward the subject's eye. Reflections from the eye are directed back through the beam-splitter to an infrared-sensitive TV camera. The high reflectivity of the human retina for infrared leads to a backlighting of the pupil, so that the camera sees the pupil of the eye as a bright, circular area (fig. 1). The camera also sees a small bright spot due to a reflection from the corneal surface. The relative positions of the center of the pupil and the corneal reflection depend on the angle of rotation of the eyeball with respect to the infrared beam. The signal processing unit uses the signal from the TV camera to compute this angle of rotation and the coordinates of the lookpoint on the instrument panel. The output of the signal processor is a set of calibrated analog signals representing the subject's lookpoint coordinates and pupil diameter. A complete description of the oculometer and test situation can be found in reference 4.

All landing approaches were started at 19 km (12 miles) from runway threshold and approximately 415 m (1360 ft) above ground level. The first 6 km (4 miles) were used by the pilot to stabilize the aircraft on the correct flight path and to check the oculometer calibration. At 13 km (8 miles) data recording was started and continued through capture and descent down the 3° glideslope, touchdown and rollout or until the approach was aborted as a result of the pilot choosing to go around.

All airline pilots used in the program were qualified Boeing 737 pilots who fly regularly for a scheduled airline. The pilots were asked to assume that they were flying an aircraft full of passengers, and if they would normally elect to go around, they should do so. All tests were conducted using the same co-pilot. The co-pilot functioned in the same manner as he would in a normal approach and provided all required call outs.

REVIEW OF PILOT OPINION AND SELECTED ALTIMETER RESEARCH

If altimeter display improvements are to be accomplished and if optimum altimeter displays are to be developed for future flight systems, it becomes imperative that we understand the problems with existing altimeters and how a pilot obtains and perceives altitude information.

Drum Pointer Altimeter Misreads

A survey was conducted by Jim Anderson, National Airline Control Safety Chairman, through the Airline Pilots Association to ascertain the percentage of National Airline pilots who have misread or observed another pilot misread the drum pointer altimeter used in National Airline's B727 aircraft. The results of the survey indicated that of the 169 pilots who responded, 137 stated that they had misread the altimeter and 134 stated that they had observed another pilot misread the altimeter (85% of each group stated that such observations had been made on more than one occasion). The survey results also indicate that a surprisingly large number of misreads (50) happen during the approach phase. Several comments of pilots relating to the drum pointer altimeter are:

1. "This altimeter takes more concentration than should be necessary to read accurately."
2. "The small drum window is a complication on the instrument and (is) quite small, often requiring a 'double look' and diverting attention from the needle. Other instruments require only a single point of visual attention to comprehend and do not divert, slow, or complicate a smoothly flowing scan."
3. "Misreads seemed to always occur at the lower altitude when attention is split between more activities."
4. "The more stressful situations produced more misreads."
5. "A quick glance after (being distracted) can usually induce a reading of 1,000 ft. off if the barrel drum is halfway between thousands."

Pilot Opinion of Altitude Importance

Pilots normally rate the altimeter as the third most looked at instrument in the aircraft (with the Flight Director being first and the airspeed indicator second). In fact, when asked, some pilots stated they spent 20 to 25% of their time on the altimeter. Studies conducted using these same pilots (ref. 4) indicate that for all test conditions they actually spent an average of between 3 to 6% of their time looking at the altimeters. The discrepancy between pilot opinion and actual time spent on the altimeter may not be as bad as it seems at first glance. Indications are that while the pilot may in fact be concerned about his altitude 25% of the time, it does not equate to spending that much time looking at the altimeter. On the straight and level portion of the approach, once having established his altitude, the pilot can use either the horizontal command bar of the Flight Director to indicate position with respect to desired altitude or other cues which indicate that a change in altitude is taking place. Upon starting the descent, additional instruments also provide altitude information. To quote a NASA test pilot, "On the glideslope the altimeter is all but relegated to a back up mode. My sources of information are first the raw glideslope data, second, command bars, and third, where present, co-pilot call outs." While the first two do not give absolute altitude information they do tell the pilot where he is with respect to his desired altitude at that point in his approach. Therefore, while a pilot may in fact spend up to 25% of his time concerned with altitude information, it is not necessary, however, that he spend all of that time looking at the altimeter.

Altimeter Research

A number of different altimeters are used in current commercial aircraft such as the three pointer, counter pointer, drum pointer, and counter drum pointer (fig. 2). The altimeter used in the current study was a drum pointer (fig. 2b). The pointer indicates altitude over a 30.5 m (1000 ft) range while the drum indicates thousands and tens of thousands of feet. One of the most comprehensive studies of time required to read the various types of altimeters (fig. 2) is reported in reference 5. In these tests, the subjects were required to read altimeter settings while engaged in a central tracking task. At random times, the experimenter would open a shutter which was covering the altimeter. The subject would read the altimeter, operate a hand switch to close the shutter and then report the altitude to the nearest 30.5 m (100 ft.) Measurements were taken of the altimeter exposure time and the accuracy of reporting the altitude. Eighteen pilots participated in the study. A total of 15 altimeter exposure trials were performed on each of the four types of altimeters (similar to those of fig. 2). The results for the drum pointer altimeter (equivalent to the one used in the airline pilot study) showed a mean exposure time of 1.38 seconds with a probability of an error of 2.4%. In those tests, the pilot was presented with a random selection of altitudes so that no history of altitude profile could be maintained; consequently, the subject pilots were required to read the entire altimeter each time it was shown.

RESULTS AND DISCUSSION

In an actual flight situation, altimeter readings are not presented to pilots in a random fashion. In fact, the pilot has a continuing altitude profile which provides a running time history; consequently, he has a prior knowledge of what to expect when he looks at the altimeter and therefore, does not have to read the entire altimeter each time he looks at the instrument. In fact, both reference 4 and reference 6 indicate that pilots when flying simulated approaches have an altimeter mean dwell time of only between .3 to .4 seconds as opposed to the 1.38 seconds found in reference 5. In addition, observation of the real time TV tapes, taken during the airline pilot study (ref. 4), shows that the pilot looked at the left side of the altimeter even though the needle was pointing to the right side. This observation coupled with the large standard deviation of mean dwell time found in the data led to a reanalysis of the altimeter data in terms of dwell times for the left side, right side, and altimeter drum window. For the above analysis, the altimeter was divided into three areas: the left side, the right side, and the altitude drum window. The left and right side divided the altimeter in half from top to bottom with no overlap. The drum window, however, overlapped a very small part of the left side and part of the right side (fig. 3). Figure 4 presents a combined dwell time histogram of the frequency distribution of individual dwells on the total altimeter. These data were taken from seven pilots who performed a total of 108 simulated ILS approaches from 13 km (8 miles) out to 30.5 (100 ft) above the runway. The abscissa is dwell time in seconds plotted on a log scale; the ordinate is percent of the total number of looks at the altimeter. The curve shows a mode at about .25 seconds with a median at .275 seconds and mean of .32 seconds. The next figure (fig. 5) presents a break out of the dwells on the left and right sides of the altimeter. This shows a characteristic difference in the dwells on the right and left sides. The left side dwells show a distribution with two peaks, one at about .1 seconds and a second at about .4 seconds. Reference 7 refers to a bimodal dwell distribution as being a characteristic of a type II instrument and defined the peaks occurring at these same dwell times as glance (.1 sec) and read (.4 sec) dwells. For the short dwell times the pilot gets only minimal information such as the direction of needle orientation. The longer dwell times are associated with reading the needle value. During the approximately 180 seconds required for an approach the needle is on the left side for only 40 or 50 seconds (on the average 25% of the time). Yet, the pilot spends approximately 48% of the time in the altimeter on the left side. It is hypothesized that the pilot can determine right side needle position and/or rate parafoveally while fixated on the left side of the altimeter. The right side of the altimeter shows a totally different shape with a single mode at .25 seconds. Reference 7 refers to a single peaked dwell distribution as a type one instrument with the pilot reading only the value to which the needle was pointing.

Of particular interest, on the right side of the altimeter, is the window which contains the drum. The data were analyzed for dwell times in the area of the drum window (fig. 3) plus ½ of a visual degree (¼ inch) surrounding the window. When the pilot looks in the drum area and the needle is overlapping the drum area, it is difficult to determine which piece of information he is reading. Figure 6 gives the dwell time histogram for the drum window area. These data show a broad peak between .1 to .25 seconds. This broad peak could be a summation of a distribution having a peak at about .1 seconds (glances) and one having a peak at .25 seconds. Reference 8 presents the dwell time histogram of subjects during text reading. The text reading data also peak at .25 seconds and have a shape that appears to be log normally distributed. To obtain an estimate of what dwell distribution remains when the text reading (in this case assumed to be needle position reading) is removed, the distribution of reference 8 was subtracted from that of figure 6. The resulting curves are plotted in figure 7. The middle curve is the one subtracted (ref. 8) and the remaining distribution forms the left and right curves. The one to the left is almost identical in distribution to the glances of reference 7 and is probably associated with needle direction estimation. The distribution on the right appears to be log normally distributed with a peak between .5 and .6 seconds. There are two possibilities to explain the distribution. In follow-on work, Dr. R. Harris (co-author of this paper) using the general aviation data reported in reference 7, found similar distributions at this peak dwell time to be associated with a control input. These data were analyzed for associated control inputs (ref. 9) by establishing a control input criterion based on amplitude and rate. When this criterion was met, the instrument at which the subject was looking and the dwell time for that look were determined. These data, however, were not found to be associated with control input. In fact, no altimeter looks occurred within .75 seconds of a control input. The second possible explanation of the dwell distribution peaking at .5 to .6 seconds is that these are the dwells in which the pilot was reading the altitude digits in the drum window. If these are associated with the pilot reads of the drum, then two implications can be drawn. First, the number of times that the altitude window is actually read is very small (approximately 3.0% of all altimeter dwells). Second, the peak occurring at .5 to .6 seconds is a display design concern since this is almost twice as long as text reading.

The longer time could either be because of digit size (the digits are the minimum size recommended in ref. 10) or it could be that reading the drum requires the pilot to interpolate between the 305 m (1000 ft) digits showing (see fig. 2b) or a combination of both factors. In any case, numbers presented on a counter which steps between thousands of feet altitude should reduce the total read time, as the pilot has only one set of digits to evaluate. This is what apparently helped reduce the reading times (reported in ref. 5) of the drum pointer from 1.38 sec. to .8 sec. for counter pointer altimeter. It would seem logical to make the counter digits as large as possible and place them on the left of the altimeter. This is the location where the pilots look most often.

CONCLUDING REMARKS

While the drum pointer altimeter may not be the best available, all altimeters share to some degree the same problems. Additional research in exactly how and why pilots glance, read, and scan altimeters should lead to better instrument design and consequently enhance safety in both commercial and general aviation aircraft.

While each pilot has an individual scan pattern which changes with instrument layout, aircraft, and flight conditions the basic time required to extract the desired components of information should be fairly constant across conditions for an instrument like the altimeter.

The results presented here indicate that:

1. Drum pointer altimeter misreads by pilots are fairly common.
2. It requires several fixations within the drum pointer altimeter to get all the information available.

3. The pilot can pick up relative needle position (right or left) in a quick glance (.1 sec.).

4. The total time spent looking at the altimeter drum is very small, 3% of the dwells within the altimeter and it requires .5 to .6 seconds to read it.

5. Additional scan research with tests specifically designed to look at altimeter design and use is needed to properly develop and evaluate future altimeters.

At this point, several improvements are indicated; first, to increase the size of the drum numbers, second, use a counter or counter/drum combination and third, place it where the pilot looks most often (on the left side of the altimeter). Some of these improvements have already been incorporated in some of the newer altimeters. Research using these newer altimeters is needed to determine if in fact they do allow the pilots to extract the needed information quickly and accurately.

REFERENCES

1. Schum, D. A., Robertson, J. A., and Mathing, W. G.: Altimeter Display and Hardware Development 1903-1960. WADC Technical Report 63288, Wright Air Development Center, Daytona, Ohio, May 1963.

2. Mitchell, T. R.: Altimeters Display Study, Part One: Summary Report; FAA-RD-72-46, May 1972.

3. Du Zeu, A. N.: Altimeters - The Way Ahead. Aircraft Engineering, p. 12-21, July 1975.

4. Spady, A. A., Jr.: Airline Pilot Scan Patterns During Simulated ILS Approaches. NASA TP 1250, October 1978.

5. Chemikoff, R. and Ziegler, P. N.: An Experimental Evaluation of Four Types of Altimeters Using Both Pilot and Non-pilot Subjects. NRL-6232, Naval Research Lab, Washington, DC, December 1964.

6. Weir, D. H., and Klein, R. H.: The Measurement and Analysis of Pilot Scanning and Control Behavior During Simulated Instruments Approaches. NASA CR-1535, 1970.

7. Harris, R. L. and Christhilf, D. M.: What Do Pilots See in Displays? Presented at the Annual Meeting of the Human Factors Society, Los Angeles, CA October 14, 1980.

8. Cunitz, R. J., and Steinman, R. M.: Comparison of Saccadic Eye Movements During Fixation and Reading. Vision Research, Vol. 9, p. 683-693, 1969.

9. Dick, A. O.: Instrument Scanning and Controlling; Using Eye Movement Data to Understand Pilot Behavior and Strategies, NASA CR 3706, September 1980.

10. McCormick, Ernest J.: Human Factors in Engineering and Design. McGraw-Hill Book Company, 1976.

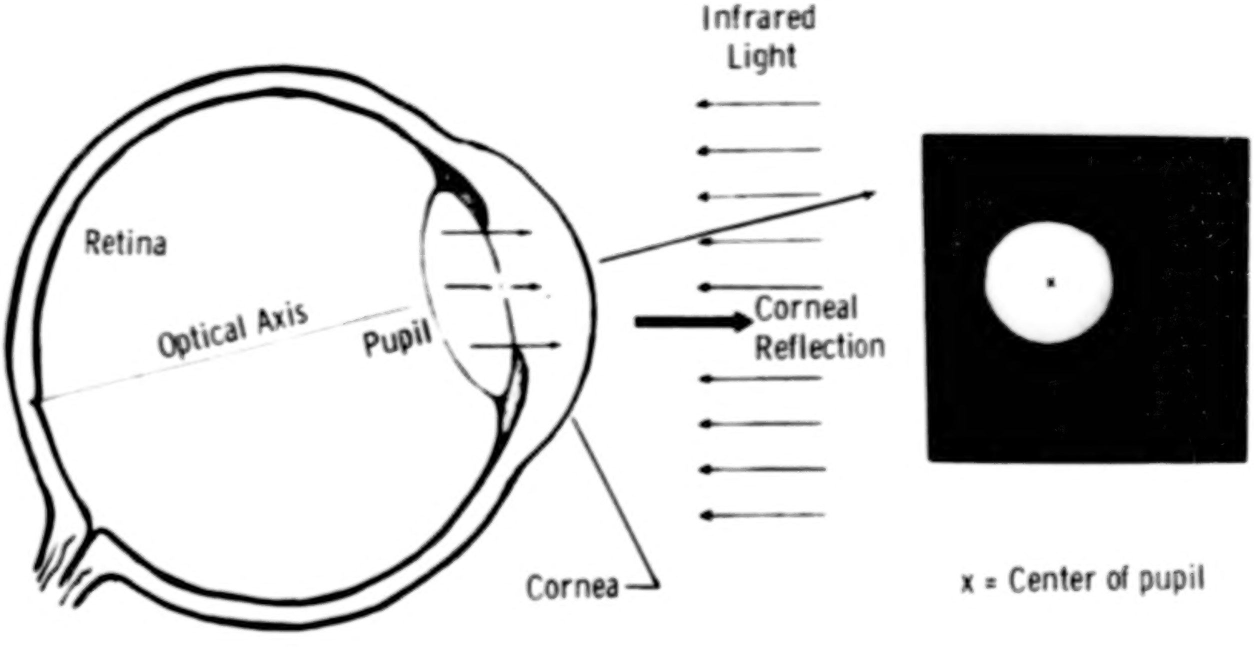
Infrared Light
Retina
Optical Axis
Pupil
Corneal Reflection
Cornea
x = Center of pupil

Figure 1.- Basic sensing principle.

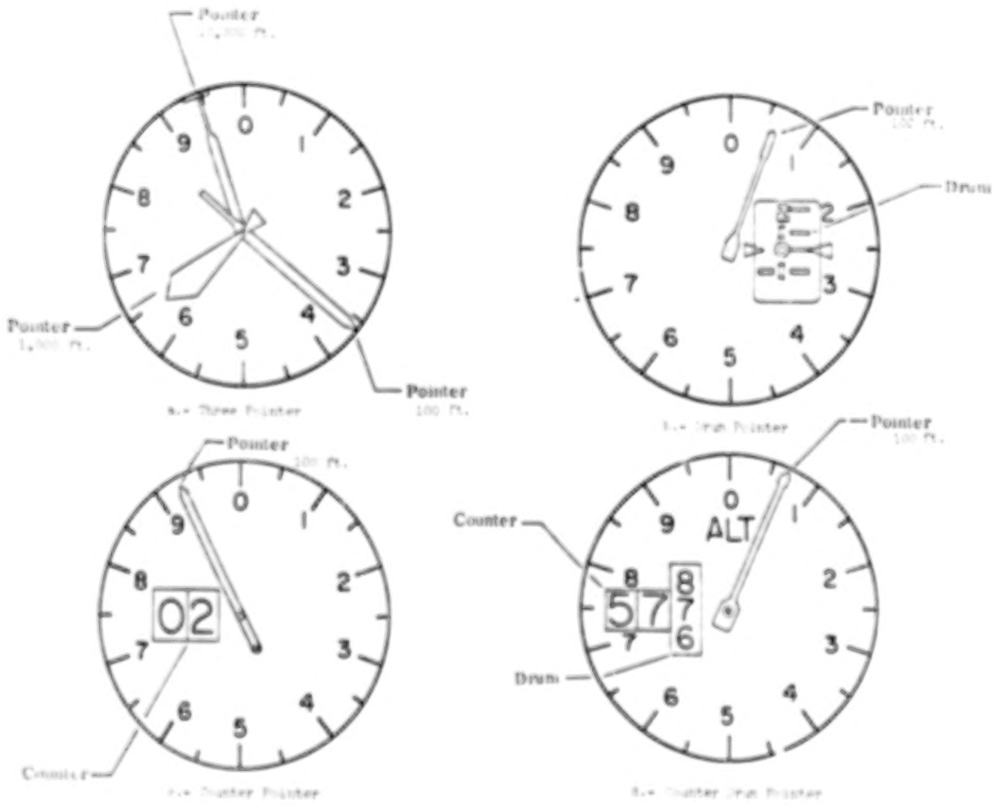
Pointer 10,000 ft.
Pointer 1,000 ft.
Pointer 100 ft.
Pointer 100 ft.
Drum
Pointer 100 ft.
Counter
Pointer 100 ft.
Counter
Drum
ALT

a.- Three Pointer

b.- Drum Pointer

c.- Counter Pointer

d.- Counter Drum Pointer

Figure 2.- Four types of altimeters. (Note: 1 ft = 0.3048 m.)

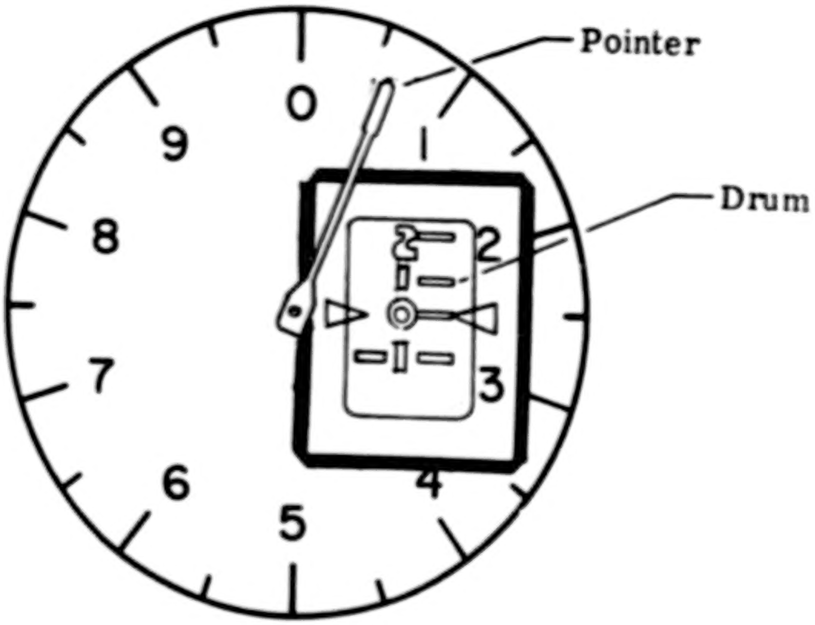
Pointer
Drum
0
1
2
3
4
5
6
7
8
9

Figure 3.- Drum pointer altimeter showing drum window area used for analysis.

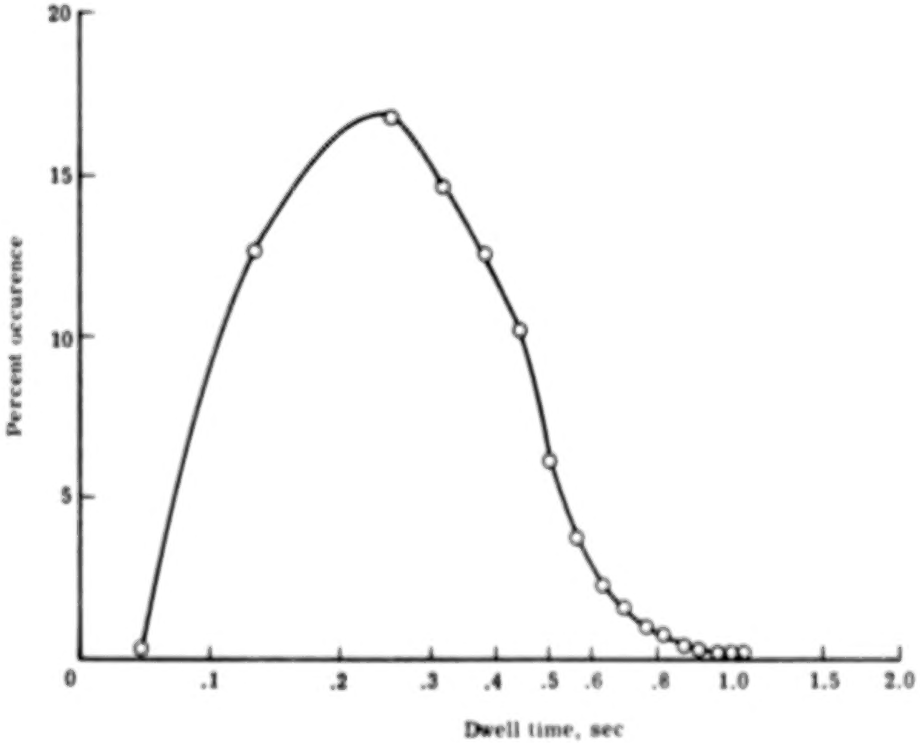

Figure 4.- Dwell time for total altimeter.

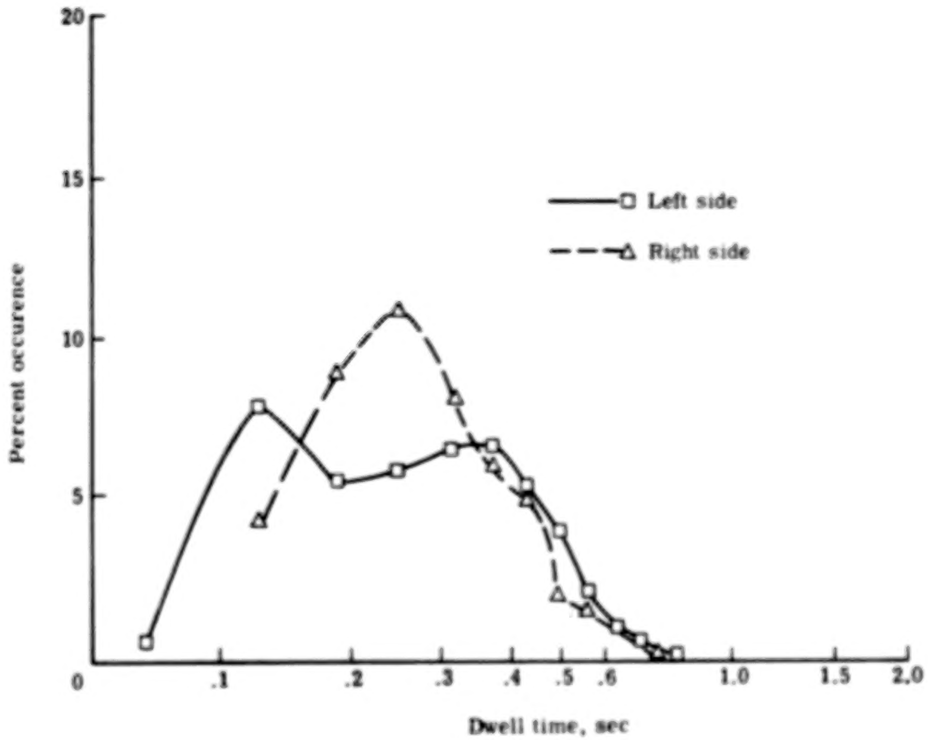

Figure 5.- Dwell time for right and left side of altimeter.

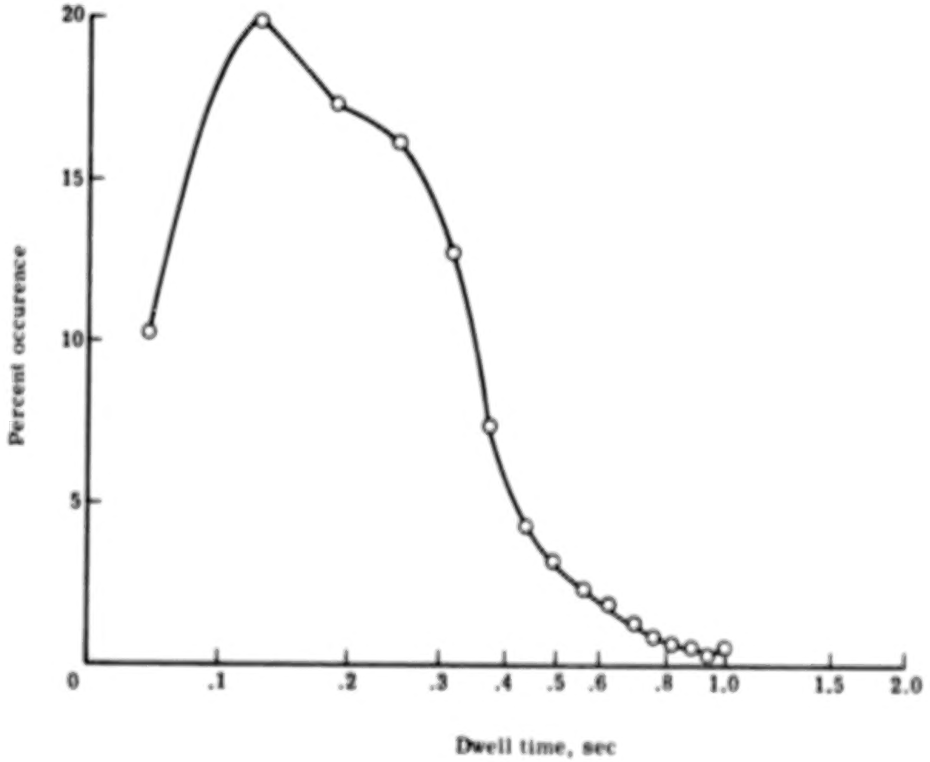

Figure 6.- Dwell time for altimeter drum area.

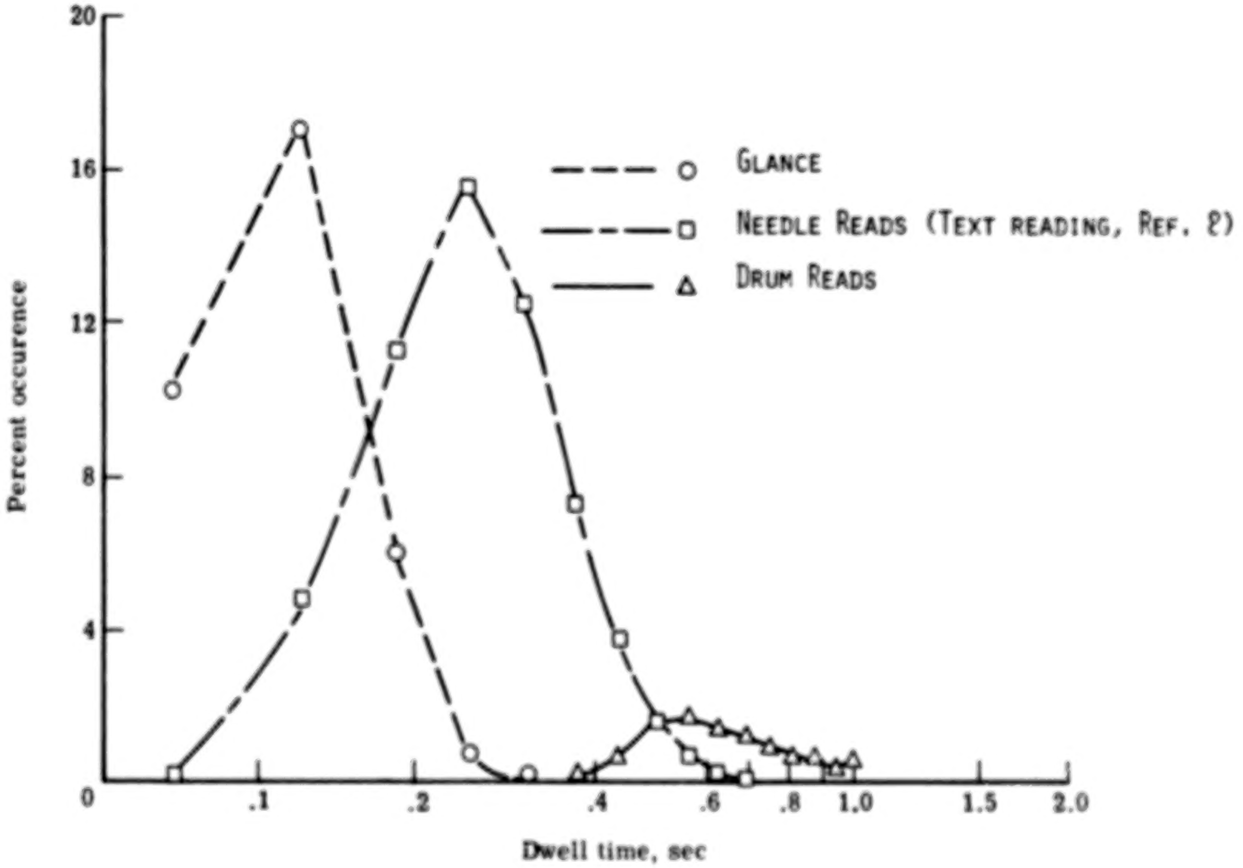

Figure 7.- Dwell time histogram of altimeter drum area showing distributions of looks.

SESSION III - ATMOSPHERIC ENVIRONMENT

BLANK PAGE

BLANK PAGE

SUMMARY OF FLIGHT TESTS OF AN AIRBORNE LIGHTNING LOCATOR SYSTEM AND COMPARISON WITH GROUND-BASED MEASUREMENTS OF PRECIPITATION AND TURBULENCE

Bruce D. Fisher and Norman L. Crabill
Langley Research Center

SUMMARY

The National Aeronautics and Space Administration is conducting research involving the operation of aircraft in and around thunderstorms. The tests described herein were conducted at the National Severe Storms Laboratory of the National Oceanic and Atmospheric Administration, in Norman, Oklahoma, during May 1978, and at the NASA Wallops Flight Center, in August 1978, using a NASA-owned twin-engine light transport aircraft. This paper includes data from an airborne lightning locator system and data relating to storm intensity obtained by the NSSL ground-based Doppler radars and the NASA Wallops SPANDAR radar. When comparing lightning locations from the airborne lightning locator system with ground-based Doppler radar measurements of reflectivity and spectrum width, the lightning locations tended to be further from the aircraft position than the Doppler radar contours, but at the same relative bearing from the aircraft as the Doppler radar contours. The results have also shown that some convective storms generate little or no lightning for a significant part of their life cycle, but can produce at least moderate turbulence. Therefore, a lack of lightning activity cannot be accepted as an inference of a corresponding lack of other hazards to the flight of aircraft through convective storms.

INTRODUCTION

Although there have been significant advances in ground-based and airborne equipment for providing information relative to severe weather, there continues to be a serious aviation safety problem associated with aircraft operations in the vicinity of severe storms. One of the problems is that of providing the pilot with information needed to avoid storm hazards which exceed the design capabilities of the airplane and its systems. As part of NASA's aviation safety research program, NASA Langley Research Center has undertaken a storm hazards research program to extend the knowledge and understanding of atmospheric processes as they affect aircraft design and operations.

The initial phase of this program, conducted during the storm season of 1978 at NSSL and NASA Wallops Flight Center, involved the preliminary evaluation of instrumentation and operational procedures around the periphery of storms using a NASA-owned twin-engine light transport aircraft. The aircraft was equipped with a commercially available lightning locator system, which was tested to determine the ability of the device to detect and locate lightning discharges, and to develop an understanding of how the device should best be used to avoid hazardous weather in flight operations. The data recorded during this program included data from the airborne lightning locator system and contours of precipitation reflectivity and radial velocity spectrum width (turbulence) from ground-based weather radars. This paper presents the results of the comparison between airborne indications of lightning and other measurements of storm hazards.

TEST EQUIPMENT AND PROCEDURES

NASA Aircraft

Physical characteristics.- The NASA test airplane was a twin-engine, high-wing, light STOL-type transport. The maximum design gross weight was 48 928 N (11 000 lb) and the aircraft weight ranged between 38 253 and 45 370 N (8 600 and 10 200 lb) during these tests. A dimensioned three-view drawing of the aircraft is given in figure 1.

Data acquisition.- Thirty-six parameters were recorded by the onboard data system. The parameters included angle of attack, angle of sideslip, static pressure, total pressure, altitude, altitude rate, total temperature, accelerations in three body axis, impact pressure, and the output of an airborne lightning-locator device. The data system included an Inertial Navigation System (INS). The following parameters from the INS were recorded: pitch, roll, and heading attitude, latitude and longitude, drift angle, crab angle, and an inertially-derived vertical acceleration.

The parameters from the INS were digitally recorded in a 16-bit stream at 20 samples/sec. The memory of the lightning locator system was sampled and recorded by the onboard data recording system 30 time/sec. Although the airborne lightning locator system was operated continually, the data were only recorded when the onboard data system was operating. The other parameters were recorded on the magnetic tape data system at 80 samples/sec by a pulse-code modulation method. All data were correlated with a time code.

Airborne lightning locator system.- As a part of these tests, a commercially available device for indicating the position of lightning strikes relative to the aircraft was installed. The device consists of a detector unit connected to an ADF antenna, a control unit, and a 7.5 cm (3-inch) diameter CRT display. The control box and display unit are shown in figure 2 as installed in the co-pilot's instrument panel. The device determines lightning location by radio direction finding on sferics and determining a line of position. The range from the aircraft along the line of position is determined by comparing the received signal wave shape and strength with an assumed lightning model. The position of the lightning is presented as a dot on the CRT. If the lightning is very intense, or very close, the device will present a series of dots along the line of position. This characteristic is known as "radial spread."

The line of position and location of the lightning strike is determined relative to the airplane position and heading at the time of the lightning strike. Thus, over a period of time, particularly with airplane heading changes, the existing CRT display of previously stored lightning locations does not represent their location relative to the new airplane position and heading. The CRT display can be erased and the indications of the lightning locations removed from the system memory by depressing the "clear" function button on the control unit. The memory section can store the location of 128 lightning signals between manual clearing of the unit. After this number of signals is recorded, additional signals overwrite the memory by replacing the oldest values with the newest. This often occurs in very electrically-active storms.

The signals used to generate the CRT display were recorded on the magnetic tape data system. Also, a video recorder was installed to record the CRT presentation. The center of the CRT is the aircraft location with a 360^0 azimuth presentation of lightning about the aircraft (figure 2). Two concentric rings about the airplane symbol represent various ranges up to 40, 100, or 200 n.mi., depending upon the position of the range selector switches on the control unit. The range setting was manually recorded by the test operator.

Transformation of lightning locations to true geographic positions.- Each lightning event detected by the airborne lightning locator in the NASA aircraft was stored by the locator system as a number pair representing the longitudinal and lateral position of the event with respect to the aircraft location at the time of the event. The memory of the system was subdivided into a 63 x 63 rectangular grid for spatially locating each lightning event. This spatial presentation was superimposed on the CRT display in the cockpit (see figure 2), with the lower left-hand corner of the display being the (1,1) matrix position, and the upper right-hand corner being the (62,62) position. Up to 128 individual lightning events could be stored and displayed by the system. After 128 points had entered the system, the new points began replacing the old points in sequential order.

For data reduction, the contents of the memory of the airborne lightning locator, and, hence, the CRT display, were digitized for the selected times of interest. The lightning rate of production for the locator was computed at 30-sec intervals after the flight. Centered on the 30-sec interval times, a program counted the number of changes in the lightning locator's memory for ±15 seconds. The number of changes counted in each interval were then divided by time to give a normalized value equivalent to the lightning rate of production in events/sec. When necessary, the sample counting intervals were shortened to eliminate changes associated with the crew manually clearing the memory. When this occurred, the shorter time interval was used for normalization. The 30-sec interval procedure was automatically interrupted in the program whenever there was a break in the data, either from turning the data recorder on and off, or from clearing the locator memory. In these instances, computations were made for +15 secs from the time the first new data appeared on tape. Subsequent computations were then made at 30-sec intervals, using this new first time as a new starting point. Every time a computation was made, the contents of the memory (and CRT) were plotted on computer drawn replicas of the CRT grid to produce a record of the lightning scenario presented to the crew by the airborne lightning locator system.

Although the basic lightning locator data used for the cockpit display were not updated for changes in aircraft position and heading, these data, in conjunction with the INS airplane position data, allowed the measured lightning locations for the reduced data to be resolved relative to fixed ground coordinates throughout time intervals of interest. For the Oklahoma flights, the transformations were made between those times corresponding to the start and stop times of the NSSL Doppler radar sample intervals. For the single flight in the vicinity of NASA Wallops, the transformations were made for the full length of the aircraft data run.

The transformation of the recorded number pairs, representing the lightning locations, to geographical locations was a five-step process: (a) conversion of the number pairs into longitudinal and lateral distances with respect to the aircraft; (b) converting the distances in step (a) into a radial and angular displacement from the aircraft; (c) computation of the angular displacement of the point from true north; (d) computation of the aircraft position with respect to the ground-based radar; and (e) transformation of the lightning point into coordinates with respect to the ground-based radar. The transformation equations used were:

For $X' > 0$

$$X_{ns} = \{(X')^2 + (Y')^2\} \sin \{90^0 - \tan^{-1} (Y'/X') + \Psi\} + X_{ac} \text{ and}$$

$$Y_{ew} = \{(X')^2 + (Y')^2\}^{1/2} \cos \{90^0 - \tan^{-1} (Y'/X') + \Psi\} + Y_{ac}$$

and for $X' < 0$

$$X_{ns} = \{(X')^2 + (Y')^2\}^{1/2} \sin \{270^0 - \tan^{-1} (Y'/X') + \Psi\} + X_{ac} \text{ and}$$

$$Y_{ew} = \{(X')^2 + (Y')^2\}^{1/2} \sin \{270^0 - \tan^{-1} (Y'/X') + \Psi\} + Y_{ac}$$

where:

X_{ns} is the north-south distance of the lightning point from a ground-based radar, positive north (km)

Y_{ew} is the east-west distance of the lightning point from a ground-based radar, positive east (km)

X' is the longitudinal distance of the lightning point from the aircraft, positive ahead (km)

Y' is the lateral distance of the lightning point from the aircraft, positive to the right (km)

Ψ is the true heading of the aircraft from the INS (deg)

X_{ac} is the north-south distance of the aircraft from a ground-based radar, positive north (km)

Y_{ac} is the east-west distance of the aircraft from a ground-based radar, positive east (km).

During calibration, it was found that the actual center of the lightning locator display and memory, which represents the aircraft position, was offset from the presumed center, and varied with the range selected. The center offsets and scale factors were used to compute X' and Y' using the equations:

$X' = (X \text{ value in memory} - X \text{ center offset}) \times (\text{scale factor})$

$Y' = (Y \text{ value in memory} - Y \text{ center offset}) \times (\text{scale factor})$

The aircraft position (X_{ac}, Y_{ac}) was found using the equations:

$X_{ac} = 111.12 \, (\text{aircraft longitude} - \text{radar longitude}) \times \cos(\text{aircraft latitude})$

$Y_{ac} = 111.12 \, (\text{aircraft latitude} - \text{radar latitude})$.

The longitude and latitude of the aircraft were taken from the INS, and the coordinates for the NSSL Norman Doppler or NASA Wallops SPANDAR radars were tabulated values.

It should be noted that the equations for X_{ns} and Y_{ew} compensated for the relative motion of the aircraft during the sample interval by using the instantaneous values of aircraft heading, longitude, and latitude. Therefore, the lightning points plotted in the figures in this paper are located at the true locations as detected by the locator system.

For comparison purposes, the aircraft ground tracks (X_{ac}, Y_{ac}) were plotted along with the lightning locations (X_{ns}, Y_{ew}) and the contours of precipitation reflectivity and spectrum width (turbulence).

NSSL/USAF Aircraft

A U.S. Air Force RF-4C aircraft was operated in a joint USAF/NSSL program to measure turbulence and wind shear within convective storm cells in Oklahoma. The RF-4C is a twin-engine, two-seat, fighter-type aircraft with the structural ruggedness and reserve power necessary for thunderstorm penetrations. A dimensioned three-view drawing of the aircraft is given in figure 3.

The following parameters were recorded by the magnetic tape data system onboard the aircraft: outside air temperature, angle of attack, angle of sideslip, normal acceleration, pressure altitude, stabilator position, radar altitude, airspeed, and magnetic heading. The instrumentation system included an AN/ASN-56 inertial navigation system (INS). The recorded INS parameters were pitch and roll angle, pitch rate, and ground speed and direction. These data were recorded at a sample rate of 21.9 samples/sec. A time code generator synchronized to WWV was used as a time base.

The aircraft track of the NSSL/USAF RF-4C aircraft was established every 20 seconds from the location of the aircraft transponder displayed on the photographically recorded WSR-57 radar plan position indicator (PPI) scope. Linear interpolation was used to position locations between scans. Aircraft and radar data were synchronized using WWV time-based checks. Digitally recorded aircraft data were computer processed and expressed in engineering units.

The vertical winds, w, in m/sec were computed using:

$$w = V_{ta}\alpha + V_{ta}\beta_a - V_{ta}\theta + \int_0^t a_z dt + w_{p,g}\ (0) + L_v\dot{\theta}$$

where:

V_{ta} = true air speed (m/sec)

α = angle of attack (rads)

β_a = sideslip angle (rads)

θ = pitch angle (rad)

a_z = aircraft vertical acceleration (m/sec^2)

$w_{p,g}$ (0) = vertical velocity of the aircraft at time T = 0 (m/sec)

$\dot{\theta}$ = pitch rate (rads/sec)

L_v = distance from accelerometer to angle of attack measurement point (m).

As another measure of turbulence, the derived equivalent gust velocity, U_{de}, was also used. This value was computed from aircraft recorded data using the general equation (from reference 1):

$$U_{de} = \frac{2W \Delta a_z}{V_e K_g \rho_o C_{L_\alpha} S_a}$$

where

W = aircraft weight (N)

Δa_z = measured aircraft incremental vertical acceleration from normal (g units)

V_e = equivalent airspeed to sea level (m/sec)

K_g = gust alleviation factor

ρ_o = air density at sea level (kg/m^3)

C_{L_α} = change in aircraft lift coefficient

S_a = aircraft wing area (m^2)

Ground-Based Radars

WSR-57 radar.- The WSR-57 weather surveillance radar is the type used in the National Weather Service network. The radar characteristics were: half-power beam width of 2.2°; wavelength of 10.6 cm; and peak power of 300 kW. The radar located at Norman, Oklahoma (see figure 4), continuously scanned all azimuth sectors at an 18°/sec rate to provide a surveillance of all storms within 300 km of Norman. The elevation angle was usually 0.5°. Every 5 min, the elevation angle was stepped in increments of 2° each revolution in order to have storm cross sections at different heights.

The radar's logarithmic receiver output was integrated and then range normalized to produce digital estimates proportional to effective reflectivity factor in dBZ. The digital estimates were quantized in six categories and displayed in a Plan Position Indicator (PPI) manner on a CRT. This PPI display was used during the test operations to help guide the NASA and USAF aircraft to storm cells of interest, and to avoid hazardous weather exceeding the capabilities of the aircraft. An MPX-7/UPX-6 surface-based aircraft transponder interrogator, located adjacent to the WSR-57 radar, provided aircraft position data (out to 400 km) which was superimposed on the WSR-57 radar scope. This display, in conjunction with telephone communications to the appropriate air traffic control centers, was used by an assigned FAA air traffic controller at NSSL to coordinate control of the two test aircraft.

Doppler radars.- A matched pair of Doppler radars, one located at Norman, Oklahoma, and another at Cimarron Airport, Oklahoma City, Oklahoma (see figure 4), are used by the NSSL to scan through storms of interest. During these tests, however, no storms entered the dual Doppler area. In fact, all the Doppler radar data shown in this paper were obtained by the Norman Doppler radar.

A Doppler radar generates a datum of reflectivity factor (a measure of rainfall rate, assuming a Marshall-Palmer distribution of droplets, in dBZ). mean radial velocity to or from the radar (in m/sec), and Doppler radial velocity spectrum width (in m/sec) for each resolution volume. The relationship of reflectivity to rainfall rate and intensity level for a typical WSR-57 weather radar used by the National Weather Service is given in table I. The spectrum width can be interpreted as a measure of turbulence. (Details on the Doppler radar parameters and measurement techniques may be found in references 2 and 3.)

The radar characteristics were: half-power beam width of 0.81°; wavelength of 10.52 cm; and peak power of 750 kW. Typically, the rotation rate was 6°/sec. Periodically, the elevation angle was stepped in increments in order to have storm cross section at different heights. For these tests, the radar resolution volume had a 1° azimuth extent, 1° elevation extent, and 150 m range extent. The first two parameters are fixed values, but the range extent can be varied from 150 m to 1 km.

The Doppler radar reflectivity data are presented in this paper as constant contours on an essentially level plane at the same altitude. Correspondingly, the Doppler spectrum width data, representing turbulence, are presented as constant contours on the same planes. The techniques used for generating this presentation are outlined below.

The reconstruction of the thunderstorms on May 11, 1978, and on June 1, 1978, from the unprocessed Doppler radar tapes consisted of three distinct analysis routines: (a) editing the unprocessed, or raw, data tape; (b) interpolating data to uniformly spaced grids on constant elevation surfaces; and (c) plotting contours of equivalent reflectivity factor (dBZ) and spectrum width (m/sec).

An interlaced sampling collection mode was used in which reflectivity samples were acquired separately from velocity samples. The interlaced sampling mode allowed the resolution of range-ambiguous echoes by identifying the true ranges and strengths of all echoes, and this information was used to unscramble the ranges associated with the velocity data, or to eliminate those data when two or more echoes were overlaid.

For the storms of May 11, and June 1, 1978, the radar sampling parameters produced an unambiguous radar range of 115 km. When range scrambling was detected at a given range gate, the reflectivity and spectrum width measurements were removed from the data set, although the reflectivity data were not scrambled. Thus, there are regions on the contoured plots where it appears the contours end abruptly.

Reflectivity was computed using the radar equation given in references 4 to 6. The spectrum width was computed using the analysis given by Zrnic'[1].

For small elevation angles ($\leq 10^\circ$), the data on constant elevation surfaces could be displayed on a plane surface with little distortion by interpolating points to a horizontal surface tangent to the radar location. The data were weighted using a Cressman filter (reference 7) applied to a prolate spheroidal interpolation volume. The vertical influence radius was made disproportionately large, keeping the horizontal radius at 1 km, and data used were taken from a single azimuthal scan at one elevation. This procedure caused a small distortion factor, which at 1° elevation, was less than 0.02 percent. Thus, by using only one elevation of data for each run, a contoured simulated PPI plot for the first trip could be constructed. Displaying data at constant elevation angle was more satisfactory than displaying data at constant height because elevation angle spacings used in data acquisition caused too many gaps in data fields at constant height.

Contours of reflectivity factor (dBZ) and spectrum width (m/sec) were created by using a least-squares fit on the 120 km x 120 km data matrix. The computed contour intervals for reflectivity factor were 10, 20, 30, 40, 45, 50, 55, and 60 dBZ. For clarity and simplicity in this paper, these contours were combined to 10-40 dBZ, and greater than 40 dBZ. For spectrum width, the contour intervals were 2, 6, 10, and 14 m/sec. Because of poor spectrum width estimation at low signal-to-noise ratios, the spectrum width at the edges of storms (reflectivity $\leq$ 10 dBZ) should be considered spurious. A good discussion on this problem is given in reference 8.

NASA Wallops SPANDAR Radar

As was the case during the NSSL flight tests, contours of constant precipitation reflectivity in dBZ were desired for the single flight in the vicinity of NASA Wallops in Virginia. The radar precipitation reflectivity measurements were made by the S-band research radar (SPANDAR) at NASA Wallops. Unlike the NSSL Doppler radar, however, the SPANDAR radar could not measure spectrum width.

The SPANDAR radar sampled precipitation intensity (reflectivity) at 1-μsec intervals out to a maximum range of approximately 75 n.mi. The peak power output was 1 MW, the pulse repetition frequency was 320, the beam width was 0.4°, and the range accuracy was 229 m (750 ft). The raw data tape of radar video was digitized following the flight, and converted to received power and rainfall rate by the radar equations. The final computation step was the correction of rainfall rate for range to give reflectivity in dBZ. The reflectivity values were averaged over surfaces of 1000 m by 1000 m for the PPI plots and over surfaces of 300 m by 300 m for vertical scans, and then plotted at the centers of each averaged area. For simplicity of analysis, the reflectivity values were computer sorted into 5-dBZ increments starting at 20 dBZ for plotting. Finally, the computer plots were further simplified to give contours of 20-30, 30-50, 50-60, and 60-65 dBZ. Details on the SPANDAR radar system and radar computations may be found in reference 9.

---

[1] Zrnic', D. S.: Spectrum Width Calculation. NSSL Memorandum for the Record, Apr. 1978. (Unpublished.)

Test Procedures

NSSL.- For all of the test flights made in conjunction with the NSSL, visual flight was maintained by the NASA aircraft, although the aircraft did fly in close proximity to active thunderstorms. The onboard data system recorded lightning activity as measured by the airborne lightning locater system while ground-based radar measurements were made of the same storm. Attempts were made to correlate the pilot visual observation of the storm system with the information provided by the lightning locator system.

The NSSL/USAF aircraft was directed through thunderstorms of interest to gather in-situ turbulence measurements. The aircraft was kept out of areas of precipitation reflectivity which exceeded 45 dBZ.

Air traffic control of the two aircraft was coordinated by a dedicated FAA air traffic controller, using the WSR-57 radar display with the superimposed aircraft transponder positions. The controller, located at NSSL, was in telephone communication with the required air traffic control facilities, and in direct radio contact with both aircraft.

The aircraft flight paths were programmed by the NASA and NSSL researchers, who were co-located with the controller. For assistance in making flight decisions, Doppler radar data were presented in direct view of the controller and researchers. These Doppler data were supplemented by closed-circuit television presentation of the latest weather satellite picture covering the area.

NASA Langley.- Following the flight test program at NSSL, the NASA aircraft returned to NASA Langley for test flights over the Chesapeake Bay during August 1978. Unlike at NSSL, the NASA aircraft penetrated a small, isolated cumulonimbus cloud which showed no electrical activity on the airborne lightning locator. The aircraft crew maintained radio communications with the local air traffic control facilities and the Flight Service Office at NASA Langley. The aircraft crew was also in radio communication with the SPANDAR radar site at NASA Wallops. Because of the limited nature of the real-time displays at the SPANDAR site, however, the NASA flight crew programmed their own flight paths. As was the case at NSSL, records were made of the airborne lightning locator system while ground-based radar measurements were made of the same storm (by the SPANDAR radar).

DISCUSSION OF RESULTS

During the 1978 storm season, a total of 14 storms were surveyed with the combined airborne data and ground-based data systems. Thirteen storms were studied in the vicinity of NSSL at Norman, Oklahoma, and one storm was studied in the vicinity of NASA Wallops in Virginia. An appreciable amount of lightning activity was measured during twelve of these storms. However, for two storms, very little lightning activity was measured or reported, yet the other hazard measurements indicated significant levels of reflectivity and turbulence. The following discussion gives typical details for storms representing these conditions. The storm of June 1, 1978, at Norman, Oklahoma, represents the general case with appreciable lightning activity, and the storms of May 11, 1978, at Norman and August 14, 1978, at NASA Wallops represent the less general case of very little lightning activity.

1978 Storm Hazards Research

Storm of June 1, 1978, at Norman, Oklahoma.- An area of scattered heavy thunderstorms formed in central Oklahoma to the north and east-southeast of Norman at 15:12 CST. The storms to the north of Norman formed a line about 50 km long. This line moved slowly to the east, with individual cells in the line propogating from 250^{o} at 7 m/sec. The storms to the southeast of Norman moved from 240^{o} at about 9 m/sec. The maximum heights of these storms never exceed 13.1 km (43 000 ft).

The airborne lightning locator system was operated and recorded continuously from 15:11:50 to 15:59:30 CST. The rate of production of lightning points detected by the airborne locator is plotted as a function of time in Figure 5, along with the start and stop times of the four Doppler radar data sample periods. The lightning events occurred at a rate more than 1 every 2 secs for most of the data period, with a peak rate of 2.4 points/sec at 15:32:16 CST. Interestingly, at 15:26 CST, the storm to the southeast seemed to intensify, while the strength of the storms to the north remained unchanged. All the storms in the area weakened in intensity from 15:41 CST until 16:00 CST. There was a corresponding decrease in lightning activity between 15:40 and 15:50 CST. However, for each of the four Doppler radar sample periods, the peak reflectivity and spectrum width values in the cells being studied were 45 dBZ and 6 m/sec, respectively.

The reflectivity contour data taken during the third Doppler radar data interval (15:41:34 - 15:46:39 CST) are given in Figure 6 for discussion of this storm as the activity is typical of the storm as a whole. A typical presentation from the airborne lightning locator during this time interval is given in Figure 7. The 74 points displayed were those contained within the system memory at 15:42:52 CST. These points had been accumulating (190 secs) since the last clear at 15:39:32 CST. New lightning points were being detected at a rate of 0.1333 points/sec over the 30-second period from 15:42:37 to 15:43:07 CST. The lightning activity was concentrated at the 2 o'clock and 5 o'clock positions at a range of 40 n.mi. This airborne display would indicate that a path to the left of the current course would avoid lightning activity.

All of the lightning points detected during the entire third Doppler radar data period are shown plotted in their true positions with respect to the Norman Doppler radar in figure 6 along with the NASA aircraft ground track during this period. The aircraft was flying to the northwest, south of several storm cells with peak reflectivities of 40 and 45 dBZ. Several storm cells of similar reflectivity levels were located to the southeast of the aircraft. Reflectivities of 45 dBZ indicate a high probability of hail within the 45 dBZ contour, and a good chance of encountering moderate turbulence somewhere within the storm cell. The relative bearings of the lightning points to the aircraft are generally the same as the relative bearings of the Doppler radar reflectivity contours to the aircraft. However, many of the measured lightning locations are shown at a greater range from the aircraft than the Doppler radar reflectivity contours.

The same measured lightning locations and aircraft ground track are shown in figure 8 with the Doppler radar spectrum width contours for the same data interval. The various storm cells contain spectrum width values ranging from 2 to 6 m/sec, corresponding to light turbulence (reference 10). As was the case with the data in figure 6, the lightning locations have the same general bearing with respect to the aircraft as the Doppler radar contours, but are also shown to be further from the aircraft than the Doppler radar contours. For this typical, electrically active thunderstorm system it can be said that the airborne lightning locator data agreed generally with the location of the most severe weather as indicated by the NSSL ground-based Doppler radar. For this storm system, the airborne lightning locator system gave sufficient information to avoid the areas of high reflectivity (precipitation) and spectrum width (turbulence).

Storm of May 11, 1978, at Norman, Oklahoma.- A line of severe thunderstorms with pea-sized hail propagated from south-central Oklahoma to the east at 7 m/sec late in the afternoon of May 11, 1978. This line extended from Duncan, Oklahoma, to 40 km southwest of Archer City, Texas. Individual cells in this line moved at 16 m/sec from 250° during four Doppler radar data collection periods from 16:23:14 to 16:52:43 CST.

Very low rates of lightning production occurred throughout this storm. Unfortunately, the significance of this fact did not become apparent until after the flight was over. The aircraft had already taken 20 mins of data earlier in the flight in the vicinity of Ponca City, Oklahoma. In order to conserve the remainder of the data recorder tape, periods of little electrical activity were not recorded, although the airborne lightning locator system was in continuous operation throughout the flight. However, data were recorded for four short intervals when the aircraft was headed towards 40-dBZ reflectivity contours to document the lack of lightning activity. The crew noted that the low level of activity was no different during the recorded periods than during the non-recorded periods.

The rate of production of lightning points detected by the airborne lightning locator system is plotted as a function of time in Figure 9 along with the start and stop times of the four Doppler radar data sample periods. The start and stop times of the single penetration by the NSSL/USAF aircraft are also plotted in figure 9. The maximum lightning production rate for this storm was only 0.0666 points/sec. The low level of activity did not change with variations in the intensity of the storm. The peak reflectivity dropped from 50-55 dBZ during the first Doppler radar interval to 40-45 dBZ during the fourth interval. High spectrum widths (greater than or equal to 10 m/sec) were observed near the core of the storm during the first, second, and fourth Doppler radar period. The maximum height of the southern-most cell under study decreased from 14.6 km (48 000 ft) at 16:10 CST to 14 km (46 000 ft) at 16:45 CST with no corresponding change in lightning activity.

The data from the fourth Doppler radar period (16:47:30 to 16:52:43 CST) were chosen for discussion because this was the only time that both airborne lightning locator data and in-situ turbulence data from the NSSL/USAF aircraft were available. A typical presentation from the airborne lightning locator system during part of the fourth interval is given in figure 10. At 16:48:09 CST, only two points were being displayed ahead of the aircraft at 40 n.mi. range. These two points had been accumulating since 16:47:40 CST, when the data recording system was turned on. The rate of production was only 0.0416 points/sec over the 24-second period from 16:47:52 to 16:48:16 CST.

The four lightning points detected during the entire fourth Doppler radar data period are shown in figure 11 along with the Doppler radar reflectivity contours and ground tracks of the NASA and NSSL/USAF aircraft with respect to the Norman Doppler radar. A similar presentation with respect to the Doppler radar spectrum width contours is given in figure 12. As was the case for the comparisons for the June 1, 1978, storm (figures 6 and 8), the airborne lightning locator data agreed with the general locations of the most severe weather, as indicated by the NSSL ground-based Doppler radar. For the storms studied in this program, when comparing lightning locations from the airborne lightning locator system with ground-based Doppler radar measurements of reflectivity and spectrum width, the airborne lightning locator system data points tended to be further from the aircraft position than the Doppler radar contours, but at the same relative bearing from the aircraft as the Doppler contours.

The actual turbulence occurring inside the storm was measured by the NSSL/USAF aircraft from 16:47:13.4 to 16:50:53.4 CST during a storm penetration from northwest to southeast at a nominal altitude of 6.1 km (20 000 ft). Time histories of maximum derived equivalent gust velocity (U_{de}) and vertical gust velocity computed from the onboard instrumentation are shown in figure 13. The reflectivity intensity through which the aircraft was flying is also plotted in figure 13 for reference, where these reflectivity values were taken from a reflectivity contour plot interpolated to a constant altitude of 0.3 km. The peak U_{de} values ranged from 7 to 9 m/sec, corresponding to a moderate level of turbulence (reference 10). During the penetration, the pilot reported moderate turbulence at 16:48:46 and 16:49:03 CST. Vertical gust velocities of ±9 m/sec were experienced during this time period. In summary, the storm of May 11, 1978, was an intense convective storm which generated little or no lightning for a significant part of its life cycle, but produced at least moderate turbulence. The airborne lightning locator system gave much less indication of lightning activity during this storm than during other storms which had similar Doppler radar contour levels of reflectivity and spectrum width. This calls into question the relationship of lightning to other measures of severe storm hazards.

Storm of August 14, 1978, at NASA Wallops.- The fourteenth, and final, storm of the 1978 storm season occurred over the Chesapeake Bay, on August 14, 1978. The research flight was made in conjunction with ground-based measurements of precipitation reflectivity by the S-band SPANDAR radar at NASA Wallops.

The rate of production of lightning points detected by the airborne lightning locator system is plotted as a function of time in figure 14, along with the times during which the four SPANDAR radar scans were made. As was the case with the Oklahoma thunderstorm of May 11, 1978, very little lightning activity was measured during the storm. The output of the airborne lightning locator system was recorded during four intervals to document the lack of activity. Although the recording system was not operated continuously, close visual observation by the crew indicated that there were no lightning events during the periods when the recorder was not operating.

During the third recording period of the airborne lightning locator system (20:10:45 to 20:16:30 GMT), the NASA aircraft penetrated what visually appeared to be a benign storm. The aircraft ground track is shown on the precipitation reflectivity contours from the SPANDAR radar scan made starting at 20:01:20.7 GMT, in figure 15. The SPANDAR radar detected a peak reflectivity of 60-65 dBZ. The maximum top of 9.1 km (30 000 ft) was detected along the 325° azimuth at 20:26:57.1 GMT; a lower top of 8.8 km (29 000 ft) was found at 20:15:04 GMT along the 320° azimuth. During the entire data run shown in figure 15, only one lightning event was detected in the vicinity of the storm contours, and is plotted in its true relative position with respect to the NASA Wallops SPANDAR radar in figure 15. Two other lightning points were recorded during the run, but both were located outside the plotted region in areas of clear air.

As the aircraft flew deeper into the storm cell, the turbulence began to increase and the rain became very heavy. The pilot executed a 90° turn to depart the storm because of the worsening conditions. The turn was apparently made when the aircraft was in an area with a reflectivity between 55 and 60 dBZ (see figure 15). A peak vertical acceleration of 0.7 g incremental was recorded at 20:12:45.7 GMT, while the aircraft was turning. This vertical acceleration peak is equivalent to a U_{de} of 5.4 m/sec (17.7 ft/sec), which is near the threshold of moderate turbulence (reference 10). The high reflectivity values were probably due to the large quantity of low altitude moisture in the atmosphere over the Chesapeake Bay, rather than by hail, as is typically the case in Oklahoma thunderstorms. (There is a slight possibility that the aircraft flew through a lower reflectivity region because of motion of the storm in the time between the radar sample and the penetration, and the difference in altitude between the aircraft altitude and the height of the radar sample.)

Of the fourteen storms studied, two storms (May 11, 1978, in Oklahoma, and August 14, 1978, in Virginia) had little lightning activity but heavy precipitation and moderate turbulence. Apparently, there are some convective storms which generate little or no lightning for a significant part of their life cycle, but can produce at least moderate turbulence. Therefore, a lack of lightning cannot be accepted as an inference of a corresponding lack of other hazards to the flight of aircraft through convective storms.

Further Storm Hazards Research

The NASA Storm Hazards Research Program did not conclude with the 1978 flight tests. During 1979, a NASA-owned F-106B aircraft was flown on the peripheries of thunderstorms in the vicinity of NASA Wallops to gain operational experience prior to actual thunderstorm penetration flights. A report on the 1979 operations is given in reference 11.

During the 1980 storm season, the F-106B made approximately 70 thunderstorm penetrations during 20 storm flights in the vicinity of NSSL and NASA Wallops. During these penetrations, the aircraft sustained 10 direct lightning strikes, whose electromagnetic properties were measured by an onboard direct-strike lightning instrumentation system described in references 11 and 12. The preliminary results from this system are given in references 13 and 14.

The flight experiments carried onboard during the 1980 mission were:

- lightning related
  - direct-strike lightning
  - lightning data logger (in cooperation with Boeing)
  - atmospheric chemistry (air sampler for N_2O)
  - lightning X-rays (University of Washington)
  - composite fin cap
- non-lightning related
  - turbulence
  - wind shear
  - storm hazards correlation.

A schematic of the mission operations with the F-106B aircraft in the vicinity of NASA Wallops is given in figure 16. This schematic shows the general layout of the experimental packages in the aircraft and the ground-based data systems which are used. It should be noted that the WSR-57 radar is located at Patuxent River, Maryland, and the radar image is transmitted by telephone line to a color television monitor in the SPANDAR radar control room. A description of the NASA Wallops instrumentation is given in a paper reference 15.

During the 1979 and 1980 storm seasons, the airborne lightning locator system was installed in the F-106B, and was used by the flight crew as a real-time guide to determine the most electrically active storm cell for penetration. Flight tests with the F-106B will continue through the 1983 storm season. During these operations, comparisons of the output of the airborne lightning locator system in the F-106B and from another locator installed at the SPANDAR radar control site will be made with the output of the lightning direction and ranging system shown in figure 16.

SUMMARY OF 1978 TEST RESULTS

NASA Langley Research Center has undertaken a storm hazards program to extend the knowledge and understanding of atmospheric processes as they affect aircraft design and operations. The initial phase of this program, conducted during the storm season of 1978 at NSSL and NASA Wallops, involved flight tests around the periphery of storms using a NASA-owned light transport aircraft equipped with a commercially available airborne lightning locator system. The results of the comparison between airborne indications of lightning and other measurements of storm hazards are:

1. There are some convective storms which generate little or no lightning for a significant part of their life cycle, but can produce at least moderate turbulence. Therefore, a lack of lightning activity cannot be accepted as an inference of a corresponding lack of other hazards to the flight of aircraft through convective storms.

2. The airborne lightning locator system data agreed generally with the location of the most severe weather as indicated by the NSSL ground-based Doppler radar. When comparing lightning locations from the airborne lightning locator system with ground-based Doppler radar measurements of reflectivity and spectrum width, the lightning locations tended to be further from the aircraft position than the Doppler radar contours, but at the same relative bearing from the aircraft as the Doppler radar contours.

ACKNOWLEDGEMENTS

The author would like to acknowledge the contributions of the staff of the National Severe Storms Laboratory in preparing the Doppler radar contours shown in this paper and in providing the descriptions of the WSR-57 and Doppler radar systems. In particular, the author would like to thank Mr. Jean T. Lee, Dr. Richard J. Doviak, and Mr. Steve Goodman.

REFERENCES

1. Pratt, Kermit G.; and Walker, Walter G.: A Revised Gust-Load Formula and a Reevaluation of VG Data Taken on Civil Transport Airplanes from 1933 to 1950. NACA Report 1206, 1954.

2. Alberty, R.; Weaver, J.; Sirmans D.; Dooley, J.; and Bumgarner, B.: Spring Program 76, Section II, NOAA Technical Memorandum ERL NSSL-83, pp. 79-130, 1977.

3. Lee, J. T.: Application of Doppler Weather Radar to Turbulence Measurements Which Affect Aircraft. FAA Report No. FAA-RD-77-145, March 1977.

4. Probert-Jones, J. R.: The Radar Equation in Meteorology, Quarterly Journal of the Royal Meteorological Society, Vol 88, pp. 485-495, 1962.

5. Doviak, R. J.; and Zrnic', D.: The Weather Radar Equation-Receiver Bandwidth Considerations. Preprints, 18th Conference on Radar Meteorology, American Meteorological Society, pp. 484-489, March 28 and 31, 1978.

6. Berger, Myron I.: A Dual Doppler Radar Investigation of Planetary Boundary Layer Winds in the Optically Clear Atmosphere. Master Science Thesis, University of Oklahoma, pp. 64-65, 1978.

7. Cressman, G. P.: An Operational Objective Analysis System. Monthly Weather Review, 87, pp. 367-374, 1959.

8. Sirmans, D.; Zrnic', D. S.; and Bumgarner, W.: Estimation of Maximum Unambiguous Doppler Velocities by Use of Two Sampling Rates. 17th Conference on Radar Meteorology, American Meteorological Society, pp. 23-28, October 1978.

9. Konrad, T. G.; and Kropfli, R. A.: Radar Derived Spatial Statistics of Summer Rain, Volume II - Data Reduction and Analysis. NASA CR-2592, September 1975.

10. Anon.: National Weather Service Operations Manual, Part D, Chapter 22, 1976.

11. Fisher, Bruce D.; Keyser, Gerald L., Jr.; Deal, Perry L.; Thomas, Mitchel E.; and Pitts, Felix L.: Storm Hazards '79 -- F-106B Operations Summary. NASA TM-81779, March 1980.

12. Pitts, F. L.; Thomas, R. M.; Zaepfel, K. P.; Thomas, M. E.; and Campbell, R. E.: In-Flight Lightning Characteristics Measurement System. Presented at FAA-Florida Institute of Technology Workshop on Grounding and Lightning Technology, Melbourne, Florida, March 1979. FAA-RD-79-6.

13. Pitts, Felix L.; and Thomas, Mitchel E.: Initial Direct-Strike Lightning Data. NASA TM-81867, August 1980.

14. Pitts, Felix L.; and Thomas, Mitchel E.: In-Flight Direct-Lightning Research. 1980 Aircraft Safety and Operating Problems, NASA CP-2170, 1981. (Paper 20 of this compilation.)

15. Carr, Robert E.; and Gerlach, John C.: Wallops Severe Storms Measurement Capability. 1980 Aircraft Safety and Operating Problems, NASA CP-2170, 1981. (Paper 15 of this compilation.)

TABLE I.- WSR-57 WEATHER RADAR REFLECTIVITY CHART

Level	Intensity Category	Radar Color	Maximun reflectivity, dBZ	Rainfall Rate			
				Stratiform		Convective	
				mm/hr	in/hr	mm/hr	in/hr
	No precipitation	White	103.5 dBm at zero range	0.0	0.0	0.0	0.0
1	Weak	Gray	30	2.54	0.1	5.08	0.2
2	Moderate	Black	41	12.7	0.5	27.9	1.1
3	Strong	White	46	25.4	1.0	55.9	2.2
4	Very Strong	Gray	50			114.3	4.5
5	Intense	Black	57			180.3	7.1
6	Extreme	White				>180.3	>7.1

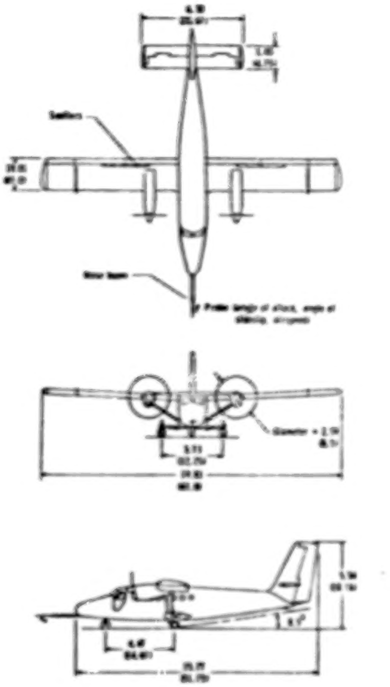

Figure 1.- Three-view drawing of NASA test airplane. All dimensions are in meters (feet).

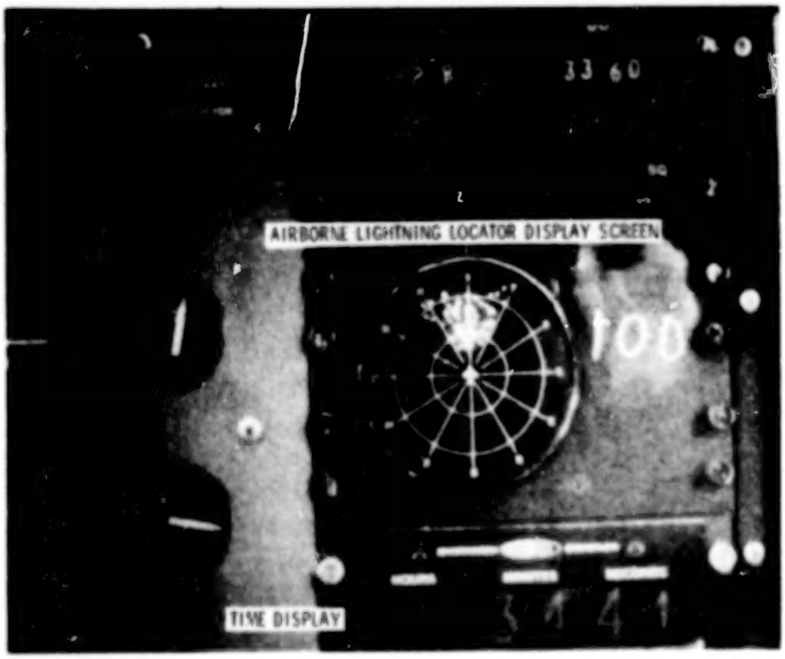
33 60
AIRBORNE LIGHTNING LOCATOR DISPLAY SCREEN
100
TIME DISPLAY
3441

Figure 2.- Airborne lightning locator display in NASA aircraft.

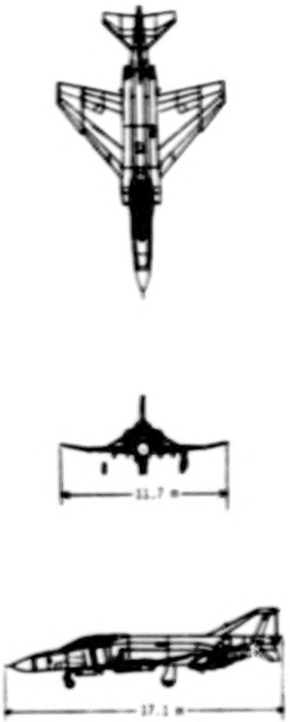

Figure 3.- Three-view drawing of U.S. Air Force RF-4C aircraft flown for NSSL.

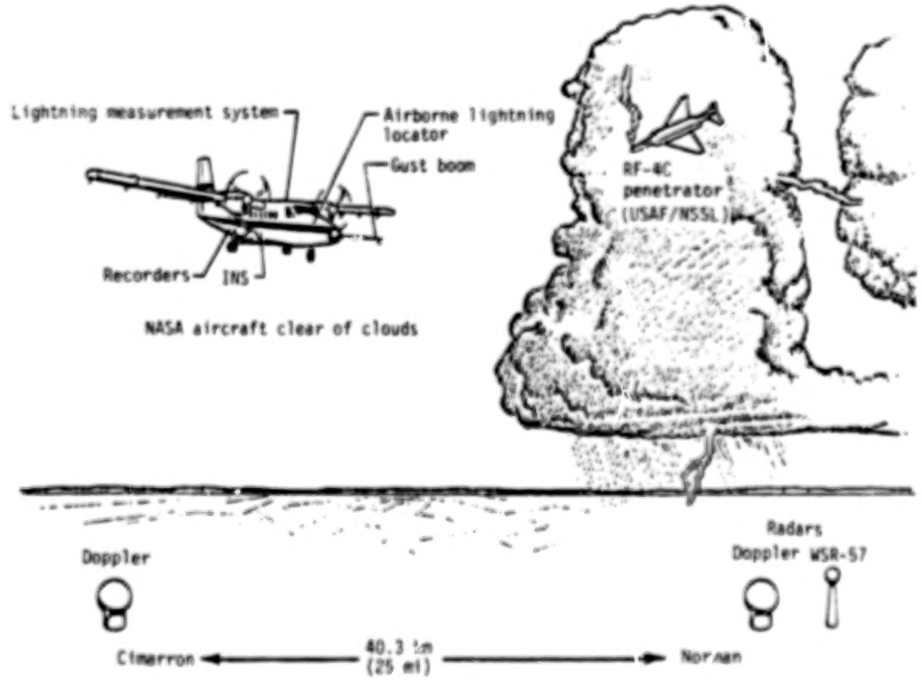
Lightning measurement system
Airborne lightning locator
Gust boom
Recorders
INS
NASA aircraft clear of clouds
RF-4C penetrator (USAF/NSSL)
Radars
Doppler
Doppler WSR-57
Cimarron
40.3 km (25 mi)
Norman

Figure 4.- Schematic of test program at National Severe Storms Laboratory during May 1978.

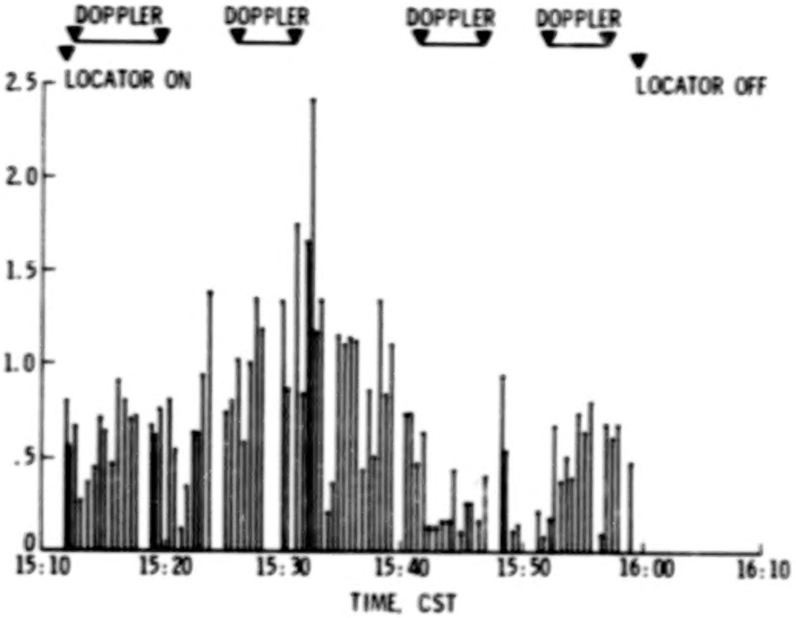

Figure 5.- Rate of production of lightning measured by airborne lightning locator system for storm of June 1, 1978.

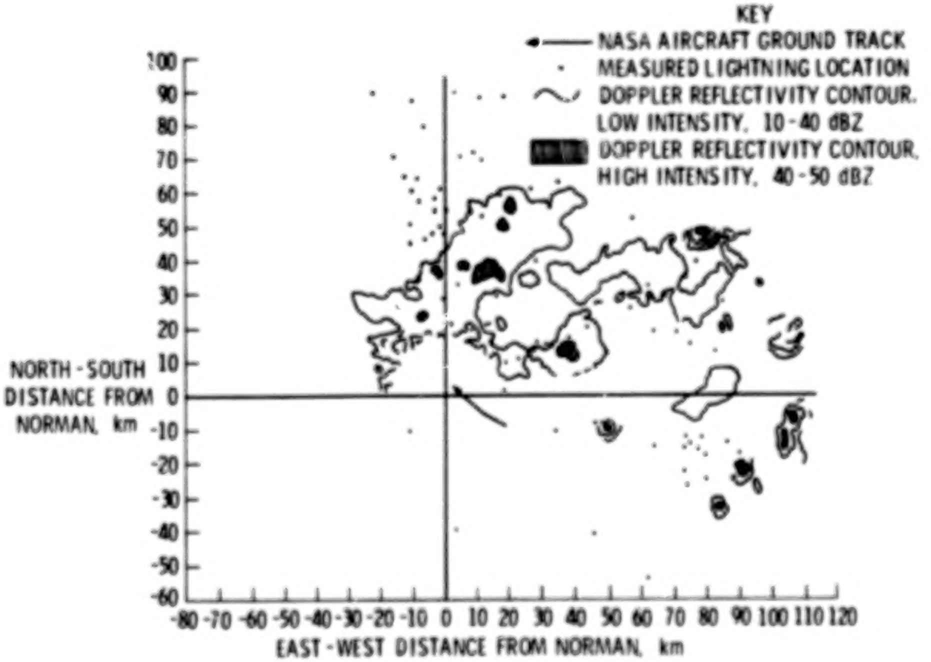
KEY
NASA AIRCRAFT GROUND TRACK
MEASURED LIGHTNING LOCATION
DOPPLER REFLECTIVITY CONTOUR, LOW INTENSITY, 10-40 dBZ
DOPPLER REFLECTIVITY CONTOUR, HIGH INTENSITY, 40-50 dBZ
NORTH-SOUTH DISTANCE FROM NORMAN, km
100
90
80
70
60
50
40
30
20
10
0
-10
-20
-30
-40
-50
-60
-80
-70
-60
-50
-40
-30
-20
-10
0
10
20
30
40
50
60
70
80
90
100
110
120
EAST-WEST DISTANCE FROM NORMAN, km

Figure 6.- Doppler radar reflectivity contours and airborne lightning locator points for third Doppler data period (15:41:34 to 15:46:39 CST) on June 1, 1978. Radar angle of 0.8°. Locator range = 40 n. mi.

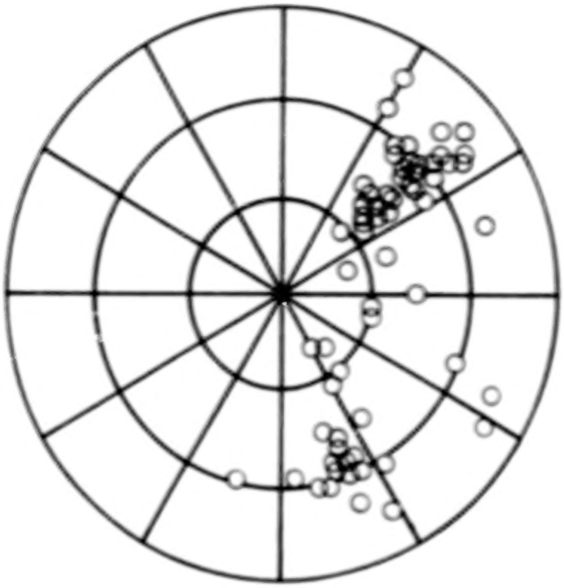

Figure 7.- Airborne lightning locator display at 15:42:52 CST, on June 1, 1978; 40 n. mi. range setting. Rate of production of 0.133 points/sec, 74 points displayed.

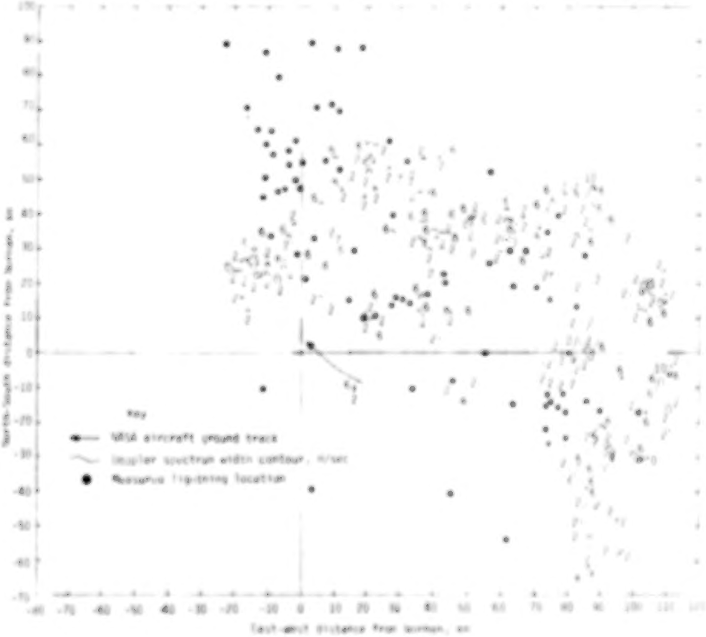

Figure 8.- Doppler radar spectrum width contours and airborne lightning locator points for third Doppler data period (15:41:34 to 15:46:39 CST) on June 1, 1978. Radar angle = 0.8°. Locator range = 40 n. mi.

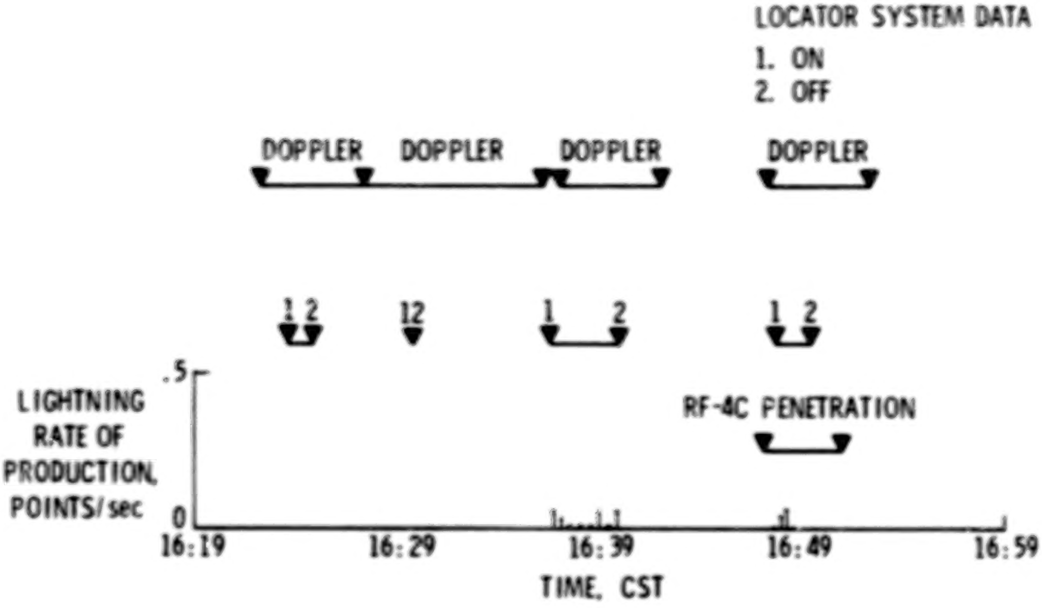

Figure 9.- Rate of production of lightning measured by airborne lightning locator system for storm of May 11, 1978.

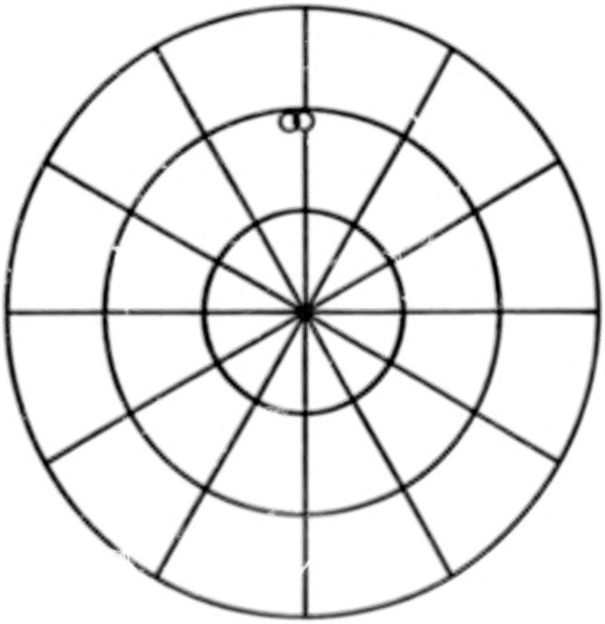

Figure 10.- Airborne lightning locator display at 16:43:09 CST on May 11, 1978; 40 n. mi. range setting. Rate of production of 0.0416 points/sec, 2 points displayed.

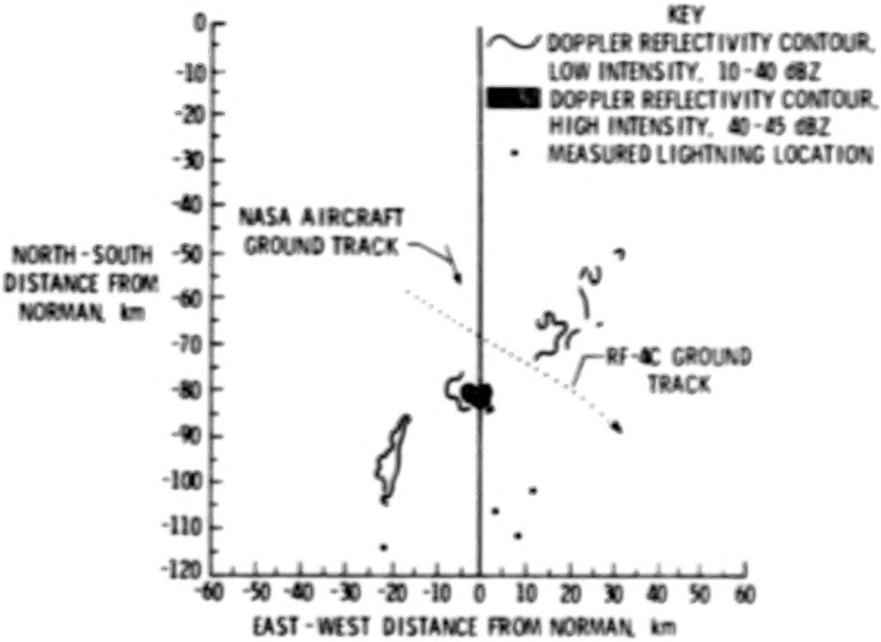

Figure 11.- Doppler radar reflectivity contours and airborne lightning locator points for fourth Doppler data period (16:43:30 to 16:52:43 CST) on May 11, 1978. Radar angle = 0.6°. Locator range = 40 n. mi.

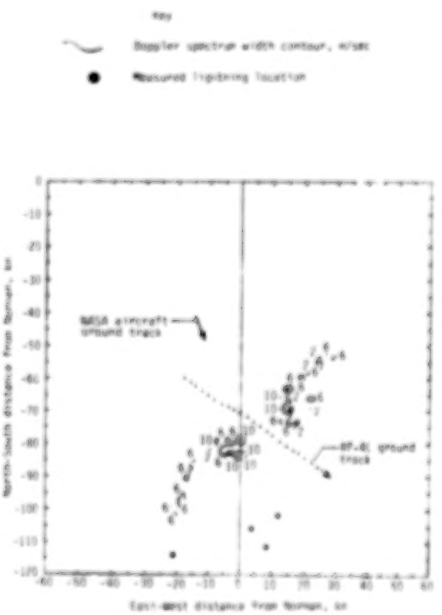

Figure 12.- Doppler radar spectrum width contours and airborne lightning locator points for fourth Doppler data period (16:43:30 to 16:52:43 CST) on May 11, 1978. Radar angle = 0.6°. Locator range = 40 n. mi.

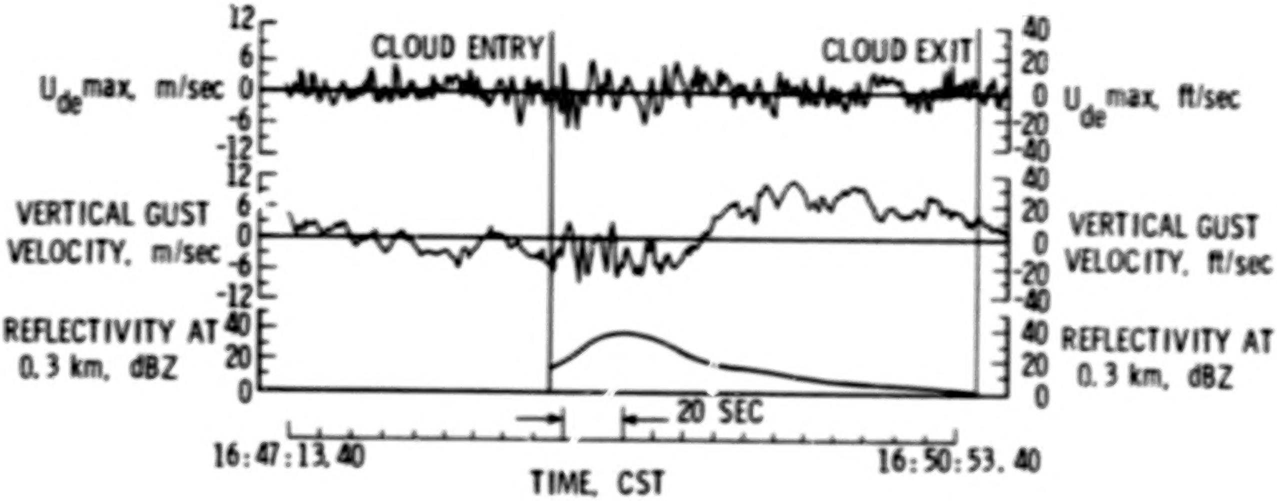

Figure 13.- Airborne turbulence measurements from NSSL/USAF aircraft and radar reflectivity along track during May 11, 1978. Nominal altitude of 6.1 km (20 000 ft) and heading of 110°.

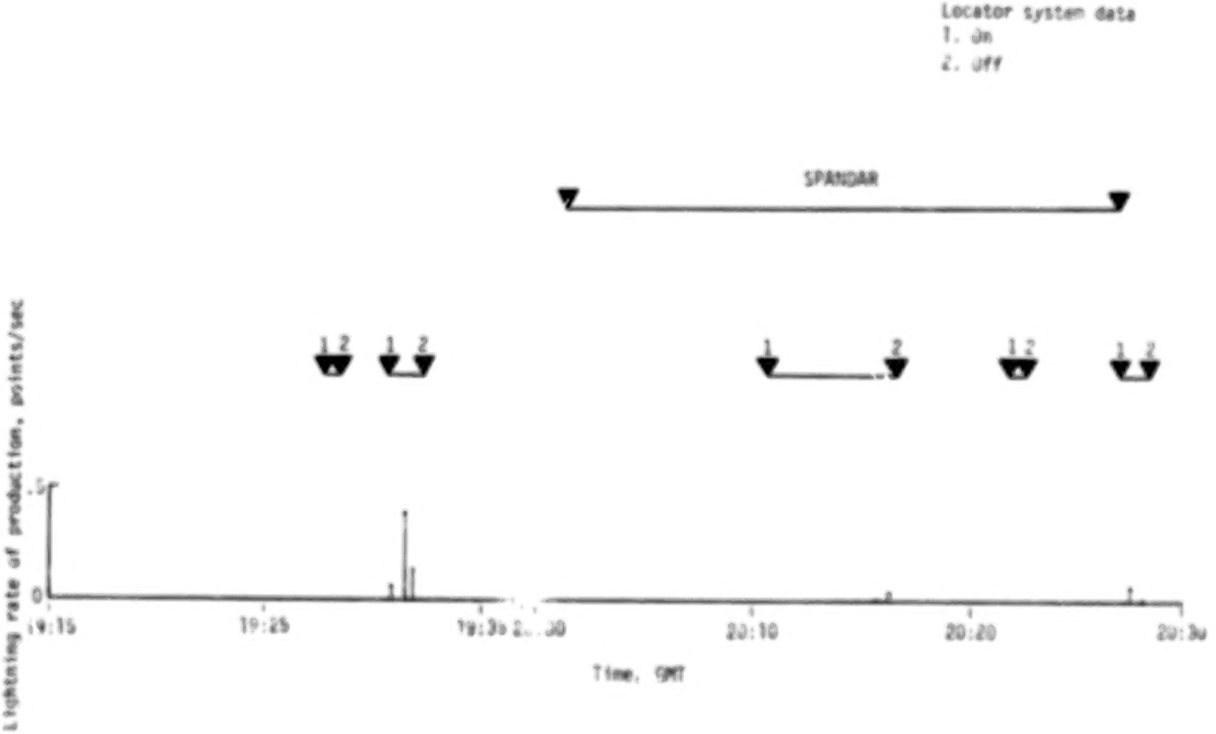

Figure 14.- Rate of production of lightning measured by airborne lightning locator system for storm of August 14, 1978.

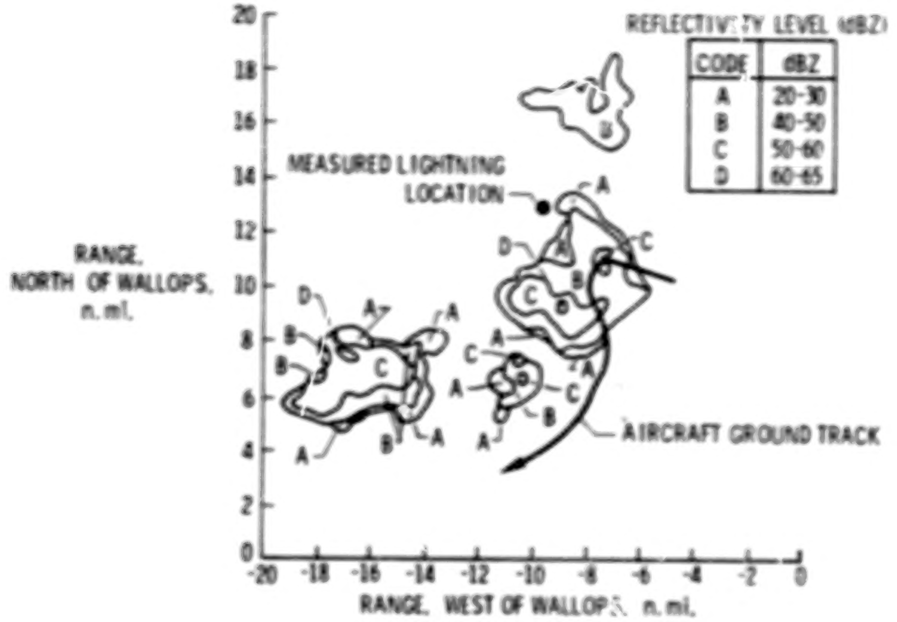

Figure 15.- SPANDAR radar reflectivity contours and airborne lightning locator point for third locator sample interval (20:10:45 to 20:16:30 GMT) on August 14, 1978. Reflectivity recorded at 20:01:20.7 GMT, elevation angle of 0.38 deg. Locator range = 40 n. mi.

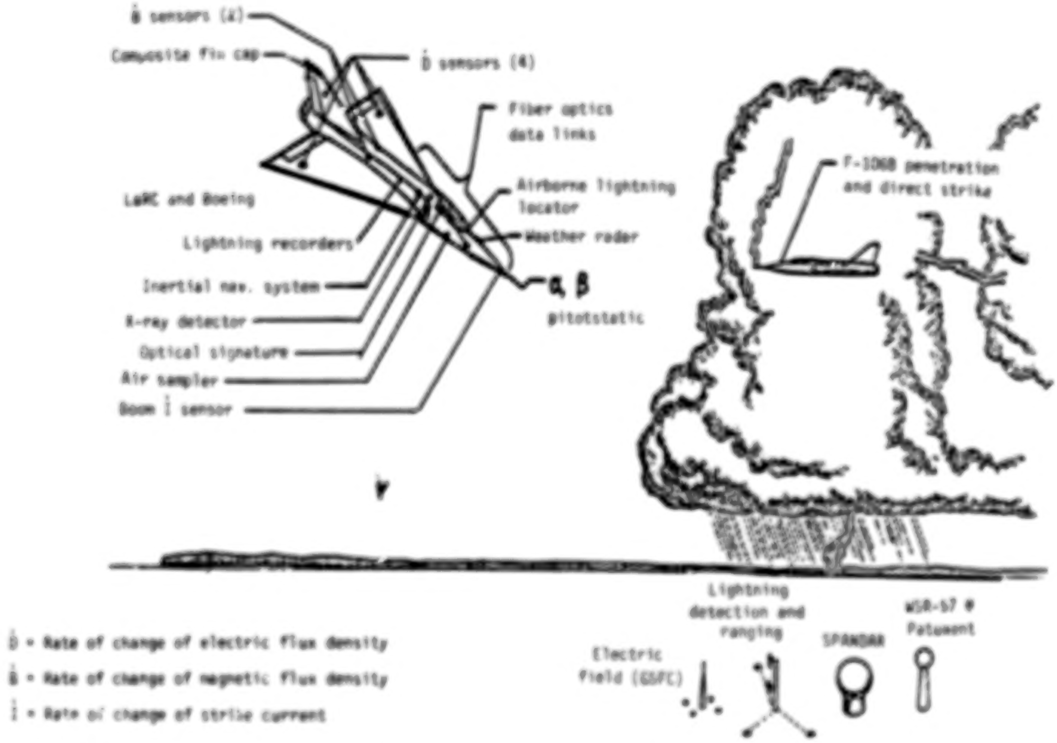
$\dot{B}$ sensors (4)
Composite fin cap
$\dot{D}$ sensors (4)
Fiber optics data links
LaRC and Boeing
Airborne lightning locator
Lightning recorders
Weather radar
Inertial nav. system
α, β pitotstatic
X-ray detector
Optical signature
Air sampler
Boom $\dot{I}$ sensor
F-106B penetration and direct strike
Lightning detection and ranging
WSR-57 @ Patuxent
SPANDAR
Electric field (GSFC)
$\dot{D}$ = Rate of change of electric flux density
$\dot{B}$ = Rate of change of magnetic flux density
$\dot{I}$ = Rate of change of strike current

Figure 16.- Schematic of storm hazards mission operations in vicinity of NASA-Wallops.

BLANK PAGE

BLANK PAGE

CONTENTS

Part 1

PREFACE . . . . iii 1/A6

1. INTRODUCTORY REMARKS 1 1/A12
Roger L. Winblade

SESSION I - TERMINAL-AREA OPERATIONS
Cochairmen: T. A. Walsh and R. [illegible] Kurkowski

2. TEST RESULTS OF FLIGHT GUIDANCE FOR FULL CONSERVATIVE DESCENTS IN A TIME-BASED METERED AIR TRAFFIC ENVIRONMENT 7 1/B4
Charles E. Knox and Leo H. Person, Jr.

3. A PILOT'S SUBJECTIVE ANALYSIS OF A COCKPIT DISPLAY OF TRAFFIC INFORMATION (CDTI) 29 1/C12
Gerald L. Keyser, Jr.

4. GUIDANCE AND CONTROL SYSTEM RESEARCH FOR IMPROVED TERMINAL AREA OPERATIONS 51 1/E6
R. M. Hueschen, J. F. Creedon, W. T. Bundick, and J. C. Young

5. OPERATIONAL CONSIDERATIONS IN UTILIZATION OF MICROWAVE LANDING SYSTEM APPROACH AND LANDING GUIDANCE 83 1/G10
William F. White and Leonard V. Clark

6. AUTOMATED PILOT ADVISORY SYSTEM TEST AND EVALUATION AT MANASSAS MUNICIPAL AIRPORT 113 2/B4
John L. Parks, Jr.

7. A METHOD FOR DETERMINING LANDING RUNWAY LENGTH FOR A STOL AIRCRAFT 127 2/C14
D. M. Watson, G. H. Hardy, J. F. Moran, and D. N. Warner, Jr.

8. FLIGHT TESTS OF IFR LANDING APPROACH SYSTEMS FOR HELICOPTERS 145 2/E4
J. S. Bull, D. M. Hegarty, L. L. Peach, J. D. Phillips, D. J. Anderson, D. C. Dugan, and V. L. Ross

9. A HEAD-UP DISPLAY FORMAT FOR TRANSPORT AIRCRAFT APPROACH AND LANDING 165 2/F10
Richard S. Bray and Barry C. Scott

MICROFILMED FROM BEST
AVAILABLE COPY

SESSION II - AVIONICS AND HUMAN FACTORS
Cochairmen: M. D. Montemerlo and A. B. Chambers

10. AN EVALUATION OF HEAD-UP DISPLAYS IN CIVIL TRANSPORT OPERATIONS 197 3/B2
John K. Lauber, Richard S. Bray, and Barry C. Scott

11. GENERAL AVIATION SINGLE PILOT IFR AUTOPILOT STUDY 201 3/B5
Hugh P. Bergeron

12. APPLICATION OF THE EPIDEMIOLOGICAL MODEL IN STUDYING HUMAN ERROR IN AVIATION 219 3/C10
Ed S. Cheaney and Charles E. Billings

13. HOW A PILOT LOOKS AT ALTITUDE 237 3/D14
Amos A. Spady, Jr., and Randall L. Harris, Sr.

SESSION III - ATMOSPHERIC ENVIRONMENT
Cochairmen: D. W. Camp and L. J. Ehernberger

14. SUMMARY OF FLIGHT TESTS OF AN AIRBORNE LIGHTNING LOCATOR SYSTEM AND COMPARISON WITH GROUND-BASED MEASUREMENTS OF PRECIPITATION AND TURBULENCE 251 3/E14
Bruce D. Fisher and Norman L. Crabill

15. WALLOPS SEVERE STORMS MEASUREMENT CAPABILITY 279 4/A3
Robert E. Carr and John C. Gerlach

16. THE 1979 CLEAR AIR TURBULENCE FLIGHT TEST PROGRAM 293 4/B3
E. A. Weaver, L. J. Ehernberger, B. L. Gary,
R. L. Kurkowski, P. M. Kuhn, and L. P. Stearns

17. PULSED DOPPLER LIDAR FOR THE DETECTION OF TURBULENCE IN CLEAR AIR 313 4/C9
E. A. Weaver, J. W. Bilbro, J. A. Dunkin, S. C. Johnson
W. D. Jones, C. E. Harris, and C. A. DiMarzio

18. FLIGHT TESTS OF A CLEAR-AIR TURBULENCE ALERTING SYSTEM 329 4/D11
Richard L. Kurkowski, Peter M. Kuhn, and Lou P. Stearns

19. CLEAR AIR TURBULENCE STUDIES WITH MICROWAVE RADIOMETERS 351 4/F5
Bruce L. Gary

20. IN-FLIGHT DIRECT-STRIKE LIGHTNING RESEARCH 359 4/F13
Felix L. Pitts and Mitchel E. Thomas

21. MAGNITUDE AND FREQUENCY OF WIND SPEED SHEARS AND ASSOCIATED DOWNDRAFTS 373 4/G13
Margaret B. Alexander and C. Warren Campbell

MICROFILMED FROM BEST
AVAILABLE COPY

WALLOPS SEVERE STORMS MEASUREMENT CAPABILITY

Robert E. Carr and John C. Gerlach
Wallops Flight Center

National Aeronautics and Space Administration

INTRODUCTION

Since its establishment in 1945, Wallops Flight Center has been a facility where both government research agencies and independent investigators from the United States and abroad can conduct a broad range of experiments. Over the years Wallops has installed a wide array of instrumentation systems and has assembled a highly trained group of personnel to support these experiments.

In this report we will discuss some of the instrumentation systems used in support of NASA's Storm Hazards Program. These systems include the Radar Atmospheric Research Facility (RARF) with its ultra-sensitive, high-resolution Space Range Radar (SPANDAR), a near real time display from the National Weather Service WSR-57 radar at NAS, Patuxent River, a Lightning Detection and Ranging System (LDAR), and a Ryan Stormscope.

We will first discuss the measurements that can be made with the systems that make them useful to the program and then describe the individual systems in some detail. Lastly, we will discuss modifications being made to prepare for the 1981 storm season.

MEASUREMENT CAPABILITIES

Wallops has available a combination of ultra-sensitive, high-resolution, multi-wavelength radar system that can detect, track, and quantify the properties of severe storms. Simultaneous measurements in the UHF (70 cm), S (10 cm), and C (5 cm) bands can be made of clouds and precipitation to deduce particle size and characteristics, including quantitive cross sections of individual hailstones and raindrops. Relative attenuation at these wavelengths can be used to calculate path integrated rainfall and water content. The track of an instrument aircraft can be displayed on a S-band reflectivity map of the individual storm cells, thus correlating in situ aircraft measurements with the overall structure of the storm. The addition of doppler processing for the S-band radar, planned for 1981, will permit investigations of velocity fields associated with thunderstorms or coastal hurricanes.

The Lightning Detection and Ranging System (LDAR) and the Ryan Stormscope can be used to study the electrical properties of storms. The LDAR system can determine the location of lightning discharges in real time and measure and record the electric field waveform for further study The Ryan Stormscope can detect and range lightning out to 320 kilometers (200 miles). The radars and the lightning detection systems should be able to detect the earliest phases of cloud electrification and precipitation.

Other weather phenomena which may be studied as precursors of storm systems or for their own interesting behavior are: sea breeze fronts, gust fronts, and tenuous regions of turbulence in the upper atmosphere.

As an integral part of any program, Wallops makes available operation meteorological support in the form of standard and special surface and upper atmosphere measurements, routine and special weather forecasting and weather briefing.

RADAR ATMOSPHERIC RESEARCH FACILITY (RARF)

The Radar Atmospheric Research Facility (RARF) consists of two separate research and development radar systems, one operating in the UHF (70 cm) band and the other in the S (10 cm) band. The facility was constructed in the late 1950's for a program involving atmospheric reentry of missile payloads. It originally included an X (3 cm) band radar which has since been dismantled. Since 1965 the facility has been used almost exclusively for atmospheric research projects. (See reference 1.) All of the ground based data collection instrumentation for the Storm Hazards Program are presently located at RARF for convenience of operation; however, in the future some may be located elsewhere.

Only the S-band radar (SPANDAR) is used in the Storm Hazards Program. It is used to survey any storm within a 100 nautical mile radius of Wallops in order to choose interesting storm cells as possible candidates for aircraft penetration, to monitor the aircraft's flight, and to display and to record radar reflectivity data from the storm the aircraft penetrates. The radar PPI scan is displayed on a 19-inch color television monitor along with the range time and the position of the aircraft. This real time PPI scan is also recorded on video tape. The PPI and RHI data scans are recorded both photographically and on digital tape.

As a supplement to the SPANDAR radar system, near real time presentation of the data from the National Weather Service WSR-57 weather radar, located at NAS, Patuxent River, Maryland, is displayed on another 19-inch color television monitor. These data are recorded when SPANDAR data are not available and at other times for documentation purposes.

A more detailed description of SPANDAR and the two display systems is given below.

SPACE RANGE RADAR (SPANDAR)

The Space Range Radar (SPANDAR) is a precision, long-range, S-band, conical scan, tracking radar. It was originally designed to collect missile reentry tracking data and deep space trajectory data. While it is still capable of performing these functions, it has been used most intensively since the middle 1960's in atmospheric research. Figure 1 is a block diagram of the SPANDAR. ble 1 gives the technical characteristics of the radar. Figures 2 and 3 are of the SPANDAR antenna and tracking console.

PANDAR has two transmitters which differ only in power output. The high- transmitter's peak power output is 5.0 megawatts with a 10 MHz bandwidth over a frequency band of 2700 to 2900 MHz. The low-power transmitter's peak power is 1.3 megawatts with a 10 MHz bandwidth over a frequency band of 2800 to 2900 MHz.

For meteorological measurements both transmitters are controlled by a frequency diversifier. The diversifier shifts the transmit frequency of each radar pulse by the reciprocal of the pulse width, thus making each pulse independent in frequency from every other pulse. The radar receiver is programmed in step with the transmitter so that echoes from each pulse are received in the proper range gate.

Frequency diversity allows for the accumulation of a large number of independent meteorological echoes at a much faster rate than normal, thus increasing the radar scan rate. It also rejects second-time around targets which fall outside the receiver bandwidth. Another advantage is that it inserts a calibration signal. In this way any receiver drift can be automatically compensated (reference 2).

The return signal from a precipitation volume is routed from the receiver to a Digital Video Integrator and Processor (DVIP) (reference 3). The DVIP is an intensity contouring device that continuously averages radar logarithmic video in range and direction to obtain quantitive estimates of mean detected precipitation returns. The accuracy of mean intensity estimates is improved over that of a logarithmic receiver by 1.0 db or less at range increments of 1 and 2 kilometers. Specifically, the DVIP (1) accepts logarithmic video over a maximum range of 80 db, (2) continuously integrates log video samples digitally in range and on a pulse-to-pulse basis in range increments of 1 and 2 kilometers, (3) provides a fixed range normalization function as part of the digital processing, (4) provides a contoured log video output of six contours of mean signal intensity to the radar PPI and to a 19-inch color television monitor, and (5) provides a separate digital output of one 8-bit binary word for each integrated video sample.

As stated earlier, the display of radar reflectivity data is used both for selection of storm cells and for investigation and for monitoring the aircraft position during flight. Aircraft position is tracked by a separate C-band tracking radar and superimposed on the SPANDAR display in real time. The position data are also recorded on digital tape for post-flight analysis.

WSR-57 DATA DISPLAY

The National Weather Service WSR-57 weather radar range normalized reflectivity is transmitted by a Radar Data Remoting System (reference 4) over a dedicated telephone line from the radar location at NAS, Patuxent River, Maryland, for display on a 19-inch color television monitor at the RARF site. The up-date time for this display is two minutes. Range time is superimposed on the display. It is possible to superimpose the aircraft track on this display; however, the ground track cannot be displayed simultaneously on the SPANDAR and the WSR-57 displays. The WSR-57 reflectivities are given in the same six discrete levels as the SPANDAR display. Figure 4 shows the TV monitors used to display weather data. The right one is normally used for SPANDAR data; the left one normally displays Pax River data.

LIGHTNING DETECTION AND RANGING (LDAR)

The LDAR was originally developed at NASA Kennedy Space Center to detect potential hazardous electrical activity that might impair missile launch operation (references 5 and 6). Wallops acquired it from Kennedy Space Center in 1979, but because of funding and manpower limitation could not put it into operation for the 1980 storm season. Our current plans are to have it operational for the beginning of the 1981 storm season.

LDAR measures the times of arrival of the pulsed RF radiation emitted by an electrical discharge. This RF radiation is detected by VHF antennas at outlying sites and relayed to a central station where the spatial location of the discharge is determined. The outlying sites normally are in a Y configuration with an antenna site at the extremities of the legs of the Y and a central site where each leg meets. The best configuration for accurate location of discharges is to have an azimuth of 120° between the baselines and with the central station located at the junction of each leg of the Y. At Wallops, geographical considerations and the availability of electrical power have caused us to deviate slightly from the 120° configuration. We have also relocated the central site to the extremities of one of the legs and placed it in the SPANDAR radar building. Figure 5 shows the layout as configured for Wallops.

Two basic measurements are made at each antenna site: the time of arrival of the pulsed RF signal and the electric field (E-field) waveform. The pulsed RF is detected by a vertically polarized, omnidirectional, 40 to 100 MHz antenna (figure 6), and the E-field signal is picked up by a circular flat plate antenna (figure 7). Signals from both antennas are transmitted to the receiving station over a 8 MHz bandwidth microwave link. At the receiving station the waveform of this lightning discharge is recorded on both digital and analog recorders. A mini-computer uses the time of arrivals to solve the hyperbolic equations to locate the position of the discharge. The range/azimuth position of the discharge is plotted as a dot on a PPI plot; the height of the discharge is plotted as a dot on two separate range/height indicators (RHI). Those discharges north of an east-west line passing through the central station are plotted on one RHI and those south of this line are plotted on another RHI.

An accuracy analysis of the LDAR system (reference 7) has shown that the symmetrical Y configuration produces a uniform low measurement error with an X, Y position accuracy within the baseline of the system of less than one percent. At distances greater than the baseline length, the accuracy decreases with distance; however, quite useable data can still be obtained at distances as far away as 110 nautical miles. Within the baseline, azimuth position can be measured with an error of less than 0.1 degree. Because of the planar orientation of the receiving stations, height is measured with a lesser accuracy than azimuth or range. Height is measured more accurately above 300 meters (1000 feet). Typically, the height error is less than 100 meters. Figure 8 shows the LDAR equipment in the SPANDAR control room.

RYAN STORMSCOPE

A Ryan Stormscope is installed in the RARF building for use in conjunction with LDAR (figure 9). The Stormscope is a four-component solid state receiving system which provides bearing and range information between aircraft and electrical discharges. Radio frequency signals, generated by electrical discharges, are picked up by a single flat-pack antenna which provides both the V and H direction loop antennas and an electrical sense antenna followed with a signal amplifier. The antenna signals are routed to the receiver where processing and control functions take place. The receiver is broadband tuned with a center frequency of 50 kHz. Azimuth of the discharge is determined from the ratio of the two crossed loop antenna inputs. Polarization of the fields is detected and processed. Signals from horizontal discharges are rejected. The range of the discharge is obtained by computer evaluation of signal strength, time to peak, decay time, spectral content, and comparison of electric and magnetic field amplitudes. (The details of the physical concept of this evaluation cannot be found in the open literature and are not provided by the company). Bearing information is displayed on a CRT monitor over 360°. Range is selected in three steps of 40, 100, and 200 nautical miles (NM). The system records and displays up to 128 individual electrical discharges, as small green dots on the CRT, and automatically updates the "oldest" discharge information with the "newest." In this manner, the display is constantly updated. If the dots are not replaced by new data, each is automatically erased after five minutes. Also, dots may be manually erased by the operator. Changes in heading and position of the aircraft will not affect data already displayed, so periodic clearing is necessary to maintain an accurate presentation with respect to the changing position of the aircraft in flight (references 6 and 8).

Several years ago, the Air Force Flight Dynamics Laboratory conducted an in-flight test program to evaluate the Stormscope performance in conjunction with a Bendix X-band airborne weather radar and a ground-based LDAR detection system operated at NASA Kennedy Space Center. The result of this comparison is given in reference 9.

PREPARATIONS FOR 1981

A major effort is being made to improve the instrumentation available for the 1981 storm season. We are cooperating with the Air Force Geophysical Laboratory, Cambridge, Massachusetts, in upgrading the SPANDAR radar to provide doppler information on the radial wind components within the storm cell. The AFGL equipment will be on the SPANDAR for only the first portion of the 1981 season. After the AFGL equipment is removed we will try to record the coherent SPANDAR signal for future processing.

Another major effort is to have the LDAR system fully installed and operating for the 1981 season.

REFERENCES

1. Cox, Ronald and Robert Masterson: Ed. Facilities for Atmospheric Research. No. 11, December 1969, NCAR Facilities Laboratory.

2. Kropfli, Robert A.: New Capabilities for the Wallops Island SPANDAR. Atmospheric Technology, NCAR, Winter 1974-1975.

3. Anon. - Digital Video Integrator and Processor (DVIP). February 1977, Enterprise Electronics Corporation.

4. Anon. - Radar Data Remoting System (RDRS). April 1979, Enterprise Electronics Corporation.

5. Poehler, H. A. and Carl L. Lennon: Lightning Detection and Ranging System LDAR System Description and Performance Objectives. NASA TM-74105, June 1979.

6. Corbin, John C., Jr.: Atmospheric Electricity and Lightning. Talk presented at the Fourth Annual Workshop on Meteorological and Environmental Inputs to Aviation Systems, March 25-27, 1980, University of Tennessee Space Institute.

7. Poehler, H. A.: A Preliminary Test of the Application of the Lightning Detection and Ranging System (LDAR) as a Thunderstorm Warning and Location Device for the FAA. NASA CR-154629, December 1978.

8. Ryan Stormscope WX-7A Weather Mapping System. Installation and Technical Manual. No. 377A200, Revision 2, January 1980.

9. Baum, R. K. and T. J. Seymour: In-Flight Evaluation of a Severe Weather Avoidance System for Aircraft. AFFDL-TM-79-45-EES, April 1979.

TABLE I.-SPANDAR TECHNICAL CHARACTERISTICS

Transmitter System:

Frequency	2700 to 2900 MHz
Frequency Resolution	1 MHz
Peak Power Output	5 MW or 1.3 MW
Pulsewidth	1, 2, or 5 Microseconds
Pulse Repetition Rate (PRF)	160, 320, 640, and 960 PPS
Pulse Coding	1 to 3 Pulses

Receiver System:

Type	Superheterodyne
Dynamic Range	70 db
Noise Figure	2.5 db
Sensitivity	-119 db
I. F. Frequency	30 MHz
Bandwidth	230 kHz, 480 kHz, 1.1 MHz
Tracking Gate	6 or 18 Microseconds

Antenna System:

Reflector	18.3 m (60 ft) Parabolic
Beamwidth	0.39°
Beam Crossover	1.5 db
Gain	52.8 db
Polarization	Circular, Vertical, or Horizontal
Antenna Temperature	30°K
Feed	NUTATING (Conical, 30 Hz)
Azimuth Coverage	360°
Elevation Coverage	90°
Tracking Rates (Az. and El.)	6° Per Second
Slew Rates (Az. and El.)	15° Per Second

Ranging and Tracking System:

Measurement Range	910 m (1000 Yds.) to 25,000 NM
Range Precision	4.57 m (± 5 Yds.)
Angle Precision	0.06°

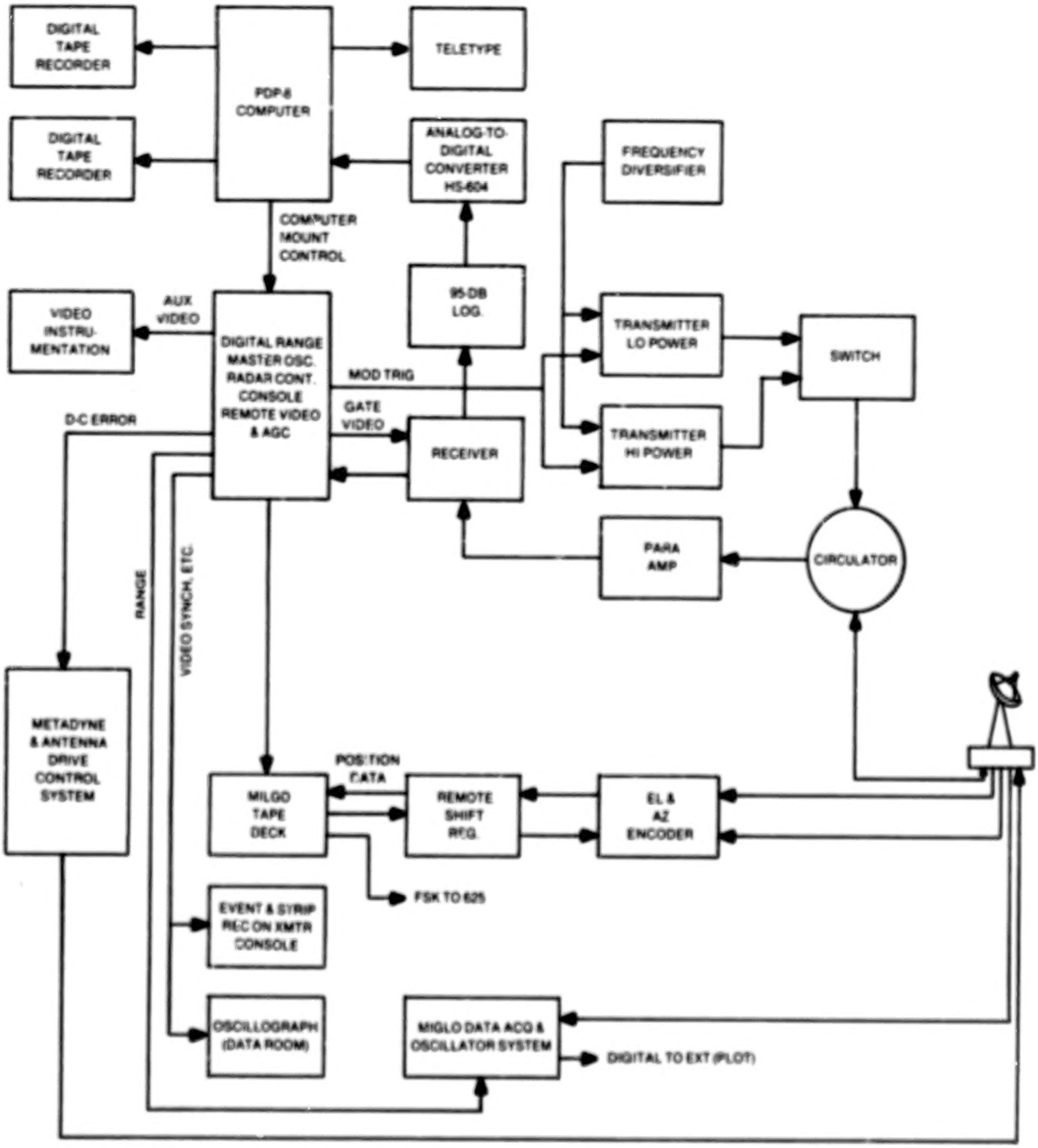
DIGITAL TAPE RECORDER
PDP-8 COMPUTER
TELETYPE
DIGITAL TAPE RECORDER
ANALOG-TO-DIGITAL CONVERTER HS-604
FREQUENCY DIVERSIFIER
COMPUTER MOUNT CONTROL
95-DB LOG.
VIDEO INSTRU-MENTATION
AUX VIDEO
DIGITAL RANGE MASTER OSC. RADAR CONT. CONSOLE REMOTE VIDEO & AGC
MOD TRIG
TRANSMITTER LO POWER
SWITCH
D-C ERROR
GATE VIDEO
RECEIVER
TRANSMITTER HI POWER
PARA AMP
CIRCULATOR
RANGE
VIDEO SYNCH, ETC.
METADYNE & ANTENNA DRIVE CONTROL SYSTEM
POSITION DATA
MILGO TAPE DECK
REMOTE SHIFT REG.
EL & AZ ENCODER
FSK TO 625
EVENT & STRIP REC ON XMTR CONSOLE
OSCILLOGRAPH (DATA ROOM)
MIGLO DATA ACQ & OSCILLATOR SYSTEM
DIGITAL TO EXT (PLOT)

Figure 1.- Space Range Radar (SPANDAR) System block diagram.

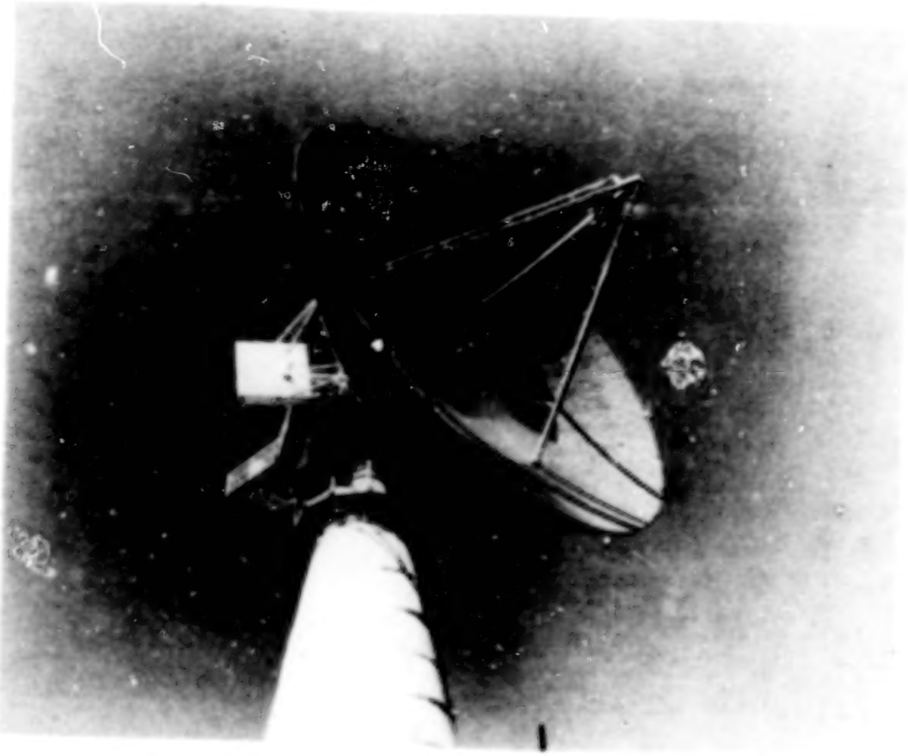

Figure 2.- SPANDAR antenna.

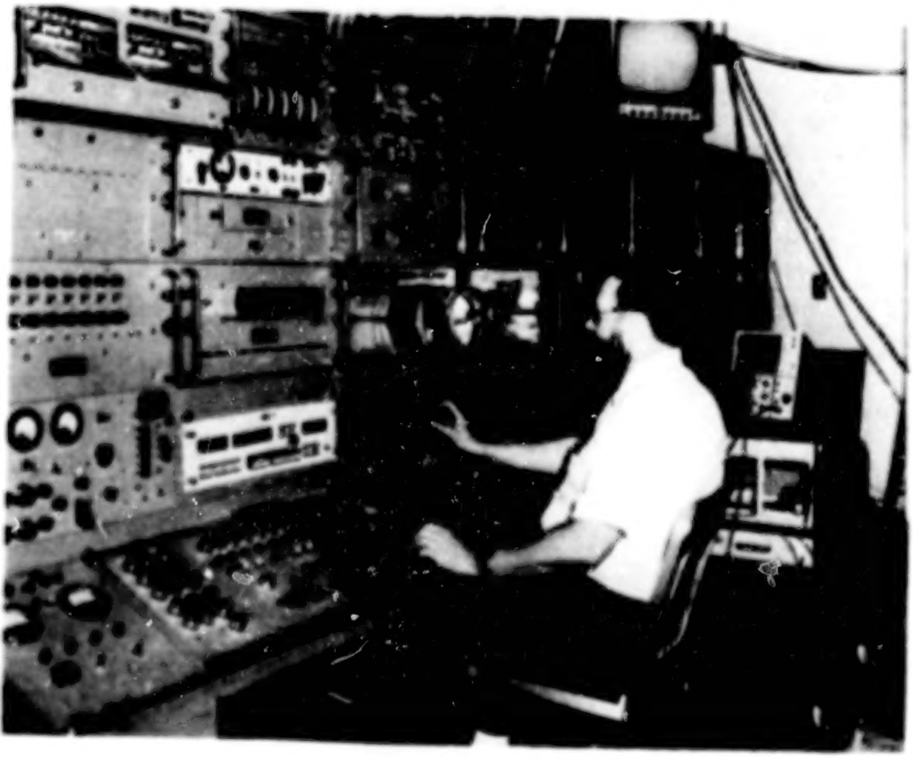

Figure 3.- SPANDAR tracking console.

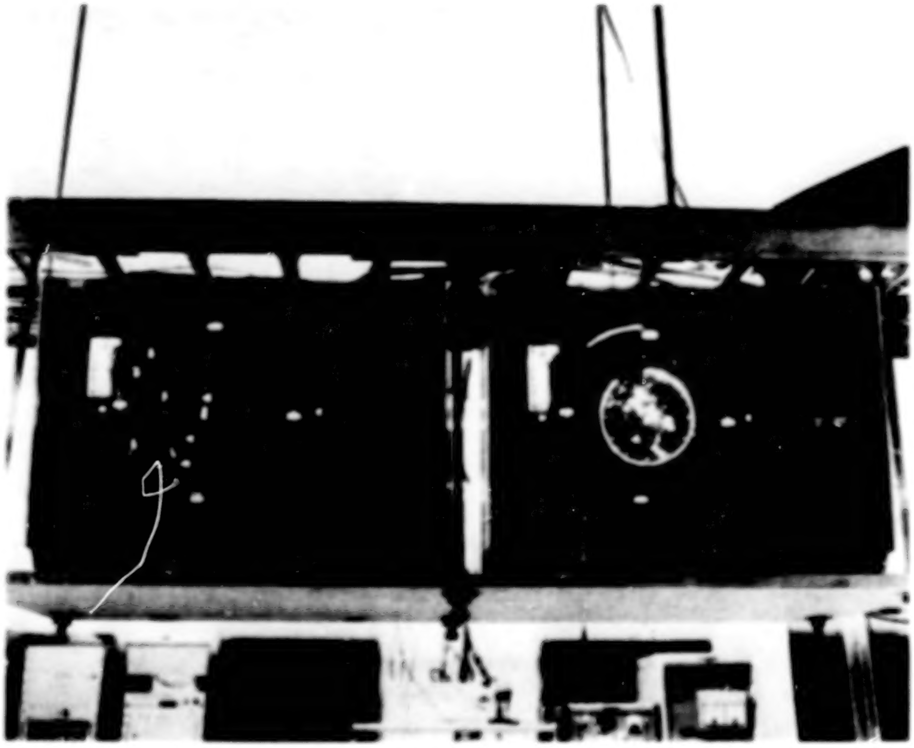

Figure 4.- Weather radar television monitors in SPANDAR control room.

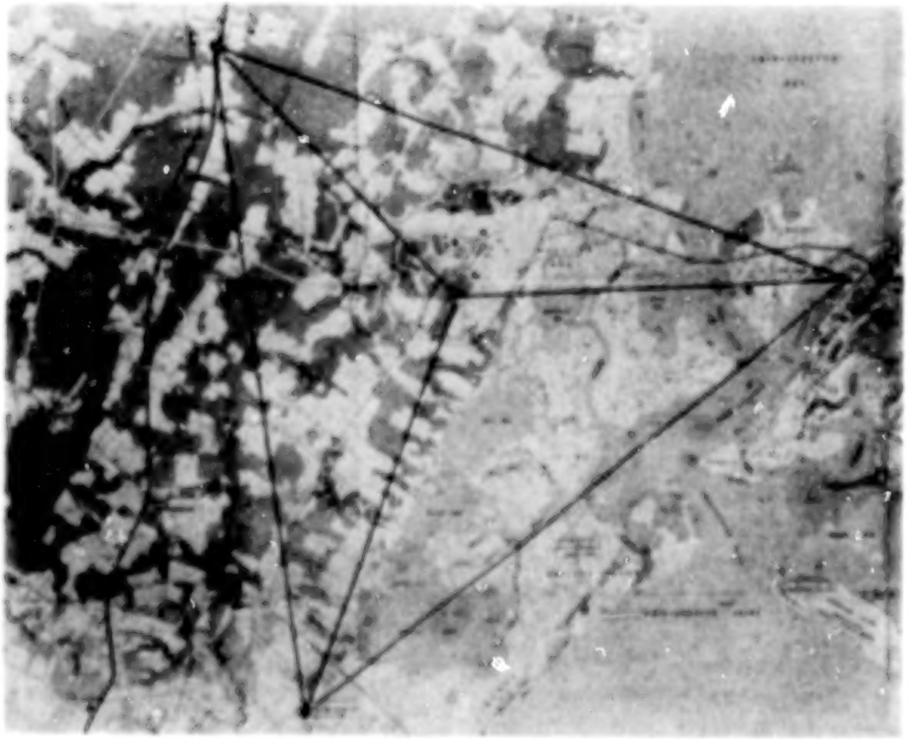

Figure 5.- LDAR antenna layout.

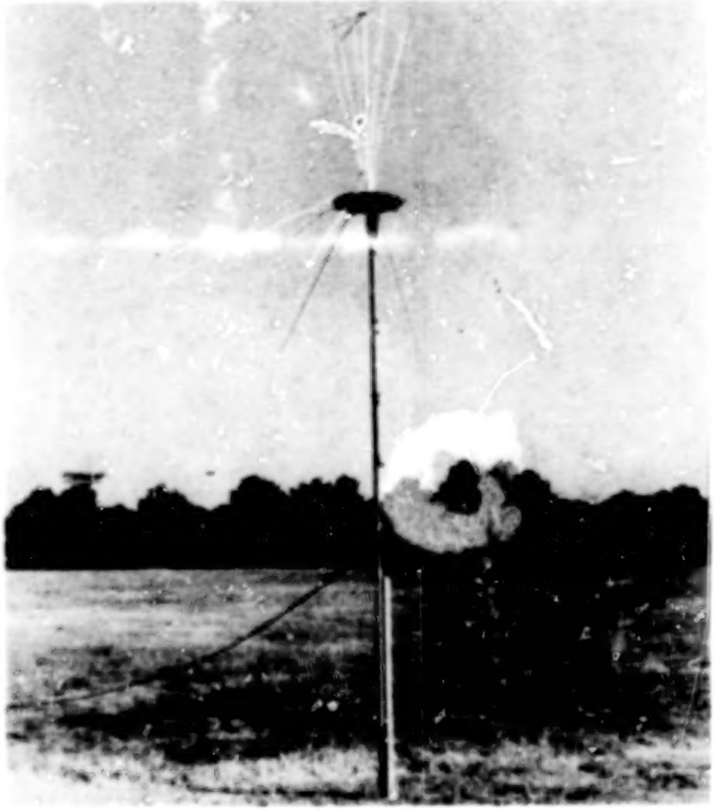

Figure 6.- LDAR RF antenna.

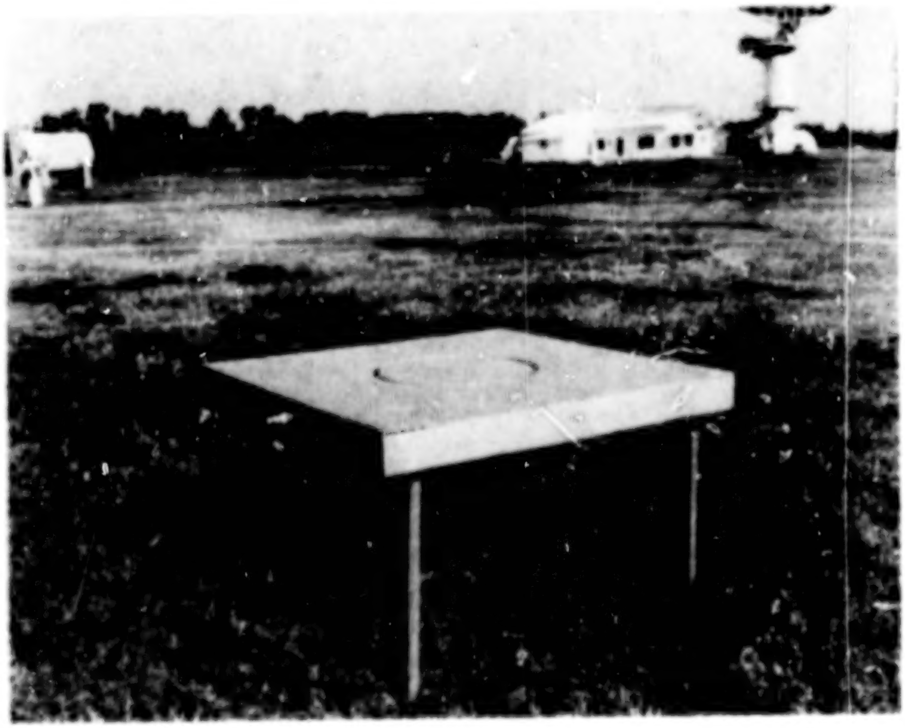

Figure 7.- LDAR e-field antenna.

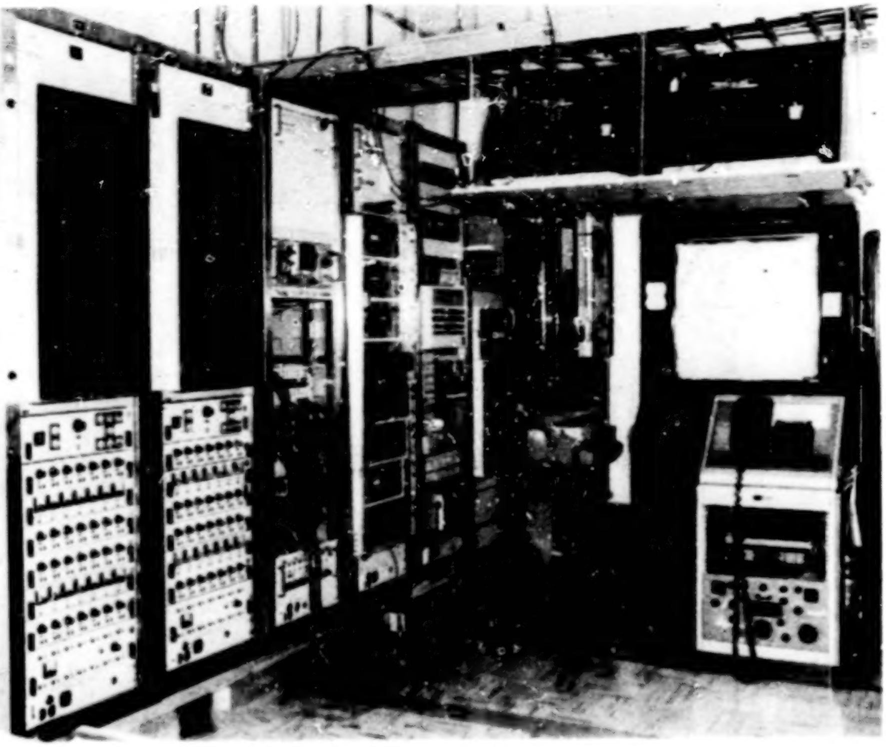

Figure 8.- LDAR receivers and data handling equipment.

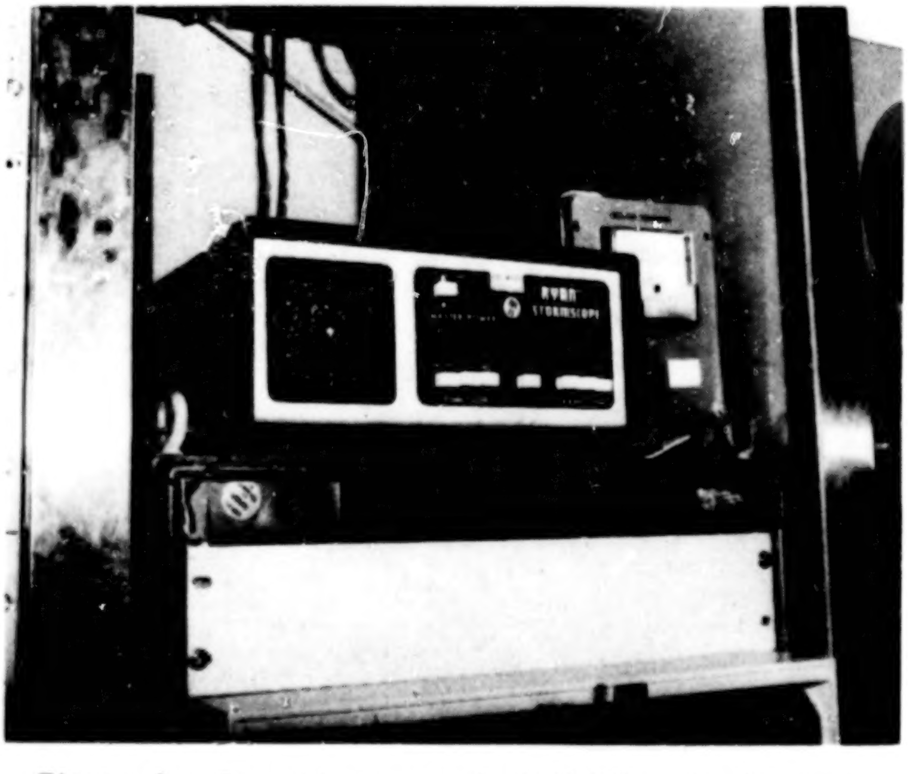
RYAN
STORMSCOPE

Figure 9.- Ryan Stormscope in SPANDAR control room.

BLANK PAGE

BLANK PAGE

THE 1979 CLEAR AIR TURBULENCE FLIGHT TEST PROGRAM

E. A. Weaver, L. J. Ehernberger, B. L. Gary, R. L. Kurkowski
National Aeronautics and Space Administration

P. M. Kuhn,* L. P. Stearns
National Oceanic and Atmospheric Administration

SUMMARY

A flight test program for Clear Air Turbulence (CAT) detection and measurement was conducted over the western part of the United States during the winter season of 1979 aboard NASA's Galileo II flying laboratory. A carbon dioxide pulsed Doppler lidar and an infrared radiometer were tested for the remote detection and measurement of CAT. Two microwave radiometers were evaluated for their ability to provide encounter warning and altitude avoidance information. A brief description is given of the program, the four flight experiments, and some examples of the data. This test program was a cooperative effort among several U. S. Government agencies, industries, and educational institutions. The Ames Research Center, Dryden Flight Research Center, Jet Propulsion Laboratory, Marshall Space Flight Center, and the Lewis Research Center of the National Aeronautics and Space Administration cooperated in the experiments in this test program.

INTRODUCTION

NASA has sponsored research and development on the Clear Air Turbulence (CAT) problem for many years. Remote detection and measurement of CAT has been one of the objectives of this research. Remote sensors have two useful features in an experiment such as this: (1) the ability to detect atmospheric features associated with CAT prior to actually entering the turbulent region, and (2) mobility, which allows the experimenter to cover large regions of the troposphere in search of CAT. In situ sensors are also useful since they allow direct measurement of the turbulence by aircraft penetration of the CAT region. In combination, these two types of probes yield more than each considered separately: the in situ sensor data is seen in a larger context, and the remote sensor data is rendered more credible by confirmation where data types overlap. The 1979 CAT Flight Test Program, sponsored by NASA's Aviation Operations Safety Technology Program, made extensive use of both sensor types. Flight evaluations were performed on four advanced technology instruments, each one measuring distinct atmospheric parameters that are related to CAT. It involved a search for CAT using detailed meteorological forecasting methods. The four instruments tested were: (1) a pulsed Doppler lidar measuring the

*Presently with Raven Systems, Inc.

velocity spectrum of air volumes, (2) an infrared (IR) radiometer monitoring the variability of line-of-sight water vapor content for the forecasting of CAT encounters, (3) a 180.1 GHz microwave radiometer also sensitive to water vapor content changes, and (4) a 55.3 GHz microwave radiometer that measured "altitude temperature profiles" for relating CAT location to inversion layers and tropopause features.

The flight test program conducted during January through March 1979 provided a common test platform for determining the performance of each CAT instrument system in a variety of turbulent and smooth air conditions, at a wide range of flight levels, and a variety of synoptic atmospheric conditions. This was not a "fly-off" test. Rather, each instrument was evaluated with due consideration given to its state of development. For example, this was an initial "concept demonstration" for the microwave radiometers as they had not been previously tested for the CAT objectives. The flight program provided an opportunity for determining the instrument-peculiar performance features. Each sensor is very briefly described and sample data are given.

TEST DESCRIPTION

The "1979 Clear Air Turbulence Flight Test Program" was conducted aboard NASA 712, a Convair 990 aircraft (ref. 1). The CV-990 was selected because of the space requirements for the lidar, and this led to the availability of space for other CAT sensors. This airborne research laboratory was based at Moffett Field, California, for these tests. It is shown in Figure 1 in its configuration with probes, special windows, and fairings for the CAT test. The infrared radiometer probe was near the front of the aircraft in the window just aft of the main entry door. It contained a small gold-coated mirror for intercepting the IR radiation in the forward direction along the flight path. The Pulsed Doppler Lidar required a special fairing containing a reflecting mirror attached to the lidar telescope which directed the infrared laser radiation outside the aircraft through a germanium window that is transparent to the CO_2 laser radiation. The microwave sensors required that aircraft windows be replaced with a material that was transparent to the sensor's radiation.

No modern laboratory can successfully sustain itself without a computer; neither can the CV-990. The Airborne Digital Data Acquisition System, located in the passenger compartment, which is the experiment area, is used for collection and real-time display of standard cockpit and experiment data. This includes information such as position, altitude, true airspeed, wind velocity, surface temperature, and accelerometer outputs. Such a laboratory requires personnel too. About 25 to 30 people were on each flight with 8 to 10 of them required for operating the flying laboratory and the remainder for operating and monitoring the experiments.

There were three investigators with CAT sensors: (1) P. M. Kuhn, whose work was supported by both NOAA and NASA, developed the infrared radiometer. It has received some testing on other NASA aircraft. (2) B. L. Gary from the

Jet Propulsion Laboratory who investigated the use of microwave radiometry applied to the CAT problem, and (3) the team associated with the pulsed Doppler lidar that was developed by the Raytheon Company for the Marshall Space Flight Center. E. A. Weaver managed this effort and also directed the flight test program.

An essential activity for a CAT flight program is the detailed analyses of synoptic weather data for the forecasting of CAT. L. J. Ehernberger from the Dryden Flight Research Center was the meteorological investigator who oversaw this investigation. The U. S. Navy, U. S. Air Force, National Weather Service, and the National Environmental Satellite Service provided the data and synoptic forecast information on a daily basis which was used for locating the potential areas of CAT. In addition, SRI International, Inc., assisted in the meteorological planning and post-flight analyses. The primary meteorological objectives were to sample CAT associated with: (1) mountain waves, (2) jet streams, (3) cirrus clouds, and (4) other pronounced wind shear zones associated with fronts, troughs, and ridges aloft. Figure 2 lists the investigators and the investigative objectives discussed above.

This test was supported by many groups including nine industrial firms, three educational institutions, and four federal government organizations. These are shown in Figure 3. The four federal government groups included the Department of Defense, Department of Commerce, Department of Transportation, and NASA, which had five centers involved (Marshall Space Flight Center, Dryden Flight Research Center, Ames Research Center, Jet Propulsion Laboratory, and Lewis Research Center). These groups worked together for 24 missions flown between January 12, 1979, and March 28, 1979. An additional six missions were flown where the CAT experiments were operated on a "noninterference basis" with nonCAT-oriented experiments, thus providing additional in-flight experience with the CAT sensors for a total of 140 flight hours.

The geographical region where the weather was monitored and studied in detail for mission planning is shown in Figure 4. The search for CAT covered an area bounded on the south by Yuma, Arizona, and El Paso, Texas; Denver, Colorado, on the east; and on the north by Great Falls, Montana, and Portland, Oregon. Flights eventually covered all of this region except for the state of Wyoming.

METEOROLOGICAL SUPPORT

Clear air turbulence is known to be generated by a wide variety of synoptic weather patterns and with diverse combinations of wind shear and static stability. Its natural occurrence can vary from elusive to unexpectedly prolific. As a consequence, it was decided to include meteorological support to: (1) help plan the program sampling objectives in terms of atmospheric structures, (2) improve the selection of flight days and routes, (3) increase continuity between flight experience and post-flight analyses, and (4) evaluate the turbulence encounters with respect to the present CAT forecasting state-of-the-art (ref. 2).

In order to accomplish the test objectives for the instruments carried onboard the CV-990, it was recognized that a number of different atmospheric conditions and turbulence situations would need to be sampled. A comprehensive list of wind shear conditions, temperature gradient profile characteristics, and synoptic patterns significant to the occurrence of CAT or to the direct physical evaluation of each instrument was prepared. This provided the forecaster with a checklist for reviewing the weather conditions each day and identifying the atmospheric regions or locations where the most significant phenomena could be sampled. Program preparation also included technical discussions between the project team and CAT experts from San Jose State University, SRI International, Inc., and the U. S. Air Force Global Weather Center. These discussions were helpful to forecasting CAT regions and to selecting the airplane sampling tracks through these regions.

The project meteorologist began the daily activity by reviewing the standard synoptic and prognostic charts and discussing any specific points of question with the duty forecaster. Selected areas of interest were then examined more closely using rawinsonde data hardcopy and pilot report bulletins available via a COMEDS (Continental U. S. Meteorological Distribution System) terminal. Upper air charts were then plotted and analyzed at selected levels and the rawinsonde data were screened for significant wind shear and temperature gradient structure. Both visual and infrared imagery were also obtained from the laserfax terminal. With these combined resources, potential sampling regions were examined in detail and the project team then selected the mission objectives and flight routing for the day.

Flight results reflected the value of utilizing all available planning tools including the detailed screening of rawinsonde wind shear and temperature gradient profiles. Of sixteen flights routed specifically to sample turbulence, eight encountered significant meteorological variations and amounts of turbulence. On the remaining eight flights, the turbulence encountered was lighter or was due to meteorological conditions which repeated similar patterns sampled on previous missions. The variety of phenomena causing the turbulence encounters included low altitude thermal instability, mechanical ridge line turbulence, mountain wave activity, vertical wind shear (at low, middle, and high altitudes), fronts aloft, and strong thermal advection into a low pressure trough. Jet stream turbulence was encountered over the Pacific Ocean west of the Baja California coast as well as over the continental U. S. In addition, the experiments obtained samples in various ambient scattering conditions associated with marine aerosols, dust, haze, and jet stream cirrus. Only one phenomenon of the initial primary objectives was not sampled - strong localized mountain wave CAT in conjunction with the jet stream at the tropopause. This resulted from an abnormally low frequency of mountain wave conditions during the test period and from emphasis on phenomena at lower altitudes.

The meteorological conditions experienced during the missions confirmed the validity of some of the classical synoptic patterns and criteria for CAT, for example, its association with positive vorticity advection. In addition, the real-time onboard wind and temperature data proved valuable to establish the airplane location relative to wind shear zones and temperature gradients charted in the preflight analyses and to select subsequent tracks and altitudes in the sampling area. Also, the unique combination of experimental instruments demonstrated the added information which may be obtained by use of similar sensors in future flight programs. For example, additional atmospheric structure information can be inferred when data are simultaneously available from radiometers having different wavelengths, lines of sight, and fields of view. Further, the combination of a vertical temperature structure radiometer and a lidar system which could potentially define the vertical wind shear would greatly advance our knowledge of gravity wave activity and CAT by defining local Richardson number and its dynamic variations. Other applications, if such instruments were developed for operational use, could include flight level selection to obtain wind and temperature conditions for optimum performance.

A wide variety of atmospheric conditions were sampled during this CAT flight test program to evaluate the feasibility of the lidar, infrared radiometer, and microwave systems for observing conditions related to CAT. These conditions were acquired by the use of detailed analysis of wind shear and temperature gradients and by the exercise of attentive mission route management as well as with the assistance of the standard meteorological forecast products and pilot reports.

INFRARED RADIOMETER

The infrared radiometer (IR) sensor system has now been tested on 3 NASA aircraft including this CV-990 test (refs. 2, 3). It has an operating spectral range in the water vapor band of 20 to 40 micrometers (ref. 4). It is a passive device similar to Forward Looking Infrared (FLIR) devices, and detects variability of water vapor content integrated along the viewing direction, which is inclined about 11° above the horizon. This variability has been found to be associated with Kelvin-Helmholtz wave action in the atmosphere, which, in the breaking stage, results in shearing and tumbling of air parcels and associated turbulence. However, it is possible to detect developing wave action and the resulting water vapor variability prior to encountering the turbulence. In contrast for nonCAT conditions in clear air, the water vapor content ahead of the aircraft is relatively constant.

The location of the IR radiometer CAT detector onboard the CV-990 is shown in Figure 1. Figure 5 shows a close-up of the 2.5-cm probe tube enclosing a gold, right angle mirror mounted in the left forward passenger window for the experiment. Figure 6 shows the sensor device, the chopper, and the signal processor which were mounted inside the aircraft. The dimensions of the sensor device are approximately 15 cm in diameter and 18 cm in length. The signal processor's size is approximately 10 cm by 15 cm by 8 cm. These three components weigh approximately 5 kg. The specifications for the IR radiometer that was flown on the CV-990 are given in Table 1. The size and weight of the IR radiometer hardware are indicative of the simplicity of its basic operation.

Signals from the atmosphere are received and only the 20 to 40 micrometer signals are fed to the radiometer amplifier. After the signals are amplified they are analyzed in the signal processor which contains the algorithms related to output signal anomaly and CAT threshold alerting. The experimenter had the option of varying the signal processing, including variable threshold levels, during the flight. When the signal activity threshold is exceeded, an alert is displayed on the experimenter's console.

A diagram of the IR radiometer system "scores" from the 1979 CAT Flight Test Program is shown in Figure 7. Ninety-four CAT alerts were given by the system and eighty separate segments of turbulence encounters were documented. Of these, only 4% of the encounters were not preceded by an alert. Out of ninety-four alerts, 18% were "false," i.e., not followed by a turbulence encounter. Other results from the experiment are as follows:

a. The device was found to give satisfactory alerts at all flight levels above 4.4 km altitude (14,500 ft).

b. Turbulence was detected up to sixty km ahead of the aircraft encounter of CAT. (This range can be varied by changing optical filters.)

c. The envelope of maximum alert time varied from one minute at 4.4 km (14,500 ft) to four minutes at 11.3 km (37,000 ft) altitude.

d. The system performs efficiently with less than 8% false alarms in clear air, i.e., when cloud effects are removed from the data. It should be noted however that the sensor was not tested specifically in cloudy conditions and that the total field of view for this IR sensor can pick up false alarms from near nonturbulent clouds such as flights in clear air just above the cloud tops. Additional testing is required to understand the effects of the near cloud conditions on the IR radiometer.

NASA has flown this CAT sensor on other aircraft during the last several years (ref. 3). Analyzing the data from all these tests, CAT alerts from two to nine minutes ahead of an encounter have been recorded at least 80% of the time at altitudes of 5.8 to 12.5 km. Considering these encouraging results, there will be further testing of the IR radiometer on NASA aircraft. The infrared radiometer is already installed on the Kuiper Airborne Observatory (C-141), and there are plans to install it on the CV-990 for use by the flight crews.

TWO MICROWAVE RADIOMETERS

This was the initial "concept feasibility" test for two microwave radiometers developed at the Jet Propulsion Laboratory for other purposes. They were made available for installation on the CV-990 aircraft, but time did not permit their configurations to be optimized for the CAT objectives so they essentially operated as originally developed. A "water vapor radiometer" was operated at a frequency of 180.1 GHz while a "temperature structure radiometer" was operated at a frequency of 55.3 GHz. A brief description of the two radiometers is given below (ref. 5).

The 180.1 GHz "water vapor radiometer" (Figure 8) is shown as it was mounted on the starboard side of the aircraft. The purpose of this was to forecast the occurrence of CAT by monitoring variations of the line-of-sight integrated water vapor content in a manner that is equivalent to that used by the IR radiometer system developed by Dr. Peter Kuhn. This radiometer has the potential advantage of not being influenced by cirrus clouds passing through the line-of-sight (and, hence it should provide fewer "false alarms" than the IR counterpart). Although the expected insensitivity to the confusing influence of cirrus clouds was demonstrated, the 180.1 GHz microwave radiometer failed to provide warnings of CAT encounters. Presumably, this can be explained by the 180.1 GHz radiometer's several fold inferiority in sensitivity to changes in water vapor when compared to the counterpart IR sensor, although a less than optimum viewing geometry (side looking) was employed by the microwave radiometer. The 180.1 GHz radiometer evaluation was done with existing hardware at very low cost and no attempt was made to optimize its configuration for CAT objectives (i.e., employing narrow beam, directing the beam to a forward azimuth, recording the data at greater than 1 Hz rate). Dramatic improvements in 180.1 GHz radiometer technology are being made, and eventually it will be possible to conduct a more meaningful evaluation of this technology for a CAT detection system.

The 55.3 GHz "temperature structure radiometer" was mounted on the port side of the aircraft looking through a high-density polyethylene window as shown in Figure 9. The purpose of the 55.3 GHz temperature structure radiometer (TSR) was to study the altitude association between CAT and unusual structures of the altitude temperature profile. The TSR measured the natural occurring thermal emission of oxygen molecules at a selection of elevation angles above and below the horizon. The raw data, consisting of sky brightness temperature versus elevation angle, was converted in real-time by a desktop calculator to something approximately equivalent to air temperature versus altitude. Altitude Temperature Profiles (ATP) were obtained every seventeen seconds. The ATP plots were subjected to a search for two types of features: (1) a sharp inflection marking the tropopause, and (2) inversion layers defined as a layer within which air temperature increases with altitude (instead of decreasing at the typical rate of -7°K/km). CAT has often been found at the tropopause and within inversion layers. The intended use of this ATP information on commercial air carriers would be to provide altitude guidance away from those altitudes that have the greatest capability for generating CAT (the inversion layers and the tropopause). Another possible use for the ATP is to combine information of the inversion layer's thickness and lapse rate in a way that may forecast, in some statistically acceptable way, the maximum level of turbulence that can be expected from the inversion layers.

The theoretical basis for associating CAT generation with inversion layers is presented in reference 6. It also presents TSR data supporting the hypothesized association of CAT with inversion layers. In Figure 10, a representative set of the data is presented. These are plots of air temperature versus altitude. The altitude coverage is from about one kilometer above flight level to one kilometer below flight level. The temperature values are differences from the static air temperature (SATM). The upper left panel is typical of the most often encountered ATP with the observed air temperature "0" decreasing uniformly from about 0.6 km below the aircraft level to 0.9 km above it. The outside air temperature is 225.4°K. The sloping pattern of colons is where the "0s" would be found for flight within a "dry adiabatic" atmosphere. It is nearly impossible to abruptly generate strong turbulence in the "dry adiabatic" condition. For flight within an isothermal atmosphere the "Os" would overlay the vertical pattern of dots. The panel on the upper right shows a shallow inversion layer above the aircraft altitude. The lower left panel corresponds to flight within an inversion layer. It is the same inversion layer as shown in the upper right panel, but it is taken 15 minutes later. The base and top altitudes for this inversion layer are -0.1 km and $\pm$0.25 km (-300 ft to $\pm$800 ft). The lapse rate within the inversion layer is approximately $+4^{\circ}$K/km. The lower right panel corresponds to flight at the tropopause. These are the first "altitude temperature profile" plots that have ever been produced using an airborne remote sensor to the authors' knowledge. The question of whether ATP generation can be done by an airborne sensor has been answered. The next question, more directly related to CAT, is whether ATP information can be useful in avoiding CAT. If CAT is really found more within inversion layers and near the tropopause, then altitude temperature profile information of the type illustrated in these panels could be useful in selecting "smooth" flight levels.

An improved TSR sensor is under construction and intended for installation on the NASA C-141 aircraft, the Kuiper Airborne Observatory. This sensor should provide a five-fold improvement in sensitivity for the measurement of air temperature. A potential several hundred hours of flight evaluation will be available during the next few years. Meaningful statistical analyses on the usefulness of a TSR type sensor for the forecasting of CAT severity and altitude avoidance should then be possible.

PULSED DOPPLER LIDAR

The pulsed Doppler lidar that was tested in this program underwent initial feasibility flight tests in 1972 and 1973. After extensive ground-based testing and modification, ground-based measurements were made of low altitude wind shears after which the lidar was reconfigured to the aircraft mode for the 1979 test (ref. 7). This is the only airborne pulsed Doppler lidar in existence. The lidar is shown in Figure 11 mounted aboard the aircraft about mid-cabin at the emergency door. The transmitter, shown in this figure, includes the master oscillator, the local oscillator, the laser amplifier, the modulator, the optical interferometer, and the telescope. Not shown, but essential to the lidar, are signal processing elements which include a minicomputer used for recording the signal and providing real-time analyses and the display of essential performance information. The range capability of the pulsed Doppler lidar is determined by the lidar's output power and the features of the atmosphere. The signal processing system has a maximum capability of 30 km in range. A signal from 20 km ahead of the aircraft is the most distant signal ever received for this lidar. The per pulse energy level is about 12 to 15 millijoules. Typical ranges are from 3 to 15 km. The atmospheric factors that have the greatest effect on the signal received are: (1) the size and number of aerosols, which provide the backscattered signal, (2) the water vapor, and (3) CO_2 content which contributes significantly to the atmospheric absorption of the CO_2 laser radiation at 10.6 micrometers.

The aerosol tracers essential for received signals were at such a low density that often signals were only received from special conditions such as a dust, cumulus, or cirrus cloud. An example of mountain wave CAT, also illustrating low aerosol density limitation, is given in Figure 12, which shows a cumulus cloud that seeds the atmosphere for the lidar. This is a cloud that cannot be seen on the aircraft's weather radar. Plotted on the geographic coordinates as a heavy black line on the left side of the figure is the flight track made on March 2, 1979, starting at 21:45 Z hours. The aircraft was at flight level 060 (1829 m (6000 ft) MSL.) on the lee side of the Techapi Mountains southeast of White Oak near Edwards Air Force Base, California. Above the flight track are plotted lines indicating the magnitude of the peak-to-peak vertical acceleration from each 5 second time period as recorded near the center of gravity of the aircraft. Using the scale shown above the plot, the length of these lines shows that the aircraft is in turbulence much of this run and especially before the cloud encounter. The lidar obtained data from the cumulus cloud and just after the cloud which is shown as the shaded area along and near the end of the flight track. This cloud is also shown in the photograph at the right. The lidar data is given below the flight track in the shaded area of the plot, representing the cloud location, and for a point just outside the cloud. It "saw" through the cloud to the west data point. The line length is the measured spectral width. This is directly proportional to the gust velocity and has been defined as the predicted gust velocity of the CAT. (There would be almost no spectral width if there were no turbulence.) The lidar data were first recorded about 60 seconds ahead of the turbulence encounter, and shown here is a predicted gust velocity of nearly 10 m/s in two locations. This is indicative of turbulence at the upper end of the moderate turbulence spectrum which is about 10.5 m/s. The scalar value for the measured spectral width is given above the plotted data. There is excellent correlation between the lidar data and the accelerometer data which shows about 0.4 g vertical acceleration in the cloud. The data comparison outside the cloud shows only about a 50% level of predicted CAT versus the actual. The only explanation, so far, for this is again the lack of aerosols outside the cloud. With the lidar's special displays a turbulence patch can be nearly tracked to the point of the aircraft encounter with it. Since the aircraft is already encountering moderate turbulence a precise encounter onset for the lidar measured turbulence cannot be defined in this data set. The picture on the right of this chart is a view of the atmosphere along the flight path ahead of the aircraft. For each CAT case there are pictures taken at the rate of one frame per second to identify these conditions for each set of data. This particular photograph was taken at 21:46:17 Z hours with the aircraft heading at 248.8° and the cloud encountered is the one in the upper part of it. Similar CAT detection sequences were experienced in cirrus clouds, haze, and in other mountain waves.

The aerosol density was low throughout the entire flight test period of 11 weeks. There were aerosol measuring experiments aboard this aircraft during these flights and some of these data are of poor quality; however, the number of large aerosols, those above one micrometer diameter, appeared to be much lower than expected. For the winter of 1979, it appears that the aerosol concentration may have been at least two orders of magnitude lower than the nominal values (ref. 8) used in the pulsed Doppler lidar design. Before definite conclusions and recommendations can be given about the potential capability of the pulsed

Doppler lidar, a better understanding of the variability of the atmospheric aerosol size distribution and density as it relates to CO_2 laser radiation is required. Only when this information is known can realistic projections be made about the future applications of this technology including a prototype system design specification. A small program called the Beta Experiment will attempt to address this problem starting in 1981. Meanwhile, the pulsed Doppler lidar is being modified to measure the wind velocity in the nonprecipitous regions of thunderstorms. This work is part of the NASA's Severe Storms and Local Weather Research and Technology Program. These initial tests are currently planned for the summer of 1981 and should add to the knowledge of the technology and enable better projections to be made concerning its future use. At this time, there are no plans to further test the lidar for detecting and measuring high altitude CAT.

CONCLUDING REMARKS

The results from the test of the IR radiometer are very encouraging. It gave CAT alerts at all flight levels although it appears to give better warning information at altitudes above 4 km. Because of its small size and weight, it is the sensor that shows strong potential for operational development and possible application to the commercial aircraft fleet. Further study is underway wherein NASA pilots will evaluate the system during the 1980-81 "CAT Season" in regular flight operations of the C-141 and CV-990 flying laboratories based at the NASA's Ames Research Center. In addition, United Airlines and the Colorado Air National Guard are considering independent evaluations of this type of CAT sensor.

The microwave temperature structure radiometer (55.3 GHz) was successful in historically providing the first "altitude temperature profiles" using an airborne sensor. The altitude temperature profile data now in hand show that on some occasions CAT is strikingly well-correlated with inversion layer altitudes whereas on other occasions CAT is encountered in the absence of near inversion layers. More flight hours of data are needed to provide estimates of the fraction of the time useful avoidance guidance can be generated from altitude temperature profile information. It is planned to further test this radiometer in a "CAT" configuration aboard NASA's C-141 aircraft.

The 180.1 GHz water vapor radiometer is apparently not sensitive enough to measure the small variations of water vapor content from which the IR CAT detector generates its warnings. Much better 180.1 GHz radiometers tailored to the CAT observing requirements could be built with present microwave technology, and would merit consideration for development in the near future.

The pulsed Doppler lidar appears to be a useful sensor for meteorological research in its present configuration which is based on 1970 technology. However, as an operational CAT sensor it is large and complex. The primary question concerns the aerosol density in the atmosphere and the backscatter coefficient or signal return from the aerosols at the CO_2 laser frequencies. In its role as a research tool, it is planned to collect velocity data on the winds in the nonprecipitous regions of thunderstorms in the summer of 1981.

The success in finding CAT during this 1979 season when the conditions for it were somewhat unfavorable is a credit to the detailed meteorological analyses and forecasting efforts used for this test, and to the routing flexibility exercised by the CV-990 flight crew. In the viewpoint of the authors, the most significant accomplishment has been to indicate the advantages of synergistic combinations of onboard remote sensors for observing the local dynamic atmospheric structure associated with gravity waves and CAT.

ACKNOWLEDGEMENTS

The authors wish to thank the more than 150 people who had a part in this test program. Especially noted are the efforts of the Raytheon Company and M&S Computing Company whose untiring efforts made the testing of the lidar a reality. The meteorological team consisting of NASA, Navy, Air Force, and NOAA personnel enabled early and exacting mission planning so essential for a successful rate of encountering CAT. The CV-990 aircraft personnel and specifically George Alger, the Mission Manager, and those associated with preparing and operating each flight, provided outstanding support to the program. The teamwork necessary for a test program of this size was outstanding and a credit to all who supported the mission. Finally, special appreciation is hereby expressed for the many years of financial and personal support provided by NASA/OAST's Aviation Safety Technology Branch.

REFERENCES

1. Weaver, E., "1979 Clear Air Turbulence Flight Test Program," March 1980, Aviation Meteorology Workshop.

2. Kuhn, P., Carcena, F., and Gillespie, C. M., Jr., "Clear Air Turbulence: Detection by Infrared Observations of Water Vapor," Science, Vol. 196, 1977, pp. 1099-1100.

3. Kurkowski, R., Kuhn, P., and Stearns, L., "Flight Tests of a Clear-Air Turbulence Alerting System," 1980 Aircraft Safety and Operating Problems, NASA CP-2170, 1981. (Paper 18 of this compilation.)

4. Kuhn, P., Nolt, I. G., Stearns, L. P., and Radostitz, J. V., "Infrared Passbands for Clear Air Turbulence Detection," Optics Letters, Vol. III, 1978, pp. 130-133.

5. Gary, B. L., "Clear Air Turbulence Studies With Microwave Radiometers," 1980 Aircraft Safety and Operating Problems, NASA CP-2170, 1981. (Paper 19 of this compilation.)

6. Gary, B., "An Airborne Remote Sensor for the Avoidance of Clear Air Turbulence," Paper presented at the AIAA 19th Aerospace Sciences Meeting, St. Louis, Mo., Jan. 12-15, 1981.

7. Weaver, E. A., Bilbro, J. W., Dunkin, J. A., Johnson, S. C., Jones, W. D., Harris, C. E., and DiMarzio, C. A., "Pulsed Doppler Lidar for the Detection of Turbulence in Clear Air, 1980 Aircraft Safety and Operating Problems, NASA CP-2170, 1981. (Paper of this compilation.)

8. McClatchey, R., Fenn, R., Selby, J., Volz, F., and Garing, J., "Optical Properties of the Atmosphere," AFCRL 72-0479, August 24, 1972.

TABLE 1 - INFRARED RADIOMETER PERFORMANCE AND OPTICAL DATA

PERFORMANCE DATA

OPERATING SPECTRAL RANGE	20 μ m TO 40 μ m
CAVITY REFERENCE TEMPERATURE	– 20 C
OUTPUT VOLTAGE	+ 10 VDC TO – 10 VDC
A TO D CONVERSION	12 BIT (5mv/bit)
NOISE EQUIVALENT POWER	2.5×10^{-8} watts
RESPONSE TIME (TIME CONSTANT)	50 Hz

OPTICAL DATA

DETECTOR TYPE	1 mm X 1 mm LITHIUM TANTALATE CHIP
OPTICAL FILTER	INTERFERENCE BAND PASS (20 TO 40 μ m)

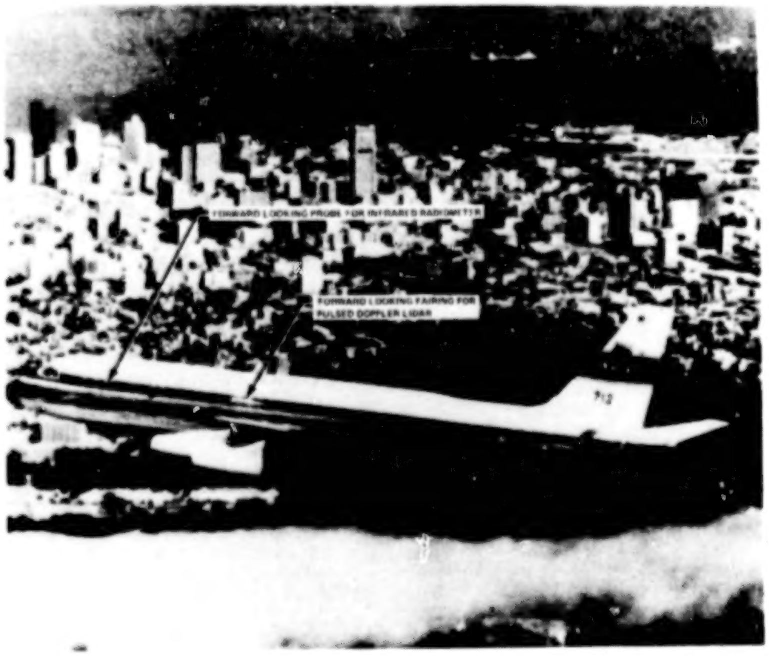
FORWARD LOOKING PROBE FOR INFRARED RADIOMETER
FORWARD LOOKING FAIRING FOR PULSED DOPPLER LIDAR
712

Figure 1.- Convair 990 aircraft.

1979 CLEAR AIR TURBULENCE (CAT) FLIGHT TEST
TEST OBJECTIVES

OBJECTIVE:

- EVALUATE 4 SENSORS FOR THE DETECTION AND MEASUREMENT OF CAT AND METEOROLOGICAL TARGETS OF OPPORTUNITY.
  - CAT FORECASTING TECHNIQUES
  - INFRARED RADIOMETER – 20 – 40 MICROMETERS
  - MICROWAVE RADIOMETERS – 180.1 GHZ
  - MICROWAVE RADIOMETERS – 55.3 GHZ
  - DOPPLER LIDAR – 10.6 MICROMETERS

TYPES OF CAT:

- MOUNTAIN WAVE
- JET STREAM
- CAT IN CIRRUS CLOUDS
- CAT IN FRONTAL WIND SHEARS, TROUGHS, RIDGES

Figure 2.- Test objectives.

1979 CAT FLIGHT TEST

NATIONAL AERONAUTICS & SPACE ADMINISTRATION

NASA HEADQUARTERS
AMES RESEARCH CENTER
DRYDEN FLIGHT RESEARCH CENTER
JET PROPULSION LABORATORY
LEWIS RESEARCH CENTER
MARSHALL SPACE FLIGHT CENTER

DEPARTMENT OF TRANSPORTATION

FAA – AIR TRAFFIC & AIRWAY FACILITIES
TRANSPORTATION SYSTEMS CENTER

INDUSTRY

BARNES ENGINEERING COMPANY
COMPUTER SCIENCES CORPORATION
EXOTIC MATERIALS
INFORMATICS PMI
M & S COMPUTING, INC.
NORTHROP SERVICES
RAYTHEON COMPANY
SRI INTERNATIONAL, INC.
UNITED AIRLINES

DEPARTMENT OF COMMERCE

NATIONAL OCEANIC & ATMOSPHERIC ADMINISTRATION

ENVIRONMENTAL RESEARCH LABS
NATIONAL WEATHER SERVICE
NATIONAL ENVIRONMENTAL SATELLITE SERVICE

DEPARTMENT OF DEFENSE

U. S. AIR FORCE

AIR WEATHER SERVICE
EDWARDS FLIGHT TEST CENTER
GLOBAL WEATHER CENTER

U. S. NAVY

MONTEREY – FLEET NUMERICAL WEATHER CENTER
MOFFET FIELD – NAVAL WEATHER DETACHMENT

EDUCATION

ALABAMA A&M UNIVERSITY
UNIVERSITY OF COLORADO
UNIVERSITY OF OREGON

Figure 3.- Groups participating in 1979 CAT flight test.

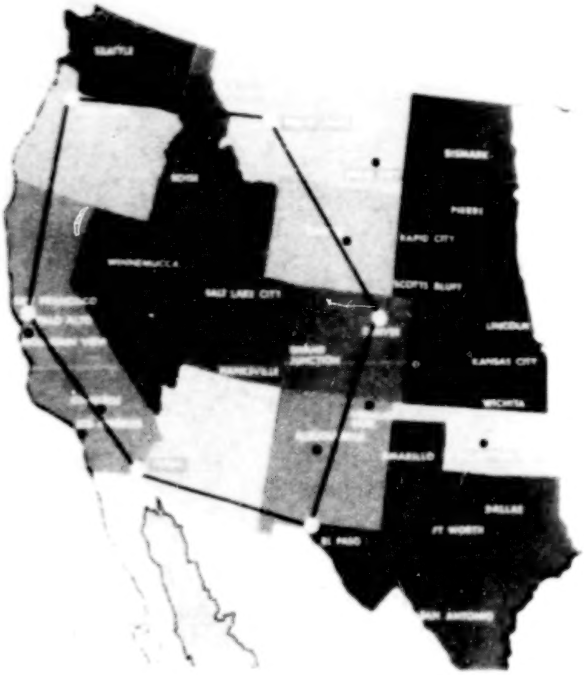
SEATTLE
BOISE
BISMARCK
PIERRE
RAPID CITY
WINNEMUCCA
SALT LAKE CITY
SCOTTS BLUFF
PALO ALTO
DENVER
LINCOLN
GRAND JUNCTION
HANKSVILLE
KANSAS CITY
WICHITA
AMARILLO
DALLAS
FT WORTH
EL PASO
SAN ANTONIO

Figure 4.- 1979 flight test region.

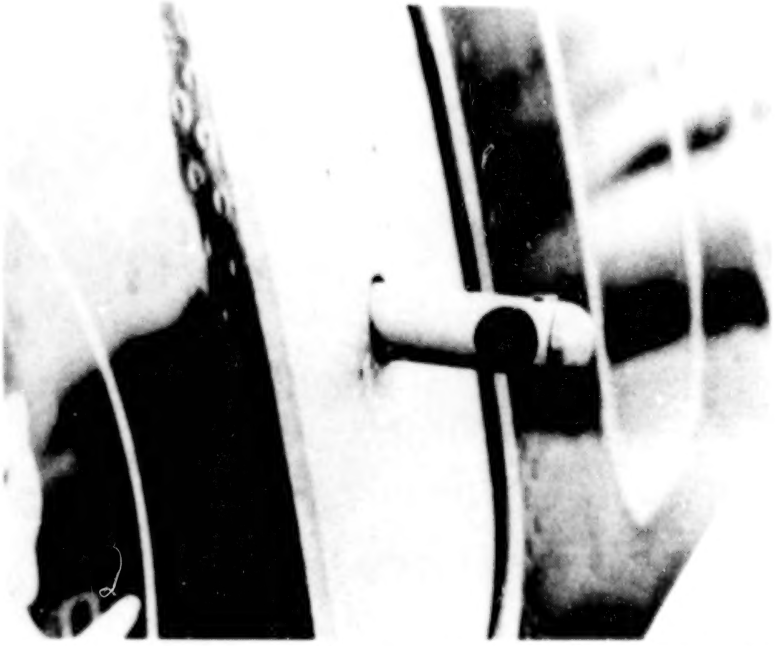

Figure 5.- Infrared radiometer forward looking probe with gold-coated mirror.

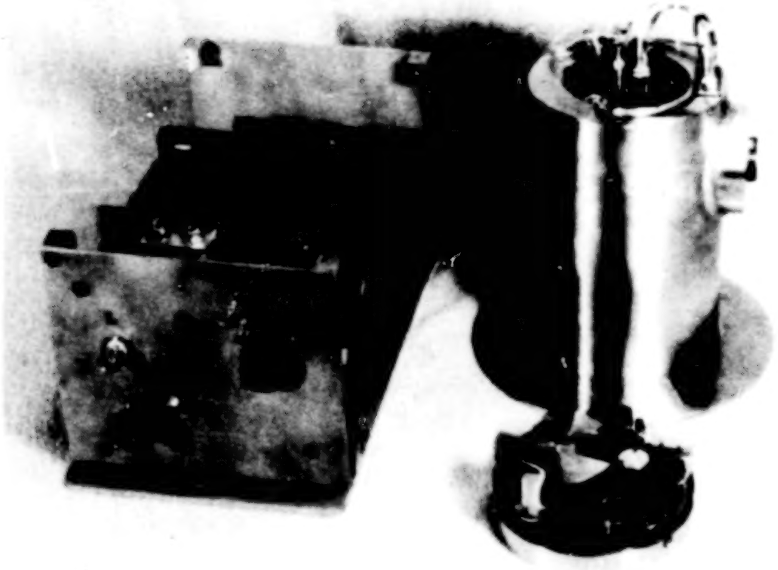

Figure 6.- Infrared radiometer sensor and chopper.

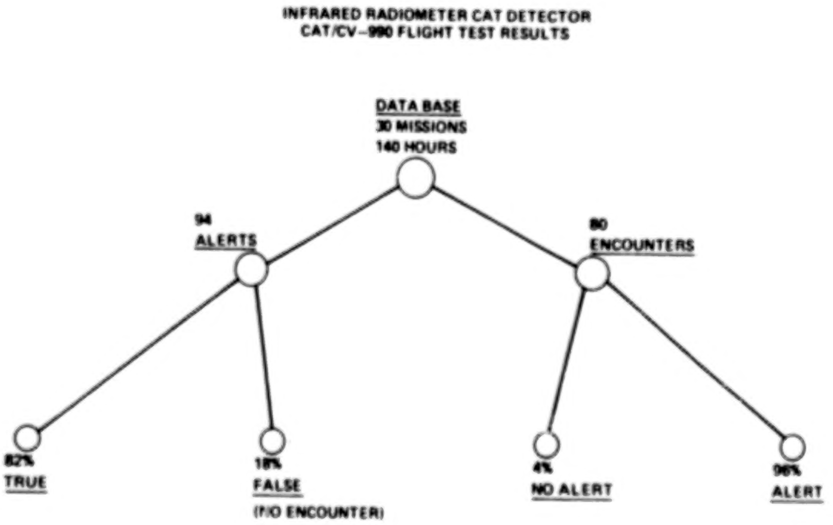
INFRARED RADIOMETER CAT DETECTOR
CAT/CV-990 FLIGHT TEST RESULTS
DATA BASE
30 MISSIONS
140 HOURS
94
ALERTS
80
ENCOUNTERS
82%
TRUE
18%
FALSE
(NO ENCOUNTER)
4%
NO ALERT
96%
ALERT

Figure 7.- Infrared radiometer flight test results on CAT data (CV-990).

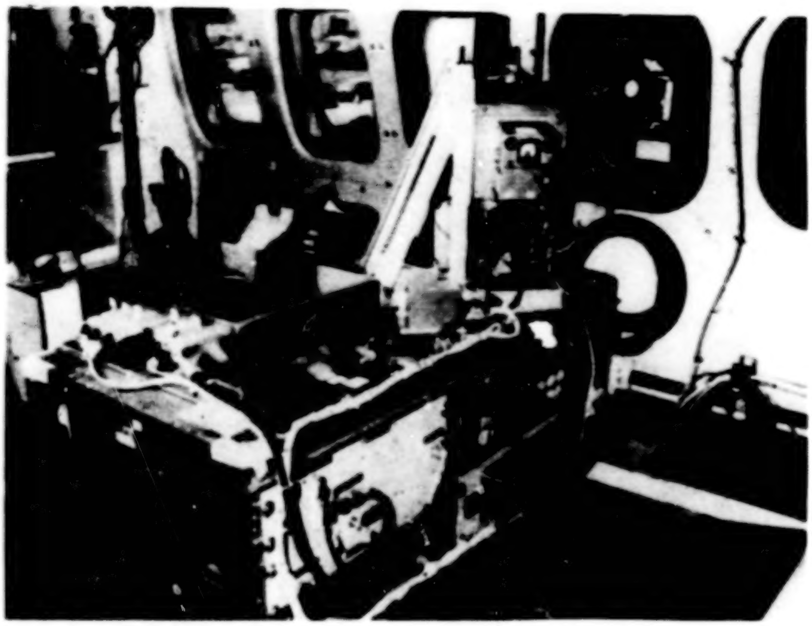

Figure 8.- Microwave radiometer in the water vapor band.

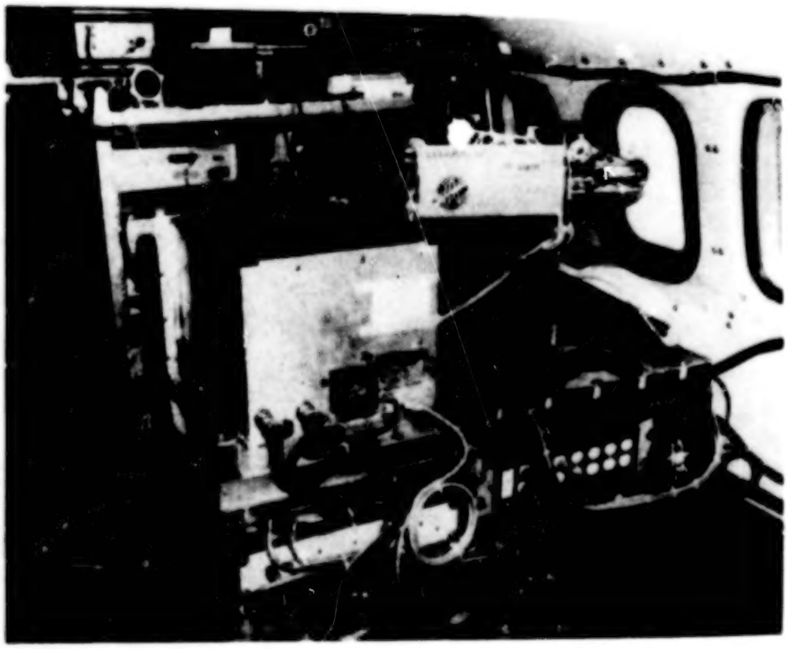

Figure 9.- Microwave radiometer in the oxygen band.

55.3 GHz MICROWAVE RADIOMETER TEMPERATURE DATA

Figure 10.- Altitude temperature profiles generated from 55.3 GHz microwave radiometer data.

EMERGENCY EXIT
DANGER

Figure 11.- Pulsed Doppler lidar using a CO_2 laser.

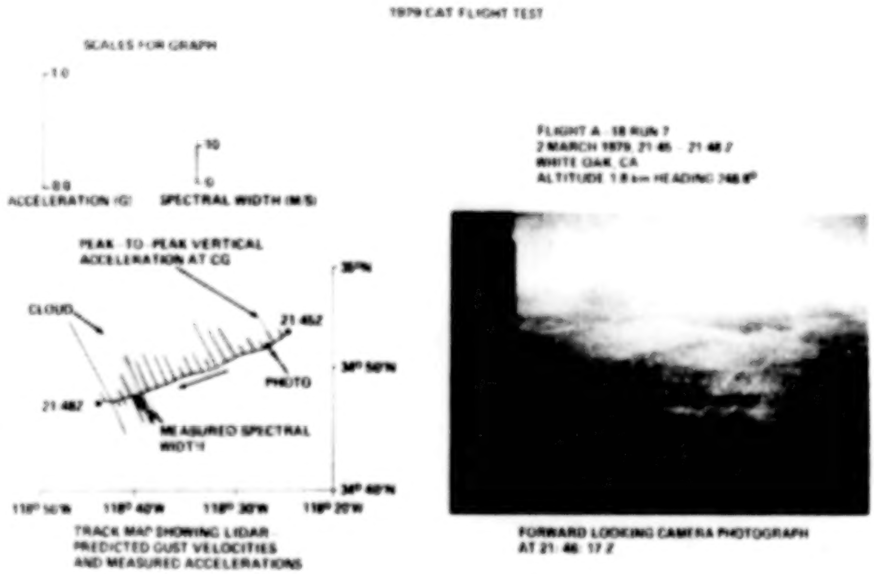
1979 CAT FLIGHT TEST
SCALES FOR GRAPH
1.0
0.0
ACCELERATION (G)
10
0
SPECTRAL WIDTH (M/S)
PEAK-TO-PEAK VERTICAL ACCELERATION AT CG
CLOUD
21:45.2
PHOTO
21:48.7
MEASURED SPECTRAL WIDTH
35°N
34° 50'N
34° 40'N
118° 50'W
118° 40'W
118° 30'W
118° 20'W
FLIGHT A-18 RUN 7
2 MARCH 1979, 21:45 - 21:48.7
WHITE OAK, CA
ALTITUDE 1.8 km HEADING 248.6°

TRACK MAP SHOWING LIDAR-PREDICTED GUST VELOCITIES AND MEASURED ACCELERATIONS

FORWARD LOOKING CAMERA PHOTOGRAPH AT 21:46:17.2

Figure 12.- CAT and cloud turbulence encounter (lidar).

BLANK PAGE

BLANK PAGE

PULSED DOPPLER LIDAR FOR THE DETECTION OF TURBULENCE IN CLEAR AIR

E. A. Weaver, J. W. Bilbro, J. A. Dunkin, S. C. Johnson, W. D. Jones
National Aeronautics and Space Administration

C. E. Harris, C. A. DiMarzio
Raytheon Company

SUMMARY

The Carbon Dioxide Pulsed Doppler Lidar System developed by the Marshall Space Flight Center was tested in 1978 and 1979 to measure turbulence in clear air. In a 1978 ground test, this remote detection system was used to measure wind shear in the gust fronts of thunderstorms at the Kennedy Space Center. The flight test of the lidar system in the winter of 1979 was for airborne measurements of clear air turbulence over the western part of the United States. A brief description of the Doppler lidar is presented in this overview along with representative data from the two tests.

INTRODUCTION

NASA, as part of the Aviation Safety Technology Program and for more than a decade, has been sponsoring research and development of carbon dioxide (CO_2) laser Doppler system technology for its application to aircraft operating problems - specifically, those problems resulting from both naturally and artificially induced adverse atmospheric environments. A pulsed Doppler lidar system was developed from this technology by the Raytheon Company for the Marshall Space Flight Center in 1979 to 1972 (ref. 1,2). Following its development, it was evaluated in an engineering checkout test to determine if it could operate in the aircraft environment and be used for the advanced detection and measurement of clear air turbulence (CAT) (ref. 3). This earlier system test was described in a paper presented at the 1976 Aircraft Safety and Operating Problems Conference (ref. 4). After the initial test, the lidar, while retaining its airborne capability, was modified for operation as a ground-based instrument system.

In 1976, the Department of Transportation asked NASA to evaluate the use of CO_2 Doppler lidars in the measurement of wind shear in the airport terminal area as part of the ongoing laser Doppler technology program. In support of this evaluation, tests of the pulsed Doppler lidar were conducted in 1978 at two locations: Oklahoma City, Oklahoma, and Kennedy Space Center (KSC), Florida. Wind velocity changes in the gust fronts of thunderstorms were measured at the normal glide slope elevation (3^o). These wind shears were clearly visible in both the real-time and post processed data displays. One data set from this test program is discussed in this paper.

After these tests the lidar was placed in its airborne configuration for a CAT flight test program. This test was conducted from January through March 1979. The objective of the test was to evaluate the lidar's performance from the airborne platform and establish its ability to provide data on the advanced detection of turbulence. Mountain wave CAT, CAT in cirrus clouds, and CAT in haze/dust were detected and measured by the lidar in advance of their encounter by the aircraft. Selected data from this flight test program are presented.

SYSTEM DESCRIPTION

The pulsed Doppler lidar was developed to measure atmospheric wind velocities and turbulence that could be hazardous to aircraft operations. Its operation is similar to that of a microwave Doppler radar. For a pulsed Doppler lidar, coherent infrared laser radiation is transmitted from the system and shifted in frequency when it is scattered by the naturally entrained aerosols in the atmosphere. The frequency of the backscattered radiation received by the system from the aerosol reflection is compared to the frequency of the outgoing laser beam by photomixing. The resulting difference frequency is the Doppler shift which is directly proportional to the line-of-sight velocity of the aerosol motion.

The lidar's transmitter, shown in Figure 1 as it was mounted on the CV-990 aircraft, is the central element of the system having a master oscillator power amplifier (MOPA) configuration. The system's simplified block diagram, shown in Figure 2, illustrates this configuration. The primary components are two lasers, the modulator, the power amplifier, an interferometer, a telescope, a detector, the signal processors, and several displays. To provide a better understanding of the system, each element in the block diagram is briefly described (ref. 5).

The master oscillator is a very stable, continuous wave CO_2 laser that provides about eight watts of linearly polarized radiation at a wavelength of 10.6 micrometers. A small portion of this radiation is used to stabilize the frequency of the master oscillator and to maintain the frequency offset of the second laser which serves as a local oscillator (LO) for the system. In the laser optical path the cadmium telluride electro-optic modulator is used to chop the radiation into a pulse train that is variable in repetition rate and in width. The pulse width can be varied between two and eight microseconds equivalent to pulse lengths of 600 to 2400 meters, while the pulse repetition rate may be varied from one pulse to two hundred pulses per second. The resultant pulse train passes through an indium-antimonide optical isolator which prevents reflections from entering the master oscillator and causes its frequency to change. The pulse train next passes through the power amplifier that has six discharge tubes cascaded to provide a gain of approximately 36 dB. Upon exiting the power amplifier the pulse train passes through a Brewster window, then through a quarter-wave plate which converts the radiation from linear to circular polarization. The pulse train finally passes into a 30 cm diameter telescope where it is expanded to approximately 24 cm, collimated, and transmitted into the atmosphere. The energy is then directed to a specific location in the atmosphere by a scanner mirror system that provides nearly hemispherical coverage for the ground-based opeartion. In the flight configuration, the energy is directed by a fixed flat from the telescope forward along the flight path of the aircraft through a 35.5 cm diameter, 1.9 cm thick germanium window that serves as an aircraft pressure bulkhead to the atmosphere.

The directed laser energy is scattered by aerosols naturally entrained in the atmospheric wind. Some of the scattered light is reflected back along the same optical path that the transmitted beam traveled. As mentioned previously, it has been Doppler shifted in frequency by an amount proportional to the radial (line-of-sight) velocity component of the aerosols. It is the measurement of this Doppler shift that allows the wind velocity component to be determined. The backscattered part of the laser radiation collected by the telescope is transmitted back through the quarter-wave plate. Because the polarization of the reflected radiation is rotated 180^o from the transmitted laser light it is reflected by the Brewster window to the detector through a combining beam splitter. Also coming to the detector through the combining beam splitter is the laser beam from the very stable LO laser. The LO is tuned to a frequency that is offset by 10 MHz from the master oscillator frequency. This allows not only the magnitude of the radial velocity to be measured, but also its direction as well.

Photomixing of the LO and the received beams occurs at the detector which is a mercury-cadmium-telluride photodiode. The signal from the detector is amplified and then passed through a filter bank to obtain the signal frequency spectra. The frequency resolution can be set for 125 kHz, 250 kHz, and 500 kHz matching pulse widths of 8, 4, and 2 microseconds. The corresponding velocity resolution is 0.6 m/s, 1.2 m/s, and 2.4 m/s. Typically, the transmitter operated at 140 pulses per second with an integration of 50 pulses. This provided 3 data sets per second with a data set consisting of the spectral distribution averaged over 50 pulses in a single range cell.

The signal from the signal processor is displayed in real time in two forms as shown in Figure 3. In this first display, which is the range velocity indicator (RVI), the wind velocity is shown as a function of range. It has a maximum range of 30 km corresponding to 200 microseconds elapsed time. The brightness of the signal is an indication of its intensity. In the second display, which is the intensity velocity indicator (IVI), the signal intensity for each velocity at a selected range is shown. The width of the spectrum at the e^{-2} point (near the spectrum base) is a measure of the turbulence or gust velocity in the selected measurement volume.

The frequency/velocity information is further processed by an online minicomputer for displays in real time and is recorded for post test analyses. Data processing after the test can be performed using both the online minicomputer and the MSFC 1108 central site computer. The parameters of the plots can vary according to the requirements of the specific investigation. This plotting capability was first used with the lidar in the wind shear test program.

WIND SHEAR FEASIBILITY TESTS

Abrupt wind speed changes over very short flight path distances can cause sudden variation in the airflow over the wing when these wind shears are encountered by aircraft. This causes the aircraft to deviate from the planned course. At times, particularly during takeoff or landing, a wind shear encounter has resulted in serious and fatal accidents. One source of hazardous wind shear is a thunderstorm with its associated gust fronts, down drafts, and turbulence. NASA is studying these and other meteorological conditions that cause the invisible wind gradients. The agency has also sponsored sensor development to remotely detect them and provide advanced warning to the pilots about these conditions before their aircraft enter the critical opeational zones of the airport.

A study of the NASA pulsed Doppler lidar applied to glide slope wind shear detection showed these measurements to be feasible (ref. 6), so the lidar was deployed to the Kennedy Space Center during the 1978 summer thunderstorm period as part of the NASA-DOT Wind Shear Test Program. The lidar was positioned 0.6 km NE of the Vertical Assembly Building and 5.5 km from the Florida Coast Line (Figure 4). It was essential that the data be collected as it would be at an airport so the lidar scanned a 320^{o} azimuth sector at an elevation of 3^{o} and at a $2\ ^{o}/s$ scan rate. During the one month test period, three storms were monitored that showed the existence of well defined gust fronts with associated wind shear. The July 29, 1978, case was selected for discussion in this paper (ref. 7).

The selected data consist of wind flow-field plots obtained from an anemometer network at KSC and the pulsed Doppler lidar velocity plots (ref. 8). The lidar plots show mean radial wind velocity as a function of scan position and range with the lidar located at the center of the plot and surrounded by circular range increments of 2 km. The areas coded 1 through 9 indicate increasing velocities toward the center of the plot and the A through I codes indicate increasing velocities away from it. Each number or letter represents a velocity bin of 2.5 m/s. Groups of 3 velocity bins are indicated by the different designs on the plots. Adjacent velocity groups are separated by solid lines.

The first wind flow-filed plot in Figure 5 indicates the penetration of the lidar scan plane by a sea breeze front at approximately 1500 EDT. This resulted in a predominant wind direction from the southeast behind the front but from the southwest preceding the front. By 1530 EDT a second sea breeze front, with wind from the northeast, has pushed into the scan plane resulting in convergence at the site - winds approaching from virtually all directions. By approximately 1600 EDT (third plot), a col had formed slightly to the west of the lidar site. At this point the wind was approaching from the west and east, but was receding to the north and south. Simultaneously, a storm was forming over the Indian River to the west and within a half hour had passed over the site and out to sea as indicated in the final plot of Figure 5.

The laser Doppler velocity data corresponding to these events are shown in Figure 6. The first of the plots, generated at 1532 EDT, indicates approaching velocities from all but a small area to the north of the site. At 1542 EDT the wind was flowing toward the north and by 1552 EDT had evolved so that the wind was flowing almost uniformly toward the northwest. Five minutes later, a high velocity approaching wind was observed to the west, while just south of it was a high velocity receding wind for a total wind speed change of approximately 25 m/s. By the next scan, a highly turbulent region was encountered with both approaching and receding velocities in excess of 16 m/s. At 1611 EDT the flow had become much more uniform with relatively high winds toward the southeast.

The wind velocity variations associated with thunderstorm gust fronts were measured on three occasions during the KSC test with the lidar. It is capable of measurements to a range of 6 km. The wind shears along a single lidar line-of-sight can be measured, but it appears that by scanning in azimuth the presence of fronts and the direction of shears are more readily identified.

LIDAR FLIGHT TEST FOR CLEAR AIR TURBULENCE

Clear air turbulence cannot be visually located because it has no feature to identify it in the atmosphere. In that sense it also resembles wind shear. CAT is considered a problem for all aircraft so areas of potential CAT are identifid on the synoptic weather charts, but avoidance of all these regions cost both time and energy while passenger injury and/or aircraft damage may result from CAT encounters. These costs have resulted in a requirement for more accurate location of CAT and providing advance warning of it. Therefore, part of NASA's CAT research effort is the development of sensors to detect and measure the severity of CAT ahead of aircraft with sufficient warning for possible evasive maneuvers by the pilot.

The requirement for a CAT sensor was the basis for a study applying CO_2 laser Doppler technology that required using recognized models for the atmosphere's optical properties (ref. 9). The study results showed that an advanced technology CO_2 pulsed laser Doppler system could meet the CAT sensor requirements so a flightworthy breadboard CO_2 pulsed Doppler lidar was developed to test the feasibility of detecting CAT. (These test results are summarized in reference 4.) Further laboratory tests were followed by modifications and ground-based tests. Then in December 1978 the lidar was installed aboard the NASA Convair 990 aircraft for CAT detection and calibration flight testing. The lidar's transmitter (Figure 1) was placed so that the telescope's forward reflecting mirror was inside the special fairing at the emergency door on the port side of the aircraft (Figure 7). Because the lidar occupied about half of the onboard floor space, three other sensors in various stages of development for application to the CAT problem were also tested. The other CAT sensors and the flight test program are further described in reference 10; however, selected information from the reference is presented as background for the lidar data cases and the test results.

When flight testing CAT detection sensors the overriding requirement is to find clear air turbulence. Once it is located the goal is to remotely detect and measure it with sensors. To locate CAT during the test program, the meteorological conditions were closely monitored daily as each flight was based on a detailed meteorological forecast covering the western part of the United States (Figure 8). For each day CAT was the first mission priority and on a CAT flight day the mission centered around the most probable CAT area. Where there was not a reasonable probability for CAT the next mission priority was CAT sensor calibration. If neither of the CAT missions could be met the nonCAT experiment objectives were followed. Based on the above mission priority, thirty flights were made between January 12 and March 28, 1979. Sixteen flights were for CAT, another eight were primarily for lidar performance and calibration in conditions other than CAT, although some CAT data were often collected, and finally, six flights were for other experiment objectives. From these flights, three data cases were selected that illustrate the lidar's capability and are representative of all the lidar CAT flight test data, and they are presented in this paper.

One of the lidar performance flight tests was to determine how the lidar signal return (measuring true airspeed) varied with altitude, especially in a relatively small geographical location, both over land and just off the coast. The meteorological conditions required for the test are a clear day with wind speeds relatively low at all flight levels from the surface to 12 km. In 1973, during a similar test along the coast, the mixing of salt particles into the upper altitudes, often in layers, was observed. These observations were made just after many frontal systems entered California from over the Pacific Ocean. In this flight test a similar frontal history occurred prior to Flight A-12 on February 12, 1979, which was a test to make an altitude profile of the lidar signal return. The test was conducted just off the California Coast near Monterey Bay. The aircraft was flown in a race track like pattern with one side about 60 km long and about 5 km between the north and south tracks. The first data were collected at an altitude of 75 m with the aircraft climbing at the end of each track. The final altitude was 10.7 km.

The results of this test are summarized in Figure 10. The CAT lidar detected air signals from 3 km ahead of the aircraft to an altitude of 2.5 km. Between 2.5 and 8.5 km there was one altitude, 4.9 km, where low level signals were collected. Signals were again detected from 8.5 to 10.7 km. These high altitude signals came from very thin cirrus cloud particles. From the data it was concluded that the many frontal systemsprior to the flight did not transport many sea salt particles to altitudes above 2.5 km. Only one possible layer was found at 4.9 km. The data collected on this flight were typical of the entire 30 flights with aerosol concentrations significantly lower than the predictions based on commonly used atmospheric models (ref. 9).

One type of CAT planned for observation during this test was the Sierra mountain wave. For this, at least 20 m/s wind speeds from a direction perpendicular to the ridge line of the mountains are minimum conditions for large CAT areas that disturb the atmosphere sufficiently to propogate the CAT to the tropopause. During the 1979 test these conditions did not occur so this type of CAT could not be observed. Mountain wave CAT, having about a one km altitude thickness, could occasionally be found near the mountain ridge line. The next two lidar data cases are both mountain wave CAT conditions observed during less than minimum wind conditions required for the Sierra wave.

On March 28, 1979, Flight A-30, mountain wave turbulence was found near Vermejo Park, NM (near the New Mexico - Colorado border). The aircraft was at flight level 152 (4600 m) and on a heading of 132° with the wind at 10 m/s from 270°. The plot in Figure 10 shows the lidar spectrum from 3 km ahead of the aircraft. There are two peaks in this spectrum at 170 m/s and 178 m/s. The narrow peak at 178 m/s is associated with the cloud shown in the photograph on the right side of Figure 10. The broad peak, centered about the true airspeed, 170 m/s, is about 8 m/s wide. (This width is often represented by a scalar value.) The broadness of this return is indicative of turbulence within the lidar beam and was one of the strongest CAT conditions detected by the lidar during the 1979 test. Only the edge of this turbulence was encountered by the aircraft because the aircraft was turned to avoid undesirable terrain features. This CAT spectrum is classified as moderate turbulence. Further evidence that CAT should exist in the area was a 12 m/s wind speed decrease within a distance of 25 km which is a wind shear conducive for moderate-to-severe turbulence. The spectral width (in this case 8 m/s) can be represented as a scalar value so that the variation of the turbulence along the flight path can be evaluated. This type of data presentation is used in the next data case.

The data shown in Figure 11 from March 2, 1979, Flight A-18, not only show the turbulence variation along the flight path but also illustrate the lack of lidar signals caused by a low atmospheric aerosol density. Shown in the photograph in Figure 11 is a cumulus cloud, not visible on the aircraft's weather radar, that provided the aerosols essential for lidar measurements. Plotted on the geographical coordinates is the flight track made on Run 7 starting at 2145Z when the aircraft was on a 248.8° heading at flight level 060 (1.8 km MSL) on the lee side of the Tehachapi Mountains. This track is southeast of White Oak, a private landing field, near Edwards Air Force Base, California. The shaded area near the west end of the flight track represents the cumulus cloud. Above the flight track are plotted lines representing the magnitude of the peak-to-peak vertical accelerations from each 5 second time period of flight as recorded by the accelerometers located near the center of gravity of the aircraft. The acceleration plots show that the aircraft was in turbulence for most of Run 7, and especially before the cloud encounter. The lidar data shown as lines below the flight track represent the measured spectral width which is directly proportional to the wind gust velocity. There are no lidar data east of the cloud because the aerosol density is too low. In the clouds however are plotted several spectral width lines, some nearly 10 m/s, indicating moderate-to-severe turbulence. The change in the lidar's gust velocities appears to follow the corresponding change in the peak-to-peak accelerations. In this data set the lidar "saw" through the cloud to a west data position and tracked this cell to the lidar's minimum range of 3 km. In comparing the data west of the cloud, the lidar predicted CAT at about half of the intensity encountered by the aircraft. So far this case is explained by the lack of sufficient aerosols needed to provide the broad spectrum that would compare more favorably with the encountered vertical acceleration. Since the aircraft is encountering moderate turbulence prior to the location of the lidar data, a precise encounter for the lidar measured turbulence cannot be shown. Similar CAT detection sequences were found in cirrus clouds and in other mountain waves where either clouds or dust provided the aerosols.

CONCLUDING REMARKS

The pulsed CO_2 Doppler lidar has been successfully demonstrated in both the ground-based and airborne flight operations. As a ground-based system, it has detected wind shears in thunderstorm gust fronts to a range of 6 km. It has also demonstrated operation under light rain conditions (5 mm/hr). Typical ranges achieved during operation as a ground-based unit were from 3 to 6 km. Ranges as far as 16 km were achieved on days with low humidity and high aerosol densities. When in the airborne configuration, the lidar detected clear air turbulence in advance of the aircraft encountering CAT. The data provided by the lidar included turbulence location and intensity with intensity being indicated by the measured spectral width which is proportional to the wind gust velocity.

Lack of aerosols inhibited operation of the lidar throughout the flight test program usually restricting measurements to low altitudes and close ranges. The ranges at which CAT was detected were inadequate to provide sufficient warning (30 s minimum, 2 to 4 min preferred). While higher per pulse energies will allow detection at longer ranges, it is uncertain at this time as to how much improvement can be realized or even how much is required to match the extreme aerosol density variation. Based on the data from the flight test, the aerosol density appears to be considerably below that predicted by the models which were used in the lidar system design. A test designed specifically to measure the backscatter profile (a function of the aerosol density, size, and composition) is planned for 1981. This test will help determine the potential for future CO_2 lidar systems.

The lidar, developed for aviation safety research involving atmospheric winds, is a unique and valuable research tool. It can provide meteorologists with heretofore unavailable data concerning the variability of the atmospheric winds. The measurement potential can be greatly increased using 1980 technology; however, extensive applications will depend upon considerable reduction in cost and size and simplification of operation.

REFERENCES

1. Jelalian, A. V., Keene, W. H., Sonnenschein, C. M., "Development of CO_2 Laser Doppler Instrumentation for Detection of Clear Air Turbulence," Raytheon Company Report ER72-4243, NASA Contract NAS8-24742, May 1972.

2. Sonnenschein, C. M., Jelalian, A. V., Keene, W. H., "Development of CO_2 Laser Doppler Instrumentation for Detection of Clear Air Turbulence," Raytheon Company Report ER70-4203, NASA Contract NAS8-24742, June 1970.

3. Harris, C. E., Jelalian, A. V., "Development of CO_2 Laser Doppler Instrumentation for Detection of Clear Air Turbulence," Raytheon Company Final Report ER78-4392-1, NASA Contract NAS8-28424, September 1979.

4. Weaver, E., Bilbro, J., Dunkin, J., Jeffreys, H., "Laser Doppler Technology Applied to Aviation Safety Problems," NASA SP-416, pp. 287-301, October 1976.

5. DiMarzio, C. A.; and Bilbro, J. W.: "An Airborne Doppler Lidar", Heterodyne Systems and Technology - Part II, NASA CP-2138, 1980, pp. 529-540.

6. Kalafus, R. M., "Wind Shear Requirements and Their Application to Laser Systems," FAA-RD-77-123, Final Report to FAA, DOT/TSC, Cambridge, MA, 1978.

7. DiMarzio, C., Harris, C., Foley, D., "Thunderstorm Velocity Measurements using A Coherent CO_2 Laser Weather Monitoring System," Raytheon Company Report, ER78-4417, NASA Contract NAS8-32555, December 15, 1978.

8. DiMarzio, C., Harris, C., Bilbro, J., Weaver, E., Burnham, D., Hallock, J., Pulsed Laser Doppler Measurements of Wind Shear," AMS Bulletin, Vol. 60, No. 9, September 1979.

9. McClatchey, R., Fenn, R., Selby, J., Volz, F., Garing, J., "Optical Properties of the Atmosphere," AFCRL 72-0497, August 24, 1972.

10. Weaver, E. A., Ehernberger, L. J., Gary, B. L., Kurkowski, R. L., Kuhn, P. M., Stearns, L. P., "The 1979 Clear Air Turbulence Flight Test Program," 1980 Aircraft Safety and Operating Problems, NASA CP-2170, 1981. (Paper 16 of this compilation.)

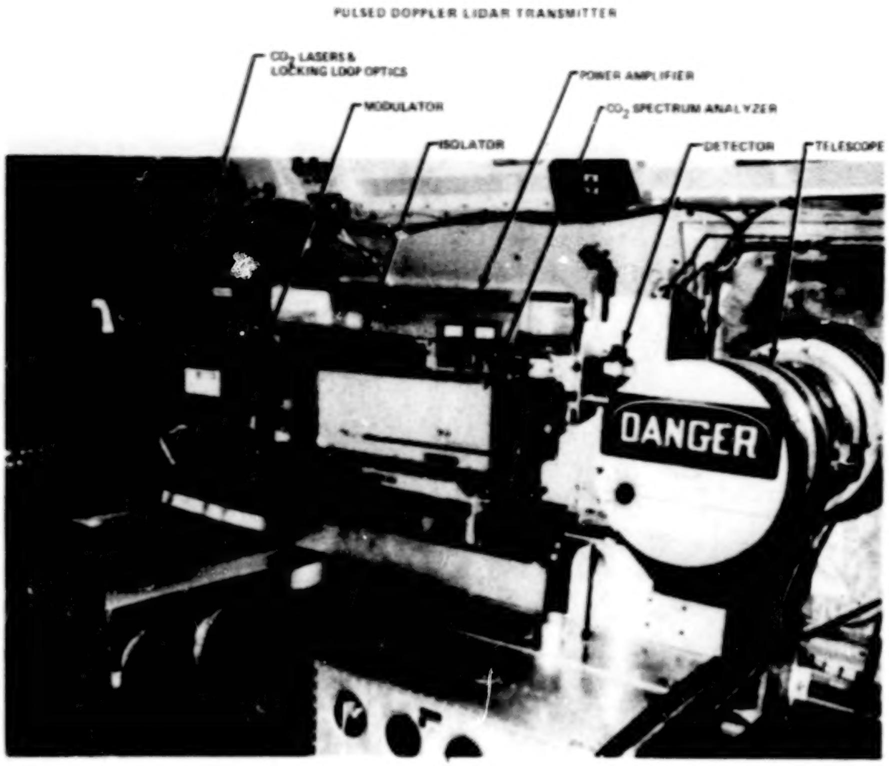
PULSED DOPPLER LIDAR TRANSMITTER
CO$_2$ LASERS & LOCKING LOOP OPTICS
MODULATOR
ISOLATOR
POWER AMPLIFIER
CO$_2$ SPECTRUM ANALYZER
DETECTOR
TELESCOPE
DANGER

Figure 1.- Pulsed doppler lidar transmiter with some components identified.

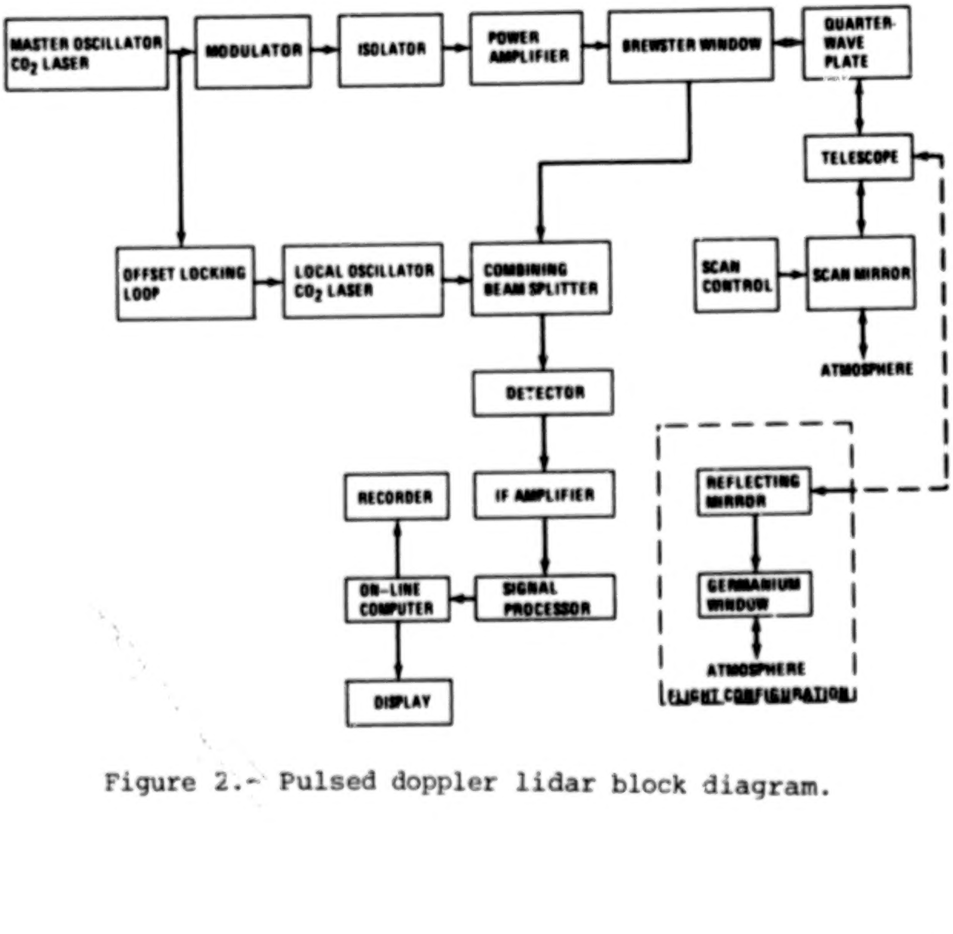
MASTER OSCILLATOR CO$_2$ LASER
MODULATOR
ISOLATOR
POWER AMPLIFIER
BREWSTER WINDOW
QUARTER-WAVE PLATE
TELESCOPE
OFFSET LOCKING LOOP
LOCAL OSCILLATOR CO$_2$ LASER
COMBINING BEAM SPLITTER
SCAN CONTROL
SCAN MIRROR
ATMOSPHERE
DETECTOR
RECORDER
IF AMPLIFIER
REFLECTING MIRROR
ON-LINE COMPUTER
SIGNAL PROCESSOR
GERMANIUM WINDOW
ATMOSPHERE
(FLIGHT CONFIGURATION)
DISPLAY

Figure 2.- Pulsed doppler lidar block diagram.

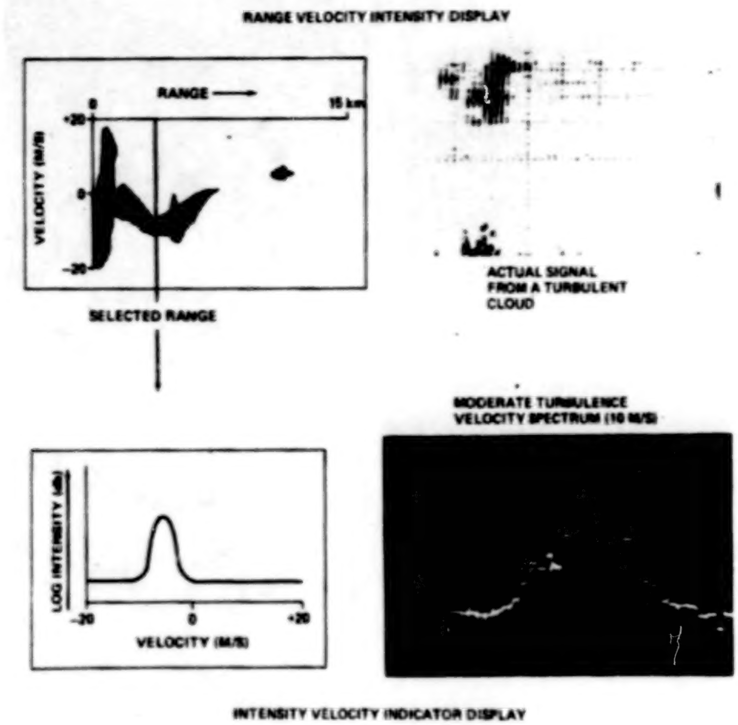

Figure 3.- CAT detection real-time displays.

KENNEDY SPACE CENTER
PULSED DOPPLER LIDAR LOCATION

Figure 4.- Kennedy Space Center lidar test site.

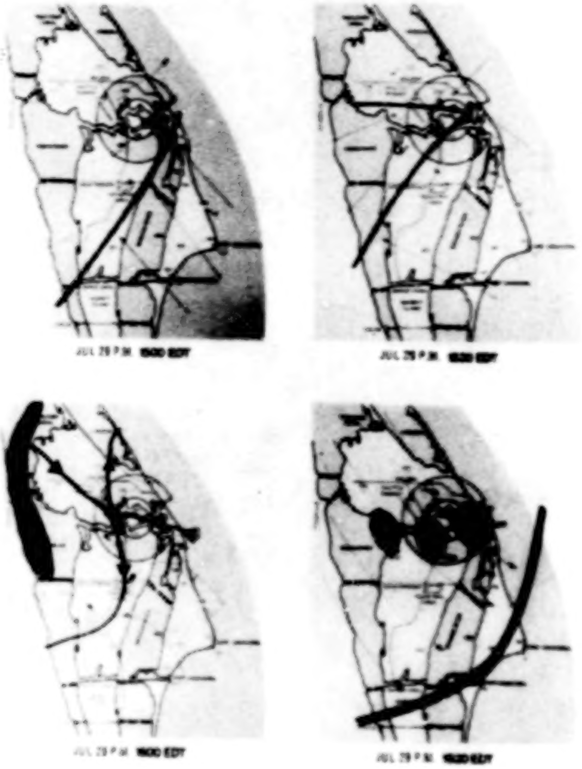

Figure 5.- Wind flow-field plots. Anemometer data, July 29, 1978.

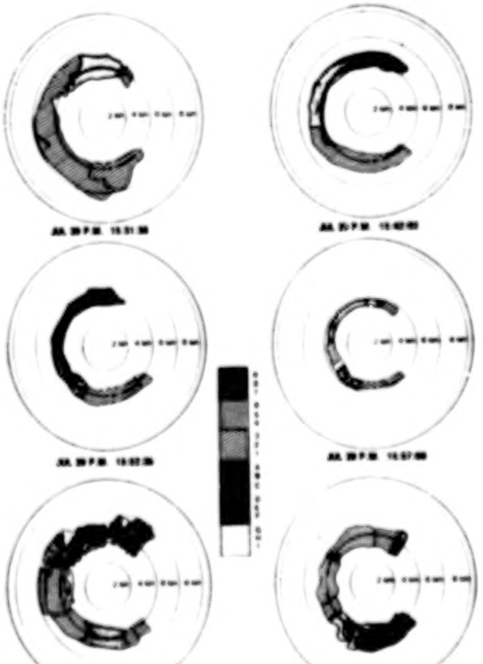

Figure 6.- Wind flow-field plots. Lidar data, July 29, 1978.

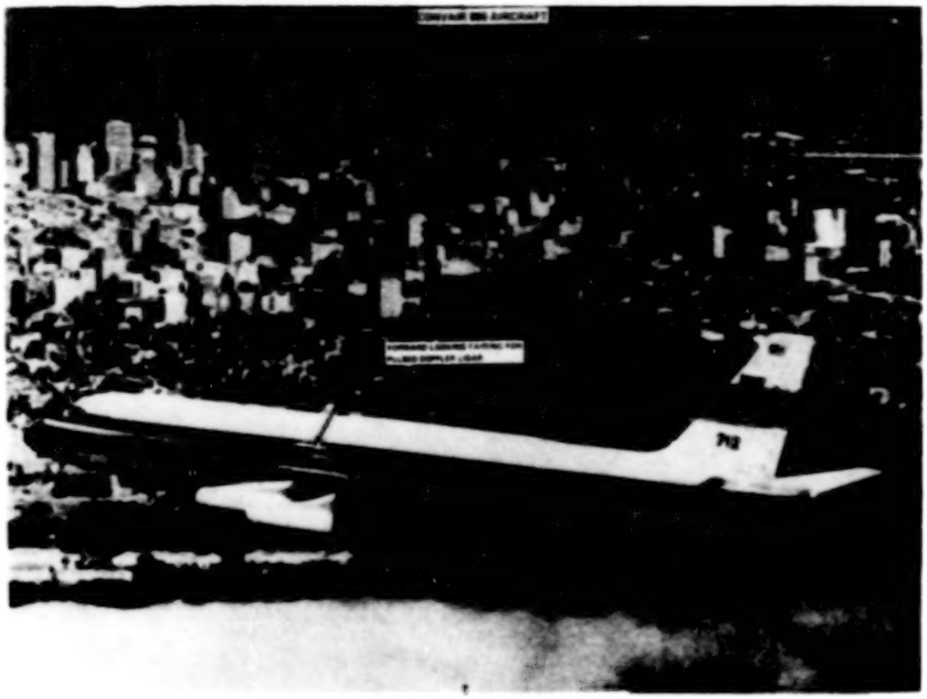

Figure 7.- Convair 990 aircraft used in clear air turbulence flight test.

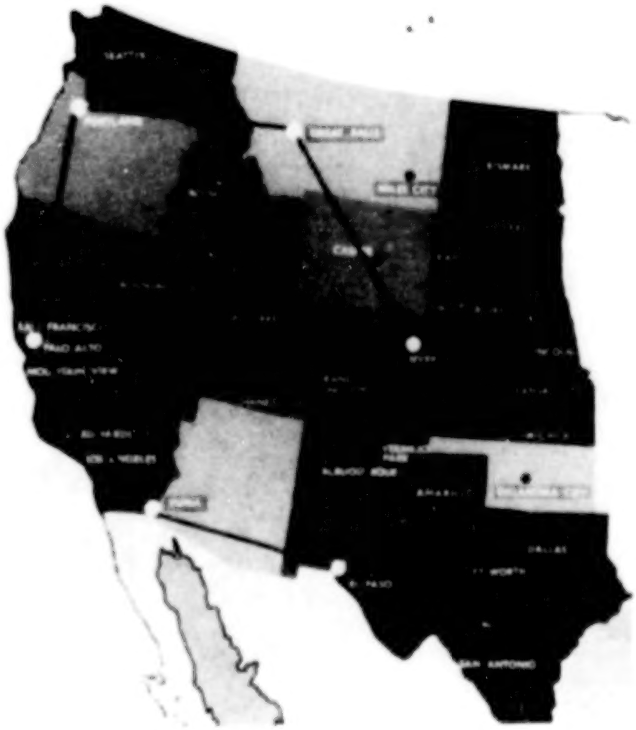
PALO ALTO
DALLAS
FT WORTH
SAN ANTONIO

Figure 8.- 1979 CAT flight test region.

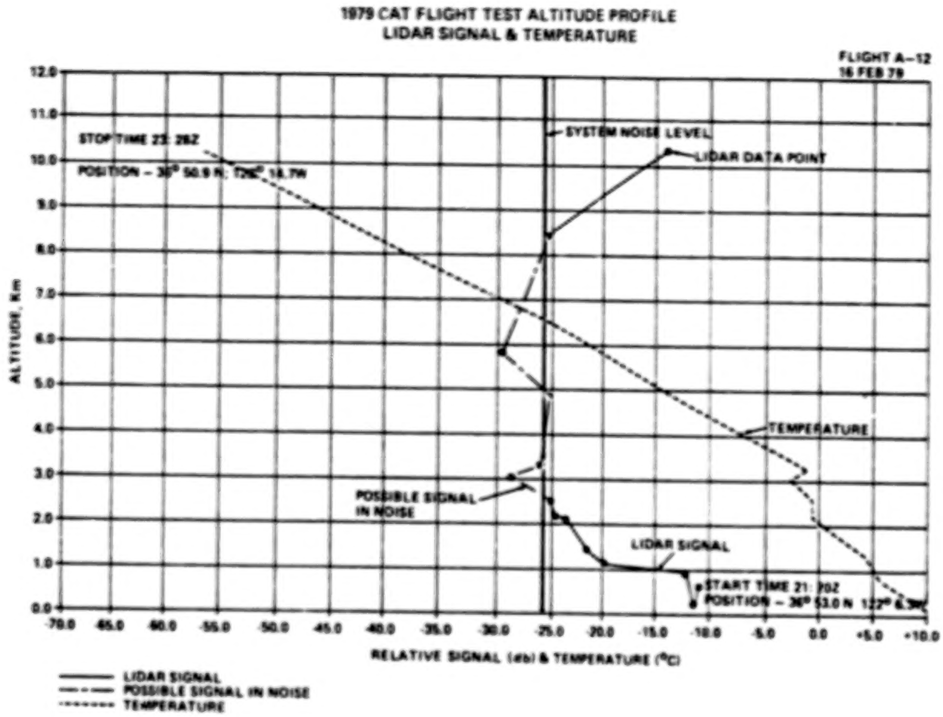

Figure 9.- Lidar signal level variation with altitude.

MOUNTAIN WAVE CAT

TRUE HEADING –	132°	1979 CAT FLIGHT A – 30, RUN 4
PRESSURE ALTITUDE –	4.6 km	28 MARCH 1979 22:20 Z
TRUE AIR SPEED –	170 M/S	VERMEJO, NM
ROLL –	29° LEFT	

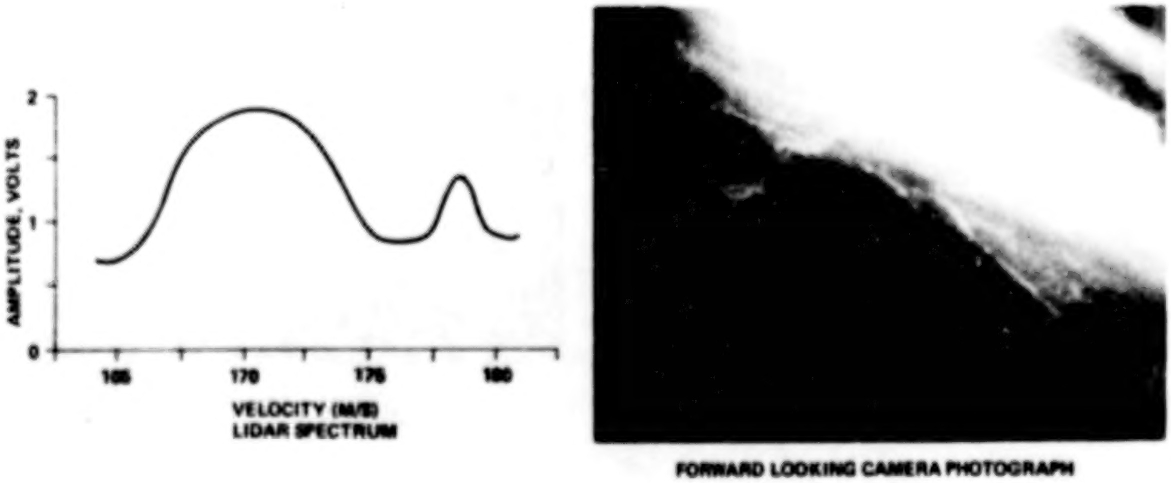

VELOCITY (M/S)
LIDAR SPECTRUM

FORWARD LOOKING CAMERA PHOTOGRAPH

Figure 10.- Pulsed doppler lidar clear air turbulence measurement.

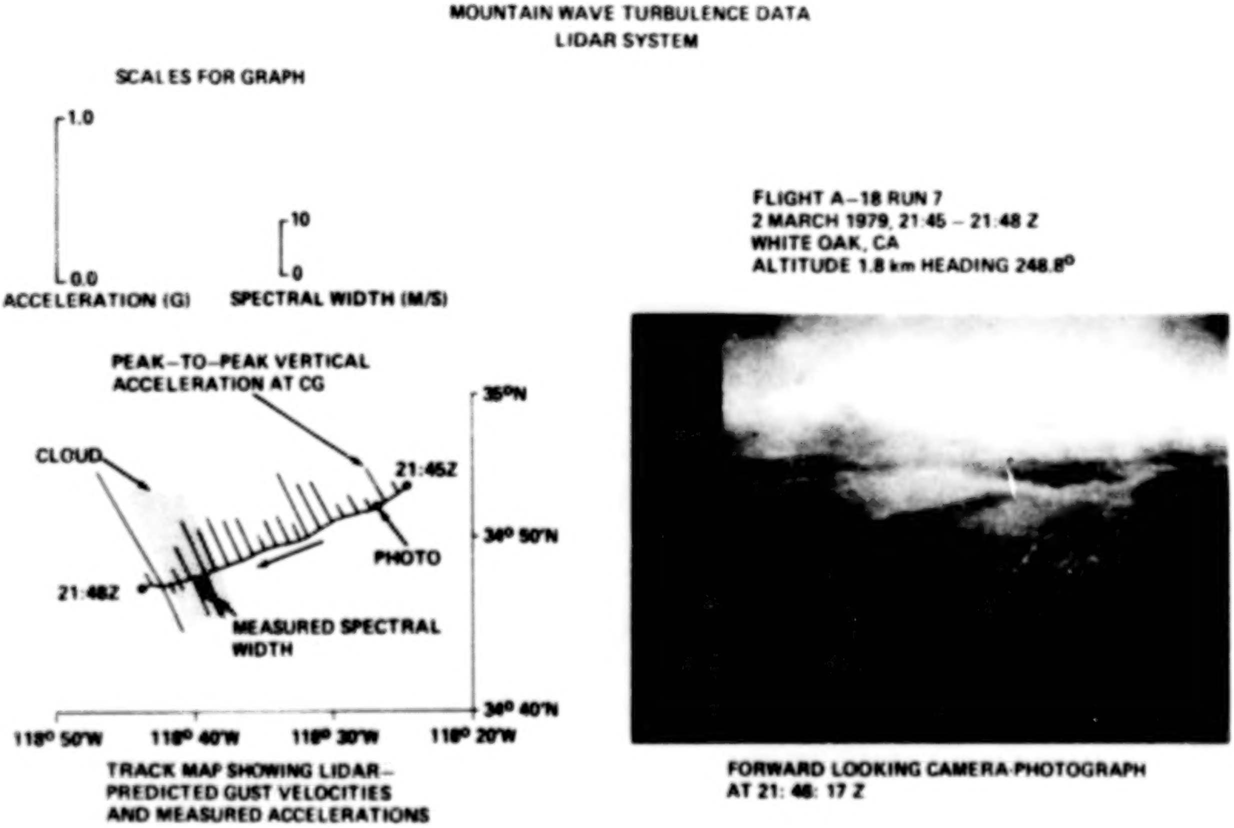
MOUNTAIN WAVE TURBULENCE DATA
LIDAR SYSTEM
SCALES FOR GRAPH
1.0
0.0
ACCELERATION (G)
10
0
SPECTRAL WIDTH (M/S)
PEAK-TO-PEAK VERTICAL ACCELERATION AT CG
CLOUD
21:45Z
PHOTO
21:48Z
MEASURED SPECTRAL WIDTH
35°N
34° 50'N
34° 40'N
118° 50'W
118° 40'W
118° 30'W
118° 20'W
TRACK MAP SHOWING LIDAR-PREDICTED GUST VELOCITIES AND MEASURED ACCELERATIONS
FLIGHT A-18 RUN 7
2 MARCH 1979, 21:45 - 21:48 Z
WHITE OAK, CA
ALTITUDE 1.8 km HEADING 248.8°
FORWARD LOOKING CAMERA-PHOTOGRAPH
AT 21: 46: 17 Z

Figure 11.- CAT and cloud turbulence encounter (lidar).

BLANK PAGE

BLANK PAGE

FLIGHT TESTS OF A CLEAR-AIR TURBULENCE ALERTING SYSTEM

Richard L. Kurkowski
Ames Research Center

Peter M. Kuhn
Raven Systems and Research, Inc.

Lois P. Stearns
NOAA-Environmental Research Laboratories

SUMMARY

Clear-air turbulence (CAT) ahead of an aircraft can be detected in real-time by an infrared (IR) radiometer. The alert time and reliability depend on the band-pass of the IR filter used and on the altitude of the aircraft. Results of flight tests, in a joint NASA/NOAA program, indicate that a band-pass of 20 to 40 μm appears optimal for alerting the aircraft crew to CAT at times before encounter of 2 to 9 min. Alert time increases with altitude, as the atmospheric absorption determining the horizontal weighting is reduced.

INTRODUCTION

Turbulence is the largest single cause of weather-related air carrier accidents in the United States. From 1962 to 1974, turbulence was either a cause of or a contributing factor in 189 of 450 weather-related cases (ref. 1). Of the 189 cases of turbulence, 68 are classified as due to clear-air turbulence (CAT). In one case in April, 1978, 11 persons were injured in a CAT encounter over Orlando, Florida.

CAT, a problem for all aircraft, cannot be seen because it usually has no cloud signature such as that evident in thunderstorm-related turbulence. CAT may develop in a standing wave caused by air moving over mountainous terrain, and is frequently associated with shear-induced Kelvin-Helmholtz (KH) atmospheric waves occurring in a statically stable atmosphere (refs. 2-4). Under certain atmospheric conditions, the character of these waves can become visible (see fig. 1). Arguments suggest that atmospheric regions characterized by internal fronts and a sloping tropopause are favored regions for KH instability and CAT formation.

Although some progress has been made in forecasting CAT, an on-board warning device is needed. Several investigators have proposed and some have flight tested on-board forward-looking CAT sensing infrared (IR) radiometers operating in the CO_2 band of the spectrum (refs. 5-8). However, these devices have been unsatisfactory because of the large number of false alarms. Presumably, this is due to the homogeneous mixture of CO_2 in the atmosphere. Some researchers suggested that CAT might be identified by the water-vapor anomalies. It is well-known that KH waves "roll up" atmospheric layers in which they form and that vertical gradients of water vapor in some regions can be as much as 20 times greater than their initial undisturbed values. A CAT sensing radiometer detecting signals in the water-vapor bands – 6.3 μm and 19.0-37.0 μm – was proposed and preliminary tests of such a radiometer system were conducted on a noninterference basis on the NASA C-141A Kuiper Airborne Observatory (fig. 2) at tropopause levels. A sketch of the aircraft flying in a CAT wave condition is shown in figure 3. Water vapor tends to concentrate in the "breaking waves" and the radiometer detects changes or gradients in water-vapor content as shown by the sample trace. This detection leads the actual encounter as shown by the accelerometer trace.

Results of these initial tests (ref. 9) to detect CAT at an altitude of 13.5 km above sea level indicated that of 51 cases, 80% were CAT alerts followed by CAT encounters, 12% were CAT alerts not followed by CAT encounters, and 8% were CAT encounters not preceded by an IR signal anomaly or CAT alert.

Based on the experience with the device used in the C-141A, a new radiometer was developed (ref. 10) specifically for use in a dedicated joint NASA/NOAA program on CAT detection research using a Learjet aircraft and, subsequently, in the NASA CV-990/CAT experiment program (ref. 11). The overall objectives of the program were to (1) study the most probable mechanisms that allow the passive detection of CAT in the water-vapor IR bands; (2) test all types of jet-level turbulence above and below the tropopause, but generally above the 500-mbar level; and (3) define a simple and reliable IR radiometer system that will alert air crews to CAT encounters 2 to 6 min before the event and one that could be built at a modest cost and that would require little maintenance.

The purpose of this paper is to present the methods and results of the on-board IR CAT detector flight-test program. The various test hardware, aircraft, and aircraft installations are described and the experimental methods are given. This is followed by the results of the flight tests for each of the test-bed aircraft: C-141A, Learjet, and CV-990.

SYMBOLS AND ABBREVIATIONS

A_o	effective detector area, cm^2
B	Planck blackbody radiance, $W/cm^2/sr$
D*	sensor detectivity, cm/Hz/W
Δf	chopping frequency, Hz
G	radiometer gain, dimensionless

g	acceleration of gravity, cm/sec^2
k	radiometer system coefficient, $W/cm^2/sr/V_o$
N	radiance, $W/cm^2/sr$
NEN	noise equivalent radiance, $W/cm^2/sr$
NEP	noise equivalent power, W
N_R	radiometer reference cavity radiance, $W/cm^2/sr$
S	slant path distance, cm
T	temperature, K
U	horizontal velocity, cm/sec
V_E	radiometer offset, V
V_o	radiometer output, V
Z	vertical distance, cm
α	radiometer half-angle aperture, deg
ν	wave number, cm^{-1}
ϕ	filter function, dimensionless
ω	solid angle, sr
θ	potential temperature, K

DESCRIPTION OF TEST EQUIPMENT

CAT Detector Sensor System

The radiance arriving at the CAT detector comes from two sources: (1) emission from the water vapor in the radiometer field of view; and (2) background emission from clouds, the air-surface interface, or hydrometers. Inhomogeneities in the water vapor crossing the radiometer cone-of-acceptance produce anomalies in the detector response and strong signal gradients which are readily detected as a sharply varying output signal. The radiance observed by the radiometer is represented by

$$N = -\int_\nu \int_s B(\nu,T)\phi(\nu) \frac{\partial \tau(H_2O)}{\partial s} \, ds \, d\nu + \int_\nu B(\nu,T_o)\phi(\nu)\tau_o(H_2O) d\nu \qquad (1)$$

Equation (1) is a representation of the radiative transfer equation. The output voltage of the CAT radiometer may be expressed as

$$V_o = \left(\frac{N - N_R}{k} \mp V_E\right)\left(\frac{1}{G}\right) \tag{2}$$

The design of the radiometer for the Learjet included a double-filter wheel arrangement. The University of Oregon/NOAA-designed filter wheel enabled the experimenters to study the ranging characteristics of several band-passes in the water-vapor spectrum. This modification, employing reststrahlen techniques, permits selection of narrower band-passes within the 20 and 40 μm ($500\ \text{cm}^{-1}$ to $250\ \text{cm}^{-1}$) spectral band. Such band-passes at, for example, 250 to $325\ \text{cm}^{-1}$, 325 to $400\ \text{cm}^{-1}$, and 400 to $500\ \text{cm}^{-1}$, were examined for CAT alert ranging. The prototype CAT radiometer flown in the Learjet experiments is shown in figure 4.

The radiometer has a noise equivalent radiance of $5\times10^{-7}\ \text{W/cm}^2/\text{sr}$ employing a blackened chopper blade as a reference and sync generator derived from a noise equivalent power of 0.12×10^{-9} W. Noise equivalent radiance (NEN) and noise equivalent power (NEP) are defined as follows:

$$\text{NEN} = \frac{\text{NEP}}{A_o \omega \phi} \tag{3}$$

where

$$\text{NEP} = \frac{1}{D^*}\sqrt{A_o \Delta f} \quad , \qquad \omega = (0.01245\ \alpha)^2 \tag{4}$$

The detector and blade were not temperature-controlled and "floated" at inside nose cone temperature. This posed no problems in flight to altitudes of 13 km (43,000 ft).

Learjet

Dedicated flight tests were conducted in 1978 using a NASA Learjet model 23 (see fig. 5). The CAT sensor was mounted in the aircraft nose beneath a special shroud (fig. 6). The radiometer was directed upward at a fixed elevation angle of from 7.5° to 15.0°. The experiment instrumentation in the Learjet cabin included a Litton model 51 inertial navigation system (INS), a computer, a data acquisition system, a vertical axis accelerometer, and a side-looking infrared true-air-temperature radiometer.

The on-board data acquisition system for the Learjet was built around the D.E.C. (Digital Equipment Corporation) LSI-II. This is a 16-bit microcomputer with 32 K words of memory. Additional memory was available on a triple floppy disk used for system, program, and data storage. The principal input-output device was a T.I. 745 terminal. A digital magnetic tape recorder was also included in the system. A basic software package was written in Fortran IV to sample the internal clock and eight channels of analog data. The accelerometer data were sampled several hundred times each second; at the end of these 1-sec intervals, maximum peak-to-peak deviations were calculated and recorded on disk or tape (or both) together with the CAT radiometer output voltage, altitude, pitch, roll, and time. The time, accelerometer peak-to-peak deviations, and radiometer output data were printed each 10 sec on the 745 terminal. The system of software included CAT forecast algorithms for real-time use of data flights as well as INS position and wind data. Several CAT forecast algorithms were programmed and examined for on-board CAT alert. These included: (1) a second-difference alert algorithm, (2) an arc-length alert algorithm, and (3) a standard-deviation alert algorithm.

Convair 990 and C-141A

Additional data were taken in the first quarter of 1979 on the Convair 990 Galileo II (fig. 7) during the NASA clear air turbulence missions (ref. 11). Concurrently with those missions and subsequent to them, data were also obtained during routine C-141A Kuiper Airborne Observatory missions.

The infrared radiometer sensor system flown on the CV-990 and on the C-141A had the characteristics shown in table 1. As stated previously, the operating spectral range is in the water-vapor band, that is, 20 to 40 µm. It is a passive device similar to forward-looking infrared (FLIR) sensors.

The location of the IR radiometer CAT detector sensor on-board the CV-990 is shown in figure 8. Figure 9 shows a close-up of the probe tube enclosing a gold-plated right-angle mirror, as mounted in the left-forward passenger window for the experiment. The elevation angle of the radiometer was kept constant at 10°. A similar installation was mounted in the sidewall of the C-141A above the main landing gear. Figure 10 shows the sensor device and chopper system, which are mounted inside the aircraft. The sensor device is about 15 cm in diameter and 18 cm in length. A diagram of the system is shown in figure 11. The radiometer sensor signals that pass through the optics section are fed to the radiometer amplifier. The signals are analyzed in the signal processor, which contains the algorithms related to output signal anomaly and CAT threshold alerting. The experimenter had the option of varying the signal processing, including variable threshold levels, during the flight. When the signal activity threshold is exceeded an alert is displayed on the experimenter's console.

All CV-990 accelerometer data were recorded at 50 Hz, and radiometer sampling data were recorded at 10 Hz. The C-141A data were logged at varying frequencies.

EXPERIMENTAL METHOD

CAT Alert

A CAT alert may be defined as a warning that CAT is ahead of the aircraft along its projected flight path. False alarms from the IR detector system may be caused by several factors. They may occur because of aircraft motion within the turbulence, by the aircraft being in a roll or turn, and by cirrus clouds or contrails. They may also be caused by electromagnetic interference (EMI) disturbing the radiometer signal and, finally, by a water-vapor disturbance that is not associated with turbulence. False alarms caused by the aircraft in turbulence, in a turn, or EMI were eliminated from the statistical analyses since these could be suppressed in a system for commercial aircraft.

Turbulence Encounter

An encounter is a function of the acceleration imposed on the aircraft by CAT and the time separation between CAT areas. Factors such as the size and speed of the aircraft change the way the aircraft reacts to turbulence. The accelerometer mounting location also affects the recorded peak-to-peak values of the turbulence. Turbulence is measured in g's (gravity values over the normal 1 g). The accelerometer numerical value was derived by taking the maximum g value of each of the 50 tape samples less the minimum value during each second. The net difference was called the "peak-to-peak" accelerometer value. For example, the accelerometer on the C-141A was mounted on the floor of the jet a little to starboard of center. Normal vibration of the aircraft does not exceed 0.02 g's. Originally, an arbitrary 0.1 g was used to define turbulence, but in checking alarms for a possible cause, it was discovered that many alerts were forecasting 0.07, 0.08, and 0.09 g's of CAT with the same vigor as a 0.2 g encounter. It was therefore decided that 0.05 g's would be defined as an encounter on the C-141A aircraft. Since encounters on this aircraft were fairly isolated, only encounters that were separated by 3 or more minutes were considered. (For a commercial version of this instrument, the experimenters believe 30 to 40 sec should be used as the minimum time interval between encounter alerts.)

The accelerometer was mounted on the floor of the Learjet near the center of gravity. The Learjet flies at greater speeds and is a lighter wing-loading aircraft than the C-141A. Consequently, it may react more strongly to a CAT encounter. The value of 0.15 g was assigned as the magnitude of an encounter for this aircraft. Various time interval criteria between CAT encounters were used.

The CV-990 accelerometer was mounted on the floor of the aircraft near the center of gravity. The value of 0.10 g peak-to-peak was assigned as the magnitude for an encounter for the CV-990. A minimum of 30 sec was used to separate encounters or false alarms, if they occurred.

Alert Algorithms

An algorithm is a procedure for solving a mathematical problem that involves a repetition of an operation. Three algorithms were evaluated for processing radiometer voltage to signal a CAT alert. They were arc-length ratio, standard deviation, and a second-difference manipulation. Each algorithm could accept a predetermined number of radiometer voltages and, after computation, compare the results to a threshold value. On the basis of the comparison the computer either signals a CAT alert condition or rejects the results as being below the CAT alert threshold. The threshold itself is the numerical minimum point or boundary at which the effect of subsequent CAT is alerted. This threshold is a value that represents a delicate balance between alerting the observer to as many of the CAT encounters as possible without allowing more false alarms than desired. It had to be experimentally determined for each algorithm in each aircraft.

FLIGHT TEST RESULTS

Learjet Flights

Selection of filters- IR transmission is a strong function of wavelength. The radiometer senses radiant emission in the water-vapor band from varying distances depending on the band-pass of the water-vapor filter. One way of determining the optimum range or "look" distance of the CAT radiometer is to examine a weighting function, which is defined as the derivative of transmittance with respect to the natural logarithm of distance. By selecting the proper filter we can adjust the "range" for the radiometer (which also depends on the altitude). The filters found to give best radiometer performance at 200 mbars (about 12 km (40,000 ft)) were BaF_2 (barium fluoride), SrF_2 (strontium fluoride), and CaF_2 (calcium fluoride). Figure 12 illustrates the calculated weighting function of the three filters used in the Learjet flight experiments. Figure 13 shows the measured band-pass response for the three types of filters. Flight research with this three-filter system began in January, 1978. Because flight data of filter comparisons showed that the SrF_2 filter gave large signal standard deviations and had a longer alert time than the other two filters, it was chosen as the prime filter for further testing.

Encounter data- Approximately 46 hr of flight testing of the CAT detector IR system were completed during the winter 1977-spring 1978 "CAT season." Most of the data flights were conducted in the Denver, Colorado, area, where mountain waves frequently cause clear-air turbulence. Data were acquired at various altitudes from 4.5 to 14 km (15,000 to 45,000 ft).

For these initial Learjet flights, the purpose was to test different filters for optimum reliability and to check on the validity of theoretical time calculations for alerts as they vary with altitude. Turbulence was encountered on about 62 occasions. CAT encounters were defined as aircraft vertical acceleration disturbances of 0.15 g or greater (peak-to-peak). No encounters were considered within turns or during the time when the computer was off. In computing alerts, resetting was necessary when a crystal was changed, when an offset was changed, after an encounter was over, and after a turn was completed. Altitude changes did not affect the alert system except in takeoff and steep descents for landing. A reset was necessary upon reaching initial flight altitude.

The g levels of CAT encountered for 56 cases were as follows: 41 were at 0.15 to 0.29 g; 10 were at 0.30 to 0.48 g; and 5 were at 0.50 g or above.

The alert scores for the flight tests on the Learjet, using the standard deviation algorithm, were as follows:

CAT alert	CAT encounter	Cases	Percent
Ability to predict encounters			
Yes	Yes	60	97
No	Yes	2	3
Totals		62	100
True/false alarm rate			
Yes	Yes	58	62
Yes	No	36	38
Totals		94	100

The Learjet radiometer was directly responsible for the large false alarm rate since the electronics displayed a small signal-to-noise ratio. The water-vapor disturbances caused by CAT overrode this effect, thus not changing the true alarm data. However, the abnormally high false alarm rate can be directly traced to the radiometer. Appropriate electronic modifications were made subsequent to these missions.

C-141A Flights

Encounter data- Initial flight experiments onboard the C-141A aircraft made it evident that a broad band-pass (19 to 37 μm) radiometer could predict subsequent turbulence encounters. A report on the initial experiments is contained in reference 9. Figure 14 shows the results obtained in 194 CAT encounters through September, 1977, for flights at an MSL altitude of 13.5 km. The data show that when using an alert algorithm based on standard deviation of the radiometer signals, 80% of the CAT encounters were predicted 6 min beforehand. The false alarm rate was 6% (a false alarm is defined as a predicted encounter that did not occur). The distribution of encounter levels in terms of peak-to-peak g acceleration is shown. The range of acceleration levels for light, moderate, severe, and extreme CAT, used for analysis, is also shown in figure 14. As would be expected, most of the encounters were classified as light or moderate. (The primary mission of the C-141A, i.e., astronomical observations, requires flight in "smooth" air, if possible, and flights are planned accordingly. In addition, most flights are at very high altitudes, well above most weather phenomena.) Results of the early airborne field trials showed that the system does achieve the desired accuracy.

In later flights, additional information was obtained regarding false alarms. In particular, during June and July, 1979, four missions were examined during no-turbulence flight using the arc-length algorithm. (The C-141A in its routine astronomy missions is airborne at a constant altitude for about 6 hr per flight. A small portion of this time is devoted to turning the aircraft so that the astronomer can track his scheduled targets. Much of the flight time, especially in the summer months, is during periods of no turbulence.) Table 2 is a summary of the no-turbulence data that were accrued during the four missions. Only segments of at least 30 min of no turbulence were considered. On June 20, during a 0.5-hr "quiet period," 3 of 5 false alarms can be associated with whispy cirrus; similarly, on July 29 during a 2.5-hr quiet period, there were 11 false alarms that can be associated with cirrus. These clouds were verified by both satellite and water-vapor radiometer readings. Thus, the net clear air flight time is 13.5 hr with 4 false alarms, or about 1 false alarm in 3.4 hr.

Performance of alert algorithms- As stated, three algorithms were studied in the program for use as CAT alerts: running calculations of standard deviations, second-difference, and arc length. Data from the C-141A were used to evaluate these algorithms. Success/false alert statistics for the three algorithms for the 194 cases were as follows:

	Alert		False alert	
	No.	Percent	No.	Percent
Standard deviation	155	80	12	6
Second-difference	134	69	12	6
Arc length	159	82	16	8

The arc length works well but is somewhat sensitive to period chosen (12 sec at 1 data point/sec was selected). The second-difference is very sensitive to the time span chosen. The standard deviation shows good performance and is insensitive to time spans for periods of 12 sec or more. The standard deviation algorithm seems to be the optimum method.

Effect of altitude on alert time- Figure 15 is a graph of the maximum times at which the Learjet and C-141A were alerted before encounters at various altitudes. A curve was plotted through the maximum data down to 5.8 km (19,000 ft). It is not a linear curve since the water-vapor transmission is not linear. The envelope created represents a small number of points and should be considered only representative. It is composed of data points from moist and dry days and thus reflects different atmospheric transmission characteristics. As shown, alert time decreases with decreasing altitude; however, an alert signal is still possible at over 2 min before the encounter at 5.8 km (19,000 ft).

CV-990 Flights

Encounter data- The data flights of the CV-990 were dedicated to the study of clear air turbulence. The aircraft crew and scientists looked for and found turbulence. The flight altitudes ranged from 4.4 to 11.3 km (14,500 to 37,000 ft). During the 30 missions and 140 hr of flight, 94 CAT alerts were given by the system and 80 separate segments of turbulence encounters were documented. Only 4% of the encounters were not preceded by an alert. Of the 94 alerts, 18% were false, that is, they were not followed by a turbulence encounter.

A diagram of the "scores" from the CV-990/CAT experiment with regard to the IR radiometer system is shown in figure 16. Other results from the experiment were as follows:

1. The device was found to give satisfactory alerts at all flight levels above an msl altitude of 4.4 km (14,500 ft).

2. Turbulence was detected at distances up to 60 km (37 miles) ahead of the aircraft. (This range can be varied by changing optical filters.)

3. The envelope of maximum alert time varied from 1 min at an altitude of 4.4 km (14,500 ft) to 4 min at 11.3 km (37,000 ft).

Analysis- The emphasis in the CV-990 data analysis was on answering the following questions:

1. Which sample rate (frequency) of the radiometer is optimum?

2. Which algorithm yields best results?

3. What time period (or number of points) yields the optimum algorithm score?

4. Are the new electronics adequate to significantly decrease the false alarm rate?

Analysis of the data led to the following answers:

1. The radiometer voltage sample rates that yield acceptable results are one and two samples per second. More frequent sampling with the use of either the standard-deviation or arc-length algorithm gives poor results.

2. Either standard deviation or arc length yield excellent forecasts and minimal false alarms. However, standard deviation seems to cause an alert to be given to some of the more severe events that the arc-length algorithm overlooks; consequently, it is recommended. A combination of the two does not improve the forecast score, however, since most of the turbulence encounters are predicted and a very small increase in the prediction is offset by a larger increase of false alarms. Therefore, either algorithm is recommended, but with the standard-deviation algorithm somewhat preferred.

3. At a sample rate of 1 sample per 2 sec, a sample-size choice of either 6 or 30 points yields the best forecast before an alarm. This may be less desirable than the 12 sec of $N = 6$. If one sample per second is used, $N = 5$ yields excellent results.

4. The improved electronics had a significant effect on the reduced false-alarm rate compared to the Learjet data.

ONGOING AND SUGGESTED FURTHER STUDY

Further study is under way wherein NASA pilots will evaluate the system during the 1980-81 CAT season (roughly November through March) during regular operations of the C-141A and CV-990 NASA flying laboratories. In addition, United Airlines and the Colorado Air Guard are considering independent evaluations of this type of CAT alert system.

Four alternatives seem worthy of further investigation to improve the detector system. They are:

1. Use a narrower field of view in the radiometer.

2. Scan in a forward mode.

3. Obtain a mosaic of the water vapor ahead of the aircraft by changing the type of detector (still within the same band-pass).

4. Use a discriminating detector.

The first of these alternatives is the least expensive. It may not improve the system; nevertheless, it should be investigated. The second alternative would add to the cost of the radiometer on a commercial level, but probably would be more effective. The third would be the most desirable, but would cost a great deal to research; however, the ultimate cost to the consumer would be almost the same as the second alternative. The microprocessing equipment may be more complex due to the pattern-identification capabilities. The fourth alternative would again require a special detector capable of looking at two forward points. This would achieve a scan-like discrimination on a small scale and would be more economical than a scanning radiometer.

SUMMARY AND CONCLUSIONS

Clear-air turbulence was detected and the air crew alerted at least 80% of the time that CAT was encountered during the studies; moreover, the alert may be signaled as many as 2 to 9 min before encounter, depending on aircraft flight level. At this time, no correlation was found between the intensity of alarm and the intensity of encounter. Also, no correlation was found between the frequency of alarm and intensity of encounter. Radiometer voltages recorded at the rate of one per second showed a slightly better alert rate than those recorded at the rate of two per second. Thresholds for alerts depend on the gain of the radiometer. They also vary slightly with the amount of moisture present. Clouds have a strong effect on the false-alarm rate of the CAT detector system. If nonturbulent (dissipating, lenticularis, or whispy cirrus) clouds are present, one may expect about one false alarm per hour. If the atmosphere is cloudless, the expectation of false alarms should not exceed a maximum of one every 3 or 4 hr. It may be concluded that the radiometer has been shown to be an effective clear-air-turbulence detecting device when cloud effects are eliminated.

REFERENCES

1. Airline Pilot (Technical Talk), vol. 46, no. 4, April 1977, p. 38.
2. Patnaik, P. C.; Sherman, F. S.; and Corcos, G. M.: A Numerical Simulation of Kelvin-Helmholtz Waves of Finite Amplitude. J. Fluid Mech., vol. 73, 1976, p. 215.
3. Reiter, E. R.: Stratospheric-Tropospheric Exchange Processes. Rev. Geophys. Space Phys., vol. 13, 1975, pp. 459-474.
4. Possiel, N.; and Scoggins, J. R.: Curvature of the Wind Profile in the Troposphere Versus Regions of CAT and non-CAT in the Stratosphere. Mon. Weather Rev., vol. 104, 1976, pp. 57-62.
5. Collis, R. H.: Method and System for Detecting Clear Air Turbulence. U.S. Patent 3,696,670, 1972.
6. Smith, S. D.; and Houghton, J. T.: Radiometer Apparatus. U.S. Patent 3,498,132, 1970.
7. Anderson, H. C.: A Measuring System. U.S. Patent 3,056,958, 1962.
8. Astheimer, R. W.: The Remote Detection of Clear Air Turbulence by Infrared Radiation. Applied Optics, vol. 9, Aug. 1970, pp. 1789-1797.
9. Kuhn, P.; Caracena, F.; and Gillespie, C. M., Jr.: Clear Air Turbulence: Detection by Infrared Observations of Water Vapor. Science, vol. 196, 1977, pp. 1099-1100.
10. Kuhn, P. M.: Improved Method and Apparatus for Detecting Clear Air Turbulence. U.S. Patent Application 950,943, Oct. 1978.
11. Weaver, Edwin A. et al.: The 1979 Clear Air Turbulence Flight Test. 1980 Aircraft Safety and Operating Problems, NASA CP-2170, 1981. (Paper 16 of this compilation.)

TABLE 1.- CV-990 AND C-141A AIRCRAFT RADIOMETER SPECIFICATIONS

Performance data	
Operating spectral range	20 to 40 µm
Cavity reference temperature	-20° C
Output voltage	+10 Vdc to -10 Vdc
A to D conversion	12 bit (5 mv/bit)
Noise equivalent power	2.5×10^{-8} W
Response time (time constant)	50 Hz
Optical data	
Detector type	1- by 1-mm lithium tantalate chip
Optical filter	band-pass, 20-40 µm

TABLE 2.- C-141A: NO-TURBULENCE AREAS DATA

Date, 1979	Cirrus included		Cirrus excluded	
	Duration, hr	No. false alarms	Duration, hr	No. false alarms
June 20	3.5	5	3.0	2
July 11	2.5	5	2.5	0
July 13	6.5	0	6.5	0
July 29	4.0	13	1.5	2
	16.5	18	13.5	4

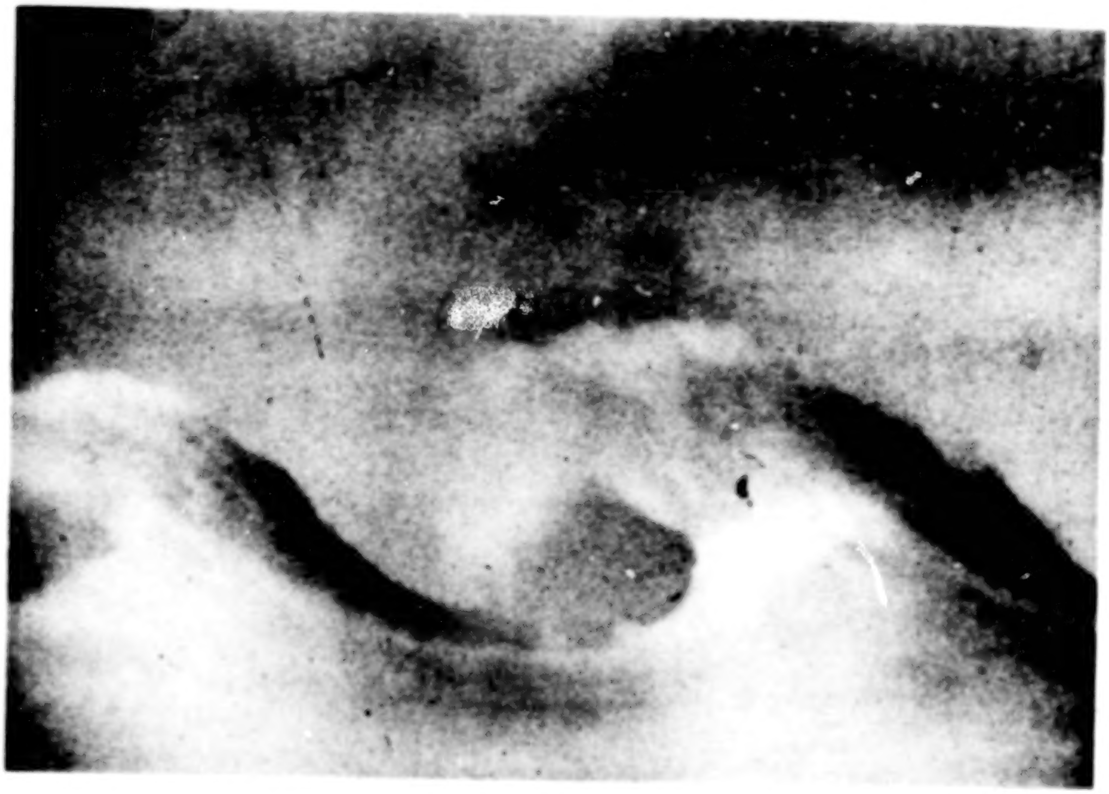

Figure 1.- Kelvin-Helmholtz atmospheric wave.

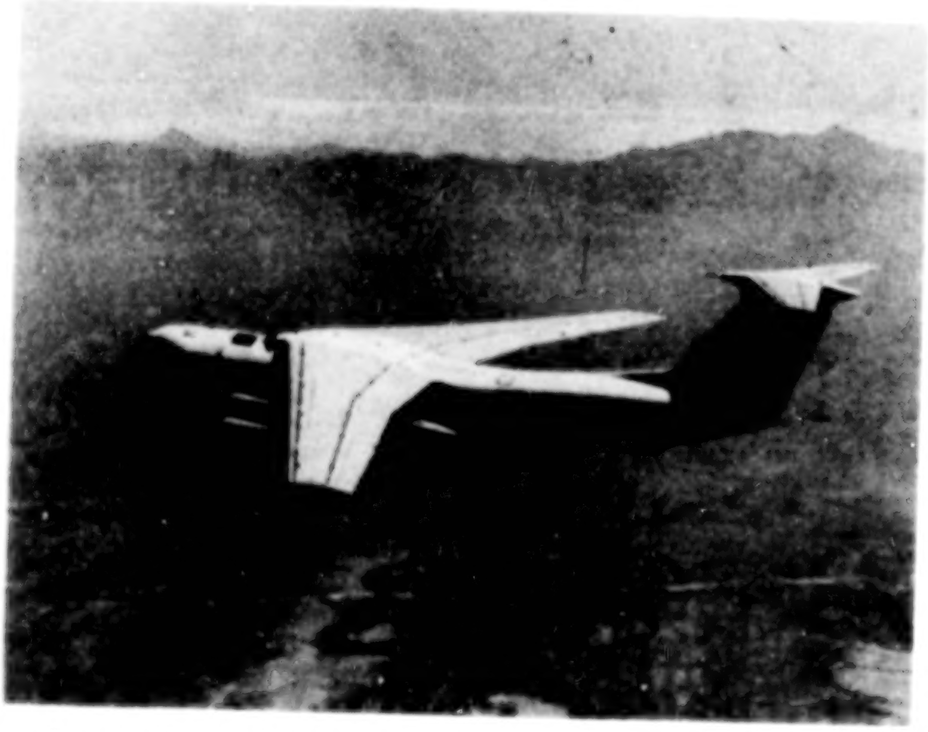

Figure 2.- NASA C-141A Kuiper Airborne Observatory.

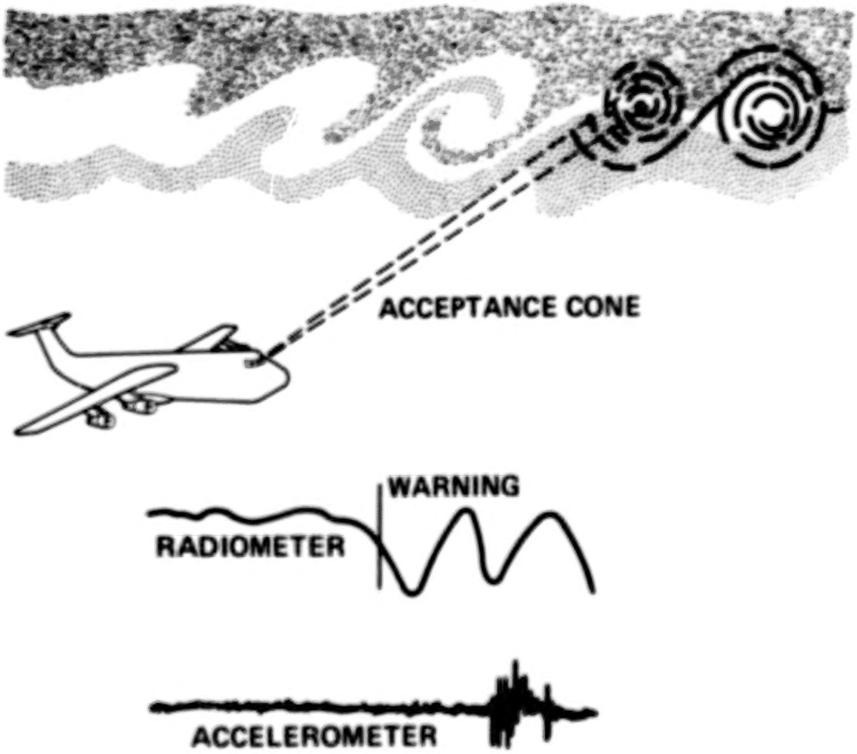
ACCEPTANCE CONE
WARNING
RADIOMETER
ACCELEROMETER

Figure 3.- CAT detection.

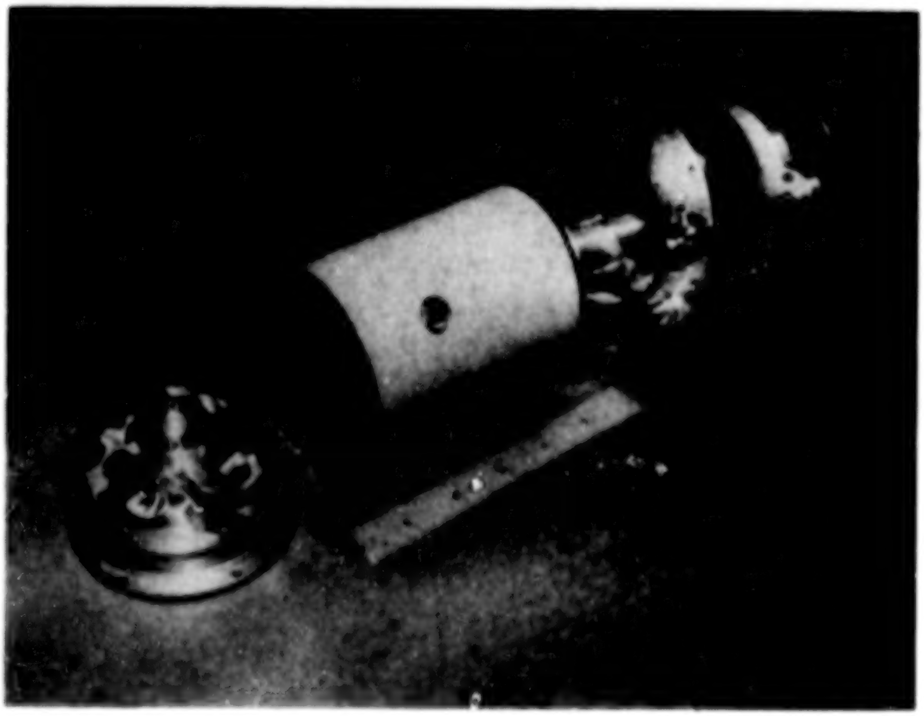

Figure 4.- CAT radiometer used in Learjet tests.

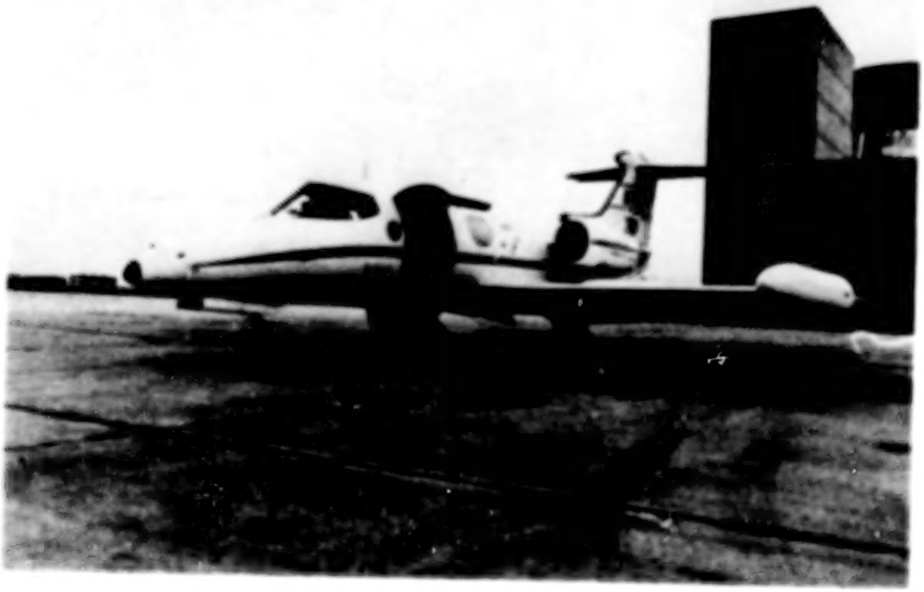

Figure 5.- NASA Learjet model 23.

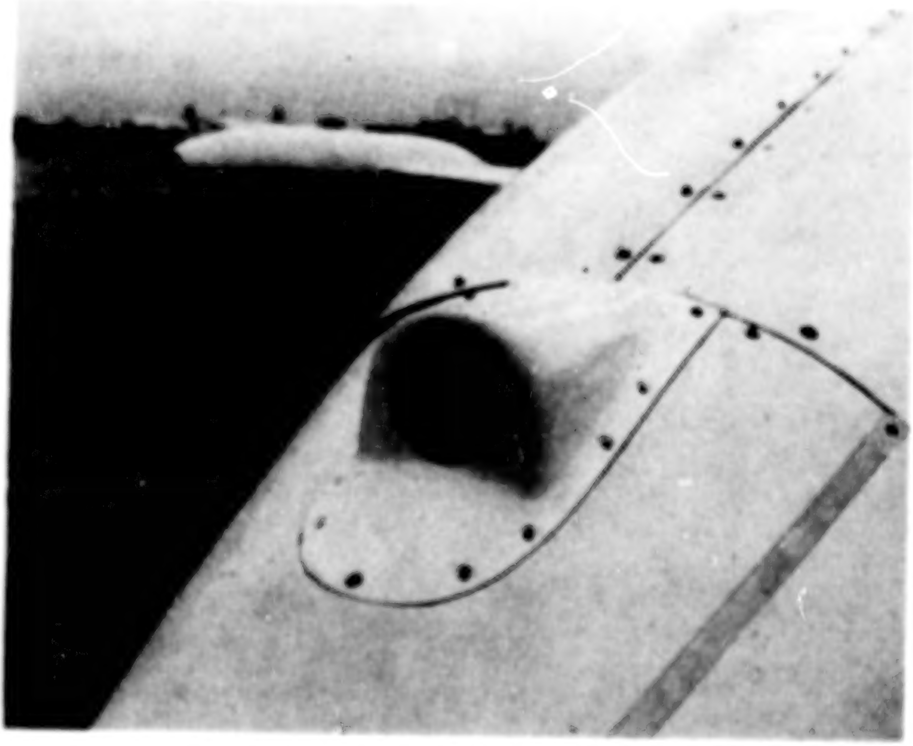

Figure 6.- CAT sensor installation on the Learjet.

Figure 7.- NASA Convair 990, Galileo II.

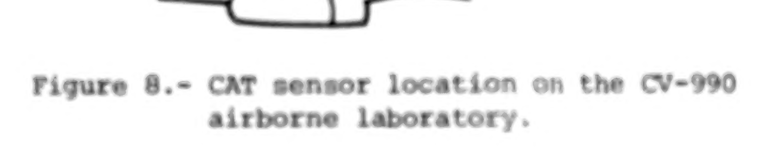
IR RADIOMETER CAT SENSOR
NASA

Figure 8.- CAT sensor location on the CV-990 airborne laboratory.

Figure 9.- CAT sensor installation on CV-990.

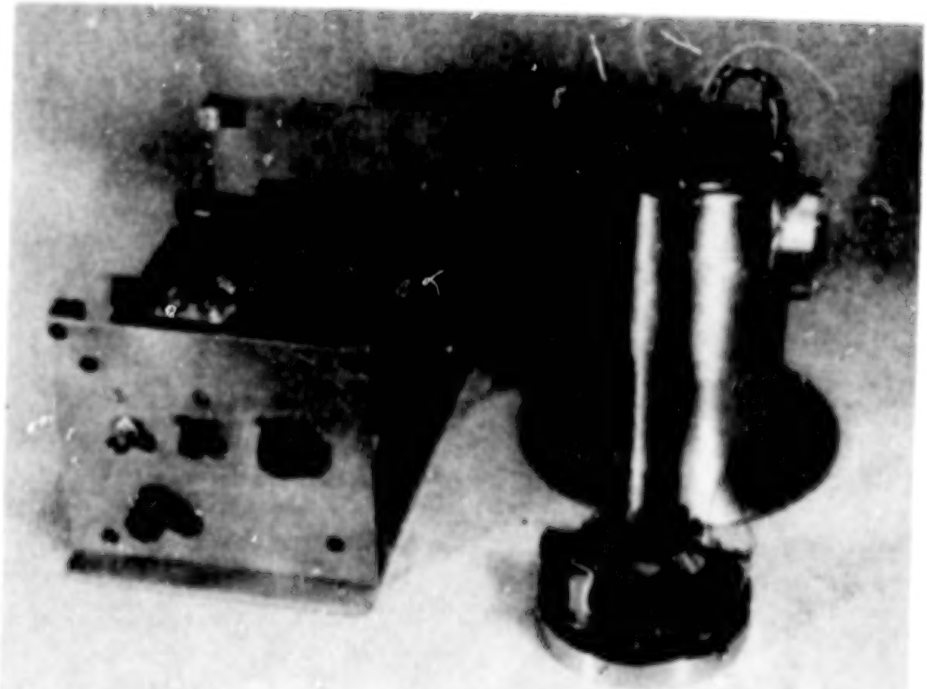

Figure 10.- CAT sensor device and chopper system.

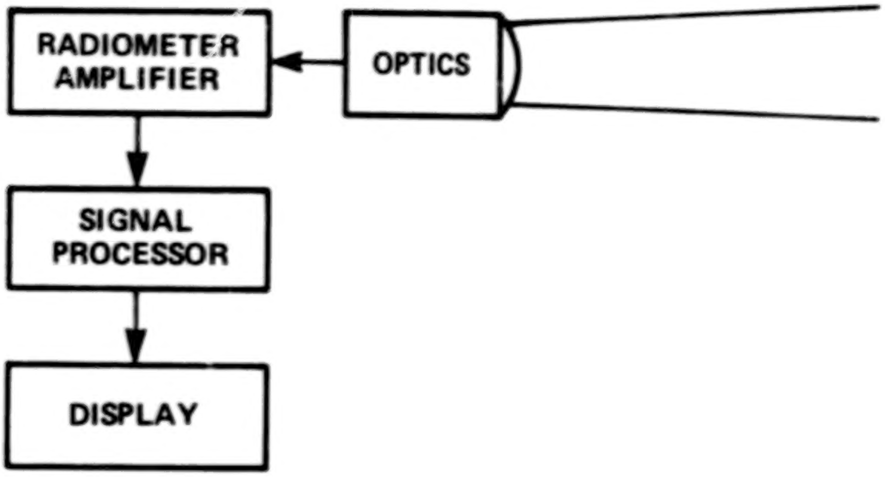
RADIOMETER AMPLIFIER
OPTICS
SIGNAL PROCESSOR
DISPLAY

Figure 11.- Infrared radiometer CAT detector system diagram.

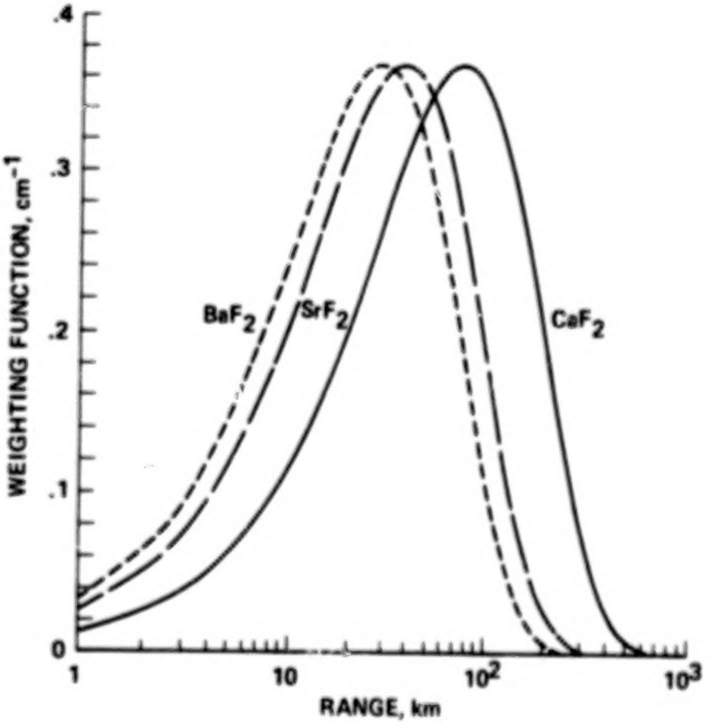

Figure 12.- Filter weighting functions.

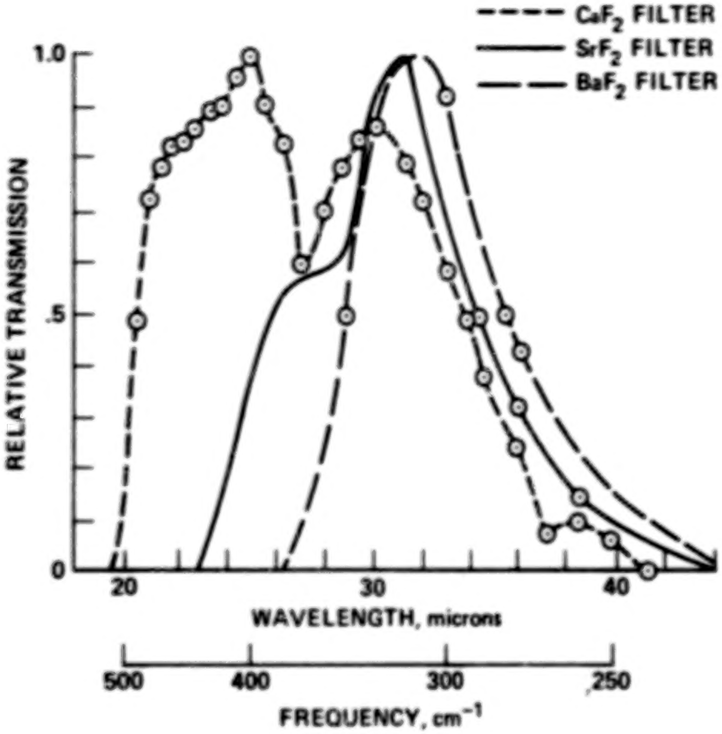

Figure 13.- Measured filter response.

• ABILITY TO PREDICT ENCOUNTER			
CAT ALERT	CAT ENCOUNTER	CASES	%
YES	YES	155	80
NO	YES	39	20
		194	100
• TRUE/FALSE ALARM RATE			
CAT ALERT	CAT ENCOUNTER	CASES	%
YES	YES	155	94
YES	NO	10	6
		165	100
• ENCOUNTER LEVELS			
G LEVEL		CASES	%
LIGHT (0.15 < 0.30)		155	80
MODERATE (0.30 < 0.50)		36	19
SEVERE (0.50 < 1.0)		3	1
EXTREME (> 1.0)		0	0
		194	100

Figure 14.- Encounter prediction statistics: C-141A data; MSL altitude 13.5 km (44,290 ft).

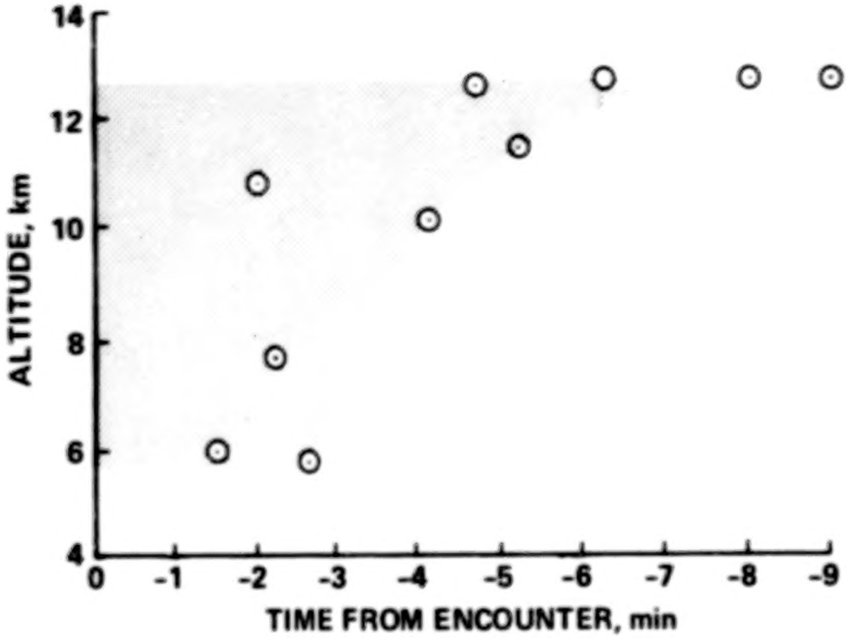

Figure 15.- Onset of alert before an encounter envelope.

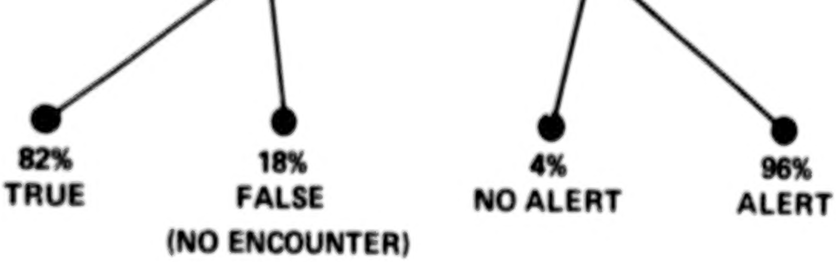
DATA BASE
30 MISSIONS
140 hours
94
ALERTS
80
ENCOUNTERS
82%
TRUE
18%
FALSE
(NO ENCOUNTER)
4%
NO ALERT
96%
ALERT

Figure 16.- Infrared radiometer CAT detector:
CAT/CV-990 flight-test results.

BLANK PAGE

BLANK PAGE

CLEAR AIR TURBULENCE STUDIES WITH MICROWAVE RADIOMETERS

Bruce L. Gary
Jet Propulsion Laboratory

SUMMARY

Two passive microwave radiometers were flown on the Ames CV-990 aircraft during the 1979 Clear Air Turbulence Mission (see reference 1 for a mission description). A 55.3 GHz radiometer was used to measure "altitude temperature profiles", and a 180 GHz radiometer was used for monitoring line-of-sight integrated water vapor content. The measurement of altitude temperature profiles was motivated by the suggestions that: 1) CAT (Clear Air Turbulence) is often found within inversion layers (Haymond, unpublished[1]) and at the tropopause, and 2) CAT severity is related to the static stability (lapse rate) of the layer within which the turbulence is generated (Haymond). The water vapor measurements were motivated by the recent success of Dr. Peter Kuhn (Reference 2) in providing warnings of CAT encounters using an IR sensor that responds to line-of-sight water vapor content. The microwave counterpart has the advantage of not being subject to the confusing influence of cirrus clouds.

INTRODUCTION

It is desirable that a CAT (Clear Air Turbulence) warning system provide the answer to three questions: when, how severe, and how to avoid. The bulk of previous sensor development has been devoted to answering "when", and usually in a qualitative manner (i.e., "soon", or "not soon"). A convincing flight demonstration of severity forecasting and avoidance guidance has not yet been conducted. To the author's knowledge, no CAT sensor is in operational use at the present time.

The intent of the 55.3 GHz sensor evaluation, which will be described briefly here, is to develop a severity forecasting and altitude avoidance capability. The intent of the 180 GHz sensor evaluation is to develop an "improved" (cirrus insensitive) version of the IR CAT warning sensor that is being flight-tested by Dr. Kuhn.

---

[1] High Altitude Clear Air Turbulence, 9WS Tech. Rep. #2, 1967, by F. Haymond.

55.3 GHz MEASUREMENTS

The 55.3 GHz radiometer is a modified version of the NIMBUS-6 SCAMS (Scanning Microwave Spectrometer) instrument. Measurements of sky brightness temperature were made at a sequence of elevation angles spaced 4 degrees apart and extending from -16 degrees to +20 degrees. Aircraft-generated parameters were measured every 2 seconds (roll, pitch, pressure altitude, static air temperature, and vertical accelerometer output). The instrument was mounted inside the cabin, with a view through a specially designed microwave-transparent window.

Sky brightness temperatures measured by the 55.3 GHz radiometer are related to the physical temperature of the oxygen molecules along the viewing direction, range-weighted in accordance with an e-folding distance of about 3-kilometers. Elevation angle scanning moves the "applicable altitude" above and below the aircraft altitude in accordance with: h=3km*sin(elevation). As a first approximation, air temperature versus altitude can be estimated from the plot of sky brightness temperature versus elevation angle, with the elevation angle re-scaled to correspond to "applicable altitude". The altitude coverage is typically 1500 m (5000 ft), centered on the aircraft altitude. The altitude resolution is approximately 10% of the altitude coverage (for the instrument described here). This is sufficient for the detection of most inversion layers with thickness exceeding 300 m (1000 ft).

Figure 1 is an example of "altitude temperature profiles" generated from the 55.3 GHz radiometer measurements in the manner described above. The left panel is the most commonly observed profile, exhibiting lapse rates (slopes) of about -7 K/km. Occasionally, the dry adiabatic lapse rate of -9.5 K/km is observed. The right panel was taken while flying within an inversion layer. Note how it is possible to read off the altitudes of the lower and upper boundary of the inversion layer. It is also possible to estimate the lapse rate within the inversion layer. Panels like these are obtained every 17 seconds of flight (3.5 km). It is therefore possible to monitor the various properties of the inversion layer, and to characterize it as unchanging or changeable.

INTERPRETATION OF 55.3 GHz MEASUREMENTS

Layers of air that exhibit an adiabatic lapse rate are unable to sustain wind shear. Sub-adiabatic layers (including inversion layers) are able to support wind shear. It is commonly thought that vertical wind shear is the energy source for the turbulent motions associated with CAT. Since large values of wind shear represent a large reservoir of energy for the production of CAT, it is natural to postulate that CAT severity bears a relationship to the magnitude of the wind shear within the layer. Since large values of wind shear can only exist within layers having large, positive lapse rates (i.e., inversion layers), it is natural to suppose that the most severe CAT will be found within inversion layers. Moreover, the greater the lapse rate of the inversion layer, the greater the severity of any ensuing turbulence. These predictions are supported by the measurements of Haymond (Ref. 1), who analyzed 4000 sorties of U2 aircraft, flying above the tropopause. It is important to independently verify these findings, especially for flight below the tropopause. The 55.3 GHz sensor is ideal for such an investigation.

The right panel of Figure 1 is one of a sequence covering a half-hour period. A case study analysis of this data set has been conducted and will be published elsewhere. To summarize, the inversion layer supported a wind shear of 28 knots, averaged 400 m (1300 ft) in thickness, and was generally isothermal when it was 400 m (1300 ft) thick. If it is assumed that the wind profile compressed and expanded as the temperature field defining the inversion layer compressed and expanded, then it is possible to calculate a Richardson number for each hypothetical thickness (Richardson number, Ri, is the ratio of stabilizing forces to overturning forces, or Ri = "potential temperature lapse rate" divided by "wind shear squared"). In this way, it is calculated that when the layer is thinner than about 210 m (700 ft), Ri will be <0.25, which is a theoretical precondition for growth of wind shear driven instabilities. The layer was observed to vary in thickness from a high of 760 m (2500 ft) to a low of 120 m (400 ft) (briefly). When it was at its shallowest, "nibbles" of turbulence were noted. Unfortunately, the aircraft 120 m below the inversion layer when these conditions occurred, and it can only be speculated that the turbulence originated, and was more severe, within the inversion layer.

The observations described in the previous paragraph are significant in several respects. First, the behavior of the inversion layer supports the theoretical portrayal of CAT being formed by the breakdown of Kelvin-Helmholtz waves, which are driven past their stability limit by conditions associated with decreasing Richardson number (to the $<1/4$ region). Second, inversion layers that are very dynamic do not always produce CAT. In other words, CAT sensors that base their "when" warnings on variability of the remotely sensed temperature field must contend with the false alarm problem. Third, if a CAT "when" warning sensor is ever found acceptable for operational use, a radiometer similar to the 55.3 GHz sensor could be deployed for the altitude location of nearby inversion layers, which could then serve for any evasive actions that the pilot deems necessary. It is important to learn how often inversion layers are the source of CAT, or else altitude changes for their avoidance would be fruitless.

During the 1979 CAT Mission there are many instances when CAT was found within inversion layers. On some occasions, during ascents or descents, there is a remarkable association between turbulence intensity and inversion layer location. However, there are many cases where CAT was encountered when the 55.3 GHz sensor did not show the presence of an inversion layer. Many flight hours were spent at low altitudes, near ridge level, searching out topography-generated turbulence. Under these circumstances, inversion layers would not be related to the origin of the turbulence in the same way that can be expected for cruise altitude events. A systematic study of the statistical association of CAT encounters with inversion layer locations will have to be conducted. Although such a study will be performed on the 1979 CAT Mission data in hand, a more definitive analysis should be available in 2 or 3 years, when a highly improved version of the 55.3 GHz radiometer is deployed for a more extensive evaluation on NASA's C-141 aircraft.

180 GHz MEASUREMENTS

The 180 GHz radiometer was borrowed from a different project, and has been described in Reference 3. The wide bandwidth channel was used during the 1979 CAT Mission. The radiometer was mounted inside the cabin, with a view through a microwave transparent window (high-density polyethelene, with 1/4 wave grooves). The viewing direction was 12 degrees elevation and 50 degrees right of forward. The antenna beamwidth was 5 degrees. The radiometer output was gated every 2 seconds, and the sensitivity was typically less than 1 K. At the frequency of 180 GHz, the atmosphere is approximately 50% transparent at an altitude of 6 km (20 000 ft) (for the viewing direction used). At 180 GHz, the principal source of opacity (and, hence, emission) is molecular water vapor. Roll compensation was not applied, which greatly complicated the task of extracting atmospheric related variations. Small frequency drifts occurred at random times, creating gain drifts, which occasionally complicated isolation of atmospheric effects. It should be noted that radiometers for operation at frequencies as high as 180 GHz are difficult to build, and their state of the art is improving rapidly.

The basis for Dr. Peter Kuhn's CAT warning capability is that shear-driven Kelvin-Helmholtz waves disturb the flatness of an interface separating overlying air masses that are characterized by different absolute humidities (Ref. 2). The variations in line-of-sight water vapor which are measured by an IR sensor in an aircraft that is underflying the interface region are revealing a process that is intimately related to the generation of CAT. I have suggested (Ref. 4), using simple geometrical arguments, that if warning times of several minutes can be generated from viewing directions that are inclined upward by 7 degrees and greater, there must be an annulus of disturbed air, surrounding the CAT region, that is recognized by the IR CAT sensor. The IR CAT sensor, in other words, issues its warning before its viewing cone intercepts that part of the air containing the CAT.

The reasoning described in the previous paragraph convinced us that, in spite of the off-forward viewing direction (that an inside-the-cabin installation would require), a fair evaluation might still be possible of the merits of a 180 GHz sensor as a forecaster of CAT encounters if it were included in the 1979 CAT Mission. As stated in the introduction, the motivation for installing and operating the 180 GHz radiometer is that it would not be subject to the confusing influence of cirrus clouds, which leads to false alarms for the IR CAT sensor. The scattering and absorbing cross section of ice crystals is orders of magnitude smaller at 180 GHz than at 30 microns, where the IR CAT sensor operates.

RESULTS OF 180 GHz MEASUREMENTS

As expected, cirrus clouds had no noticeable effect on the 180 GHz radiometer output. This much had been demonstrated on previous flights by Waters (private communication, 1977).

A few of the 100 total hours of 180 GHz data have been cleansed of roll-related fluctuations. Plots of RMS variation were constructed, and correlations with light and moderate CAT encounters were sought. No correlations were found! Dr. Peter Kuhn, whose IR CAT sensor was installed on the same aircraft, reports successful warnings throughout the 1979 CAT Mission.

There are 6 differences between the 180 GHz radiometer and the IR CAT sensor that can be considered as potential explanations for the difference in their performance:

1. Sensitivity, 10 versus 5 microns of precipitable water vapor (estimated)
2. Beamwidth, 5 degrees versus 2 degrees
3. Off-forward viewing direction, 50 degrees versus 0 degrees
4. Elevation, 12 degrees versus 7 degrees
5. Sampling rate, 2 seconds versus 0.1 second
6. Sensitivity to roll variations

Item 4 is probably not important. Item 1 is perhaps more important than it appears. The 180 GHz radiometer output was definitely "radiometer noise" limited, and not "sky noise" limited, whereas the IR CAT radiometer appears to have been "sky noise" limited! Although the sampling rates appear to be significantly different, the IR CAT sensor is reported to produce warnings when the raw data stream is converted to a sequence of 1-second averages. Indeed, the earlier data from this sensor (Ref. 2) shows variability on time-scales far longer than 2 seconds, during times that are associated with flight through turbulence. At this time, there is no unique explanation for the difference in performance between the two sensors.

A greatly improved 180 GHz radiometer could be built with present technology. It is possible that all the shortcomings in performance relative to the IR CAT sensor, that are listed above, could be overcome. (It should not be forgotten, however, that any microwave counterpart to an IR sensor can be expected to cost more to produce.) The principal result of the 180 GHz flight experience is that any microwave counterpart to the IR CAT sensor will have to be significantly better than the 180 GHz radiometer described above.

CONCLUDING REMARKS

The 55.3 GHz airborne radiometer is the first of its type. It was used to measure, for the first time, "altitude temperature profiles". The sequence of profiles, spaced 17 seconds apart (3.5 km), enable inversion layer and tropopause properties to be studied. On some occasions, the altitude distribution of CAT severity correlated remarkably well with inversion layer location. On other occasions, turbulence was not located within 55.3 GHz measured inversion layers. These may be cases of topography-generated CAT, where inversion layers would not necessarily be expected. Evidence has been obtained supporting the hypothesis that CAT is generated within layers containing levels of wind shear that cannot be supported by the layer's lapse rate; i.e., that Kelvin-Helmholtz wave breakdown can generate CAT.

The 180 GHz radiometer failed to warn of CAT events. It is suggested that the radiometer's sensitivity (1 K) was inadequate for detecting the small variations in line-of-sight water vapor content, which are reportedly responsible for the success of Dr. Peter Kuhn's IR CAT warning sensor. The 180 GHz radiometer was not affected by cirrus clouds, which should justify its continued consideration for future sensor development.

ACKNOWLEDGEMENTS

This paper presents the results of one phase of research carried out at the Jet Propulsion Laboratory, California Institute of Technology, under NASA Contract NAS7-100, sponsored by the Aviation Safety Technology Branch, Office of Aeronautics and Space Technology, National Aeronautics and Space Administration. It is a pleasure to extend thanks to the Ames Research Center's Medium Altitude Missions Branch for their professional support of our experiment, and to George Alger, the Mission Manager, for his competent handling of the many problems that came his way. I would also like to express gratitude to Jack Enders, whose farsighted management of the Aviation Safety Technology Branch made this project possible.

REFERENCES

1. Weaver, E. A.; Ehernberger, L. J.; Gary, B. L.; Kurkowski, R. L.; Kuhn, P. M.; Stearns, L. P.: 1979 Clear Air Turbulence Flight Test Program. 1980 Aircraft Safety and Operating Problems, NASA CP-2170, 1981. (Paper 16 of this compilation.)

2. Kuhn, P.: Clear Air Turbulence: Detection by Infrared Observations of Water Vapor. Science, 196, pp. 1099-1100, 1977.

3. Waters, J. W.; Gustincic, J. J.; Kakar, R. K.; Kerr, A. R.; Roscoe, H. K.; and Swanson, P. N.: The Microwave Limb Sounder Experiment: Observations of Stratospheric and Mesospheric H_2O. Interhemispheric Survey of Minor Upper Atmospheric Constituents During October-November 1976, NASA TM X-73630, 1977, pp. 31-44.

4. Gary, B.: Progress Report Notes for Clear Air Turbulence Studies. Presentation at CAT Workshop #1, MSFC, June 1979.

DAY UT ALT PCH ROLL
223 214655 17900 1 6 4 4 3 3
254 3 254 6 42
LAPS SATM TB FILE

The JPL airborne passive microwave sensor that was test-flown in a NASA research aircraft demonstrated that "altitude temperature profiles" can be measured remotely, and in real time. The panel on the left shows that from 610 m (2000 ft) below aircraft to 910 m (3000 ft) above, observed air temperature "0" decreased uniformly with altitude. The dashed horizontal line, corresponding to aircraft altitude (8476 m (27 810 ft) for this panel), has the temperature scale coded with semicolons 10 K apart. Temperature at aircraft altitude is 225.4 K. The sloping pattern of semicolons correspond to an "adiabatic" atmosphere, in which it is nearly impossible to generate turbulence. The panel on the right illustrates an inversion layer at aircraft altitude (5456 m (17 900 ft)). The boundaries of the layer are at 90 m (300 ft) below and 400 m (1300 ft) above. If a "yes/no" type of turbulence detector shows that CAT is imminent, the pilot could use the information contained in this panel to request an assignment to a lower altitude, and thereby underfly the region of greatest turbulence.

Figure 1.- Clear air turbulence studies with microwave radiometers.

BLANK PAGE

IN-FLIGHT DIRECT-STRIKE LIGHTNING RESEARCH

Felix L. Pitts and Mitchel E. Thomas
NASA Langley Research Center

SUMMARY

The NASA Langley Research Center is performing in-flight direct-strike lightning research to better define the lightning-generated electromagnetic environment affecting aircraft. The research program uses an F-106B aircraft which operates in a thunderstorm environment and is specially instrumented for lightning electromagnetic measurements. The instrumentation system is reviewed and typical results recorded by the research instrumentation during simulated-lightning ground tests performed for a safety survey are presented. Several examples of data obtained during the summer of 1980 are presented and future plans are discussed.

INTRODUCTION

The NASA Langley Research Center is performing in-flight direct-strike lightning research using a specially instrumented F-106B aircraft. The intent of this research is to refine the characterization of the lightning-generated electromagnetic environment affecting aircraft. The projected use of digital avionic systems, along with composite aircraft structure, compounds lightning-related problems. Digital avionic systems are potentially more susceptible to upset by electrical transients than previous generation systems and the composite structure may not provide electrical shielding equivalent to that provided by metal aircraft in the past. Future design processes will thus require lightning-protection assessment techniques for digital avionic systems operating in electromagnetically nonoptimum structures. A necessary requirement of potential assessment techniques (which may range from purely analytical, through simulation, to actual hardware tests) is a refined definition of the lightning electromagnetic hazard. Recent discussion and review (ref. 1) supplemented by ground-based measurements (ref. 2) has indicated that the rise times of lightning electromagnetics are around one order of magnitude faster than those used in current lightning-protection criteria.

The intent, rationale, and design goals of the instrumentation system developed at NASA Langley Research Center to aid in-flight lightning-hazard characterization are described in reference 3. The present report contains a review of the actual instrumentation system implementation, presents results recorded by the research instrumentation during simulated lightning testing, which was part of a safety survey of the aircraft, and presents and compares the initial direct-strike lightning data with the simulation data.

INSTRUMENTATION SYSTEM OVERVIEW

The instrumentation concept shown in figure 1 consists of a number of electromagnetic sensors which measure the electromagnetic fields during the lightning process. The data are then recorded in a shielded, isolated instrumentation enclosure. A photograph of the instrumentation system with its cover removed is shown in figure 2. The system is mounted in the missile bay of the F-106B.

Specially expanded Biomation transient waveform recorders (ref. 4), which operate at a 10-nanosecond sample interval and 6-bit resolution, provide a unique capability for recording lightning electromagnetic transients. The basic Biomation Model 6500 recorder memory was increased by over two orders of magnitude to allow a significant data window recording of 1.3 milliseconds of data at 10-nanoseconds resolution. Photographs of the expanded Biomation front panel and the memory expansion are shown in figures 3 and 4. Upon acquisition of strike data by the transient waveform recorder, the data are automatically transferred to the data formatter and thence to the instrumentation recorder for permanent storage. The transient recorder is then automatically reset to acquire data from the next strike.

The wide-band RCA video recorder has 6-MHz bandwidth and is capable of recording continuously for 24 minutes. This continuous recorder is used to provide information on the overall lightning scenario.

The sensors used in the lightning instrumentation system are derived from designs developed for nuclear electromagnetic pulse measurements. (See ref. 5.) The sensors measure the rate of change of strike current to the noseboom (I-Dot) along with the rate of change of electric and magnetic flux density (D-Dot, B-Dot) at a number of locations as shown in figure 5. The sensor response to rates of change of the lightning electromagnetic characteristics (as opposed to the current and fields, directly) accentuates the recording of the higher frequency components of the lightning process. Since the magnitudes of induced voltages (and currents) are proportional to rates of change of the lightning electromagnetic characteristics, enhanced definition of the more interesting (from an induced-effects viewpoint) portion of the spectrum is obtained. The sensor sensitivity is calculated based on sensor geometry (ref. 6) and then checked using a parallel-plate transmission-line calibrator. Figures 6, 7, and 8 are photographs of the I-Dot, B-Dot, and D-Dot sensors, respectively; figure 9 is a photograph of the flat-plate transmission-line calibrator.

Power system isolation for the instrumentation is obtained using a motor-generator set. A 3-phase, 208-V, 400-Hz, 13-kVA electric motor external to the enclosure drives a nonconducting flexible coupler to a 12.5-kVA, 120/208-V, 3-phase, 400-Hz AC generator located within the enclosure to power the system.

The sensor-recorder configuration used in the initial flight configuration is shown in table I, which also summarizes the data channel bandwidths, thresholds, and full-scale values.

SIMULATED LIGHTNING GROUND TEST

A simulated lightning safety survey test was performed on the aircraft to assess potential problems concerning aircraft systems safety. These tests were conducted by Lightning Technologies, Inc., and no safety hazards were disclosed by the tests. The safety survey tests also provided an opportunity for "end-to-end" instrumentation system fidelity and noise immunity tests. The tests were performed with the aircraft engine running and all flight systems operating on aircraft power. The instrumentation system measured and recorded the fields and currents on the aircraft in response to a current pulse of known amplitude and waveform (as determined from an external current transformer measurement) which was generated with a high-voltage capacitor discharge apparatus attached to the noseboom. The current exited from the aircraft tail and was returned to the generator using symmetrical return wires as shown in the test setup photograph of figure 10. During these tests, the instrument system sensitivity was increased by one order of magnitude over the initial flight configuration to accommodate the relatively low capability of the test generator compared with the nominal lightning characteristics assumed for data channel scaling. In addition, the channel assignments were altered as shown in table II to utilize the increased time resolution of the transient recorder for monitoring the I-Dot sensor.

Typical responses of the I-Dot, D-Dot forward, and B-Dot longitudinal sensors are shown in figures 11 to 14. Figure 11 shows I-Dot sensor response to an input current to the noseboom. The input was a damped sinusoidal current oscillating at 86 000 Hz with a peak amplitude of 10 500 amperes. The I-Dot measurement agrees with the rate of change of input current within about 10 percent. Polarity of the I-Dot measurement is negative for conventional current increasing out of the noseboom, as was the case for this test. Figures 12 and 13 show in greater detail the response of the I-Dot and D-Dot forward sensors to the first cycle of input current.

Figure 14 shows the response of the B-Dot sensor to a damped sinusoidal input current to the aircraft noseboom. The input was a damped sinusoidal current oscillating at 86 000 Hz with a peak amplitude of 14 250 amperes. The magnitude of the B-Dot measurement is about 35 percent of the amplitude calculated for this input current to a simple cylinder with a radius of 1 meter (approximate fuselage radius). The presence of the aircraft wing alters the magnetic field which would be obtained from a simple cylinder. The relative position of the return wires causes intensification of current in the wing, thereby reducing the field at the location of the B-Dot sensor.

During subsequent tests, sensor cables were terminated in dummy 50-ohm loads, in lieu of the sensors, to investigate the noise immunity of the instrumentation system. The system did not respond during these tests, which indicates that the noise level would be at least one order of magnitude below the flight configuration threshold.

LIGHTNING DATA

The aircraft sustained three strikes while in the vicinity of the National Severe Storms Laboratory, Norman, Oklahoma, on June 17, 1980. The strikes occurred with the aircraft at an altitude of 4800 meters at a speed of 300 knots; the approximate freezing level was at the aircraft operating altitude. The detailed waveforms of these strikes were reported in reference 7; these strikes were not particularly energetic in that the magnetic characteristics (I-Dot, B-Dot) did not exceed system thresholds, and only information from the forward D-Dot sensor was recorded. The portions of the preceding strike data records with the largest rates of change of electric flux density are shown in figures 15 and 16.

The aircraft was struck a total of ten times during the 1980 campaign with five of these occurring in rapid succession during one flight on September 3, 1980. Data processing, interpretation and analysis of the data are continuing; the following observations are offered at this point: (1) the utility of the derivative (D-Dot) sensor is clearly demonstrated by examining the amplitude resolution of the "faster" changing portions of figures 15 and 16 during the first microsecond of the event; and (2) the data indicate significant changes in the strike electric characteristics during submicrosecond intervals.

FUTURE PLANS

The capability of the recording system is being significantly increased. A new transient recorder with 12 data channels of similar characteristics to the expanded Biomation transient recorder is being obtained as is an analog video recorder with a 15-MHz bandwidth. This increased capability will allow a much more complete characterization of the lightning-generated electromagnetic environment.

Upon acquisition of a statistically significant data base for strike characterization (which is not near at hand), considerable effort will be required to assess the significance and interpret the data as concerns future aircraft designs.

REFERENCES

1. Clifford, Don W.; Krider, E. Philip; and Uman, Martin A.: A Case for Submicrosecond Rise-Time Lightning Current Pulses for Use in Aircraft Induced Coupling Studies. 1979 IEEE International Symposium on Electromagnetic Compatibility. San Diego, Calif., Oct. 9-11, 1979, pp. 143-149.

2. Weidman, C. D.; and Krider, E. P.: Submicrosecond Risetimes in Lightning Radiation Fields. Lightning Technology, NASA CP-2128, 1980, pp. 29-38.

3. Pitts, F. L., et al.: In-Flight Lightning Characteristics Measurement System. Federal Aviation Administration - Florida Institute of Technology Workshop on Grounding and Lightning Technology, FAA-RD-79-6, Mar. 1979, pp. 105-111.

4. Thomas, Robert M., Jr.: Expanded Interleaved Solid-State Memory for a Wide Bandwidth Transient Waveform Recorder. Lightning Technology, NASA CP-2128, 1980, pp. 119-129.

5. Baum, C. E., et al.: Sensors for Electromagnetic Pulse Measurements Both Inside and Away from Nuclear Source Regions. IEEE Trans. Electromagn. Compat., vol. EMC-20, no. 1, Feb. 1978.

6. Trost, Thomas F.; and Zaepfel, Klaus P.: Broadband Electromagnetic Sensors for Aircraft Lightning Research. Lightning Technology, NASA CP-2128, 1980, pp. 131-152.

7. Pitts, Felix L.; and Thomas, Mitchel E.: Initial Direct Strike Lightning Data. NASA TM-81867, 1980.

TABLE I. - INITIAL FLIGHT CONFIGURATION

Sensor	Recorder	Sample Rate (Bandwidth)	P-P Full Scale	Threshold
$\dot{D}$ Forward	Transient	100 MHz (50* MHz)	±24.5 A/m^2	+4.9 A/m^2
$\dot{B}$ Longitudinal	Transient	100 MHz (50* MHz)	±8695 T/s	+1739 T/s
$\dot{D}$ Right Wing	Wide-band Analog	(6 MHz)	±28 A/m^2	±2.8 A/m^2
$\dot{I}$	Wide-band Analog	(6 MHz)	$\pm 4.7 \times 10^{10}$ A/s	$\pm 4.7 \times 10^{9}$ A/s

*Four-pole linear phase low pass filter 3 db point at 50 MHz.

TABLE II. - GROUND TEST CONFIGURATION

Sensor	Recorder	Sample Rate (Bandwidth)	P-P Full Scale	Threshold
$\dot{D}$ Forward	Transient	100 MHz (50* MHz)	±2.45 A/m^2	+0.49 A/m^2
$\dot{B}$ Longitudinal	Wide-band Analog	(6 MHz)	±870 T/s	±87 T/s
$\dot{D}$ Tail	Wide-band Analog	(6 MHz)	±2.45 A/m^2	±.245 A/m^2
$\dot{I}$	Transient	100 MHz (50* MHz)	$\pm 4.7 \times 10^{9}$ A/s	$+0.94 \times 10^{9}$ A/s

*Four-pole linear phase low pass filter 3 db point at 50 MHz.

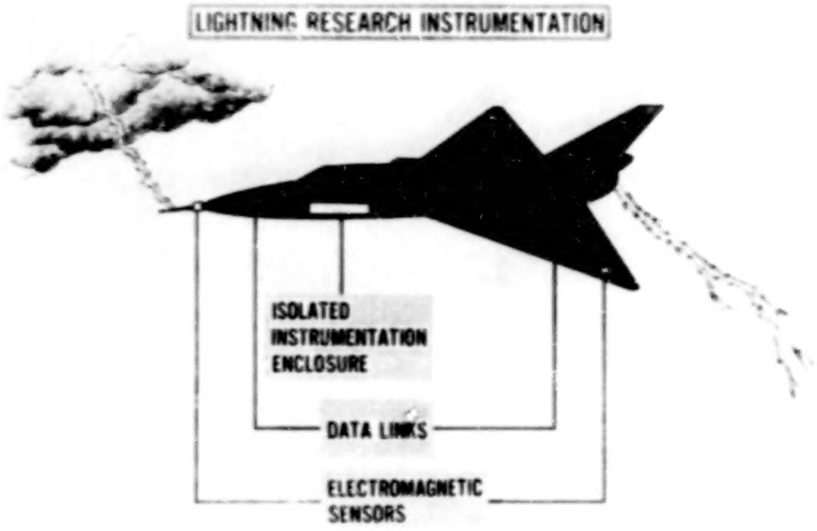
LIGHTNING RESEARCH INSTRUMENTATION
ISOLATED INSTRUMENTATION ENCLOSURE
DATA LINKS
ELECTROMAGNETIC SENSORS

Figure 1.- Instrumentation system concept.

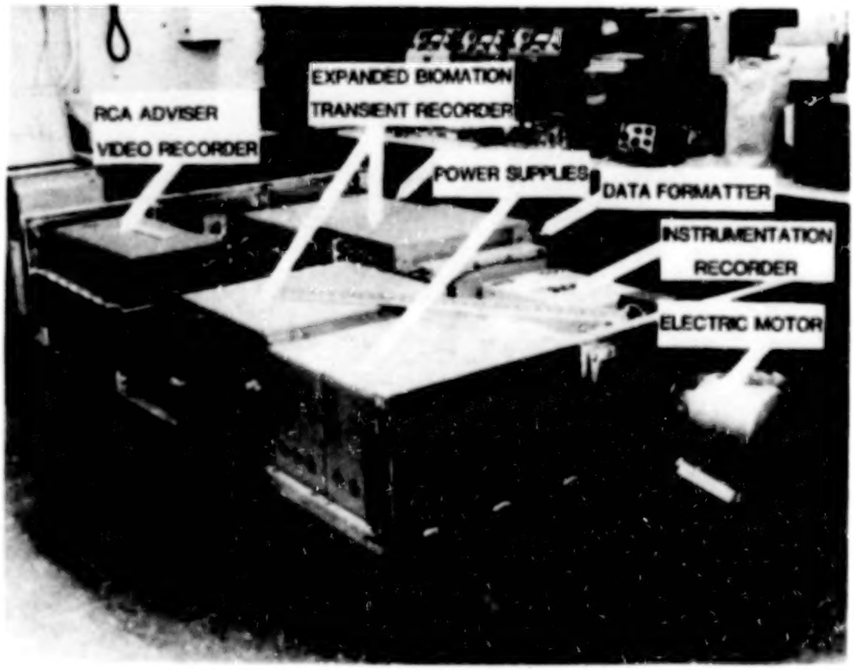
RCA ADVISER VIDEO RECORDER
EXPANDED BIOMATION TRANSIENT RECORDER
POWER SUPPLIES
DATA FORMATTER
INSTRUMENTATION RECORDER
ELECTRIC MOTOR

Figure 2.- Instrumentation system.

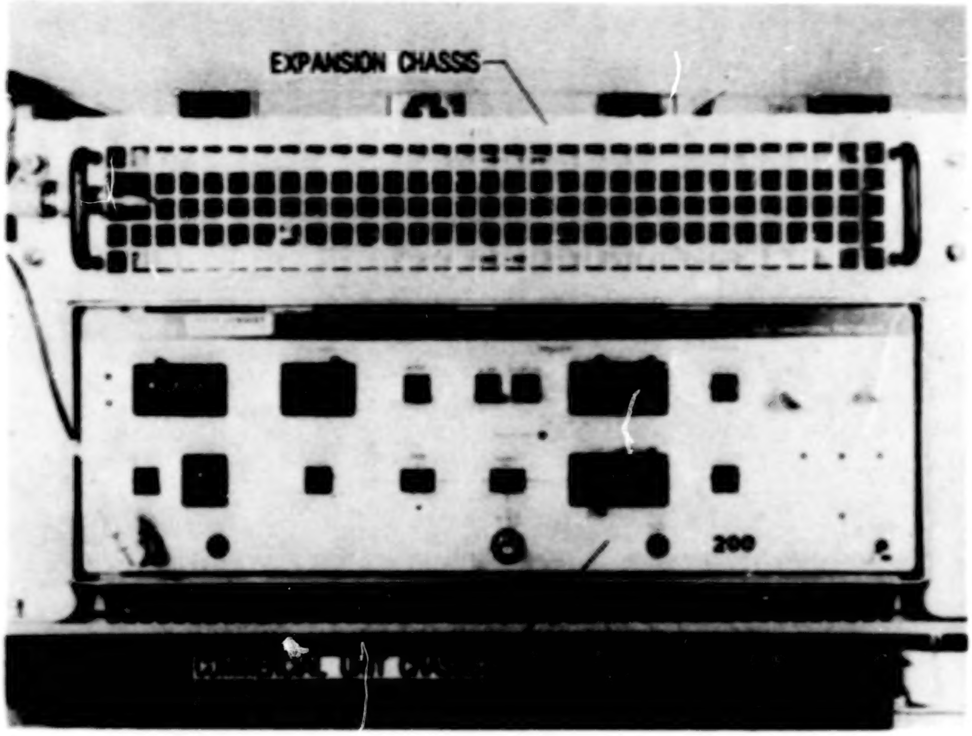
EXPANSION CHASSIS
200

Figure 3.- Expanded waveform recorder.

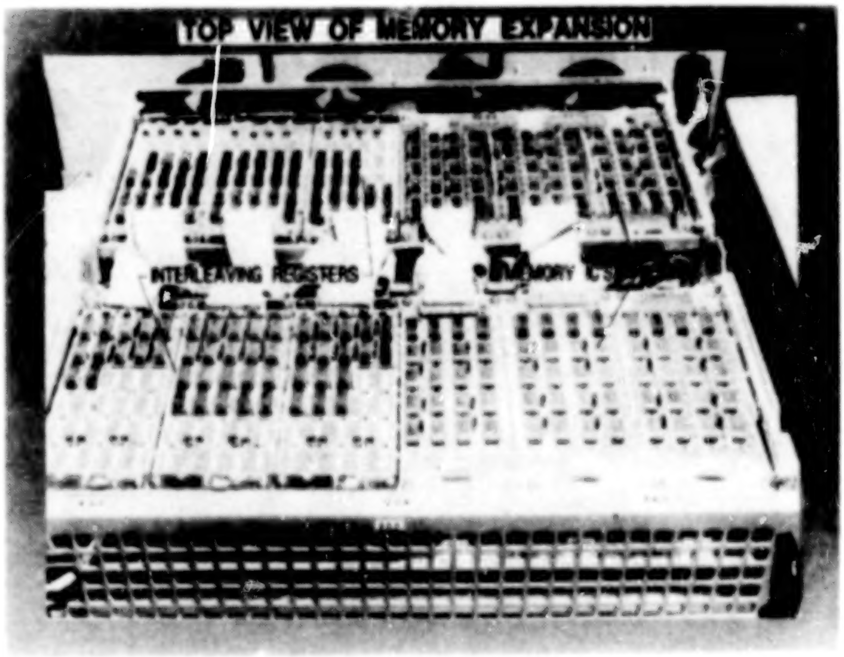
TOP VIEW OF MEMORY EXPANSION
INTERLEAVING REGISTERS
MEMORY IC'S

Figure 4.- Expanded memory.

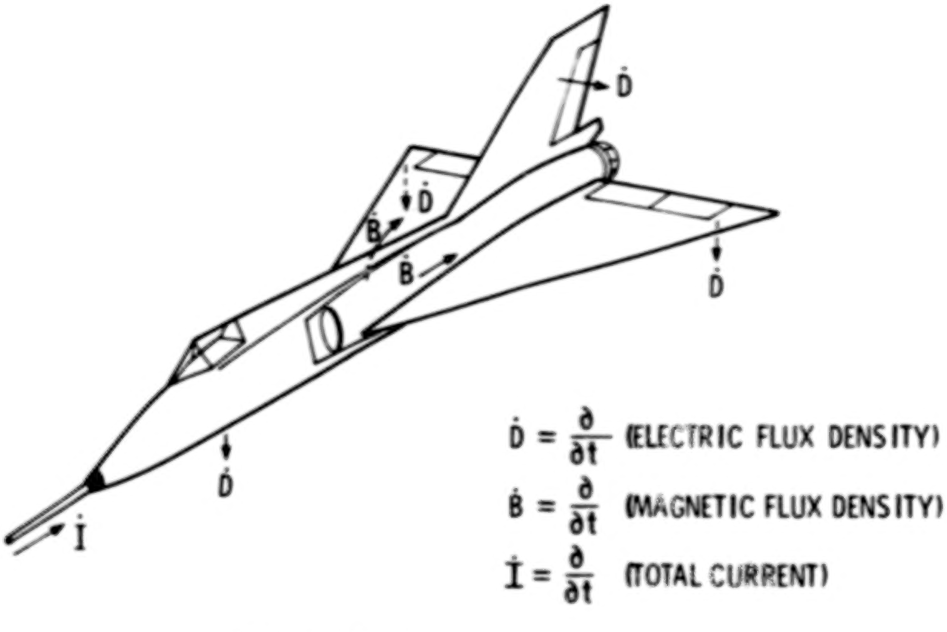
$\dot{D}$
$\dot{D}$
$\dot{B}$
$\dot{B}$
$\dot{D}$
$\dot{D}$
$\dot{I}$
$\dot{D} = \frac{\partial}{\partial t}$ (ELECTRIC FLUX DENSITY)
$\dot{B} = \frac{\partial}{\partial t}$ (MAGNETIC FLUX DENSITY)
$\dot{I} = \frac{\partial}{\partial t}$ (TOTAL CURRENT)

Figure 5.- Sensor locations.

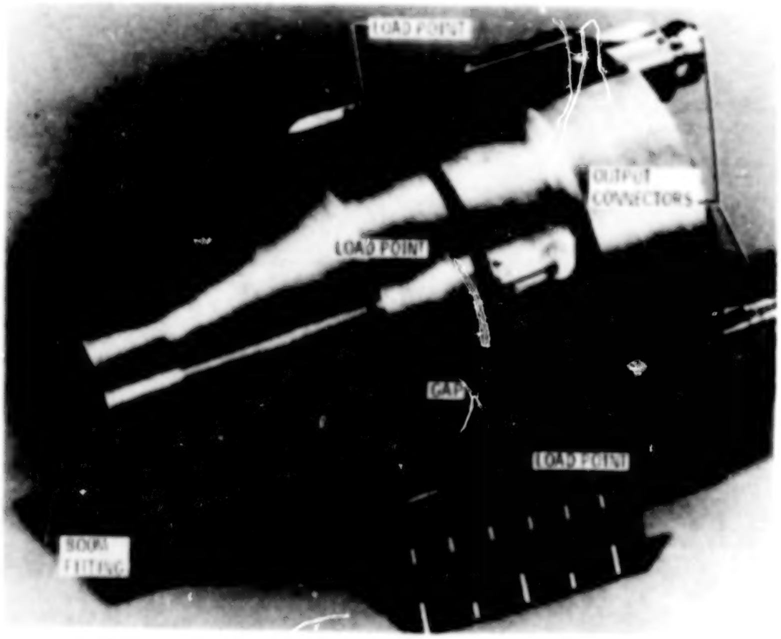
LOAD POINT
OUTPUT CONNECTORS
LOAD POINT
GAP
LOAD POINT
BOOM FITTING

Figure 6.- I-Dot sensor.

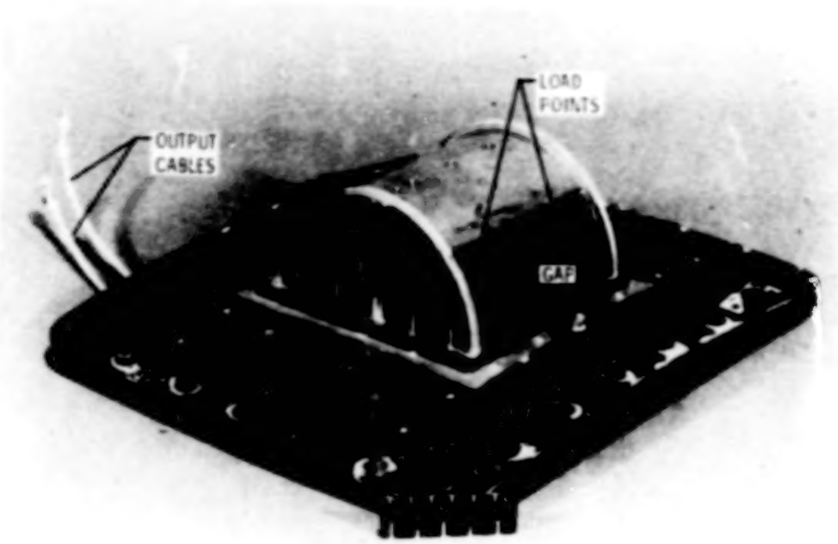
LOAD POINTS
OUTPUT CABLES
GAP

Figure 7.- B-Dot sensor.

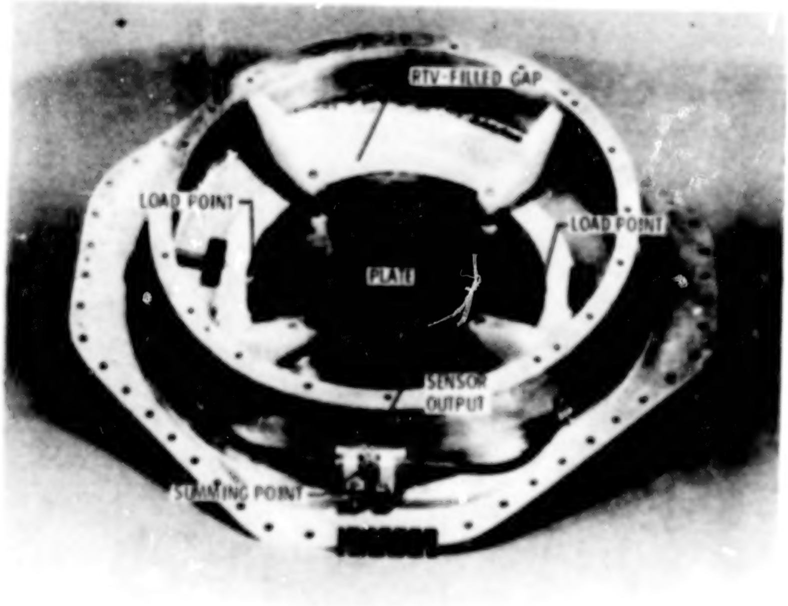
RTV-FILLED GAP
LOAD POINT
LOAD POINT
PLATE
SENSOR OUTPUT
SUMMING POINT

Figure 8.- D-Dot sensor.

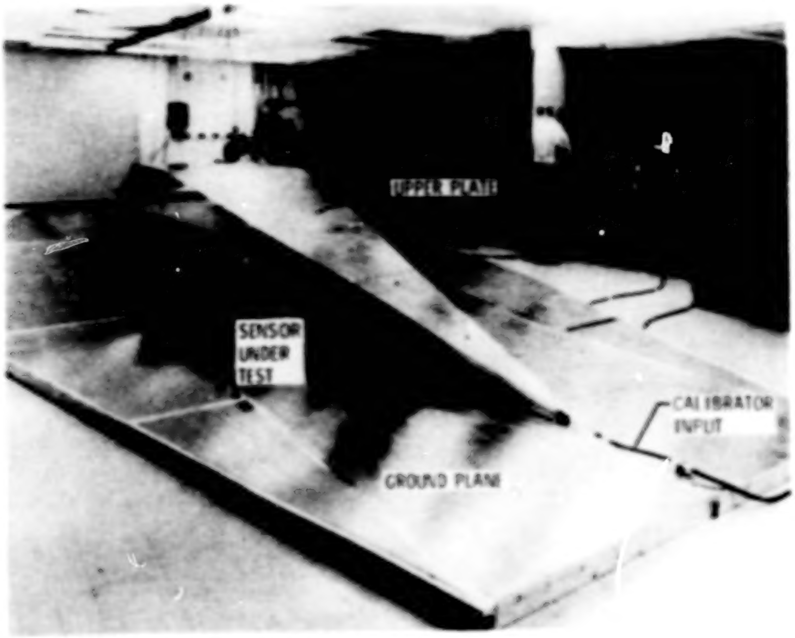
UPPER PLATE
SENSOR UNDER TEST
CALIBRATOR INPUT
GROUND PLANE

Figure 9.- Flat-plate transmission-line calibrator.

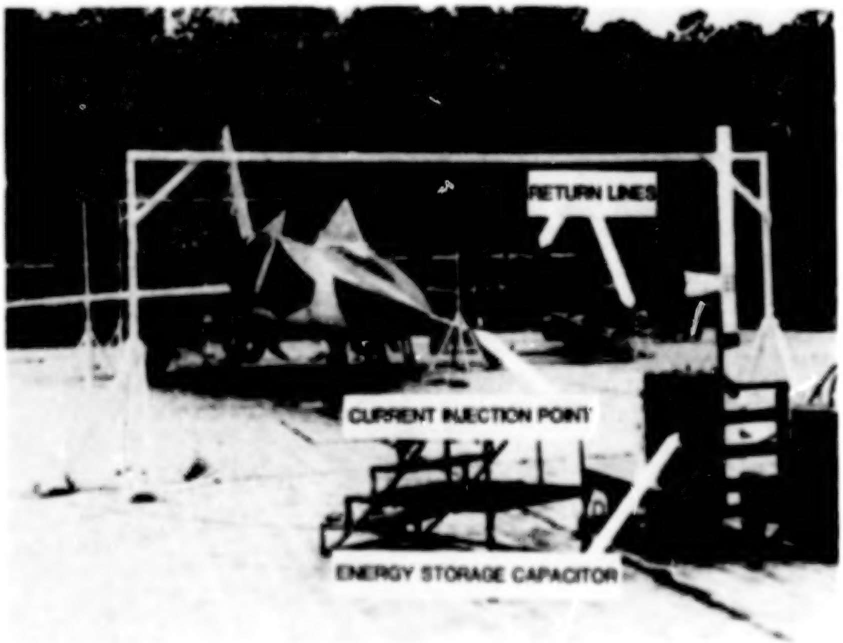
RETURN LINES
CURRENT INJECTION POINT
ENERGY STORAGE CAPACITOR

Figure 10.- Simulated lightning ground test.

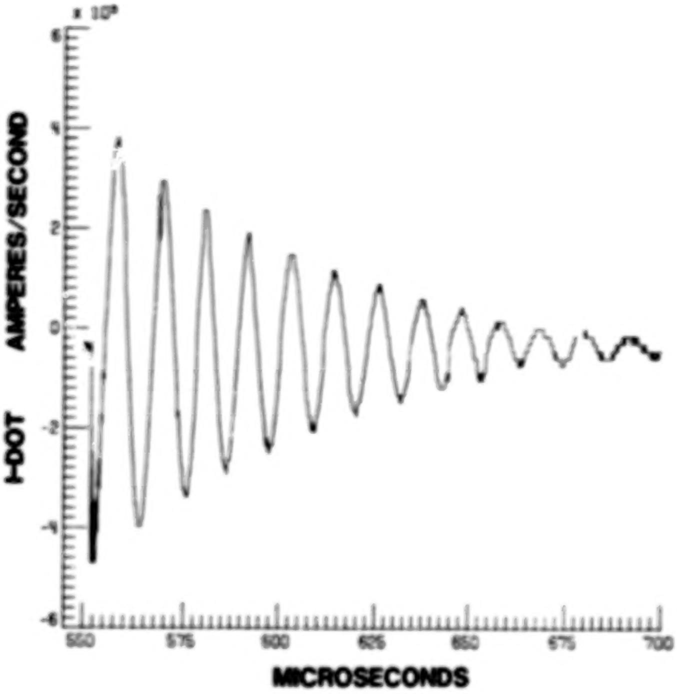

Figure 11.- I-Dot sensor response.

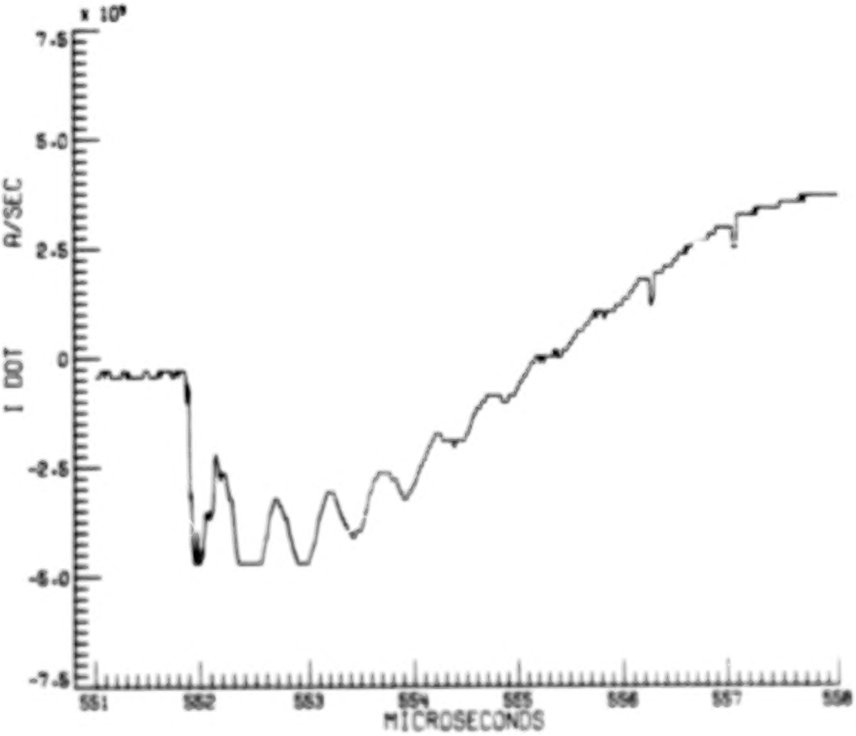

Figure 12.- I-Dot sensor response, expanded time scale.

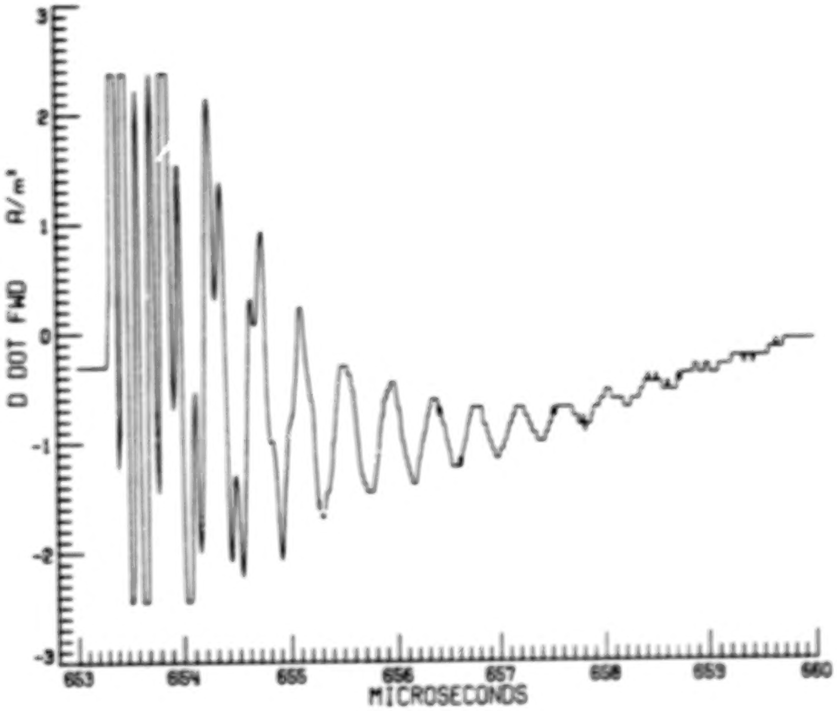

Figure 13.- D-Dot sensor response.

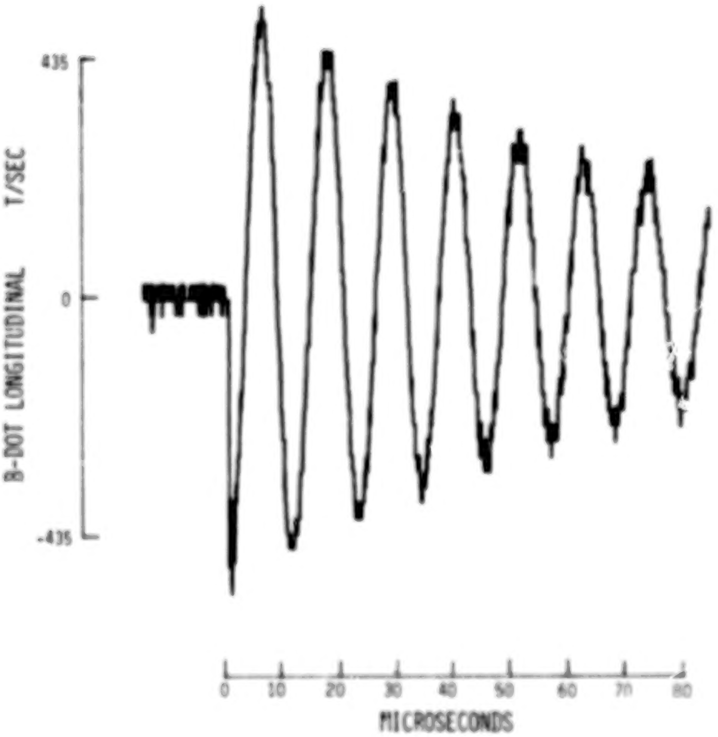

Figure 14.- B-Dot sensor response.

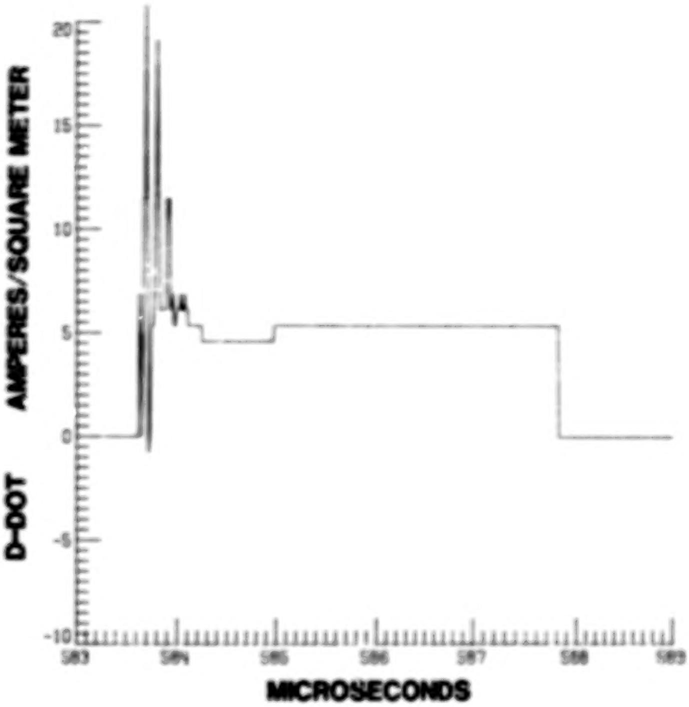

Figure 15.- Direct-strike D-Dot record A.

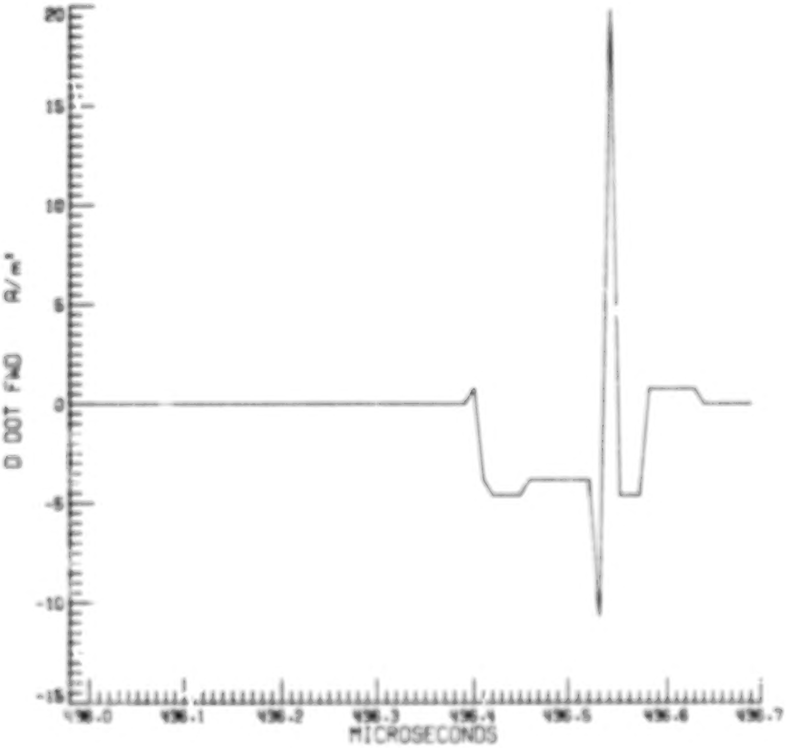

Figure 16.- Direct-strike D-Dot record B.

MAGNITUDE AND FREQUENCY OF WIND SPEED SHEARS AND ASSOCIATED DOWNDRAFTS

Margaret B. Alexander and C. Warren Campbell
Atmospheric Sciences Division
Space Sciences Laboratory
Marshall Space Flight Center, Alabama 35812

SUMMARY

Information on wind shear and downdraft interaction in the lowest 150 m of the Earth's atmosphere is required for simulating their effect on ascent and descent of conventional aircraft under hazardous conditions. Both of these wind conditions have similar effects on aircraft. Previous studies indicate that a 5 knot downdraft is comparable to a 5 knot per 30.5 m (100 ft) wind shear with regard to the effect on large sweptwing transport-type aircraft. Magnitudes equal to or in excess of these values can have a significant effect on aircraft during take-off and landing. Data are presented indicating the frequency of occurrence of wind shear and downdrafts together with information on the simultaneous occurrence of these two phenomena. The source of these data is the NASA 150-Meter Ground Winds Tower Facility at the Kennedy Space Center, Florida.

INTRODUCTION

Atmospheric conditions in the vicinity of airports are a primary concern of aviation meteorology. Turbulence, wind shear, and vertical motion (updrafts/downdrafts) are low-level conditions known to be hazardous to high-performance aircraft during takeoff/climbout and approach/landing operations. All can and frequently do occur simultaneously. Thus, a requirement exists for information on these conditions below 150 m (500 ft) relative to magnitude, frequency and simultaneity of occurrence.

Although short-term wind measurement accuracy is vital in the study of low-level conditions, relatively little high-resolution data from aircraft and/or meteorological towers are available. Data acquired at the NASA 150-Meter Ground Winds Tower Facility at Kennedy Space Center, Florida, provided simultaneous horizontal wind speeds at eight levels and vertical speeds at four levels for analysis to determine characteristics of typical horizontal shears and associated downdrafts.

The analysis of meteorological tower data provides a basis for simulating aircraft ascent and descent under adverse conditions. Data of this type are valuable because theoretical model simulation of wind shears, intermittent downdrafts, or turbulence phenomena in the planetary boundary layer is subject to certain technical difficulties. These difficulties relate to the nonisotropy of the turbulence and the failure of the turbulence to conform to Gaussian probability distributions. Multilayer tower data can be used to create realistic approach and departure wind conditions.

The simultaneous occurrence of wind shear and downdrafts can cause serious problems for approaching and departing aircraft. Understanding statistical properties of these simultaneous occurrences enables accurate simulations.

BACKGROUND

A serious problem in aviation meteorology is wind events during airport operations for departing and approaching aircraft. It is known that the danger from shear events encountered by large, sweptwing, jet-powered aircraft increases below an altitude of 150 m (500 ft). Ramsdell and Powell (1973) state that the behavior of the wind in the last 30 m of descent, in particular between 30 and 15 m during which some aircraft travel approximately 300 m in 4 to 5 s, is most important to a descending aircraft. To ascertain the relative effects, Snyder (1968) simulated an aircraft on final approach and subjected it to the three events of sudden horizontal wind shear, downdraft, and an airspeed drop. Using Snyder's analog computer study and a simple flow model, Kalafus (1978) achieved results consistent with Snyder's: That a 5 kphf ($0.08\ s^{-1}$) shear is a typical average shear that would be associated with a 5 kt ($2.57\ ms^{-1}$) downdraft and that a 10 kt ($5.15\ ms^{-1}$) downdraft is comparable to a 10 kphf ($0.17\ s^{-1}$) shear appears to be a reasonable assumption.

The analysis presented here demonstrates the properties of simultaneously occurring wind shears and downdrafts. To this end, high resolution data from the NASA tower facility were analyzed. Downdrafts were measured at 150, 60, 18, and 10 meters, and shear determinations were made for the 150-120, 90-60, 60-30, and 30-3 m layers.

DATA

To understand and describe wind shear effects on the safety of flight operations in the terminal area, available data from aircraft and meteorological towers should be exploited to the fullest. This analysis used high-resolution wind profile measurements recorded at the NASA 150-Meter Ground Winds Tower Facility. The NASA Tower Facility, depicted in Figure 1 and described by Kaufman and Keene (1968), is located at the Kennedy Space Center approximately midway between Launch Complex 39B and the Space Shuttle runway. Placement of the meteorological sensors on the tower is shown in Figure 2. Eight tests acquired in March, July,

CONTENTS

Part 1

PREFACE . . . . iii 1/A6

1. INTRODUCTORY REMARKS 1 1/A12
Roger L. Winblade

SESSION I - TERMINAL-AREA OPERATIONS
Cochairmen: T. A. Walsh and R. L. Kurkowski

2. TEST RESULTS OF FLIGHT GUIDANCE FOR FUEL CONSERVATIVE DESCENTS IN A TIME-BASED METERED AIR TRAFFIC ENVIRONMENT 7 1/B4
Charles E. Knox and Lee H. Person, Jr.

3. A PILOT'S SUBJECTIVE ANALYSIS OF A COCKPIT DISPLAY OF TRAFFIC INFORMATION (CDTI) 29 1/C12
Gerald L. Keyser, Jr.

4. GUIDANCE AND CONTROL SYSTEM RESEARCH FOR IMPROVED TERMINAL AREA OPERATIONS 51 1/E6
R. M. Hueschen, J. F. Creedon, W. T. Bundick, and J. C. Young

5. OPERATIONAL CONSIDERATIONS IN UTILIZATION OF MICROWAVE LANDING SYSTEM APPROACH AND LANDING GUIDANCE 83 1/G10
William F. White and Leonard V. Clark

6. AUTOMATED PILOT ADVISORY SYSTEM TEST AND EVALUATION AT MANASSAS MUNICIPAL AIRPORT 113 2/B4
John L. Parks, Jr.

7. A METHOD FOR DETERMINING LANDING RUNWAY LENGTH FOR A STOL AIRCRAFT 127 2/C14
D. M. Watson, G. H. Hardy, J. F. Moran, and D. N. Warner, Jr.

8. FLIGHT TESTS OF IFR LANDING APPROACH SYSTEMS FOR HELICOPTERS 145 2/E4
J. S. Bull, D. M. Hegarty, L. L. Peach, J. D. Phillips, D. J. Anderson, D. C. Dugan, and V. L. Ross

9. A HEAD-UP DISPLAY FORMAT FOR TRANSPORT AIRCRAFT APPROACH AND LANDING. 165 2/F10
Richard S. Bray and Barry C. Scott

MICROFILMED FROM BEST
AVAILABLE COPY

SESSION II - AVIONICS AND HUMAN FACTORS

Cochairmen: M. D. Montemerlo and A. B. Chambers

10. AN EVALUATION OF HEAD-UP DISPLAYS IN CIVIL TRANSPORT OPERATIONS 197 3/B2
John K. Lauber, Richard S. Bray, and Barry C. Scott

11. GENERAL AVIATION SINGLE PILOT IFR AUTOPILOT STUDY 201 3/B6
Hugh P. Bergeron

12. APPLICATION OF THE EPIDEMIOLOGICAL MODEL IN STUDYING HUMAN ERROR IN AVIATION 219 3/C10
Ed S. Cheaney and Charles E. Billings

13. HOW A PILOT LOOKS AT ALTITUDE 237 3/D14
Amos A. Spady, Jr., and Randall L. Harris, Sr.

SESSION III - ATMOSPHERIC ENVIRONMENT

Cochairmen: D. W. Camp and L. J. Ehernberger

14. SUMMARY OF FLIGHT TESTS OF AN AIRBORNE LIGHTNING LOCATOR SYSTEM AND COMPARISON WITH GROUND-BASED MEASUREMENTS OF PRECIPITATION AND TURBULENCE 251 3/E14
Bruce D. Fisher and Norman L. Crabill

15. WALLOPS SEVERE STORMS MEASUREMENT CAPABILITY 279 4/A3
Robert E. Carr and John C. Gerlach

16. THE 1979 CLEAR AIR TURBULENCE FLIGHT TEST PROGRAM 293 4/B3
E. A. Weaver, L. J. Ehernberger, B. L. Gary,
R. L. Kurkowski, P. M. Kuhn, and L. P. Stearns

17. PULSED DOPPLER LIDAR FOR THE DETECTION OF TURBULENCE IN CLEAR AIR 313 4/C9
E. A. Weaver, J. W. Bilbro, J. A. Dunkin, S. C. Johnson
W. D. Jones, C. E. Harris, and C. A. DiMarzio

18. FLIGHT TESTS OF A CLEAR-AIR TURBULENCE ALERTING SYSTEM 329 4/D11
Richard L. Kurkowski, Peter M. Kuhn, and Louis P. Stearns

19. CLEAR AIR TURBULENCE STUDIES WITH MICROWAVE RADIOMETERS 351 4/F5
Bruce L. Gary

20. IN-FLIGHT DIRECT-STRIKE LIGHTNING RESEARCH 359 4/F13
Felix L. Pitts and Mitchel E. Thomas

21. MAGNITUDE AND FREQUENCY OF WIND SPEED SHEARS AND ASSOCIATED DOWNDRAFTS 373 4/G13
Margaret B. Alexander and C. Warren Campbell

MICROFILMED FROM BEST
AVAILABLE COPY

September and October 1973 between 0800 and 1600 EST provided 5-second data intervals (one interval every 100 s during each approximately 2 h test). Table 1 presents the date, start and end time, number of intervals and measurements per level, and peak horizontal wind speed and downdraft per test.

The data record consisted of 457 intervals from the Automatic Data Acquisition System, described by Traver, et al. (1972). This system sampled each wind sensor at a rate of 10 samples per second, digitally recorded, and real-time processed the 22,800 wind speeds per level. These speeds at six tower levels provided the differences to determine wind shears for four 30 m layers in the lowest 150 m of the Earth's atmosphere, i.e., 150-120, 90-60, 60-30 and 30-3 m. These layers bracketed the simultaneous vertical wind speed (updraft/downdraft) measurements at the 150, 60, 18 and 10 m levels. Table 2 is a tabulation by levels of the frequency and maximum values of the vertical motion. Table 3 presents a percentage frequency distribution of the magnitudes of the downdrafts in Table 2.

Because of the infrequent occurrence of downdrafts $\geq$10 kts ($\geq$5.15 ms^{-1}) in the eight tests, results from a previous analysis (Alexander 1977) of maximum vertical gusts recorded at the facility are also included. A continuous record of six 10-minute computational sequences per hour for one year of maximum horizontal wind speed and maximum updraft and downdraft revealed 274 occurrences of downdrafts $\geq$10 kts for the four levels. Table 4 lists the maximum values of updraft/downdraft by months, seasons and levels for the one-year data record. Table 5 presents the frequency of occurrence of maximum 10-minute interval vertical motion $\geq$10 kts ($\geq$5.15 ms^{-1}) by seasons and levels.

Unfortunately, the 10-minute sampling period did not permit the determination of simultaneous occurrence of shear and associated downdraft. However, for each occurrence of a maximum downdraft $\geq$10 kts in a 10-minute interval at each level, wind shear was determined for the associated layer and interval from the maximum horizontal wind speeds to give some indications relative to the intent of this analysis.

RESULTS

Vertical wind shear is defined to be the change of wind speed with height and is determined by means of two anemometers mounted at different heights on a tower. Spatially varying shears, determined for four layers of the atmosphere from 3 to 150 m, were derived by algebraically subtracting the wind speed at the lower level of the layer from the speed at the upper level and dividing by the distance between levels, i.e.,

$$\frac{WS_U - WS_L}{d_{(U-L)}} = \frac{\Delta WS}{\Delta d} .$$

Previously, Alexander and Camp (1979) derived maximum and mean values and frequency of wind shears greater than 0.1 s^{-1} as a function of the following six vertical layers at the facility:

WIND SPEED SHEAR

Layer (m)	Obs. (f)	Max (s^{-1})	Mean (s^{-1})	>0.1 s^{-1} (f)	>0.1 s^{-1} (%)
150-120	3950	0.160	0.022	72	1.82
120-90	3150	0.173	0.030	75	2.38
90-60	3150	0.327	0.039	184	5.84
60-30	3950	0.387	0.047	602	15.24
30-18	3950	0.792	0.099	1278	32.35
18-3	3950	0.713	0.185	2465	62.39

Simultaneously occurring downdrafts at four levels and associated shears are tabulated. Table 6 presents a percentage frequency distribution of >3.89 kt (2.0 ms^{-1}) downdrafts at four levels as a function of wind shear for associated layers for the 457 5-second data intervals.

A tabulation was made of maximum downdraft ($\geq$9.7 kts (5.0 ms^{-1})) per 10-minute interval for a one-year data record as a function of maximum horizontal wind speed. It should be noted that surface winds are generally classsified as

Class	Wind Speed (kts)	Wind Speed (ms^{-1})
Low	0<9.7	0<5
Moderate	9.7<19.4	5<10
High	19.4<35.0	10<18
Gale-force	35.0<64.1	18<33
Hurricane	$\geq$64.1	$\geq$33 .

Table 7 presents a frequency distribution of this tabulation of 274 downdrafts $\geq$9.7 kts (5.0 ms^{-1}) by levels and wind speed classes. Table 8 is a percentage frequency distribution of these downdrafts as a function of wind shear derived from maximum wind speed per interval.

An additional analysis of the joint probability data was done. The wind shear and downdrafts were checked for independence by comparing the joint probability density with the product of the probability density for downdrafts and the probability density for wind shears. The two are approximately equal. This indicates that windshear and downdraft are independent quantities; i.e., one does not affect the other. In other words, if a range of values of downdrafts is selected and a corresponding probability density of wind shears measured, and then another range of values of downdrafts selected, the corresponding probability density of wind shears will be the same as before.

To further check these results, correlation coefficients between wind shear and downdrafts were measured. Values less than 0.1 were obtained, with some values positive and some values negative. These small values appear to indicate independence of the two parameters.

CONCLUSIONS

Regarding magnitudes and frequencies of wind speed shears and associated downdrafts in the lowest 150 m of the atmosphere, the conclusions of this analysis are the following:

(1) From instantaneous measurements during horizontal wind speeds of gale-force and below intensity, vertical motion at the 10, 60 and 150 m levels was approximately 60 percent downward and 40 percent upward. At the 18 m level the percentages were reversed. Updraft maxima were an order of magnitude or two greater than downdrafts at all levels.

(2) Frequency of vertical motion $\geq$9.7 kts ($\geq 5\ \mathrm{ms}^{-1}$) for a year at four levels was 338 occurrences upward and 274 downward. Approximately 90 percent of these updrafts occurred at the 18 m level almost equally during summer and winter, and 65 percent of the downdrafts were at the 150 m level during summer.

(3) Magnitudes of 83 percent of the 274 downdrafts $\geq$9.7 kts ($\geq 5\ \mathrm{ms}^{-1}$) were in the range of 9.7<11.7 kts ($5<6\ \mathrm{ms}^{-1}$), with only 1 percent in the highest magnitude range of 15.6<17.5 kts ($8<9\ \mathrm{ms}^{-1}$).

(4) Data from sources such as the Kennedy Space Center 150-Meter Ground Winds Tower Facility provide useful information for simulating aircraft approaches and departures under adverse conditions. These data are valuable because of the difficulty of theoretical model wind simulations near the ground.

(5) Models for simulating aircraft ascent and descent under adverse conditions should show simultaneously occurring wind shears and downdrafts to be independent and uncorrelated.

This analysis certainly lends support to the beliefs that the need for information concerning atmospheric conditions is most important over the lowest 150 m and that short-term wind measurement accuracy is vital in detecting and identifying hazards to aircraft flight operations in terminal areas.

REFERENCES

Alexander, Margaret B., 1977: An Analysis of Maximum Vertical Gusts Recorded at NASA's 150-Meter Ground Winds Tower Facility at Kennedy Space Center, Florida. NASA TM 78139.

Alexander, Margaret B. and Dennis W. Camp, 1979: Magnitude and Frequency of Wind Speed Shears from 3 to 150 Meters. Space Sciences Laboratory, NASA/MSFC, Preprint Series No. 79-115.

Kalafus, Rudolph M., 1978: Wind Shear Requirements and Their Application to Laser Systems. FAA-RD-77-123.

Kaufman, John W. and Lester F. Keene, 1968: NASA's 150-Meter Meteorological Tower Located at Kennedy Space Center, Florida. NASA TM X-53699.

Ramsdell, J. V. and D. C. Powell, 1973: Meteorological Information for V/STOL Operations in Built-Up Urban Areas -- An Analysis. FAA-RD-72-135.

Snyder, C. T., 1968: Analogue Study of Longitudinal Response to Wind Shear and Sustained Gusts During Landing Approach. NASA TN D-4447.

Traver, Wilson B., Thomas E. Owen, and Dennis W. Camp, 1972: An Automatic Data Acquisition System for the 150-Meter Ground Winds Tower Facility, Kennedy Space Center. NASA TM X-64708.

TABLE 1.- FIVE-SECOND DATA INTERVAL TESTS SUMMARY

Date 1973	Time LST Start	Time LST End	Number 5 s Obs./ Intervals	Number 5 s Obs./ Level	Maximum Wind Speed Horizontal (kts)	Maximum Wind Speed Horizontal (ms^{-1})	Maximum Wind Speed Downward (kts) (<)	Maximum Wind Speed Downward (ms^{-1})
March 13	0842	1144	74	3700	31	16	12	6
March 14	0932	1234	73	3650	35	18	8	4
July 3	1606	1752	28	1400	51	26	10	5
July 3	1431	1655	50	2500	39	20	8	4
Sept 20	1025	1310	61	3050	20	10	6	3
Sept 24	0812	0945	21	1050	20	10	6	3
Sept 26	1552	1856	75	3750	33	17	8	4
Oct 5	1214	1518	75	3750	30	15	8	4

TABLE 2.- FREQUENCY AND MAXIMUM VALUES OF VERTICAL MOTION IN FIVE-SECOND INTERVAL TESTS

Level (m)	Frequency (f) Up	Frequency (f) Down	Percent (%) Up	Percent (%) Down	Maximum (kts) Up	Maximum (kts) Down	Maximum (ms^{-1}) Up	Maximum (ms^{-1}) Down
150	9657	13143	42.36	57.64	7.04	9.93	3.62	5.11
60	9952	12848	43.65	56.36	7.85	7.25	4.04	3.73
18	13721	9079	60.18	39.82	10.34	7.48	5.32	3.85
10	8296	14504	36.39	63.61	5.77	5.17	2.97	2.66

TABLE 3.- PERCENTAGE FREQUENCY DISTRIBUTION OF DOWNWARD MAGNITUDES

Level (m)		Frequency (f)						Percent (%)					
	kts	$0_{<2}$	$2_{<4}$	$4_{<6}$	$6_{<8}$	$8_{<10}$	$10_{<12}$	$0_{<2}$	$2_{<4}$	$4_{<6}$	$6_{<8}$	$8_{<10}$	$10_{<12}$
	ms^{-1}	$0_{<1}$	$1_{<2}$	$2_{<3}$	$3_{<4}$	$4_{<5}$	$5_{<6}$	$0_{<1}$	$1_{<2}$	$2_{<3}$	$3_{<4}$	$4_{<5}$	$5_{<6}$
150		10074	2782	252	26	6	3	76.65	21.17	1.92	0.20	0.05	0.02
60		9651	2571	549	77	0	0	75.12	20.01	4.27	0.60	0	0
18		7314	1667	94	4	0	0	80.56	18.36	1.04	0.04	0	0
10		10366	3983	155	0	0	0	71.47	27.46	1.07	0	0	0

TABLE 4.- MAXIMUM VALUES OF VERTICAL MOTION IN 10-MINUTE INTERVALS

DATA BY MONTHS, SEASONS, AND LEVELS

Season Month	Updrafts (kts) (ms^{-1})								Downdrafts (kts) (ms^{-1})							
Level (m)																
Winter	150		60		18		10		150		60		18		10	
Oct	9.5	4.9	9.1	4.7	11.5	5.9	7.6	3.9	10.7	5.5	10.3	5.3	9.9	5.1	7.4	3.8
Nov	9.7	5.0	5.8	3.0	11.5	5.9	8.0	4.1	8.0	4.1	10.9	5.6	10.7	5.5	9.3	4.8
Dec	12.4	6.4	9.5	4.9	11.9	6.1	8.6	4.4	8.7	4.5	9.9	5.1	9.9	5.1	5.4	2.8
Jan	11.7	6.0	7.0	3.6	16.1	8.3	8.2	4.2	7.6	3.9	9.5	4.9	8.4	4.3	6.0	3.1
Feb	5.4	2.8	8.9	4.6	18.1	9.3	10.3	5.3	11.1	5.7	16.7*	8.6	10.3	5.3	9.9	5.1
Mar	4.9	2.5	8.9	4.6	18.3*	9.4	11.1*	5.7	7.8	4.0	15.0	7.7	12.2*	6.3	10.3*	5.3
Summer																
Apr	16.3*	8.4	8.2	4.2	18.7	8.6	8.9	4.6	12.6	6.5	16.3	8.4	11.1	5.7	8.9	4.5
May	11.5	5.9	9.9	5.1	12.2	6.3	7.0	3.6	13.6	7.0	12.1	6.2	10.1	5.2	7.8	4.0
Jun	11.9	6.1	7.8	4.0	11.9	6.1	8.2	4.2	12.4	6.4	15.0	7.7	10.3	5.3	9.7	5.0
Jul	9.5	4.9	10.7*	5.5	12.2	6.3	8.9	4.6	15.2*	7.8	11.1	5.7	9.3	4.8	6.6	3.4
Aug	11.5	5.9	8.6	4.4	12.1	6.2	8.2	4.2	12.2	6.3	9.3	4.8	8.9	4.6	7.2	3.7
Sep	13.0	6.7	7.8	4.0	11.7	6.0	7.2	3.7	11.7	6.0	10.3	5.3	10.3	5.3	8.9	4.6

*Level Maximum

TABLE 5.- FREQUENCY OF OCCURRENCE OF MAXIMUM VERTICAL MOTION ≥10 KTS ($\geq 5.15\ ms^{-1}$) IN 10-MINUTE INTERVALS DATA.

	Updrafts			Downdrafts		
Level (m)	Winter (Oct-Mar)	Summer (Apr-Sep)	(f) Total	Winter (Oct-Mar)	Summer (Apr-Sep)	Total
150	13	18	31	2	179	181
60	1	3	4	23	55	78
18	160	141	301	6	5	11
10	2	0	2	3	1	4
Total	176	162	338	34	240	274

TABLE 6.- PERCENTAGE FREQUENCY DISTRIBUTION OF SHEARS VERSUS DOWNDRAFTS

≥3.89 KTS (≥2.0 ms^{-1}) IN 5-SECOND INTERVALS

	SHEARS						DOWNDRAFTS						
Layer (m)	ΔWS (kts)	ΔWS (ms^{-1})	ΔWS/Δd (s^{-1})	Level	Freq.	(kts)	3.89<5.00	5.00<6.01	6.01<7.00	7.00<8.01	8.01<9.00	9.00<9.99	TOTAL
				150	287	(ms^{-1})	2.00<2.57	2.57<3.09	3.09<3.60	3.60<4.42	4.42<4.63	4.63<5.14	
150-120	0<1.9	0<1.0	0<.033				48.43	11.15	1.05	4.88	0.35	1.39	67.25
	1.9<3.9	1.0<2.0	.033<.067				14.29	8.01	1.39	0.70	0.70		25.09
	3.9<5.8	2.0<3.0	.067<.100				5.23	1.39	0.35				6.97
	5.8<7.8	3.0<4.0	.100<.133				0.70						0.70
90-60	0<1.9	0<1.0	0<.033	60	626		28.12	8.15	5.75	0.64			42.66
	1.9<3.9	1.0<2.0	.033<.067				26.20	6.87	3.19				36.26
	3.9<5.8	2.0<3.0	.067<.100				14.70	1.44	0				16.14
	5.8<7.8	3.0<4.0	.100<.133				1.92	0.37	0				2.24
	7.8<9.7	4.0<5.0	.133<.167				0.96	0	0				0.96
	9.7<11.7	5.0<6.0	.167<.200				0.64	0.64	0.48				1.76
60-30				60	626								
	0<1.9	0<1.0	0<.033				27.80	6.07	3.19	0			37.06
	1.9<3.9	1.0<2.0	.033..067				26.84	6.87	3.04	0.32			37.07
	3.9<5.8	2.0<3.0	.067<.100				6.87	2.40	1.92	0.32			11.51
	5.8<7.8	3.0<4.0	.100<.133				5.43	0.96	0.80				7.19
	7.8<9.7	4.0<5.0	.133<.167				3.99	0.64	0.16				4.79
	9.7<11.7	5.0<6.0	.167<.200				1.60	0.64					2.24
	11.7<13.6	6.0<7.0	.200<.233				0.16	0					0.16
30-3													
	0<1.9	0<1.0	0<.033	18	98		0	0					0
	1.9<3.9	1.0<2.0	.033<.067				16.33	1.02					17.35
	3.9<5.8	2.0<3.0	.067<.100				22.45	1.02	1.02	2.04			26.53
	5.8<7.8	3.0<4.0	.100<.133				13.27	0					13.27
	7.8<9.7	4.0<5.0	.133<.167				12.24	0					12.24
	9.7<11.7	5.0<6.0	.167<.200				12.24	1.02					13.26
	11.7<13.6	6.0<7.0	.200<.233				11.22	5.10					16.32
	13.6<15.6	7.0<8.0	.233<.267				1.02	0					1.02
30-3													
	0<1.9	0<1.0	0<.033	10	155		9.68	0					9.68
	1.9<3.9	1.0<2.0	.033<.067				16.77	0.65					16.77
	3.9<5.8	2.0<3.0	.067<.100				25.16	1.94					25.81
	5.8<7.8	3.0<4.0	.100<.133				24.52	0.65					26.46
	7.8<9.7	4.0<5.0	.133<.167				12.90	1.94					13.55
	9.7<11.7	5.0<6.0	.167<.200				3.87						5.81
	11.7<13.6	6.0<7.0	.200<.233				0.65						0.65
	13.6<15.6	7.0<8.0	.233<.267				1.29						1.29

TABLE 7.- MAXIMUM HORIZONTAL WIND SPEED CLASSES VERSUS DOWNDRAFTS

≥9.7 KTS (≥5.0 ms^{-1}) IN 10-MINUTE INTERVALS DATA

	Maximum WS				Downdrafts			
Level (m)	Class	(kts)	(ms^{-1})	(kts)	9.7<11.7	11.7<13.6	13.6<15.6	15.6<17.5
				(ms^{-1})	5<6	6<7	7<8	8<9
150	Low	0<9.7	0<5		2	0	0	
	Moderate	9.7<19.4	5<10		93	16	0	
	High	19.4<35.0	10<18		53	12	2	
	Gale-force	35.0<64.1	18<33		2	0	1	
60	Low	0<9.7	0<5		0	0	0	0
	Moderate	9.7<19.4	5<10		24	2	1	1
	High	19.4<35.0	10<10		36	5	2	1
	Gale-force	35.0<64.1	18<33		4	0	1	1
18	Low	0<9.7	0<5		0	0		
	Moderate	9.7<19.4	5<10		1	1		
	High	19.4<35.0	10<18		6	0		
	Gale-force	35.0<64.1	18<33		3	0		
10	Low	0<9.7	0<5		0			
	Moderate	9.7<19.4	5<10		1			
	High	19.4<35.0	10<18		2			
	Gale-force	35.0<64.1	18<33		1			

TABLE 8.- PERCENTAGE FREQUENCY DISTRIBUTION OF SHEARS VERSUS DOWNDRAFTS

≥9.7 KNOTS (≥5.0 ms^{-1}) IN 10-MINUTE INTERVALS DATA

Layer (m)	ΔWS (kts)	ΔWS (m/sec)	ΔWS/Δd (s^{-1})	Level (m)	Freq. (f)	(kts)	9.7<11.7	11.7<13.6	13.6<15.6	15.6<17.5	Total
						(m/sec)	5<6	6<7	7<8	8<9	
150-120				150	181						
	0<1.9	0<1.0	0<.033				72.93	12.71	1.66		87.30
	1.9<3.9	1.0<2.0	.033<.067				8.84	2.21			11.05
	3.9<5.8	2.0<3.0	.067<.100				1.10	0.55			1.65
	5.8<7.8	3.0<4.0	.100<.133								
90-60											
	0<1.9	0<1.0	0<.033	60	78		60.26	7.69	3.85	0	71.80
	1.9<3.9	1.0<2.0	.033<.067				17.95	0	1.28	2.56	21.79
	3.9<5.8	2.0<3.0	.067<.100				3.85	0	0	0	3.85
	5.8<7.8	3.0<4.0	.100<.133				0	1.28	0	1.28	2.56
60-30											
	0<1.9	0<1.0	0<.033	60	78		50.00	5.13	1.28	2.56	58.97
	1.9<3.9	1.0<2.0	.033<.067				25.64	2.56	0	1.28	29.48
	3.9<5.8	2.0<3.0	.067<.100				6.41	1.28	3.85	0	11.54
	5.8<7.8	3.0<4.0	.100<.133								
30-3											
	0<1.9	0<1.0	0<.033	18	11		9.09	0			9.09
	1.9<3.9	1.0<2.0	.033<.067				9.09	9.09			18.18
	3.9<5.8	2.0<3.0	.067<.100				27.27				27.27
	5.8<7.8	3.0<4.0	.100<.133				9.09				9.09
	7.8<9.7	4.0<5.0	.133<.167				18.18				18.18
	9.7<11.7	5.0<6.0	.167<.200				18.18				18.18
30-3											
	0<1.9	0<1.0	0<.033	10	4		0				0
	1.9<1.9	1.0<2.0	.033<.067				25.00				25.00
	3.9<5.8	2.0<3.0	.067<.100				25.00				25.00
	5.8<7.8	3.0<4.0	.100<.133				0				0
	7.8<9.7	4.0<5.0	.133<.167				50.00				50.00
	9.7<11.7	5.0<6.0	.167<.200				0				0

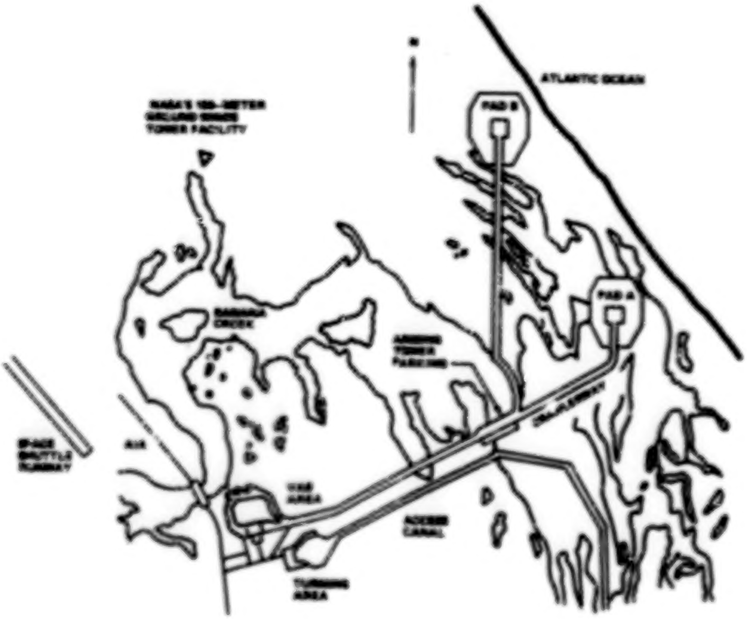
NASA'S 150-METER GROUND WINDS TOWER FACILITY
N
ATLANTIC OCEAN
PAD B
PAD A
BANANA CREEK
SPACE SHUTTLE RUNWAY
VAB AREA
BARGE CANAL
TURNING AREA

Figure 1.- NASA's 150-Meter Ground Winds Tower Facility and Launch Complex 39B, Kennedy Space Center, Florida.

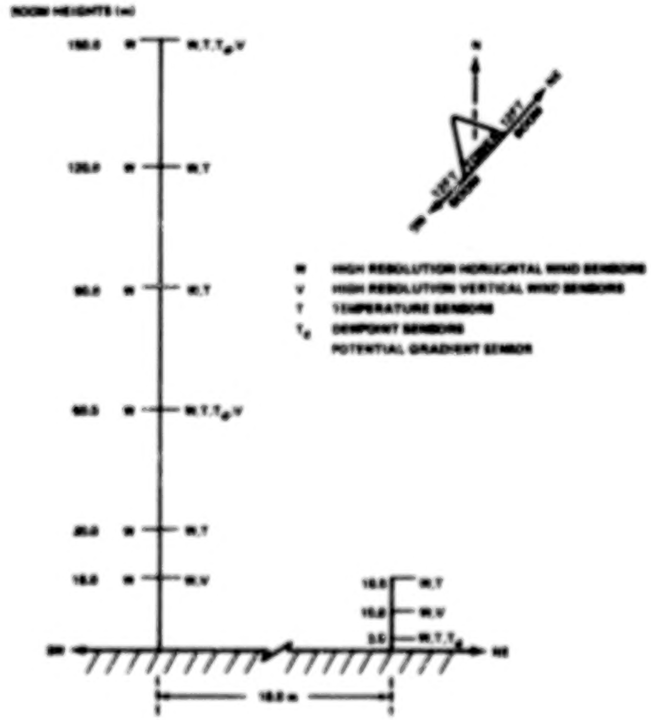
BOOM HEIGHTS (m)
150.0
120.0
90.0
60.0
30.0
18.0
W
W,T,T_d,V
W,T
W,V
N
W HIGH RESOLUTION HORIZONTAL WIND SENSORS
V HIGH RESOLUTION VERTICAL WIND SENSORS
T TEMPERATURE SENSORS
T_d DEWPOINT SENSORS
POTENTIAL GRADIENT SENSOR

Figure 2.- Placement of sensors on NASA's 150-Meter Ground Winds Tower Facility at Kennedy Space Center, Florida. (Note: 1 ft = 0.3048 m.)

1. Report No.
NASA CP-2170, Part 1

2. Government Accession No.

3. Recipient's Catalog No.

4. Title and Subtitle
1980 AIRCRAFT SAFETY AND OPERATING PROBLEMS

5. Report Date
March 1981

6. Performing Organization Code
505-44-23-03

7. Author(s)
Joseph W. Stickle, Compiler

8. Performing Organization Report No.
L-14254

9. Performing Organization Name and Address
NASA Langley Research Center
Hampton, VA 23665

10. Work Unit No.

11. Contract or Grant No.

12. Sponsoring Agency Name and Address
National Aeronautics and Space Administration
Washington, DC 20546

13. Type of Report and Period Covered
Conference Proceedings

14. Sponsoring Agency Code

15. Supplementary Notes

16. Abstract

NASA maintains a continuing research effort on aircraft safety and operating problems. Periodic reports to the aviation community, usually 3 to 5 years apart, are presented in conference form with subsequent publication of the proceedings. This document contains the NASA program presented at the 1980 Aircraft Safety and Operating Problems Conference held at the Langley Research Center, Hampton, VA, November 5-7, 1980. Sessions for the conference included: Terminal-Area Operations; Avionics and Human Factors; Atmospheric Environment; Operating Problems and Potential Solutions; Flight Experiences and Ground Operations; and Acoustic and Noise Reduction.

17. Key Words (Suggested by Author(s))

Airplanes
Flight operations
Crashworthiness
Safety
Terminal area
Environment

18. Distribution Statement
Unclassified - Unlimited

Subject Category 03

19. Security Classif. (of this report)
Unclassified

20. Security Classif. (of this page)
Unclassified

21. No. of Pages
389

22. Price
A17

384

For sale by the National Technical Information Service, Springfield, Virginia 22161

END

June 18, 1981